Trinity College Dublin
Coláiste na Tríonóide, Baile Átha Cliath
The University of Dublin

Combination radiotherapy and immunotherapy: effects on the immune landscape of oesophageal adenocarcinoma and the multimodal therapeutic paradigm

May 2022

A dissertation submitted to the University of Dublin, Trinity College for the degree of Doctor of Philosophy

Noel Edward Donlon

Student number: 07397143

Department of Surgery

Trinity Translational Medical Institute

St. James's Hospital Campus

Trinity College Dublin.

Under the supervision of Prof Joanne Lysaght.

Head of Department; Prof John V Reynolds.

This work is supported by CROSS charity.

Declaration

I declare that this thesis has not been submitted as an exercise for a degree at this or any other university and it is entirely my own work. I agree to deposit this thesis in the University's open access institutional repository or allow the Library to do so on my behalf, subject to Irish Copyright Legislation and Trinity College Library conditions of use and acknowledgement.

Noel E Donlon

May 2022

Acknowledgements

I gratefully acknowledge the CROSS charity funding, without which this work could not have been undertaken. It is a pleasure to thank the many people who made this thesis possible.

I would like to sincerely thank Prof Joanne Lysaght who has at every step of this journey provided constant support, advice and guidance. Her scientific mind, knowledge in the field and enthusiasm to develop new concepts and ideas have made this entire process even more rewarding. Joanne has always allowed me the scope to explore new concepts and new avenues which allowed the project to diversify which undoubtedly led to a better end product.

It is near impossible to articulate the depth of gratitude I must attribute to Prof John Reynolds who has been a constant source of support as a mentor in both clinical practice and academia. His clinical, academic and scientific prowess is exemplary of a rounded surgeon. He has always been supportive and a constant source of encouragement and challenges me to be better. The opportunities he has afforded me, the patience, respect and guidance have allowed me to evolve. He has an incredible work ethic, is dedicated to his patients and enhancing the world of surgery, I can only aspire to his insight, energy and vision.

I would also like to especially thank Dr. Margaret Dunne who was an incredible support in all aspects of this project and I am indebted to her for this. We worked together on a number of projects and she is an all round great person and scientist.

I would also like to thank Jacintha O' Sullivan, Melissa Conroy, Stephen Maher and Niamh Lynam Lennon who were all constant sources of support and mentoring throughout.

I would like to express my gratitude in particular to Maria Davern. We have been working alongside each other for the majority of this journey. Her knowledge, ability, collegiality, friendship and her personality are all that anyone needs to succeed and undoubtedly, she will have an incredible future ahead. I must also thank Andrew Sheppard and Fiona O' Connell who have constantly helped me in every aspect along the way. To all my other friends and colleagues in the lab especially Tim Nugent, Rebecca O'Brien, Aisling Heeran, Croi Buckley, Jason Mc Grath, Eimear Mylod, Laura Kane, I look forward to catching up with you soon at the next night out, it has been a pleasure working alongside you.

I would also like to thank Prof Narayanasamy Ravi and Ms Claire Donohoe, both of whom are excellent surgeons, academics, teachers, mentors, and have a work ethic that is inspiring. To Sinead the data manager, you are a fantastic and crucial component of the department. To Jenny our CNS, your care for patients is incredible, and you always went above and beyond to help me and your humour knows no bounds.

Finally, I would like to thank my entire family for their never ending support in everything I do. To my parents, you have provided for everyone of us and always

ensured we have everything we need to succeed in every facet of life. The opportunities you have provided us and sacrifices you have made have enabled us to develop and the gratitude we all have to you both is incomprehensible. To my brothers Paul and Kieran, sister Josephine, thank you for always being there for me, supporting, encouraging and helping me. I would like to mention my uncle Mel who sadly passed away this year unexpectedly and my auntie Pauline who have looked after me and my siblings as we have grown up. I must also mention my godparents, Patsy and Josephine, who provided me some of the fondest memories of my entire childhood years. You are both fantastic people. Sadly, Josephine passed away just before my viva and this work is dedicated to the memory of both Josephine and my late uncle Mel.

Abstract
The incidence of cancer of the oesophagus and the gastro-oesophageal junction (GEJ) has increased exponentially in the western world over the last half century. Oesophageal adenocarcinoma (OAC) is now the dominant subtype, heavily influenced by western diets and obesity. Despite advances in the multimodal therapeutic strategies to treat the disease, the overall survival remains poor, primarily due to its indolent nature and consequently metastatic or inoperable disease at presentation. For early-stage disease, there are new endotherapies obviating the need for resection, which carries significant morbidities and mortality. However, in locally advanced disease, neoadjuvant chemo(radio)therapy is the gold standard of treatment in the form of FLOT chemotherapy or CROSS chemoradiotherapy. The response rates remain quite poor with suboptimal pathological responses to these current standards of treatment.
The current work highlights that oesophageal adenocarcinoma is an immunogenic cancer and also suggests the potential synergistic effects between radiation and immunotherapy as a viable and realistic treatment option for oesophageal adenocarcinoma in the curative setting. Furthermore, the perioperative immunosuppressive period provides further rationale for use of immune checkpoint blockade (ICB) in conjunction with the current conventional therapies to propagate anti-tumour immunity and shift away from an immunosuppressive milieu.
Radiation at conventional and fractionated dosing induces upregulation of immune checkpoints and significant expression of Damage Associated Molecular Patterns (DAMPs) *in vitro* and *ex vivo,* and radiation therapy was demonstrated to reduce the expression of angiogenesis promoters, which is crucial to mitigate the risk of metastatic disease for upper gastrointestinal cancers. Furthermore, the use of immune checkpoint blockade in combination with radiation synergistically reduced viability in radioresistant cells in this study. Further efforts are needed to understand the nature of radiotherapy-induced immune responses.
This body of work demonstrates that the hostile features of the tumour microenvironment of hypoxia and nutrient deprivation induce the upregulation of a range of immune checkpoints proteins, representing therapeutic potential with single or double agent ICBs that target the PD-1 and CTLA-4 axes. There was also a significant upregulation in IFN-γ and IL-12 by T cells as a consequence of radiation, which was significantly higher under conditions of the tumour microenvironment (TME). The cytolytic assay, which represented an *in vitro* model of T cell killing at the tumour site following radiation, shows promise of the synchronised and potent anti-tumour effect of combining radiation with immune checkpoint blockade, with significantly increased cytolysis evident with ICB and radiation, particularly noted with 4Gy radiation and Pembrolizumab.
This work also highlighted that the TME is more immunosuppressive than the lymph node microenvironment (LNME), and that nodal involvement surpasses both clinical and pathological tumour staging for prognostication purposes, highlighting the pivotal role of the tumour draining lymph node in OAC pathogenesis. There was also observed evidence of the rewiring of the Tumour Draining Lymph Node (TDLN) toward pre-metastatic niche orchestrated perhaps by the neighbouring TME with increases in immune checkpoint expression, a potential therapuetic target in the curative setting.
In the perioperative study, it was highlighted that there was a prevailing Th2-like immunophenotype post-surgery. Therefore, shifting the balance in favour of a Th1-like phenotype would offer a potent therapeutic approach to promote cancer regression and prevent recurrence in the adjuvant setting and could potentially propagate anti-tumour

immune responses perioperatively if ICBs were administered in the immediate neoadjuvant setting.
Consequently, with the promising results from the checkmate 577 trial, this body of work paves the way for further studies and appropriate trial design for the use of ICBs in the multimodal treatment of locally advanced disease in the neoadjuvant, adjuvant and curative setting and warrants further interrogation.

Publications

First author

Radiotherapy, immunotherapy, and the tumour microenvironment: Turning an immunosuppressive milieu into a therapeutic opportunity. Donlon NE, Power R, Hayes C, Reynolds JV, Lysaght J. Cancer Lett. 2021 Apr 1;502:84-96. doi: 10.1016/j.canlet.2020.12.045. Epub 2021 Jan 12. PMID: 33450360.

Radiation and Immunotherapy in Upper Gastrointestinal Cancers: The Current State of Play. Donlon NE, Power R, Hayes C, Davern M, Reynolds JV, Lysaght J. Int J Mol Sci. 2021 Jan 22;22(3):1071. doi: 10.3390/ijms22031071. PMID: 33499003; PMCID: PMC7865314.

The tumour immune microenvironment in oesophageal cancer. Davern M*, **Donlon NE*,** Power R, Hayes C, King R, Dunne MR, Reynolds JV. Br J Cancer. 2021 Aug;125(4):479-494. doi: 10.1038/s41416-021-01331-y. Epub 2021 Apr 26. PMID: 33903730; PMCID: PMC8368180. **denotes equal contribution.*

Modern oncological and operative outcomes in oesophageal cancer: the St. James's hospital experience. Donlon NE, Ravi N, King S, Cunninhgam M, Cuffe S, Lowery M, Wall C, Hughes N, Muldoon C, Ryan C, Moore J, O'Farrell C, Gorry C, Duff AM, Enright C, Nugent TS, Elliot JA, Donohoe CL, Reynolds JV. Ir J Med Sci. 2021 Feb;190(1):297-305. doi: 10.1007/s11845-020-02321-4. Epub 2020 Jul 21. PMID: 32696244.

The Prognostic Value of the Lymph Node in Oesophageal Adenocarcinoma; Incorporating Clinicopathological and Immunological Profiling. Donlon NE*, Davern M*, Sheppard A, Power R, O'Connell F, Heeran AB, King R, Hayes C, Bhardwaj A, Phelan JJ, Dunne MR, Ravi N, Donohoe CL, O'Sullivan J, Reynolds JV, Lysaght J. Cancers (Basel). 2021 Aug 9;13(16):4005. doi: 10.3390/cancers13164005. PMID: 34439160. **denotes equal contribution.*

Linking Circulating Serum Proteins with Clinical Outcomes in Esophageal Adenocarcinoma-An Emerging Role for Chemokines. Donlon NE, Sheppard A, Davern M, O'Connell F, Phelan JJ, Power R, Nugent T, Dinneen K, Aird J, Greene J, Nevins Selvadurai P, Bhardwaj A, Foley EK, Ravi N, Donohoe CL, Reynolds JV, Lysaght J, O'Sullivan J, Dunne MR. Cancers (Basel). 2020 Nov 13;12(11):3356. doi: 10.3390/cancers12113356. PMID: 33202734; PMCID: PMC7698106.

The Impact of Esophageal Oncological Surgery on Perioperative Immune Function; Implications for Adjuvant Immune Checkpoint Inhibition. Donlon NE, Davern M, Sheppard AD, O'Connell F, Dunne MR, Hayes C, Mylod E, Ramjit S, Temperley H, Mac Lean M, Cotter G, Bhardwaj A, Butler C, Conroy MJ, O'Sullivan J, Ravi N, Donohoe CL, Reynolds JV, Lysaght J. Front Immunol. 2022 Jan 27;13:823225. doi: 10.3389/fimmu.2022.823225. PMID: 35154142; PMCID: PMC8829578.

The impact of radiotherapy on the immune landscape in oesophageal adenocarcinoma. Noel E Donlon*, Maria Davern*, Andrew Sheppard, Fiona O' Connell, Aisling B Heeran, Anshul Bhardwaj, Christine Butler, Narayanasamy Ravi, Claire L Donohoe, Niamh Lynam Lennon, Margaret R Dunne, Stephen G Maher,

Jacintha O' Sullivan, John V Reynolds, Joanne Lysaght. *denotes equal contribution. *World J Gastroenterol* 2022; 28(21): 2302-2319 [DOI: 10.3748/wjg.v28.i21.2302].

The immune response to major gastrointestinal cancer surgery and potential implications for adjuvant immunotherapy. N. E. Donlon, M. Davern, C. Hayes, R. Power, A. D. Sheppard, C. L. Donohoe, J Lysaght, J V Reynolds. Critical Reviews in Haematology/Oncology. 2022 Vol. 175 Pages 103729. DOI: https://doi.org/10.1016/j.critrevonc.2022.103729

Adverse Biology in Adenocarcinoma of the Esophagus and Esophagogastric Junction Impacts Survival and Response to Neoadjuvant Therapy Independent of Anatomic Subtype. Donlon NE, Elliott JA, Donohoe CL, Murphy CF, Nugent T, Moran B, King S, Ravi N, Reynolds JV. Ann Surg. 2020 Nov;272(5):814-819. doi: 10.1097/SLA.0000000000004184. PMID: 32657924.

FLOT-regimen Chemotherapy and Transthoracic en bloc Resection for Esophageal and Junctional Adenocarcinoma. Donlon NE, Kammili A, Roopnarinesingh R, Davern M, Power R, King S, Chmelo J, Phillips AW, Donohoe CL, Ravi N, Lowery M, Mueller CL, Cools-Lartigue J, Ferri LE, Reynolds JV. Ann Surg. 2021 Jul 26. doi: 10.1097/SLA.0000000000005097. Epub ahead of print. PMID: 34310355.

CROSS versus FLOT regimens in Esophageal and Esophagogastric Junction Adenocarcinoma: A propensity-matched comparison reveals equivalent oncologic outcomes but differential impact on respiratory complications and tolerance. Donlon N.E., Moran B, Kammili A, Donohoe CL, Ravi N, Lowery M, Mueller CL, Cools-Lartigue J, Ferri LE, Reynolds JV. Accepted; Annals of Surgery Nov 2022.

Prophylactic negative wound therapy in laparotomy wounds (PROPEL trial): randomized controlled trial. Donlon NE, Boland PA, Kelly ME, Schmidt K, Cooke F, Neary PM, Barry KM, Reynolds JV. Int J Colorectal Dis. 2019 Nov;34(11):2003-2010. doi: 10.1007/s00384-019-03398-9. Epub 2019 Sep 16. PMID: 31529194.

The Use of Clinical Parameters as Adjuncts to Endoscopic Evaluation of Mural Thickening on Conventional Computed Tomography in Diagnosing Malignancy. Donlon NE, Kelly ME, Zafar M, Boland PA, Davis C, Wei Teh J, Corless K, Khan W, Khan I, Waldron R, Barry K. Dig Surg. 2021;38(3):230-236. doi: 10.1159/000514777. Epub 2021 Mar 30. PMID: 33784697.

Embolization or disruption of thoracic duct and cisterna chyli leaks post oesophageal cancer surgery should be first line management for ECCG-defined type III chyle fistulae. Donlon NE, Nugent TS, Power R, Butt W, Kamaludin A, Dolan S, Guiney M, Mc Eniff N, Ravi N, Reynolds JV. Ir J Med Sci. 2021 Aug;190(3):1111-1116. doi: 10.1007/s11845-020-02396-z. Epub 2020 Oct 11. PMID: 33040261.

Robotic versus laparoscopic anterior resections for rectal and rectosigmoid cancer: an institutional experience. Donlon NE, Nugent TS, Free R, Hafeez A, Kalbassi R, Neary PC, O'Riordain DS. Ir J Med Sci. 2021 Apr 13. doi: 10.1007/s11845-021-02625-z. Epub ahead of print. PMID: 33846946.

Predictive value of CRP/albumin ratio in major abdominal surgery. Donlon NE, Mohan H, Free R, Elbaghir B, Soric I, Fleming C, Balasubramanian I, Ivanovski I, Schmidt K, Mealy K. Ir J Med Sci. 2020 Nov;189(4):1465-1470. doi: 10.1007/s11845-020-02238-y. Epub 2020 May 2. PMID: 32361882.

Negative appendicectomy rates as a quality measure in a regional surgical unit: a retrospective review. Donlon NE, Kelly ME, Sheppard A, Davern M, Nugent TS, Boland PA, Corless K, Khan W, Khan I, Waldron R, Barry K. Ir J Med Sci. 2021 May;190(2):755-761. doi: 10.1007/s11845-020-02360-x. Epub 2020 Sep 11. PMID: 32915371.

Should MRI Be the Imaging Modality of Choice in Suspected Appendicitis During Pregnancy?Donlon NE, Kelly ME, Davern M, Sheppard A, Nugent T, Durand M, Mehigan BJ, Larkin JO, McCormick PH. Ir Med J. 2019 Dec 16;112(10):1018. PMID: 32311244.

Last author

The oncogenic and clinical implications of lactate induced immunosuppression in the tumour microenvironment. Hayes C, Donohoe CL, Davern M, **Donlon NE.** Cancer Lett. 2021 Mar 1;500:75-86. doi: 10.1016/j.canlet.2020.12.021. Epub 2020 Dec 23. PMID: 33347908.

Hypoxia and its impact on the tumour microenvironment of gastroesophageal cancers. King R, Hayes C, Donohoe CL, Dunne MR, Davern M, **Donlon NE.** World J Gastrointest Oncol. 2021 May 15;13(5):312-331. doi: 10.4251/wjgo.v13.i5.312. PMID: 34040696; PMCID: PMC8131902.

Co-authored

Tissue distribution of γδ T cell subsets in oesophageal adenocarcinoma. Melo AM, Mylod E, Fitzgerald V**, Donlon NE,** Murphy DM, Foley EK, Bhardwaj A, Reynolds JV, Doherty DG, Lysaght J, Dunne MR, Conroy MJ. Clin Immunol. 2021 Aug;229:108797. doi: 10.1016/j.clim.2021.108797. Epub 2021 Jul 15. PMID: 34273585.

Fractalkine Elicits Chemotactic, Phenotypic, and Functional Effects on CX3CR1^{+}CD27^{-} NK Cells in Obesity-Associated Cancer. Mylod E, Melo AM**, Donlon NE,** Davern M, Bhardwaj A, Reynolds JV, Lysaght J, Conroy MJ. J Immunol. 2021 Aug 15;207(4):1200-1210. doi: 10.4049/jimmunol.2000987. Epub 2021 Jul 28. PMID: 34321227.

Chemotherapy regimens induce inhibitory immune checkpoint protein expression on stem-like and senescent-like oesophageal adenocarcinoma cells. Davern M, **Donlon NE,** Sheppard A, Connell FO, Hayes C, Bhardwaj A, Foley E, Toole DO, Lynam-Lennon N, Ravi N, Reynolds JV, Maher SG, Lysaght J. Transl Oncol. 2021 Jun;14(6):101062. doi: 10.1016/j.tranon.2021.101062. Epub 2021 Mar 22. PMID: 33765543; PMCID: PMC8008239.

Cooperation between chemotherapy and immune checkpoint blockade to enhance anti-tumour T cell immunity in oesophageal adenocarcinoma. Davern M, **Donlon**

NE, O' Connell F, Sheppard AD, Hayes C, King R, Temperley H, Butler C, Bhardwaj A, Moore J, Bracken-Clarke D, Donohoe C, Ravi N, Reynolds JV, Maher SG, Conroy MJ, Lysaght J. Transl Oncol. 2022 Mar 30;20:101406. doi: 10.1016/j.tranon.2022.101406. Epub ahead of print. PMID: 35366537; PMCID: PMC8976141.

PD-1 and TIGIT blockade differentially affect tumour cell survival under hypoxia and glucose deprived conditions in oesophageal adenocarcinoma; implications for overcoming resistance to PD-1 blockade in hypoxic tumours. Davern M, Fitzgerald MC, Buckley CE, Heeran AB, **Donlon NE,** McGrath J, O' Connell F, Deshpande MR, Hayes C, MacDonald J, Sheppard AD, Reynolds JV, Maher SG, Lynam-Lennon N, Murphy B, Lysaght J. Transl Oncol. 2022 May;19:101381. doi: 10.1016/j.tranon.2022.101381. Epub 2022 Mar 1. PMID: 35245832; PMCID: PMC8894275.

Safety, efficacy, and cost-effectiveness of minimally invasive esophagectomies versus open esophagectomies: an umbrella review. Ramjit SE, Ashley E, **Donlon NE,** Weiss A, Doyle F, Heskin L. Dis Esophagus. 2022 May 22:doac025. doi: 10.1093/dote/doac025. Epub ahead of print. PMID: 35596955.

Resection of oesophageal and oesophagogastric junction cancer liver metastases - a summary of current evidence. Weiss ARR, **Donlon NE,** Schlitt HJ, Hackl C. Langenbecks Arch Surg. 2022 May;407(3):947-955. doi: 10.1007/s00423-021-02387-3. Epub 2021 Dec 3. PMID: 34860291; PMCID: PMC9151540.

PD-1 inhibitors in esophageal cancer: a systematic review of the oncological outcomes associated with PD-1 blockade and the evolving therapeutic paradigm. Whooley J, Alazzawi M, **Donlon NE,** Bolger JC, Robb WB. Dis Esophagus. 2021 Sep 23:doab063. doi: 10.1093/dote/doab063. Epub ahead of print. PMID: 34553222.

Chemokine-targeted therapies: An opportunity to remodel immune profiles in gastro-oesophageal tumours. O'Donovan C, Davern M, **Donlon NE,** Lysaght J, Conroy MJ. Cancer Lett. 2021 Sep 8;521:224-236. doi: 10.1016/j.canlet.2021.09.005. Epub ahead of print. PMID: 34506844.

Radiation-induced Bystander Effect (RIBE) alters mitochondrial metabolism using a human rectal cancer *ex vivo* explant model. Heeran AB, Berrigan HP, Buckley CE, Bottu HM, Prendiville O, Buckley AM, Clarke N, **Donlon NE,** Nugent TS, Durand M, Dunne C, Larkin JO, Mehigan B, McCormick P, Brennan L, Lynam-Lennon N, O'Sullivan J. Transl Oncol. 2021 Jan;14(1):100882. doi: 10.1016/j.tranon.2020.100882. Epub 2020 Oct 23. PMID: 33129115; PMCID: PMC7586242.

Investigating the susceptibility of treatment-resistant oesophageal tumours to natural killer cell-mediated responses. Mylod E, McKenna E, Davern M, Barr MP, **Donlon NE**, Bibby BAS, Bhardwaj A, Reynolds JV, Lysaght J, Maher SG, Conroy MJ. Clin Exp Med. 2022 Apr 1. doi: 10.1007/s10238-022-00811-6. Epub ahead of print. PMID: 35364779.

COVIDSurg Collaborative; GlobalSurg Collaborative. Timing of surgery following SARS-CoV-2 infection: an international prospective cohort study. Anaesthesia. 2021 Jun;76(6):748-758. doi: 10.1111/anae.15458. Epub 2021 Mar 9. PMID: 33690889; PMCID: PMC8206995.

Obesity and anastomotic leak rates in colorectal cancer: a meta-analysis. Nugent TS, Kelly ME, **Donlon NE**, Fahy MR, Larkin JO, McCormick PH, Mehigan BJ**.** Int J Colorectal Dis. 2021 Sep;36(9):1819-1829. doi: 10.1007/s00384-021-03909-7. Epub 2021 Apr 1. PMID: 33796958.

Management of chyle leaks following esophageal resection: a systematic review. Power R, Smyth P, **Donlon NE,** Nugent T, Donohoe CL, Reynolds JV. Dis Esophagus. 2021 Mar 16:doab012. doi: 10.1093/dote/doab012. Epub ahead of print. PMID: 33723611.

Body composition is associated with operative and oncologic outcomes in the management of retroperitoneal and trunk soft tissue sarcoma. Boyle EA, Elliott JA, McIntyre TV, Barnes ME, **Donlon NE,** Umair M, Gillis AE, Ridgway PF. Am J Surg. 2021 Aug 8:S0002-9610(21)00464-5. doi: 10.1016/j.amjsurg.2021.08.005. Epub ahead of print. PMID: 34389158.

Acidosis significantly alters immune checkpoint expression profiles of T cells from oesophageal adenocarcinoma patients. Maria Davern*, **Noel E. Donlon*,** Conall Hayes, Ross King, Robert Power, Andrew Sheppard, Gillian Cotter, Michael MacLean, Hugo Temperley, Melissa J. Conroy, Christine Butler, Fiona O' Connell, Anshul Bhardwaj, N Ravi, Dara Bracken-Clarke, Claire L. Donohoe, John V. Reynolds, Margaret Dunne, Joanne Lysaght. Accepted Translational Oncology. *denotes equal contribution. Cancer Immunol Immunother. 2022 Jun 16. doi: 10.1007/s00262-022-03228-y. Epub ahead of print. PMID: 35708739.

The Protein Secretome Is Altered in Rectal Cancer Tissue Compared to Normal Rectal Tissue, and Alterations in the Secretome Induce Enhanced Innate Immune Responses. Heeran AB, Dunne MR, Morrissey ME, Buckley CE, Clarke N, Cannon A, **Donlon NE,** Nugent TS, Durand M, Dunne C, Larkin JO, Mehigan B, McCormick P, Lynam-Lennon N, O'Sullivan J. Cancers (Basel). 2021 Feb 2;13(3):571. doi: 10.3390/cancers13030571. PMID: 33540635; PMCID: PMC7867296.

Prospective study of surgical site infections post-open esophageal cancer surgery, and the impact of care bundles. Raftery NB, Murphy CF, **Donlon NE,** Heneghan H, Donohoe CL, King S, O'Connell B, Ravi N, Reynolds JV. Dis Esophagus. 2021 Feb 16:doaa136. doi: 10.1093/dote/doaa136. Epub ahead of print. PMID: 33590037.

RETAINER Collaborative Group; Irish Surgical Research Collaborative. International snapshot study exploring the impact of COVID-19 on elective inguinal hernia repair. Br J Surg. 2021 Sep 27;108(9):e301-e1173. doi: 10.1093/bjs/znab198. PMID: 34333632; PMCID: PMC8385828.

Outcomes following colonic stenting for malignant left-sided bowel obstruction: a systematic review of randomised controlled trials Boland PA, Kelly ME, **Donlon NE,** Rausa E, Beddy DP, McCormick PH, Mehigan BJ, Larkin JO.. Int J Colorectal Dis.

2019 Oct;34(10):1625-1632. doi: 10.1007/s00384-019-03378-z. Epub 2019 Sep 2. PMID: 31475316.

Management options for chronic anal fissure: a systematic review of randomised controlled trials. Boland PA, Kelly ME**, Donlon NE,** Bolger JC, Larkin JO, Mehigan BJ, McCormick PH. Int J Colorectal Dis. 2020 Oct;35(10):1807-1815. doi: 10.1007/s00384-020-03699-4. Epub 2020 Jul 25. PMID: 32712929.

Gastro-cholecysto-colic fistula. Case report of an idiopathic case, and management approach. Irwin S, **Donlon NE,** Mohan H, Reynolds JV. J Surg Case Rep. 2020 Aug 26;2020(8):rjaa162. doi: 10.1093/jscr/rjaa162. PMID: 32864091; PMCID: PMC7449391.

Obscure gastrointestinal bleeding resulting from small bowel neoplasia; A case series. Teh JW, Fowler AL, **Donlon NE,** Khan W, Khan IZ, Waldron M, Barry K. Int J Surg Case Rep. 2019;60:87-90. doi: 10.1016/j.ijscr.2019.05.006. Epub 2019 May 10. PMID: 31207533; PMCID: PMC6580013.

Research articles under revisions/preparation

The impact of radiation on DAMP expression in oesophageal adenocarcinoma. Authors: Noel E Donlon, Maria Davern, Andrew Sheppard, Fiona O' Connell, Melissa Conroy, Narayanasamy Ravi, Claire L Donohoe, John V Reynolds, Joanne Lysaght. Manuscript under preparation, submitting to Diseases of the Esophagus October 2022.

Radiation, immune checkpoint blockade and the tumour microenvironment. Authors: Noel E Donlon, Maria Davern, Andrew Sheppard, Fiona O' Connell, Melissa Conroy, Narayanasamy Ravi, Claire L Donohoe, John V Reynolds, Joanne Lysaght. Manuscript under preparation, submitting to Cancer Letters October 2022.

Single Centre Experience in Implementation of Endoscopic Surveillance Protocol after Oesophagectomy. Authors: Ahmed Kamaludin, **Noel E Donlon,** Matthew Kavanagh, John V Reynolds, Claire L Donohoe. Under review Diseases of the Esophagus.

FLOT and CROSS chemotherapy regimens alter the frequency of CD27+ and CD69+ T cells in oesophagogastric adenocarcinomas; implications for combination with immunotherapy. Authors: Maria Davern, **Noel E. Donlon**, Andrew S. Sheppard, Klaudia Majcher, Fiona O' Connell, Aisling B. Heeran, Malika Grant, Robert A. Farrell, Conall Hayes, Melissa J. Conroy, Emma Foley, Dermot O' Toole, Anshul Bhardwaj, Narayanasamy Ravi, John V. Reynolds, Stephen G. Maher, Joanne Lysaght. Under revisions Translational Oncology.

Targeting inhibitory immune checkpoint proteins in oesophageal adenocarcinoma patients to enhance anti-tumour T cell immunity. Authors: Maria Davern, **Noel E. Donlon,** Andrew S. Sheppard, Fiona O' Connell, Conall Hayes, Melissa J. Conroy, Emma Foley, Dermot O' Toole, Anshul Bhardwaj, Narayanasamy Ravi, John V. Reynolds, Stephen G. Maher, Joanne Lysaght. Submitted to Journal of Immunotherapy for Cancer August 2022.

Nutrient deprivation and hypoxia alter T cell immune checkpoint expression; potential impact for immunotherapy. Authors: Maria Davern, **Noel E. Donlon,** Conall Hayes, Ross King, Andrew Sheppard, Gillian Cotter, Hugo Temperley, Melissa J. Conroy, Christine Butler, Fiona O' Connell, Anshul Bhardwaj, N Ravi, Claire L. Donohoe, John V. Reynolds, Joanne Lysaght. Manuscript under preparation, submitting to Cancer Immunology and Immunotherapy October 2022.

PD-1 immune checkpoint blockade enhances FLOT chemotherapy toxicity in oesophageal adenocarcinoma cells via immune-independent mechanisms. Authors: Maria Davern, **Noel E. Donlon,** Andrew Sheppard, Gillian Cotter, Michael MacLean, Hugo Temperley, Melissa J. Conroy, Christine Butler, Fiona O' Connell, Anshul Bhardwaj, N Ravi, Dara Bracken-Clarke, Claire L. Donohoe, John V. Reynolds, Margaret Dunne, Joanne Lysaght. Manuscript under preparation, submitting to Cancer Letters October 2022.

PD-1 and TIGIT blockade differentially affect tumour cell survival under hypoxia and glucose deprived conditions in oesophageal adenocarcinoma; implications for overcoming resistance to PD-1 blockade in hypoxic tumours. Authors: Maria Davern, Croí Buckley, Claire Fitzgerald, Aisling B. Heeran, **Noel E. Donlon**, Andrew S. Sheppard, Malvika Dreshpande, Fiona O' Connell, John V. Reynolds, Stephen G. Maher, Joanne Lysaght. Submitting to Cancers August 2022.

The secretome of visceral adipose tissue from oesophageal adenocarcinoma patients promotes an IL-17-like pro-inflammatory T cell phenotype which is attenuated by immune checkpoint blockade. Authors: Maria Davern, Dara Bracken-Clarke, **Noel E. Donlon,** Andrew D. Sheppard, Fiona O' Connell, Klaudia Majcher, Melissa J. Conroy, Eimear Mylod, Christine Butler, Claire Donohoe, Anshul Bhardwaj, Narayanasamy Ravi, Ashanty Melo, John V. Reynolds, Joanne Lysaght. Manuscript under preparation, submitting to Journal for Immunotherapy of Cancer October 2022.

The secretome of tumour-draining lymph nodes, omentum and liver promote a metastatic phenotype in oesophageal adenocarcinoma cells via chemokine receptor signalling axes; a role for CXCR4, CCR1 and CX3CR1 to target metastasis. Authors: Maria Davern*, Katelynn Cahill*, **Noel E. Donlon,** Caoimhe Guaghan, Andrew Sheppard, Christine Butler, Fiona O' Connell, Eimear Mylod, Ashanty Melo, Klaudia Majcher, Maria Kavanagh, Anshul Bhardwaj, N Ravi, Dara Bracken-Clarke, Claire L. Donohoe, John V. Reynolds, Melissa J. Conroy, Joanne Lysaght. Manuscript under preparation, submitting to Cancer Letters October 2022. *denotes equal contribution.

Radiation alters chemokine receptor signalling which alters migration and anti-tumour phenotypes of T cells in oesophageal adenocarcinoma. Authors: Maria Davern, Cillian O' Donovan, **Noel E. Donlon**, Caoimhe Guaghan, Eimear Mylod, Andrew Sheppard, Christine Butler, Fiona O' Connell, Anshul Bhardwaj, N Ravi, Dara Bracken-Clarke, Claire L. Donohoe, John V. Reynolds, Joanne Lysaght, Melissa J. Conroy. Manuscript under preparation, submitting to Cancer Immunology and Immunotherapy October 2022.

Presentations

National

Trinity Translational Medicine Institute Precision Medicine Cancer Symposium, Dublin, Ireland, 15th February 2019 3-minute flash presentation; Immunotherapy and radiotherapy: a double edged sword?

The Irish Association for Cancer Research Annual Conference, (Breakthrough Cancer Research Session, poor survival rate cancers session) virtual conference, 24th-26th March 2021. Title: Timing is everything; Harnessing the double edge sword of surgery with immunotherapy in the perioperative phase.

Sir Peter Freyer memorial lecture & surgical virtual symposium, 4th-5th September 2021. Title: Perioperative immunosuppression in Oesophageal cancer; a new therapeutic target?

Sir Peter Freyer memorial lecture & surgical virtual symposium, 4th-5th September 2021. Title: Enhancing Radiation Induced Immunogenicity In The Multimodal Treatment Of Oesophageal Cancer: A Bench To Bedside Approach

Sylvester O' Halloran Virtual Perioperative Symposium, Ireland, 5th - 6th March 2021. Title: The cytolytic effect of ionising radiation and immunotherapy in oesophageal cancer.

Sir Peter Freyer memorial lecture & surgical virtual symposium, 6th-7th September 2019. Plenary session. Title: Immunotherapy, radiotherapy and the tumour microenvironment.

Waterford October meeting 2019. Plenary Session. Title: Immunotherapy in Upper Gastrointestinal Cancer.

Sylvester O' Hallorhan 1st-2nd March 2019. ASIT Prize section. Title: The effect of conventional therapies on anti-tumour immune responses in oesophageal cancer.

International

Oral

11th NE National Colorectal Forum Newcastle upon Tyne 19th November 2019. Title: The immune landscape of Upper GI cancers.

Association of Surgeons of Great Britain and Ireland Short paper series 26th August 2020. Title: Enhancing responses to current treatment strategies in Oesophageal Cancer. A novel approach to a not so novel disease.

Association of Surgeons of Great Britain and Ireland Virtual Congress 4th-8th May 2021. Title: The immune landscape of the Tumour draining lymph node and the Tumour Microenvironment in oesophageal; A novel therapeutic target

European Surgical Association 23rd – 25th May 2021. Title: FLOT-regimen Chemotherapy and Transthoracic en bloc Resection for Esophageal and Junctional Adenocarcinoma.

Poster

Association of Surgeons of Great Britain and Ireland Virtual Congress 4th-8th May 2021. Title. From bench to bedside; A rationale for Immunotherapy in the adjuvant setting for Oesophageal cancer.

International Society of Diseases of the Esophagus September 27th – 30th 2021. Title: Non-Alcoholic fatty liver disease and the hepatic response to surgery among patients with Esophageal adenocarcinoma.

International Society of Diseases of the Esophagus September 27th – 30th 2021. Title: The immune response to Esophageal Cancer Surgery: Implications for Postoperative Adjuvant Immunotherapy.

International Society of Diseases of the Esophagus September 27th – 30th 2021. Title: Radiation, Immunotherapy and the Tumour Microenvironment in Esophageal cancer.

EACR Defence is the Best Attack 2021, virtual conference, 16th-17th February 2021. Title: The importance of Incorporating clinicopathological and Immunomodulatory features of Tumour draining lymph nodes in identifying new targets into multimodal therapy for Oesophageal Adenocarcinoma.

EACR 2021 Poster presentation 9th – 12th June 2021. Title: Timing is everything; Manipulating the surgery induced immunosuppressive milieu into a therapeutic target.

Annual Irish Association for Cancer Research Conference, Belfast, Ireland, 20th-22nd February 2019. Title: The effect of radiation on DAMP expression in oesophageal adenocarcinoma.

Defence is the Best Attack: Immuno-Oncology Breakthroughs, Barcelona, Spain, 11th-13th March 2019. Title: The impact of ionising radiation on the tumor microenvironment in oesophageal cancer.

8th ImmunoTherapy of Cancer Conference (iTOC8), young researcher session 8th-9th October 2021. Title: Impact of major oncologic surgery on immune responses in the immediate post-operative setting in oesophageal adenocarcinoma patients; a guide to harnessing the double-edged sword of cancer surgery

Awards

National University of Ireland Galway/Mayo University Hospital Academic Research Trainee Winner 2018.

Beacon Hospital Research Fund 2018-2019 €10,000.

Strattice mesh research Bursary €1,000 Oct 2018.

Association of Surgeons in Training Scientific Prize Sylvester O' Hallorhan Meeting March 2019.

William O' Keefe Waterford Meeting Prize October 2019.

TTMI Collaborative Pilot Study Awards €6,000 March 2020.

The William O' Keefe lecture October 2021.

Bank of Ireland research fund €52,000 Jan 2022.

TTMI Collaborative Pilot Study Awards €6,000 March 2022.

Figures

Tables

List of Abbreviations

ALA	Alpha linolenic acid
ATP	Adenosine Triphosphate
APC	Antigen presenting cell
CAFs	Cancer-associated fibroblasts
COX	Cyclooxygenase
cRPMI	complete Roswell Parks Memorial Institute
CAF	Cancer Associated Fibroblast
CTC	Circulating tumour cell
CTLs	Cytotoxic T Lymphocytes
CTLA4	Cytotoxic T-lymphocyte associated protein 4
DAMP	Danger-associated molecular patterns
DC	Dendritic cell
dCRT	Definitive Chemoradiotherapy
DHA	Docosahexaenoic acid
DTCs	Disseminated tumour cells
EBRT	External beam radiotherapy
EDTA	Ethylene-diamine tetra-acetic acid
EMT	Epithelial to mesenchymal transition
EPA	Eicosapentaenoic acid
ESPEN	European Society for Clinical Nutrition and Metabolism
GORD	Gastro-oesophageal reflux disease
HIF-1α	hypoxia inducible factor 1
HMGB1	High mobility group box 1
HR	Hazards ratios
ICB	Immune checkpoint blockade
IFN-γ	Interferon-gamma
IL	Interleukin
iNOS	inducible nitric oxide synthase
IL-1Ra	IL-1 receptor antagonist
ITT	Intention to treat
LAG-3	Lymphocyte Activation Gene-3
LNCM	Lymph node conditioned media
MDSCs	Myeloid-derived suppressor cells
MHC	Major Histocompatability complex
MSD	Meso Scale Diagnostics, USA
MSI-H/dMMR	Microsatellite instability-high/deficiency mismatch repair
NET	Neutrophil extracellular trap
NK	Natural killer
NSCLC	Non-small cell lung cancer
OAC	Oesophageal Adenocarcinoma
OS	Overall survival
OSCC	Oesophageal Squamous Cell Cancer
PD-1	Programmed cell death protein 1
PD-L1	Programmed Death-Ligand 1
PD-L2	Programmed Death-Ligand 2
PBMC	Peripheral Blood Mononuclear Cell
PBS	Phosphate Buffered Saline
pCR	Pathologic complete response

PFS	Progression-free survival
PGE2	Prostaglandin E2
PUFA	Polyunsaturated fatty acids
RCT	Randomised Control Trial
ROS	Reactive Oxygen Species
SIRS	Systemic inflammatory immune response
TAM	Tumour Associated Macrophages
TCM	Tumour Conditioned Media
TCR	T Cell Receptor
TDLN	Tumour-draining lymph node
TGF-β	Transforming growth factor β
TH	Transhiatal
Th1	T helper type 1
Th2	T helper type 2
TIGIT	T cell immunoreceptor with Ig and ITIM domains
TIL	Tumour Infiltrating Lymphocyte
TIM-3	T cell immunoglobulin and mucin-domain containing-3
TLR	Toll-like receptor
TMB	Tumour mutational burden
TME	Tumour microenvironment
TNF-α	Tumour necrosis factor α
Tregs	Regulatory T cells
TRAEs	Treatment related adverse events TRAEs
TSP	Tumour stroma percentage

Table of contents

Chapter 1 Introduction

Chapter 2; Materials and methods

Chapter 1
Introduction

Donlon NE, Power R, Hayes C, Davern M, Reynolds JV, Lysaght J. Radiation and Immunotherapy in Upper Gastrointestinal Cancers: The Current State of Play. Int J Mol Sci. 2021 Jan 22;22(3):1071.

Donlon NE, Ravi N, King S, Cunninhgam M, Cuffe S, Lowery M, Wall C, Hughes N, Muldoon C, Ryan C, Moore J, O'Farrell C, Gorry C, Duff AM, Enright C, Nugent TS, Elliot JA, Donohoe CL, Reynolds JV. Modern oncological and operative outcomes in oesophageal cancer: the St. James's hospital experience. Ir J Med Sci. 2021 Feb;190(1):297-305

Donlon NE, Power R, Hayes C, Reynolds JV, Lysaght J. Radiotherapy, immunotherapy, and the tumour microenvironment: Turning an immunosuppressive milieu into a therapeutic opportunity. Cancer Lett. 2021 Apr 1;502:84-96.

1.1 Overview of oesophageal cancer treatment and survival in Ireland

Cancer of the oesophagus and the gastro-oesophageal junction (GEJ) has markedly increased in incidence in the western world over the last forty years (1, 2). Of the two main pathological types, adenocarcinoma (OAC) and squamous cell cancer (SCC), OAC dominates this increasing trend, and is strongly associated with an increased prevalence in modern western society of gastro-oesophageal reflux disease (GORD) and obesity (3). Despite advances in diagnosis and treatment, overall survival is traditionally poor, in part because many patients present with metastatic or inoperable disease which is incurable, or cannot be treated due to co-morbidity or age, and in part because the treatment itself can result in mortality. For patients with locally advanced disease who can be treated with curative intent, randomised clinical trials (RCTs) over the last decade show improved outcomes for patients who have neoadjuvant therapy prior to surgery, either combination chemotherapy and radiation therapy, or chemotherapy alone, and the reported 5 year survival in this context is between 40 to 50 per cent (4-6).

Surgery is the mainstay of treatment in the curative setting, in particular for OAC. Radical resection for cancer of the oesophagus is an exemplar of complex surgery, with relatively high risks of major morbidity and mortality (7, 8). In recent decades, perhaps directly linked with national and regional policies and increasing centralization of complex cancer surgery, as well as advances in risk assessment and perioperative care, operative mortality has decreased, with reported rates of less than 4% from the best series (9). In spite of modern advances in minimally invasive approaches to oesophageal cancer, and robotic-assisted approaches, operative morbidity remains high, with associated significant costs, resource requirement, a protracted impact on health related quality of life and possible link to adverse oncologic outcomes (10, 11). The most

common major complications are respiratory, in up to 40% of patients, cardiac arrhythmias at between 10 to 25%, and anastomotic leak rates, from 3% to 26% (11, 12).

In Ireland, centralization of cancer surgery is mandated since 2007 by the National Cancer Control Programme (NCCP), with four designated oesophageal centres, at St. James's Hospital, Beaumont Hospital, Mercy University Hospital (set to transition to Cork University Hospital), and Galway University Hospital. The aforementioned Cancer Survival in High –Income Countries (SURVMARK-2) on behalf of the International Cancer Benchmarking Partnership (ICBP), which compared population registry data from seven high income countries from 1995 to 2014, revealed an encouraging finding in Ireland, with a doubling of age standardized net survival from 10.9% between 1995-1999 to 21.9% between 2010-2014 (13). In this context, Ireland is highlighted as having one of the most adverse stage distributions, but the highest survival for early stage diseases, the third lowest proportion of patients diagnosed at an early stage and similar positive findings for gastric cancer (7). Several factors may be involved, including an increased cohort with an earlier diagnosis, improved curative treatment regimens and decreased treatment-related deaths. Centralisation *per se* may also have enabled this progress. When comparing 2009-2013 with 2014-2018 there were 256 and 219 patients treated, respectively. There was no significant demographic change evident, or co-morbidity profile, however Transhiatal (TH) resections increased from 20.7% to 33.33% ($p<0.01$) representing early stage disease pick up potentially as a consequence of the Barretts surveillance programme. Clinical stage III, with predicted nodal disease, decreased from 36.72% to 33.79% in the first and second period, respectively ($p=0.5$). Surgery up front decreased from 38.7% to 27.33% ($p<0.01$) in successive periods, respectively, and perioperative chemoradiotherapy as a percentage increased from 22.3% to 40.26% ($p<0.001$). There was no significant difference in

pathological stage between both time periods. Despite the continued multimodal therapy in the approach to oesophageal cancer, the median survival with nodal involvement carries with it a median survival of less than three years and less than 18 months in N3 disease (Figure 1.1).

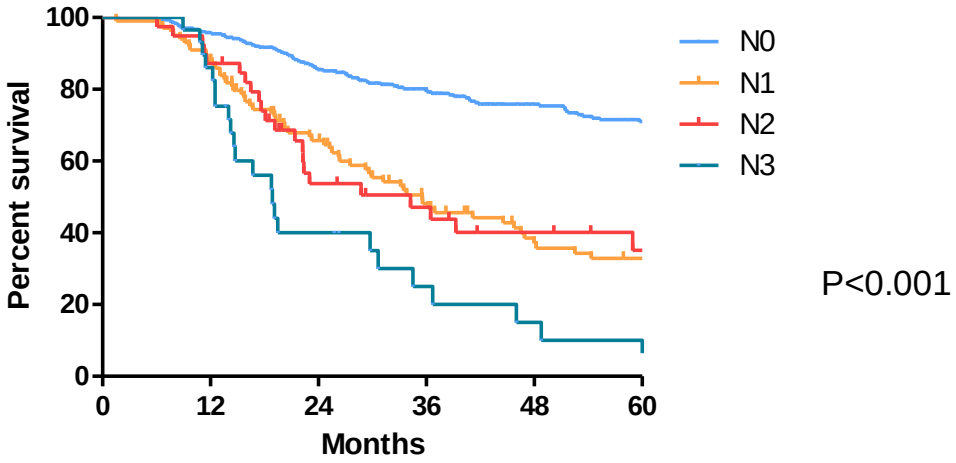

	N0			N1			N2			N3		
Survival (years)	No at risk	Deaths	% survival	No at risk	Deaths	% survival	No at risk	Deaths	% survival	No at risk	Deaths	% survival
1	308	13	96	99	12	88	39	5	87	29	4	86
3	290	46	79	86	35	49	34	14	48	24	15	27
5	194	20	70	39	11	34	14	3	36	5	3	11

Median Survival; N0 – Not reached, N1 – 35.57 Months, N2 – 34.23 Months, N2 18.9 Months.

Figure 1.1; Patient Survival according to Nodal Status *(Donlon et al. Modern oncological and operative outcomes in oesophageal cancer: the St. James's hospital experience. Ir J Med Sci. 2021 Feb;190(1):297-305)*

The evolution of published outcomes for patients undergoing curative surgery in Ireland is also of interest. A high impact RCT from this centre, published in *The New England Journal of Medicine* in 1996, of 113 patients recruited between 1990-1995, comparing surgery alone with multimodal therapy, reported a 3 year survival of 32% in the

multimodal cohort, and just 6% in the surgery only group (14). In subsequent reports from our Centre, on three time periods, 1990-1998, 1999-2003, and 2004-2008, the five year disease specific survival was 28%, 35%, and 44%, respectively (9). A report from Galway University Hospital, of 126 patients undergoing surgery between 1994 and 2008, reported a 5 year survival of 29% (15). The current survival rate reflect a continued evolution of improved outcomes from this centre in the modern era. Importantly, 230 patients with early pre-invasive (n=130) or early invasive cancer (n=100) during this period were treated by endotherapy. Prior to this study period many of these patients, particularly those with early mucosal cancer, or multifocal high grade dysplasia, would have been offered oesophagectomy, thus underlining further the modern evolution of improved survival rates. Unfortunately, in the contemporary era, despite these advances, it is not these early tumours that we continue to struggle to treat, it is advanced disease that still carries a dismal prognosis and it is this cohort of patients we must attempt to improve the available multimodal therapies to enhance the surgeons armamentarium.

1.2 Radiation therapy in the multimodal treatment of oesophageal cancer

After years of effort to harness the immune system for the treatment of cancer, the advent of antibodies which target 'immune checkpoints', including programmed cell death protein 1 (PD-1) and cytotoxic lymphocyte antigen 4 (CTLA-4), has increased interest in immunological aspects of conventional therapies. These immune checkpoint inhibitors (ICIs), including pembrolizumab, tislelizumab, nivolumab (anti PD-1) and ipilimumab (anti CTLA-4), have led to dramatic and durable clinical responses in diverse cancers (16). As previously mentioned, cancers of the upper gastrointestinal tract

(UGI) are common globally and account for a disproportionately high incidence of cancer-related mortality. In 2019, UGI malignancies accounted for 9% of cancer diagnoses and 13.5% of cancer related deaths worldwide (17). The response rates for clinically approved ICIs in melanoma and non-small cell lung cancer are approximately 20-40% (17), however, in UGI cancers this decreases to 10-15% and ICIs are therefore largely confined to salvage treatment of advanced disease with its use in the neoadjuvant and curative setting confined to select cases (18).

Radiotherapy has been one of the pillars for the management of neoplastic burden in cancer patients for over a century. It is used as a treatment modality in approximately 50% of cancer patients in the neoadjuvant, adjuvant, curative or palliative settings (19). Tri-modality treatment of surgery, chemotherapy and radiotherapy is the standard of care in oesophageal adenocarcinoma (OAC) and oesophageal squamous cell carcinoma (OSCC), while in gastric cancer (GC) adjuvant chemotherapy use depends on surgical margins and the extent of lymph node involvement (20). Radiation triggers DNA damage-induced cell death in cancer cells but can also modify the antigenicity and the adjuvanticity of tumours. This is by activating cytosolic DNA sensors, inducing immunogenic cell death, enhancing neoantigen expression and modulating the tumour microenvironment (TME) (21). Therefore, combining immuno-oncology approaches with radiation could boost response to ICI and radiotherapy in UGI cancers (Fig 1.2).

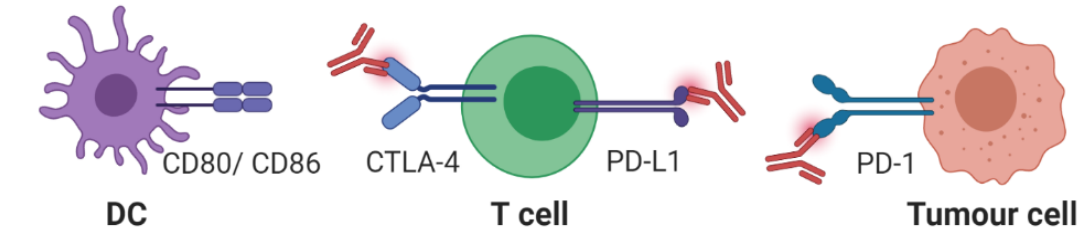

Combination strategies of ICIs in UGI cancers

Locally advanced disease
- with neoadjuvant chemoradiotherapy e.g. CROSS (& followed by surgery) – phase I/II clinical trials ongoing
- as adjuvant therapy in post-operative patients – phase II trials completed
- following definitive chemoradiotherapy (dCRT) – may prime tumours for ICI treatment – phase III trials ongoing

Metastatic/recurrent setting
- as single agent – approved for 2nd/3rd line
- with first-line chemotherapy – can prolong OS
- with radiation – no completed studies in UGI yet (clinical trials recruiting)

Figure 1.2; Combination strategies of ICIs in UGI cancers. Immune checkpoint inhibitors (ICIs) are under investigation in a variety of settings in upper gastrointestinal (UGI) cancers, including in conjunction with surgery, chemotherapy, radiation therapy, and multimodal combinations.

Traditionally, radiotherapy research has focused on radiation induced biological effects on cancer cells, with little focus on the surrounding stroma. However, cancer cells can reprogram the local environment to induce a tumourigenic milieu. The tumour microenvironment (TME) is composed of blood vessels, extracellular matrix, cancer-associated fibroblasts (CAFs) and a range of immune cells including T and B lymphocytes, tumour-associated macrophages (TAMs), natural killer (NK) cells and myeloid derived suppressor cells (MDSCs) (22). A growing body of evidence suggests the TME is not only important in cancer development and progression, but is altered dynamically in response to radiotherapy. As these changes may be critical in

determining treatment success or failure, a deeper knowledge of the TME following radiotherapy is needed to understand radioresistance and develop effective combination strategies. In this body of work, we discuss the effect of radiation on the stroma, the vasculature and immune cell composition of the TME. We outline a 'double edged sword' effect, where radiation can induce both immunogenic and immunosuppressive changes in the immune microenvironment. Finally, we propose how this milieu can be therapeutically targeted using a combination of radiation and immune-based approaches to optimise radiation induced microenvironment remodelling.

1.3 Mechanisms of synergy

1.31 The Abscopal Effect

The "abscopal effect", first described in 1953 by Mole, refers to regression of metastases outside the primary radiation field post irradiation (21). This is not frequently observed in tumours treated with radiotherapy alone; a phase II trial of 60 patients with head and neck cancer did not report any abscopal responses as a secondary endpoint (23). However, abscopal responses appear to occur more commonly when ICIs are used alongside radiotherapy, both in experimental models and clinical studies. In a mouse model of melanoma, CTLA-4 blockade alongside hypofractionated radiotherapy led to an abscopal effect (24). Radiotherapy and PD-1 blockade has also seen abscopal responses in mouse models of melanoma, renal cell carcinoma and thoracic cancers (25). This has also been reported clinically, most prominently in melanoma patients treated with PD-1 blockade (26). A pooled analysis of two clinical trials of ICIs in non-small cell lung cancer, found that the additional of radiotherapy increased the response rate of unirradiated lesions, and was associated with prolonged survival – suggesting that this

phenomenon can confer a clinical benefit (27). The mechanism of the abscopal effect is not clear, and relies on mostly preclinical data, but it is hypothesised that radiation induced cell death can release tumour antigens from the primary lesion. These antigens may be taken up by antigen-presenting cells (APCs), which migrate to lymph nodes to prime naïve $CD4^+$ and $CD8^+$ T cells (28). The activated $CD8^+$ cytotoxic T cells then travel to both the primary irradiated tumour and the non-irradiated metastatic site, where cognate tumour antigens are recognised, and this can trigger systemic immune-mediated elimination of malignant cells.

1.32 Immunogenic Cell Death

Radiotherapy can augment the adjuvanticity of tumours through induction of immunogenic cell death. This promotes successful tumour antigen processing and presentation via the release of damage-associated molecular patterns (DAMPs) to break peripheral tolerance and subsequent killing of tumour cells (29). These DAMPs include calreticulin, ATP and HMGB1, and all are increased by radiotherapy. Calreticulin acts as a pro-phagocytic signal and opposes the anti-phagocytic survival signal of CD47 (30). HMGB1 activates TLR4 and promotes antigen cross-presentation by blocking degradation of phagosomes (31). ATP released into the TME binds to the P2X7 purinergic receptor on antigen-presenting cells. This activates the NLRP3 inflammasome, releasing IL-1β, which is important for cytotoxic T cells priming (32). Therefore, the precise delivery of radiotherapy can convert a tumour into an *in-situ* vaccine, whereby neoantigens are released, and DAMPs enable efficient antigen presentation and effector immune cell function. (Fig 1.3)

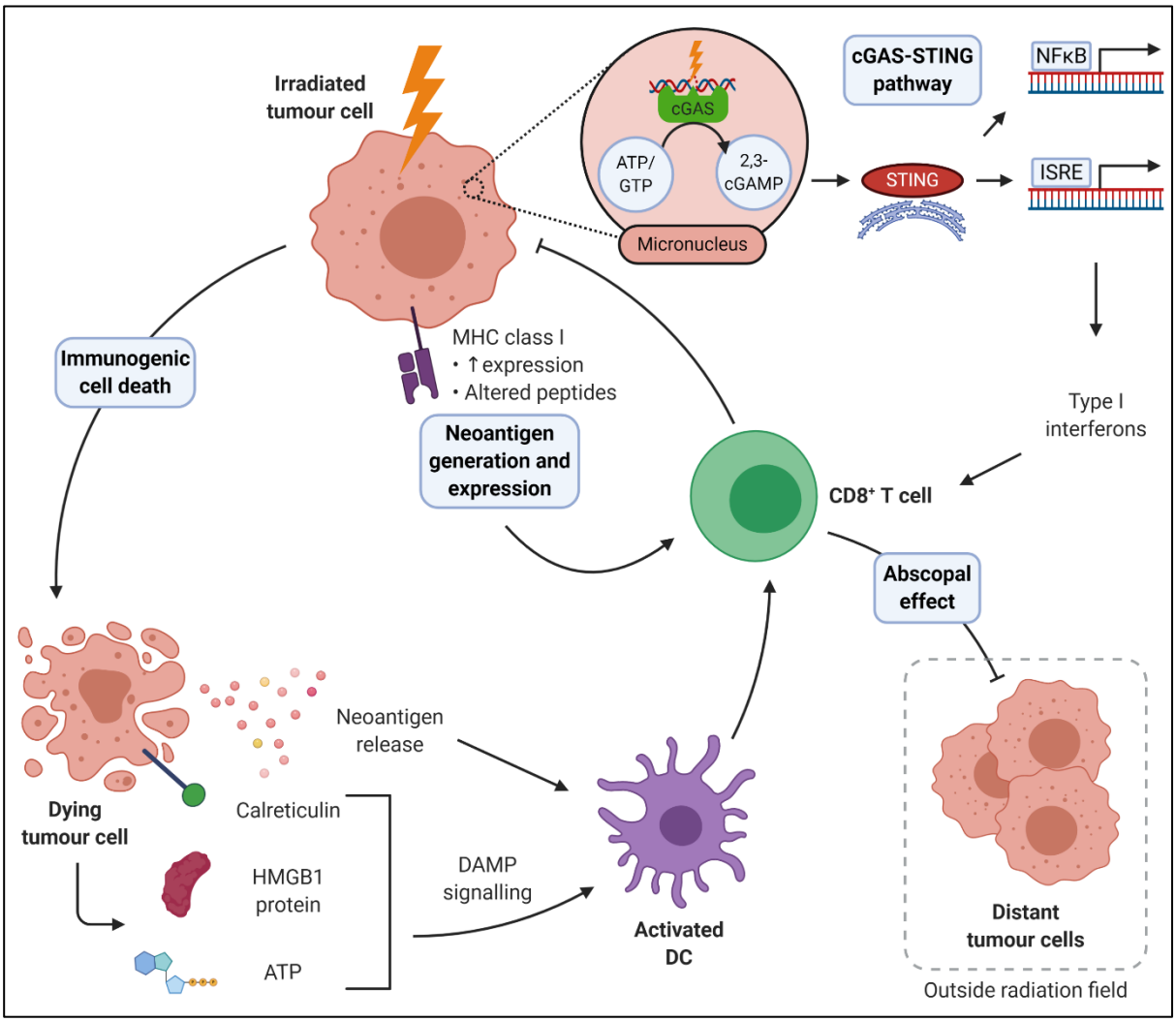

Figure 1.3; Immunogenic effects of radiation therapy. Radiation can augment anti-tumour immunity in several ways. Damage and death of cancer cells leads to release of tumour neoantigens and damage-associated molecular patterns (DAMPs) such as calreticulin, high motility group box 1 (HMGB1) protein, and ATP which activate dendritic cells (DCs) to prime and stimulate CD8+ T cells responsible for cancer cell detection and elimination. Moreover, radiation can increase the expression and alter the array of peptides presented on major histocompatibility (MHC) class I proteins, which CD8+ T cells use to identify transformed cells. Radiation-induced DNA damage can activate the cGAS-STING pathway leading to type I interferon production which enhances CD8+ T cell activity. Beyond local effects, radiation may induce systemic anti-tumour immunity if tumour-specific CD8+ T cells migrate to metastatic lesions; regression of distant tumour cells outside the radiation field is known as the abscopal effect.

1.33 Neoantigen Generation and Expression

Elimination of tumour cells by cytotoxic T cells requires antigen presentation on MHC-I molecules. An accumulating body of evidence suggests that the tumour mutational burden (TMB) and neoantigen load predicts clinical response to ICIs (33). Radiation increases tumour cell MHC-I expression (34) and radiotherapy also expands the intracellular peptide pool, altering cellular MHC-I associated peptide profiles while upregulating presentation of existing peptides (35, 36). Radiation-induced DNA damage activates a cellular stress response, promoting transcription and expression of neoantigens (37). In Non-Small Cell Lung Cancer (NSCLC), the *KPNA2* gene, a member of the nuclear transporter family, is involved in the nucleocytoplasmic transport pathway of a variety of tumour-associated proteins. Its expression is upregulated by radiation, and peptide fragments trigger activation and IFN production in the patient's $CD8^+$ T cells, therefore radiotherapy increases presentation of existing neoantigens, encouraging a $CD8^+$ T cell response (37).

Neoantigens can be divided into clonal neoantigens, present in all tumour cells and are potent drivers of anti-tumour immunity, and subclonal neoantigens which are only present in a subset of tumours cells and are less immunogenic (33). There is a concern that even if radiotherapy induced DNA damage elicits an effective antigen specific response it will only kill a small subset of tumour cells leaving the bulk of the tumour cells behind. Preclinical models suggest that radiotherapy in combination with ICIs is associated with increased diversity of the TCR repertoire. However, these tumours are dominated by a small number of high frequency T cells clones, suggesting an immune response is mounted against just a few clonal neoantigens (38).

1.4 The Tumour Microenvironment

The mass of non-malignant cells and stromal tissue surrounding cancerous cells is referred to as the tumour microenvironment (TME), which is composed of numerous cell types including cancer-associated fibroblasts, endothelial cells, pericytes and a wide range of innate and adaptive immune cells (39). Radiotherapy promotes a chemokine milieu amenable to T cell infiltration, including the secretion of CXCL16, which binds to CXCR1 on Th1 cells and activates $CD8^+$ T cells (40). In murine lung models, a combination of radiation and Ataxia Telangiectasia Mutated and RAD3 (ATR) inhibition promotes transcription of CXCL10, which binds to the immunostimulatory CXCR3 receptor on T cells (34). Radiation also upregulates ICAM-1 and NKG2D ligands *in vivo* (41). Once T cells have infiltrated a tumour, MHC-I, ICAM-1, RAE-1γ and NKG2D promote T cell arrest, tumour cell engagement and were found to be essential for the efficacy of a combination of radiotherapy and CTLA-4 blockade in mice (41). Radiation also increases production of CCL5, which acts to recruit pro-inflammatory $CCL2^+CCL5^+$ macrophages both inside the tumour and in the peripheral circulation (42). Low dose radiation promotes vascular renormalisation, which could be useful in immune-excluded tumours, where stromal elements prevent effector immune cells from accessing the tumour parenchyma (43). Radiation can also promote polarisation of M2-macrophages to an M1 pro-inflammatory phenotype (43). M1-macrophages secrete Th1 cytokines (IFN-γ, IL-12) and enhance $CD8^+$ T cell activity. These M1-macrophages express high levels of inducible nitric oxide synthase (iNOS+) allowing nitric oxide dependent vessel normalisation (44).

However, these immunostimulatory aspects of radiotherapy can be counterbalanced by suppressive signalling. Regulatory T (T_{reg}) cells are a therapeutic target for anti-tumour immunity; naturally occurring $FoxP3^+$ T_{reg} cells suppress immunity by direct cell to cell

contact and inducible T_{reg} cells secrete TGF-β and IL-10 which promote immune escape (45). These immunosuppressive elements are upregulated by radiotherapy, and their presence has been linked to poor response to ICIs in diverse patient cohorts (45, 46). Myeloid-derived suppressor cells (MDSCs: $Gr1^{+}CD11b^{+}$) are potent inhibitors of cytotoxic T cell function (47). Radiotherapy can upregulate CCL2, which binds to the CCR2 receptor to promote MDSC accumulation in the TME (48). Radiation also dampens effector T cell responses as a result of increased PD-L1 expression mediated by IFN-γ(49). Overall, this highlights a double edged sword in the context of radiotherapy, representing an important mechanism of radioresistance, while simultaneously promoting sensitivity to checkpoint blockade. As such, radiotherapy can have a dual effect on the TME, both enhancing the accumulation of effector and suppressive T cell and myeloid cell populations (Figure 1.4).

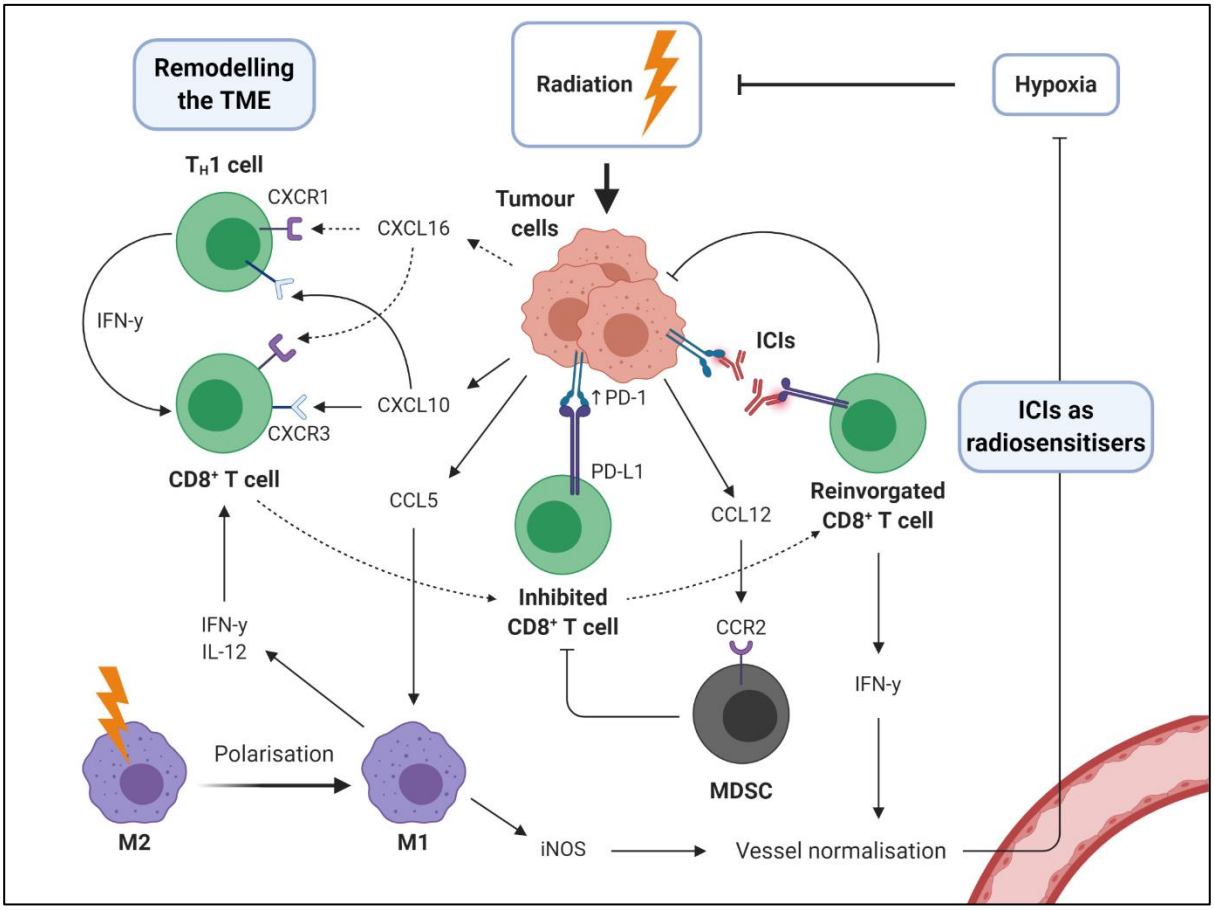

Figure 1.4; Radiation therapy can shape the immune response just as immunotherapy can shape the response to radiation therapy. Radiation induces production of a variety of chemokines that can facilitate and antagonise the anti-tumour response: T cells and M1 macrophages contribute to tumour elimination and can be recruited by CXCL16 or CXL10, and CCL5, respectively; myeloid-derived suppressor cells (MDSCs) are immunosuppressive and can be recruited by radiation-induced expression of CCL12. Immune checkpoint inhibitors (ICIs) boost anti-tumour immunity by disrupting suppressive signalling molecules such as PD-1, PD-L1 and CTLA-4 (latter not shown). By recruiting T cells (via aforementioned mechanisms) radiation therapy can augment this phenomenon. Furthermore, cytokines released by immune cells including IFN-γ from $CD8^+$ T cells can promote tumour vessel normalisation counteracting hypoxia which promotes radioresistance: thus, by enhancing T cell responses ICIs can act as radiosensitisers.

1.5 Immunotherapy as a Radiosensitiser

Although the current focus of combining radiation and immunotherapy is to boost response to ICIs, emerging evidence indicates that immunotherapy itself is a potent radiosensitiser. The dysfunctional vasculature within tumours promotes radioresistance as a result of the hypoxic environment (47). The lack of oxygen is responsible for the suppression of apoptosis during radiotherapy, as low oxygen availability limits ROS generation. Paradoxically, radiation itself can lead to the disruption of *in vivo* vascular systems around tumours, inducing a hypoxic response and activating hypoxia-inducible factor 1 (HIF1), thus reducing the generation of intratumoural ROS (50). Hypoxia upregulates HIF-1, activating anaerobic glycolysis which produces lactate and antioxidants (51). These antioxidants scavenge ROS, impeding radiation induced cell death, and lactate promotes immunotherapy resistance (52). Recent data indicate that immunotherapy can normalise poorly formed, leaky hypoxia-promoting vessels in the TME. In preclinical models of breast and colon cancer, anti-PD-1 and anti-CTLA-4 therapy resulted in tumour regression, increased perfusion and reduced tumour hypoxia (53). This vessel normalisation was mediated by IFN-γ producing $CD8^+$ T cells. The angiostatic effects of IFN-γ may be related to reduced ‘αVβ3 integrin dependent endothelial cell activation and survival (54), and was correlated with preclinical efficacy of anti PD-1 therapy (53, 54). Another *in silico* analysis found an association between immune-stimulating gene pathways (including *Ackr1, Il1r1, Il6st* and *Socs2*) and vessel normalisation related genes, such as decreased expression of *Vegfa* and increased expression of *Angpt1/Angpt2* (55). In response to ICIs, Th1 cells produce IFN-γ to normalise vessels and reduce hypoxia through increased pericyte coverage, decreased leakiness and decreased hypoxia. This suggests that ICIs remodel the tumour vasculature, augmenting their own efficacy and potentially acting as a radiosensitiser.

1.6 Clinical Trials of Radiation and Immunotherapy in UGI cancer

1.61 Single agent Immunotherapy

Single agent ICI trials in UGI cancers have delivered modest results. The ATTRACTION-2 phase III trial found that nivolumab (anti-PD-1) improved overall survival (OS; 5.3 vs 4.1 months in the placebo group, $p<0.0001$) in heavily pretreated gastric cancer (GC) or gastroesophageal junction cancer regardless of PD-L1 expression (56). The KEYNOTE-059 phase II study evaluated pembrolizumab (anti-PD-1) versus chemotherapy in previously treated gastric cancer (GC) or gastroesophageal junction cancer, with the objective response rate (ORR) of 11.6%, with a longer median duration of response in PD-L1$^+$ patients (16.3 vs 6.9 months) (57). Based on these results, in 2018 the FDA granted accelerated approval of pembrolizumab in the third line treatment of recurrent GC or gastroesophageal junction cancer that overexpresses PD-L1 with a Combined Positive Score [CPS] $\geq$ 10, as determined by a U.S. Food and Drug Administration (FDA)-approved test, with disease progression after one or more prior lines of systemic therapy as identified in KEYNOTE-181. Clinical efficacy of ICIs in OSCC is slightly more encouraging, with KEYNOTE 181, a phase III trial reporting that as second line treatment, the median OS with pembrolizumab vs chemotherapy was similar in the intention to treat (ITT) group (7.1 vs 7.1 months) and longer in the SCC (8.2 vs 7.1 months) and PD-L1 CPS $\geq$10 groups (9.3 vs 6.7 months) (58). A trend was observed favouring responses in OSCC, forming the basis for the 2019 FDA approval of pembrolizumab in the second line treatment of metastatic PD-L1$^+$ OSCC. More recently, the ATTRACTION-3 phase III trial of second line nivolumab vs chemotherapy confirmed this OS benefit (10.9 months vs 8.4 months, $p = 0.019$), further supporting the place of PD-1 inhibition in metastatic OSCC (59). Approved indications of immunotherapy in gastroesophageal cancer are therefore confined to the second- or

third-line treatment of metastatic disease. However, more recent data from the CheckMate-649 and KEYNOTE-590 studies indicates that the addition of nivolumab (median OS: 14.4 vs 11.1, HR 0.71, $p < 0.0001$) or pembrolizumab (median OS: 12.4 vs 9.8, HR 0.73, $p < 0.0001$) to first line chemotherapy in metastatic UGI cancers can prolong overall survival (60, 61). This suggests that combining ICIs with more traditional treatment modalities can improve outcomes in gastroesophageal cancers.

Prospective clinical data of combining immunotherapy and radiation are in a nascent phase; phase III trials have not been published outside of prostate and non small cell lung cancer (NSCLC). The phase III PACIFIC trial investigated durvalumab (anti PD-L1) following chemoradiotherapy in locally advanced NSCLC (62). Compared to placebo, durvalumab improved overall survival (28.3 vs 16.2 months) and both arms had similar rates of treatment related adverse events. A phase III trial in metastatic castration resistant prostate cancer found no benefit of ipilimumab (anti CTLA-4) following a single 8 Gy dose of radiation of up to five bone metastases (63). In gastroesophageal cancers, trials are in early stages and the majority are ongoing. Clinical investigation focuses on three settings: disease treatable by surgical resection, definitive chemoradiotherapy and palliative treatment in the metastatic setting with timing of delivery and ideal combination multimodal therapies yet to be elucidated.

1.62 Locally Advanced Disease

Locally advanced, nonmetastatic UGI cancers are optimally treated by surgical resection. This is accompanied by the CROSS neoadjuvant chemoradiotherapy regimen consisting of carboplatin, paclitaxel and 41.4 Gy external beam radiotherapy (EBRT) (59). However, only 15% of patients display a pathologic complete response (pCR) and trials are investigating if the addition of ICIs can improve response rates and patient

outcomes (Table 1.1). One example is phase I trial (NCT03044613) of pembrolizumab (anti PD-1) in combination with the CROSS regimen in stage II/II OAC, OSCC or GEJC. Primary endpoints are pCR rate and treatment related adverse events (TRAEs). Preliminary results for the first 10 patients show an encouraging pCR rate of 40%, with acceptable toxicity and no delays in surgery (60). A larger (n=28) phase II trial of pembrolizumab in OSCC has reported a pCR rate of 46.1%, with 82% of patients surviving at 12 months (61). However, 2/28 patients did not undergo surgery and two treatment related deaths were reported due to acute lung injury emphasising the need for TRAE monitoring. Another approach is the use of adjuvant ICIs in postoperative patients to better control micro-metastatic disease. A phase II trial has evaluated durvalumab (anti PD-L1) in OAC or GEJC previously treated with external beam radiotherapy (EBRT) with residual disease following tri-modality treatment of surgery and chemoradiation (NCT02639065). Early results indicate that adjuvant durvalumab is safe with few dose limiting toxicities (62). Relapse free survival in this single arm study was 79.2%, which compares favourably to historical rate of 50%. These encouraging results further underscore the need for more data in the adjuvant setting.

Table 1.1. Ongoing clinical trials of radiation and immunotherapy in operable disease.

Identifier	Phase	N	Disease setting	Treatment	Radiation	Primary Endpoint
NCT03792347	I	20	Stage II/III OSCC	Pembrolizumab, carboplatin, and paclitaxel	41.4Gy in 23 fractions	TRAEs
NCT02844075	II	18	Stage II/III OSCC	Pembrolizumab, carboplatin, and paclitaxel	41.4Gy in 23 fractions	pCR rate *
NCT03257163	II	40	Stage II/III dMMR or EBV^+ GC	Neoadjuvant pembrolizumab Adjuvant Capecitabine and pembrolizumab	Conventional Fractionation	RFS
NCT03064490	II	38	Stage II/III GC or OAC	Pembrolizumab, carboplatin, and paclitaxel	41.4 Gy in 23 fractions	pCR rate
NCT02730546	I/II	68	Stage II/III GC or GEJC	Pembrolizumab, carboplatin, and paclitaxel	41.4 Gy in 23 fractions	pCR rate PFS
NCT03044613	I	25	Stage II/III OAC,	Nivolumab and carboplatin and paclitaxel	41.4 Gy in 23 fractions	TRAEs *

			OSCC or GEJC			
NCT03776487	I/II	30	Stage II/III GC or GEJC	FOLFOX + Nivolumab + ipilimumab followed by surgical resection	50 Gy in 25 fractions	TRAEs
NCT02962063	II	35	Stage II/III GEJC and GC	Neoadjuvant Durvalumab and mFOLFOX Adjuvant durvalumab	50 Gy in 28 fractions	TRAEs pCR rate
NCT04159974	II	56	Stage II/III OAC or GEJC	Durvalumab, carboplatin and paclitaxel	41.4 Gy in 23 fractions	pCR rate TRAEs
NCT02639065	II	23	Stage II/III OAC or GEJC with residual disease	Durvalumab	41.4 Gy in 23 fractions	TRAEs * DLTs
NCT03490292	I/II	24	Stage II/III OSCC or OAC	Avelumab + Carboplatin, paclitaxel	41.4 Gy in 23 fractions	DLT pCR

Abbreviations: TRAEs, treatment related adverse effects; pCR, pathological complete response; DLT, dose limiting toxicity; OAC, oesophageal adenocarcinoma; OSCC, oesophageal squamous cell carcinoma; GEJC, gastroesophageal junction adenocarcinoma; dMMR, deficient mismatch repair; Gy, Gray; RFS, relapse free survival.

1.63 Definitive Chemoradiotherapy

Definitive chemoradiotherapy (dCRT) is an alternative standard of care in OSCC and is also employed in localised OAC deemed unsuitable for surgery. A 50.4 Gy EBRT is delivered in 25 fractions, accompanied by 5-FU and cisplatin or FOLFOX (5-FU, folinic acid and oxaliplatin). dCRT may promote immunogenic changes in tumours, priming tumours for ICI treatment to further enhance local and distant tumour control. The randomised, doubled blinded, phase III KEYNOTE-975 trial is evaluating pembrolizumab with traditional dCRT in localised but inoperable OSCC, OAC and GEJC (NCT04210115). The primary endpoints are overall survival and event free survival, and results could define a new standard of care in the dCRT setting. Other ongoing trials are evaluating dual checkpoint blockade (anti PD-1 and anti CTLA-4; NCT03437200), and sequential nivolumab and cetuximab (anti EGFR) with concomitant dCRT.

1.64 Systemic Treatment of Advanced Disease

Combining ICIs and radiation in the recurrent or metastatic setting seeks to activate the abscopal response, priming antigen specific $CD8^+$ T cells against tumours outside the radiation field. The few radio-immunotherapy trials in metastatic UGI cancers are at an early stage and seek to investigate toxicities and mechanisms of response. One example, a phase II trial of pembrolizumab and 30 Gy conventional fractionated radiotherapy is recruiting patients with metastatic gastroesophageal cancers (NCT03544736). Primary endpoints aim to quantify the abscopal response; changes in $CD8^+$ TILs at the irradiated site, and changes in MDSCs and Tregs at peripheral metastases will be measured. Another approach is a combination of nivolumab and high dose brachytherapy to deliver 16 Gy over 2 fractions (NCT02642809), and durvalumab with concomitant chemoradiotherapy in the palliative setting (NCT03544736).

1.7 Optimising Radiation Parameters within Immunotherapy

1.71 Radiation Dose

Conventional fractionated radiation is delivered in small 1.8-2 Gy daily fractions. For example, the CROSS regimen for OAC and OSCC involves 41.4 Gy given in 23 fractions of 1.8 Gy each, five days per week (64). Recent advances in radiation technique and delivery, including intensity modulated radiotherapy (IMRT), volumetric-modulated arc therapy (VMAT) and proton beam therapy allow delivery of higher radiation doses, while minimising acute and long-term toxicity. This has allowed a shift to 'hypo-fractionated' approaches, ranging from 5-10 Gy over three to five fractions to single doses of up to 24 Gy using stereotactic body radiotherapy (SBRT). SBRT employs advanced imaging, immobilisation techniques and real-time organ motion tracking, used to ablate oligometastatic disease. Hypofractionated radiotherapy can minimise toxicity while maintaining efficacy, favoured in oesophageal cancer patients unfit to receive definitive chemoradiation therapy (65).

It is postulated that conventional fractionation can have immunosuppressive effects in the TME by recruiting MDSCs, Treg cells and M2-macrophages, potentially mediated by TGF-β upregulation (66). However, this conventional fractionation can also have the immunogenic effect of normalising the tumour vasculature (43). Higher radiation doses per fraction (>6 Gy) have more profound immunological effects, including facilitating maturation of APCs, increasing T cell infiltration, enhancing MHC-I expression and tumour peptide presentation, and upregulation of immunostimulatory signals like Fas and ICAM on tumour cells (66, 67). However, the immunogenic effects of high dose radiation seems to have a limit; higher ablative doses (>12-18 Gy) induce *TREX1*, an exonuclease that degrades cytoplasmic DNA (68). This negatively regulates the cGAS-STING pathway that is vital in radiation-induced immunogenicity. For this reason,

hypofractionated radiotherapy (eg. 3 x 8 Gy doses) has the most potential as a favourable immunomodulator (68). (Fig 1.5)

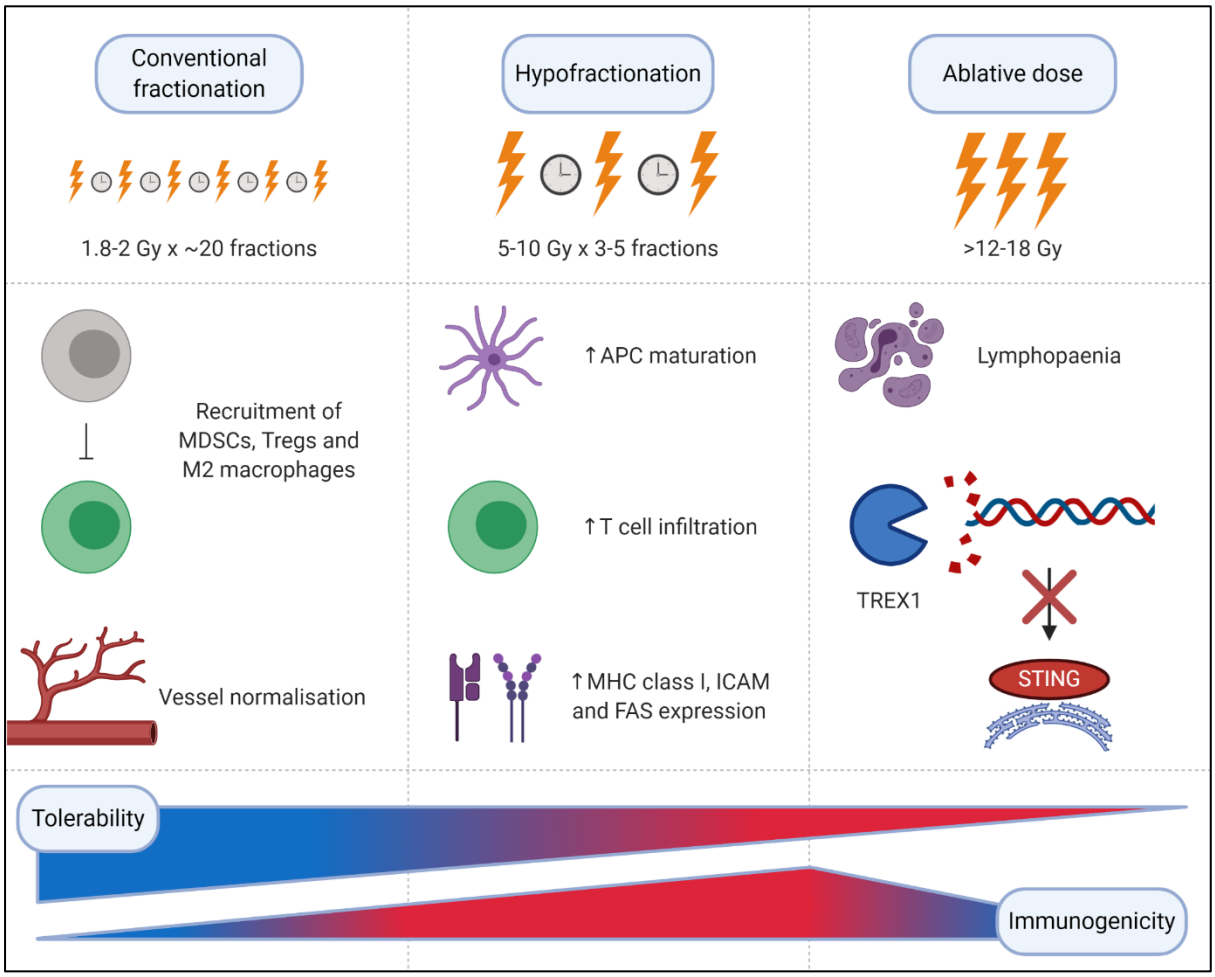

Figure 1.5; Optimising radiation dose and delivery for optimal immunogenicity. Small doses of radiation delivered in conventional fractionated radiotherapy are believed to have immunosuppressive effects in the tumour microenvironment; accumulation of immunosuppressive cell types such as myeloid-derived suppressor cells (MDSCs), regulatory T cells (Tregs) and M2 macrophages repress anti-tumour immunity. This immunosuppressive effect is somewhat counterbalanced by the normalising effect low dose radiation has on the tumour vasculature. Higher doses of radiation, such as those used in hypofractionation, can have a stimulatory immunogenic effect mediated by increased antigen presenting cell (APC) maturation, in addition to augmented T cell infiltration and enhanced expression of immunogenic proteins including MHC class I, ICAM and FAS on tumour cells. However, once the dose of

radiation surpasses 12-18 Gy, immunogenicity is compromised: TREX1, an exonuclease, is induced leading to degradation of cytoplasmic DNA, thus negatively regulating the cGAS-STING pathway.

1.72 Radiation Timing

The immunological effects of radiation are time-dependent. *In vitro* there is an increase in the MHC-I peptide pool after 8 hours, lasting for 11 days (35). Clinical samples show increased activated dendritic cells during the first week, potentially correlating with radiation-induced antigen presentation (69). Populations of activated and proliferating T cells declined in the first week but increased after the third week of therapy, supporting radiation as an *in situ* vaccine (69). These time-dependent effects can be exploited in the clinic. Multivariable analysis in the PACIFIC trial found that ICI initiation <2 weeks following chemoradiotherapy was associated with greater overall survival (62). This survival benefit when ICI is initiated concurrently or shortly after radiation was also found in a retrospective analysis of 750 patients (70). This suggests that radiation may 'prime' the tumour for optimal immunotherapy efficacy, a principle that could be employed to maximise ICI efficacy in gastroesophageal cancers.

1.8 Radiation Adverse Effects

Radiotherapy is associated with a host of adverse effects, but radiation-induced lymphopenia (RIL) is most relevant to ICI treatment. Lymphocytes are critical for the anti-tumour immune response, and T cell-deficient mice are unable to mount abscopal responses (71). Indeed, RIL is an independent predictor of poor overall survival in UGI cancers (72). In addition to combination chemotherapy, the radiotherapy target volume is a key determining factor in incidence of RIL. This is due to radiation doses to sites of lymphopoiesis (bone marrow) or lymphocyte storage (spleen, lymph nodes) (66).

Advances in fractionation may ameliorate this adverse effect; in two pancreatic cancer cohorts, hypofractionated radiotherapy delivered by SBRT was associated with less RIL when compared to standard fractionation (1.8 Gy), highlighting that hypofractionated approaches may also have favourable toxicity as well as efficacy (73, 74). As well as direct depletion of lymphocytes, elective irradiation of draining lymph nodes has additional detrimental effects (75). Compared to irradiating the primary tumour alone, elective nodal irradiation is associated with altered intratumuoral chemokine expression and $CD8^+$ T cell trafficking, as this was correlated with poorer survival in a combination of radiation and immunotherapy (75). Immunotherapy carries a risk of immune-related adverse events (irAEs), including potentially life-threatening pneumonitis. Radiation-induced lung injury is defined by pneumonitis and fibrosis and is a common dose limiting toxicity of radiotherapy in UGI cancers. Therefore, a combination of radiation and immunotherapy could increase incidence and severity of this adverse effect (66). The KEYNOTE-001 reported a higher rate of ICI-related pneumonitis in those that had previously received thoracic radiation, and several case reports have been published of severe pneumonitis in patients treated with ICI and SBRT (76). In the PACIFIC trial, both the durvalumab and placebo arms had similar incidence of pneumonitis (62), so further data is needed to achieve a balance between safety and efficacy in UGI cancers.

1.9 IMMUNOGENIC EFFECTS OF RADIATION

1.91 Infiltration and Activation of T cells

The cytokine milieu is critically important for the immune cell composition of the TME and is altered following radiotherapy. Effector $CD8^+$ T cells, interferon (IFN)-γ expression, T helper 1 cells (Th1) cells and NK cells have potent anti-tumour effects.

These cells express the CXC-chemokine receptor 3 (CXCR3) which binds to Th1 chemokines CXC-chemokine ligand 9 (CXCL9) and CXCL10, which allow migration into tumours (77). In mice, radiation promotes transcription of CXCL10, which can bind to CXCR3 and promote migration of $CD8^+$ effector T cells (78). $CD11c^+CD8\alpha^+$ BATF-lineage DCs were found to be important in this CXCL10 and CXCL9 production (79). Another preclinical study found the addition of cisplatin to radiation and anti-PD-1 therapy can promote abscopal responses, and this was contingent on CXCL10/CXCR3-mediated $CD8^+$ T cell recruitment (80). Radiation can also induce the release of CXCL16 by tumour cells, which binds CXCR6 on Th1 cells and $CD8^+$ T cells to encourage tumour infiltration (40). In addition to chemokines, radiation affects leukocyte infiltration through changes in cell adhesion molecule (CAM) expression. IL-1β, TNF-α and type I and II interferons are upregulated in response to radiation (81). These cytokines induce the upregulation of ICAM-1 and VCAM-1 on tumour endothelium (82, 83), promoting migration of lymphocytes into the tumour parenchyma.

Radiotherapy can upregulate signals in the TME that promote effector $CD8^+$ T cell mediated killing of tumour cells as $CD8^+$ T cells recognise tumour cells by presentation of neoantigens on major histocompatibility complex (MHC)-I complex and radiation increases its expression on tumour cells (35). Radiation alters the intracellular peptide pool, which can alter the repertoire of cellular MHC-I associated peptide profiles (34, 35). DNA damage caused by radiotherapy induces cellular stress, which can elevate expression of poorly expressed neoantigens (36). An example is *KPNA2* in non-small-cell lung cancer (NSCLC), where expression was upregulated by radiation, and peptide fragments trigger IFN production in patient-derived effector T cells (37). Other molecules including ICAM-1 and MIC A/B (an NKG2D ligand) are upregulated by radiation *in vivo* and are important in $CD8^+$ T cell mediated killing. (37). In mice, MHC-I, ICAM-1, RAE-

1γ and NKG2D are central in T cell functional arrest, immune synapse formation and tumour regression in response to a combination of radiation and anti CTLA-4 therapy. Therefore, inflammatory remodelling in the microenvironment following radiation allows enhanced recruitment and activation of effector T cells and enhanced immunogenicity in tumours (Figure 1.6).

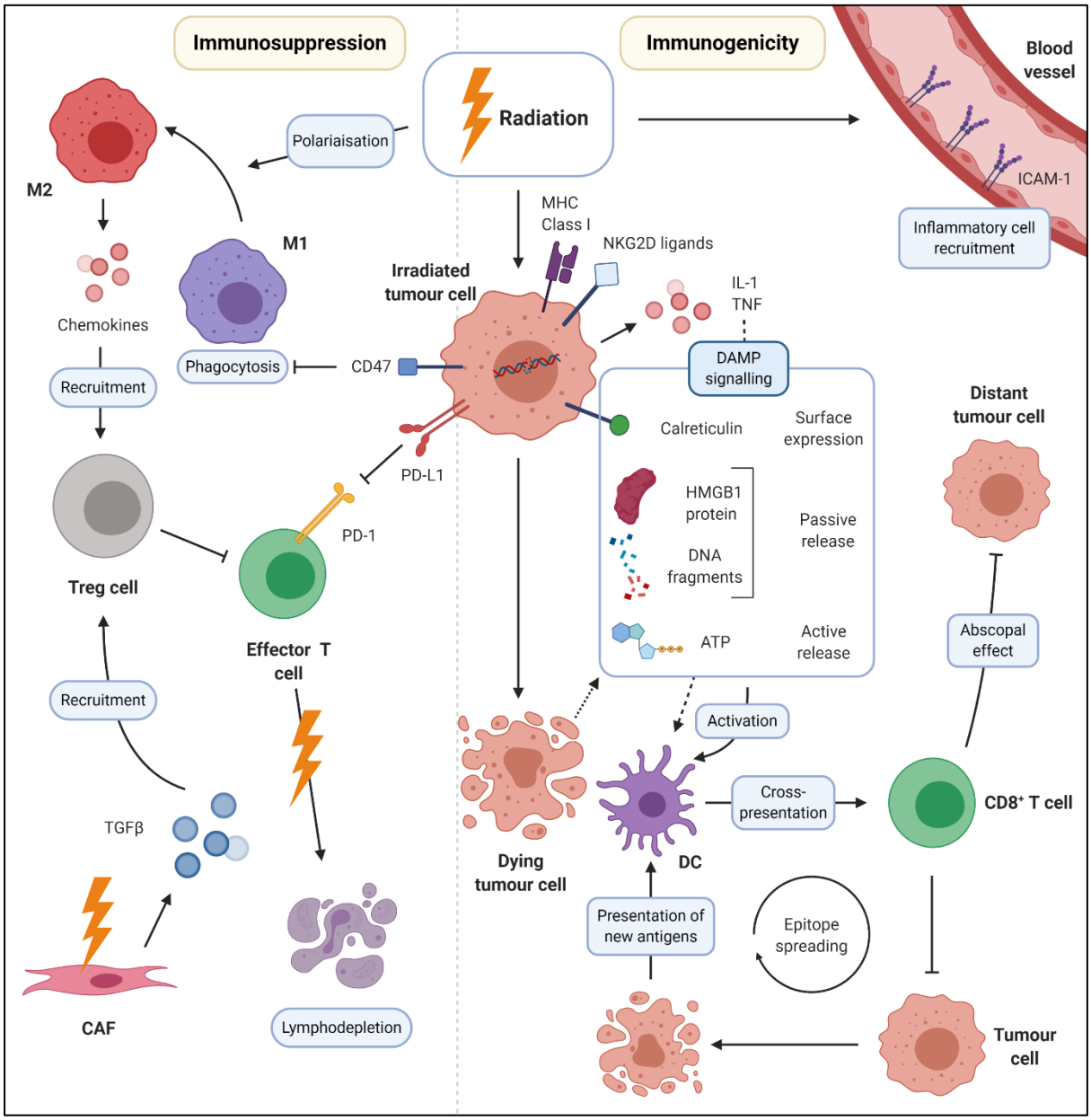

Figure 1.6. Double-edged sword of radiotherapy: immunosuppression and immunogenicity. DNA damage induced by radiation therapy (RT) leads to tumour cell

stress and death if the former surpasses a cell's reparative capacity. Radiation can promote cell death by up-regulating major histocompatibility (MHC) class I and NKG2D ligands which T cells and natural killer (NK) cells recognise respectively. Furthermore, damaged cells express and release damage-associated molecular patterns (DAMPs): calreticulin expressed on the cell surface, and release of intracellular molecules including high-mobility group box 1 (HMGB1), DNA and ATP by passive or active mechanisms activating antigen presenting cells such as dendritic cells (DCs) a key step in adaptive immunity. Cytokine release, including interleukin (IL)-1 and tumour necrosis factor (TNF), by irradiated tumour cells also contributes to DC activation. DCs can cross-present tumour antigens to $CD8^+$ T cells. $CD8^+$ T cells mature into cytotoxic lymphocytes and drive destruction of tumour cells; this process can lead to the phenomenon of epitope spreading as new antigens are released and presented following destruction of heterogeneous cancer cells. Tumour-specific activated T lymphocytes can mediate regression of distant tumours which may not have been irradiated themselves: known as the abscopal effect. Irradiation of tumour blood vessels leads to increased expression of leucocyte adhesion molecules such as intercellular adhesion molecule 1 (ICAM-1) facilitating recruitment of anti-tumour immune cells. RT can also favour polarisation of M1 macrophages towards a pro-tumour M2 phenotype in addition to activating cancer-associated fibroblasts (CAFs). Chemokines released by M2 macrophages and transforming growth factor-β (TGF-β) secreted by CAFs work in tandem to recruit regulatory T (Treg) cells which suppress anti-tumour immunity. RT also causes a relative increase in these immunosuppressive cell types by driving apoptosis of effector lymphocytes known as lymphodepletion. Furthermore, induction of co-inhibitory molecules on tumour cells such as programmed death-ligand 1 (PD-L1) and CD47 suppress effector lymphocyte activity and phagocytosis by macrophages and DCs, respectively. PD-L1 mediates this effect via interactions with programmed cell death protein 1 (PD-1) on lymphocytes.

1.10 THE TUMOUR STROMA AND VASCULATURE

1.10.1 Endothelial Cells

The vascular component of the TME is composed of endothelial cells, pericytes and supportive stroma. The tumour vasculature and endothelial cells are perhaps the most well studied component of TME following radiation, but changes depend on dose, fractionation, as well as the type and location of the tumour (22). Radiation induces endothelial cell dysfunction, which is characterised by increased permeability, detachment and apoptosis (84, 85) and is associated with the expression of acid sphingomyelinase, which in turn induces endothelial cell apoptosis (86). This promotes a prothrombotic state, encouraging platelet aggregation, microthrombus formation and adhesion of inflammatory cells with transmigration into the interstitial space (87). Radiation can induce a senescent phenotype in endothelial cells (88), where suppression of angiogenesis, oxidative stress and inflammation contribute to long term vascular dysfunction (89). Radiation induced endothelial cell death can also promote anti-tumour immune signals, including CXCL16, which activates macrophages and T cells (40). Pro-survival processes in cancer cells can be upregulated following endothelial cell irradiation. For example, tumour cells may secrete vascular endothelial growth factor (VEGF) and fibroblast growth factor (FGF), promoting survival of endothelial cells, maintaining vascular function post radiation which in turn can promote cancer progression (90). Endothelial cells also induce other pro-survival processes, including the phosphatidylinositol 3-kinase (PI3K)/Akt pathway (91) and overexpression of the $\alpha_v\beta_3$ integrin, which promotes radioresistance with epithelial mesenchymal transition (EMT). (92). Finally, adhesion molecule expression, such as focal adhesion kinase (FAK), which is important in the regulation of integrin signaling, cell adhesion, migration and proliferation of cells and its downstream effector paxillin are increased following

irradiation, which may help adherence of tumour cells and the initiation of the metastatic cascade (93). In summary, activation, apoptosis and senescence of the endothelium can have pleotropic pro- and anti-tumour effects.

1.10.2 The Tumour Vasculature

Understanding the functional impact of radiation on the tumour vasculature is key to maximise therapeutic efficacy. On a macroscopic level, irradiation of the vasculature results in dose dependent destruction of blood vessels, especially potent at the level of the microvessel network (94). This, in turn, reduces vascular density and the distance between functioning vessels to promote an area of vessels with hypoperfusion. Vessels become thicker, with intimal proliferation and an increased risk of atherosclerotic changes (95). Later changes include fibrosis and medial necrosis and high doses of radiation may induce a permanent reduction in blood flow, implying that the post radiation effects are irreversible (96). Vessels in the TME may arise through angiogenesis, vasculogenesis or vessel co-option and may lack basement membrane or supporting pericytes, increasing radiosensitivity of the local TME vasculature (97). Moreover, endothelial cells in the TME have high proliferation rates, which increases inherent radiosensitivity (98).

Similar to normal tissue, high dose radiation promotes acid sphingomyelinase dependant endothelial apoptosis, microvascular damage and tumour cell death in melanoma and fibrosarcoma xenografts (99). Subsequent tumour revascularisation is by vasculogenesis, a less efficient method of vessel development compared to angiogenesis and occurs through hypoxia inducible factor 1α (HIF-1α) dependant and HIF-1α independent mechanisms (100). HIF-dependant induction of stromal cell derived factor (SDF-1) production in the TME is required for recruitment of matrix metalloprotease 9 (MMP-9)

bone marrow derived cells through the CXCR4 chemokine receptor (101). Radiation can also activate a novel pathway of HIF-1α independent SDF-1 induction to promote endothelial cell migration (102). Inhibiting CXCR4 reduces vasculogenesis and prevents tumour recurrence post radiotherapy (100), suggesting another pathway of vessel remodelling which could be targeted by radiosensitisers.

1.10.3 Hypoxia

The dysfunctional microvasculature, inherent to the TME, contributes to radioresistance by promoting hypoxia and radiation-induced microvascular damage further potentiates this as shown in Figure 1.7(103). Hypoxia correlates with tumour recurrence and poor prognosis in response to radiotherapy (104), and hypoxia directly and indirectly leads to radioresistance through a number of mechanisms. Firstly, hypoxia supports development of a cancer stem cell like phenotype through epigenetic reprogramming (105), and has been shown to encourage radioresistance in pancreatic cancer models (106). Secondly, low intracellular levels of oxygen prevent radiation induced reactive oxygen species production (ROS), which is responsible for the indirect method of radiation induced DNA damage (107). Additionally, hypoxia leads to accumulation and stabilisation of HIF-1α (108), which has been demonstrated in irradiated glioma cells, promoting angiogenesis and tumour progression (109). This, amongst other pathways, activates anaerobic glycolysis by expression of pyruvate kinase isoform M2, aldolase A, enolase and lactate dehydrogenase (110, 111). Anaerobic glycolysis involves conversion of pyruvate to lactate which is then secreted into the TME to prevent feedback inhibition. Lactate levels in the TME diminish T and NK cell activation, leading to immune escape and resistance to radiotherapy (112, 113). Lactate also upregulates the HIF-1α pathway, creating a futile cycle of radio- and immune resistance (114). HIF-1α also upregulates the pentose phosphate and the serine synthesis pathway, which increase the production of NADPH

(115). NADPH is vital in the glutathione dependent antioxidant pathway and upregulation further impedes ROS induced cell death in the irradiated TME (115).

The HIF pathway can also modify the immune microenvironment. HIF-1α dependent production of the chemokine CCL28 in hepatocellular carcinoma cells recruits T_{reg} cells to the TME (116). This dampens effector T cell function and promotes angiogenesis. Hypoxia also leads to recruitment of TAMs with an M2 phenotype through p38 mitogen activated protein kinase (MAPK) signalling (117). In response to hypoxia, TAMs can inhibit T cell proliferation in a HIF-1α dependent manner and targeted deletion of HIF in myeloid cells reduced tumour growth in mouse models of breast cancer (118). HIF-1α can also regulate MDSC differentiation and function (119), while signals secreted from hypoxic tumours can promote the establishment of a premetastatic niche by MDSC recruitment and suppression of NK cell cytotoxicity (120). Hypoxia induced accumulation of these suppressive cell populations in the TME is a potent means of radioresistance.

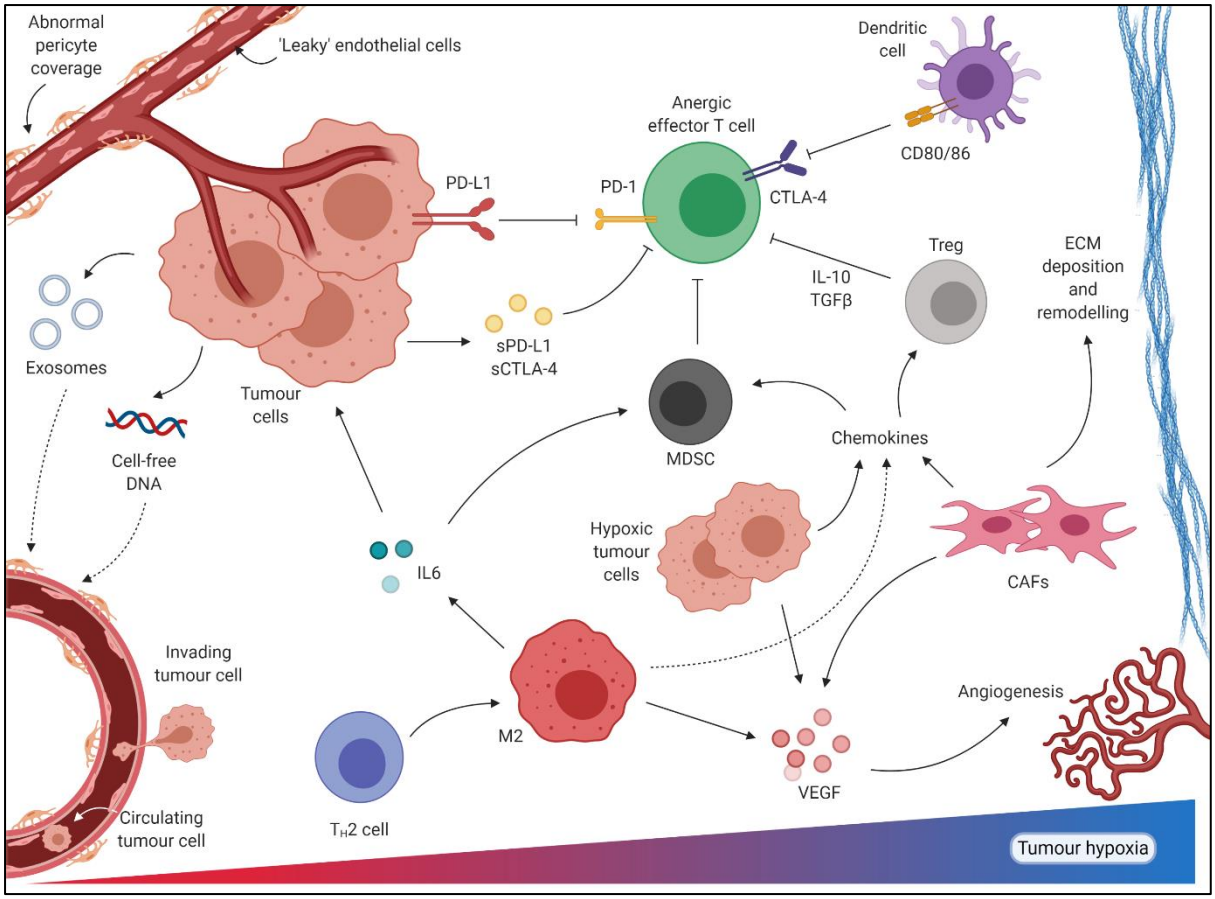

Figure 1.7. The tumour microenvironment: a team effort. A key concept in tumourigenesis and progression is the corruption of surrounding stromal and immune cells and soluble mediators to form a network, dubbed the tumour microenvironment, that aids, nourishes and protects the tumour. A major role of the tumour microenvironment is to subvert anti-tumour immunity. This can be achieved by the expression of immune checkpoints such as programmed death 1 (PD-1) or cytotoxic T-lymphocyte antigen 4 (CTLA-4) which induce anergy following ligation with their ligands programmed death ligand 1 (PD-L1) and CD80/86, respectively. Tumours can also release soluble immune checkpoints, including sPD-L1 and sCTLA-4, to dampen anti-tumour responses. Recruitment of immunosuppressive cell types such as regulatory T (Treg) cells and myeloid-derived suppressor cells (MDSCs) is encouraged by expression of chemokines and cytokines from transformed cells, M2 macrophages and

cancer-associated fibroblasts (CAFs) and act to limit effector lymphocyte responses. CAFs are also critical in the remodelling of the tumour microenvironment by depositing extracellular matrix (ECM) and promoting angiogenesis through expression of vascular endothelial growth factor (VEGF) under hypoxic conditions along with tumour cells and macrophages. Stromal remodelling and angiogenesis are key facets of tumour progression: remodelling of the ECM promotes invasion and metastasis while the nascent vasculature facilitates nutrient and oxygen delivery. Additionally, tumour blood vessels are characterised by dysfunctional endothelium and abnormal pericyte coverage leading to increased vessel permeability; these factors assist the intravasation of potential metastatic seedlings as well as exosomes and cell-free DNA which can circulate in the blood and prime pre-metastatic niches.

1.10.4 Cancer Associated Fibroblasts

Cancer associated fibroblasts (CAFs) are a heterogeneous population that make up the majority of stromal cells in many carcinomas. CAFs secrete extracellular matrix proteins and cytokines (such as SDF-1 and TGF-β) that have diverse immunomodulatory roles but generally promote tumour progression (121, 122). Radiation can recruit CAFs and the irradiated TME myofibroblasts undergo phenotypic transformation to CAFs (123). The role of CAFs in the immune response to radiotherapy is poorly understood, largely due to heterogeneity in CAF function. CAFs are predominantly immunosuppressive and can contribute to radioresistance by secretion of TGF-β to induce a radioresistant cancer stem cell-like phenotype (106). Cancer stem cells (CSC) represent an individual subpopulation within a tumour exhibiting the capacity to self-renew and differentiate, rendering CSCs resistant to various therapies including radiation therapy (124). CAFs can also secrete RNA containing exosomes that interact with tumour cell RIG-I, a pattern recognition receptor, and activates STAT1 dependent signalling,

which facilitates transcriptional responses to NOTCH3 and expands therapy resistant tumour-initiating cells to potentiate radioresistance in breast cancer (125). Radiation induced DNA damage can potentiate immune resistance, by conferring a senescence CAF phenotype, via the release of different factors by CAFs mediating fibrosis, EMT/invasion and treatment resistance, promoting tumour cell survival by promoting immunomodulation, metabolism, ECM remodelling, autophagy and treatment resistance to radiation therapy through a β_1 integrin mediated mechanism (126, 127). However, further work is needed to characterise the specific immunosuppressive role of irradiated CAFs in this context.

1.11 THE EFFECT OF RADIATION DOSING AND FRACTIONATION

As alluded to previously, conventional fractionated radiation is delivered in small 1.8-2Gy daily fractions. Recent advances in radiation technique and delivery, including intensity modulated radiotherapy (IMRT), volumetric-modulated arc therapy (VMAT) and proton beam therapy allow delivery of higher radiation doses while minimising acute and long-term toxicity (64). This has allowed a shift to 'hypo-fractionated' approaches, ranging from 5-10 Gy over three to five fractions to single doses of up to 24 Gy using stereotactic ablative radiotherapy (SABR) or stereotactic body radiotherapy (SBRT) (128). Different cellular responses in the TME depend on the dose of radiation delivered, mediated in part, by the intrinsic radioresistance of different immune cells (129). The sensitivity of T cells to radiation depends on their activation state; resting lymphocytes are more radiosensitive than activated forms. T_{reg} cells are more radioresistant than other T cells, allowing persistence following radiation, while B lymphocytes are highly radiosensitive (129). Macrophages are more resistant to radiation than monocytes under

high (>30 Gy) radiation doses, however, this dosing reduces the co-stimulatory receptor expression in immature DCs, down-regulating the expression of CD86 and CD80 compromising their ability to capture and present antigens (130).

1.12 Dosing, Fractionation, and Immunity

Conventional fractionated radiotherapy is designed to exploit vulnerabilities in DNA repair and cell cycle arrest as described in Figure 1.8, but the fractionation required for the most effective anti-tumour immune response is yet to be determined. Conventional fractionation mainly promotes cell death through mitotic catastrophe and apoptosis, which may be effective in promoting tumour regression but is more tolerogenic with less release of DAMPs (131). This is also associated with increased MDSCs and T_{reg} cells in the TME (132). Low dose radiotherapy also promotes tumour associated macrophage (TAM) accumulation, but may also promote the polarisation of TAMs to an immunogenic M1 phenotype (43) and a Th1 cytokine milieu (133). Therefore, despite these putative immunosuppressive effects, conventional radiation doses induce some level of anti-tumour immunity, as tumour antigen specific T cells have been isolated in prostate (134) and colorectal (135) cancer patients receiving radiation treatment.

There is evidence that hypofractionated radiotherapy (eg. 3x8 Gy) promotes more immunogenic changes in the TME. Upregulation of MHC-I on tumour cells and expanding the peptide repertoire is dose 'dependant', having an effect at >4 Gy in melanoma and >8-20 Gy in colon cancer cells (35). Upregulation of ICAM-1 on tumour cells, as well as the CD95 death receptor are also contingent on radiation dose (136). Hypofractionated radiotherapy (10 Gy) can promote cell death by necrosis and senescence, which is a more immunogenic form of cell death compared to apoptosis (31). Immunogenic cell death promotes the release of DAMPs potentiating the presentation of neoantigens released. Indeed, hypofractionated (10 Gy) radiation has been found to

enhance DC maturation compared to conventional fractionation in mice (137). These immunogenic effects may have implications for combining with ICIs. In mouse models of oral cancer, a hypofractionated regimen (2x8 Gy) induced greater $CD8^+$ T cell infiltration and reduced MDSC accumulation compared to low dose radiotherapy (1.8-2 Gy) (138). Furthermore, anti-PD-1 therapy reversed adaptive immune resistance and promoted $CD8^+$ dependant local and distant tumour regression.

High ablative doses (>20 Gy), such as those delivered by SABR/SBRT have been shown to dramatically increase T cell priming, $CD8^+$ T cell infiltration and the induction of tumour regression in breast, lung and melanoma mouse models (139, 140). Another preclinical study in an inherent poorly immunogenic colon cancer mouse model found a similar increase in $CD8^+$ infiltration compared to extended fractionation regimen, alongside MDSC depletion (141). These immunogenic effects of ablative radiotherapy are not universal. In combination with anti-CTLA-4 therapy, hypofractionated (3x8 Gy) radiotherapy was superior to an ablative (20 Gy) dose in promoting T cell infiltration and local and distant tumour regression (24). Consistent with this, higher ablative doses (>18-20 Gy) of radiation induce TREX1, as mentioned previously, an exonuclease that degrades cytoplasmic DNA and abrogates STING mediated IFN production and reduces $Batf3^+$ antigen presentation in mice (68). A single ablative dose may also lead to MDSC recruitment (42), further highlighting that there may a ceiling on radiation's dose dependant immunogenicity.

1.13 Dosing, Fractionation and the Tumour Vasculature

Radiation dosing and fractionation also have divergent effects on the tumour vasculature. Low doses of radiation not only normalise vessels but even stimulate angiogenesis and vasculogenesis through VEGF and SDF-1/CXCR12 signalling (102). Low dose radiation can normalise dysfunctional vessels of the TME, promoting inducible nitric oxide

synthase (iNOS) and an M1-phenotype in TAMs, allowing NO dependant vascular normalisation (43). The subsequent Th1 pattern of cytokines allows recruitment of $CD8^+$ T cells and tumour rejection in mouse models. Therefore, conventional radiation fractionation may be useful in immune-excluded tumours, where a dense stroma prevents effector T cells from accessing the tumour parenchyma (142).

Ablative doses of radiation leads to the destruction of the tumour vasculature. High doses (>8-10 Gy) of radiation delivered through SBRT/SABR promote endothelial cell apoptosis, through direct DNA damage and induced acid sphingomyelinase (99). Although this disruption of the tumour vasculature can lead to cancer cell death, they may generate regions of hypoxia and promote radioresistance (50, 104, 107). A computational model of tumour growth probability found that single ablative doses result in impaired local control of hypoxic tumours compared to hypofractionated regimens. (50). Therefore, the choice of radiation may be tailored based on the specific goals of microenvironment modification, whether destruction or normalisation of vessels is favoured.

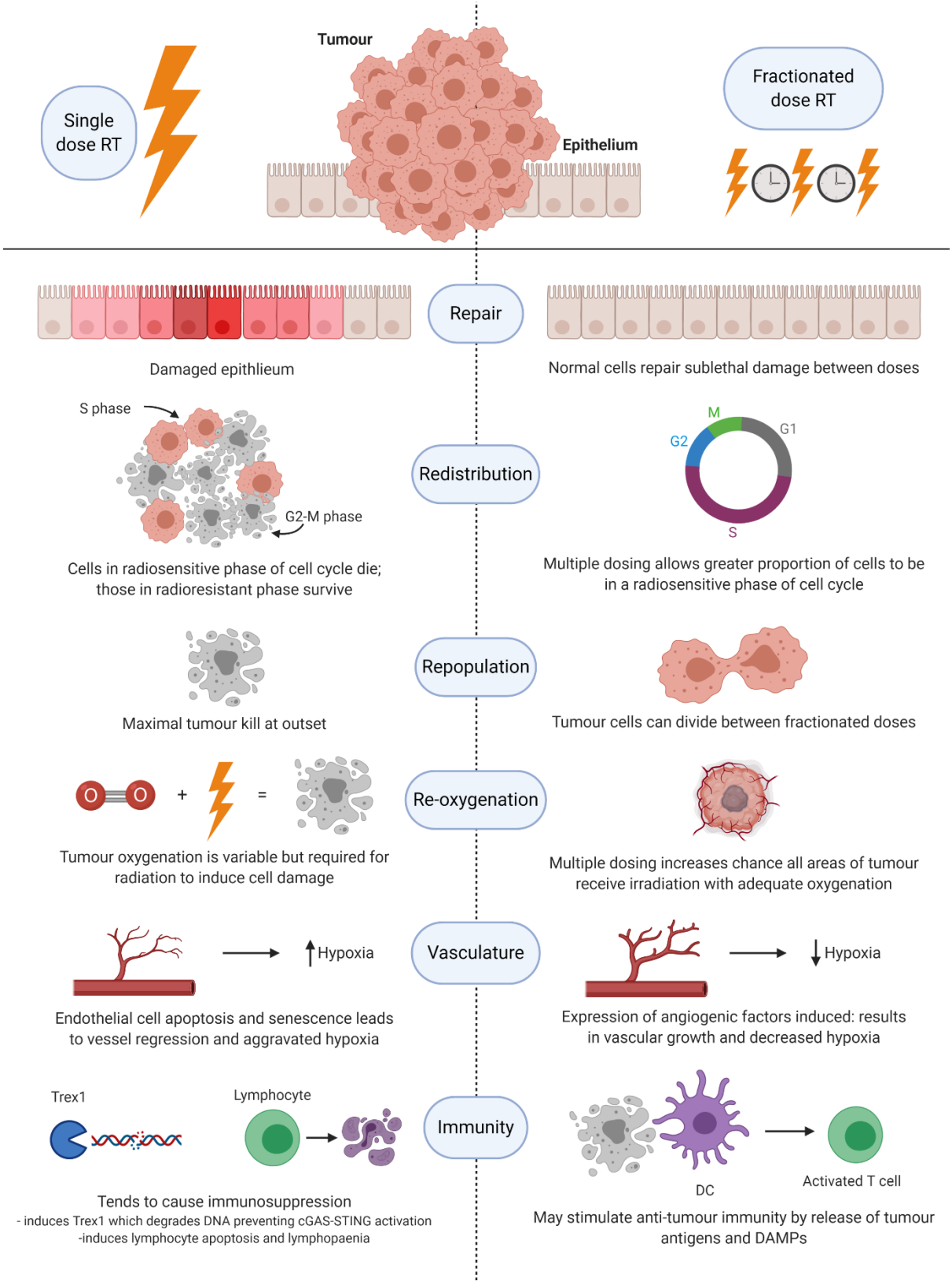

Figure 1.8. Fractionation: more than the sum of its parts. Radiation therapy (RT) can be administered to patients in a variety of regimens: single or fractionated dose. In contrast to a high dose of radiation administered at a single time-point, fractionated RT

entails division of the total radiation dose into multiple, smaller doses which are administered to a patient over a period of several days. Rationing the dose allows normal cells to recover or repair sublethal DNA damage whereas administering a high single dose often overwhelms a cell's ability to repair itself leading to toxicity. Cancer cells are often characterised by defective or repressed DNA repair, and therefore, single and fractionated radiation exposure leads to accumulation of genomic aberrations driving cell death. The radiosensitivity of tumour cells varies depending on progress through the cell cycle, with cells in S phase most radioresistant compared to those in G2-M phase. Administering multiple doses of radiation subjects a higher proportion of cells to radiation in the appropriate cell cycle phase in a concept known as redistribution. However, the gaps between fractionated treatments provide an opportunity for tumours to repopulate – this effect is mitigated somewhat by administering a single dose of radiation. RT is highly dependent on the oxygenation status of a tumour as oxygen free radicals are a major mediator of cell damage; however, malignant tumours are renowned for their hostile hypoxic microenvironments which can limit the success of RT. Additionally, the location of the hypoxic areas within tumours are highly variable, therefore, fractionating the dose increases the number of cells with adequate oxygenation (re-oxygenation) and the number of cells killed. High dose radiation causes regression of tumour blood vessels; however, the ensuing lack of perfusion may aggravate tumour hypoxia leading to angiogenesis and tumour progression. Conversely, fractionated low dose RT may induce vascular growth and normalisation via pro-angiogenic factor expression with resultant normoxia. While the differing effects of RT dosing regimens on the immune system have yet to be fully elucidated it seems that a high single dose of radiation contributes to immunosuppression within the tumour microenvironment while the fractionated RT appears to have immunostimulatory effects. High dose radiation can induce expression of TREX1 which degrades DNA fragments that otherwise would have triggered cytokine production via the cGAS-STING pathway. Moreover, high dose radiation is inherently lymphotoxic and lymphopenia often follows such treatments. In contrast, fractionated low dose RT may stimulate adaptive immune responses via release of tumour antigens and damage-associated molecular patterns (DAMPs) which prime DCs to activate anti-tumour T cells.

1.14 THE MICROENVIRONMENT AS A THERAPEUTIC TARGET

Radiation has profound effects on the composition and organisation of the TME, depending on the dose, location and tumour type. The immunogenic effects of radiotherapy promote tumour regression, whereas recruitment of immunosuppressive cell populations and exacerbation of tumour hypoxia can engender a radioresistant phenotype. Boosting these positive effects while mitigating these undesirable effects can be exploited to improve clinical responses.

1.15 Immune Checkpoint Blockade and the microenvironment

The induction of immunogenic cell death, enhanced neoantigen expression and presentation, cGAS-STING activation and $CD8^+$ T cell activation and infiltration provide preclinical rationale for combinatorial approaches of radiation and immune checkpoint blockade (ICB). Radiation can also increase tumour and immune cell expression of PD-L1, thought to be related somewhat to $CD8^+$ T cell derived IFN-γ secretion (143). This is a method for adaptive immune resistance to radiotherapy which can be overcome by PD-1/PD-L1 blockade (38). The expression of PD-L1 was found to be essential for ICB efficacy in some preclinical models (144) and a robust predictor of benefit of ICB in clinical trials (145), suggesting that radioresistance may also sensitise tumours to checkpoint inhibition. These immunogenic effects of radiation are more pronounced in hypofractionated radiotherapy or SBRT, but these doses promote vessel destruction, potentially exacerbating tumour hypoxia. Interestingly, anti PD-1 and anti-CTLA-4 therapy can result not only in tumour regression, but can also reduce tumour hypoxia (53). This vessel normalisation was mediated by IFN-γ producing $CD8^+$ T cells and was correlated with clinical efficacy. Another *in silico* analysis found that gene expression

related to vessel normalisation correlates with immunostimulatory pathways with Th1 derived IFN-γ normalising vessels (55). This reduces hypoxia *in vivo* and provides evidence of the symbiotic relationship between ICB and RT, through mutually favourable remodelling of the microenvironment.

Prospective clinical data combining immunotherapy and radiation are in a nascent phase; phase III trials have not been published outside of prostate and non-small cell lung cancer (NSCLC). The phase III PACIFIC trial investigated durvalumab (anti-PD-L1) following chemoradiotherapy in locally advanced NSCLC (62). Compared to placebo, durvalumab improved overall survival (28.3 vs 16.2 months, hazard ratio 0.68, p=0.0025) and both arms reported similar rates of treatment related adverse events (NCT02125461). A phase III trial in metastatic castration resistant prostate cancer found no survival benefit of ipilimumab (anti-CTLA-4) following a single 8 Gy dose of radiation, but a benefit in the combination arm was reported among those with favourable prognostic features (63). These trials have employed conventional fractionation or a single dose, whereas preclinical data indicate that hypofractionated RT has most potential in combination with ICB. One phase I trial of pembrolizumab (anti-PD-1) alongside hypofractionated radiotherapy (3 × 8 Gy) in metastatic solid tumours has reported early results (146). No dose limiting toxicities were observed and three patients displayed durable or complete responses to therapy. However, another trial of a similar regimen in bladder cancer was terminated early due to adverse events, highlighting the potential toxicity issues of this combination (147). Efficacy data is eagerly awaited from ongoing trials of hypofractionated radiation and immunotherapy in NSCLC (NCT04351256), melanoma (NCT03646617), renal cell carcinoma (NCT04090710) and glioblastoma (NCT03743662).

1.16 Soluble Factor Inhibition

Targeting chemokines has the potential to mitigate the immunosuppressive effects of MDSCs, T_{regs} and TAMs on the irradiated immune microenvironment. MDSCs are recruited following radiation due to interactions of CCL2/CCR2 and CCL2/CCR5, and inhibition of these chemokine axes can increase response to radiotherapy in preclinical models (148). This approach is being evaluated in a phase I/II trial, combining a CCR2/5 dual antagonist (BMS-813160) with anti PD-1 therapy and hypofractionated RT (5 x 6.6 Gy) in pancreatic cancer (NCT03767582). T_{reg} cells are recruited by CCL2 and TGF-β in an immunosuppressive TME. Targeting TGF-β alongside hypofractionated RT (3 x 7.5 Gy) has been examined in a phase I trial of metastatic breast cancer (149). This combination was well tolerated with seven grade 3/4 adverse events in 5/11 patients in the 1mg/kg arm and in 2/12 patients in the 10mg/kg arm, respectively. In addition to this, the higher dose cohort had favourable immune markers and a longer median survival of 16 months than those in the lower dose cohort of 7.57 months.

Production of adenosine by CD73 is a potent means of T_{reg} induced immunosuppression and a recent preclinical study reported that combining CD73 inhibition with radiation promotes DC infiltration and tumour rejection in combination with anti-PD-L1 and anti-CTLA-4 therapy (150). Anti-CD73 therapy alongside PD-L1 blockade and SBRT is being investigated in an ongoing breast cancer trial by Institut Curie (France) & Jules Bordet Institute (Belgium) in collaboration with AstraZeneca (NCT03875573).

1.17 The DNA Damage Response

Cancer-associated DNA damage response (DDR) defects can be targeted to amplify radiation induced DNA damage (151). Checkpoint kinase 1 (CHK1), WEE1 and ataxia telangiectasia and Rad3- related protein (ATR) are involved in the S phase and G2/M

arrest following DNA damage (152). Inhibiting this pathway leads to premature M phase entry and results in increased micronuclei formation when combined with radiation, which can enhance the STING induced type I interferon release (153). Studies in mice indicate that AZD6738, an ATR inhibitor, potentiates radiation induced type I interferon production and modifies the TME; with an increase in $CD8^+$ T cells, NK cell and DC infiltration noted alongside MDSC depletion compared to controls (34, 154). A phase I trial is evaluating the addition of AZD6738 as a radiosensitiser to palliative radiotherapy (155). Another approach, the combination of a WEE1 inhibitor alongside RT and PD-1 blockade enhanced the efficacy of $CD8^+$ T cell mediated cytotoxic activity in mice (156). DNA protein kinase (DNA-PK) is involved in non-homologous end joining repair of double strand DNA breaks (151), and although it has not been studied preclinically alongside RT and ICB, clinical trials evaluating this triplet combination are ongoing (NCT04068194, NCT03724890). As these strategies of DDR inhibition represents a novel approach to amplify the immunogenic effects of radiation, it may prove useful as a radiosensitiser alone or to further optimise the combination of radiotherapy and ICB.

1.18 Future directions

Despite the success in leveraging the combination of immunotherapy for the treatment of upper gastrointestinal cancers, several issues are outstanding. There is a lack of studies that directly compare the immunogenicity of different dosing and fractionation regimens. This is seen in both preclinical studies and clinical trials, and not specific to gastrointestinal cancers. Some studies vary the entire dose of radiation but do not ascertain whether this dose would be better delivered in a single ablative dose, a hypofractionated regimen or conventional 1.8-2 Gy fractionation. Well-controlled preclinical studies would provide more clarity on the subtle effects of different

fractionation, while a multi-arm clinical trial would be useful to determine the optimal dosage regimen for clinical practice. These trials should also have translational study endpoints including abscopal response and changes in $CD8^+$ TILs, T_{reg} cells and MDSCs levels in the irradiated and peripheral sites. This would involve dissecting the mechanisms of action and resistance to immuno-radiotherapy, and provide mechanistic data specific to upper GI cancers. Finally, there is a need for more trials in the advanced disease setting. In contrast to single agent ICB, most trials of ICB and radiotherapy are in locally advanced, resectable disease where chemoradiotherapy is a standard of care. However, outcomes are worst in the refractory disease setting and response rates to single agent ICB are low (157). This highlights an unmet need for trials in this cohort, which could stand to benefit most of this symbiotic combination.

1.19 Conclusion

The advent of immune checkpoint blockade has shifted the paradigm in the treatment of solid tumours, but the impact of ICIs on patient outcomes in UGI cancers has been limited. Radiotherapy has the potential to augment responses to ICI through cGAS-STING signalling, immunogenic cell death, upregulation of neoantigen expression and through inflammatory remodelling of the immune microenvironment. Given the extensive pre-existing use of radiation and the modest activity of single agent immunotherapy, gastroesophageal cancers are poised to greatly benefit from a combination of ICIs and radiotherapy. However, questions remain surrounding methods of optimising the radiation dose and timing while minimising toxicity. Most ongoing clinical trials employ conventional radiation fractionation, although preclinical data suggest that hypofractionated regimens are favourable in terms of toxicity and efficacy.

Signalling events following radiotherapy have profound effects in altering the immune landscape of the TME. Advances have been made in recent years to untangle the biology of radiation induced anti-tumour immunity and how this knowledge can be used to design rational therapeutic approaches. However, issues remain regarding the paradoxical effects of radiation in recruiting suppressive cell populations, the complex effects that radiation invokes on the tumour vasculature and the radiation dosage and fractionation that influences these effects. Although hypofractionated regimens display the most promising immunomodulation in preclinical studies, there is a lack of prospective clinical data that directly compare different approaches. Questions remain around the best way to promote immunostimulatory effects of radiotherapy while minimising immunosuppression. We propose that combining radiation with immunotherapy is a promising approach to shift this balance and exploit the microenvironment's untapped therapeutic potential. A better understanding of variability in response to immune checkpoint blockade is also required. Future trials should incorporate correlative endpoints to identify predictive biomarkers of response as this will help to select patients likely to benefit from radiation and immunotherapy and facilitate a precision oncology approach.

The five specific aims of this thesis are to:

1. Evaluate the impact of radiotherapy on Immune checkpoint expression *in vitro* and *ex vivo* under normal conditions and those of the tumour microenvironment.

2. Evaluate the impact of conventional chemo(radio)therapy on the immune profile of matched tumour and lymph nodes.

3. Evaluate the impact of major oncological surgery on the post operative immune response.

4. Evaluate the impact of conventional chemotherapy and chemoradiotherapy on DAMP expression in pre treatment and post treatment whole blood and tumour biopsies. This study will also evaluate the impact of the tumour microenvironment on DAMP and immune checkpoint expression.

5. Evaluate the impact of radiotherapy and the tumour microenvironment on Oesophageal cancer patient T cell function and the immune profile in pre- and post- conventional treatments.

Chapter 2: Materials and methods

2.1 Reagents

The chemicals and reagents utilised in this thesis were stored as per manufacturers' instructions. Solutions including distilled water were autoclaved following preparation. Calibrated Gilson pipettes were used for the precise transfer of liquid volumes up to 1ml (Gilson S.A., France). All cell culture reagents were purchased from Lonza (Basel, Switzerland) unless otherwise stated. All cell culture flasks and plates were purchased from Sarstedt (Wexford, Ireland), unless otherwise stated.

2.2 Ethical approval

Ethical approval was granted from the Tallaght University Hospital/St. James's Hospital Ethics Committee and the Beacon Hospital Ethics Committee (Project ID: 0215). All patients were consented for sample requisition prospectively and informed written consent for sample and data acquisition from patients or from healthy donors was obtained. This study was carried out in accordance with the World Medical Association's Declaration of Helsinki guidelines on medical research involving human subjects. Patient samples were pseudonymised in line with GDPR and data protection policies to protect the privacy and rights of the patients.

2.3 Prospective specimen collection

This study consisted of samples collected at 3 timepoints;

1. Tumour tissue samples and whole blood were obtained from a cohort of consecutive patients prior to neoadjuvant therapy (Chemotherapy or Chemoradiotherapy) at the time of endoscopy or clinic appointment at St James's Hospital or Beacon Hospital under the

care of the Upper Gastrointestinal Surgical service. This was a cross site study and was carried out in collaboration with Maria Davern and Andrew Sheppard.

2. Tumour and whole blood was also collected from patients post-FLOT chemotherapy (docetaxel, oxaliplatin, leucovirin and 5-fluorouracil) treated and post-CROSS chemoradiotherapy (carboplatin, paclitaxel and 41.6 Gy irradiation) at time of an en bloc oesophagectomy for oesophageal and junctional adenocarcinoma (Siewert any).

3. Whole blood and serum samples were also collected immediately pre-operatively (POD 0), days 1, 3, 7 and week 6 post-operatively. This study included patients treated with curative intent only.

Samples were obtained in accordance with the ethically-approved standard operating procedure in the department. Patient samples were collected over a three-year period from 2018-2020 inclusive.

Prospective databases containing detailed clinicopathological, demographic, staging, treatment, and follow-up information for all patients were maintained. The database consists of all patients with a diagnosis of oesophageal cancer, junctional or otherwise at St James's Hospital which were recorded prospectively. Patient details were cross referenced and accurate logging of information confirmed by a dedicated database manager who worked in conjunction with the clinical teams and the dedicated multidisciplinary conferences in order to maximise the validity of the database. The relevant patient demographics, data relating to clinicopathological stage and outcomes were included for the population of interest. Tumour, node and metastasis descriptors and the staging classification used for this analysis were those defined in the eighth edition of the American Joint Committee on Cancer staging manual (AJCC, 2018) The group was evaluated based on Mandard TRG status applied throughout, with TRG 1 indicating no

residual cancer cells, TRG 2 indicating rare residual cells, TRG 3 representing an increase in the number of residual cancer cells, but with fibrosis l predominating, TRG 4 where cancer outgrows fibrosis, and TRG 5 represents a complete absence of regressive changes. Adverse tumour biological features were defined as poor differentiation, the presence of lymphatic invasion, vascular invasion and perineural invasion in the resected specimen.

2.4 Pre-operative quantification of serum immune proteins

Serum samples were collected from OAC patients, snap frozen and cryopreserved at –80^{o}C until further analysis. Serum proteins were quantified using a V-PLEX Human Biomarker 54-plex enzyme-linked immunosorbent assay (ELISA) kit, spread across 7 discrete assays (Meso Scale Diagnostics, USA). These assays quantified the secretions of the following 54 proteins: CRP, CCL11 (eotaxin), CCL26 (eotaxin-3), FGF (basic), GM-CSF, ICAM-1, IFN-γ, IL-10, IL-12/IL-23p40, IL-12p70, IL-13, IL-15, IL-16, IL-17A, IL-17A/F, IL-17B, IL-17C, IL-17D, IL-1RA, IL-1α, IL-1β, IL-2, IL-21, IL-22, IL-23, IL-27, IL-3, IL-31, IL-4, IL-5, IL-6, IL-7, IL-8, IL-8, IL-9, CXCL10 (IP-10), CCL2 (MCP-1), CCL13 (MCP-4), CCL22 (MDC), CCL3 (MIP-1α), CCL4 (MIP-1β), CCL20 (MIP-3α), PlGF, SAA, CCL17 (TARC), Tie-2, TNF-α, TNF-β, TSLP, VCAM-1, VEGF-A, VEGF-C, VEGF-D and VEGFR-1/Flt-1. All assays were run as per manufacturer's recommendations, with an alternative protocol of overnight serum incubation being used for all assays except Vascular Injury and Angiogenesis, which were run in a single day. All results were reported in pg/ml. This work was carried out in collaboration with Margaret Dunne and Fiona O'Connell.

2.5 Post-operative Quantification of serum immune proteins

Serum samples were collected from those patients who completed their neoadjuvant treatment regimens and were handled according to MSD (Meso Scale Diagnostics, USA) multiplex protocols. To assess angiogenic, vascular injury, pro-inflammatory, cytokine, chemokine and immune checkpoint secretions, custom 54 V-plex ELISA and U-PLEX ELISA kits, separated across 10 discrete assays were used (Meso Scale Diagnostics, USA). The multiplex kit was used to quantify a total of of 59 analytes including: CD27, CD276, CD28, CD40L, CRP, CTLA-4, Eotaxin, Eotaxin-3, FGF(basic), Flt-1, GITR, GITRL, GM-CSF, IFN-γ, IL-10, IL-12p40, IL-12p70, IL-13, IL-15, IL-16, IL-17A,IL-17A/F, IL-17B, IL-1RA, IL-1α, IL-1β, IL-2, IL-21, IL-22, IL-23, IL-27, IL-31, IL-4, IL-6, IL-8, IL-9, IP-10, LAG3, MCP-1 ,MCP-4, MDC, MIP-1α, MIP-1β, MIP-3α, OX40, PD1, PD-L1 , PD-L2, PIGF, TARC, Tie-2, TIGIT, TIM-3, TNF-α, TNF-β, TSLP, VEGF-A, VEGF-C, VEGF-D. All assays were run as per manufacturer's recommendations, with an overnight supernatant incubation protocol used for all assays except Angiogenesis Panel 1 and Vascular Injury Panel 2 which were run according to the same day protocol. Analyte concentrations were calculated using Discovery Workbench software (version 4.0). Values outside the kits limit of detection were not reported.

2.6 Histological assessment of matched OAC donor tissues

Routine haematoxylin and eosin (H&E) stained sections from diagnostic biopsy material from serum-matched OAC donors were reviewed by 2 pathologists (JA and KD), who were blinded to clinical outcomes. Inflammatory cell density and tumour stroma percentage were assessed in tissue fragments containing invasive carcinoma. Inflammatory cell density was classified as either absent/low-grade (mild/patchy increase in inflammatory cells) or high-grade (prominent inflammatory infiltrate and/or

involvement and destruction of cancer cell islands). The presence of eosinophils, neutrophils, lymphocytes and plasma cells was also assessed and similarly classified as either absent/low-grade or high-grade. The tumour stroma percentage (TSP) was assessed by estimating the proportion of stroma as a percentage of the visible field from an area of carcinoma, excluding areas of mucin deposition or necrosis. Tumours were classified as low TSP if stroma accounted for 50% of the visible field. Similarly, they were classified as high-TSP if stroma accounted for 50% of the visible field.

2.7 Cell culture

2.7.1 Cell lines

OGJ cells (OE33, and an in-house developed isogenic model of radiosensitive OE33P and radioresistant OE33R cells (158)) used in this study were obtained from the European Collection of Cell Cultures. The OE33 cell line was established from a 73-year old female patient with adenocarcinoma of the lower oesophagus. The tumour was poorly differentiated and characterised as stage IIA. The OE19 cell lines was established in 1993 from an adenocarcinoma of gastric cardia/oesophageal gastric junction of a 72-year old male patient. The tumour was identified as pathological stage III (UICC) and showed moderate differentiation.

The FLO-1 cell line was obtained from our colleagues at the Peter Mc Callum Cancer Centre in Victoria Australia in addition to a liver metastasis generated cell line on site. The FLO-1 cell line was established from a primary distal oesophageal adenocarcinoma in a 68 year-old Caucasian male in 1991. The Y chromosome could not be detected in this cell line by short tandem repeat (STR)-PCR analysis when tested at the ECACC. It is a known phenomenon that due to the increased genetic instability of cancer cell lines the Y

chromosome can be rearranged or lost resulting in lack of detection. The cell line is identical to the source provided by the depositor based on the STR-PCR analysis.

2.8 Mycoplasma testing

Mycoplasma testing was performed on all cell lines received from outside institutions and tested every 4 months thereafter alongside in-house cell lines. These cells were tested for mycoplasma infection using the MycoAlert® mycoplasma detection assay (Lonza). This assay exploits the activity of certain mycoplasmal enzymes, which react in the absence of mycoplasma and can then be detected by measuring the ratio of the level of ATP in sample before the addition of the substrate. Cells were passaged in antibiotic free media for two passages before carrying out the assay. Briefly, 2ml of culture medium was transferred into a centrifuge tube and centrifuged at 200 × g for 5 minutes to pellet floating cells. 100µL of the cleared supernatant was then transferred into a luminescence compatible plate. 100µL of MycoAlert® reagent was added to each sample for 5 minutes and a 1 second integrated reading was taken on the luminometer (reading A) (Victor™, Perkin Elmer, Columbus, OH). 100µl of MycoAlert® substrate was then added to each sample for 10 minutes and a second reading was taken (reading B). The ratio of reading B to reading A was used to determine the presence of mycoplasma in the cell culture medium. Cells infected with mycoplasma produced ratios greater than 1. Cells that tested positive for the presence of mycoplasma and frozen aliquots were discarded and the incubator in which they were stored was cleaned thoroughly.

2.9.1 Cell line subculture

OE-33, OE19 and FLO-1 cells were maintained in Roswell Park Memorial Institute (RPMI) 1640 medium which was supplemented with 10% (v/v) foetal bovine serum (FBS) and penicillin streptomycin (50 U/ml penicillin 100µg/ml streptomycin). Cells were incubated in 25cm^2 or 75cm^2 vented flasks at 37°C in a humidified atmosphere with 5% CO_2. Cells were examined daily using an inverted phase-contrasted Nikon microscope (Nikon Corp., Tokyo, Japan). Sub-culturing was performed when the cells reached 80-90% confluency. Adherent cells were detached for sub-culturing by trypsinisation. The growth medium was decanted and the cells were washed with 10ml of 0.01 M phosphate buffered saline (PBS) (13.8mM NaCl, 2.7mM KCl, pH 7.4) to remove residual FBS. 1ml (25cm^2 flasks) or 2ml (75cm^2 flasks) of trypsin ethylene-diamine tetra-acetic acid (EDTA) (0.05% (w/v) trypsin, 0.02% (w/v) EDTA) was added to the flasks. Flasks were incubated at 37°C for approximately 5 minutes to allow the cells to detach from the flask surface. 10ml of complete medium (medium containing 10% FBS) was then added to the flasks to inactivate the trypsin. Cells were transferred to a sterile tube and pelleted by centrifugation. (Thermo lEC, Needham heights, MA, USA) at 1300 x g for 3 minutes. The supernatant was then discarded and the cell pellet re-suspended in 10ml of complete medium. This suspension was used to seed fresh flasks at a number of different ratios. Complete medium (5 or 10ml was added to the cells in 25cm^2 and 75cm^2 flasks respectively). All cell culture experiments were carried out using cell lines within 10 passages. Cell stocks were stored under liquid nitrogen in a cryofreezer (NuAire Corp., Plymoth, MN, USA) or in a -80°C freezer. Stocks were prepared from cells growing in the exponential phase at less than 80% confluency. To prepare frozen stocks, cells were washed in 10ml PBS and trypsinised as above. 5-10ml of complete medium was added to the trypsinised cells and the cells were re-suspended 5% (w/v) dimethyl sulphoxide

(DMSO) in complete media. 750µ1 of DMSO solution was added for each cryovial of cells to be frozen. The solution was applied in a drop-wise manner to the cells during re-suspension.

2.9.2 Cryopreservation of cell line stocks

Cryovials were placed at -20°C overnight before being transferred to -80°C for short term storage. For long-term storage, vials were transferred to liquid nitrogen. Cryovials were removed from liquid nitrogen and placed at 37°C to thaw rapidly. Cells were transferred to a fresh 25cm flask, to which 5ml of complete media had been added. Cells were incubated at 37°C for 24 hours. Media was replaced the following day to remove any dead cells and residual DMSO. Flasks were maintained and passaged as previously described. Cell waste was decontaminated for 24 h using Haztab chlorine tablets.

The optimised seeding densities for cell lines are listed in Table 2.1.1.

Table 2.1.1 Seeding densities used for cell lines

Cells	plate size	Seeding density
OE33 cells	Flat 96 well plate	5×10^3 cells/ml
OE33 cells	Flat 12 well plate	0.1×10^6 cells/ml
FLO-1, FLO-1 LM cells	Flat 96 well plate	5×10^3 cells/ml
FLO-1, FLO-1 LM cells	Flat 12 well plate	0.1×10^6 cells/ml

2.10 PBMC isolation by density gradient centrifugation

Peripheral blood mononuclear cell (PBMC) isolation was carried out by density gradient centrifugation using lymphoprep solution (Axis-Shield) at room temperature. The procedure was carried out under sterile conditions in a laminar flow cabinet (Microflow Biological Safety Cabinet) which was turned on 10 mins prior to use to achieve a sterile atmosphere. Blood was diluted 1:1 in PBS solution (Gibco). The diluted blood solution was carefully layered on top of lymphoprep solution (Axis-Shield) so as to not break the lymphoprep-blood interface (1:2 ratio of lymphoprep:diluted blood). The sample was centrifuged at 2000 RPM for 25 mins with the brake off (centrifuge, Thermo Scientific Heraeus Megafuge 40). Following centrifugation, the different blood cells separated into distinct layers based on their relative densities. The layer containing the PBMCs was a white cloudy layer (buffy layer) and contained monocytes and lymphocytes. The buffy layer was removed and washed twice with PBS. The supernatant was discarded and the resulting cell pellet was vortexed and resuspended in 1 ml of cRPMI. PBMCs were then counted as described in section 2.11 and plated at 1 x 10^6 cells in 1 ml of cRPMI per well in a 24 well plate (Sarstedt) or at 2 x 10^5 cells in 200 µl of cRPMI per well in a 96 well plate (Sarstedt) and incubated overnight to rest the cells at 37˚C, 5% CO_2 (ESCO cell culture, CO_2 incubator, Medical Supply Company).

Flat bottomed plates (96- or 12-well) were coated with 50 µl and 200 µl, respectively of goat anti-mouse IgG (5 µg/ml in PBS) and incubated overnight at 4°C. Wells were washed twice with PBS and coated with 200 µl of anti-CD3/anti-CD28 antibody solution (anti-CD3 5µg/ml BioLegend and anti-CD28 Ancell diluted 1:1000 dilution) and incubated for 2h at 37°C. Wells were washed with PBS and cells were seeded in 100 µl of cRPMI with IL-2 (100 units/ml, ImmunoTools, Germany) at a density of 1 x 10^6 cells/ml.

Table 2.1.2

Cells	plate size	Seeding density
PBMCs	Flat 96 well plate	2 x 10^5 cells/ml
PBMCs	Flat 24 well plate	1 x 10^6 cells/ml

2.11 Cell counting

Cell counting was carried out using a bright-line haemocytometer (Hausser Scientific, PA, USA). Cell viability was examined using a trypan blue dye exclusion assay. 180ul of trypan blue was mixed with 20ul of cell suspension and was added to the counting chamber of the slide. Viable cells were unstained due to their exclusion of trypan blue, whereas dead cells stained blue due to their distorted membranes. The number of viable cells was counted in each of the four quadrants of the haemocytometer. The number of cells/ml was then calculated using the following equation: Cells/mL = average cell number x 10 x 10^4 counted then divided by 4 which represents the number of fields counted on the haemocytometer. 10 = dilution factor 10^4 = constant.

2.12 Nutrient deprivation and hypoxia treatment

2.12.1 Nutrient deprivation and hypoxia treatment of cells lines

OE33 cells were cultured in complete RPMI (cRPMI, 10% FBS, 1% P/S), serum-free RPMI (0% FBS, 1% P/S), glucose-free RPMI (Gibco (11560406), 10% FBS, 1% P/S), dual glucose-free and serum deprived RPMI (Gibco, 0% FBS, 1% P/S) under normoxic

conditions (37°C, 5% CO_2, 21% atmospheric O_2) or hypoxic conditions (37°C, 5% CO_2, 0.5% O_2) for 48h using the H35 Don Whitley hypoxia station (Don Whitley Scientific).

2.12.2 Nutrient deprivation and hypoxia treatment of OGJ donor PBMCs

5-day anti-CD3/CD28 expanded PBMCs were seeded at a density of 1 x 10^6 cells/ml in 100 µl of media in a 96 well round bottomed plate (not pre-coated with anti-CD3/28) for an additional 24h in complete RPMI (cRPMI, 10% FBS, 1% P/S), serum-free RPMI (0% FBS, 1% P/S), glucose-free RPMI (Gibco, 10% FBS, 1% P/S), dual glucose-free and serum deprived RPMI (Gibco, 0% FBS, 1% P/S) under normoxic conditions (37°C, 5% CO_2, 21% atmospheric O_2) or hypoxic conditions (37°C, 5% CO_2, 0.5% O_2) using the H35 Don Whitley hypoxia station. PBMCs were then harvested for flow cytometry staining.

2.13 Flow cytometry staining

2.13.1 Whole blood staining

100 µl of whole blood was added to two FACS tubes with extracellular fluorochrome-conjugated antibodies and incubated for 15 min at room temperature in the dark. Without washing off the antibodies, red cells were lysed using red blood cell lysing solution (Biolegend, USA), according to manufacturer's recommendations: 500 µl of red blood cell lysing solution was added to stained and unstained blood at a concentration of 1X and vortexed (BD Biosciences, USA, 10X concentration). Red blood cell lysing solution was diluted using distilled water to dilute a 10X solution down to a 1X solution. Tubes

were incubated in the dark for an additional 15 mins at room temperature. Cells were washed twice with FACS buffer. Cells were washed with PBS and stained with zombie aqua viability dye (BioLegend, USA) for 20 mins (1:1000 dilution using PBS). Cells were fixed for 15 min in 1% paraformaldehyde solution (Santa Cruz Biotechnology, USA) and resuspended in FACs buffer and acquired using BD LSR Fortessa flow cytometer (BD Biosciences) using BD FACs Diva Software Version 8.0. Data was analysed using FlowJo v10 software (TreeStar Inc.).

2.14 Cell line and PBMC flow cytometry staining

Trypsinised cells, PBMCs, or digested tumour biopsies were transferred to FACs tubes (BD Biosciences, USA) and washed twice with PBS and stained with Zombie aqua, NIR or violet viability dye (BioLegend, USA using an overall 1:1000 dilution of Zombie viability dye using PBS) for 15 minutes in the dark at room temperature. Cells were then sequentially stained with appropriate antibodies for 15 minutes in the dark at room temperature: calreticulin-AF488 (Bio-techne, USA), HMGB-1-PE, MIC-A/B-APC, CD45RA-PE/Cy7, CD45RO-BV510, CD3-APC, CD3-PerCP, CD4-BV510, CD4-APC, CD69-BV605, TIGIT-BV605, PD-L2-BV421 (Biolegend, USA), CD69-PE, CD62L-FITC, CD8-BV421, or CD4-PerCpCy5.5, CD27-APEefluor780 (eBioscience, USA) (Table 2.3). Cells were washed with FACs buffer and fixed with 1% paraformaldehyde solution (diluted with PBS), washed with FACs buffer, resuspended in FACs buffer and acquired using BD LSR Fortessa flow cytometer (BD Biosciences) or Cells using the BD FACs CANTO II flow cytometer and BD FACs Diva Software. Data was analysed using FlowJo v10 software (TreeStar Inc.).

LN biopsies were stained with zombie aqua viability (Biolegend, USA) and the following cell surface antibodies: PD-L1 PE and CD8 BV421 (BD Biosciences, USA), TIM-3 Biobright FITC and CD3 APC (Miltenyi, USA), TIGIT PE/Cy7 and PD-1 APC/Cy7 (Biolegend, USA) and CD4 PerCpCy5.5 (eBiosciences, USA). Cells were fixed using 1% paraformaldehyde solution (Santa Cruz, USA), washed and resuspended in FACs buffer and acquired using BD FACs CANTO II (BD Biosciences) using Diva software version10 and analysed using FlowJo v10 software (TreeStar Inc.).

Table 2.3 Volume of extracellular fluorochrome-conjugated antibodies added per sample.

Antibody	Company	Concentration per well/tube
PD-L1-FITC	BD Biosciences (USA)	2 µl
PD-L2-PE	Biosciences (USA)	2 µl
TIM-3-ViobrightFITC	Miltenyi (Germany)	2 µl
LAG-3-FITC	BioLegend (USA)	2 µl
PD-1-PE/Cy7	BioLegend (USA)	2 µl
TIGIT-PE/Cy7	BioLegend (USA)	2 µl
CTLA-4-PECy5.5	BioLegend (USA)	2 µl
CD8-BV421	BioLegend (USA)	1 µl
CD3-PerCpCy5.5 or CD3-APC or CD3-FITC or CD3-PEeluor610	BioLegend (USA)	1 µl
CD4-APC or CD4-BV510	BioLegend (USA)	1 µl
CD4-PercPCy5.5	eBiosciences (USA)	1 µl
CD62L-FITC	BD Biosciences (USA)	1 µl
CD69-PE	BD Biosciences (USA)	1 µl

CD69-BV605	BioLegend (USA)	1 µl
PD-L2-BV421	BioLegend (USA)	2 µl
HMGB1-PE	BioLegend (USA)	2 µl
Calreticulin-AF405	BioLegend (USA)	2 µl
CD45RA-PE/Cy7	BioLegend (USA)	1 µl
CD45RO-BV510	BioLegend (USA)	1 µl
CD27-APCefluor780	eBiosciences (USA)	1 µl

2.15 Intracellular flow cytometry staining

For intracellular cytokine staining PBMCs were treated with phorbol. 12-myristate 13-acetate (PMA) (10 ng/ml, Sigma Aldrich, USA) and ionomycin (1 µg/ml, Sigma Aldrich, USA) for the last 4h of the incubation. 2 µl of anti-CD107a-PE (BD Biosciences, USA) was added during stimulation. For the final 3h of the incubation PBMCs were treated with brefeldin A (10 µg/ml, eBiosciences). Cells were harvested, washed in FACs buffer and intracellular cytokines were assessed using a Fixation/Permeabilisation kit (BD Biosciences), as per manufacturer's recommendations. Cells were stained with cell surface antibodies (CD8-BV421, CD3-APC or CD3-PerCP, CD4-PerCP, CD4-APC or CD4-BV510 (Biolegend, USA)) washed, permeabilised, and then stained for intracellular cytokines: IFN-γ-BV510, IL-4-PE/Cy7, IL-10-PE, IL-2-FITC (Biolegend, USA) (Table 2.4). Cells were washed with FACs buffer, fixed with 1% paraformaldehyde solution, resuspended in FACs buffer and acquired using the BD FACs CANTO II flow cytometer and BD FACs Diva Software. Data was analysed using FlowJo v10 software (TreeStar Inc.).

Table 2.4 Volume of intracellular fluorochrome-conjugated antibodies added per sample.

Antibody	Company	Volume per well/tube
IL-2-FITC	BioLegend (USA)	2 µl
IFN-γ-BV510	BioLegend (USA)	2 µl
IL-10-PE	BioLegend (USA)	2 µl
IL-4-PE/Cy7	BioLegend (USA)	2 µl

2.16 Generation of conditioned media

2.16.1 Generation of tumour biopsy conditioned media

Resected post-FLOT or post-CROSS OGJ tumour explants (n=11) of ~2–3 mm^3 were transferred into 1 ml of serum-free M199 media (Gibco), supplemented with gentamicin and cultured for 24 h at 37°C, 5% CO_2. The resulting tumour conditioned media (TCM) was harvested and stored at −80°C until required. Patient demographics are shown in **Table 2.2**. Protein content was assessed by BCA assay for normalisation.

Lymph node (LN) biopsies (n=9) were cultured in a 12 well plate in L-15 (Leibovitz) Lonza™ BioWhittaker™ X-vivo media for 24 hrs *ex vivo* at 37ºC, 5% CO_2. LN tissue was divided into four equal quadrants to ensure adequate distribution of immune cells. These were confirmed to be benign through formal histological assessment by the St James' Hospital Histopathology department. The resulting LNCM was harvested and stored at −80ºC until required.

Table 2.2 Patient Demographic Table for generating tumour biopsy conditioned media.

Patient Demographic Table	N=11
Age (years)	65.5
Sex ratio (M:F)	6:4
Diagnosis (no. patients)	
OGJ	10
Clinical tumour stage[a] (no. patients)	
T0	1
T1	1
T2	1
T3	7
T4	1
Clinical nodal status[a] (no. patients)	
Positive	6
Negative	5
Received neoadjuvant FLOT	45.5%
Received neoadjuvant CROSS CRT	54.5%
Did not receive neoadjuvant treatment	0%

2.17

Irradiation

Cell lines, tumour tissue, PBMCs and lymph node were irradiated using the X-Ray generator RS225 system (Gulman Medical, UK). The instrument was upper-heated for 45 min prior to irradiation and irradiated with bolus dosing of 2 Gy, 10 Gy, 20 Gy, fractionated dosing 3 x 2 Gy, 3 x 4 Gy, 3 x 8 Gy, or mock irradiated (cells were placed into the irradiator but not irradiated). For irradiation of the hypoxic plates, these were placed in mini hypoxia chambers and transferred to the irradiator and subsequently transferred back after receiving the appropriate dose of radiation.

2.18 OAC tumour tissue dissociation

Tumour tissue was cut into small 2-3 mm^3 pieces. Tumour tissue biopsy was digested in collagenase type IV solution (50 µl type IV collagenase (1 mg/ml, Sigma-Aldrich) in 5 ml of HBSS buffer) at 37ºC on a shaker for 20-30 mins with maximum agitation. The digested biopsy solution was filtered using 70 µm nylon mesh filter into a 50 ml tube (Fisher Scientific) to separate filtered cells from tissue debris. Filters were washed with 5 ml of HBSS buffer. Cells were washed twice with FACS buffer at room temperature. 100 µl of vortexed cell pellet was transferred to a FACS tube and cells were stained according to the flow cytometry staining protocol.

2.19 Cytolysis assay for assessing lymphocyte-mediated killing of OGJ cells

The cytolysis assay was carried out as previously reported (159). Treatment naïve OGJ patient-derived PBMCs were isolated using density gradient centrifugation and expanded using plate bound anti-CD3 (10 µg/ml, Biolegend, USA) and anti-CD28 (10 µg/ml, Ancell, USA) and recombinant human IL-2 (100 units/ml, Immunotools, Germany) for

5 days, (n=6, duplicate technical replicates). OE33 cells were seeded at a density of 5 x 10^3 cells/100 µl of media in a flat 96 well plate and incubated overnight at 37˚C, 5% CO_2. FLO-1 and FLO-1 LM cells were seeded at a density of 5x10^3 cells /100ul of media also. The media was replaced and PBMCs were co-cultured with tumour cells in an effector:target ratio of 5:1 and 10:1, 20:1 for 48h in the absence or presence of radiation. Tumour cells and PBMCs were also cultured alone as controls to account for an increase in cell viability during treatment. At 48h 5µl of CCK8 (Sigma, USA) was added to each well and the optical density at 450 nm and 650 nm (reference wavelength) was measured using the Versa Max microplate reader (Molecular Devices, Sunnyvale, CA, USA) to determine viable cell numbers using the following formula: (viability tumour cell-lymphocyte co-culture)-(viability PBMCs alone)/ (viability untreated tumour cells alone) x 100 = % live cells.

2.20 Collection of serum

Whole blood was collected using vacutainer tubes suitable for collecting serum (BD Biosciences). Filled red top blood collection tubes were positioned upright after the blood was drawn at room temperature. Bloods were centrifuged in a horizontal rotor (swing-out head) for 20 minutes at 1300 x g at room temperature. Serum was pipetted into labelled cryovials, filling the vials in sequential order. The caps were then closed on the vials tightly. This process was completed within 1 hour of centrifugation. The aliquots were then all placed upright in a -80ºC freezer or in liquid nitrogen.

2.21 BrdU assay

Cells were seeded at a dilution of 5 x 10^3 / well in 96-well plates in the appropriate complete media and allowed to adhere overnight at 37°C. Following the overnight incubation in serum-depleted media (0.5% FBS), cells were treated for 24 hours with the appropriate inhibitors. Cell proliferation was then assessed using a BrdU cell proliferation ELISA (Roche Diagnostics Ltd., Sussex, UK). The basis of this assay is as follows; following culturing of the cells in 96-well plates, BrdU is added to the cells, and the cells are re-incubated. During this labelling period, the pyrimidine analogue BrdU is incorporated in place of thymidine into the DNA of proliferating cells. The anti-BrdU POD antibody then binds to the BrdU incorporated in newly synthesised cellular DNA. The immune complexes are then detected by subsequent substrate reaction. 10µl of a 1:1000 dilution of BrdU labelling solution was added to each well for 4 hours at 37°C. The media was then removed and the cells fixed and denatured with 200µl of a fixative solution for 30 minutes at room temperature (RT). 100ul anti-BrdU-POD (mouse monoclonal antibody, peroxidise conjugated) working solution was then added to each well for 5-10 minutes (or until colour change was sufficient for photometric detection). Absorbance was measured on an Alpha Flour Plus plate reader (Tecan Trading AG, Switzerland) at 450nm with a reference wavelength of 690nm. Wells containing cells but no BrdU label were used to subtract background absorbances and percentage increase/ decrease in proliferation was calculated relative to untreated cells.

2.22 Cell viability assay

A CCK-8 assay (Sigma, USA) was used to assess the effect of ionising radiation on the viability of OE33P and passage matched OE33R cells. Additionally, the effect of

nivolumab, pembrolizumab, atezolizumab, dual nivolumab-atezolizumab or pembrolizumab-atezolizumab in the absence or presence of radiation (at both hypofractionation and bolus dosing clinically relevant regimens) on the viability of OE33P and R cells was also assessed using a CCK-8 assay. OAC cells (5×10^3) were seeded in a 96 well plate at 37°C, 5% CO_2 overnight. Cells were treated with bolus dosing or three consecutive fractionated doses of radiation with an interval of 24hrs using the X-Strahl RS225 irradiator. Additionally, cells were treated with or without radiation in the absence or presence of single agent pembrolizumab (10 ug/ml), atezolizumab (10 ug/ml), nivolumab (10 ug/ml) or dual atezolizumab (10 ug/ml) and nivolumab (10 ug/ml) dual atezolizumab (10 ug/ml) and pembrolizumab (10 ug/ml) 12hrs following the first dose of radiation. Untreated, non irradiated samples were used as controls for the experiment. The optical density at 450 nm and 650 nm (reference wavelength) was measured using the Versa Max microplate reader (Molecular Devices, Sunnyvale, CA, USA) to determine viable cell numbers. Data were analysed from three independent experiments.

2.23 Statistical Analysis

Data were analysed using GraphPad Prism 5 software (GraphPad Prism, San Diego, CA, USA) and SPSS® (version 22.0) software (SPSS, Chicago, IL, USA). The normality of the data was assessed and non-parametric test were used where appropriate. Continuous variables were compared using unpaired t tests (Mann-Whitney test for non-parametric data). Association of categorical variables (differences for dichotomous variables between groups) was assessed using chi-square test. Correlations between variables were assessed using the Spearman and Pearson correlation coefficients as appropriate and was carried out in collaboration with Fiona O' Connell at TCD. All data are expressed as mean ± the standard error of the mean (SEM), which is the standard deviation of the

distribution of sample mean. When the SEM is small, it indicates that the distribution of the sample means has less error estimating the true mean. SEM is calculated as the standard deviation of the original sample divided by the square root of the sample size. Significance was determined by analysis of variance (ANOVA), or Students *t*-test. A probability (p) of < 0.05 was considered to represent a significant difference between groups. The *t*-test was used to compare the means of two groups. In cases where data was paired (i.e untreated versus treated), a paired *t*-test was used for statistical analysis. Otherwise, an unpaired *t*-test was used. When population variances were unequal, Welch correction was applied. For statistical analysis involving 3 or more groups, the ANOVA test was used. Tukey post-hoc analysis was performed following ANOVA to determine statistical significance between individual groups. Survival statistics were calculated using Kaplan-Meier method and the log rank test was used to assess differences in survival between groups. Survival time was measured from the date of diagnosis to the date of an event or last follow-up. Disease-specific survival was assessed in all cases. A significance level of 0.05 was used for all analyses and all p values reported are two-tailed.

Chapter 3: The impact of conventional and hypofractionated radiotherapy on the immune checkpoint expression in oesophageal adenocarcinoma

The impact of radiotherapy on the immune landscape in oesophageal adenocarcinoma. Noel E Donlon*, Maria Davern*, Andrew Sheppard, Fiona O' Connell, Aisling B Heeran, Anshul Bhardwaj, Christine Butler, Narayanasamy Ravi, Claire L Donohoe, Niamh Lynam Lennon, Margaret R Dunne, Stephen G Maher, Jacintha O' Sullivan, John V Reynolds, Joanne Lysaght. *denotes equal contribution. *World J Gastroenterol* 2022; 28(21): 2302-2319 [DOI: 10.3748/wjg.v28.i21.2302].

3.1 Introduction

Oesophageal adenocarcinoma (OAC) is rapidly increasing in incidence in the western world, and five year survival rates rarely exceed 40% (160). Multimodal therapy alongside surgical resection has become standard of care for locally advanced cancer of the oesophagus or the oesophagogastric junction (161). One treatment option is the CROSS regimen, which includes preoperative administration of carboplatin and paclitaxel with concomitant radiotherapy (RT) (162). In Europe, radiation is delivered in 23 fractions of 1.8 Gray (Gy), giving a total dose of 41.4 Gy but this varies worldwide, with North American centres delivering up to 50-51.4 Gy (163), while Asian regimens can feature cumulative doses of 60 Gy (164).

Hypofractionated radiotherapy refers to radiation which is delivered in fewer fractions of 2.4 to 5 Gy, but often achieving the same cumulative dose (165). This has the potential to reduce costs, increase patient comfort, and could be more effective compared to conventional treatment (166). Randomised trials in breast and prostate cancer have found that both high- (≥5 Gy per fraction) and moderately (2.4-3.4 Gy per fraction) hypo-fractionated RT is non-inferior to traditional regimens in terms of overall survival (166-169). As RT is a mainstay of treatment, and oesophageal malignancies are associated with considerable morbidity, there is interest in evaluating whether this paradigm can be applied in the upper gastrointestinal context.

Disappointingly, a pathologic complete response to treatment is observed in less than 30% of patients with oesophageal cancer undergoing chemoradiotherapy (170), and it is this small subgroup of responders who benefit most in terms of survival (171). More effective strategies are therefore required. One emerging approach is combining chemoradiotherapy with immune checkpoint blockade (ICB). The most widely used ICB

involves blocking the interaction of programmed cell death protein 1 (PD-1) on T cells and programmed cell death ligand 1 (PD-L1) on tumour cells (172), and seeks to re-invigorate anti-tumour cytotoxic T cells (173). Phase III trials of single agent ICB have delivered mixed results in chemorefractory advanced oesophago-gastric cancer (157), but some recent encouraging results have been reported in earlier stage disease (61, 174).

Radiation can sensitise tumours to immunotherapy through three main mechanisms (175). First, radiation can increase neoantigen expression and induce immunogenic cell death, whereby release of damage associated molecular patterns (DAMPs) results in more efficient tumour antigen presentation and immune stimulation (29). Second, radiation induced DNA damage can activate the cGAS-STING cytosolic DNA sensor, resulting in type I interferon production (176, 177). Finally, RT can result in remodelling of the tumour microenvironment (TME), promoting infiltration of immune cells (151). The latter effect is particularly affected by radiation dosage and some limited preclinical evidence suggests that hypofractionated RT can have more immunostimulatory effects than conventional fractionation (175). However, most studies to date have focused on more inherently immunogenic tumour models such as melanoma or NSCLC, or common malignancies such as breast or colon cancer. There are a number of clinical studies evaluating hypofractionation in the context of squamous cell cancer of the oesophagus, however, data is lacking for OAC. To our knowledge, there are no translational studies characterising immune response in OAC in the context of immunotherapy and thus was the premise for this study.

The aim of this study was to;

1. Assess the effects of bolus dosing and hypofractionated RT on immune checkpoint expression in oesophageal cancer cells *in vitro* and *ex vivo* and correlat this with clinical outcomes.

2. Evaluate immune checkpoint expression *in vitro* following bolus and hypofractionated radiotherapy dosing under conditions of hypoxia and nutrient deprivation in the TME. .

3. Thirdly, to assess the synergistic effects of ICB and radiation on OAC cell lines was also assessed.
4. Evaluate the effects of radiation on the release of angiogenic markers, cytokines, co-stimulatory molecules and soluble checkpoints.

Through this, it is aimed to enhance the understanding of the interplay between immunotherapy, radiation and the TME in oesophageal cancer, with the goal of identifying the most effective radiation dosing strategy to combine with immunotherapy.

3.2 Results

3.2.1 Immune checkpoint expression in a passage matched parental cell line and isogenic model of radioresistance following bolus and hypofractionated radiotherapy dosing.

In order to ascertain if different expression levels of immune checkpoint proteins were detectable in a radiosensitive (OE33P) and radioresistant (OE33R) oesophageal adenocarcinoma cells at baseline and in response to different doses of radiation, cells were stained with antibodies for a range of immune checkpoint proteins and assessed by flow cytometry. All cell lines including mock irradiated controls were stained and assessed by flow cytometry 24hrs following the last dose of radiation. There was a significantly higher expression of checkpoints PD-1 and its ligands PD-L1, PD-L2, and TIGIT in the parental cell line compared to the passage matched radioresistant cell line (Figure 3.1).

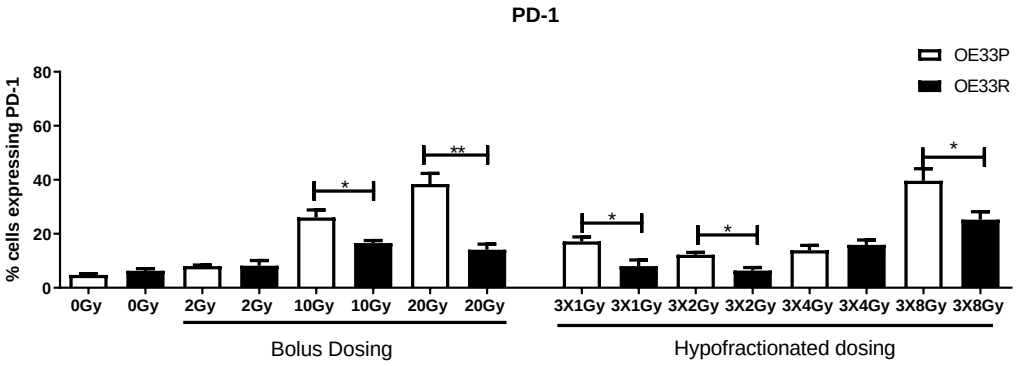
PD-1
OE33P
OE33R
% cells expressing PD-1
0
20
40
60
80
0Gy 0Gy 2Gy 2Gy 10Gy 10Gy 20Gy 20Gy
3X1Gy 3X1Gy 3X2Gy 3X2Gy 3X4Gy 3X4Gy 3X8Gy 3X8Gy
Bolus Dosing
Hypofractionated dosing

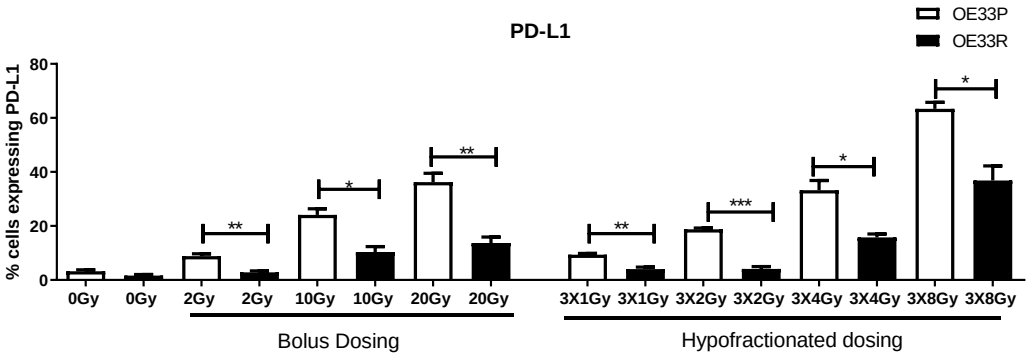
PD-L1
OE33P
OE33R
% cells expressing PD-L1
0
20
40
60
80
0Gy 0Gy 2Gy 2Gy 10Gy 10Gy 20Gy 20Gy
3X1Gy 3X1Gy 3X2Gy 3X2Gy 3X4Gy 3X4Gy 3X8Gy 3X8Gy
Bolus Dosing
Hypofractionated dosing

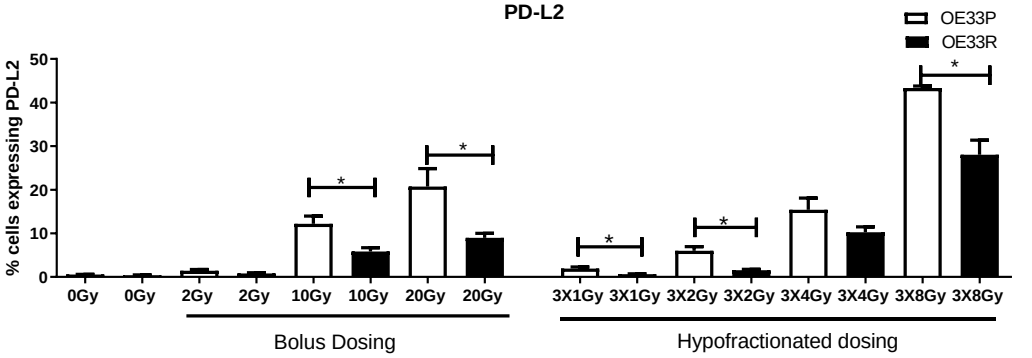
PD-L2
OE33P
OE33R
% cells expressing PD-L2
0
10
20
30
40
50
0Gy 0Gy 2Gy 2Gy 10Gy 10Gy 20Gy 20Gy
3X1Gy 3X1Gy 3X2Gy 3X2Gy 3X4Gy 3X4Gy 3X8Gy 3X8Gy
Bolus Dosing
Hypofractionated dosing

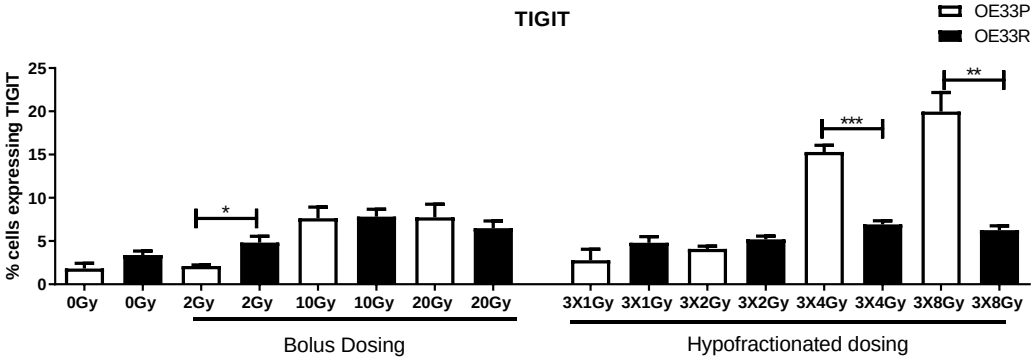
TIGIT
OE33P
OE33R
% cells expressing TIGIT
0
5
10
15
20
25
0Gy 0Gy 2Gy 2Gy 10Gy 10Gy 20Gy 20Gy
3X1Gy 3X1Gy 3X2Gy 3X2Gy 3X4Gy 3X4Gy 3X8Gy 3X8Gy
Bolus Dosing
Hypofractionated dosing

Figure 3.1: Inhibitory immune checkpoints are expressed at a higher level on parental cells than the passage matched radioresistant cell line. OE33P and OE33R cell lines were screened for the surface expression of PD-1, PD-L1, PD-L2 & TIGIT by flow cytometry. Graph shows mean % expression (±SEM) (n=3). *p<0.05, **p<0.01, ***p<0.001 by unpaired parametric t-test.

There is a significantly higher expression of PD-1 in the OE33P cell line than in the OE33R cell line at 10 Gy (26±2.86 vs 16.6±0.91) p<0.05, 20 Gy (38.47±3.88 vs 14.07±2.13) p<0.01, 3x1 Gy (17.17±16.67 vs 8.04±2.26) p<0.05, 3x2 Gy (12.2±0.9 vs 6.33±1.18) p<0.05, and 3x8 Gy (39.63±4.47 vs 25.23±2.97) p<0.05 (Figure 3.1).

There is a significantly higher expression of PD-L1 in the OE33P cell line than in the OE33R cell line at 2 Gy (8.1±0.91 vs 2.82±0.55) p<0.01, 10 Gy (24.1±2.27 vs 10.4±1.95) p<0.05, 20 Gy (36.23±3.26 vs 13.72±2.15) p<0.01, 3x1 Gy (9.34±0.48 vs 4.04±0.72) p<0.01, 3x2 Gy (18.77±1.2 vs 4.12±1.86) p<0.001, 3x4 Gy (33.23±3.59 vs 15.77±1.27)p<0.05, and 3x8 Gy (63.33±2.47 vs 36.8±5.43) p<0.05 (Figure 3.1).

There is a significantly higher expression of PD-L2 in the OE33P cell line than in the OE33R cell line at 10 Gy (12.21±1.74 vs 6.84±1.1) p<0.05, 20 Gy (20.74±4.13 vs 8.97±1.04) p<0.05, 3x1 Gy (1.9±0.4 vs 0.64±0.25) p<0.05, 3x2 Gy (6.1±2.31 vs 1.56±1.46) p<0.05, and 3x8 Gy (43.33±3.32 vs 28.03±3.33) p<0.05 (Figure 3.1).

There is a significantly higher expression of TIGIT in the OE33P cell line than in the OE33R cell line at 3x4 Gy (15.3±0.78 vs 6.93±1.41) p<0.001, and 3x8 Gy (19.97±2.22 vs 6.25±0.51) p<0.01, with a significantly higher expression at 2 Gy on the OE33R cell line (4.82±0.78 vs 2.12±0.65) p<0.05 (figure 3.1).

3.22 Immune Checkpoint Expression on OE33 P and OE33 R (model of radioresistance) cells following bolus and hypofractionated radiotherapy dosing with conditions of the Tumour Microenvironment (TME) of nutrient deprivation and Hypoxia.

Both glutamine and glucose are essential for T cell activation, and are essential for their differentiation, proliferation, and overall function. Cancer cells induce a highly metabolic state and preferentially utilise all nutrients available therefore limiting any potential nutrient supply to cells involved in anti-tumour immunity propagating a pro-tumourigenic milieu. Of note, hypoxic cancer cells produce signalling molecules that promote the transformation of fibroblasts into cancer associated fibroblasts (CAFs) and dysregulation of all immune cells in such a way that supports progression and subsequent metastases (178, 179). For example, fibroblasts can be transformed into tumour-specific CAFs, vascularisation process facilitates cancer progression, and antitumour immune function becomes generally repressed. There are variable levels of hypoxia in the tumour and hence three levels of oxygenation were utilised for the experiments.

In order to determine the effects of the hostile tumour microenvironment, oxygenation at 5% constituting mild hypoxia and 0.5% constituting severe hypoxia were chosen to simulate the varying levels of reduced oxygenation *in vivo*, along with nutrient deprivation in the form of glucose and glutamine deprivation and evaluate the expression of PD-1 and its ligands PD-L1, PD-L2 and TIGIT in OE33P and passage matched OE33R cells with or without radiation.

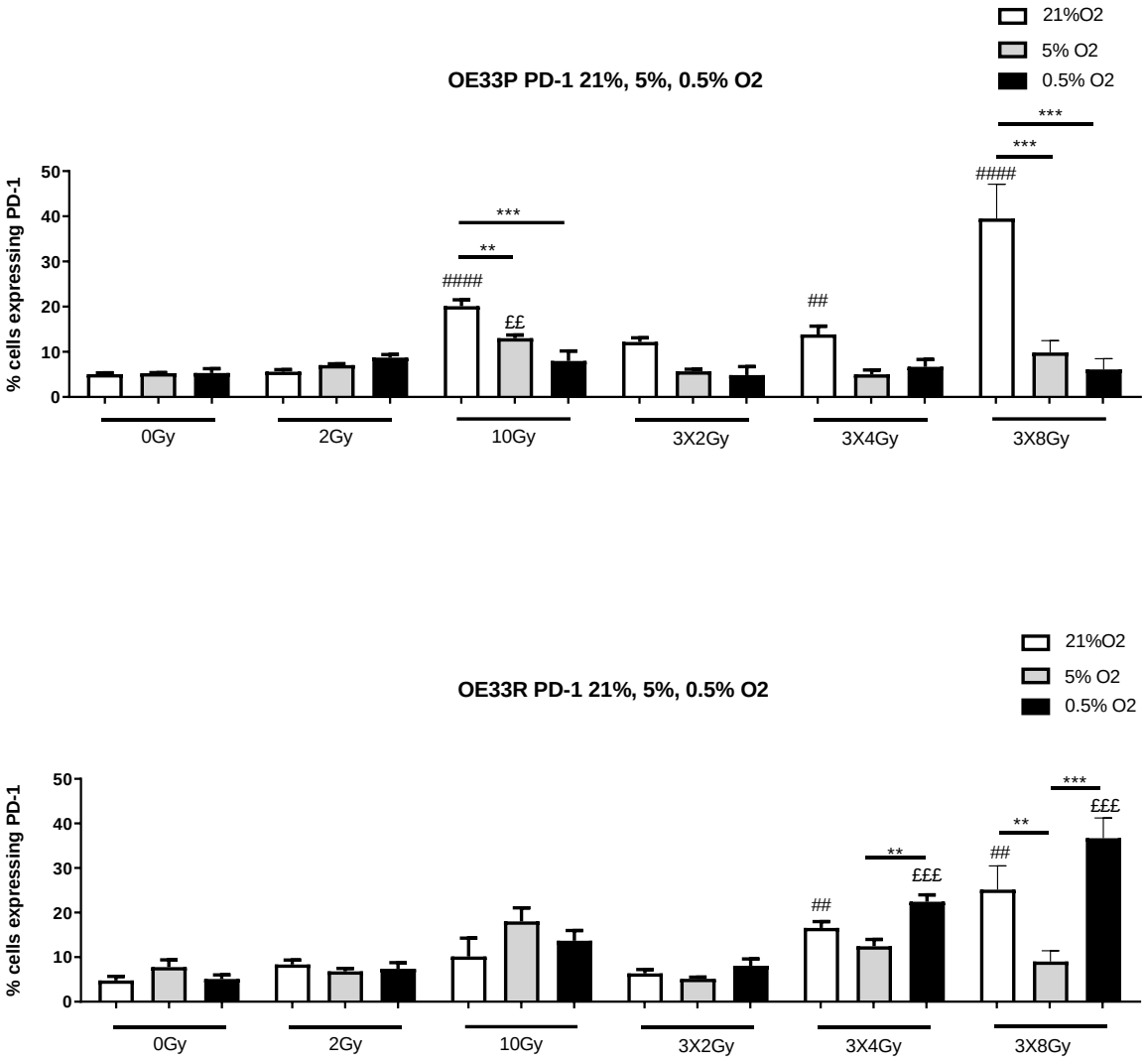

Figure 3.2 OE33P and OE33R cell lines were screened for the surface expression of PD-1 by flow cytometry. Bolus dosing was administered once daily over three consecutive days. Cancer cells were stained 24hrs following the last fraction of radiation. Tukey's multiple comparison testing. Graph shows mean % expression (±SEM) (n=3). 21%=Normal oxygenation, 5%=mild hypoxia, 0.5%=severe hypoxia. * denotes comparison between oxygen levels for each radiation dosing regimen, ** $p<0.01$, *** $p<0.001$. # denotes comparison of dosing with 0 Gy at 21% O_2, ## $p<0.01$, ### $p<0.001$, #### $p<0.0001$. £ denotes comparison of dosing with 0 Gy at 5% O_2, £ $p<0.05$, ££ $p<0.01$, £££ $p<0.001$.

In the OE33P cell line, there was a significant increase in expression of PD-1 with 10 Gy irradiation (26±2.86), $p<0.001$, fractionated dosing 3x4 Gy (13.87±1.82) $p<0.01$, and 3x8 Gy (39.63±4.47) $p<0.001$ compared to non-irradiated cells (3.27±0.87) . There was a significant increase in expression of PD-1 with 10 Gy at 5% O_2 (13.03±0.69) compared

to 0 Gy 5% O_2 (4.9±0.96) p<0.01. There was a significantly higher expression of PD-1 at 10 Gy 21% O_2 (26±2.86) compared to 5% O_2 (13.03±0.78) p<0.01, and compared to 10 Gy 0.5% O_2 (7.99±2.21) p<0.01. There was a significantly higher expression of PD-1 at 3x8 Gy normal oxygenation (39.5±4.4) compared to 3x8 Gy 5% O_2 (9.86±1.5) p<0.001, and 3x8 Gy 0.5% O_2 (6.08±1.37) p<0.001. (Figure 3.2).

In the OE33 R cell line there was a significant increase in expression of PD-1 with 3x4 Gy irradiation (15.93±1.96), p<0.01, and 3x8 Gy (25.23±2.97) compared to non-irradiated cells (0 Gy) (4.7±0.4) p<0.01 respectively. There was a significant increase in expression of PD-1 with 3x4 Gy at 0.5% O_2 (22.44±1.54), p<0.001, 3x8 Gy at 0.5% O_2 (36.67±2.64) compared to 0 Gy 0.5% O_2 (5.1±0.89) p<0.001. There was a significant increase in expression of PD-1 with 3x4 Gy at 0.5% O_2 (22.44±1.54) compared to 3x4 Gy 5% O_2 (12.43±1.43) p<0.01. There was a significantly higher expression of PD-1 at 3x8 Gy with normal oxygen concentrations (25.23±2.97) compared to 3x8 Gy 5% O_2 (9.01±1.4) p<0.01. There was a significantly increased expression of PD-1 at 3x8 Gy 0.5% O_2 (36.67±2.64) compared to 3x8 Gy 5% O_2 (9.01±1.4) p<0.01). Figure 3.2).

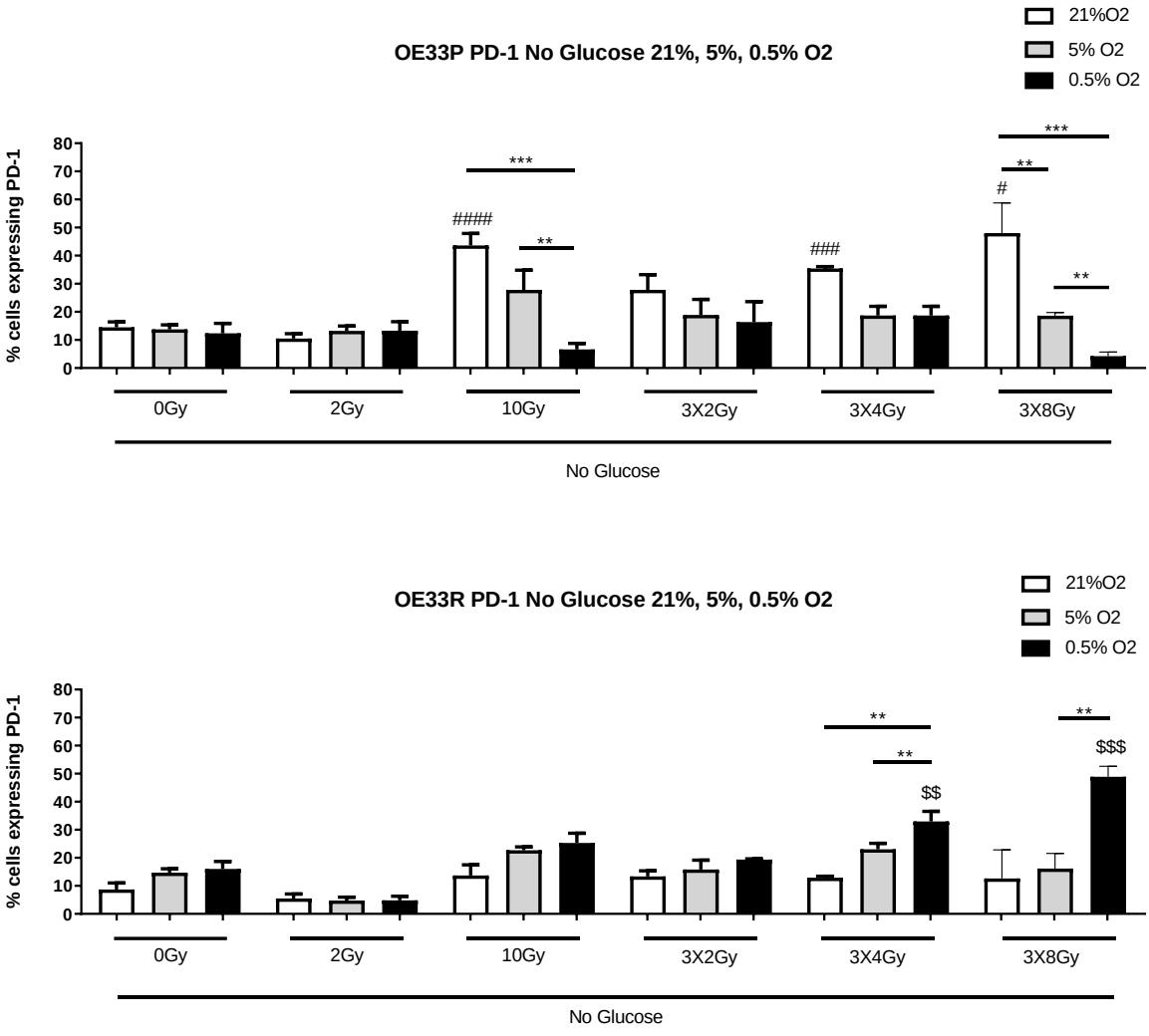

Figure 3.3 OE33P and OE33R cell lines were screened for the surface expression of PD-1 by flow cytometry under conditions of glucose deprivation. Bolus dosing was administered once daily over three consecutive days. Cancer cells were stained 24hrs following the last fraction of radiation. Tukey's multiple comparison testing. Graph shows mean % expression (±SEM) (n=3). 21%=Normal oxygenation, 5%=mild hypoxia, 0.5%=severe hypoxia. * denotes comparison between oxygen levels for each radiation dosing regimen, ** $p<0.01$, *** $p<0.001$. # denotes comparison of dosing with 0 Gy at 21% O_2, ### $p<0.001$, #### $p<0.0001$. $ denotes comparison of dosing with 0 Gy at 0.5% O_2, $$ $p<0.01$, $$$ $p<0.001$.

In the OE33P cell line, there was a significant increase in expression of PD-1 with 10 Gy irradiation no glucose (43.6±4.33), $p<0.0001$, fractionated dosing 3x4 Gy no glucose (35.43±1.21) $p<0.001$, and 3 x8 Gy no glucose (48.03±6.02) compared to non-irradiated cells (14.5±1.95) $p<0.05$. There was a significant increase in expression of PD-1 with

3x4 Gy at 0.5% O_2 no Glucose (18.67±3.28) and 3x8 Gy at 0.5% O_2 (48.03±6.21) compared to 0 Gy 5% O_2 no Glucose (4.9±0.96) $p<0.01$. There was a significantly higher expression of PD-1 at 10 Gy 21% O_2 (26±2.86) compared to 5% O_2 (13.03±0.78) $p<0.01$, and compared to 10 Gy 0.5% O_2 (7.99±2.21) $p<0.01$. There was a significantly higher expression of PD-1 at 3x8 Gy normal oxygenation (39.5±4.4) compared to 3x8 Gy 5% O_2 (9.86±1.5) $p<0.001$, and 3x8 Gy 0.5% O_2 (6.08±1.37) $p<0.001$. (Figure 3.3).

In the OE33 R cell line there was a significant increase in expression of PD-1 with 3x4 Gy irradiation no glucose 0.5% O_2 (32.97±3.58), $p<0.01$, and 3x8 Gy no glucose 0.5% O_2 (48.9±2.16) compared to non-irradiated cells 0 Gy 0.5% O_2 (8.68±2.33) $p<0.01$. There was a significant increase in expression of PD-1 with 3x4 Gy no glucose at 0.5% O_2 (32.97±3.58), compared to 3x4 Gy no glucose at 5% O_2 (23±2.2) $p<0.01$,and 3x4 Gy no glucose 21% O_2 (12.9±0.53) $p<0.01$. There was a significant increase in expression of PD-1 with 3x8 Gy no glucose at 0.5% O_2 (48.9±2.16) compared to 3x8 Gy no glucose 5% O_2 (16.17±3.2) $p<0.01$. (Figure 3.3.)

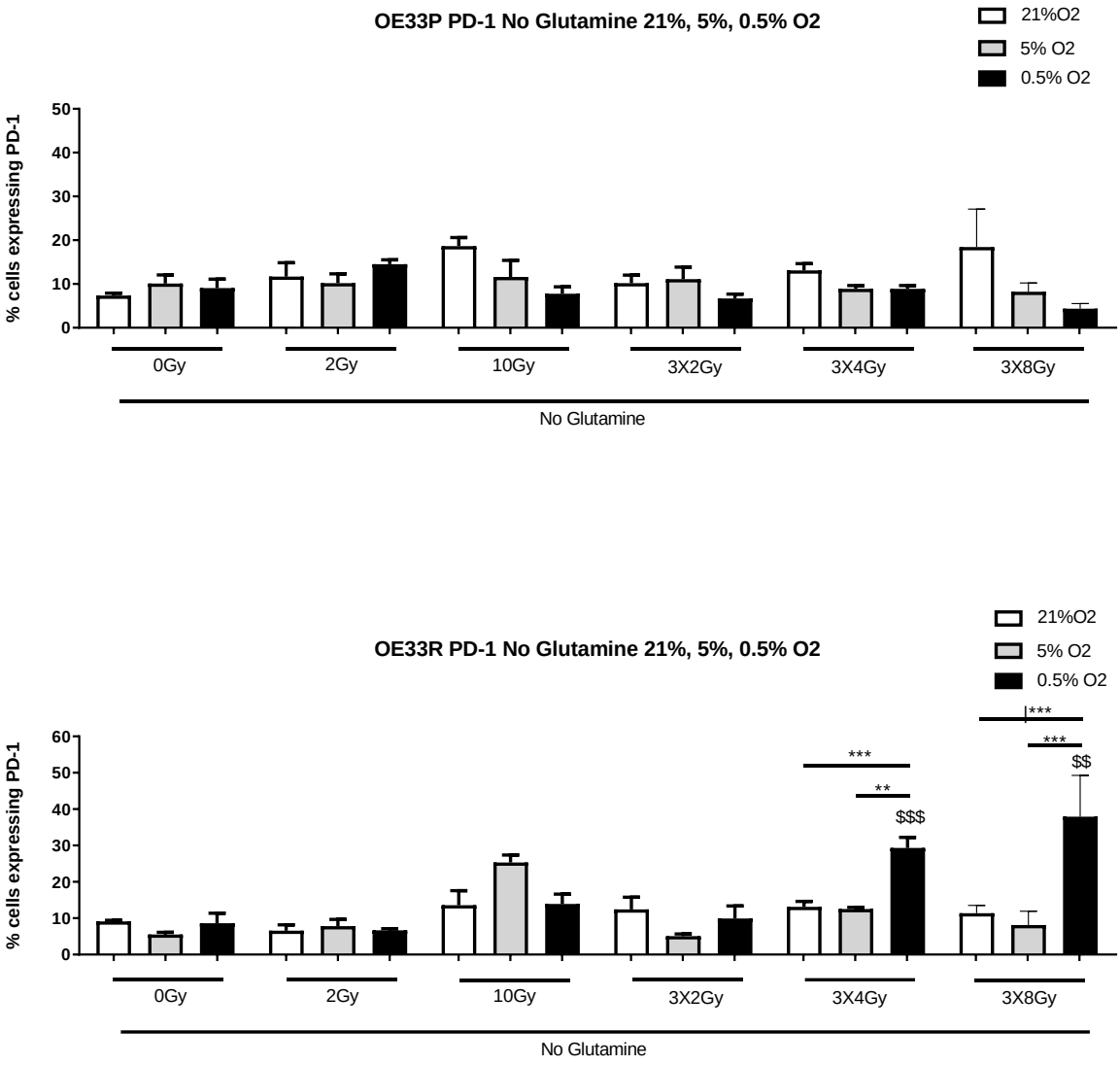

Figure 3.4 OE33P and OE33R cell lines were screened for the surface expression of PD-1 under conditions of glutamine deprivation by flow cytometry. Bolus dosing was administered once daily over three consecutive days. Cancer cells were stained 24hrs following the last fraction of radiation. Tukey's multiple comparison testing. Graph shows mean % expression (±SEM) (n=3). 21%=Normal oxygenation, 5%=mild hypoxia, 0.5%=severe hypoxia. * denotes comparison between oxygen levels for each radiation dosing regimen, ** p<0.01, *** p<0.001. # denotes comparison of dosing with 0 Gy at 21% O_2, # p<0.05, ## p<0.01, ### p<0.001, #### p<0.0001. $ denotes comparison of dosing with 0 Gy at 0.5% O_2, $$ p<0.01, $$$ p<0.001.

In the OE33 R cell line there was a significantly higher expression of PD-1 with 3x4 Gy no glutamine at 0.5% O_2 (29.33±2.8) and 3x8 Gy no glutamine at 0.5% O_2 (37.95±6.53) compared to 0 Gy no glutamine at 0.5% O_2 (8.63±2.76). There was a significantly higher expression of PD-1 at 3x4 Gy no glutamine at 0.5% O_2 (29.33±2.8) compared to 3x4 Gy

no glutamine normoxia (13.1±1.53) p<0.001) and 3x4 Gy no glutamine 5% O_2 (12.53±0.43) p<0.01). There was a significantly higher expression of PD-1 at 3x8 Gy no glutamine at 0.5% O_2 (37.95±6.53) compared to 3x8 Gy no glutamine normoxia (11.35±1.25) p<0.001) and 3x8 Gy no glutamine 5% O_2 (8.14±2.2) p<0.001). (Figure 3.4)

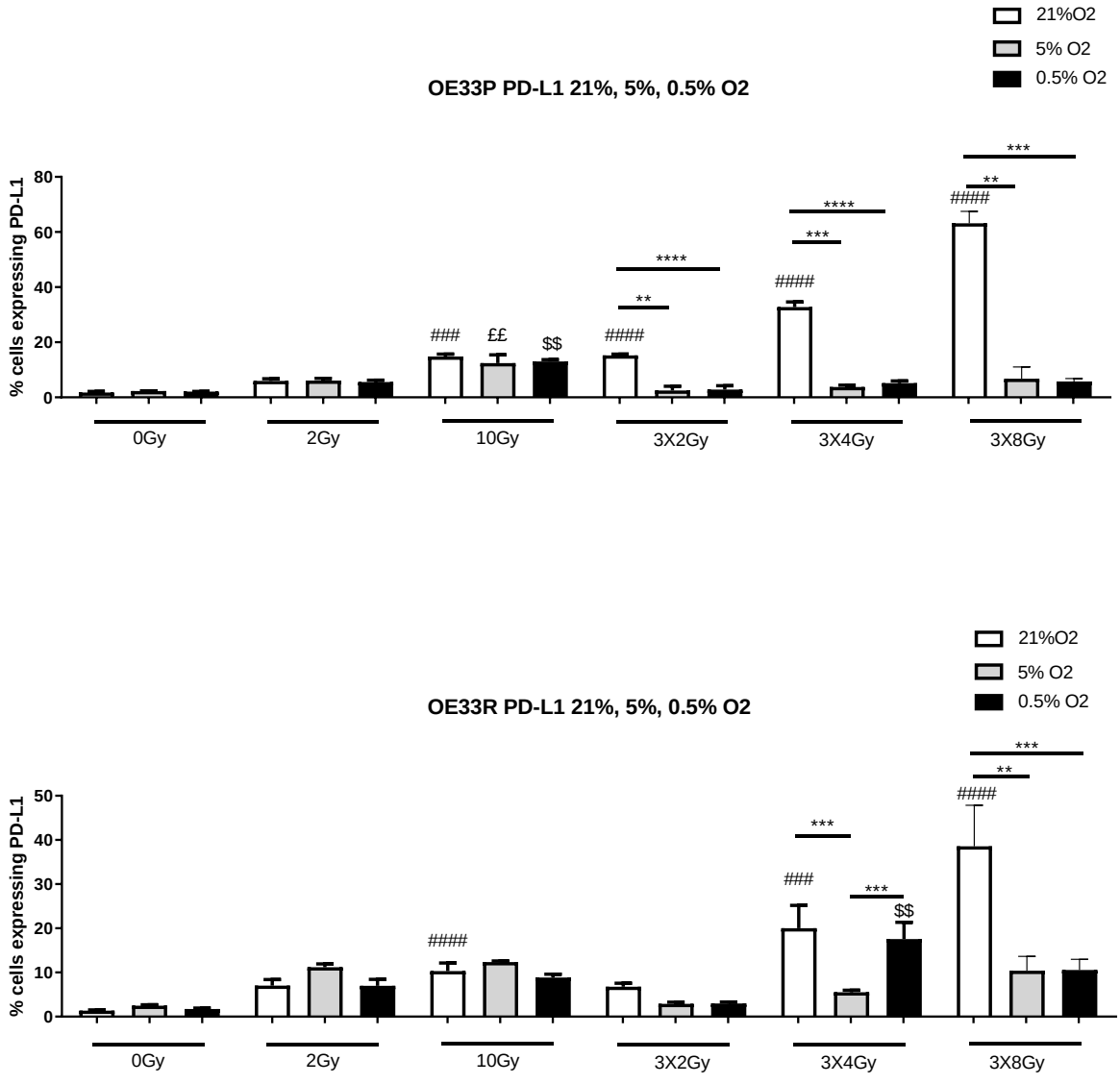

Figure 3.5 OE33P and OE33R cell lines were screened for the surface expression of PD-L1 by flow cytometry. Bolus dosing was administered once daily over three consecutive days. Cancer cells were stained 24hrs following the last fraction of radiation. Tukey's multiple comparison testing. Graph shows mean % expression (±SEM) (n=3). 21%=Normal oxygenation, 5%=mild hypoxia, 0.5%=severe hypoxia. * denotes comparison between oxygen levels for each radiation dosing regimen, ** p<0.01, *** p<0.001. # denotes comparison of dosing

with 0 Gy at 21% O_2, ### p<0.001, #### p<0.0001. £ denotes comparison of dosing with 0 Gy at 5% O_2, ££ p<0.01. $ denotes comparison of dosing with 0 Gy at 0.5% O_2, $$ p<0.01.

In the OE33P cell line, there was a significant increase in expression of PD-L1 with 10 Gy irradiation (24.1±2.27), p<0.001, fractionated dosing 3x2 Gy (18.77±0.49), p<0.0001, 3x4 Gy (33.23±5.89) p<0.0001, and 3x8 Gy (63.33±2.47) p<0.001 compared to non-irradiated cells (3.25±0.47) . There was a significant increase in expression of PD-L1 with 10Gy at 5% O_2 (12.4±0.33) and 10Gy at 0.5% O_2 (13.03±0.69) compared to 0Gy 5% O_2 (2.28±0.32) p<0.01 and 0 Gy 0.05%(2.07±0.68) p<0.01. There was a significantly higher expression of PD-L1 at 3x2 Gy 21% O_2 (18.77±0.49) compared to 3x2 Gy 5% O_2 (2.49±1.58) p<0.01, and compared to 3x2 Gy 0.5% O_2 (2.83±1.37) p<0.001. There was a significantly higher expression of PD-L1 at 3x4 Gy normal oxygenation (33.23±5.89) compared to 3x4 Gy 5% O_2 (3.77±0.68) p<0.001, and 3x4 Gy 0.5% O_2 (5.15±0.82) p<0.0001. There was a significantly higher expression of PD-L1 at 3x8 Gy normal oxygenation (63.33±2.47) compared to 3x8 Gy 5% O_2 (6.73±2.49) p<0.001, and 3x8 Gy 0.5% O_2 (5.74±0.63) p<0.001. (Figure 3.5).

In the OE33 R cell line there was a significant increase in expression of PD-L1 with 10 Gy (10.4±1.96) p<0.001, 3x4 Gy irradiation (15.17±1.27), p<0.001, and 3x8 Gy (36.8±5.43) p<0.001 compared to non-irradiated cells 0 Gy (2.2±0.8) . There was a significant increase in expression of PD-L1 with 3x4 Gy (15.17±.27), compared to 3x4 Gy 5% O_2 (5.52±0.47) p<0.01 and 3x4 Gy 0.5% O_2 (14.56±2.27) compared to 3x4 Gy 5% (5.52±0.47) p<0.01. There was a significant increase in expression of PD-1 with 3x8

Gy at 0.5% O_2 (36.8±5.43) compared to 3x8 Gy 5% O_2 (10.88±1.38) p<0.001 and 3x8 Gy 0.5% O_2 (10.58±1.48). (Figure 3.5.)

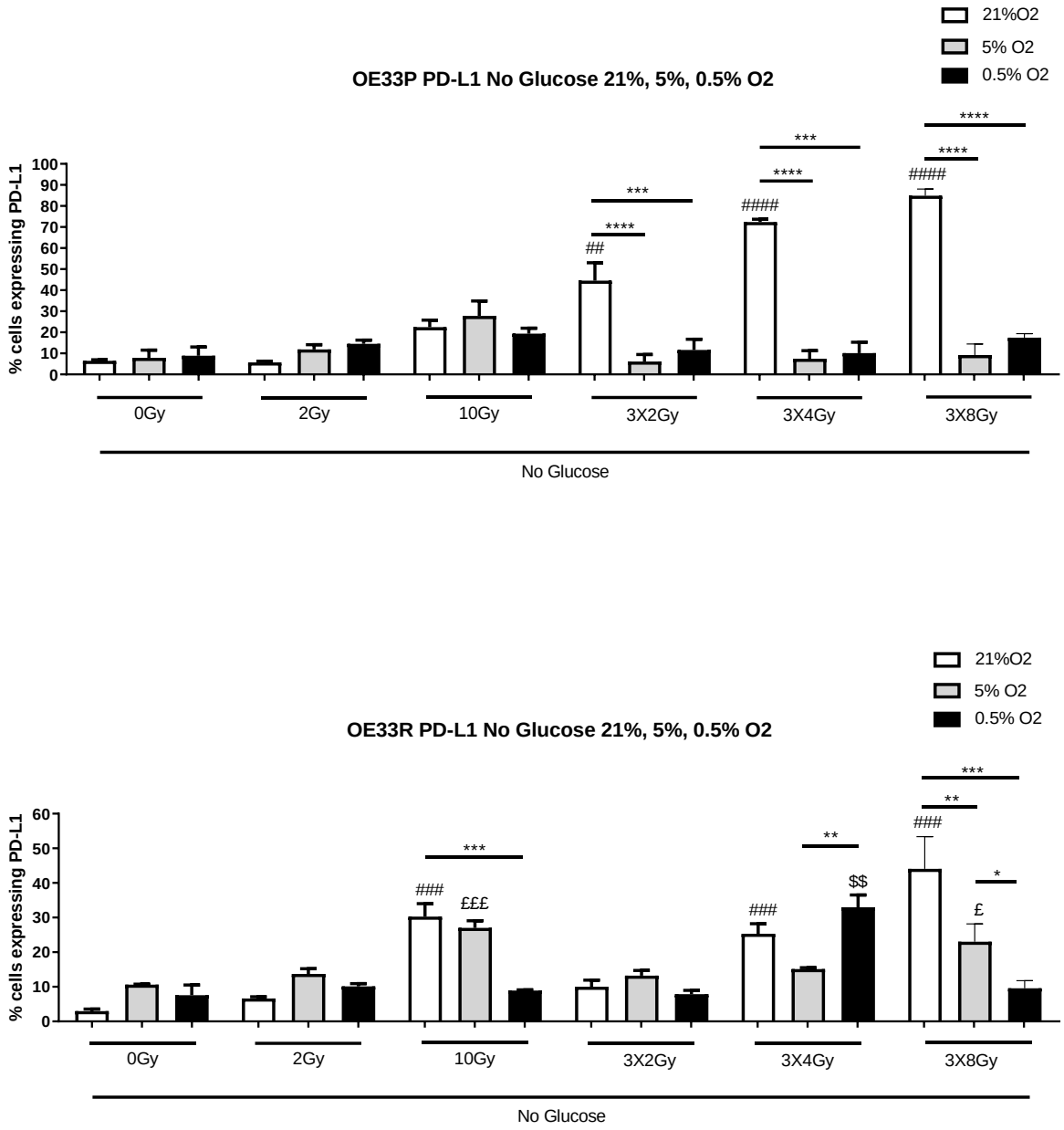

Figure 3.6 OE33P and OE33R cell lines were screened for the surface expression of PD-L1 by flow cytometry under conditions of glucose deprivation. Bolus dosing was administered once daily over three consecutive days. Cancer cells were stained 24hrs following the last fraction of radiation. Tukey's multiple comparison testing. Graph shows mean % expression (±SEM) (n=3). 21%=Normal oxygenation, 5%=mild hypoxia, 0.5%=severe hypoxia. * denotes comparison between oxygen levels for each radiation dosing regimen, * p<0.05, ** p<0.01, *** p<0.001, ****p<0.0001. # denotes comparison of dosing with 0 Gy at 21% O_2, ## p<0.01, ### p<0.001, #### p<0.0001. £

denotes comparison of dosing with 0Gy at 5% O_2, £ $p<0.05$, £££ $p<0.001$. $ denotes comparison of dosing with 0 Gy at 0.5% O_2, $$ $p<0.01$.

In the OE33P cell line, there was a significant increase in expression of PD-L1 with fractionated dosing 3x2 Gy irradiation no glucose (44.55±8.58) $p<0.01$,, 3x4 Gy no glucose (72.37±1.3) $p<0.0001$, and 3x8 Gy no glucose (48.03±6.02) $p<0.0001$ compared to non-irradiated cells (8.49±1.83) . There was a significant increase in expression of PD-L1 with 3x2 Gy no glucose (44.55±8.58) compared to 3x2 Gy at 5% O_2 no Glucose (6.09±3.4) and 3x2 Gy at 0.5% O_2 (11.58±5.09) $p<0.001$, $p<0.001$. There was a significantly higher expression of PD-L1 at 3x4 Gy no Glucose (72.37±1.3) compared to 3x4 Gy 5% O_2 (7.43±3.85) $p<0.001$, and 3x4 Gy 0.5% O_2 (10.16±5.14) $p<0.0001$. There was a significantly higher expression of PD-L1 at 3x8 Gy no glucose normal oxygenation (48.03±6.02) compared to 3x8 Gy no glucose 5% O_2 (9.25±2.99) $p<0.0001$, and 3x8 Gy no glucose 0.5% O_2 (17.47±1.11) $p<0.0001$. (Figure 3.6).

In the OE33 R cell line there was a significant increase in expression of PD-L1 at 10 Gy no glucose (30.27±3.75), $p<0.001$, 3x4 Gy irradiation no glucose (25.33±2.9), $p<0.001$, and 3x8 Gy no glucose (44.09±5.37) $p<0.001$ compared to non-irradiated cells 0 Gy (2.95±0.6) . There was a significant increase in expression of PD-L1 with 10 Gy no glucose (30.27±3.75) compared to 10 Gy no glucose at 5% O_2 (8.9±0.21) $p<0.001$, and 3x4 Gy no glucose 0.5% O_2 (32.97±3.58) compared to 3x4 Gy no glucose 5% O_2 (15.1±1.1) $p<0.01$. There was a significant increase in expression of PD-L1 with 3x8 Gy no glucose O_2 (44.09±5.37) compared to 3x8 Gy no glucose 5% O_2 (23.03±2.97) $p<0.01$

and 3x8 Gy no glucose 0.5% O_2 (9.58±1.28) p<0.001 and 3x8 Gy no glucose 5% O_2 (23.03±2.97) and 3x8 Gy no glucose 0.5% O_2 (9.58±1.28) p<0.001. Figure 3.6.

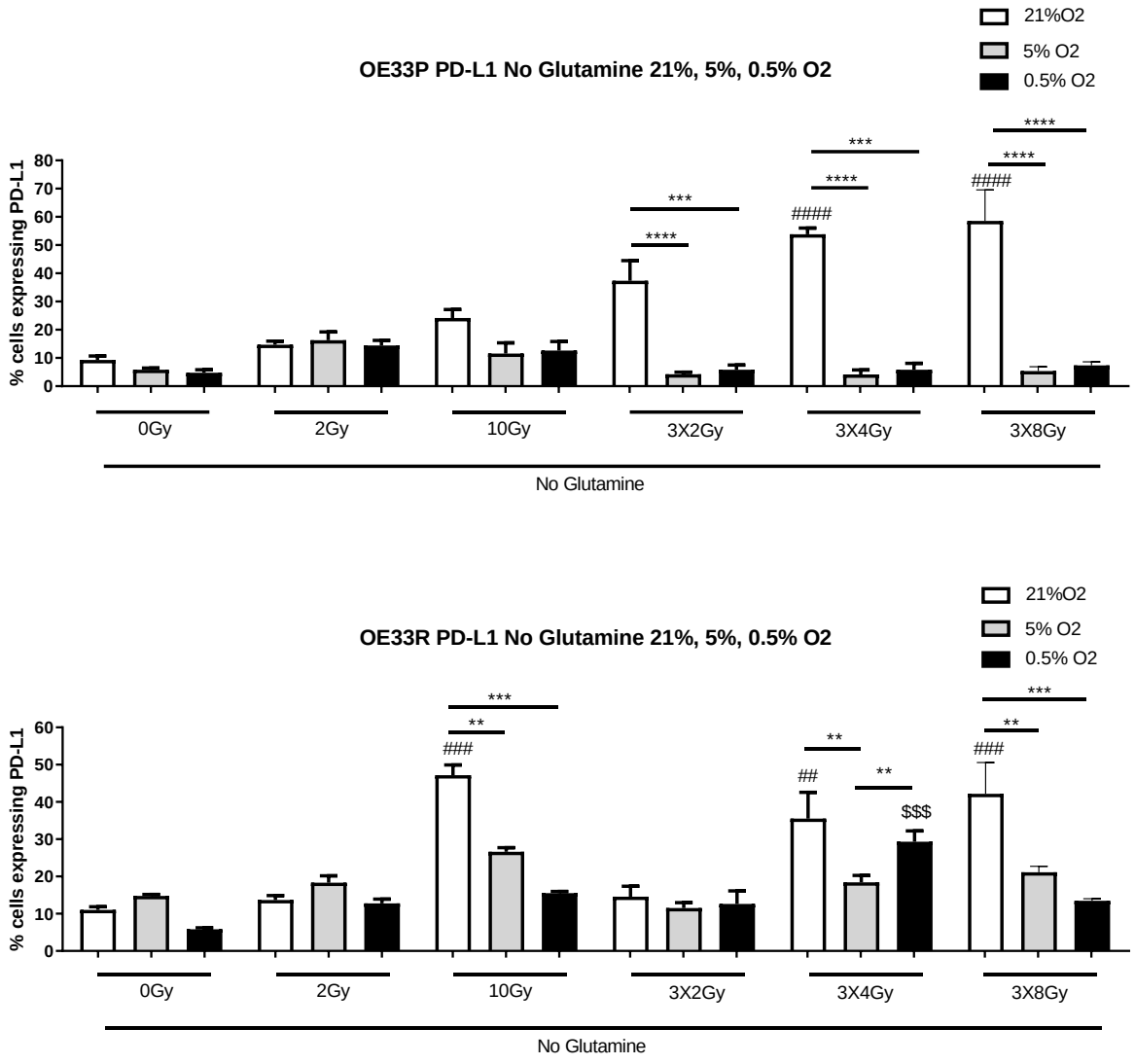

Figure 3.7 OE33P and OE33R cell lines were screened for the surface expression of PD-L1 under conditions of glutamine deprivation by flow cytometry. Bolus dosing was administered once daily over three consecutive days. Cancer cells were stained 24hrs following the last fraction of radiation. Tukey's multiple comparison testing. Graph shows mean % expression (±SEM) (n=3). 21%=Normal oxygenation, 5%=mild hypoxia, 0.5%=severe hypoxia. * denotes comparison between oxygen levels for each radiation dosing regimen, ** p<0.01, *** p<0.001, **** p<0.0001. # denotes comparison of dosing with 0 Gy at 21% O_2, ## p<0.01, ### p<0.001, #### p<0.0001. $ denotes comparison of dosing with 0 Gy at 0.5% O_2, $$$ p<0.001.

In the OE33 P cell line there was a significantly higher expression of PD-L1 at 3x4 Gy no glutamine (53.8±2.26) and 3x8 Gy no glutamine (58.57±6.35) compared to 0 Gy no glutamine (5.82±0.62) $p<0.001$, $p<0.01$, $p<0.001$. There was a significantly higher expression of PD-L1 at 3x8Gy no glutamine (58.57±6.35) $p<0.0001$, compared to 3x8 Gy no glutamine 5% O_2 (5.36±0.97) and 3x8 Gy 0.5% O_2 (7.35±0.76) $p<0.0001$.

In the OE33 R cell line there was a significantly higher expression of PD-L1 with 10 Gy no glutamine (47.17±2.17), $p<0.0001$, 3x4 Gy no glutamine (18.43±1.83), $p<0.01$, 3x8 Gy no glutamine (42.17±4.85) compared to 0 Gy no glutamine (11.02±0.45) and also with 3x4 Gy no glutamine at 0.5% O_2 (31.33±2.8) compared to 0 Gy no glutamine at 0.5% O_2 (5.82±0.22), $p<0.001$. There was a significantly higher expression of PD-L1 at 10 Gy no glutamine (47.17±2.17) compared to 10 Gy 5% O_2 (26.63±1.11) and 10 Gy 0.5% O_2 (15.53±1/35) $p<0.01$, $p<0.001$. There was a significantly higher expression of PD-L1 at 3x8 Gy no glutamine (42.17±4.85) compared to 3x8 Gy 5% O_2 (21.13±0.92) and 3x8 Gy 0.5% O_2 (13.47±0.32). (Figure 3.7)

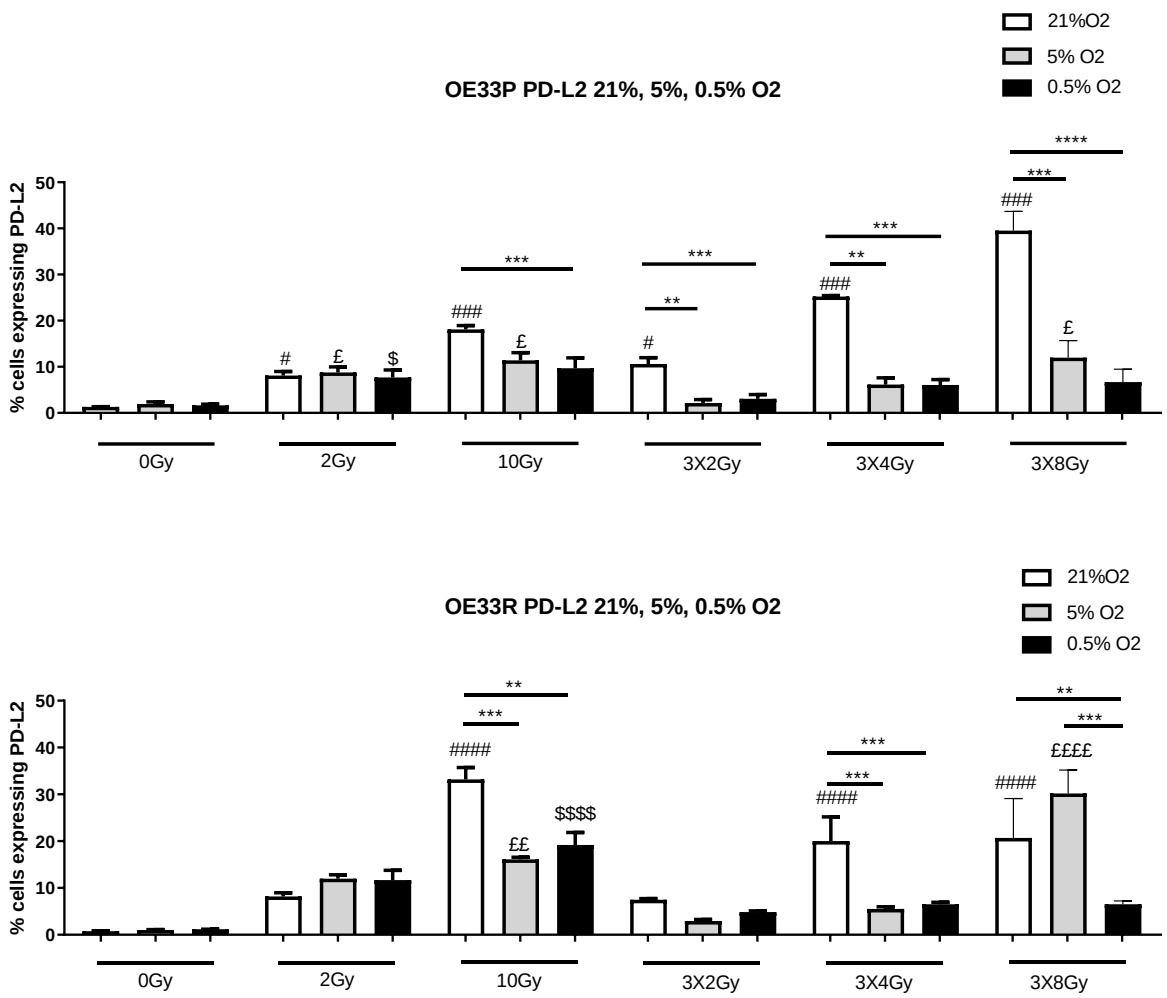

Figure 3.8 OE33P and OE33R cell lines were screened for the surface expression of PD-L2 by flow cytometry. Bolus dosing was administered once daily over three consecutive days. Staining of cancer cells took place 24hrs after last fraction of radiation. Tukey's multiple comparison testing. Graph shows mean % expression (±SEM) (n=3). 21%=Normal oxygenation, 5%=mild hypoxia, 0.5%=severe hypoxia. * denotes comparison between oxygen levels for each radiation dosing regimen, ** $p<0.01$, *** $p<0.001$, **** $p<0.0001$. # denotes comparison of dosing with 0 Gy at 21% O_2, ### $p<0.001$, #### $p<0.0001$. £ denotes comparison of dosing with 0Gy at 5% O_2, £ $p<0.05$, ££ $p<0.001$, ££££ $p<0.0001$. $ denotes comparison of dosing with 0Gy at 0.5% O_2, $ $p<0.05$, $$$ $p<0.001$.

In the OE33P cell line, there was a significant increase in expression of PD-L2 with 2 Gy (8.1±0.97) $p<0.05$, 10 Gy irradiation (18.1±0.85), $p<0.0001$, fractionated dosing 3x2 Gy (10.62±1.35), $p<0.05$, 3x4 Gy (25.23±1.87) $p<0.001$, and 3x8 Gy (39.5±2.43) $p<0.001$ compared to non-irradiated cells (1.3±0.92). There was a significant increase in

expression of PD-L2 with 10 Gy (18.1±0.85) compared to 10 Gy at 5% O_2 (9.65±0.23) $p<0.001$. There was a significantly higher expression of PD-L2 at 3x2 Gy 21% O_2 (10.62±1.35) compared to 3x2 Gy 5% O_2 (2.14±0.74) $p<0.01$, and compared to 3x2 Gy 0.5% O_2 (3.06±0.92) $p<0.001$. There was a significantly higher expression of PD-L2 at 3x4 Gy normal oxygenation (25.23±1.87) compared to 3x4 Gy 5% O_2 (6.16±1.45) $p<0.01$, and 3x4 Gy 0.5% O_2 (6.08±1.16) $p<0.001$. There was a significantly higher expression of PD-L2 at 3x8 Gy normal oxygenation (39.5±2.43) compared to 3x8 Gy 5% O_2 (12±2.13) $p<0.001$, and 3x8 Gy 0.5% O_2 (6.7±1.6) $p<0.001$. (Figure 3.8).

In the OE33 R cell line there was a significant increase in expression of PD-L2 with 10 Gy (33.17±2.58) $p<0.001$, 3x4 Gy irradiation (20.01±4.87), $p<0.0001$, and 3x8 Gy (20.7±4.84) $p<0.0001$ compared to non-irradiated cells 0 Gy (0.98±1.1).. There was a significantly higher expression of PD-L2 at 3x4 Gy normal oxygenation (20.01±4.87) compared to 3x4 Gy 5% O_2 (5.52±0.48) $p<0.001$, and 3x4 Gy 0.5% O_2 (6.51±0.56) $p<0.001$. There was a significantly higher expression of PD-L2 at 3x8 Gy normal oxygenation (20.7±4.84) compared to 3x8 Gy 0.5% O_2 (6.5±0.42) $p<0.001$ (Figure 3.8).

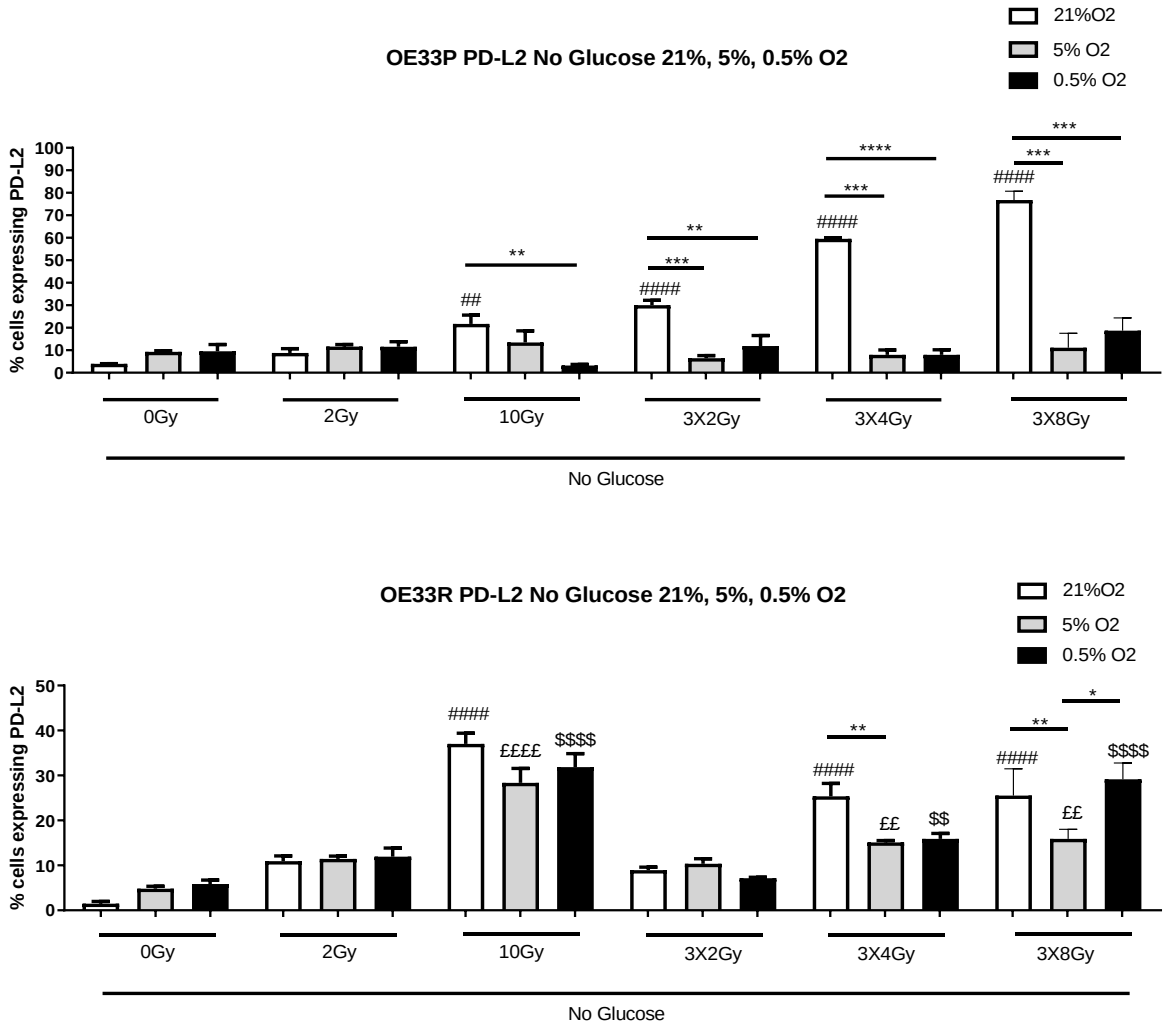

Figure 3.9 OE33P and OE33R cell lines were screened for the surface expression of PD-L2 by flow cytometry under conditions of glucose deprivation. Bolus dosing was administered once daily over three consecutive days. Cancer cells were stained 24hrs following the last fraction of radiation. Tukey's multiple comparison testing. Graph shows mean % expression (±SEM) (n=3). 21%=Normal oxygenation, 5%=mild hypoxia, 0.5%=severe hypoxia. * denotes comparison between oxygen levels for each radiation dosing regimen, * $p<0.05$, ** $p<0.01$, *** $p<0.001$, **** $p<0.0001$. # denotes comparison of dosing with 0 Gy at 21% O_2, ## $p<0.01$, #### $p<0.0001$. £ denotes comparison of dosing with 0 Gy at 5% O_2, ££ $p<0.01$, ££££ $p<0.0001$. $ denotes comparison of dosing with 0Gy at 0.5% O_2, $$ $p<0.01$, $$$$ $p<0.0001$.

In the OE33P cell line, there was a significant increase in expression of PD-L2 with 10 Gy no glucose (21.73±3.93) $p<0.01$, fractionated dosing 3x2 Gy irradiation no glucose (30.07±2.12), $p<0.0001$, 3x4 Gy no glucose (59.53±1.15) $p<0.0001$, and 3x8 Gy no glucose (76.8±2.27) $p<0.001$ compared to non-irradiated cells (3.96±1.3). There was a

significant increase in expression of PD-L2 with 3x2 Gy no glucose (30.07±2.12) compared to 3x2 Gy at 5% O_2 no Glucose (6.43±1.21) and 3x2 Gy at 0.5% O_2 (11.89±4.66) $p<0.01$, $p<0.001$. There was a significantly higher expression of PD-L2 at 3x4 Gy no Glucose (59.53±1.15) compared to 3x4 Gy 5% O_2 (7.98±2.67) $p<0.001$, and 3x4 Gy 0.5% O_2 (7.96±2.26) $p<0.001$. (Figure 3.9).

In the OE33 R cell line there was a significant increase in expression of PD-L2 at 10 Gy no glucose (37.03±2.37), $p<0.001$, 3x4 Gy irradiation no glucose (25.33±2.9), $p<0.001$, and 3x8 Gy no glucose (25.53±3.44) $p<0.001$ compared to non-irradiated cells 0 Gy (1.51±0.51) . There was a significant increase in expression of PD-L2 with 10 Gy no glucose at 5% O_2 (28.33±3.22), $p<0.001$, 3x4 Gy no glucose 5% O_2 (15.1±0.44) $p<0.01$, and 3x8 Gy no glucose 5% O_2 (15.9±1.22) $p<0.01$ compared to 0 Gy no glucose 5% O_2 (4.8±0.55). Figure 3.9.

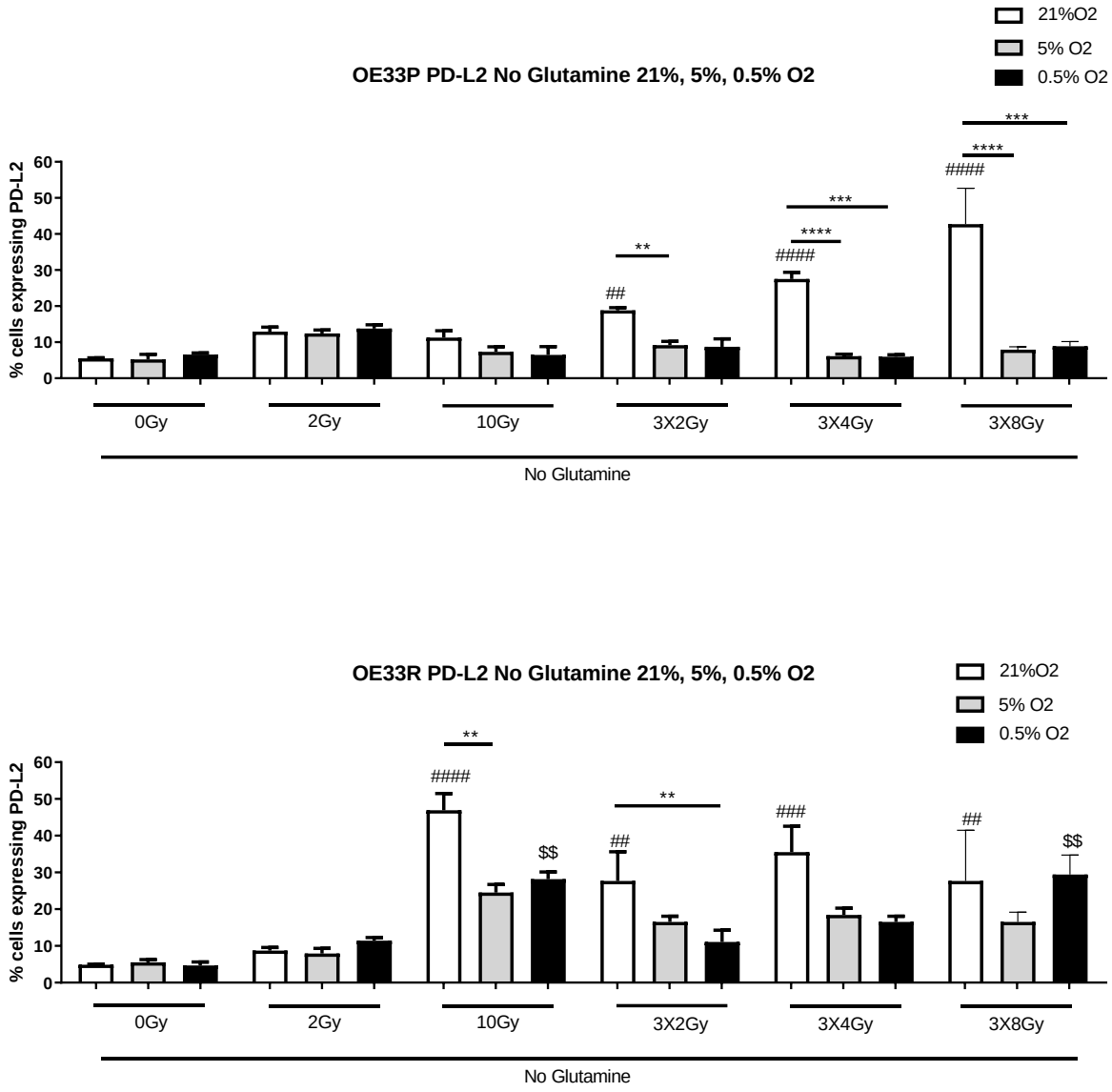

Figure 3.10 OE33P and OE33R cell lines were screened for the surface expression of PD-L2 under conditions of glutamine deprivation by flow cytometry. Bolus dosing was administered once daily over three consecutive days. Staining of cancer cells took place 24hrs after last fraction of radiation. Tukey's multiple comparison testing. Graph shows mean % expression (±SEM) (n=3). 21%=Normal oxygenation, 5%=mild hypoxia, 0.5%=severe hypoxia. * denotes comparison between oxygen levels for each radiation dosing regimen, ** p<0.01, *** p<0.001 **** p<0.0001. # denotes comparison of dosing with 0 Gy at 21% O_2, ## p<0.01, ### p<0.001, #### p<0.0001. $ denotes comparison of dosing with 0 Gy at 0.5% O_2, $$ p<0.01.

In the OE33 P cell line there was a significantly higher expression of PD-L2 at 3x2 Gy no glutamine (18.8±0.98), p<0.01, 3x4 Gy no glutamine (27.5±1.91) p<0.0001, and 3x8 Gy no glutamine (42.73±5.73) p<0.0001compared to 0 Gy no glutamine (5.5±0.18).

There was a significantly higher expression of PD-L2 at 3x2 Gy no glutamine (18.8±0.98) compared to 3x2 Gy no glutamine 5% O_2 (59.18±1.17) There was a significantly higher expression of PD-L2 at 3x4 Gy no glutamine (27.5±1.91) compared to 3x4 Gy no glutamine 5% O_2 (6.13±1.51) and 3x4 Gy 0.5% 02 (5.99±0.58) p<0.0001, p<0.0001.

In the OE33 R cell line there was a significantly higher expression of PD-L2 with 10 Gy no glutamine (46.93±4.56), p<0.0001, 3x2 Gy no glutamine (27.67±6.76), p<0.01, 3x4 Gy no glutamine (35.53±7.06), p<0.001, 3x8 Gy no glutamine (27.67±7.97) compared to 0 Gy no glutamine (4.87±0.15) , expression of PD-L2 at 10 Gy no glutamine (47.17±2.17) compared to 10 Gy 5% 02 (26.63±1.11) (Figure 3.10)

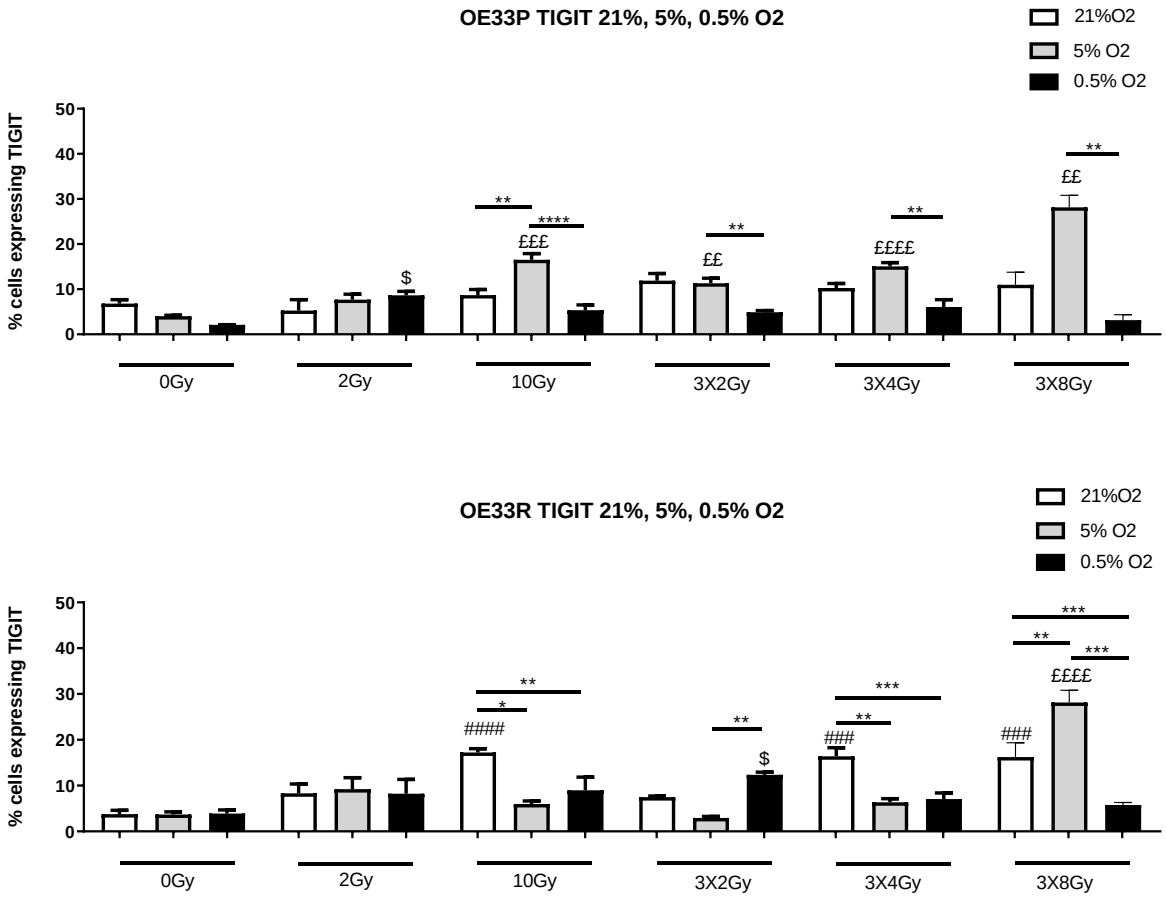

Figure 3.11 OE33P and OE33R cell lines were screened for the surface expression of TIGIT by flow cytometry. Bolus dosing was administered once daily over three consecutive days. Cancer cells were stained 24hrs following the last fraction of radiation.

Tukey's multiple comparison testing. Graph shows mean % expression (±SEM) (n=3). 21%=Normal oxygenation, 5%=mild hypoxia, 0.5%=severe hypoxia. * denotes comparison between oxygen levels for each radiation dosing regimen, * $p<0.05$, ** $p<0.01$, *** $p<0.001$ **** $p<0.0001$. # denotes comparison of dosing with 0Gy at 21% O_2, ### $p<0.001$, #### $p<0.0001$. £ denotes comparison of dosing with 0Gy at 5% O_2, ££ $p<0.01$, £££ $p<0.001$ ££££ $p<0.0001$. . $ denotes comparison of dosing with 0Gy at 0.5% O_2, $ $p<0.05$.

In the OE33 P cell line there was a significant increase in expression of TIGIT with 10 Gy 5% O_2 (16.53±1.37) $p<0.001$, 3x2 Gy irradiation 5% O_2 (11.3±1.14), $p<0.01$, 3x4 Gy 5% O_2 (15.87±0.68) $p<0.0001$, and 3x8 Gy 5% O_2 (28.13±1.54) $p<0.01$ compared to non-irradiated cells 0 Gy (4.04±0.17) .

In the OE33R cell line, there was a significant increase in expression TIGIT with 10 Gy irradiation (7.64±1.28), fractionated dosing 3x4 Gy (15.3±0.8) and 3x8 Gy (19.97±2.2) compared to non-irradiated cells (1.82±0.6) $p<0.0001$, $p<0.001$, $p<0.001$ respectively. There was a significantly higher expression of TIGIT at 3x4 Gy normal oxygenation (15.3±0.8) compared to 3x4 Gy 5% O_2 (6.36±0.97) $p<0.001$, and 3x4 Gy 0.5% O_2 (7.06±1.16) $p<0.01$. (Figure 3.11).

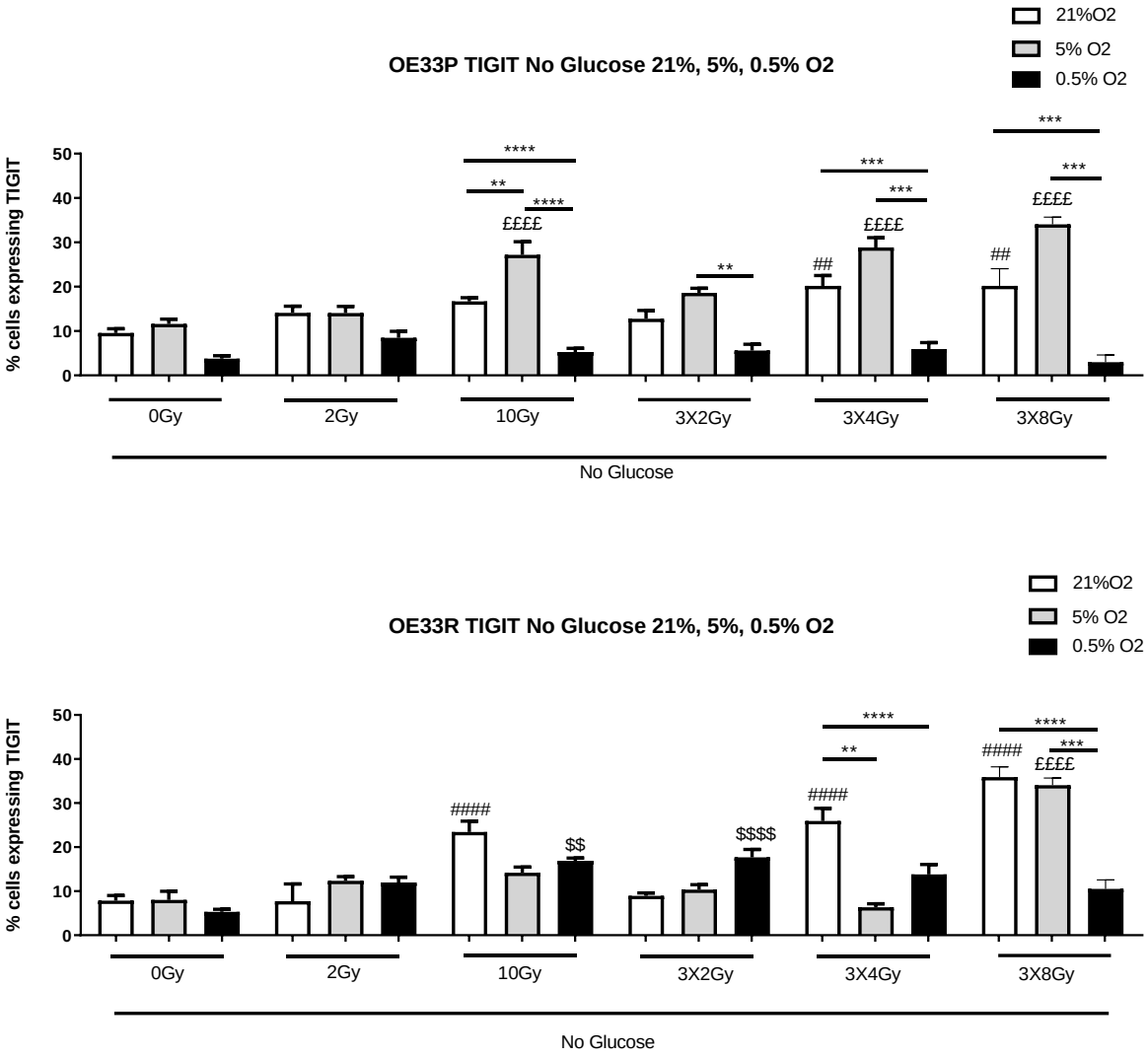

Figure 3.12 OE33P and OE33R cell lines were screened for the surface expression of TIGIT by flow cytometry under conditions of glucose deprivation. Bolus dosing was administered once daily over three consecutive days. Cancer cells were stained 24hrs following the last fraction of radiation. Tukey's multiple comparison testing. Graph shows mean % expression (±SEM) (n=3). 21%=Normal oxygenation, 5%=mild hypoxia, 0.5%=severe hypoxia. * denotes comparison between oxygen levels for each radiation dosing regimen, ** p<0.01, *** p<0.001 **** p<0.0001. # denotes comparison of dosing with 0 Gy at 21% O_2, ## p<0.01, #### p<0.0001. £ denotes comparison of dosing with 0 Gy at 5% O_2, ££££ p<0.0001. $ denotes comparison of dosing with 0 Gy at 0.5% O_2, $$ p<0.01, $$$$ p<0.0001.

In the OE33P cell line, there was a significant increase in expression of TIGIT with 10 Gy no glucose 5% O_2 (27.92±2.95) p<0.0001, fractionated dosing 3x4 Gy no glucose 5%

O_2 (28.83±2.22) p<0.0001, and 3x8 Gy no glucose 5% O_2 (34.97±0.93) p<0.001 compared to non-irradiated cells (11.61±1.09) . (Figure 3.12).

In the OE33 R cell line there was a significant increase in expression of TIGIT at 10 Gy no glucose (23.43±2.43), p<0.001, 3x4 Gy irradiation no glucose (25.93±2.89), p<0.001, and 3x8 Gy no glucose (35.9±1.35) p<0.001 compared to non-irradiated cells 0 Gy (7.85±1.18) . There was a significant increase in expression of TIGIT with 10 Gy no glucose at 0.5% O_2 (16.9±0.61), p<0.01, 3x2 Gy no glucose 0.5% O_2 (17.7±2.82) p<0.0001compared to 0 Gy no glucose 0.5% 02 (5.3±0.61). Figure 3.12.

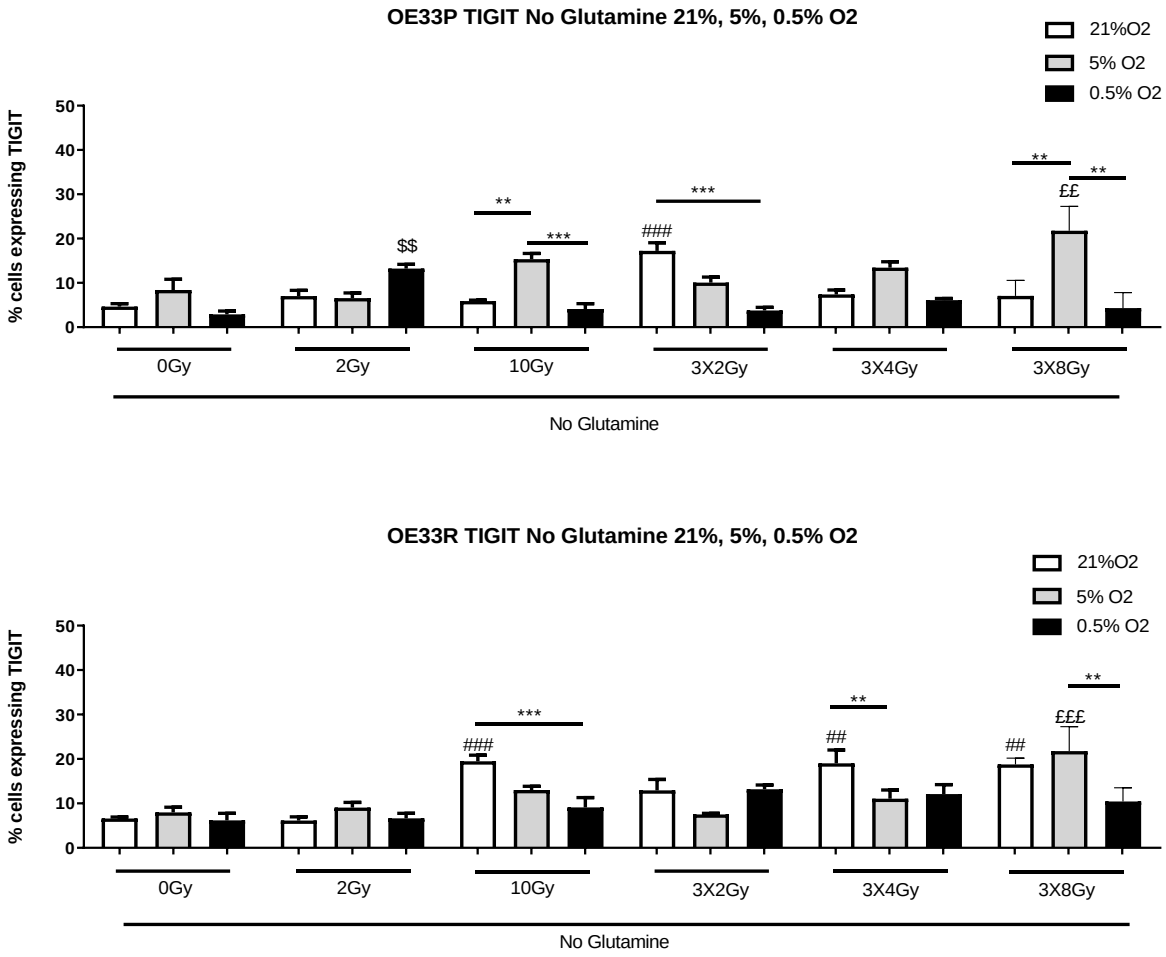

Figure 3.13 OE33P and OE33R cell lines were screened for the surface expression of TIGIT under conditions of glutamine deprivation by flow cytometry. Bolus dosing was administered once daily over three consecutive days. Cancer cells were stained 24hrs following the last fraction of radiation. Tukey's multiple comparison testing. Graph shows mean % expression (±SEM) (n=3). 21%=Normal oxygenation, 5%=mild hypoxia, 0.5%=severe hypoxia. * denotes comparison between oxygen levels for each radiation dosing regimen, ** p<0.01, *** p<0.001. # denotes comparison of dosing with 0 Gy at 21% O_2, ## p<0.01, ### p<0.001. £ denotes comparison of dosing with 0 Gy at 5% O_2, ££ p<0.01, £££ p<0.001. $$ denotes comparison of dosing with 0 Gy at 0.5% O_2 $$ p<0.01.

In the OE33 P cell line there was a significantly higher expression of TIGIT at 3x2 Gy no glutamine (17.23±1.83) compared to 0 Gy no glutamine (4.64±0.66) p<0.001. There was a significantly higher expression of TIGIT at 3x2 Gy no glutamine (17.23±1.83) compared to 3x2 Gy no glutamine 0.5% O_2 (3.77±0.72) p<0.001.

In the OE33 R cell line there was a significantly higher expression of TIGIT with 10 Gy no glutamine (19.47±1.4), 3x4 Gy no glutamine (19.03±3.01), 3x8 Gy no glutamine (18.77±0.81) compared to 0 Gy no glutamine (6.6±0.32) $p<0.001$, $p<0.01$, $p<0.01$. There was a higher expression of TIGIT at 3x4 Gy no glutamine (19.03±3.01) compared to 3x4 Gy no glutamine 5% O_2 (11.04±1.99) $p<0.01$. (Figure 3.13)

3.23 Cell viability in the context of radiation and immune checkpoint blockade

It is clear from the above experiments that radiation induces increased expression of immune checkpoints *in vitro,* hence, it is of interest to determine if radiation along with immune checkpoint blockade reduces cell viability of these cancer cell lines.

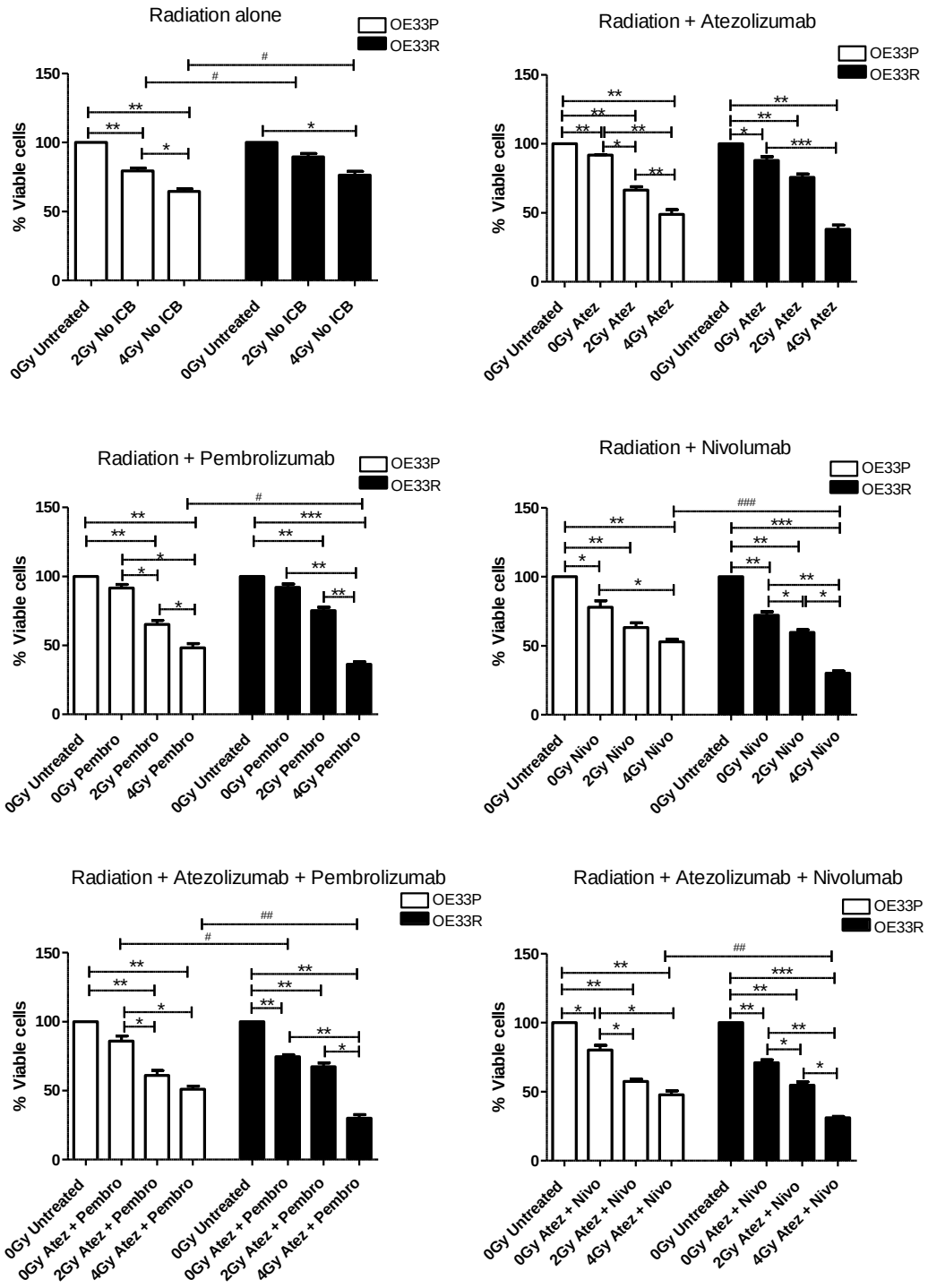

Figure 3.14: Ionising radiation with immune checkpoint blockade results in a greater reduction in cell viability when compared to either modality alone. The % viability (±SEM) of OE33P and OE33R cells were assessed using a CCK8 assay with or without radiation (0, 2 or 4 Gy) and in the presence or absence of immune checkpoint

inhibitors Atezolizumab (Atez), Pembrolizumab (Pembro), Nivolumab (Nivo) or in combination (n=3). * <0.05, ** <0.01, *** <0.001 paired t-test. # <0.05, ## <0.01, ### <0.001 unpaired t test.

Immune checkpoint blockade alone reduced the viability of both OE33P and OE33R cell lines. Through the multimodal use of both anti-PD-1 and anti-PD-L1 therapies with ionising radiation, this resulted in a synergistic reduction in viability in both cell lines. (Figure 3.14). Both anti-PD-1 and anti-PD-L1 therapies were efficacious in reducing viability of the OE33P and OE33R cancer cell lines.

In the OE33P cell line, 2 Gy radiation alone reduced viability to 78.49%±2.05, ($p<0.01$) and 4 Gy to 35.48%±2.08, ($p<0.01$) compared with unirradiated cells and there was a significant reduction in viability when comparing 2 Gy to 4 Gy ($p<0.05$). In the OE33R cell line, 4 Gy reduced viability to 63.33%±2.67, ($p<0.05$). Both 2 Gy and 4 Gy radiation resulted in a significantly greater reduction in viability in the OE33P cell line compared to the OE33R ($p<0.05$) (Figure 3.14).

Compared with untreated cells, when the OE33P cells were treated with Atezolizumab alone, viability was reduced to 91.3%±0.3, ($p<0.01$) and with the addition of 2 Gy radiation viability reduced to 66.57%±2.4, ($p<0.01$) and to 48.92%±5.76, ($p<0.01$) with 4 Gy radiation. Compared with untreated OE33R cells, viability of OE33R cells treated with Atezolizumab alone was reduced to 88%±2.65, ($p<0.05$), with the addition of 2 Gy radiation viability was reduced to 75.67%±2.33, ($p<0.01$) and 38%±3.06, ($p<0.01$) with 4 Gy radiation (Figure 3.14).

In the OE33P cells, Pembrolizumab treatment alone reduced viability to 91.54% (±2.67) compared with the untreated cells, however with the addition of 2 Gy radiation viability reduced to 65.36%±2.81, ($p<0.01$) and 48.18%±3.2, ($p<0.01$) with 4 Gy radiation when

compared to untreated OE33P cells. When the OE33R cells were treated with Pembrolizumab, viability was reduced to 92%±2.52), but the addition of 2 Gy radiation significantly reduced viability to 75.33%±2.33, ($p<0.01$) and 36.33%±1.67, ($p<0.001$) with 4 Gy radiation. 4 Gy radiation with Pembrolizumab resulted in a significantly greater reduction in viability in the radioresistant OE33R cell line compared to the radiosensitive OE33P cell line ($p<0.05$) (Figure 3.14).

In the OE33P cells Nivolumab reduced viability to 77.94%±4.79, ($p<0.05$) and with the addition of 2 Gy radiation viability reduced to 63.21%±3.41, ($p<0.01$) and 52.98%±1.82, ($p<0.01$) with 4 Gy radiation compared with untreated OE33P cells. When the OE33R cells were treated with Nivolumab, viability was reduced to 72%±2.62, ($p<0.01$) and with the addition of 2 Gy radiation viability reduced to 59.67%±1.86, ($p<0.01$) and 30%±1.73, ($p<0.001$) with 4 Gy radiation compared with untreated OE33R cells. Treatment with 4 Gy radiation and Nivolumab resulted in a significantly greater reduction in viability in the OE33R cell line compared to the radiosensitive cell line ($p<0.001$) (Figure 3.14).

In the OE33P cells, combination Atezolizumab and Pembrolizumab reduced viability to 85.94%±3.79) but the addition of 2 Gy radiation significantly reduced viability to 61.1%±3.44, ($p<0.01$) and 51.07%±2.27, ($p<0.01$) with 4 Gy radiation compared with untreated OE33P cells. When the OE33R cells were treated with combination Atezolizumab and Pembrolizumab, viability was significantly reduced to 74.67%±1.33, ($p<0.01$), and with the addition of 2 Gy radiation viability was reduced to 67.33%±2.73, ($p<0.01$) and 30%±2.52, ($p<0.01$) with 4 Gy radiation. 4 Gy radiation with combination Atezolizumab and Pembrolizumab resulted in a significantly greater reduction in viability in the OE33R cell line compared to the radiosensitive cell line ($p<0.01$) (Figure 3.14).

In the OE33P cells combination Atezolizumab and Nivolumab reduced viability to 80.18% ±3.48, ($p<0.05$) and with the addition of 2 Gy radiation reduced viability further to 57.48% ±1.64, ($p<0.01$) and 47.63%±3.11, ($p<0.01$) with 4 Gy radiation, compared with untreated OE33P cells. When the OE33R cells were treated with combination Atezolizumab and Nivolumab, viability was reduced to 71%±2.08, ($p<0.01$) and with the addition of 2 Gy radiation viability reduced to 54.67%±2.4, ($p<0.01$) and 31%±1.03, ($p<0.001$) with 4 Gy radiation compared with untreated OE33R cells. Treatment with 4 Gy radiation and combination Atezolizumab and Nivolumab resulted in a significantly greater reduction in viability in the OE33R cell line compared to the OE33P cell line ($p<0.01$) (Figure 3.14).

3.24 Profiling immune checkpoint expression in fresh patient tissue samples

As alluded to, the *in vitro* data revealed an increase in immune checkpoint expression on OAC cells post irradiation. To determine if this held true in *ex vivo* OAC tumour tissue, we profiled immune checkpoint expression post irradiation with 2 Gy and 4 Gy. Subcohorts of patients demonstrated an upregulation and others a downregulation in checkpoint expression upon exposure to conventional radiation doses and hypofractionation for $CD3^+$, $CD3^+CD4^+$, $CD3^+CD8^+$ tumour-infiltrating T cells.

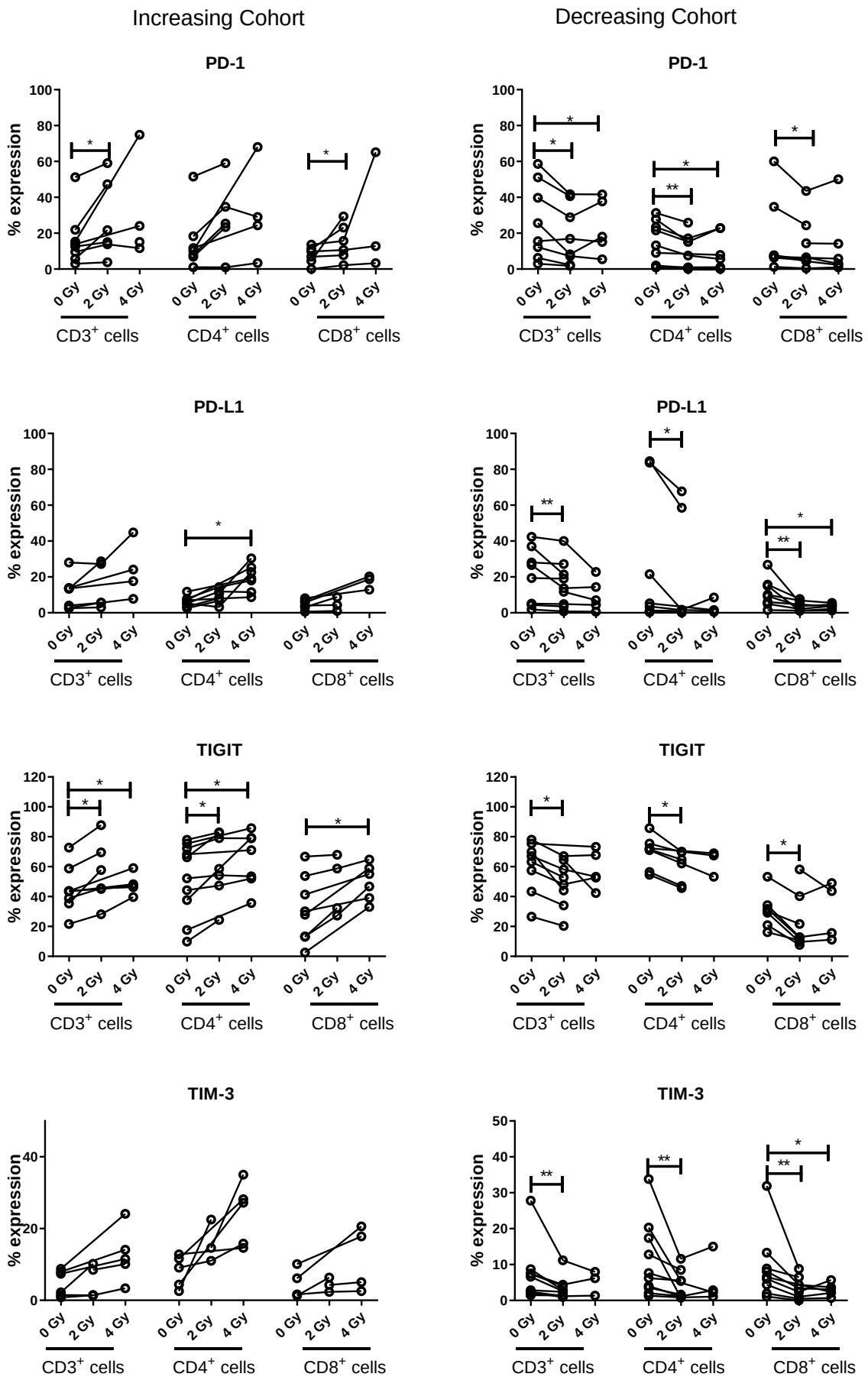
Increasing Cohort
Decreasing Cohort
PD-1
PD-L1
TIGIT
TIM-3
% expression
0 Gy
2 Gy
4 Gy
CD3+ cells
CD4+ cells
CD8+ cells

Figure 3.15: Divergent effects of ionising radiation on immune checkpoint expression *ex vivo* in OAC tumour biopsies. Inhibitory immune checkpoints are expressed at a higher level with conventional and hypofractionated dosing regimens in one subcohort (n=8 treatment naïve samples), while expressed at a lower level in the other subcohort (n=9 treatment naïve samples). Tumour infiltrating T cells from OAC patients were screened for the surface expression of PD-1, TIGIT, TIM-3 and PD-L1 *ex vivo* following treatment with 0, 2 or 4 Gy radiation, by flow cytometry. *p<0.05, **p<0.01, ***p<0.001 by Wilcoxon signed rank test.

There was a significant increase in the percentage expression of $CD3^+PD\text{-}1^+$ and $CD3^+CD8^+PD\text{-}1^+$ T cells in tumour tissue when irradiated with 2 Gy (26.76±8.8 vs 16.62±5.4 compared to 0Gy and 14.8±4.1 vs 7.7±2.01 at 0 Gy, respectively, p<0.05). There was a significant increase in the percentage expression of $CD3^+CD4^+$ $PD\text{-}L1^+$ cells with 4 Gy radiation (19.4±2.9 vs 6.27±1.02 at 0Gy, p<0.05). There was a significant increase in $CD3^+TIGIT^+$ and $CD3^+CD4^+TIGIT^+$ expression with both 2 Gy (55.6±8.6 vs 40.12±5.4 and 61.29±8.2 vs 52.17±7.7 respectively, p<0.05) and 4 Gy radiation dosing regimens (48.06±3.1 vs 40.12±5.4 and 65.16±6.9 vs 52.17±7.9 respectively, p<0.05) when compared with unirradiated cells, and an increase in $CD3^+CD8^+$ $TIGIT^+$ expression following 4 Gy irradiation (49.55±4.9 vs 31.07±7.7, p<0.05). (Figure 3.15)

In the cohort of patients which displayed a reduction in immune checkpoint protein expression following radiation, there was a significant decrease in expression of PD-1 by $CD3^+$, $CD3^+CD4^+$ and $CD3^+CD8^+$ cells in tumour tissue when irradiated with 2 Gy vs 0 Gy (18.44±5.9 vs 26.48±7.5, p<0.05; 10.33±3.4 vs 14.46±3.9, p<0.01; 12.96±5.1 vs 17.77±8.2, p<0.05, respectively) and PD-1 expression by $CD3^+$ and $CD3^+CD4^+$ when irradiated with 4 Gy vs 0 Gy (21.06±6.9 vs 26.48±7.5 and 10.04±4.2 vs 14.46±3.9 respectively, p<0.05). There was also a significant decrease $CD3^+$, $CD3^+CD4^+$ and

$CD3^+CD8^+$ cells expressing PD-L1 (15.6±4.2 vs 20.6±5.5, $p<0.01$; 18.73±11.5 vs 25.1±13.1, $p<0.05$; and 4.13±0.9 vs 11.17±2.8, $p<0.05$, respectively) , TIGIT (48.61±5.6 vs 60.13±6.2, 59.88±4.5 vs 69.57±4.1, 21.67±6.4 vs 30.76±4.5 respectively, $p<0.05$) and TIM-3 (3.24±0.9 vs 6.86±2.5, 4.07±1.3 vs 10.91±3.3 and 3.37±119 vs 9.13±3.1 respectively, $p<0.01$) with 2 Gy radiation. Similar findings were identified with 4 Gy irradiation compared to basal expression by $CD3^+CD8^+$ for PD-L1 (3.51±0.6 vs 11.17±2.8, $p<0.05$) and TIM-3 (2.93±0.7 vs 9.13±3.1, $p<0.05$). (Figure 3.15)

3.25 Clinical correlations

In order to understand potential clinical implications of these cohorts with increased and decreased immune checkpoint expression post radiation, clinicopathological correlations were examined based on patient tumour stage, adverse features of tumour biology, radiation and immune checkpoint positivity (Table 3.1). There was a positive correlation at baseline with PD-1^+CD3^+ cells and lymphovascular invasion ($p=0.04$). In terms of tumour staging, clinically there was a positive association of increasing tumour stage and PD-$L1^+CD3^+$ ($p=0.02$) at baseline, PD-$L1^+CD3^+$, TIM-3^+CD3^+ and TIM-3^+CD4^+ at 2 Gy, and $TIM3^+CD8^+$ at 4 Gy ($p<0.05$). There was a negative association between PD-1^+CD8^+ at 2 Gy ($p=0.01$). In terms of clinical nodal status, there was a positive association with nodal positivity and PD-$L1^+CD4^+$ at baseline ($p<0.001$) and PD-1^+CD4^+, TIM-3^+CD4^+, TIM-3^+CD8^+ at 4 Gy ($P<0.05$). Pathologically, advancing tumour stage was negatively associated with $TIGIT^+CD3^+$ at 2 and 4 Gy ($p<0.01$). Pathological nodal positivity was associated with PD-$L1^+CD4^+$ at baseline at 0 Gy, and $TIGIT^+CD3^+$ at 4 Gy ($p<0.01$). It was negatively associated with PD-$L1^+CD8^+$ cells and $TIGIT^+CD3^+$ cells at 2 Gy ($p<0.05$).

Table 3.1: Correlations of clinicopathological characteristics of OAC patients with CD3+, CD3+CD4+ and CD3+CD8+ cells expressing ICs in tumour biopsies.

Clinical Factor	IC Expression	Radiation Dose	Spearman *r*	*p* Value (Two-Tailed)
Lymphovascular invasion	PD-1 CD3+	0 Gy	0.6396022	0.046435
Clinical T stage	PD-L1 CD3+	0 Gy	0.6411189	0.024659
	PD-1 CD8+	2 Gy	-0.7	0.016471
	PD-L1 CD3+	2 Gy	0.7768986	0.004908
	TIM-3 CD3+	2 Gy	0.7171372	0.012993
	TIM-3 CD4+	2 Gy	0.7171372	0.012993
	TIM-3 CD8+	4 Gy	0.6963106	0.025293
Clinical N stage	PD-L1 CD4+	0 Gy	0.8568931	0.00037
	PD-1 CD4+	4 Gy	0.7311262	0.016282
	TIM-3 CD4+	4 Gy	0.6614951	0.037241
	TIM-3 CD8+	4 Gy	0.6614951	0.037241
Pathological T stage	TIGIT CD3+	2 Gy	-0.739574	0.014492
	TIGIT CD3+	4 Gy	-0.8964215	0.006267
Pathological N stage	PD-L1 CD4+	0 Gy	0.6510135	0.041473
	PD-L1 CD8+	2 Gy	-0.6443043	0.044345
	TIGIT CD3+	2 Gy	-0.7471188	0.013014
	TIGIT CD4+	4 Gy	0.8981774	0.006011

Positive values indicate positive correlation, negative values indicate negative correlation. Spearman's correlation. Only significant data shown. Spearman r=0.4-0.59 moderate, 0.6-0.79 strong and 0.8-1 very strong.

3.26 Release of angiogenic markers, cytokines, co-stimulatory molecules and soluble checkpoints post irradiation in tumour conditioned media.

Given the complex interplay in the tumour microenvironment between immunosuppressive factors and anti-tumour immunity, the expression of cytokines, immune checkpoints, co-stimulatory molecules, markers of angiogenesis and vascular injury with and without radiation was assessed using MSD multiplex ELISAs with data normalized to total protein from tumour biopsies.

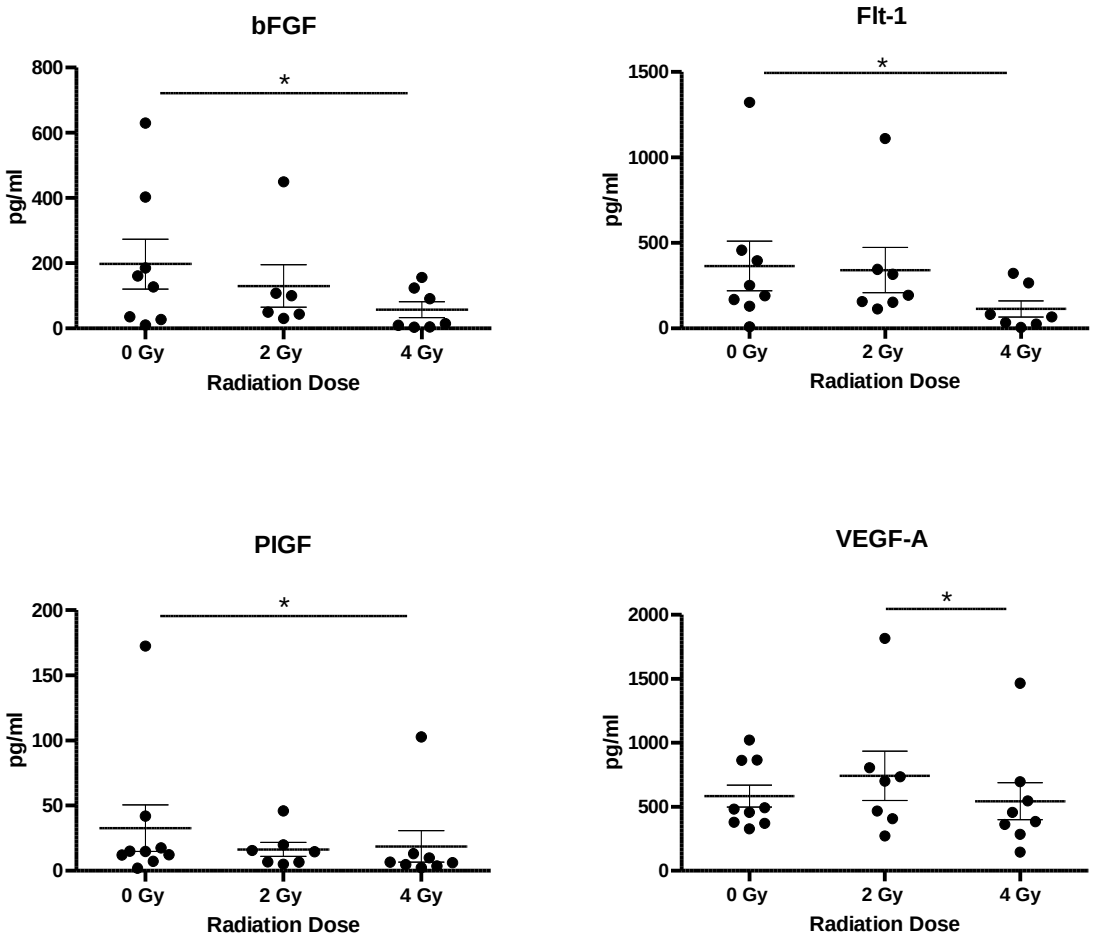

Figure 3.16: Angiogenic markers FLT-1, bFGF, PIGF and VEGF-A decrease significantly with 4Gy radiation (n=9). Normalisation using total protein using the BCA assay and refer to the samples as tumour biopsies, TCM collected at 24 h and analysed by MSD multiplex ELISA. Conditioned media generated using OAC patient

tumour was screened for FLT-1, bFGF, PIGF, VEGF-A and CRP by Multiplex ELISA. *p<0.05, by Wilcoxon signed rank test.

The administration of 4 Gy radiation was effective in significantly reducing angiogenic markers over that of untreated 0 Gy tissue; bFGF (57.7±24.5 vs 197.5±76.2, p<0.05), FLT-1 (113.5±47.7 vs 364.7±145.8, p<0.05), PIGF (18.7±12.1 vs 32.8±17.8, p<0.05). A significant reduction in VEGF-A was observed at 4 Gy radiation relative to 2 Gy. (522.8±144.2 vs 583.7±86.2, p<0.05). (Figure 3.16).

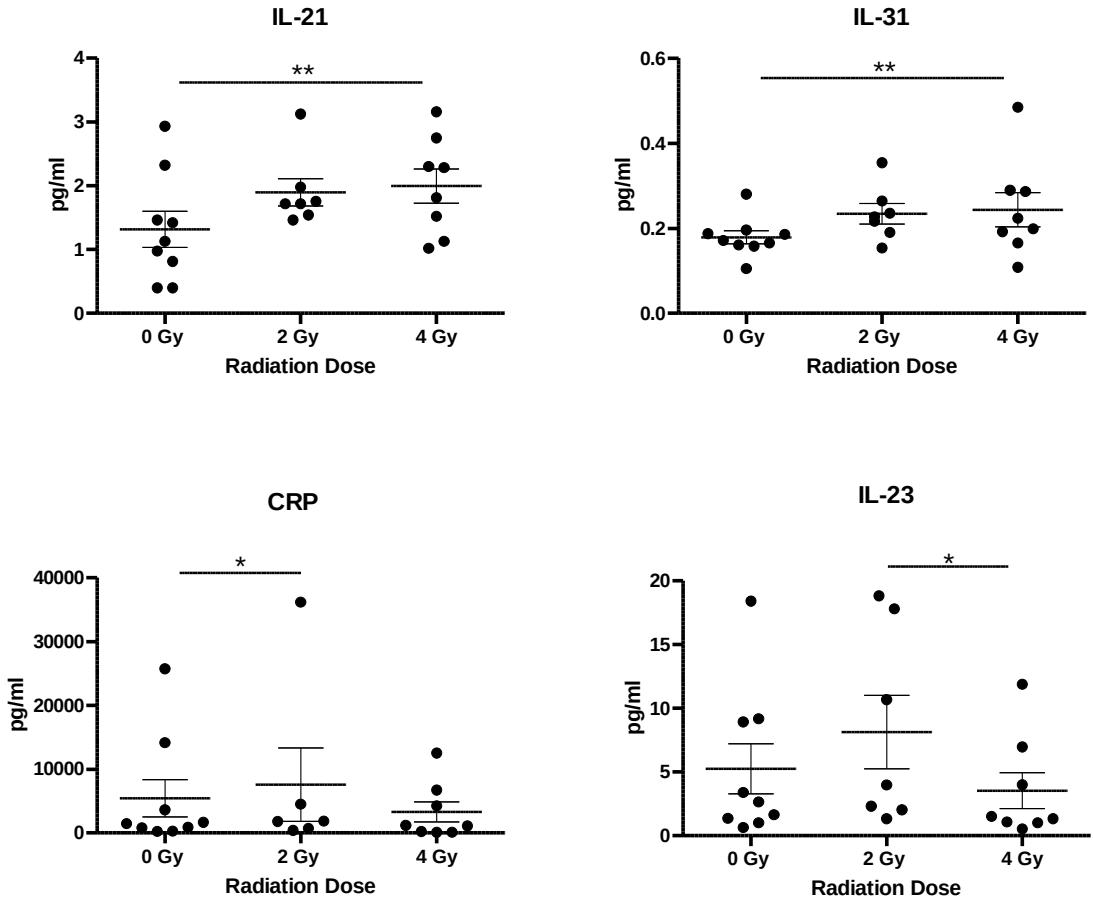

Figure 3.17: The cytokines IL-21 and IL-31, and CRP increase with ionising radiation while IL-23 decreases. OAC patient tumour conditioned media were screened for IL-21, IL-23, IL-31 and CRP by Multiplex ELISA (n=9). *p<0.05, **p<0.01, ***p<0.001. Wilcoxon signed rank test to compare expression between basal levels and dosing regimens.

There was a significant increase in the level of IL-21 (1.98±0.3 vs 1.3±0.3, $p<0.01$) and IL-31 (0.24±0.04 vs 0.18±0.02, $p<0.01$) with the administration of 4 Gy radiation compared to 0 Gy with a significant decrease in IL-23 (3.53±1.4 vs 5.24±1.9, $p<0.05$) following 4 Gy radiation compared with 2 Gy. CRP, a marker of vascular injury increased significantly with 2 Gy radiation dosing compared to untreated 0 Gy tissue (7568±5750 vs 5425±2925, $p<0.05$) but was reduced with 4 Gy compared to non-irradiated tissue (Figure 3,17).

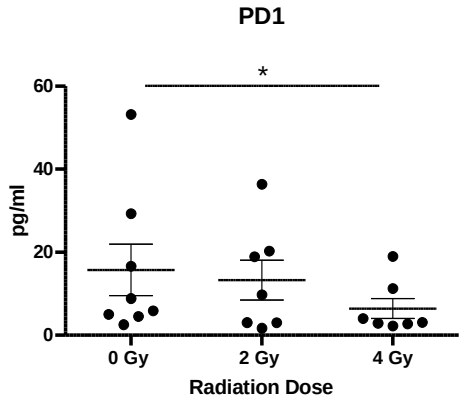
PD1
*
60
40
20
0
pg/ml
0 Gy
2 Gy
4 Gy
Radiation Dose

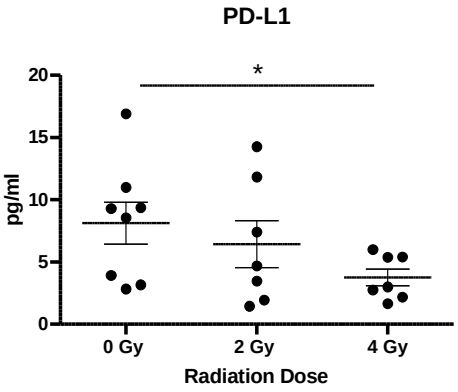
PD-L1
*
20
15
10
5
0
pg/ml
0 Gy
2 Gy
4 Gy
Radiation Dose

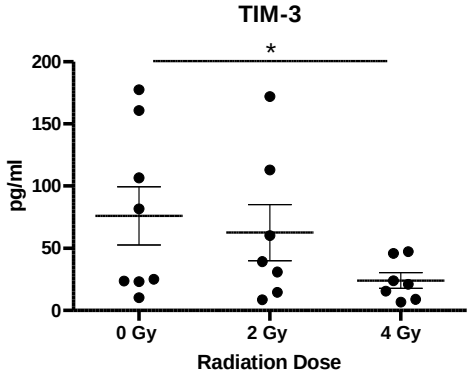
TIM-3
*
200
150
100
50
0
pg/ml
0 Gy
2 Gy
4 Gy
Radiation Dose

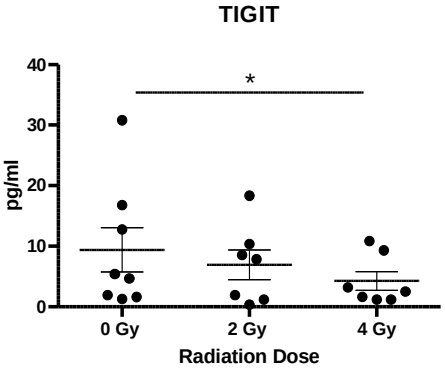
TIGIT
*
40
30
20
10
0
pg/ml
0 Gy
2 Gy
4 Gy
Radiation Dose

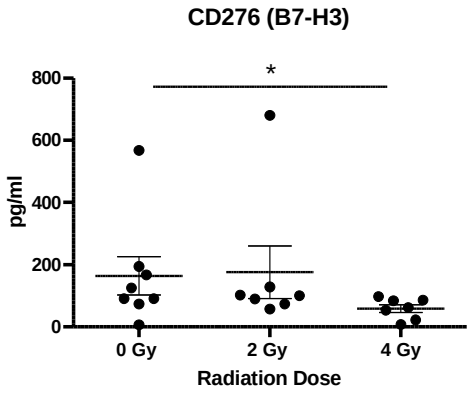
CD276 (B7-H3)
*
800
600
400
200
0
pg/ml
0 Gy
2 Gy
4 Gy
Radiation Dose

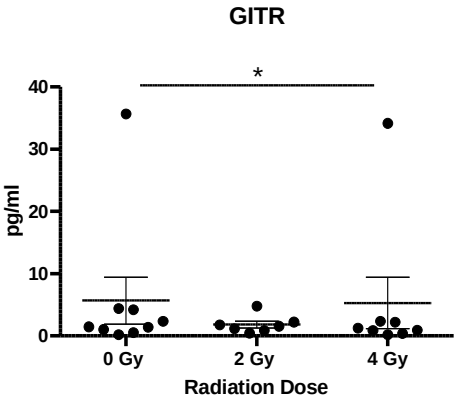
GITR
*
40
30
20
10
0
pg/ml
0 Gy
2 Gy
4 Gy
Radiation Dose

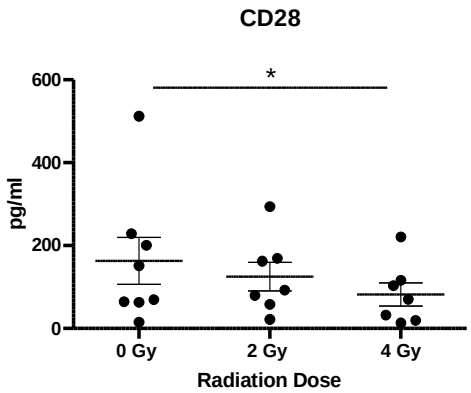
CD28
*
600
400
200
0
pg/ml
0 Gy
2 Gy
4 Gy
Radiation Dose

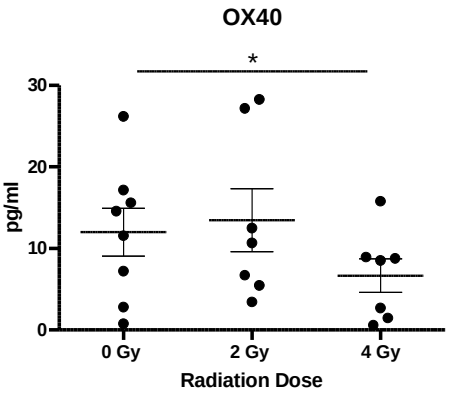
OX40
*
30
20
10
0
pg/ml
0 Gy
2 Gy
4 Gy
Radiation Dose

Figure 3.18: The soluble inhibitory checkpoints PD-1 and its ligand PD-L1, TIGIT, TIM3, immunosuppressive molecule and checkpoint CD276 (B7-H3) and costimulatory molecules CD28, OX40 and GITR significantly decrease with fractionated radiotherapy (n=8). OAC patient's tumour conditioned media were screened for PD-1, PD-L1, TIM-3, TIGIT, CD276, GITR, OX40 and CD28 by Multiplex ELISA. *p<0.05, **p<0.01, ***p<0.001 by Wilcoxon signed rank test.

In terms of immune checkpoint receptor and ligand expression, there was a significant reduction in levels of soluble PD-1 (6.44±2.4 vs 15.72±6.2, p<0.05), PD-L1 (3.76±0.7 vs 8.12±1.7, p<0.05), TIM-3 (24.11±6.2 vs 76.02±23.5, p<0.05), TIGIT (4.26±1.5 vs 39±3.6, p<0.05) and CD276 (58.81±12.8 vs 164.3±61.02, p<0.05) in the tumour conditioned media following 4 Gy radiation compared with 0 Gy. In addition, 4 Gy radiation also induced a significant decrease in the release of the soluble co-stimulatory molecules CD28 (82.18±27.7 vs 163.2±56.3, p<0.05), GITR (5.27±4.1 vs 5.7±3.8, p<0.05) and OX-40 (6.7±2.1 vs 11.9±2.9, p<0.05) compared to untreated tissue 0 Gy (3.18).

3.27 Discussion

The intuitive appeal of modulating the immune system to generate an effective anti-tumour response is so profound that the idea emerged contemporaneously with the field of cellular immunology itself. At the most fundamental level, harnessing the immune system to boost anti-tumour immunity consists of two processes amenable to manipulation: these being the stimulus and the subsequent response. The most logical way to perturb the quality or quantity of antigenic load is by inducing preferential killing of tumour cells, either systemically with chemotherapy or locally with radiation therapy. Increasing the antigenic load and facilitating immune activation with optimal kinetics may achieve a synergistic anti-tumour response, producing an effect on the immune system more definitive and durable than either approach alone. In this context, the landmark Checkmate-577 trial demonstrated significantly improved disease free survival in the adjuvant setting of resectable gastroesophageal cancer (180). The findings of increased checkpoint expression *in vitro and ex vivo* through the use of radiation in the current body of work provides promising translational therapeutic rationale for their use in the multimodal paradigm. Ionizing radiation therapy (RT) has been shown to enhance the priming and effector phases of the antitumor T cell response rendering it an attractive therapy to combine with PD-1/PD-L1 inhibitors (181). However, inherently radioresistant tumours may pose a particular therapeutic dilemma, as they may not have a similar synergism with ICB as radiosensitive tumours. Ionising radiation is currently under investigation in metastatic oesophageal cancer with pembrolizumab (NCT02642809) and is currently under investigation in the curative setting with neoadjuvant trimodal therapy of Pembrolizumab and chemoradiotherapy in oesophageal squamous cell carcinoma (NCT03792347), with a similar trial investigating durvalumab and chemoradiotherapy in SCC and OAC (NCT02735239). The SKY-SKRAPER-07 trial

is currently evaluating anti-PD-L1 Atezolizumab with anti-TIGIT therapy following chemoradiotherapy in advanced oesophageal cancer (NCT04543617). Interestingly, a recent study by Zhao *et al.,* reported that TIM-3 expression was associated with PD-1 positivity, and high $CD8^+$ TIL density as an independent risk factor for recurrence free and overall survival in oesophageal SCC (182).

The hostile features of the tumour microenvironment nutrient deprivation and hypoxia and all have profound effects on the IC with significant upregulation of TIGIT, PD-1 and its ligands. It is known that nutrient deprivation and hypoxia have a significant impact on the cellular composition of the TME, negatively influencing anti-tumour immune responses. The hypoxic microenvironment which prevails promotes the recruitment of regulatory T cells through induction of expression of the chemokine CCK- 28 and enhances the immunosuppressive microenvironment and hence are promising targets for immune checkpoint blockade to shift the balance in favour of anti-tumour immunity.

The clinically important observation in this study that half of the patients assessed displayed a reduction in immune checkpoint expression post radiotherapy is an interesting caveat, one which suggests very different susceptibility to ICB in combination with radiotherapy and therefore, the stratification of patients into potential responders and non-responders should be addressed. In the same vein, the activation of cGAS-STING signaling, which has been recognized to potentiate systemic anti-tumour immunity and subsequent tumour rejection by dual radiotherapy and checkpoint blockade administration is promising even in those with checkpoint downregulation. A study by Vanpouille-Box *et al.,* highlighting the importance of the cGAS-STING pathway in response to combination radiotherapy and immunotherapy, reported the knockdown of cGAS in murine cancer cells abrogated the priming of $CD8^+$ T cells in tumour-draining

lymph nodes and spleen, and prevented the infiltration of abscopal tumours by $CD8^+$ T cells (68). Importantly, the synergistic and significant reduction in viability of radioresistant OAC cancer cells which we observed in this study following the dual administration of immune checkpoint inhibitors and ionising radiation is very promising. With respect to the use of hypofractionation in the curative setting for oesophageal cancer, there is a growing body of evidence demonstrating the safety and efficacy of this approach (183). There are studies demonstrating a survival benefit of this approach particularly in the context of metastatic nodal disease. In one such study, hypofractionated radiotherapy (HFR) combined with paclitaxel chemotherapy for the treatment of post-surgery tracheoesophageal groove lymph node (TGLN) metastasis demonstrated improved overall survival (OS) in the HFR group compared with that of the conventional dosing group (24.2 months (95% CI, 16.2-32.1 months) vs. 11.8 months (95% CI, 9.2-14.4 months), p=0.024) (184). Importantly, there was no statistical difference in the incidence of grade 3-4 events including radiation pneumonitis between these two groups (grades 3-4, 16.0 vs. 7.1%; P = 0.314) (184).

Vascular endothelial growth factor (VEGF) is a mitogen that plays a crucial role in angiogenesis and lymphangiogenesis and Ramucirumab is approved for use in advanced gastroesophageal cancer patients. In colorectal cancer, anti-VEGF agents have demonstrated a survival benefit when combined with chemoradiotherapy, however development of resistance is very common (185). This may be attributable to the development of compensatory mechanisms of resistance, such as hypoxia-triggered upregulation of other proangiogenic factors, like placental growth factor (PIGF) (186). VEGF, bFGF (basic fibroblast growth factor) and PIGF are major pro-angiogenic factors associated with cancer angiogenesis and tumourigenesis and Flt-1, also known as vascular endothelial growth factor receptor 1 (VEGFR-1), is a high-affinity tyrosine

kinase receptor for VEGF. It is involved in tumour growth and metastasis, most likely via stimulation of macrophage-lineage cells (187). PIGF/Flt-1 signaling plays an important role in colorectal cancer progression through increasing the phosphorylation of p38 MAPK, thereby upregulating MMP9 expression; resulting in increasing cellular migration/invasion. Therefore blocking PIGF/Flt-1 signalling may have therapeutic potential in lower gastrointestinal cancers (188). In the current study radiation therapy was demonstrated to reduce the expression of these promoters of angiogenesis, which is crucial in the mitigating the risk of metastatic disease for upper gastrointestinal cancers.

The subset of cytokines expressed post radiation and in response to immunotherapy treatment play a key role in determining the subsequent immune response elicited. In this study the OAC tumour tissue released significantly more anti-tumour IL-21 and IL-31 in response to radiation. IL-21 is produced by a range of activated $CD4^+$ T helper cells, including Th1 and Th17 cells, activated NKT cells and T follicular helper cells (189). It promotes B cell differentiation into plasma cells, regulates immunoglobulin production, reshaping the tumour microenvironment and influencing the proliferation and/or effector function of both $CD4^+$ and $CD8^+$ T cells, while limiting the differentiation of Tregs (190). IL-21 has potent anti-tumour effects due to its ability to expand the pool of cytotoxic $CD8^+$ T cells through the induction of an early differentiation phenotype, NK cells and NKT cells (191). IL-31 is an immunoregulatory cytokine that is mainly produced by activated T helper (CD4) and cytotoxic T (CD8) cells, with a study demonstrating that mice infused with IL-31 exhibited a reduction in tumour growth and in the number of pulmonary metastatic lesions, highlighting the potential use of IL-31 to offset the risk for metastatic disease development (192). Similarly, in a mouse model of breast cancer, cytotoxic T cell activity is increased, whereas the levels of $CD4^+$ T cells, MDSCs and tumour-associated macrophages are decreased in IL-31-expressing tumours, with cellular

changes accompanied by a cytokine profile associated with antitumour immunity (193). While both IL-21 and IL-31 significantly increased in the tumour conditioned media, the expression of IL-23, which has been documented to promote tumour metastases decreased. IL-23 has metastases promoting properties through the suppression of anti-tumour functions of T cells and the anti-metastatic function of NK cells (194). In addition to this, IL-23 was found to be overexpressed in many human cancers including colorectal and gastric cancer, and was found to be a negative prognostic indicator (195). Of note CRP, an acute phase protein and marker of vascular injury was found to increase with 2 Gy radiation in our study. Epidemiologic studies suggest that elevated circulating levels of CRP are associated with poor prognosis in patients with several types of solid cancers. Similarly, in apparently healthy individuals from the general population, elevated levels of CRP are associated with increased future risk of cancer of any type including lung, colorectal and gastric cancers due to chronic low inflammatory states, which is of particular relevance in oesophageal adenocarcinoma (196). Therefore, the exact role of CRP in response to radiotherapy and immunotherapy requires further study.

Co-stimulatory and immune checkpoint molecules can have both immunostimulatory and immunosuppressive effects. In this study a range of soluble immune checkpoint receptors and ligands were significantly downregulated following 4 Gy radiation treatment of OAC tumour explants. However, the role of soluble receptors and ligands on immune regulation and cancer treatment is largely unknown. In this study we observed a significant down regulation of PD-1, PD-L1, TIM-3 and TIGIT and this was paralleled by a concomitant increase in OAC cell line surface expression and a cohort of OAC tumour explants, which may go some way to explain the decrease in the soluble forms of these immune checkpoint proteins post irradiation. B7-H3 (also known as CD276) is an

immune checkpoint molecule in the epithelial mesenchymal transition (EMT) pathway, with many cancers exhibiting aberrant overexpression and such upregulation is associated with aggressiveness and a poor clinical prognosis (197). Furthermore, there are studies demonstrating a crucial role for B7-H3 in promoting carcinogenesis and metastasis and playing an essential role in cell proliferation, invasion and migration (197-199). CD276 serves as a T cell inhibitor to promote tumour proliferation and invasion, rather than CD276 acting as a T cell stimulatory molecule as previously thought (200). In addition, soluble B7-H3 was found to promote the invasion and metastasis of pancreatic carcinoma cells through the TLR4/NF-κB pathway (50). Overall, additional studies are required in gastroesophageal cancers to determine the true function of soluble immune checkpoint proteins and how they pertain to treatment response and immune regulation.

The co-stimulatory molecule CD28 is essential in the augmentation of T cell activation and metabolism, driving tumour-infiltrating T cell glycolysis to promote inflammation. It is antagonized by the inhibitory and checkpoint immunotherapy receptors CTLA-4 and PD-1 (201). In the current study, soluble CD28 is reduced with radiation, which may be immunosuppressive. Soluble CD80-Fc (where extracellular domains of human or mouse CD80 are fused to the Fc domain of IgG1) have been found to sustain IFN-γ production by human and murine PD-1^+ activated T cells even in the presence of PD-$L1^+$ human or mouse tumour cells (202). Soluble Glucocorticoid-induced TNF receptor (GITR), which was reduced in this study, is an emerging immunotherapy target expressed at high levels on regulatory T cells (203, 204). Recent phase 1 trials have demonstrated the safe pharmacological profile of agonistic anti-GITR antibodies, with ongoing phase II trials currently evaluating its combination with radiotherapy and anti-PD-1 therapy (NCT04225039). New promising approaches are focuses on the activation of co-

stimulatory pathways to enhance antitumour immune responses. GITR activation can promote effector T cell function and inhibit regulatory T cell (Treg) function (203), and may also provide theoretical basis for the clinical application of combinations with monoclonal antibody therapy such as bFGF in molecular targeted therapies (205).

Lastly, OX40 has a critical role in the maintenance of an immune response beyond the initial few days boosting T cell clonal expansion, effector differentiation, and survival (206). OX40 activation could augment the downstream signaling of TCR mainly through the PI3-K/PKB pathway, accounting for T cell division, survival and cytokine production. OX40 activated in conjunction with TCR signaling could increase calcium influx, promote nuclear factor of activated T cells (NFAT) activation and enhance several cytokines secretion, such as IL-2, IL-4, IL-5, and IFN-γ (207). OX40 triggering regressed Treg cells, allowing DCs to reach the draining lymph nodes and prime the specific CD8 lymphocytes response to the tumour (208). There is also a phase 1/2 trial combining monoclonal antibody agonist of OX40 (MEDI6469) with stereotactic body radiation therapy (SBRT) in 1-2 fractions of 10-25 Gy each in breast cancer patients with lung or liver metastases (NCT01862900). However, in the current study radiation induces a downregulation of OX40 in tumour conditioned media which may indeed be an immunosuppressive consequence of radiation therapy and one which requires further investigation. Again, further studies are needed to elucidate the functions of soluble co-stimulatory molecules as they may have alternate functions compared with their cell membrane bound counterparts in the tumour microenvironment.

The advent of immunotherapy using ICIs has had a significant impact in the treatment of melanoma and NSCLC and is now expanding to the treatment of gastrointestinal malignancies with positive results in the Checkmate 577 trial in the adjuvant setting. However, there remains many issues to be interrogated including an optimized

radiotherapy methodology for use in combination with ICIs. Although a large number of preclinical and clinical studies suggest optimal schemes for dose-fractionation, and timing of radiotherapy delivery and target delineation, there is no universal consensus applicable to the clinical setting. In the current study, immune checkpoint blockade in combination with radiation synergistically reduces viability in radioresistant cells and Nivolumab appears most efficacious. The significant upregulation of Immune checkpoints in response to conditions of the TME also represent a robust rationale for the use of ICB in this scenario. However, further efforts are needed to understand in depth the nature of radiotherapy-induced immune responses. In addition, radiotherapy-induced lymphopenia may suppress reinvigoration by ICIs, thus protocols that can minimize lymphopenia need careful design for maximal therapeutic potential. Finally, further efforts to identify biomarkers to guide the selection of patients who are appropriate for these treatment modalities are urgently required with next-generation sequencing-based profiling of tumour mutation burden, immune gene expression signatures and T cell receptor repertoire potential avenues to elucidate this.

Chapter 4: The prognostic value of the lymph node in oesophageal adenocarcinoma and the impact of major oesophageal oncological surgery on the perioperative immune landscape

The Prognostic Value of the Lymph Node in Oesophageal Adenocarcinoma; Incorporating Clinicopathological and Immunological Profiling. Donlon NE*, Davern M*, Sheppard A, Power R, O'Connell F, Heeran AB, King R, Hayes C, Bhardwaj A, Phelan JJ, Dunne MR, Ravi N, Donohoe CL, O'Sullivan J, Reynolds JV, Lysaght J. Cancers (Basel). 2021 Aug 9;13(16):4005. doi: 10.3390/cancers13164005. PMID: 34439160. **denotes equal contribution.*

The Impact of Esophageal Oncological Surgery on Perioperative Immune Function; Implications for Adjuvant Immune Checkpoint Inhibition. Donlon NE*, Davern M*****, Sheppard AD, O'Connell F, Dunne MR, Hayes C, Mylod E, Ramjit S, Temperley H, Mac Lean M, Cotter G, Bhardwaj A, Butler C, Conroy MJ, O'Sullivan J, Ravi N, Donohoe CL, Reynolds JV, Lysaght J. Front Immunol. 2022 Jan 27;13:823225. doi: 10.3389/fimmu.2022.823225. PMID: 35154142; PMCID: PMC8829578. **denotes equal contribution.*

The immune response to major gastrointestinal cancer surgery and potential implications for adjuvant immunotherapy. N. E. Donlon*, M. Davern*, C. Hayes, R. Power, A. D. Sheppard, C. L. Donohoe, J Lysaght, J V Reynolds. Crit Rev Oncol Hematol. 2022 Jul;175:103729. doi: 10.1016/j.critrevonc.2022.103729. Epub 2022 May 31. PMID: 35662586. **denotes equal contribution.*

4.1 Introduction

The integral pillar in the multimodal treatment of locally advanced oesophageal adenocarcinoma is surgery in combination with chemotherapy alone or chemoradiotherapy, as established by the FLOT-4 trial and CROSS randomised control trials respectively (4, 6). Despite advances in treatment, the 5-year overall survival remains below 20% and is significantly impacted upon by tumour biology and nodal involvement (209, 210). In addition, tumour response to neoadjuvant treatment can predict overall survival (OS), with a major pathologic response associated with a significant improvement in OS compared to no response or minor pathologic changes following neoadjuvant therapy in gastro-oesophageal cancers (211). Unfortunately, only 1 in 4 of adenocarcinoma patients will achieve a complete pathological response to neoadjuvant therapies and it is this subgroup that gains the survival benefit from systemic therapy (212, 213). The potential benefits of neoadjuvant therapy include downstaging of the primary tumour, facilitating complete surgical resection and eradicating occult micrometastases (214). It is therefore important to identify those that are at a high risk of recurrence after perioperative therapy, as these patients may benefit from alternative regimens. As treatment is associated with substantial morbidity, early identification of non-responders could reduce the toxicity burden of minimally effective systemic therapies. In addition to this, recurrence rates remain high, with one study of 1147 patients with resected oesophageal adenocarcinoma or squamous cell carcinoma demonstrating recurrences in 38% of patients, with 83% of these within the first 2 years (215). The factors responsible for this include genomic and epigenomic instability, immune evasion, angiogenesis and micro-metastatic dissemination.

Surgery as the crucial therapeutic approach for oesophageal cancer may disrupt the tumour microenvironment and may be permissive of tumour-cell shedding and

production of pro-angiogenic and growth factors (216). This perioperative timeframe is postulated to be pivotal in determining long-term cancer outcomes, disproportionally with its short duration (days to weeks). It may enhance the risk of progression of pre-existing micrometastases and the initiation of new metastases - the main cause of cancer-related mortality, while simultaneously compromising immune control over residual malignant cells (217).

The lymphatic system has been recognised as a route of metastasis for over 150 years (218-220) and clinical nodal status (cN) is part of the preoperative staging of oesophageal cancer. Curative surgery includes lymph node dissection and (221) pathological staging of resected nodes (ypN) has been shown to independently predict survival for oesophageal cancer patients (170, 222-225). In addition to nodal status, histological tumour regression following treatment, measured by different tumour regression grade (TRG) scales, can predict overall survival (170, 171, 225-227). However, in a secondary analysis of a randomised trial, only nodal status was an independent prognostic factor (228). The downgrading of nodal status following neoadjuvant treatment (where ypN is less than cN) also positively correlates with survival (229), particularly in patients that do not display a local response in their primary tumour (171). However, it has been reported that those with nodal downstaging have shorter median survival than node-negative patients before treatment (229, 230).

In addition to their role in tumour metastasis and as a prognostic factor, tumour-draining lymph nodes (TDLNs) are important in the anti-tumour immune response (231). Priming of anti-tumour of $CD4^+$ and $CD8^+$ T cells by dendritic cells (DCs) occurs in the lymph node, a critical step in the cancer immunity cycle that is potentiated by anti-CTLA-4 immune checkpoint blockade (ICB) (232, 233). However, TDLNs are rich in tumour derived factors such as IL-6, TGF-β, prostaglandin E2 and VEGF, which promote an

immunosuppressive milieu (231). In melanoma, breast and cervical cancer, the lymph node microenvironment (LNME) promotes an immature and suppressive immune cell phenotype, through increased Treg and MDSC infiltration as well as by a generalized state of enhanced T cell anergy. In addition, LN-resident (LNR) dendritic cell (DC) subsets show lower levels of activation compared with that of migratory DC subsets (234-236), subsequently attenuating T cell activation, thus promoting tumour progression and metastasis (237). In this altered cytokine milieu, $CD4^+$ T cells do not differentiate into effector T cells but instead differentiate into peripheral regulatory T (T_{reg}) cells that restrain anti-tumour immunity (238). The LNME is emerging as an important substrate for immune checkpoint blockade (ICB); in mouse models, ablation or surgical resection of sentinel lymph nodes reduces immune cell infiltration in the primary tumour and reduced the efficacy of anti PD-1 and anti PD-L1 therapy (239). Collectively, these studies highlight the complex yet critical role of TDLNs in promoting or inhibiting anti-tumour immunity and mediating response to ICB (240). Furthermore, elective nodal irradiation in mice reduces chemokine expression in the tumour microenvironment (TME) and subsequent intratumoural $CD8^+$ T cell infiltration resulting in reduced ICB efficacy (75). This also has therapeutic implications, as local delivery of ICB to TDLNs in mice had similar efficacy to intratumoural delivery (241). However, the LNME has yet to be examined in the context of oesophagogastric adenocarcinoma. Understanding the LNME niche would help inform the development of rationale immunotherapeutic strategies to boost response rates to ICB and conventional therapies in oesophagogastric adenocarcinomas (157, 242, 243).

In the current era of surgical oncology emphasizing personalized therapy, immune checkpoint blockade (ICB) can unleash cells of the immune system that recognize and are poised to attack cancer cells. This will enhance systemic anti-tumour immunity of

cells which are ordinarily held in check by molecular and cellular pathways that suppress their activation and effector functions. This potentiates anti-tumour immunity and mediates durable cancer regression for a cohort of patients, exposing a panoply of new antigens for potential immune recognition. The seminal observation that blocking the prototypical immune checkpoint receptor cytotoxic T-lymphocyte antigen-4 (CTLA-4) could mediate tumour regression in murine models (232) led to the clinical development and approval of anti-CTLA-4 as a treatment for patients with advanced melanoma (244). The CheckMate 577 trial provides compelling evidence for adjuvant anti-PD-1 therapy (nivolumab) in patients with residual disease after multimodal therapy, with a doubling of disease-free survival compared with placebo (180). However, despite these promising results, the optimal timing for delivery of immunotherapies in the neoadjuvant and adjuvant setting to achieve a synergy between both immunostimulation and anti-metastatic effects is yet to be elucidated (245). At this time, it is also unclear whether immunotherapy has therapeutic benefit during the potentially immunosuppressive perioperative period (246). In theory however, harnessing the peri-operative period provides a therapeutic window to potentially arrest metastatic growth, enhance immune cell mediated immunity, immunological perturbations and achieve metabolic reprograming of the tumour microenvironment (TME) already initiated by neoadjuvant therapies, potentially improving long-term survival rates in patients with cancer (247, 248).

The complex biology of immune checkpoint pathways still contains many mysteries, and the full activity spectrum of checkpoint blocking drugs, and the study of the interaction of (chemo)radiation, surgery and relevant immune pathways may help fine-tune and standardize adjuvant therapy protocols for incorporating immunotherapies (249, 250). In the context of oesophageal cancer, studies/trials should also extend to patients with no

residual disease as they have a 30-40% risk of relapse, hence adjuvant anti-PD-1 therapy may clearly have a role in this cohort.

In this study, we investigated the prognostic implications of clinical and pathologic nodal status in a large single centre cohort of patients with locally advanced resectable oesophagogastric cancer. We also sought to immunophenotype the perioperative period in oesophagogastric cancer patients to elucidate the potential immunostimulatory and/or immunosuppressive effects of surgery with the goal of identifying potential therapeutic windows and targets in the adjuvant setting to reduce recurrence rates and prolong survival for these patients. We profiled immune checkpoint (IC) expression on T cells residing in the TDLN and infiltrating-tumour tissue of oesophagogastric adenocarcinoma patients. Furthermore, the inflammatory, angiogenic, cytokine and chemokine profile of the LNME and TME in oesophagogastric cancer patients is investigated and correlated with clinicopathologic outcomes. The hypothesis being that the TME is more immunosuppressive compared to the lymph node microenvironment and marrying clinicopathological characteristics with immune profiling remains pivotal to unwinding the complex interplay in the TME. This information will help provide a fundamental understanding of the LNME and TME in oesophagogastric adenocarcinoma patients in order to better inform future therapeutic approaches.

Specific aims:

1. Examine the effect of nodal positivity on overall survival in oesophageal adenocarcinoma.

2. Profile the immune checkpoint receptors and ligands on tumour-infiltrating T cells compared to tumour-draining lymph nodes.

3. Profile the expression of cytokines, chemokines, growth factors, markers of angiogenesis and vascular injury in tumours compared to tumour-draining lymph nodes.

4. Examine the impact of major oesophageal oncological surgery on circulating lymphocytes, circulating CTLs, effector memory and central memory T cells in the immediate post-operative period in OAC patients.

5. Determine the implications of major oesophageal oncological surgery on immune checkpoints, DAMP expression perioperatively.

6. Immunophenotyping of Th1/Th2 responses and assessment of markers of angiogenesis and vascular injury in the peri-operative period.

4.2 Results

4.2.1 Nodal status in OAC patients demonstrates superior prognostication than pathological complete response in predicting overall survival

Data for 702 patients was obtained from a prospectively maintained database between 2001-2016, of these 356 were classified as node negative, with a higher proportion of the N0 cohort having a Siewert type I tumour (60%). An *en bloc* radical oesophagectomy was performed in 50% of N0, 66% N1, 48% of N2 and 53% of N3 disease burden (Table 4.1.1). On pathologic assessment of resected specimens, N0 had earlier T stage disease, with 54% being (y)p or pT0/T1, compared with 18% for N1, 9% for N2 and 7% for N3 ($p < 0.001$). N0 and N1 were significantly associated with Barrett's oesophagus, 55% and 49% respectively ($p < 0.001$), with signet ring and mucinous features more frequent in N2 and N3. N0 was associated with less adverse features of tumour when compared to those with nodal positivity. Adverse features consisted of poor differentiation, perineural, lymphatic and vascular invasion, with a novel 3 grouping stratification of 0, 1-2, 3-4 adverse features previously described by our department (209). Linking adverse pathology with nodal status, 52%, 42% and 6% of N0 were in the 0, 1-2, and 3-4 group respectively, compared with 16%, 58% and 26% for N1, 6%, 51%, and 43% for N2 and 5%, 44% and 51% for N3 ($p < 0.001$). Chemoradiation was the most commonly utilised neoadjuvant treatment modality across all nodal status. Mandard TRG after neoadjuvant therapy was significantly better in N0, with 25% either TRG 1 or 2, compared with 14% in N1, 12% in N2 and 8% in N3. Clinical and Pathologic Demographics per Nodal Burden are outlined in Table 4.1.1.

Table 4.1.1. Clinical characteristics of OAC patients included in this study.

	pN0 N=356	**pN1 N=154**	**pN2 N=47**	**pN3 N=145**	***P*-value**
Clinical characteristics					
Age, mean (SD)	63.62 (10.47)	62.97 (10.03)	65.02 (10.09)	63.22 (10.85)	0.64
Sex					
Female	62	24	6	28	0.71
Male	294	130	41	117	
BMI, kg m^{-2}, mean (SD)	27.47 (4.58)	27.32 (4.35)	28.65 (4.62)	26.81 (4.54)	0.78
Obese	218	97	33	74	0.15
Current smoker	156	6	18	49	0.38
Diabetes	4	18	8	16	0.74
Hypertension	106	40	9	39	0.43
Dyslipidemia	62	20	9	12	0.046
ASA grade,					
ASA I	139	57	13	51	
ASA II	166	78	23	77	0.37
ASA III	51	19	11	17	
Siewert Classification					
Siewert I	217	76	19	48	
Siewert II	77	48	11	39	**<0.001**
Siewert III	62	30	17	58	
Treatment characteristics					
Neoadjuvant therapy					

Surgery first	186	106	24	79	**0.005**
	170	48	23	66	
Neoadjuvant regimen					
Chemotherapy	59	39	7	39	**0.04**
Chemoradiation	127	67	17	40	
Surgery type					
2-stage esophagectomy	197	101	23	77	
3-stage esophagectomy	27	10	0	15	**<0.001**
Transhiatal	78	12	7	7	
esophagectomy	54	31	17	46	
Extended total					
gastrectomy					
Clinical and Pathologic Staging					
Clinical T stage					
1	112	14	2	4	
2	58	21	6	19	
3	183	114	38	114	**<0.001**
4	3	5	1	8	
Clinical N stage					
0	256	87	28	57	
1	87	57	15	73	**<0.001**
2	12	9	3	11	
3	1	1	1	4	
Proximal Margin Clear	353	149	46	133	**<0.001**
Distal Margin Clear	353	146	44	131	**<0.001**
Radial Margin Clear	305	112	36	71	**<0.001**
Lymphatic invasion	51	100	35	119	**<0.001**
Venous invasion	65	66	27	92	**<0.001**
Perineural invasion	25	35	16	50	**<0.001**
	110	59	23	84	**<0.001**

Poor or undifferentiated grade (poor versus other)	173	58	17	34	**<0.001**
Barrett's oesophagus	25	13	4	32	**<0.001**
Signet Ring	33	18	6	34	**<0.001**
Mucinous features	194	75	18	47	**<0.001**
Barrett's in Tumour					
Adverse feature grading					
No adverse features	184	25	3	7	
1 or 2 adverse features	151	90	24	64	**<0.001**
3 or 4 adverse features	21	39	20	74	
Pathologic stage					
(y)pT0	37	1	1	3	
(y)pT1	154	26	3	7	**<0.001**
(y)pT2	67	29	7	14	
(y)pT3	92	87	34	105	
(y)pT4	6	11	2	16	
Tumour regression grade N					
(%)	40	1	1	1	
TRG 1	51	20	5	12	**<0.001**
TRG 2	54	40	7	19	
TRG 3	33	33	8	30	
TRG 4	9	13	4	17	
TRG 5					
CAP					
R0	335	133	37	95	**<0.001**
R1	21	21	10	50	
RCPATH					
R0	302	109	34	79	**<0.001**
R1	54	45	13	66	

Recurrence	97	83	29	115	**<0.001**
Median Survival Months	Not reached	49.7 months	34.2 months	15.4 months	**<0.001**
1 Year Survival 3Year Survival 5 Year Survival	94 78 67	86 54 45	83 48 38	67 21 11	**<0.001**

N0=0 nodes involved, N1=1-2 nodes involved, N2=3-6 nodes involved, N3=7 or greater. BMI=Body mass index, ASA=American Society for Anaesthesiologists, CAP=College of American Pathologists, RCPATH=Royal College of Pathologists United Kingdom.

Adverse features of tumour biology including perineural invasion, vascular invasion, differentiation nodal positivity, and neoadjuvant treatment were significant by multivariate analysis on overall survival. (Table 4.1.2).

Table 4.1.2: Univariable and Multivariable Analysis for overall survival.

	Univariable			Multivariable		
	HR	CI	P value	HR	CI	P value
Barretts History	1.44	1.138-1.821	**<0.001**	1.680	0.919-3.072	0.09
Neoadjuvant treatment	1.528	1.211-1.928	**<0.001**	1.434	1.177-1.746	**<0.001**
pN (node negative vs positive)	1.577	1.104-1.747	**<0.001**	1.399	1.151-1.703	**<0.001**
Perineural Invasion	1.601	1.257-2.039	**<0.001**	1.475	1.125-1.935	**0.005**
Vascular Invasion	1.548	1.219-1.465	**<0.001**	0.527	0.316-0.879	**0.01**
Differentiation (Poor versus other)	1.584	1.245-2.017	**<0.001**	1.582	1.098-1.595	**0.02**

For the entire cohort classified by nodal status (Figure 4.1.1), the median overall survival was not reached for N0, 49.7 months for N1, 34.2 months for N2, and 15.4 months for N3 with 5- year survival of 67%, 45%, and 38% and 11% respectively ($p < 0.001$).

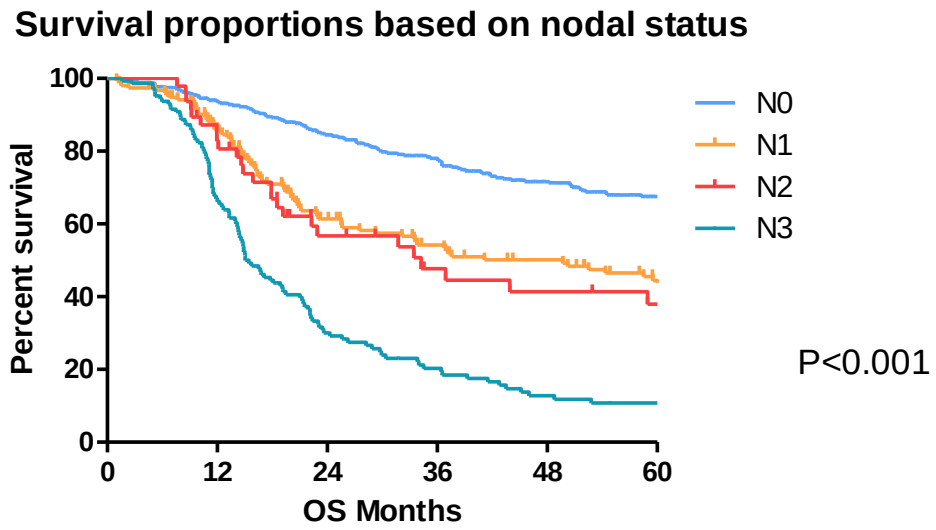

Overall number of surviving OAC patients based on nodal status.

	N0			N1			N2			N3		
Survival (years)	No at risk	Deaths	% survival	No at risk	Deaths	% survival	No at risk	Deaths	% survival	No at risk	Deaths	% survival
1	356	22	94	154	21	86	47	8	83	145	46	67
3	317	49	78	124	43	54	38	14	48	89	58	21
5	225	28	67	67	11	45	15	3	38	22	10	11

Fig. 4.1.1. Survival proportions of OAC patients based on nodal status (N0=node negative, N1=1-2 Nodes, N2=3-6 Nodes, N3=>7). Overall Survival was visualized using Kaplan–Meier curves. Log-rank (Mantel–Cox) tests were performed to assess median survival time differences between groups. Any nodal disease burden significantly reduces overall survival with proportional reduction per stage of dissemination. Median Survival; N0; Not Reached, N1; 49.7 months, N2; 34.23 months, N3; 15.43 months

Patients with positive clinical nodal status (based on Endoscopic Ultrasound and or Positron Emission tomography (PET)) but pathologically node negative had improved survival compared to those who were clinically and pathologically node positive ($p<0.001$) (Figure 4.1.2).

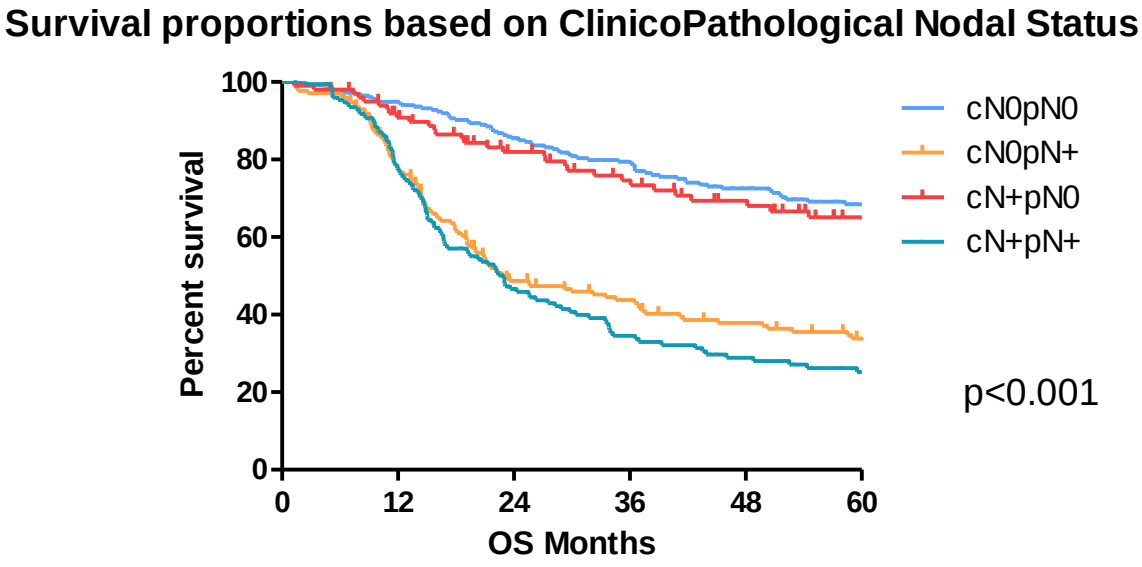

Overall survival of OAC patients based on Clinicopathological nodal status.

	cN0pN0			cN+pN0			cN0pN+			cN+pN+		
Survival (years)	No at risk	Deaths	% survival	No at risk	Deaths	% survival	No at risk	Deaths	% survival	No at risk	Deaths	% survival
1	256	13	95	100	9	91	172	38	77	174	37	78
3	231	35	79	86	14	75	126	52	44	125	63	35
5	166	21	68	59	7	65	61	13	34	43	11	26

Fig. 4.1.2. Survival proportions of OAC patients based on clinicopathological nodal status. Overall Survival was visualized using Kaplan–Meier curves. Log-rank (Mantel–Cox) tests were performed to assess median survival time differences between groups. Median Survival; cN0pN0; Not reached, cN+pN0; 124.6 months, cN0pN+; 22.93, cN+pN+; 22.5 months

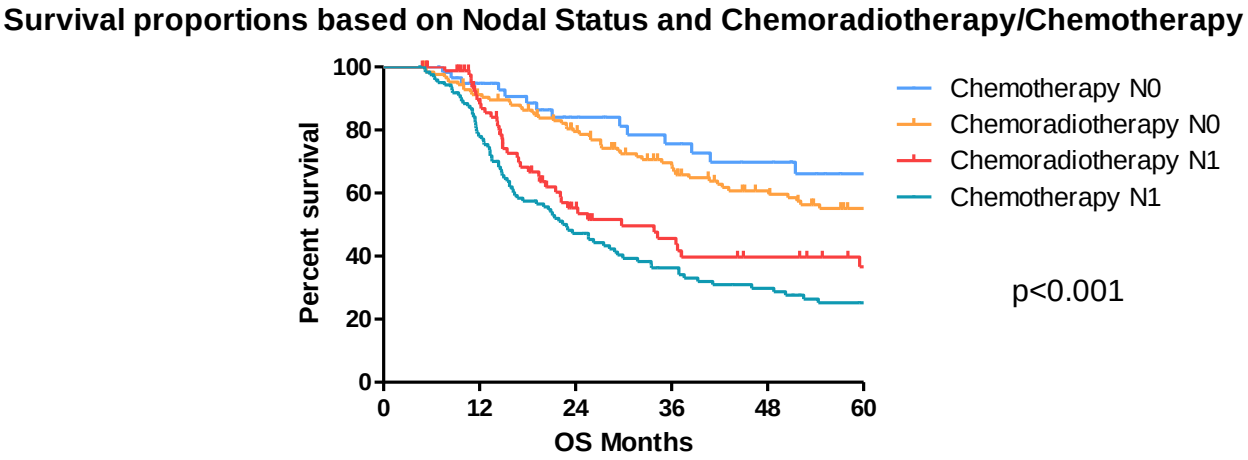

Overall survival of OAC patients based on nodal status and treatment received (chemoradiotherapy/chemotherapy).

	Chemotherapy N0			Chemoradiotherapy N0			Chemotherapy N+			Chemoradiotherapy N+		
Survival (years)	No at risk	Deaths	% survival	No at risk	Deaths	% survival	No at risk	Deaths	% survival	No at risk	Deaths	% survival
1	59	3	95	127	11	91	85	8	90	124	26	78
3	50	8	76	112	25	70	66	28	46	89	45	36
5	27	3	66	73	14	55	23	4	37	34	10	25

Fig. 4.1.3. Survival proportions of OAC patients based on nodal status and treatment received (chemoradiotherapy/chemotherapy). Overall Survival was visualized using Kaplan–Meier curves. Log-rank (Mantel–Cox) tests were performed to assess median survival time differences between groups. Median Survival; pN0 Chemotherapy; 79.2months, pN0 Chemoradiotherapy; 71.64 months, pN+ Chemotherapy; 22.9 months, pN+ Chemoradiotherapy; 29.73 months.

In patients treated with neoadjuvant chemotherapy the median survival in patients who were pN0 was 79.2 months compared to 71.64 months in those treated with chemoradiotherapy. On the contrary, in patients who were pN+ treated with neoadjuvant

chemotherapy, the median survival was 22.9 months compared to 29.73 months in those treated with chemoradiotherapy (Figure 4.1.3). Interestingly, patients who were node negative had a higher median survival than those with a pCR on final histological analysis to neoadjuvant therapy and significantly better than those who were node positive on final histology (p<0.001) (Figure 4.1.4).

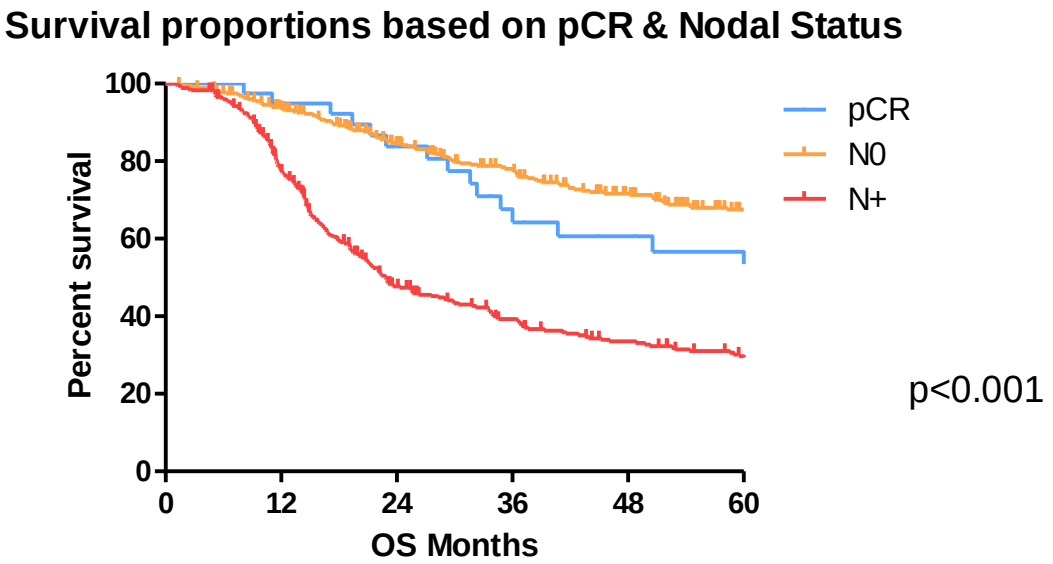

Fig. 4.1.4. Survival proportions of OAC patients based on nodal status and pathologic complete response. pCR refers to complete pathological response on histological analysis, N0-node negative, N+-node positive. Significantly reduced overall survival with nodal disease. Median Survival; pCR; Not reached, N0; 124.6 months, N+; 22.9 months.

4.2.2 Inhibitory immune checkpoint receptors and ligands are expressed at significantly higher levels on tumour-infiltrating T cells compared to tumour-draining lymph nodes.

Inhibitory ICs play important roles in suppressing anti-tumour immunity and with the recent approval of two PD-1 inhibitors, pembrolizumab and nivolumab, for treating oesophagogastric adenocarcinomas, it is important we develop a deeper understanding of

IC expression profiles in adenocarcinoma patients. IC expression on T cells infiltrating OAC tumour tissue and in the TDLN were profiled to determine the level of target expression in multimodal therapy. Representative dot plots for gating strategy are demonstrated in figure 4.2.1.

Overall, a higher percentage of T cells expressing inhibitory ICs was found within tumour tissues compared to TDLNs and this pattern was consistent across $CD4^+$ T helper and $CD8^+$ cytotoxic T cell compartments (Figure 4.2.2). Significantly higher percentages of $CD3^+CD4^+TIM\text{-}3^+$ cells were found in tumour tissue compared with TDLNs (6.5 ± 2.3 vs. 0.7 ± 0.4%, $p<0.05$). Similar trends were observed for $CD3^+CD4^+PD\text{-}1^+TIM\text{-}3^+$ cells (4.5 ± 1.4 vs. 0.5 ± 0.2%, $p<0.05$), (Figure 4.2.2).

A higher percentage of $CD3^+CD8^+PD\text{-}1^+$ cells were located intratumourally compared to the corresponding lymph node tissue (19.9 ± 5.9 vs 6.09 ± 2.1%, $p<0.05$) (Figure 4.2.2). Similar trends were observed for $CD3^+CD8^+TIM\text{-}3^+$ cells (8.5 ± 3.6 vs 1.7 ± 0.7%, $p<0.05$) (Figure 4.2.2). Interestingly, $CD3^+CD8^+$ cells co-expressing both PD-1 and PD-L1 were found at a higher frequency in tumour-infiltrating tissue compared with TDLNs (12.5 ± 6.0 vs. 0.2 ± 0.1%, $p<0.05$). Similar trends were observed for $CD3^+CD8^+TIGIT^+TIM\text{-}3^+$ cells (17.2 ± 7.6 vs. 0.8 ± 0.4%, $p<0.05$) (Figure 4.2.2).

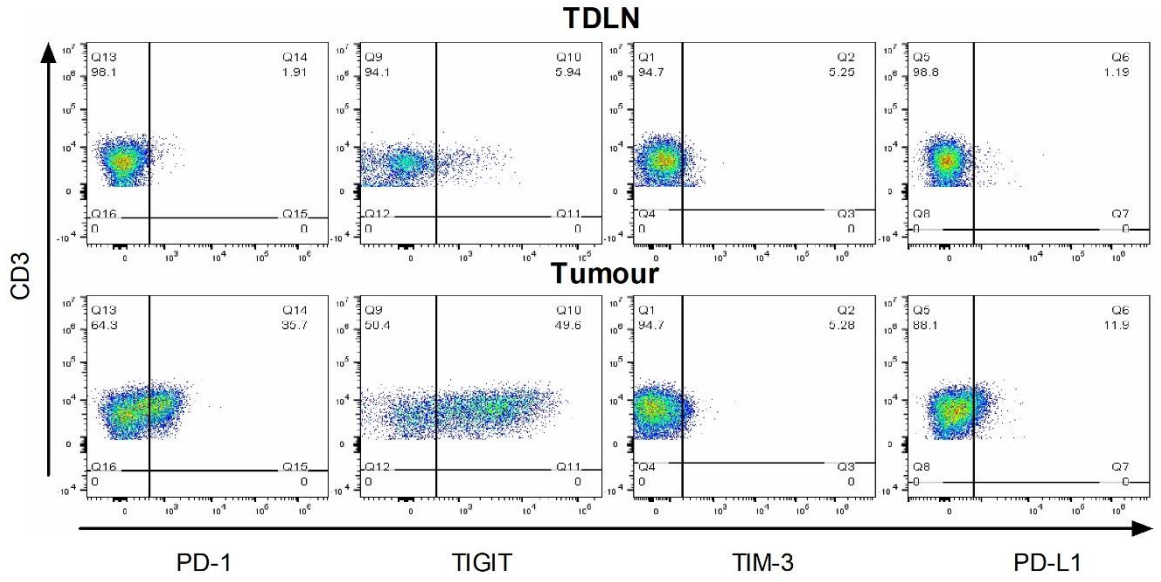

Figure 4.2.1; Representative dot plots of gating strategy used for TDLN and tumour expression of immune checkpoints PD-1, TIGIT, TIM-3 and PD-L1.

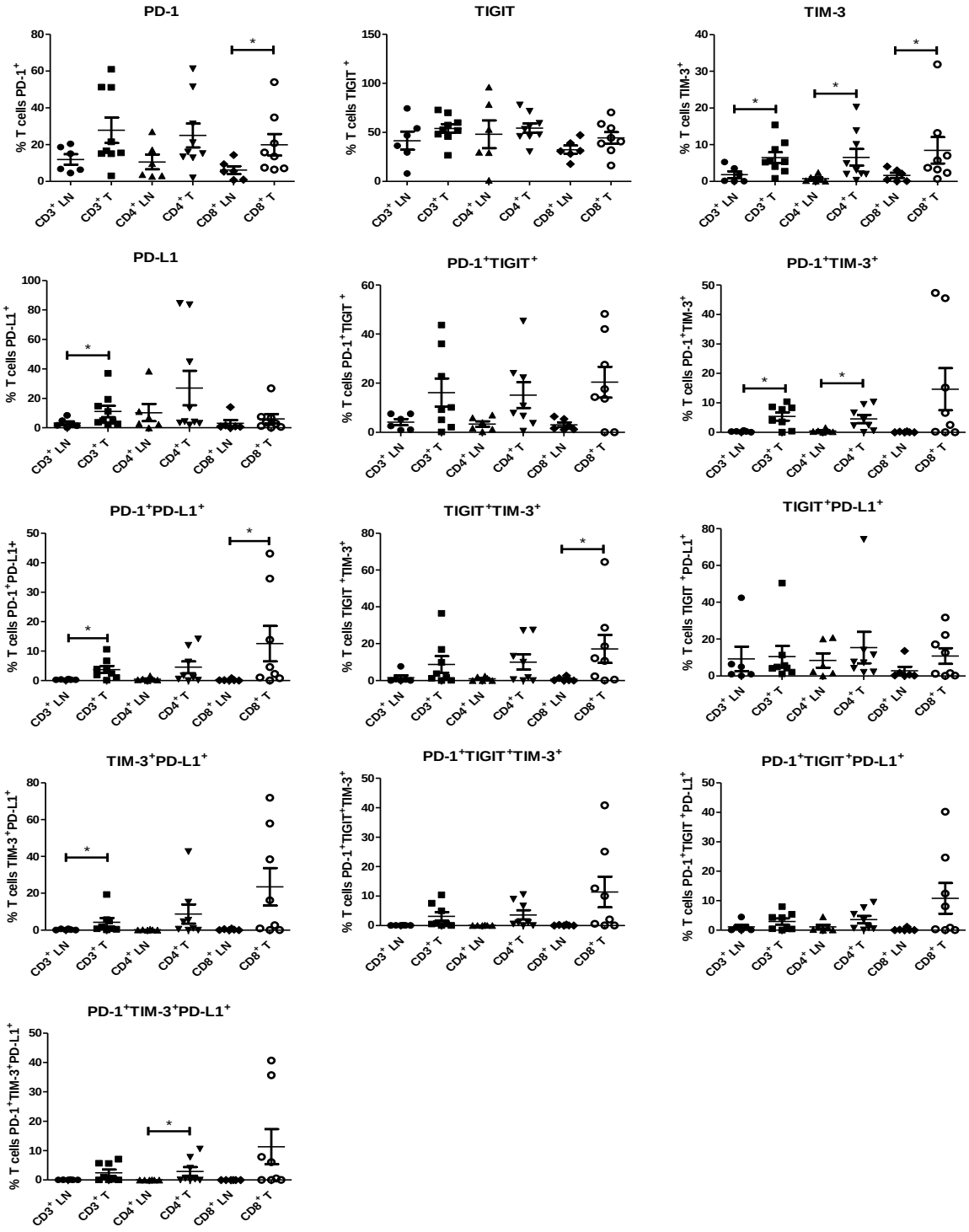

Fig. 4.2.2. Inhibitory IC receptors and ligands are expressed at significantly higher levels on tumour-infiltrating T cells compared to T cells present in tumour-draining lymph nodes. $CD3^+$, $CD3^+CD4^+$, $CD3^+CD8^+$ cells in tumour-draining lymph nodes (n=6) and infiltrating tumour tissues (n=9) in OAC patients were screened for the surface expression of PD-1^+, TIGIT$^+$, TIM-3^+ and PD-L1^+ *ex vivo* by flow cytometric analysis. Tumour draining lymph nodes and tumour specimens were post-treatment and taken at surgical resection. Mann Whitney test was used to compare expression between lymph node and tumour compartment. *$p<0.05$. LN: lymph node and T: tumour.

4.2.3 Ionising radiation has a differential impact on cytokine expression in the tumour draining lymph node with a significantly higher expression of IL-2 and IL-10.

Table 4.2. Samples were collected from patients at surgical resection and handled according to MSD (Meso Scale Diagnostics, USA) multiplex protocols. **Analyte in lymph node with or without radiation.** ***Wilcoxon rank test.***

Analyte	LNM 0 Gy vs 2 Gy **N=5** *p Value*	LNM 2 Gy vs 4 Gy **N=5** *p Value*	LNM 0 Gy vs 4 Gy **N=6** *p Value*
Angiogenesis and vascular injury			
bFGF	0.25	0.37	0.62
Flt-1	0.18	0.62	0.81
PIGF	0.12	0.12	0.62
Tie-2	0.25	0.37	0.87
VEGF-C	0.25	0.62	0.87
VEGF-D	0.25	1	0.81
CRP	0.31	0.82	1
SAA	0.62	1	0.81
ICAM-1	0.31	0.62	1
VCAM-1	0.06	0.31	0.62
Cytokines, Chemokines and Growth Factors			
IL-17A/F	0.62	0.75	0.75
IL-17B	0.25	0.75	0.5
IL-17C	0.06	0.62	0.06
IL-17D	0.31	0.31	0.81
IL-3	0.12	0.62	0.62
IL-9	0.25	0.75	0.25
TSLP	0.62	0.12	0.12
IL-1RA	0.31	0.43	0.62
GM-CSF	0.81	0.43	0.31
IL-12p40	0.87	0.25	1
IL-15	0.06	0.81	0.43
IL-16	0.31	1	0.31
IL-17A	1	0.81	0.81
IL-1α	0.12	0.43	0.81
IL-5	0.62	0.81	0.31
IL-7	0.81	0.81	0.62
TNF-β	0.06	1	0.31
VEGF	1	0.81	0.06
IL-21	0.62	0.43	0.62
IL-22	0.87	0.32	0.12
IL-23	1	1	1

IL-27	0.12	1	0.31
IL-31	0.12	0.62	0.12
MIP-3a	0.43	0.12	0.31
IFN-γ	0.62	0.06	0.02
IL-10	0.04	0.12	0.12
IL-12p70	0.81	0.62	0.43
IL-13	1	0.81	0.31
IL-1B	0.06	0.06	0.06
IL-2	0.03	0.02	0.06
IL-4	0.81	0.62	0.31
IL-6	0.18	0.62	0.81
IL-8	0.81	0.31	0.31
TNFα	0.18	0.81	0.62
Eotaxin	0.12	0.04	0.06
Eotaxin-3	0.06	0.43	0.06
IP-10	0.43	1	0.18
MCP-1	1	0.81	0.62
MCP-4	0.62	1	0.81
MDC	0.31	0.31	0.31
MIP-1α	1	0.31	1
MIP-1β	0.62	0.81	0.81
TARC	1	0.43	1

There was a significantly higher expression of IL-2 and IL-10 in the draining lymph node post 2 Gy ionising radiation ($p<0.05$) compared to non-irradiated lymph node tissue and a significantly higher expression of IFN-γ post 4 Gy ionising radiation compared to non irradiated tissue ($p<0.05$) (Table 4.2), with no significant difference between al other analytes.

4.2.4 Correlations between the tumour conditioned media, lymph node conditioned media and clinicopathological features

Within TDLNs, the frequency of T cells expressing inhibitory ICs positively correlated with a worse TRG (TRG 3 and above), advanced clinical T stage and lymphovascular invasion and negatively correlated with treatment response determined by PET/CT (Figure 4.3.1: Corr plots generated in collaboration with Fiona O'Connell, Dept. Sugery, TCD).

The percentage of $CD3^+CD8^+PD\text{-}1^+TIGIT^+$ cells in TDLNs positively correlated with TRG ($p<0.05$), (Figure 4.3.1). Similarly, the percentage of $CD3^+$ cells in the TDLN expressing TIM-3 and PD-1 and $CD3^+CD4^+$ cells expressing TIM-3 positively correlated with advanced clinical T stage ($p<0.05$), (Fig 4.3.1). The percentage of T cells expressing inhibitory ICs within TDLNs positively correlated with lymphovascular invasion (Figure 4.3.1); $CD3^+TIM\text{-}3^+$, $CD3^+TIM\text{-}3^+PD\text{-}L1^+$, $CD3^+CD4^+TIM\text{-}3^+$, $CD3^+CD8^+TIM\text{-}3^+$, $CD3^+CD8^+TIGIT^+TIM\text{-}3^+$, $CD3^+CD8^+TIM\text{-}3^+PD\text{-}L1^+$ and $CD3^+CD8^+PD\text{-}1^+TIGIT^+TIM\text{-}3^+$ cells in TDLNs positively correlated with lymphovascular invasion ($p<0.05$) (Figure 4.3.1).

Negative correlations were observed for the percentage of $CD3^+PD\text{-}1^+TIGIT^+$, $CD3^+CD4^+TIGIT^+$, $CD3^+CD4^+PD\text{-}1^+TIGIT^+$, $CD3^+CD4^+PD\text{-}1^+TIM\text{-}3^+$ and $CD3^+CD4^+TIGIT^+PD\text{-}L1^+$ cells within the TDLN with treatment response, measured by PET/CT (Figure 4.3.1). $CD3^+CD4^+PD\text{-}1^+TIGIT^+$ cells in TDLNs negatively correlated with clinical nodal involvement ($p<0.05$) (Figure 4.3.1).

Additionally, tumour-infiltrating $CD3^+PD\text{-}1^+TIGIT^+$ and $CD3^+CD4^+PD\text{-}1^+TIGIT^+$ cells negatively correlated with TRG ($p<0.05$), (Figure 4.3.2). $CD3^+CD8^+PD\text{-}1^+$ and $CD3^+CD8^+TIGIT^+$ cells positively correlated with tumour nodal metastasis, determined by EUS and PET/CT (Figure 4.3.2).

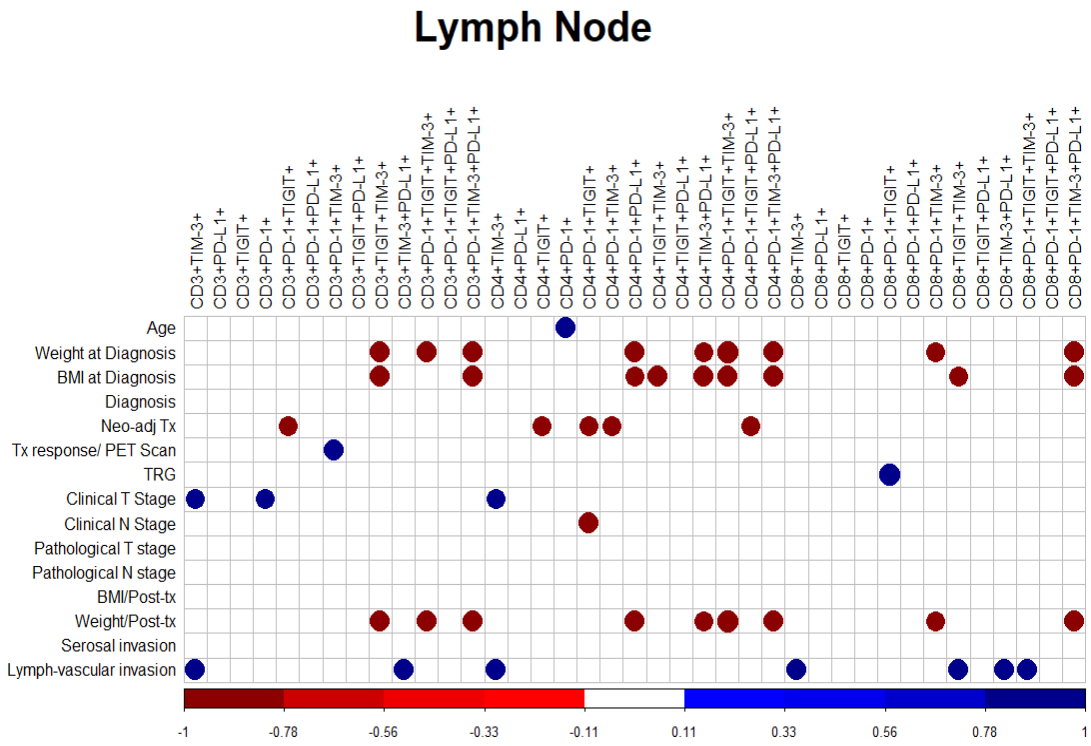

Fig. 4.3.1. The percentage of CD3$^+$TIM-3$^+$ and CD3$^+$PD-1$^+$ T cells present in tumour-draining lymph nodes positively correlates with tumour stage determined by PET/CT. Corrplots illustrating the correlation values for the percentage of CD3$^+$, CD3$^+$CD4$^+$ and CD3$^+$CD8$^+$ cells expressing inhibitory ICs present in tumour draining lymph nodes correlated with clinical demographics and characteristics. Patient clinical features included age, weight (pre-treatment, kg), BMI (pre-treatment, kg/m^2), treatment response (determined by radiographic features using PET/CT), tumour regression grade (TRG), clinical tumour stage and nodal involvement, pathological tumour stage and nodal involvement, BMI (post-treatment, kg/m^2), weight (post-treatment, kg), serosal invasion and lymph-vascular invasion. Expression of ICs was determined by flow cytometry. Blue indicates a positive correlation, red negative correlation. Only significant data are shown. *p<0.05.

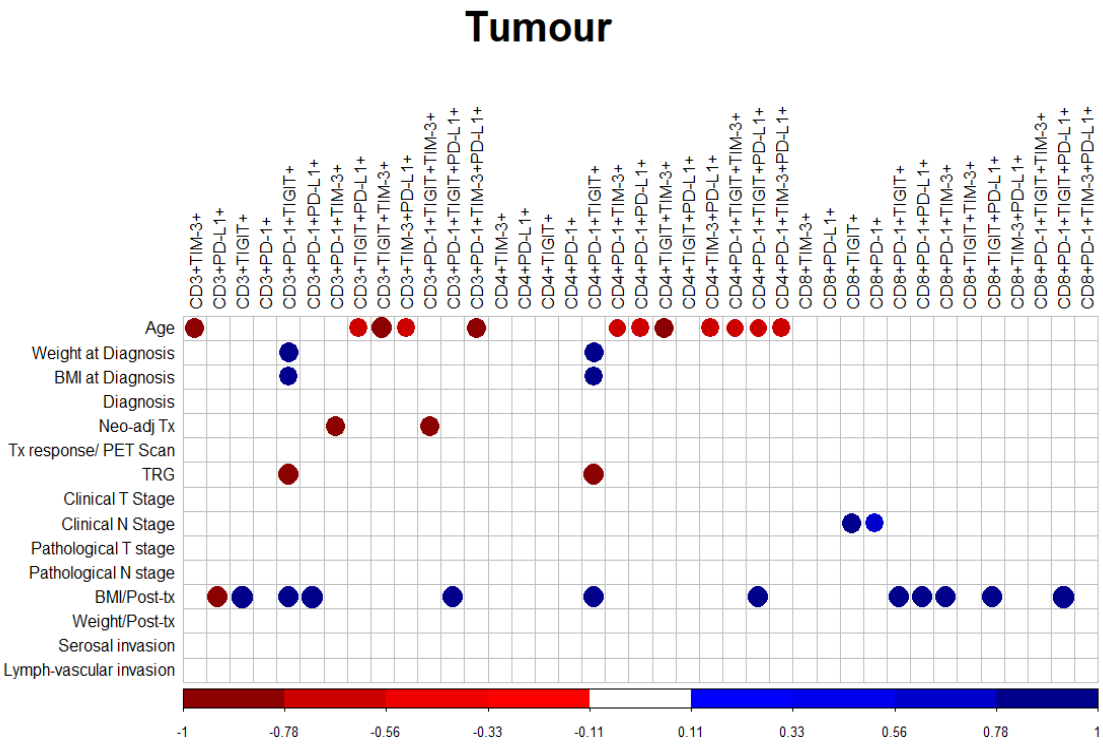

Fig. 4.3.2. The percentage of tumour-infiltrating CD8$^+$PD-1$^+$ and CD8$^+$TIGIT$^+$ T cells positively correlates with tumour nodal metastasis determined by PET/CT. Corrplots illustrating the correlation values for the percentage of CD3$^+$, CD3$^+$CD4$^+$ and CD3$^+$CD8$^+$ cells expressing inhibitory ICs present in infiltrating-tumour tissue in OAC patients correlated with clinical demographics and characteristics. Patient clinical features included age, weight (pre-treatment, kg), BMI (pre-treatment, kg/m^2), tumour type (OAC=0 or OGJ=1), neo-adjuvant treatment received (CROSS=0 and FLOT=1), treatment response (determined by radiographic features using PET/CT), tumour regression grade (TRG), clinical tumour stage and nodal involvement, pathological tumour stage and nodal involvement, BMI (post-treatment, kg/m^2), weight (post-treatment, kg), serosal invasion and lymph-vascular invasion. Expression of ICs was determined by flow cytometry. Blue indicates a positive correlation, red negative correlation. Spearman correlation. Significant data shown only. Spearman r=0.4-0.59 moderate, 0.6-0.79 strong and 0.8-1 very strong. *p<0.05.

4.2.5 IFN-γ and IL-21 are significantly lower in the TME compared to the LNME in OAC patients

Lymph node conditioned media (LNCM) and Tissue conditioned media (TCM) from OAC patients were screened for a panel of cytokines and chemokines with important roles in either promoting or inhibiting anti-tumour immunity to test the hypothesis that the tumour microenvironment confers a more immunosuppressive milieu.

Levels of the anti-tumour cytokine IFN-γ was lower in the TME (17.4 ± 16.4) compared to the LNME (67.9±63.7) $p<0.05$, However, the levels of IL-9, IL-27, and bFGF were significantly higher within the TME (6.32±2.92, 76.92±97.3, 102.4±112,) compared to the LNME (2.11±1.9, 51.63±94.6, 45.28±44.32) of OAC patients ($p<0.05$) (Figure 4.4) The levels of all other analytes were detected at comparable levels between the LNCM and TCM from OAC patients (Table 4.3).

Correlative analysis was also conducted in collaboration with Fiona O' Connell to determine if the levels of these anti-tumour or pro-tumour analytes correlated with clinical features of the tumour. Levels of pro-inflammatory cytokines; IL-1β, TNF-α, TNF-β and IL-17-A/F in the LNCM negatively correlated with advanced clinical T stage ($p<0.05$). Moreover, the levels of chemokines responsible for recruiting pro-inflammatory immune cells including Eotaxin, MCP4, MDC, MIP-1α and TARC in LNCM also negatively correlated with advanced clinical T stage ($p<0.05$). In addition, high levels of IL-27 and IL-5 and the chemokine IL-16 (responsible for recruiting CD4 T cells) in the LNCM negatively correlated with advanced clinical tumour stage ($p<0.05$) (Figure 4.5.1).

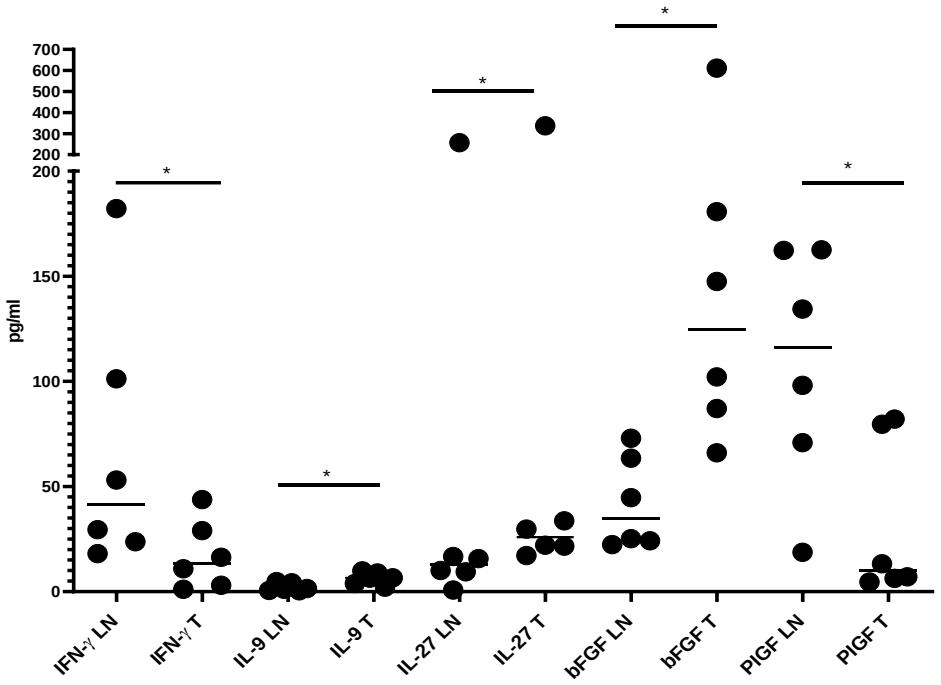

Fig. 4.4. Levels of IFN-γ, IL-9, IL-27 and soluble bFGF were significantly higher within the TME compared to the LNME, whereas, PIGF is significantly higher within the LNCM of OAC patients. Tumour-draining lymph node (n=6) and tumour tissue biopsies (n=6) from OAC patients were cultured for 24h *ex vivo* to generate lymph node conditioned media (LNCM) and tumour conditioned media (TCM), respectively. The LNCM and TCM was screened for a panel of pro-angiogenic and vascular damage mediators using a 54-multiplex assay. LNCM = lymph node conditioned media, TCM = tumour conditioned media. LN: lymph node and T: tumour. *Wilcoxon rank test*, *<0.05.

Analyte	Tumour pg/ml (SD)	Lymph Node pg/ml (SD)	P Value n=6 per group Wilcoxon matched-pairs sign rank test
Angiogenesis			
VEGF-C	19.87 (12.5)	12.21 (8.576)	0.44
VEGF-D	17.87 (25.82)	23.92 (18.67)	0.68
CRP	6532 (10565)	7783 (6127)	1
ICAM-1	17082 (29191)	13791 (15118)	0.69
SAA	467.4 (351)	1797 (1041)	0.07
VCAM-1	21811 (39119)	18926 (24064)	0.69
Cytokines, Chemokines and Growth Factors			
IL-10	553.8 (503.9)	728.7 (557.2)	0.43
IL-12p70	10.14 (7.28)	15.52 (8.99)	0.21
IL-13	12.28 (4.91)	33.75 (37.33)	0.27
IL-1β	28.15 (35.64)	25.73 (52.2)	0.98
IL-2	4.044 (2.39)	4.76 (2.18)	0.69
IL-4	5.79 (4.27)	9.31 (4.58)	0.16
IL-6	1049 (892.7)	1513 (756.8)	0.22
IL-8	1420 (517.3)	1364 (635.2)	0.84
TNFα	11.02 (6.52)	10.06 (5.84)	0.98
GM-CSF	51.1 (85.44)	33.97 (66.85)	0.44
IL-12p40	48.51 (77.96)	38.57 (51.39)	0.84
IL-15	1.71 (1.91)	1.01 (1.22)	0.98
IL-16	919.6 (1372)	1690 (1241)	0.44
IL-17A	18.03 (25.08)	19.88 (19.24)	0.84
IL-1a	56.81 (101.2)	23.24 (42.84)	0.44
IL-5	1.29 (1.92)	1.13 (1.31)	0.56

IL-7	1.86 (1.09)	4.77 (6.92)	0.43
TNFβ	1.12 (1.99)	1.31 (2.32)	0.31
IL-17A/F	8.45 (7.3)	4.44 (7.98)	0.69
IL-17B	8.08 (7.06)	2.232 (2.145)	0.13
IL-17C	15.94 (19.33)	4.24 (2.94)	0.16
IL-17D	46.29 (45.92)	48.95 (30.54)	0.97
IL-1RA	3268 (1789)	1623 (1851)	0.56
IL-3	28.69 (22.91)	10.91 (9.47)	0.31
TSLP	20.42 (19.53)	34.38 (35.83)	0.43
IL-21	0.32 (0.28)	1.09 (1.14)	0.06
IL-22	3.83 (6.4)	128 (334.7)	0.69
IL-23	1.26 (0.92)	4.06 (7.78)	0.84
IL-31	0.07 (0.05)	0.1 (0.08)	0.31
MIP-3α	280.2 (579)	211 (330.3)	0.69

Table 4.3 Analyte in matched tumour and lymph node. ***Wilcoxon rank test.***

Tumoural levels of IL-9 negatively correlated with clinical nodal staging as determined by pre-operative staging investigations EUS and PET/CT. Additionally, members of the pro-inflammatory IL-17 family including IL-17A/F, IL-17B and IL-17C as well as anti-angiogenic IL-3 in the TME negatively correlated with clinical nodal staging as determined by EUS and PET/CT.

In contrast with the LNME, high levels of pro-inflammatory chemokines in the TME including Eotaxin-3, MCP-1, MCP-4 and TARC positively correlated with adverse tumour features such as lymphatic and vascular invasion. The levels of pro-inflammatory TNF-α in the TME positively correlated with tumour nodal metastasis ($p<0.05$) (Figure 4.5.1).

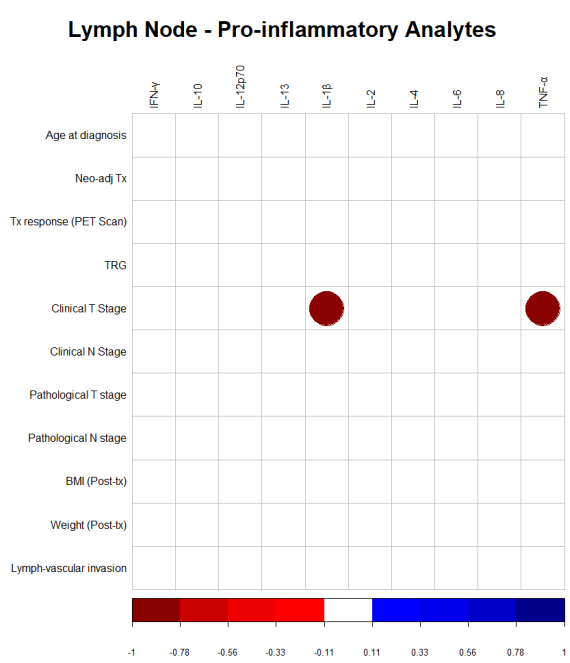
Lymph Node - Pro-inflammatory Analytes
IFN-γ
IL-10
IL-12p70
IL-13
IL-1β
IL-2
IL-4
IL-6
IL-8
TNF-α
Age at diagnosis
Neo-adj Tx
Tx response (PET Scan)
TRG
Clinical T Stage
Clinical N Stage
Pathological T stage
Pathological N stage
BMI (Post-tx)
Weight (Post-tx)
Lymph-vascular invasion
-1
-0.78
-0.56
-0.33
-0.11
0.11
0.33
0.56
0.78
1

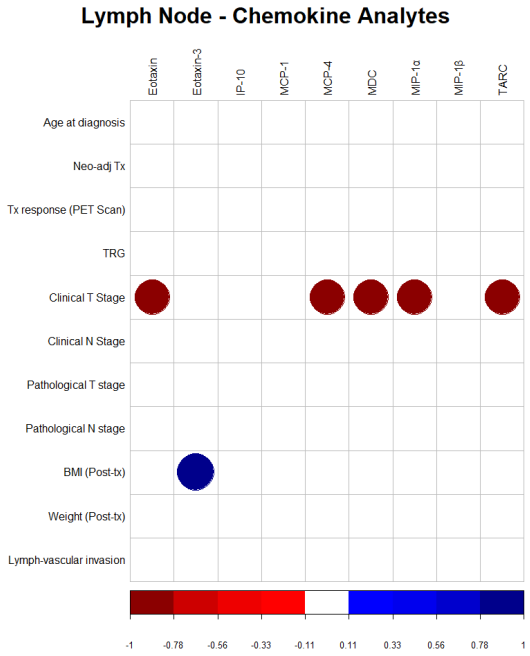
Lymph Node - Chemokine Analytes
Eotaxin
Eotaxin-3
IP-10
MCP-1
MCP-4
MDC
MIP-1α
MIP-1β
TARC
Age at diagnosis
Neo-adj Tx
Tx response (PET Scan)
TRG
Clinical T Stage
Clinical N Stage
Pathological T stage
Pathological N stage
BMI (Post-tx)
Weight (Post-tx)
Lymph-vascular invasion
-1
-0.78
-0.56
-0.33
-0.11
0.11
0.33
0.56
0.78
1

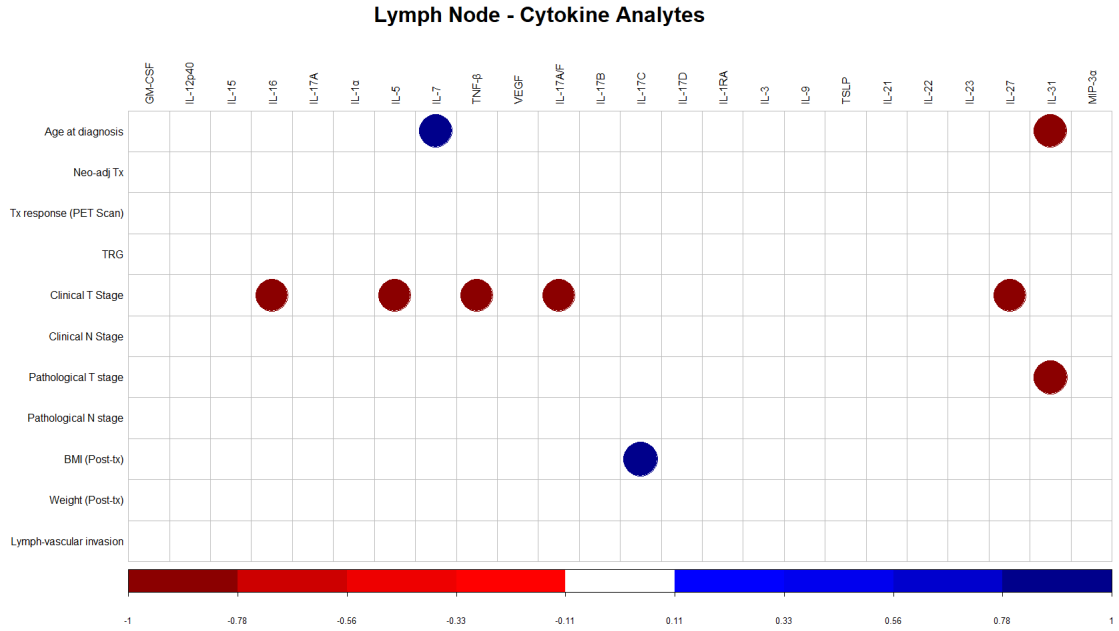
Lymph Node - Cytokine Analytes
GM-CSF
IL-12p40
IL-15
IL-16
IL-17A
IL-1α
IL-5
IL-7
TNF-β
VEGF
IL-17A/F
IL-17B
IL-17C
IL-17D
IL-1RA
IL-3
IL-9
TSLP
IL-21
IL-22
IL-23
IL-27
IL-31
MIP-3α
Age at diagnosis
Neo-adj Tx
Tx response (PET Scan)
TRG
Clinical T Stage
Clinical N Stage
Pathological T stage
Pathological N stage
BMI (Post-tx)
Weight (Post-tx)
Lymph-vascular invasion
-1
-0.78
-0.56
-0.33
-0.11
0.11
0.33
0.56
0.78
1

Fig. 4.5.1. Levels of pro-inflammatory cytokines IL-1β and TNF-α in tumour-draining lymph nodes inversely correlated with clinical T stage. Corrplots illustrating the correlation values for the levels of pro-inflammatory mediators, chemokines and cytokines in OAC tumour-draining lymph nodes correlated with clinical demographics and characteristics. Patient clinical features included age, weight (pre-treatment, kg), BMI (pre-treatment, kg/m^2), tumour type (OAC=0 or OGJ=1), neo-adjuvant treatment received (CROSS=0 and FLOT=1), treatment response (determined by radiographic features using PET/CT), tumour regression grade (TRG), clinical tumour stage and nodal involvement, pathological tumour stage and nodal involvement, BMI (post-treatment, kg/m^2), weight (post-treatment, kg), serosal invasion and lymph-vascular invasion. Blue indicates a positive correlation, red negative correlation. Spearman correlation. Significant data shown only. Spearman r; 0.4-0.59 moderate, 0.6-0.79 strong and 0.8-1 very strong. *$p<0.05$.

Anti-tumour IL-15 within the TME negatively correlated with pathological T stage ($p<0.05$), whereas, VEGF levels negatively correlated with pathological T stage ($p<0.05$) (Figure 4.5.1). The levels of IP-10 and IL-31 positively correlated with lymphatic and vascular invasion and pathological nodal status, respectively ($p<0.05$), (Figure 4.5.2).

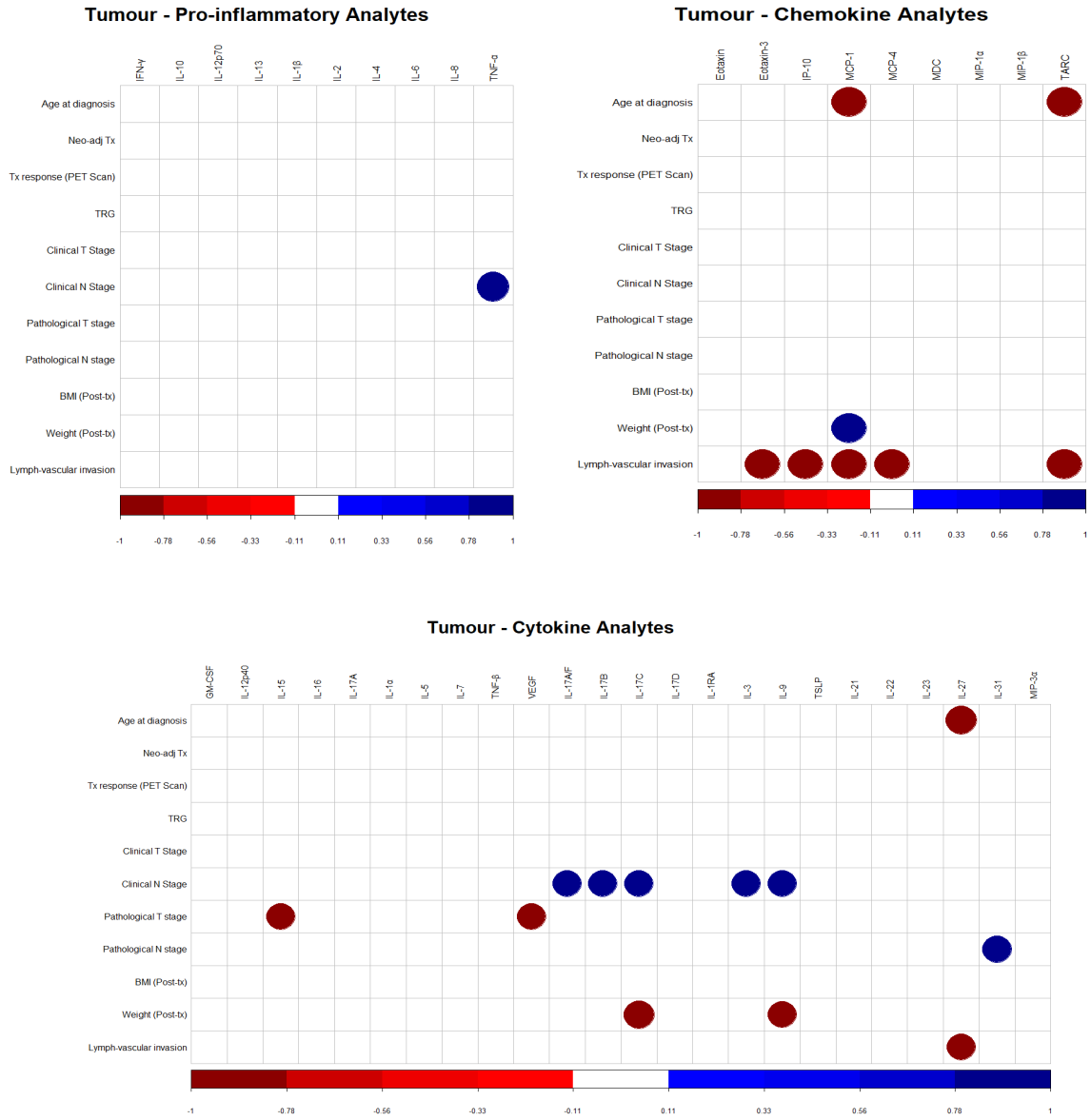

Fig. 4.5.2. A Th17 cytokine signature in OAC tumour tissue positively correlates with clinical T stage. Corrplots illustrating the correlation values for the levels of pro-inflammatory mediators, chemokines and cytokines in OAC tumour correlated with clinical demographics and characteristics. Patient clinical features included age, weight (pre-treatment, kg), BMI (pre-treatment, kg/m^2), tumour type (OAC=0 or OGJ=1), neo-adjuvant treatment received (CROSS=0 and FLOT=1), treatment response (determined by radiographic features using PET/CT), tumour regression grade (TRG), clinical tumour stage and nodal involvement, pathological tumour stage and nodal involvement, BMI (post-treatment, kg/m^2), weight (post-treatment, kg), serosal invasion and lymph-vascular invasion. Blue indicates a positive correlation, red negative correlation. Spearman correlation. Significant data shown only. Spearman r 0.4-0.59 moderate, 0.6-0.79 strong and 0.8-1 very strong. *p<0.05.

The LNME and TME was assessed for pro-angiogenic and vascular damage analytes and levels of soluble bFGF was significantly higher within the TME compared with the LNME ($p<0.05$). Interestingly, PIGF was significantly higher within the LNME than the TME of OAC patients ($p<0.05$). Flt-1 within the LNME negatively correlated with advanced clinical tumour stage ($p<0.05$) (Figure 4.6).

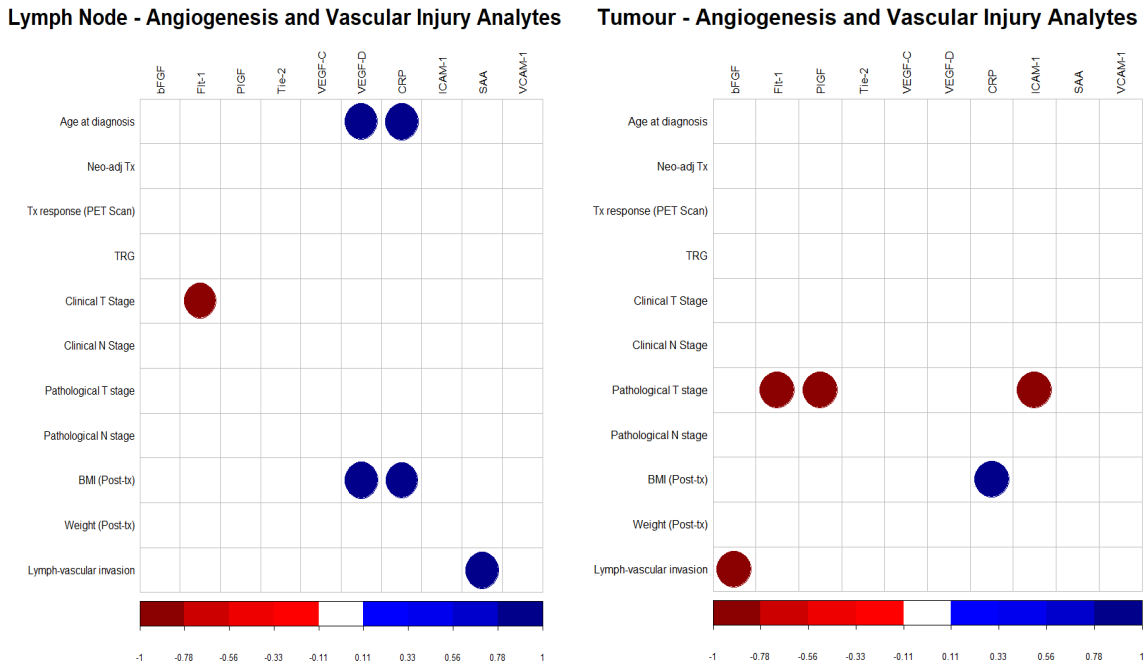

Figure 4.6. Levels of SAA in OAC tumour-draining lymph nodes positively correlate with lymphovascular invasion. Corrplots illustrating the correlation values for the levels pro-angiogenic and vascular injury cytokines in OAC tumour-draining lymph nodes and OAC tumour tissue correlated with clinical demographics and characteristics. Patient clinical features included age, weight (pre-treatment, kg), BMI (pre-treatment, kg/m^2), tumour type (OAC=0 or OGJ=1), neo-adjuvant treatment received (CROSS=0 and FLOT=1), treatment response (determined by radiographic features using PET/CT), tumour regression grade (TRG), clinical tumour stage and nodal involvement, pathological tumour stage and nodal involvement, BMI (post-treatment, kg/m^2), weight

(post-treatment, kg), serosal invasion and lymph-vascular invasion. Expression of ICs was determined by flow cytometry. Blue indicates a positive correlation, red negative correlation. Spearman correlation. Significant data shown only. Spearman r 0.4-0.59 moderate, 0.6-0.79 strong and 0.8-1 very strong. *$p<0.05$.

SAA levels in the LNME positively correlated with lymphovascular invasion. Similarly, tumour levels Flt-1, PIGF and ICAM-1 negatively correlated with pathological tumour stage ($p<0.05$). Additionally, bFGF levels negatively correlated with lymphovascular invasion ($p<0.05$), (Figure 4.6).

4.2.6 A pro-inflammatory and pro-angiogenic TME identifies OAC patients with reduced Overall Survival (OS).

Using the same panel of cytokines and pro-angiogenic mediators that were profiled in the LNCM and TCM from OAC patients, we also investigated the association between the level of these analytes in OAC tumour tissue with OS at the mRNA level using data from The Cancer Genome Atlas (TCGA). Interestingly, we found that high levels of pro-inflammatory and pro-angiogenic IL-8 ($p=0.0246$), IL-6 ($p=0.0246$) and Flt1 ($p=0.0269$) identified OAC patients with a reduced OS (Figure 4.7.1). No other significant correlations with survival outcomes were identified.

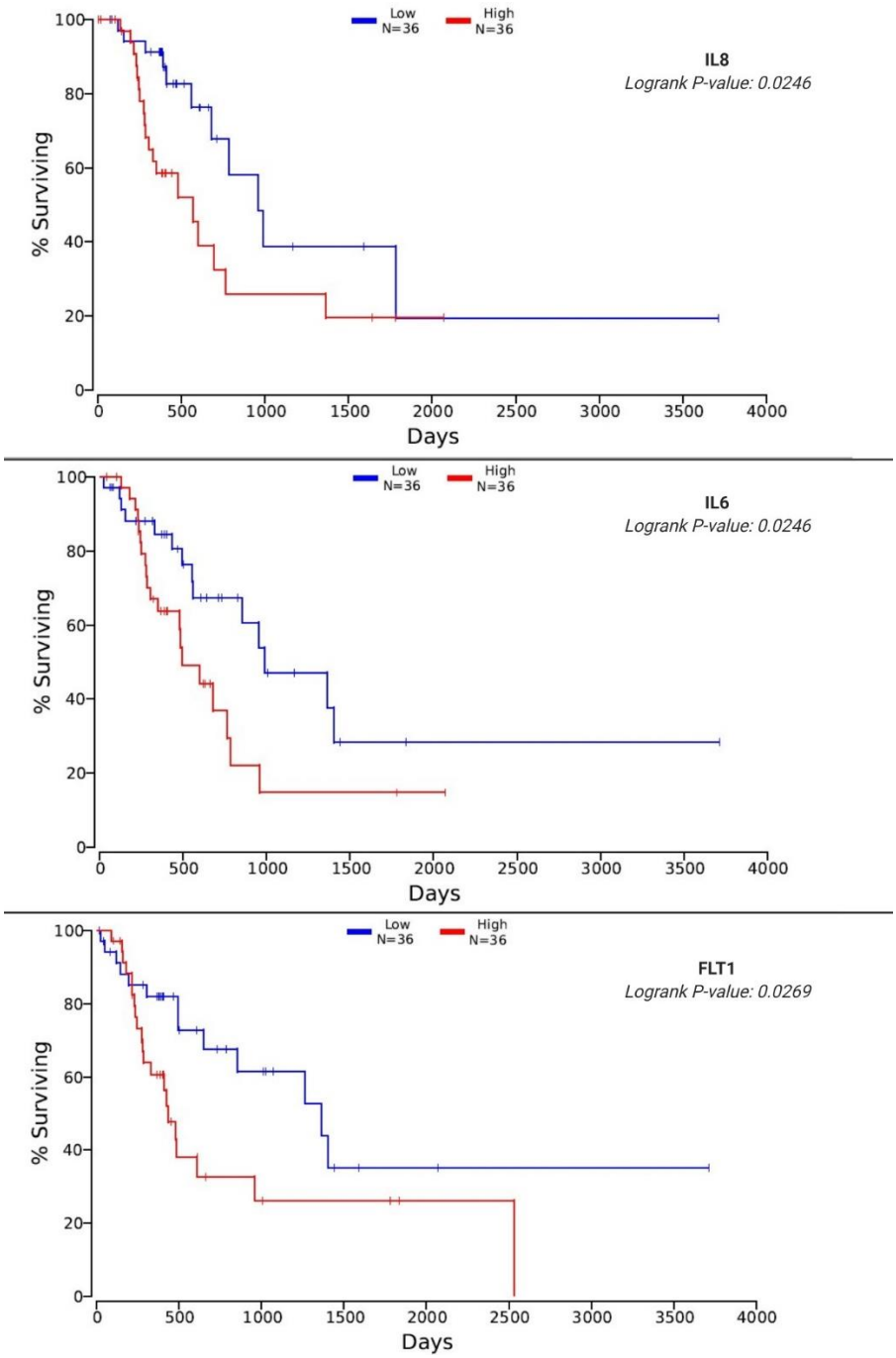

Fig. 4.7.1: High levels of IL-8, IL-6 and Flt1 mRNA in OAC tumour tissue identify OAC patients with reduced OS. Kaplan Meier curves showing OAC patients with low versus high mRNA levels of IL-8, IL-6 and Flt1 in OAC tumour tissue against OS in days (n=72). Overall Survival was visualized using Kaplan–Meier curves. Log-rank (Mantel–Cox) tests were performed to assess median survival time differences between groups.

Moreover, we also investigated whether mutations in these analytes from OAC tumour tissue were associated with a reduced PFS and OS using data from the TCGA. Mutations in genes mediating pro-inflammatory processes including CCL26, IL-31 and IL-17C as well as mutations in CCL22, a Treg chemotactic factor were associated with reduced PFS. (Figure 4.7.2, $p<0.05$).

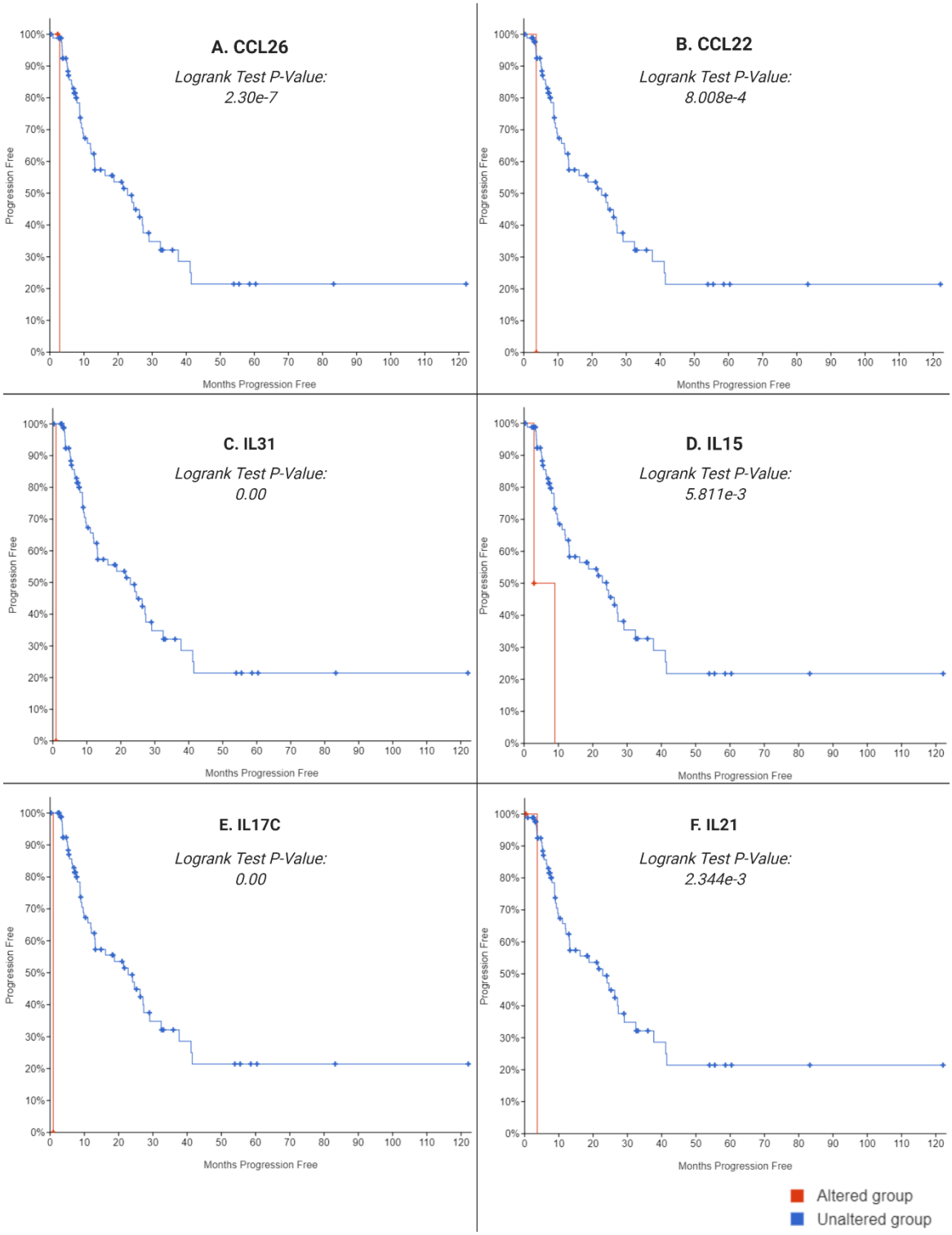

Fig. 4.7.2: Mutations in CCL26, CCL22, IL-31, IL-15, IL-17C and IL-21 identify OAC patients with significantly reduced PFS. Kaplan Meier curves showing OAC patients with mutated (altered) versus wild-type (unaltered) gene expression of **CCL26, CCL22, IL-31, IL-15, IL-17C and IL-21** in OAC tumour tissue against PFS in months (n=87).

Mutations in anti-tumour IL-15 and IL-21 also identified OAC patients with significantly reduced PFS (Figure 4.7.2, $p<0.05$). Similarly, mutations in CCL26, CCL22, IL-31 and IL-17C but not IL-15 or IL-21 identified OAC patients with significantly reduced OS. In addition, mutations in another important anti-tumour gene IL-1RN encoding IL-1RA also identified OAC patients with significantly reduced OS (Figure 4.7.3, $p<0.05$)

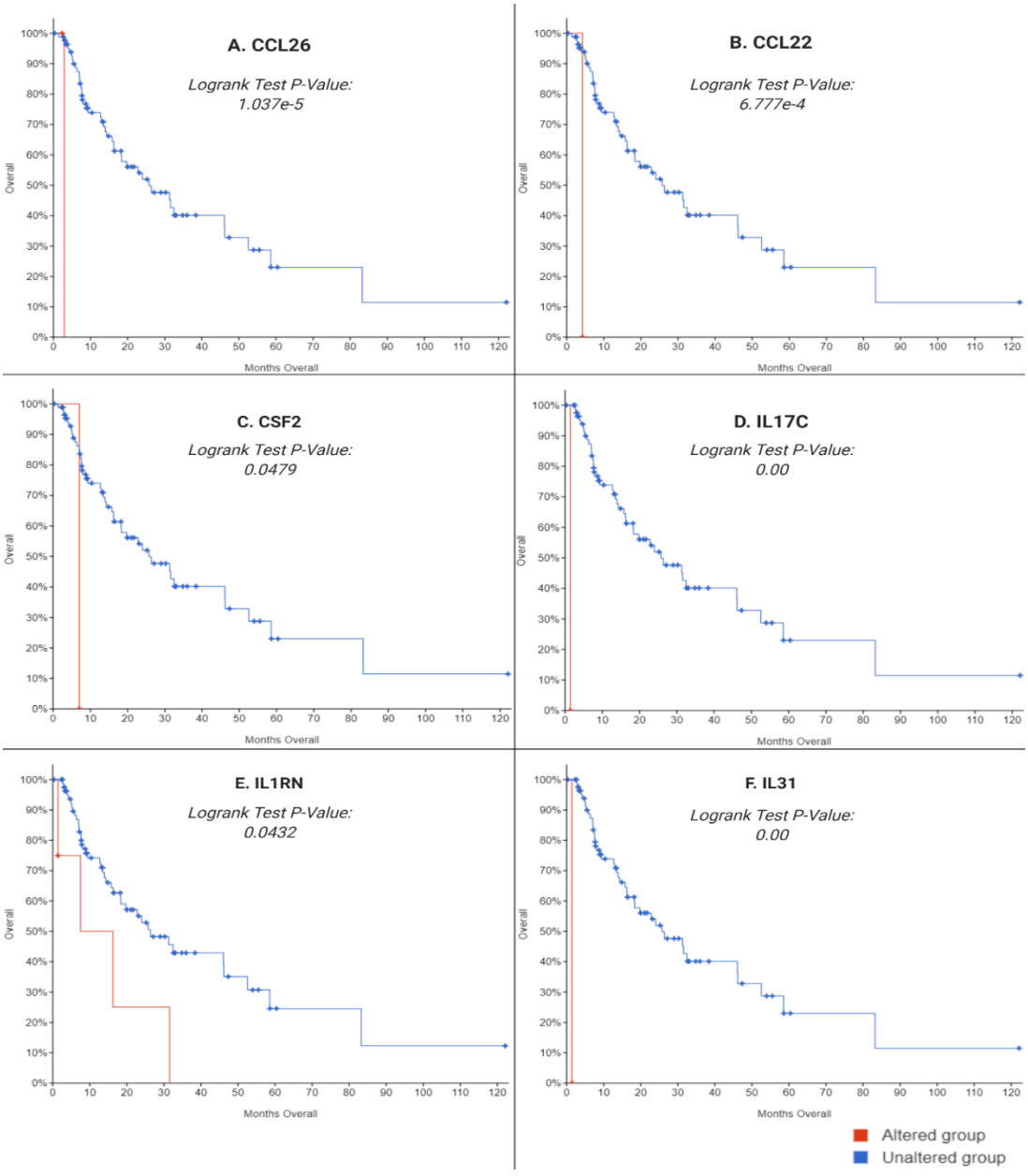

Fig. 4.7.3: Mutations in CCL26, CCL22, CSF2, IL-17C, IL-1RN and IL-31 identify OAC patients with significantly reduced OS. Kaplan Meier curves showing OAC patients with mutated (altered) versus wild-type (unaltered) gene expression of CCL26, CCL22, CSF2, IL-17C, IL-1RN and IL-31 in OAC tumour tissue vs OS in months (n=87).

4.2.7 Post operative study; Patient demographics

The aim of this study was to evaluate the impact of major oncological surgery on the immediate perioperatively immune microenvironment and determine if it is immunosuppressive. A total of 11 adenocarcinoma patients whole blood and serum for all study time points were included for analysis. The time points were preoperatively (POD 0), post operative day 1, (POD 1), POD3, POD7, week 6 post operatively. 73% (n=8) were male and the median age was 66.72 years (SD 10.26). There was one R1 resection, 73% of tumours were poorly differentiated and 91% of patients had at least one adverse feature of tumour biology (209). 10 patients underwent neoadjuvant therapy with 7 patients receiving FLOT chemotherapy, of which 6 patients tolerated all pre-operative cycles. One patient had FOLFOX and 2 patients has CROSS chemoradiotherapy (Table 4.4). Four patients in the cohort have had recurrence thus far with two local and two systemic. 80% of patients had a tumour regression grade (TRG) of 3 or greater as defined by Mandard. In terms of final histology, 63% were T3, and 45% were node positive. For complications, 5 patients had Grade III or greater as defined by the Clavien Dindo classification. There were no post-operative deaths.

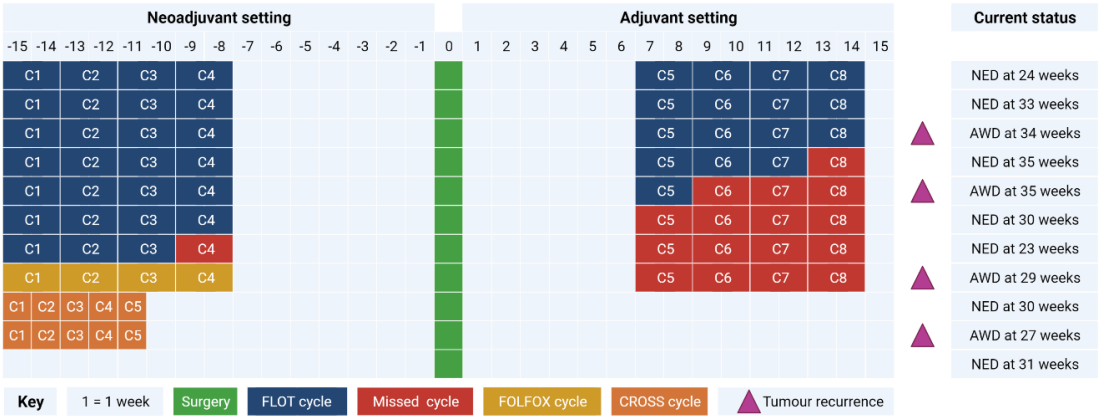

Table 4.4 Treatment modalities, cycles tolerated, tumour recurrence. NED:No evidence of disease, AWD:Alive with disease. Treatment Modalities; CROSS chemoradiotherapy, FLOT Chemotherapy, N=11.

There was a strong positive correlation between circulating levels of Tie 2 and anastomotic leaks on post operative day 1 (POD 1), and pneumonia at POD 7 and week 6. Lymphatic invasion positively correlated with PD-1 and TIGIT expression and CD27, IL-17RA and MCP-1 expression correlated with perineural invasion preoperatively. MCP-4 correlated with perineural invasion at POD 1 and POD 3 whereas IP-10 and VEGF-A positively correlated with perineural invasion at POD 7.Venous invasion correlated with CTLA-4 and IL-15 expression at POD 7 and IL-13 and week 6 (Figure 4.8).

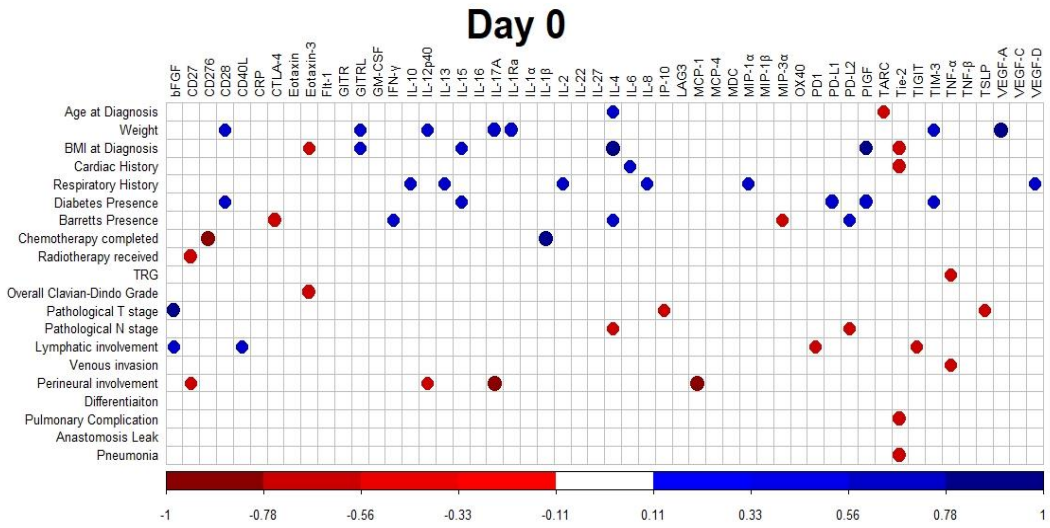

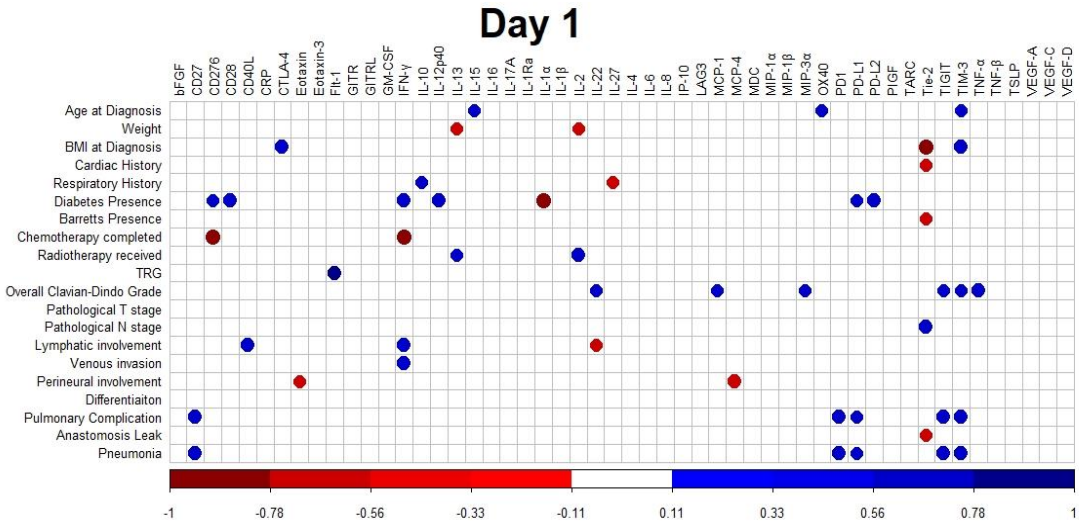
Day 1
bFGF CD27 CD276 CD28 CD40L CRP CTLA-4 Eotaxin Eotaxin-3 Flt-1 GITR GITRL GM-CSF IFN-γ IL-10 IL-12p40 IL-13 IL-15 IL-16 IL-17A IL-1Ra IL-1α IL-1β IL-2 IL-22 IL-27 IL-4 IL-6 IL-8 IP-10 LAG3 MCP-1 MCP-4 MDC MIP-1α MIP-1β MIP-3α OX40 PD1 PD-L1 PD-L2 PlGF TARC Tie-2 TIGIT TIM-3 TNF-α TNF-β TSLP VEGF-A VEGF-C VEGF-D
Age at Diagnosis
Weight
BMI at Diagnosis
Cardiac History
Respiratory History
Diabetes Presence
Barretts Presence
Chemotherapy completed
Radiotherapy received
TRG
Overall Clavian-Dindo Grade
Pathological T stage
Pathological N stage
Lymphatic involvement
Venous invasion
Perineural involvement
Differentiaiton
Pulmonary Complication
Anastomosis Leak
Pneumonia
-1 -0.78 -0.56 -0.33 -0.11 0.11 0.33 0.56 0.78 1

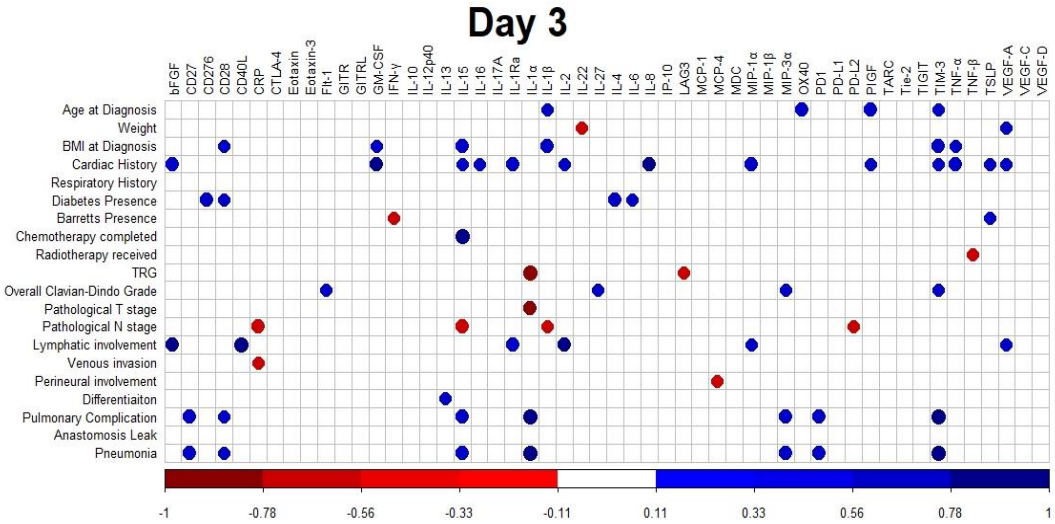
Day 3
bFGF CD27 CD276 CD28 CD40L CRP CTLA-4 Eotaxin Eotaxin-3 Flt-1 GITR GITRL GM-CSF IFN-γ IL-10 IL-12p40 IL-13 IL-15 IL-16 IL-17A IL-1Ra IL-1α IL-1β IL-2 IL-22 IL-27 IL-4 IL-6 IL-8 IP-10 LAG3 MCP-1 MCP-4 MDC MIP-1α MIP-1β MIP-3α OX40 PD1 PD-L1 PD-L2 PlGF TARC Tie-2 TIGIT TIM-3 TNF-α TNF-β TSLP VEGF-A VEGF-C VEGF-D
Age at Diagnosis
Weight
BMI at Diagnosis
Cardiac History
Respiratory History
Diabetes Presence
Barretts Presence
Chemotherapy completed
Radiotherapy received
TRG
Overall Clavian-Dindo Grade
Pathological T stage
Pathological N stage
Lymphatic involvement
Venous invasion
Perineural involvement
Differentiaiton
Pulmonary Complication
Anastomosis Leak
Pneumonia
-1 -0.78 -0.56 -0.33 -0.11 0.11 0.33 0.56 0.78 1

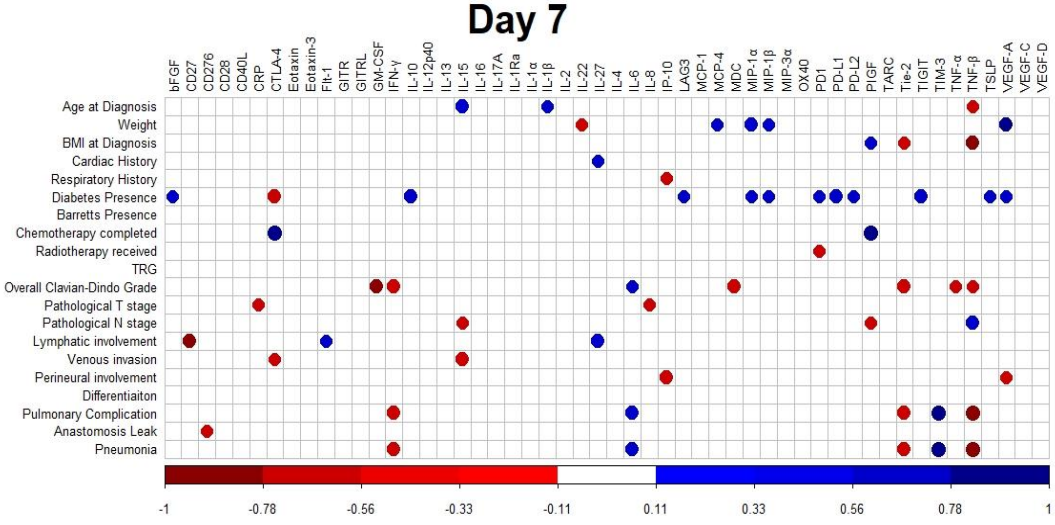
Day 7
bFGF CD27 CD276 CD28 CD40L CRP CTLA-4 Eotaxin Eotaxin-3 Flt-1 GITR GITRL GM-CSF IFN-γ IL-10 IL-12p40 IL-13 IL-15 IL-16 IL-17A IL-1Ra IL-1α IL-1β IL-2 IL-22 IL-27 IL-4 IL-6 IL-8 IP-10 LAG3 MCP-1 MCP-4 MDC MIP-1α MIP-1β MIP-3α OX40 PD1 PD-L1 PD-L2 PlGF TARC Tie-2 TIGIT TIM-3 TNF-α TNF-β TSLP VEGF-A VEGF-C VEGF-D
Age at Diagnosis
Weight
BMI at Diagnosis
Cardiac History
Respiratory History
Diabetes Presence
Barretts Presence
Chemotherapy completed
Radiotherapy received
TRG
Overall Clavian-Dindo Grade
Pathological T stage
Pathological N stage
Lymphatic involvement
Venous invasion
Perineural involvement
Differentiaiton
Pulmonary Complication
Anastomosis Leak
Pneumonia
-1 -0.78 -0.56 -0.33 -0.11 0.11 0.33 0.56 0.78 1

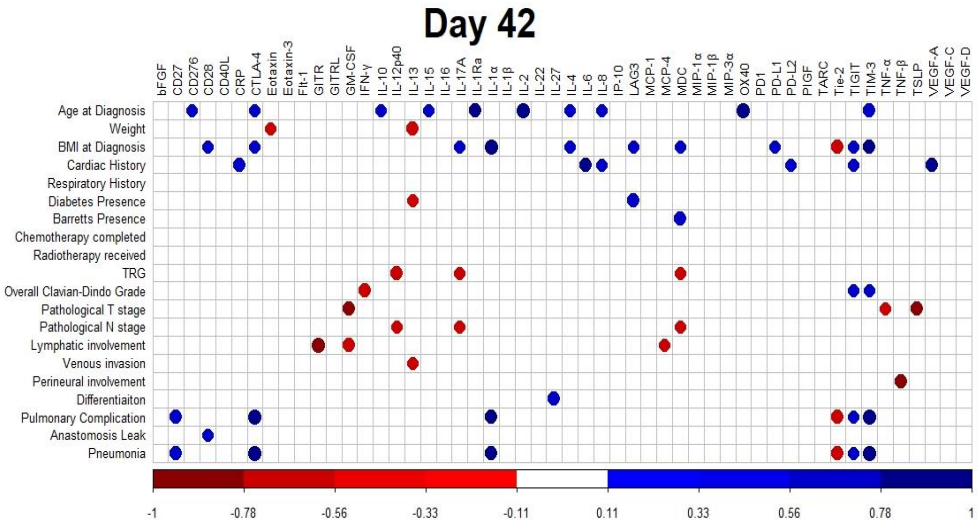

Figure 4.8. Corrplots illustrating the correlation values for MSD data in OAC patients with clinical demographics and characteristics. Patient clinical features included age, weight (pre-treatment, kg), BMI (pre-treatment, kg/m^2), tumour type (OAC=0 or OGJ=1), neo-adjuvant treatment received (CROSS=0 and FLOT=1), treatment response (determined by radiographic features using PET/CT), tumour regression grade (TRG), clinical tumour stage and nodal involvement, pathological tumour stage and nodal involvement, BMI (post-treatment, kg/m^2), weight (post-treatment, kg), serosal invasion and lymph-vascular invasion. Expression of ICs was determined by flow cytometry. Blue indicates a positive correlation, red negative correlation. Spearman correlation. Significant data shown only. Spearman r 0.4-0.59 moderate, 0.6-0.79 strong

4.2.8 Alterations in circulating T cells in the post-op setting

There was a decrease in total lymphocytes in the immediate post-operative phase at day 1 ($p<0.05$) and week 1 ($p<0.01$), with a decrease in the CD3 compartment at day 1

(p<0.05) when compared to pre operative levels. There was an increase in CD8 cytotoxic lymphocytes at week 6 (p<0.05) when compared to pre operative levels (Figure 4.9).

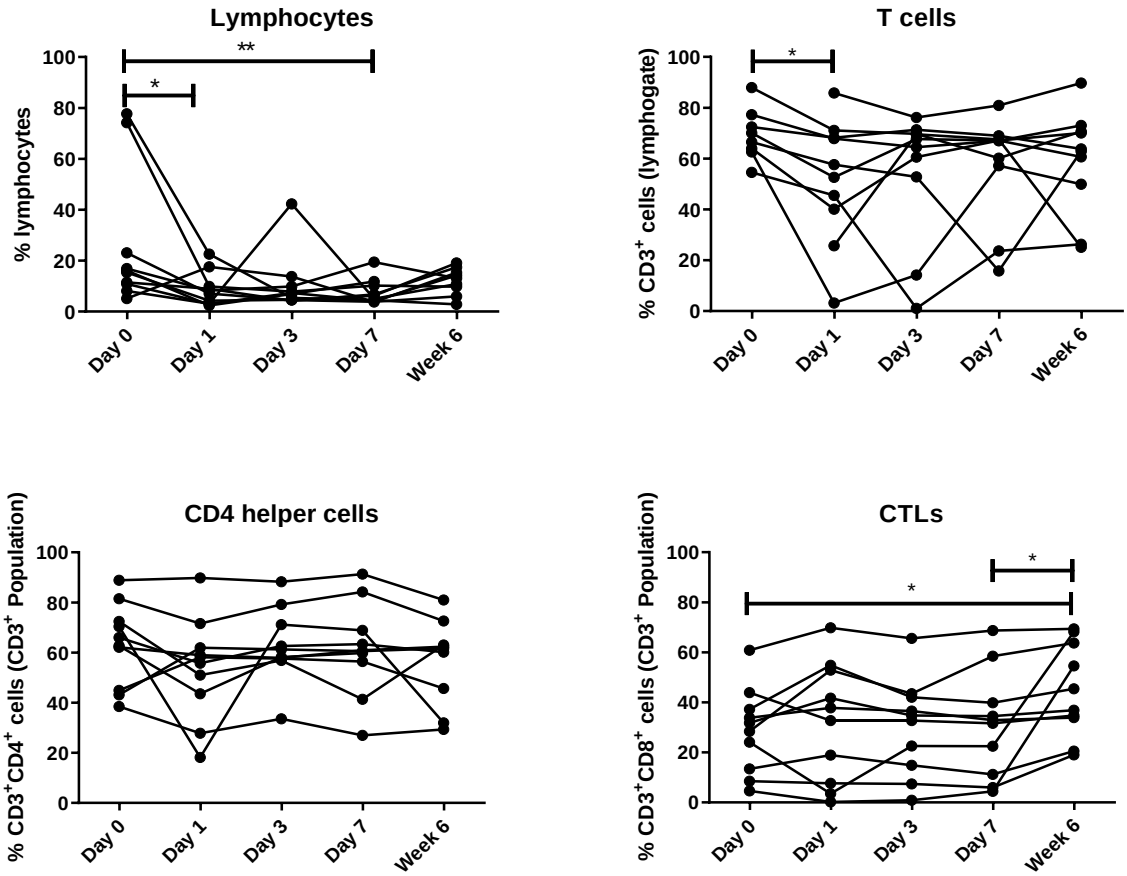

Figure 4.9. The percentage of circulating lymphocytes, $CD3^+$, $CD3^+CD4^+$ and $CD3^+CD8^+$ cells was determined by flow cytometry in OAC patients on the day of tumour resection prior to surgery (Day 0) and on post-operative days 1, day 3, day 7 and week 6 (n=11). Paired, non-parametric t-test *p<0.05 and **p<0.01.

There was a significant decrease in expression of CD62L on $CD3^+CD8^+$ cells from pre-operative levels to POD 3 (p<0.01), a significant decrease in CD69 on $CD3^+CD4^+$ cells from POD 0 to post-operative week 6 (p<0.05) and from POD 1 to post op week 6 (p<0.05), and a significant increase in CD27 on $CD3^+$, $CD3^+CD4^+$, and $CD3^+CD8^+$ cells

from pre-operative levels to POD 7 ($p<0.01$), POD 1 to POD 7 ($p<0.01$) and from POD 3 to POD 7 ($p<0.05$). There was a significant decrease in CD45RA on $CD3^+CD4^+$ cells from POD 0 to POD 1 ($p<0.05$) and week 6 post-operatively ($p<0.05$) and a significant decrease in CD45RA on $CD3^+CD8^+$ cells on day 3 post-operatively ($p<0.01$) compared to pre-operative levels and also from POD 1 to POD 3 ($p<0.05$) (Figure 4.10).

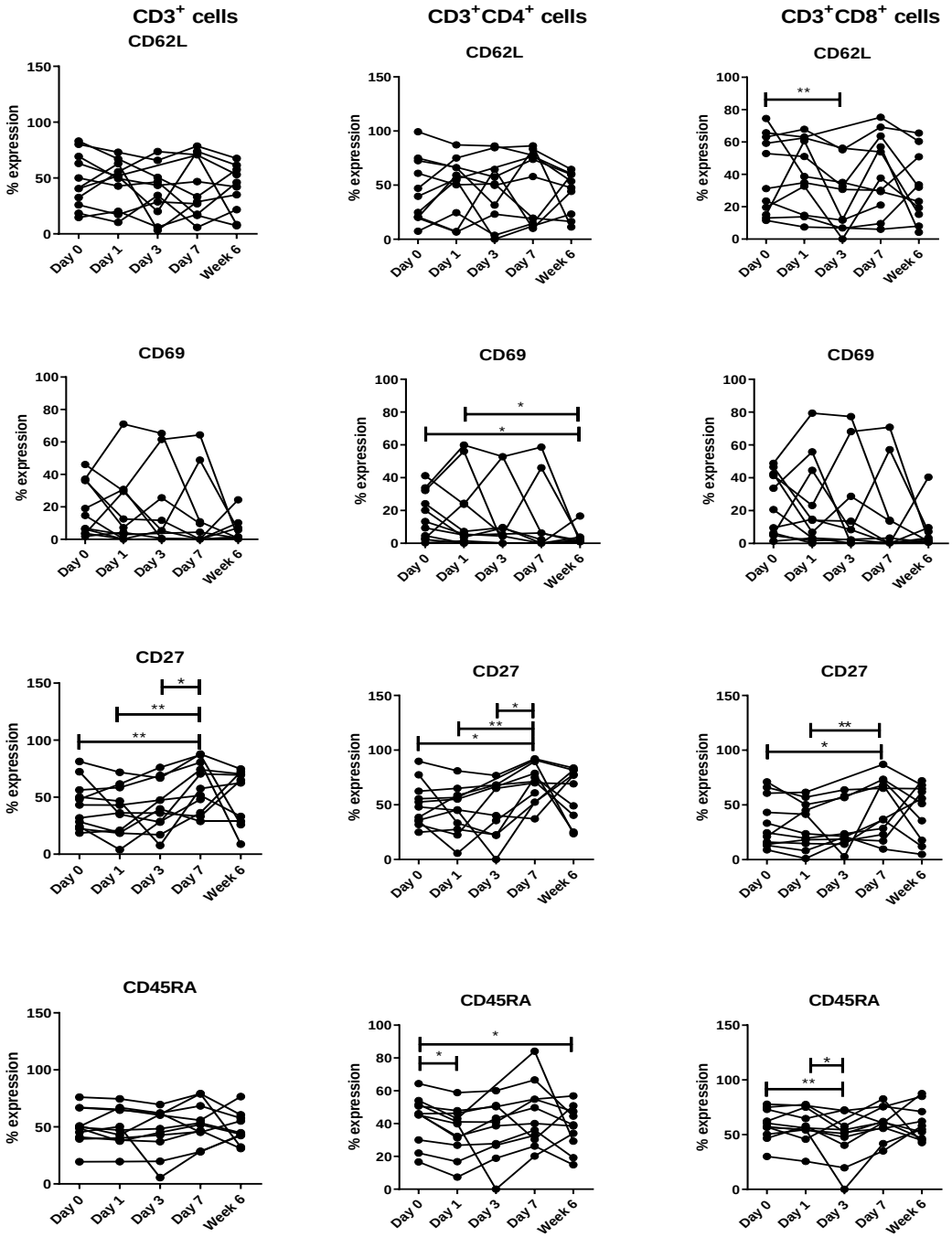

Figure 4.10. The frequency of circulating $CD27^+$ T cells increases sequentially in the immediate post-operative period peaking on day 7 in OAC patients. Expression of T cell activation markers (CD62L, CD69, CD27 and CD45RA) were assessed on the surface of circulating $CD3^+$, $CD3^+CD4^+$ and $CD3^+CD8^+$ cells in OAC patients on the day of tumour resection prior to surgery (Day 0) and on post-operative days 1, day 3, day 7 and week 6 by flow cytometry (n=11). Paired, non-parametric t-test *$p<0.05$ and **$p<0.01$.

There was a significant increase in naïve T cells in the peripheral circulation in the CD3 compartment from pre-operative levels to POD 7 ($p<0.001$), POD 1 to POD 7 ($p<0.01$) and POD 3 to POD 7 ($p<0.01$) (Figure 4.11). There was also a significant increase in $CD3^+CD4^+$ naïve T cells from POD 1 to POD 7 ($p<0.05$) and from POD 3 to POD 7 ($p<0.05$). Finally, there was a significant increase in $CD3^+CD8^+$ naïve T cells at POD 7 compared to preoperative levels ($p<0.05$), from POD 1 to POD 7 ($p<0.01$), and from POD 3 to POD 7 ($p<0.01$). In contrast, there was a significant decrease in $CD3^+CD4^+$ effector memory T cells from POD 1 to POD 3 ($p<0.05$) and also a significant decrease in $CD3^+CD8^+$ effector memory T cells from pre-operative levels to POD 7 ($p<0.05$), from POD 1 to POD 7 ($p<0.01$), and again from POD 1 to POD 7 ($p<0.05$). There was a significant decrease in $CD3^+$ and $CD3^+CD4^+$ central memory T cells from pre-operative levels to POD 7 ($p<0.01$) and from POD 1 to POD 7 ($p<0.05$), and $CD3^+CD8^+$ central memory T cells from POD 1 to POD 3 ($p<0.01$) and from POD 1 to POD 7 ($p<0.05$). (Figure 4.11)

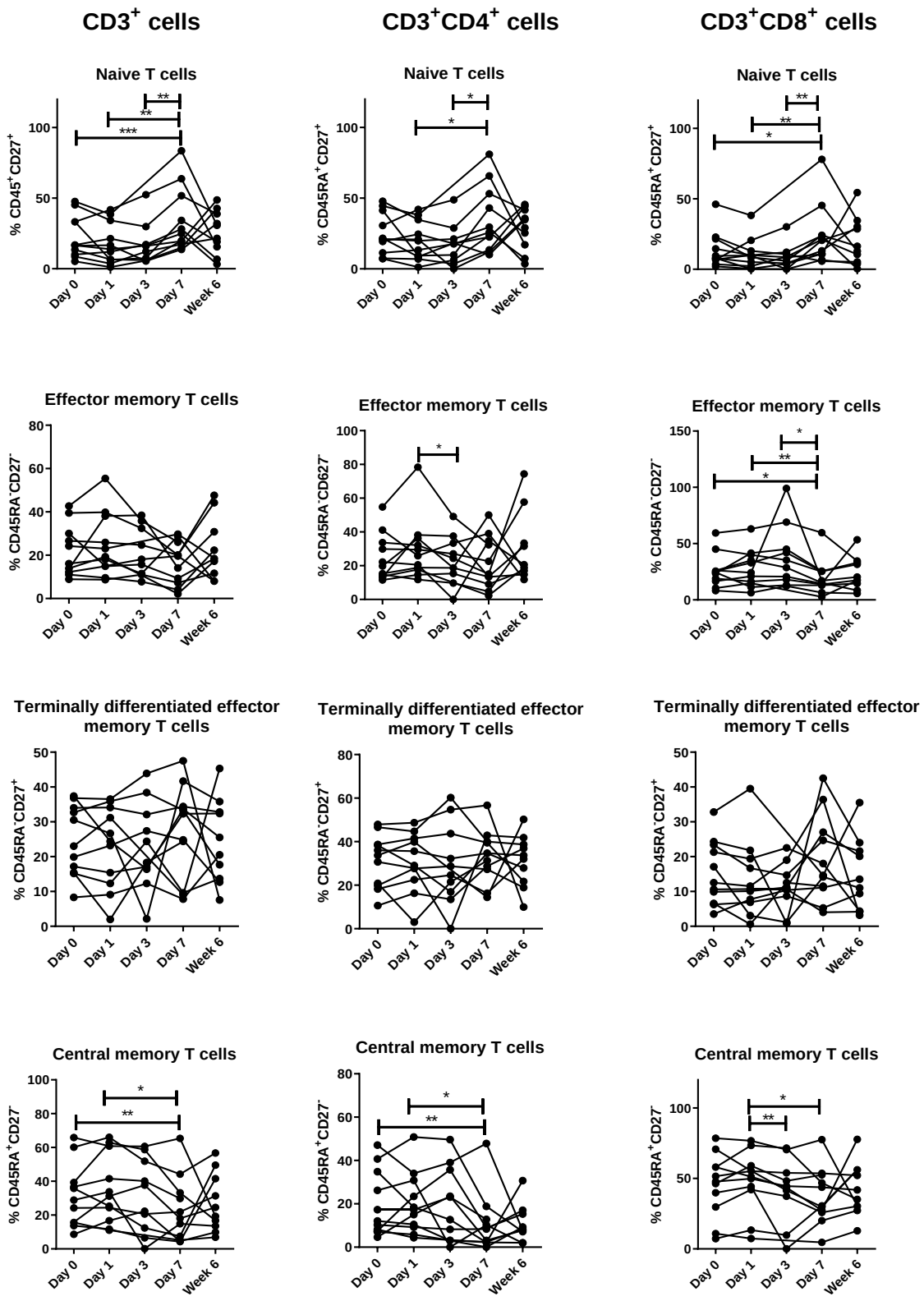

Figure 4.11. There is a sequential decrease in the percentage of effector memory and central memory T cells in circulation and an increase in the percentage of naïve T

cells in peripheral circulation of OAC patients in the immediate post-operative period. The percentage of peripheral blood naïve ($CD45RA^+CD27^+$), central memory ($CD45RA^+CD27^-$), effector memory ($CD45RA^-CD27^-$) and terminally differentiated effector memory ($CD45RA^-CD27^+$) $CD3^+$ cells, $CD3^+CD4^+$ and $CD3^+CD8^+$ cells in OAC patients, was determined on the day of surgery prior to tumour resection (Day 0) and on post-operative days 1, day 3, day 7 and week 6 by flow cytometry (n=11). Wilcoxon ranked test. *p<0.05, **p<0.01 and ***p<0.001.

There was an overall decrease in immune checkpoint expression globally, with a significantly reduced expression of $CD3^+CD4^+PD\text{-}1^+$ from POD-7 to week 6 (p<0.05). There was a significant decrease in expression of TIM-3 in the $CD3^+CD8^+$ compartment from preoperative to post-op week six (p<0.01), from POD 3 to POD 7 (p<0.05) and from POD 7 to post op week 6 (p<0.01). There was a significant decrease in LAG-3 expression across all three T cell compartments post operatively with a decrease from POD 0 to POD 3 (p<0.01), POD 1 to POD 3 (p<0.05), and from POD 1 to POD 7 (p<0.05) in the $CD3^+$ compartment. There was a significant decrease in $CD3^+CD4^+LAG\text{-}3^+$ from preoperative levels to POD 3 (p<0.01), POD 7 (p<0.01) and week 6 (p<0.05), with a decrease from POD 1 to POD 7 (p<0.05) and week six (p<0.05). Similarly, there was a significant decrease in $CD3^+CD8^+LAG\text{-}3^+$ from POD 0 to POD 3 (p<0.01) and from POD 1 to POD 3 (p<0.05). For PD-L1, there was a significant reduction in expression on $CD3^+$ cells from pre-operative levels to week 6 (p<0.05) and $CD3^+CD4^+$ cells from pre-operative levels to post-operative week 6 (p<0.05) and from POD 1 to post-operative week 6 (p<0.05), whereas there was a significant reduction in PD-L2 expression in the cytotoxic T cell compartment from pre-operative levels to POD 3 (p<0.05) and from POD 3 to post-operative week 6 (p<0.01). There was significantly less CTLA-4 expression by

$CD3^+CD4^+$ from POD 7 to post op week 6 ($p<0.05$) and $CD3^+CD8^+$ cells from preoperative levels to post op week 6 ($p<0.05$) (Figure 4.12).

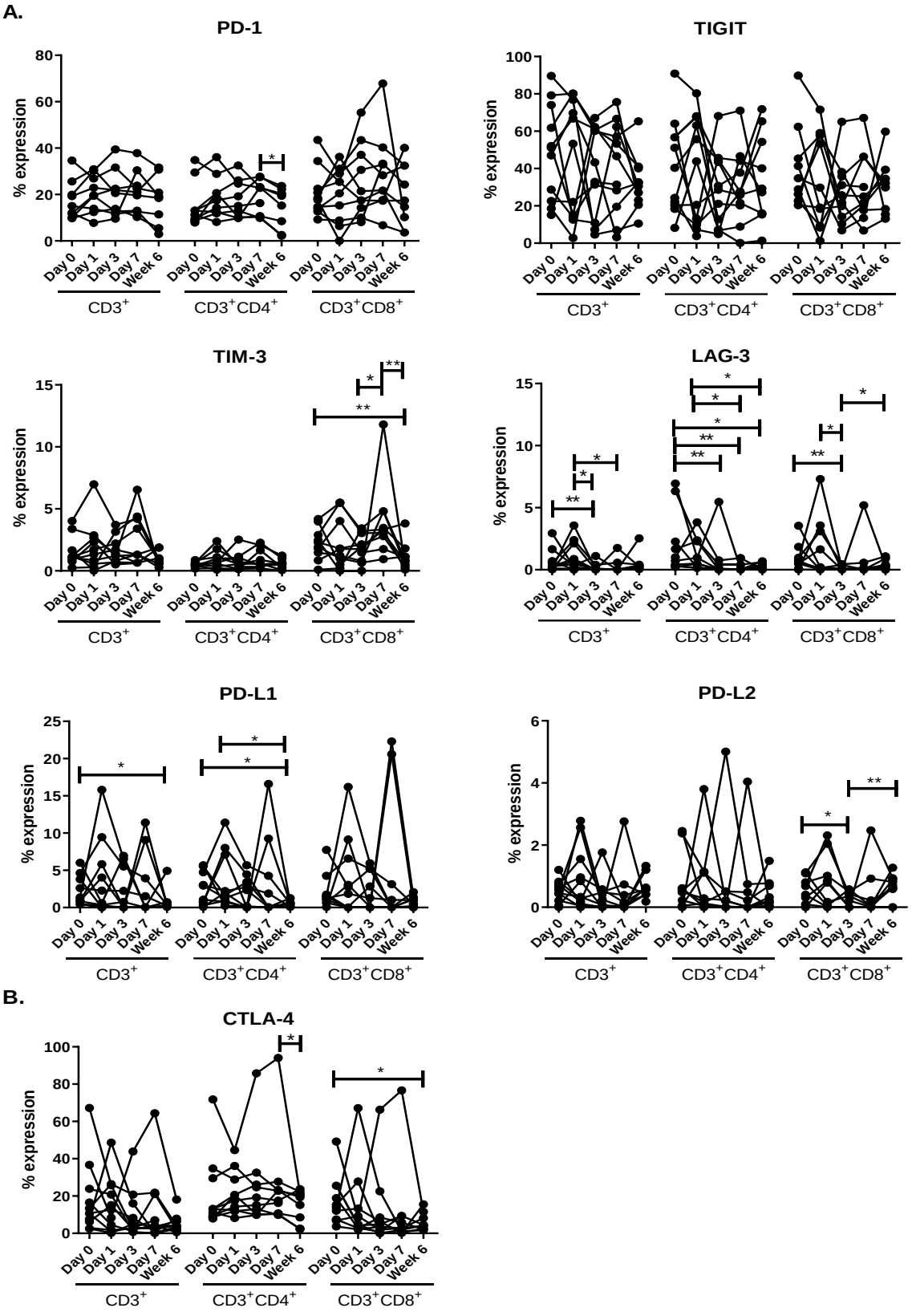

Figure 4.12. The expression of CTLA-4 on the surface of circulating CD4$^+$ T cells decreases 6 weeks post-operatively in OAC patients. Expression of inhibitory immune checkpoints (PD-1, TIGIT, TIM-3, LAG-3 and CTLA-4, PD-L1 and PD-L2) were assessed on the surface of circulating CD3$^+$, CD3$^+$CD4$^+$ and CD3$^+$CD8$^+$ cells in OAC patients on the day of tumour resection prior to surgery (Day 0) and on post-operative days 1, day 3, day 7 and week 6 by flow cytometry (n=11). Paired, non-parametric t-test *p<0.05 and **p<0.01.

There was a significant decrease in the expression of DAMPS (Calreticulin and HMGB1) across all three T cell compartments compared to pre-operative basal levels. There was a decrease in the frequency of CD3$^+$ Calreticulin expressing cells from preoperative levels to POD 3 (p<0.05), and POD 7 (p<0.05), with a decrease in CD3$^+$CD4$^+$ Calreticulin from pre-operative levels to POD 7 (p<0.01) and again similarly in CD3$^+$CD4$^+$CD8$^+$ from preoperative levels to POD 3 (p<0.05). In terms of HMGB1 there was a significant decrease in CD3$^+$, CD3$^+$CD4$^+$ and CD3$^+$CD8$^+$ positivity from pre-operative levels to POD 3 (p<0.01) and POD 7 (p<0.05). (Figure 4.13).

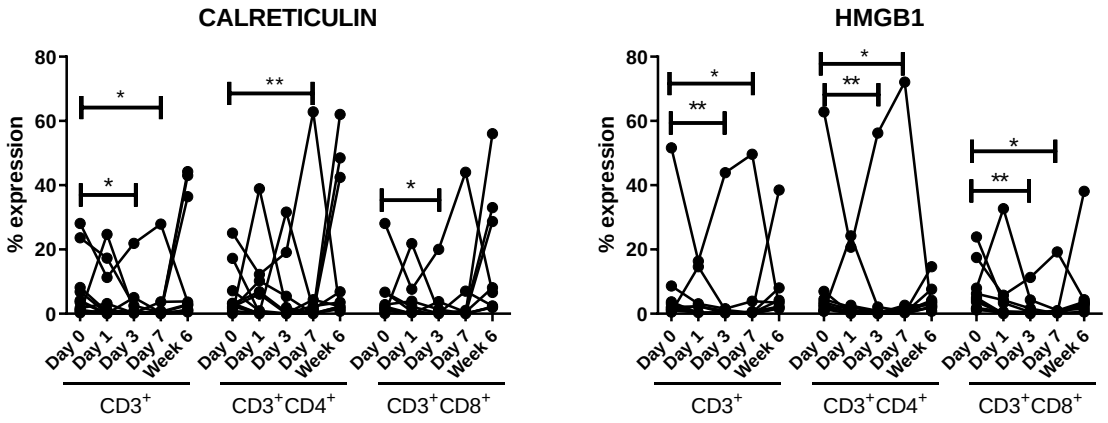

Figure 4.13. The expression of DAMPs on the surface of circulating T cells decreases in the immediate post-operative setting in OAC patients. Expression of HMGB1 and Calreticulin on the surface of circulating $CD3^+$, $CD3^+CD4^+$ and $CD3^+CD8^+$ cells in OAC patients on the day of tumour resection (Day 0), on post-operative days 1, day 3, day 7 and week 6 was assessed by flow cytometry (n=11). Paired, non-parametric t-test *p<0.05 and **p<0.01.

4.2.9 Multiplex Dataset; The impact of major oesophageal oncological surgery on cytokines, chemokines, soluble checkpoints, inflammatory and angiogenic markers.

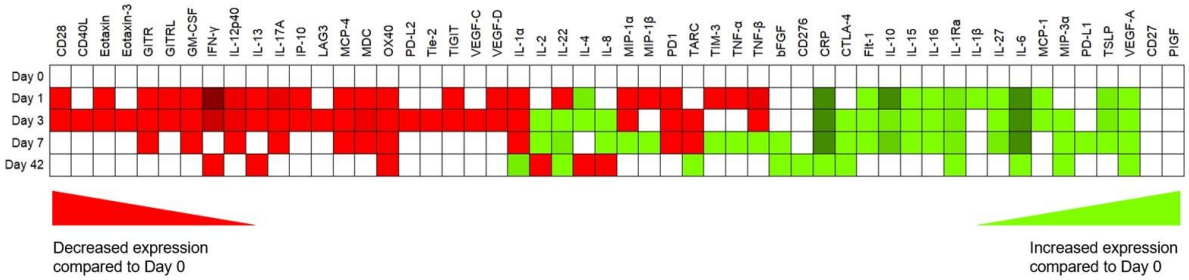

Table 4.5; Multiplex ELISA data, with trends in expression (green is increased, red is decreased) for cytokines, chemokines, soluble checkpoints, inflammatory and angiogenic markers for the entire cohort (n=11).

There were a total of 59 analytes in the ELISA dataset across the study timepoints with variability in trends across the data in terms of expression and this is represented in Table 4.5.

There was a significant decrease in the Th1 mediators IFN-γ, IL-12p40, TNF-α and an increase in IL-1RA, which acts as an immunosuppressive mediator (Figure 4.14). There was a significant decrease in IFN-γ and IL-12p40, IP-10 and IL-1RA at POD 1 (p<0.001), POD 3 (p<0.01) and POD 7 (p<0.05), with an increase in IFN-γ at post op week 6 compared to POD 1 (p<0.001) (Figure 4.14). The co-stimulatory immune checkpoints

GITR, CD276, CD28 and CD40L decrease in the immediate post-operative period before returning to pre-operative levels. The levels of GITR, CD276, CD28 and CD40L decrease at POD 1 ($p<0.05$) and POD 3 ($p<0.01$) compared to pre-operative levels with a significant increase in expression of these markers at week 6 compared to POD 3 ($p<0.001$). (Figure 4.14)

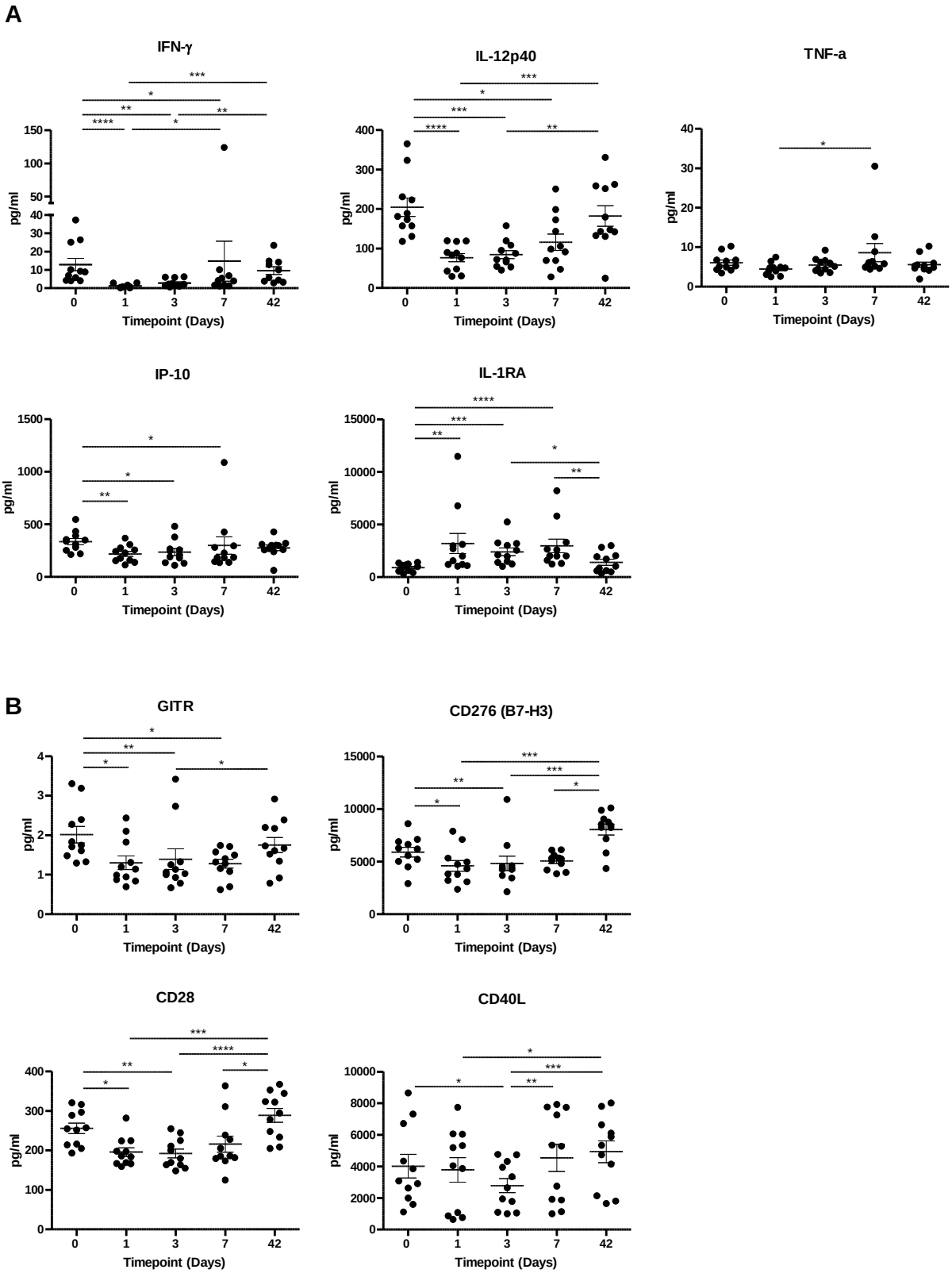

Figure 4.14. Levels of soluble Th1 mediators and co-stimulatory immune checkpoints significantly decrease in the immediate post-operative setting before

returning to baseline at 6 weeks. Preoperatively, POD 1, 3 and 7 and week 6 serums from OAC patients (n=11) were screened for a panel of soluble (**A**) Th1 mediators (IFN-γ, IL-12 p40, TNF-α, IL-1RA and IP-10) and soluble (**B**) co-stimulatory molecules (GITR, CD276, CD28, CD40L) by ELISA. Friedman test, *p<0.05, **p<0.01, ***p<0.001.

On the contrary there was an increase in the Th2 mediators IL-4, IL-6, IL-10, IL-27, soluble chemokine ligands and pro-inflammatory mediators responsible for promoting pro-tumour immune cells; MCP-1, MIP-1α, MIP-1β and IL-16 (figure 4.14.1). There was a significantly higher levels of IL-4 on POD 1 compared to post op week 6 ($p<0.01$), and POD 3 compared to POD 7 ($p<0.05$) and week 6 ($p<0.001$). There was a significantly higher levels of IL-6 on POD 1 compared to pre-operative levels ($p<0.001$), POD 7 ($P<0.01$) and week 6 ($p<0.001$). There was a significantly higher expression of IL-6 at POD 3 ($p<0.001$) compared to week 6 and pre-operative levels ($p<0.001$) and POD 7 compared to basal levels ($p<0.01$) and week 6 ($p<0.01$). There was a significantly higher expression of IL-10 at POD 1 ($p<0.001$), POD 3 ($p<0.05$) and POD 7 ($p<0.01$) compared to basal levels, with a significantly higher expression at POD 1 compared to week 6 ($p<0.001$) (figure 4.14.1). There was also a significantly higher expression of IL-27 at POD 1 ($p<0.01$), POD 3 ($p<0.001$) and POD 7 ($p<0.001$) compared to basal levels. There was a significantly higher expression of MCP-1 at POD 3 compared to POD 7 (<0.01), week 6 ($p<0.05$) and POD 0 ($p<0.05$). There was a significantly higher expression of MIP-1α and MIP-1β at POD 7 compared to POD 1 ($p<0.01$), with a higher expression of IL-16 at POD 1 ($p<0.01$) and POD 3 ($p<0.01$) compared to basal levels with a significant reduction at week 6 compared to POD 1 ($p<0.01$) and POD 3 ($p<0.01$).

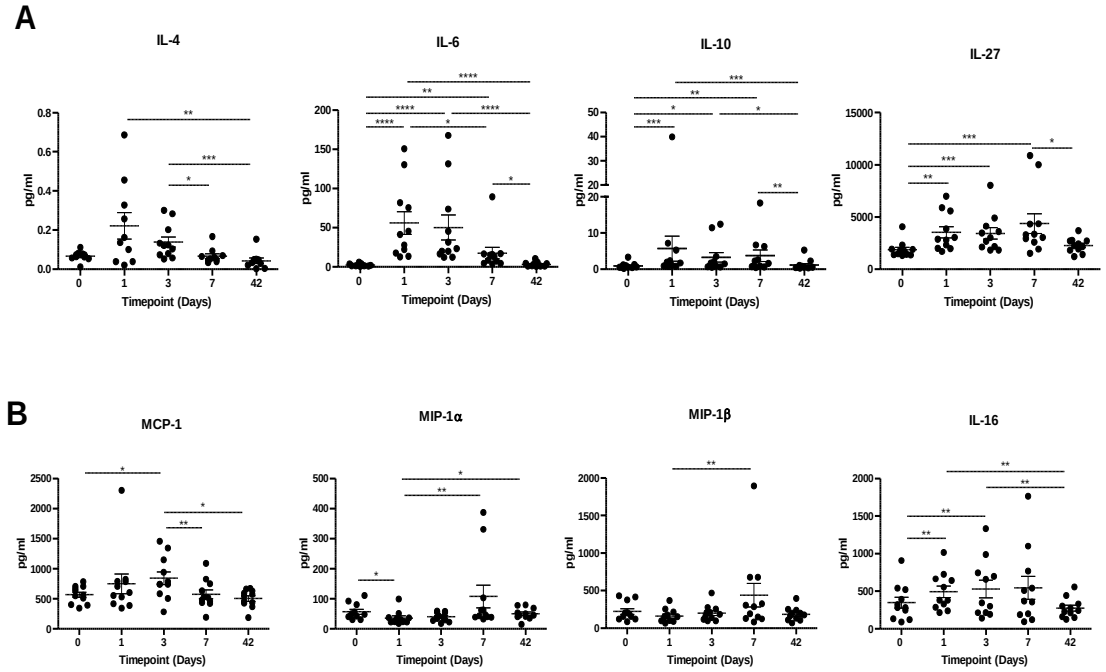

Figure 4.14.1. Levels of soluble Th2 mediators and tumour-promoting pro-inflammatory cytokines significantly increased in the immediate post-operative setting before returning to baseline at week 6. POD 0, 1, 3 and 7 and week 6 serums from OAC patients (n=11) were screened for a panel of soluble (**A**) Th2 mediators (IL-4, IL-6, IL-10, IL-27) and (B) soluble chemokine ligands and pro-inflammatory mediators responsible for promoting pro-tumour immune cells (MCP-1, MIP-1α, MIP-1β and IL-16) by ELISA. Friedman test, *p<0.05, **p<0.01, ***p<0.001, ****p<0.0001.

There were contrasting trends in the soluble checkpoints with an increase in PD-L1, CTLA-4 and TIM-3 immediately post operatively, whereas PD-1, PD-L2, TIGIT and LAG-3 all reduced significantly in the immediate post-operative setting (Figure 4.15). There was a significant increase in PD-L1 ($p<0.01$), CTLA-4 ($p<0.05$), and TIM-3 ($p<0.05$) at POD 7 compared to pre-operative levels. There was an increase in PD-L1 at POD 3 compared to pre-operative levels ($p<0.01$). There was a significant increase in TIM-3 levels at POD 7 ($P<0.01$) and week 6 ($P<0.01$) compared to POD 1. There was a

significant decrease in expression of PD-1 ($p<0.001$), PD-L2 ($p<0.01$), and TIGIT ($p<0.05$) at POD 1, POD 3 and POD 7 compared to pre-operative levels with a significant increase in expression of these markers from POD 1 to post op week six ($p<0.01$). There was a significant increase in PD-1, PD-L2, TIGIT and LAG-3 from POD 3 to week 6 ($p<0.01$).

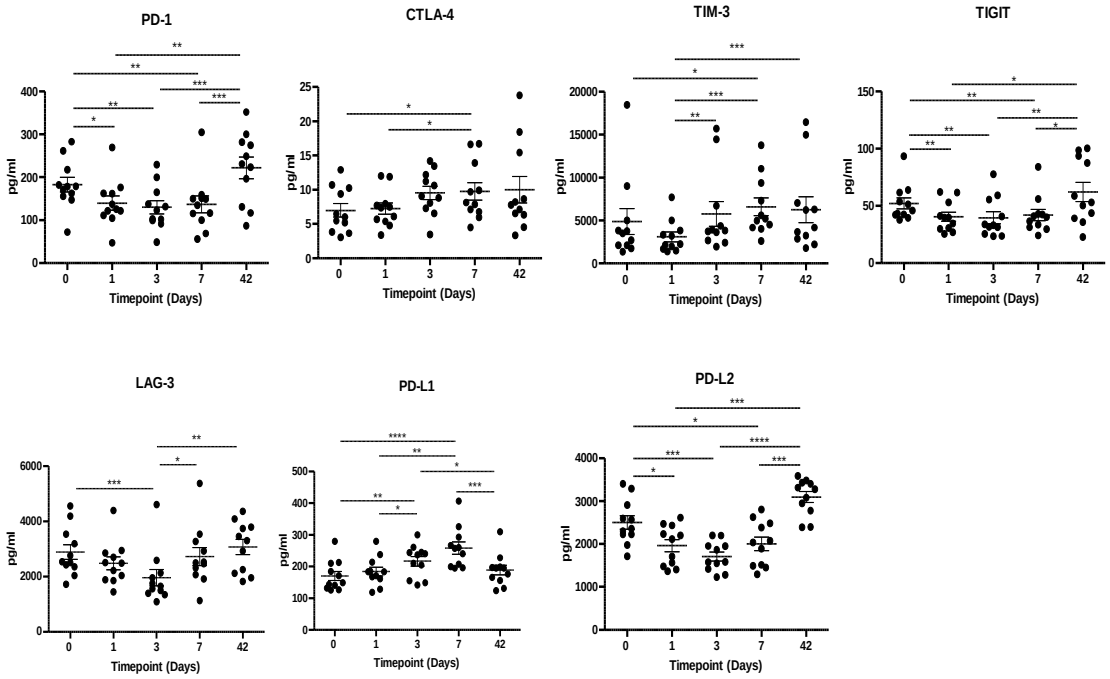

Figure 4.15. Circulating levels of soluble PD-L1, CTLA-4 and TIM-3 significantly increased whereas levels of circulating soluble PD-1, PD-L2, TIGIT and LAG-3 significantly decreased in the immediate post-operative setting before returning to baseline at 6 weeks. POD 0, 1, 3 and 7 and week 6 serums from OAC patients (n=11)

were screened for a panel of soluble inhibitory immune checkpoints PD-1, CTLA-4, TIM-3, TIGIT, LAG-3, PD-L1 and PD-L2 by ELISA. Friedman test, *p<0.05, **p<0.01, ***p<0.001. ****p<0.0001.

There was a significant increase in circulating levels of pro-angiogenic and pro-metastatic markers VEGF-A, VEGF-C, PIGF and Flt-1, with a decrease in VEGF-D and Tie-2, with a return to pre-operative levels at week 6 (Figure 4.16). There was a significantly higher expression of VEGF-A and VEGF-C at POD 3 (P<0.05) and POD 7 (P<0.001) compared to pre-operative levels and a significantly lower expression of VEGF-A at week 6 compared to POD 7 (P<0.01). PIGF was significantly higher at POD 7 compared to preoperative levels. (p<0.05), with FLT-1 significantly higher at POD 1 (P<0.001) and POD 3 (P<0.01) compared to basal levels. VEGF-D was significantly lower at POD 1 (P<0.001) and POD 3 (P<0.01) compared to basal levels. It was however, significantly higher at week six compared to POD 3 (P<0.01) and POD 1 (P<0.001). Tie 2 was significantly lower at POD 3 (P<0.001) and POD 7 (P<0.01) compared to preoperative levels.

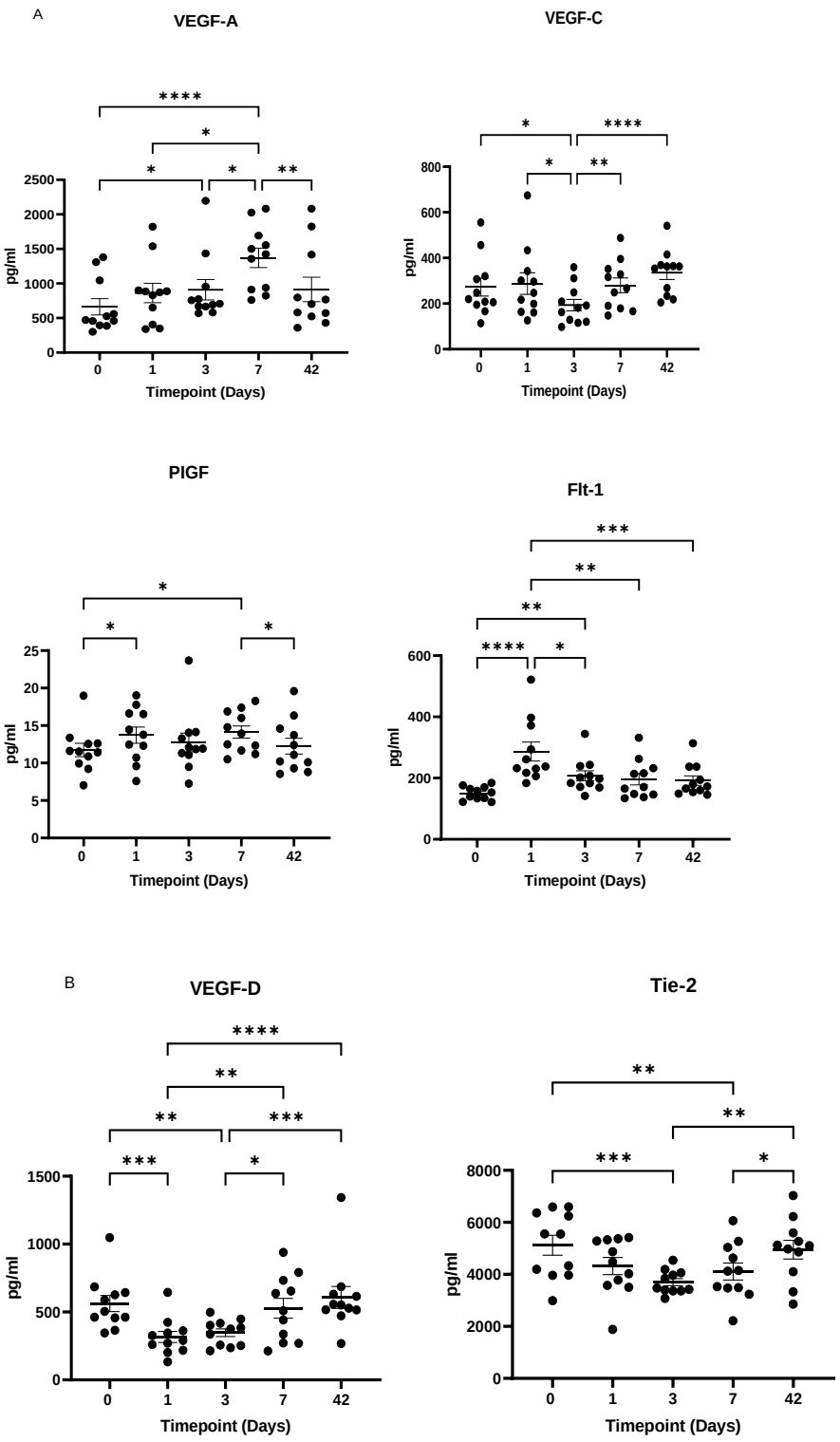

Figure 4.16. Circulating levels of pro-angiogenic and pro-metastatic VEGF-A, VEGF-C, PIGF and Flt-1 significantly increased whereas levels of circulating pro-angiogenic mediators VEGF-D and Tie-2 significantly decreased in the immediate post-operative setting. POD 0, 1, 3 and 7 and week 6 serums from OAC patients (n=11)

were screened for a panel of soluble pro-angiogenic and pro-metastatic mediators (**A**) VEGF-A, VEGF-C, PIGF, FLT-1, (B) VEGF-D and Tie-2 by ELISA. Friedman test, *p<0.05, **p<0.01, ***p<0.001, p<0.0001.

4.3 Discussion

We have demonstrated that the presence of nodal metastases has superior prognostic value than clinical tumour stage and TRG in OAC patients. This further highlights that the TDLN may play a pivotal role in orchestrating anti-tumour responses and subsequent treatment response in OAC patients and complements previous studies. This study is the first of its kind to longitudinally profile systemic anti-tumour immunity and circulating pro-metastatic mediators in oesophageal adenocarcinoma patients perioperatively. A number of issues remain with the current multimodal treatment for these patients, namely, poor treatment responses to the current gold standards, upstaging after neoadjuvant treatment, tolerance and toxicities. In addition to this, poor uptake in the adjuvant setting secondary to the significant morbidity of the surgical deconditioning of the patient and also an understandable reluctance to use therapies post operatively, which have had such poor regression results in the neoadjuvant setting (251). A further caveat being the doubling of the incidence of serious adverse events in chemotherapy cohorts when compared with immunotherapy trials for oesophageal cancer demonstrating the promise of immune checkpoint blockade due to reduced toxicities (252, 253).

Identifying patients at risk of relapse following surgery for OAC remains a challenge, but histological assessment of surgical specimens is an attractive means of predicting response. TRG 1-2, as determined by the Mandard or Becker systems, has a robust association with OS and disease free survival in resected specimens (170, 171, 225-227).

Pathological tumour extent in the resected specimen (pT) is also associated with recurrence and survival in OAC. Our results are in agreement with this, as TRG and pT stage are significant prognostic markers in patients following neoadjuvant treatment. In a *post hoc* analysis of the MAGIC trial of perioperative chemotherapy in resectable oesophagogastric cancer, both TRG1-2 and nodal status were negatively related to survival (228). However, after multivariate adjustment, it was only the presence of lymph node metastasis that was an independent predictor of OS (HR: 3.36; 95% CI, 1.70 to 6.63). Interestingly, a machine learning model developed to predict the risk of recurrence following neoadjuvant treatment found that the number of lymph node metastases was the most important variable in the model, with lymphovascular invasion second (254). This is similar to our findings as we demonstrate that nodal status has superior prognostic value compared to pT and TRG for patients treated with both chemoradiotherapy and perioperative chemotherapy.

A greater understanding of the relationship between the immune microenvironments of the tumour and lymph node will be useful in understanding response to chemoradiotherapy and future immunotherapy. Harnessing the power of TDLNs may also boost the clinical outcomes following ICB. Indeed, ongoing clinical trials are investigating the role of ICB alongside neoadjuvant chemoradiotherapy in locally advanced, operable gastroesophageal adenocarcinoma (NCT02730546, NCT03044613) (157). The LNME has been suggested to be an immunosuppressive niche. In one study, a mouse model of lung adenocarcinoma demonstrated that the LNME skews tumour antigen specific $CD4^+$ differentiation into regulatory T cells, thus promoting tumour immune escape (238). In human patients, lymph node metastases are associated with suppression of the $CD1a^+$ DC subset, a cellular population that is efficient at cross-presenting neoantigens to $CD8^+$ T cells. This immunosuppressive feature of the LNME

was correlated to local tumour recurrence (219). This also corresponded to an increased CD4:CD8 T cell ratio, and enrichment of regulatory T cells in the local nodal microenvironment in metastatic disease. This finding has since been replicated in breast and cervical cancer (236, 255), where DC suppression was associated with impaired T cell effector function.

Our data is broadly in agreement with these studies, however, we not only analysed the immune profile of the LNME, but also compared it to the immune microenvironment of primary tumour samples, demonstrating that the TME exhibited greater immunosuppression compared to the LNME. We found that the TME had higher levels of infiltrating T cells co-expressing multiple ICs, which typically denote T cell exhaustion, compared to the LNME. The presence of IC expression by T cells in the LNME was previously reported in one study of cervical cancer patients, but it was not compared with the TME (236). Using cytokine profiling, we also found that the TME had significantly lower levels of IL-21 and IFN-γ, compared to the LNME. This suggests a more suppressive immune landscape, as IFN-γ induces MHC molecule expression, promotes DC antigen presentation as well and encouraging $CD8^+$ T cell responses (256). Interestingly, in the KEYNOTE-028 clinical trial an IFN-γ gene expression signature was predictive of response to ICB in OAC patients, underscoring its role in the immune response to OAC (257). Similarly, IL-21 is produced by NK cells and $CD4^+$ T cells, driving tumour eradication in the kidney and skin (258), but has yet to be associated with the immune response in OAC. Levels of IL-9 and IL-27 were significantly higher in the LNME compared to the TME, with both having mixed or tumour promoting effects in terms of cancer progression (77). Collectively, our findings indicate greater immunosuppression in the TME compared to the LNME, which could explain why intact TDLNs are indispensable for the clinical activity of ICB in mouse models (239, 240).

However, the presence of exhausted T cells within a tumour does point toward a pre-existing antigen-specific anti-tumour immune response, a pre-requisite for response to ICBs.

The levels of immunosuppression in the LNME may also have clinical implications, as the presence of suppressed DC subsets in the TDLNs are negatively associated with recurrence and disease free survival in melanoma and breast cancer (234, 237). In our study, the frequency of $CD3^+TIM\text{-}3^+$ and $CD3^+PD\text{-}1^+$ cells present in TDLNs positively correlated with clinical tumour stage and the percentage of tumour-infiltrating $CD3^+CD8^+PD\text{-}1^+$ and $CD3^+CD8^+TIGIT^+$ cells positively correlated with clinical tumour nodal metastasis. These findings highlight the central role of the TDLNs in immune-mediated disease, control and potentially represent new methods of biomarker-driven patient stratification. Furthermore, PD-1, TIM-3 and TIGIT expression represent mechanisms of immune escape in OAC and perhaps ICBs targeting PD-1, TIM-3 and TIGIT may represent a more effective and personalised rational approach for treating oesophagogastric cancer patients

Although traditionally cancer cells were thought to spread to distant organs from lymph nodes through lymphatic vessels, recent preclinical studies suggest that cancer cells can invade local nodal blood vessels to enable a mixed haematogenous metastatic dissemination (218, 219). Thus, markers of angiogenesis and blood vessel formation may prove useful in understanding the metastatic potential of the TDLN. Levels of pro-angiogenic and wound healing markers including bFGF, PIGF and SAA were significantly higher within the LNME than the TME. These mediators play important roles in promoting wound healing, angiogenesis and tumour growth and therefore, may play a role in remodelling the TDLN into a tumour permissive niche enabling nodal metastasis. Levels of the vascular damage protein bFGF were significantly higher within

the TME compared with the LNME. Known functions of bFGF include enhancement of tumour cell proliferation, survival, motility and wound healing (86). Previous studies in oesophageal cancer demonstrated that bFGF overexpression is associated with a risk of tumour recurrence and reduced OS post-surgical resection, suggesting bFGF may play an important role in TME remodelling and enhancement of tumour progression (259).

The TCGA analysis of 72 primary OAC tumour samples which revealed high levels of pro-inflammatory and pro-angiogenic IL-6, IL-8 and Flt-1 in the TME identified OAC patients with reduced OS and represents a viable option for biomarkers or potential surrogates of survival. After further interrogation to determine if they correlate with treatment response, they may be incorporated into active stratification of patients into treatment arms.

In addition, pro-inflammatory chemokines in the TCM including Eotaxin-3, MCP-1, MCP-4 and TARC positively correlated with adverse tumour features such as lymphatic and vascular invasion. Collectively, this data highlights the detrimental role of tumour-promoting inflammation in OAC pathogenesis. Tumour-promoting inflammation is one of the enabling hallmarks of cancer and plays important roles in therapy resistance and tumour progression (260) . Interestingly, our study suggests that inflammation within the LNME may be beneficial as the levels of pro-inflammatory cytokines and chemokines negatively correlated with advanced tumour stage and further supports the hypothesis of tumour-promoting inflammation. The TDLN is a key orchestrator of anti-tumour immunity and therefore, a heightened state of immune activity would be expected within the LNME. This also highlights that anti-cancer, immune promoting therapies should be developed to target the TDLN and not just the TME.

The role of Th17 cells in cancer is controversial, with studies suggesting both pro- and anti-tumour effects in diverse cancer types (261). In this study, a Th17 cytokine signature within the TME positively correlated with clinical T stage suggesting perhaps a detrimental role for Th17 cells in OAC pathogenesis. In addition, TCGA analysis showed that mutations in the IL-17C gene was associated with significantly reduced OS and PFS in OAC patients. This finding is in agreement with prior work that detailed enrichment of Th17 cells in the TME of both gastric and oesophageal cancer (262, 263). Interestingly, the levels of soluble pro-inflammatory mediators positively correlated with the levels of pro-angiogenic mediators in both the TME and the LNME.

In summary, nodal involvement demonstrated superior prognostic value than clinical and pathological tumour staging, and soluble mediators within the LNME and TME correlated with clinical tumour stage suggesting the important role of both the LNME and TME in OAC progression and pathogenesis. These results also highlight the immunosuppressive nature of the TME demonstrated by higher percentages of T cells co-expressing multiple ICs in the TME compared to the LNME. However, the higher levels of pro-angiogenic mediators found within the LNME suggests an attempt by the local TME to remodel the TDLN toward a pre-metastatic permissive niche. Moreover, tumour-promoting inflammation was pinpointed as an adverse prognostic factor, however, a pro-inflammatory LNME negatively correlated with adverse tumour features. T cells in the LNME and TME expressing inhibitory ICs positively correlated with clinical tumour stage and clinical nodal involvement, respectively, which suggests that combination therapeutic blockade of PD-1, TIM-3 and TIGIT may have therapeutic rationale for boosting response rates in OAC.

The second part of this study assessed the immediate post-operative immune setting to identify potential therapeutic windows to enhance response to ICIs and reduce tumour

recurrence. The decrease in circulating lymphocytes in the immediate post-operative phase followed by the increase in cytotoxic lymphocytes at week 6 is intriguing in the context of the checkmate-577 trial data, as they found that the timing of adjuvant nivolumab after surgery has an impact on treatment efficacy, specifically >10 wk compared with < 10 wk, with Hazards ratios (HR) (95% CI) of 0.66 (0.52-0.84) and 0.84(0.57-1.22), respectively. Although a better physical recovery as the authors suggest may be key, a direct immunologic explanation such as increased circulating $CD8^+$ cells 6 weeks post-surgery from our study may be plausible, allowing more time for recovery of the patient's immune system post-chemo(radio)therapy treatment. However, the increased frequency of circulating CTLs 6 weeks post-surgery, might also reflect a build-up of CTLs in circulation in parallel with reduced homing of CTLs to the site of tumour excision, due to the removal of tumour-derived chemotactic signalling. This highlights a possible double-edged sword of surgery that not only removes immunosuppressive mediators but also anti-tumour factors, which might contribute to immune escape of residual pro-metastatic tumour cells and chemo(radio) resistant tumour cells that remain post-treatment and resection. However, it is unclear if the increase in circulating T cells 6 weeks post-surgery is due to a lack of homing to the tumour or perhaps a greater recovery of the immune system and subsequent increased production of CTLs which may reflect the hosts efforts to overcome the immunosuppressive effects of surgery.

It has been demonstrated that $CD69^+CD103^+$ tissue-resident memory T cells (T_{RM}), are non-recirculating cells residing in peripheral tissues and mediate tumour protection by promoting the tumour-immune equilibrium through the secretion of cytokines. Within the present study, a significant decrease in $CD3^+CD4^+CD69^+$ cells was observed at week six, potentially due to the removal of the immunosuppressive tumour. In addition to this, T_{RM} cells express inhibitory checkpoint molecules and may serve as potential targets for

cancer immunotherapy (264). It has also been demonstrated that an increase the early memory T cells including naïve T cells and effector cells is essential for efficient tumour killing especially for adoptive cancer immunotherapy (265). Thus, a system-level understanding of the mechanisms underlying the differentiation of effector and memory T cells is of increasing importance for developing immunological strategies against various tumours. (266). Furthermore, T cells with a naïve phenotype from TCR transgenic mice demonstrated enhanced anti-tumour activity following adoptive cell transfer compared with their mature T cell counterparts (267). In the current study, there was an increase in naïve T cells and a decrease in effector memory and central memory T cells in the immediate perioperative period and may reflect the adaptation of the host immune system to overcome the immunosuppressive milieu or indeed that the immunosuppressive environment has been removed.

The immune system recognizes and is poised to eliminate cancer, but is held in check by inhibitory immune checkpoint receptors and ligands and this is a mechanism co-opted by cancer to enhance immune evasion. These immune checkpoint pathways normally maintain immune homeostasis and self-tolerance to limit collateral healthy tissue injury immune responses. Drugs interrupting immune checkpoints, such as anti-CTLA-4, anti-PD-1, anti-PD-L1, and in early development anti-LAG-3 and anti-TIM-3, can unleash anti-tumour immunity and mediate durable cancer responses and regression. The complex biology of immune checkpoint pathways still contains many mysteries, and the full activity spectrum of immune checkpoint-blocking drugs, used alone or in combination, based on the principles of precision medicine, vis a vis the right patient for the right drug, is currently the subject of intense study.

The expression of the inhibitory immune checkpoint PD-1 on circulating T cells was highest in the immediate post-operative setting and significantly decreased by week 6 and

this is important in the context that programmed death-1 (PD-1) upon interaction with its ligand PD-L1, plays cardinal roles for induction of immune evasion in cancer cells (268). Similar trends were found for surface expression of CTLA-4, TIM-3, LAG-3, PD-L1 and PD-L2 on T cells with no significant change in TIGIT expression on the surface of T cells and suggests ICB as a target in the perioperative period.

There was a significant effect of surgery on the levels of circulating soluble immune checkpoints with a significant decrease in circulating levels of soluble PD-1, LAG-3, PD-L2, TIGIT, and TIM-3 in immediate post-operative setting, which return to baseline 6 weeks post operatively and this may reflect removal of their source of production through tumour excision and tumour-infiltrating immune cells. Soluble immune checkpoints may be a good or poor prognostic indicator depending on the soluble immune checkpoint in question, however, little is known about their function in particular for soluble TIGIT and PD-L2 (269). Studies have implicated immunosuppressive roles for the three soluble immune checkpoints that were increased in the immediate post-operative setting: sPD-L1, sCTLA-4 and sTIM-3, suggesting that in this context their increase in the immediate post-operative setting may be a reflection of the pleiotropic immunosuppressive effects of surgery.

Soluble PD-L1 decreases IFN-γ secretion by T cells and induces T cell apoptosis (270). Regulatory T cells are a prominent source of soluble CTLA-4, which has potent inhibitory properties suppressing IFN-γ-mediated Th1 immune responses (271). The biological effects of sTIM-3 are unknown, however, a study by Ge *et al.*, identified sTIM-3 as a negative prognostic indicator in osteosarcoma patients (272). In contrast, studies have indicated immunostimulatory roles for soluble PD-1 and LAG-3, which were both decreased in the immediate post-operative setting, further substantiating the hypothesis that surgery induces immunosuppression immediately post-operatively.

Soluble PD-1 and soluble LAG-3 were good prognostic indicators in non-small cell lung cancer (273) and gastric cancer patients, respectively (274). Moreover, Fougeray *et al.*, identified soluble LAG-3 protein as an immunopotentiator for therapeutic vaccines (275). Soluble LAG-3 binds to MHC class II inducing maturation of monocyte-derived dendritic cells *in vitro* and is used as a vaccine adjuvant to induce CD4 Th1 and CD8 T cell responses *in vivo* (275). Collectively this suggests that the surgery-induced downregulation of circulating levels of soluble PD-1 and LAG-3 may again be a reflection of surgery-induced immunosuppression. Interestingly, in this study patients with higher levels of circulating soluble LAG-3 in the post-operative setting (POD 3) had a better response to neoadjuvant CRT treatment determined by the Mandard pathological scoring system (TRG) (Supplemental Figure 1).

Chemotherapy and radiation therapy (RT) are standard therapeutic modalities for patients with oesophageal cancers and can induce forms of immunogenic cell death with subsequent release of tumour-derived antigens as well as danger signals, that could be captured for triggering anti-tumour immune responses (276). In the current study, intriguingly there is an increase in the expression of both DAMPS, calreticulin and HMGB1 in all three T cell compartments in the immediate post-operative period, which would suggest an anti-tumour response. However, paradoxically in a study on patients undergoing cytoreductive surgery, increased plasma levels of DAMPs were associated with immune suppression and postoperative infections in patients undergoing cytoreductive surgery (277, 278). Therefore, the concomitant increase in soluble checkpoints and DAMPS may represent the perfect timing for administration of immune checkpoint blockade to offset the prevailing immunosuppressive milieu.

This current study suggests an immunosuppressive milieu perioperatively with reduced Th1 cytokines in the immediate post-operative setting compared to pre-operative levels, upsetting the equilibrium through surgical stress and excision of the tumour burden with a reduction in IFN-γ, IL-12p40, CD28, CD40L and TNF-α. In addition, IP-10 (CXCL-10) which is an important chemokine ligand in recruiting anti-tumour Th1 cells and polarising the immune response to a Th1 phenotype, is significantly reduced perioperatively. There is a simultaneous increase in Th2 pro-tumour cytokines in the immediate post-operative setting, with a significant increase in IL-4, IL-10, IL-16, IL-1RA and MCP-1 before returning to preoperative levels at week 6. Immunosuppressive IL-10 inhibits the differentiation and activation of DCs, which are key activators of anti-tumour effector cells of the adaptive immune system, including cytotoxic $CD8^+$ T cells (279). Notably, this switch from a Th1 tumour-suppressive phenotype, which aids cytotoxic $CD8^+$ T cells in tumour rejection, to a Th2 tumour-promoting "regulatory" phenotype, which blocks $CD8^+$ T cell activity, is a characteristic outcome in the inflammatory, immune-suppressive tumour microenvironment (280). Myeloid-derived suppressor cells and macrophages recruited to the tumour microenvironment from the bone marrow by tumour cells and Tregs are also potent suppressors of anti-tumour immunity, when they are converted to an immunosuppressive phenotype by cytokines such as IL-10, which was found to increase perioperatively in our study and TGF-β (281) which are secreted by tumour tissue as well as other immune and stromal cells to promote recruitment and suppression of many immune cell types (282).

Interestingly, in parallel to the switch in Th1 to Th2 immunity observed in the systemic circulation, we also observed a concomitant increase in the levels of circulating soluble PD-L1 and significant decrease in circulating levels of PD-L2. PD-L1 plays an important role in dampening Th1 immune responses whereas PD-L2 is has been shown to play a

specific role in dampening Th2 responses (283). Collectively, these findings suggest that soluble PD-L1 and PD-L2 might play an important role in regulating the wound healing responses triggered by surgical excision, which is often characterised by a switch from pro-inflammatory immune responses to an anti-inflammatory immune response (246).

Specific chemokine ligands MIP-1α and MIP-1β, which recruit pro-inflammatory tumour-promoting myeloid immune cells (284), increased in the immediate post-op setting returning to baseline by week 6 and may represent a systemic pro-tumourigenic niche in the immediate post-operative period. In addition to this, high levels of MIP1-α on day 3 correlated with lymphatic invasion. MIP1-α has been implicated in promoting tumour metastasis to lymph nodes in oral squamous cell carcinoma (285). In addition, MIP1-α induced migration of MCF-7 breast cancer cells *in vitro* (286). Considering the findings of this study in the context of the existing literature MIP1-α may play an important role in promoting metastasis to lymph nodes in the immediate post-operative setting in OAC patients.

Metastatic disease is the leading cause of death among cancer patients and involves a complex and inefficient process, with a high rate of recurrence in oesophageal cancer, especially in the first 18 months (215, 287). Every step of the metastatic process can be rate limiting and is influenced by non-malignant host cells interacting with the tumour cell. Over a century ago, experiments first indicated a link between the immune system and metastasis (288). This phenomenon, called concomitant immunity, indicates that the primary tumour induces an immune response, which may not be sufficient to destroy the primary tumour, but prevents the growth of a secondary tumour or metastases. Since that time, many different immune cells have been shown to play a role in both inhibiting and promoting metastatic disease. There is a significant increase in CD276, an immune checkpoint molecule post operatively which peaked at week six. CD276 is aberrantly

overexpressed in many types of cancer, and such upregulation is generally associated with a poor clinical prognosis. There is also evidence to indicate an intricate role for CD276 (B7H3) in promoting carcinogenesis and metastasis (198, 289). VEGF-A and PIGF, are major pro-angiogenic factors associated with *cancer* angiogenesis and are pro-tumourigenic, while *Flt-1*, also known as vascular endothelial growth factor receptor 1 (VEGFR-1), is a high-affinity tyrosine kinase receptor for VEGF involved in *tumour* growth and metastasis (187). PIGF/Flt-1 signalling is integral in colorectal cancer progression through increasing the phosphorylation of p38 MAPK, thereby upregulating MMP9 expression; resulting in increasing cellular migration/invasion (186). There is an initial increase in these markers in the immediate post-operative setting which may represent a systemic pro-metastatic niche, which might be priming distal organs for metastatic dissemination and/or promoting the growth of micrometastatic deposits into overt secondary tumours. This is particularly telling in the fact that four of the cohort have already developed metastatic disease. VEGF-A circulating levels positively correlated with lymphatic invasion on day 3, with levels of circulating FLT-1 on day 1 positively correlating with a poor TRG. Importantly, three of those patients who developed metastatic disease had the highest expression of soluble PD-1, PD-L1 and TIM-3 perioperatively with a peak on day 7 and 2 of this cohort had significant increases in angiogenic markers at day 3 and day 7 post operatively.

Important clinical insights into the dynamic alterations in systemic immunity in the immediate 6-week post-operative window are provided offering guidance for the optimal scheduling of ICB with oncologic surgery. The prevailing immunosuppressive effect of surgery in the immediate post-operative window wherein a switch from Th1-Th2 immunity is observed including a significant rise in systemic tumour-promoting inflammatory and pro-metastatic mediators as early as 1-day post-surgery which returned

to baseline by week 6. This suggests that administering ICB in this 6-week post-operative window may shift the balance in favour of a Th1 phenotype offering a potent therapeutic approach for reducing tumourigenesis and promoting cancer regression. However, if ICB is administered pre-maturely post-operatively this may hamper healing as anti-inflammatory Th2-like immunity is critical in resolving the pro-inflammatory wound healing process and this carries potential implications of increased post-operative complications (290). Consequently, this body of work paves the way and provides guidance for further clinical studies to determine the optimal time to introduce ICB in the immediate neoadjuvant or adjuvant setting to propagate anti-tumour immunity whilst minimising the risk to increasing post-operative complications.

Chapter 5: The impact of radiation, hypoxia and nutrient deprivation on Damage Associated Molecular Pattern (DAMP) expression and cell viability

5.1 Introduction

The fundamental purpose of radiotherapy is the induction of maximal local tumour cell death and the abrogation of clonogenic survival, while sparing normal cells (291). In contemporaneous terms, radiotherapy remains a pillar of cancer treatment in the curative and neoadjuvant setting for oeosphageal cancer (4) and moreover it has become apparent that such conventional therapy can modulate the intimate cross-talk between tumours and systemic immunity and thus will determine anti-tumour responses (292). However, the crucial issue or radio-resistance owing to intrinsic mechanisms or acquired resistance remain to be overcome (293). A main factor related to radioresistance is the presence of cancer stem cells (CSC) within tumours, which are responsible for metastases, relapses, radiation therapy failure and a poor prognosis in cancer patients, and tumour heterogeneity plays an important role in acquired radiation resistance (294). Nonetheless, radiotherapy has been redefined as a partner for cancer immunotherapy and has shown promise notably in targeting metastatic tumours through the coveted abscopal effect and also may be exploited through the potential synergistic effect of the combination of these therapeutic modalities in overcoming radioresistance. (295).

One of the most promising effects of radiotherapy is immunologic cell death and the release damage-associated molecular patterns (DAMPs), which are able to trigger cancer cells and other cells within the tumour microenvironment (TME), which can induce suppression or promotion of tumour growth (296) One of the critical effects of DAMPs is the activation of dendritic cells (DC's). The exposure of DCs to some DAMPs leads to maturation of primed DCs, leading to their activation and successful presentation of antigens to $CD8^+$ T cells (297). The activation of $CD8^+$ T cells, known as cytotoxic T lymphocytes (CTLs) can directly kill tumour cells, trigger the recruitment of additional anti-tumour cells, release anti-cancer cytokines and inhibit tumour growth (298).

Calreticulin, one of the most widely known DAMPs is an endoplasmic reticulum resident protein with different roles including chaperone activity and maintenance of Ca^{2+} homeostasis and functionally regulates protein synthesis, cell proliferation, adhesion, invasion and nuclear transport (299, 300).

High mobility group box 1 (HMGB1) is another well-known DAMP molecule, and binds to toll-like receptor 4 (TLR4) on DCs, promoting antigen cross-presentation on the surface of T cells (301). Enhanced release of HMGB1 and increased calreticulin expression are important for priming antigen-specific T cell responses, thereby promoting synergistic effect between radiation and immunotherapy (302).

The role of the tumour microenvironment (TME) in cancer progression is evolving and garnering increased interest in the field where anti-tumour functions are downregulated, fundamentally in response to tumour-derived signals (303). Simultaneously, immune cells in the tumour microenvironment fail to exercise anti-tumour effector functions, and are often co-opted to promote tumour growth (304). The TME consists of an abundance of cancer cells of different metabolic phenotypes, reflecting fluctuating nutrient availability, to ensure their viability and propagation (305). Indeed, hypoxia is a common feature of tumour development and progression of solid tumours and is largely due to the rapid growth of tumour cells. Therefore, cancer and stromal cells often have restricted access to nutrients and oxygen (306). Most solid tumours have regions either permanently or transiently subjected to hypoxia because of dysregulated vascularisation and inconsistent supply (307). Often, hypoxia leads to their dysregulation in a way that supports cancer growth: fibroblasts can be transformed into tumour-prone cancer-associated fibroblasts (CAFs), ECM remodelling supports metastases, vascularisation process facilitates angiogenesis, and antitumour immune function becomes generally suppressed (303). Glucose and glutamine are central metabolites for catabolic and

anabolic metabolism, which is under investigation for diagnostic methodology and therapeutic potentials to overcome the often prevailing precarious immunosuppressive microenvironment (308). In the same vein, hypoxia may promote a number of events in the tumour microenvironment that can lead to the expansion and propagation of aggressive clones from heterogeneous tumour cells and thereby promote a lethal phenotype (309).

It must also be borne in mind tumour antigens need to be made accessible to the immune system, and the presence of adjuvants facilitating the recruitment, differentiation, and activation of antigen-presenting cells (APCs) in the microenvironment is essential for the successful priming of anti-tumour immunity (310). To this end, the orchestration of immunogenic forms of tumour cell death are known to release damage-associated molecular patterns (DAMPs), including Calreticulin and HMGB1, promoting the recruitment and maturation of APCs (311). The mode of cell death resulting from ionizing irradiation is not congruent and is dependent on the irradiation dose, the fractionation regimen, and the genetic repertoire of the irradiated cells, many of which remain to be elucidated (312). A number of studies have examined the initial steps of anti-tumour immune priming by fractionated and bolus radiation delivery (20 Gy, 4 × 2 Gy, 2 Gy, 0 Gy) with cell lines of triple-negative breast cancer *in vitro* and *in vivo* (310).

The aims of this chapter was to;

1. Evaluate the impact of fractionated and bolus dosing regimen radiotherapy and conditions of the tumour microenvironment on DAMP expression *in vitro*.
2. Evaluate the impact of conventional treatment modalities on DAMP expression *ex vivo* pre and post treatment.
3. Perform clinical correlations with DAMP expression on patient samples.

4. Examine the effect of ionising radiation, nutrient deprivation and immune checkpoint blockade on cell viability.

5.2 Results

5.2.1 Damage Associated Molecular Pattern Expression in an isogenic model of radioresistance following bolus and hypofractionated radiotherapy dosing.

In order to ascertain if different expression levels of DAMPs were detectable on radiosensitive (OE33P) and radioresistant (OE33R) oesophageal adenocarcinoma cell lines at baseline and following different doses of radiation, cells were stained with antibodies for a range of DAMPs and assessed by flow cytometry.

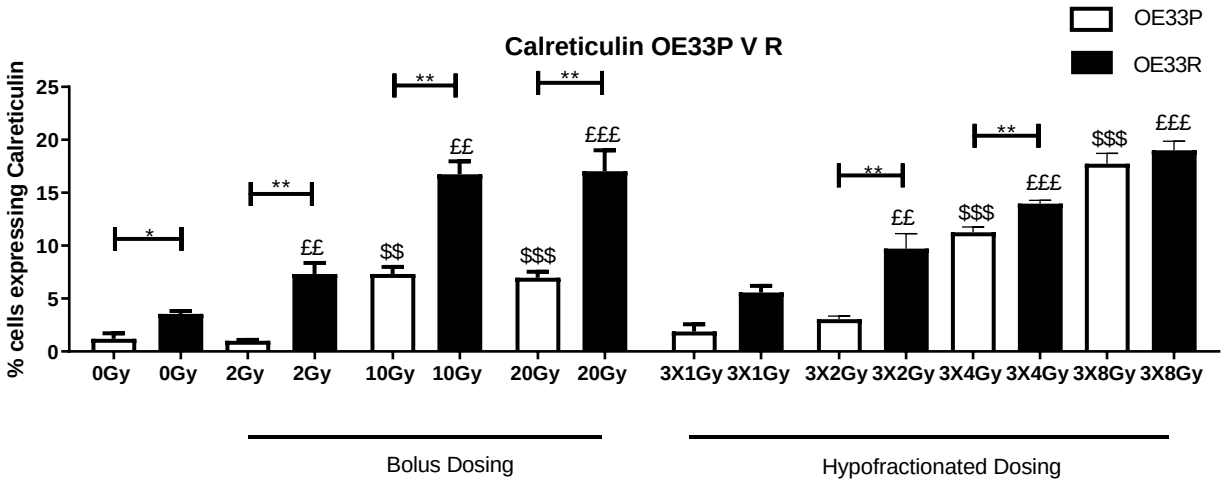

Figure 5.1 Calreticulin is expressed at a higher level on the OE33R cell line compared to the OE33P cell line. OE33P & OE33R cell lines were screened for the surface expression of Calreticulin by flow cytometry. Tukey's multiple comparison testing. Graph shows mean % expression (±SEM) (n=3). * denotes comparison of OE33P and OE33R, * P<0.05, ** p<0.01. £ denotes comparison of dosing with 0 Gy on OE33P, £ p<0.05, ££ p<0.01, £££ p<0.001. $ denotes comparison of dosing with 0 Gy on OE33R, $ P<0.05, $$ P<0.01, $$$ P<0.001.

In the OE33 P cell line, there was a significantly higher expression of Calreticulin in response to 10 Gy (7.33±0.66), 20Gy (6.96±0.56), 3x4 Gy (11.27±0.49) and 3x8 Gy (17.73±0.98) compared to 0 Gy (1.2±0.53) $p<0.01$, $p<0.001$, $p<0.001$, $p<0.001$ respectively (Figure 5.1).

In the OE33 R cell line, there was a significantly higher expression of Calreticulin in response to 2 Gy (7.32±1.03), 10 Gy (16.73±1.24), 20 Gy (17.03±1.97), 3x2 Gy (9.71±1.42), 3x4 Gy (16.1±0.32) and 3x8 Gy (19±0.87) compared to 0 Gy (3.56±0.26) $p<0.01$, $p<0.01$, $p<0.001$, $p<0.01$, $p<0.001$, $p<0.002$ respectively. There was a significantly higher expression of Calreticulin in the OE33R cell line at 0 Gy (3.56±0.26), 2 Gy (7.32±1.03), 10 Gy (16.73±0.32), 20 Gy (17.03±1.97), 3x2 Gy (9.71±1.42), 3x4 Gy (16.1±1.1) compared to 0Gy in the OE33 P cell line (1.2±0.52) $p<0.05$, 2 Gy (1.01±0.08) $p<0.01$, 10 Gy (7.33+/-0.66) $p<0.01$, 20 Gy (6.96+/-0.56), $p<0.01$, 3x2 Gy (3.05+/-0.28) $p<0.01$, 3x4 Gy (11.27+/-0.49) $p<0.01$ (Figure 5.1). Further significance between the dosing regimens are available in Appendix Table 1.

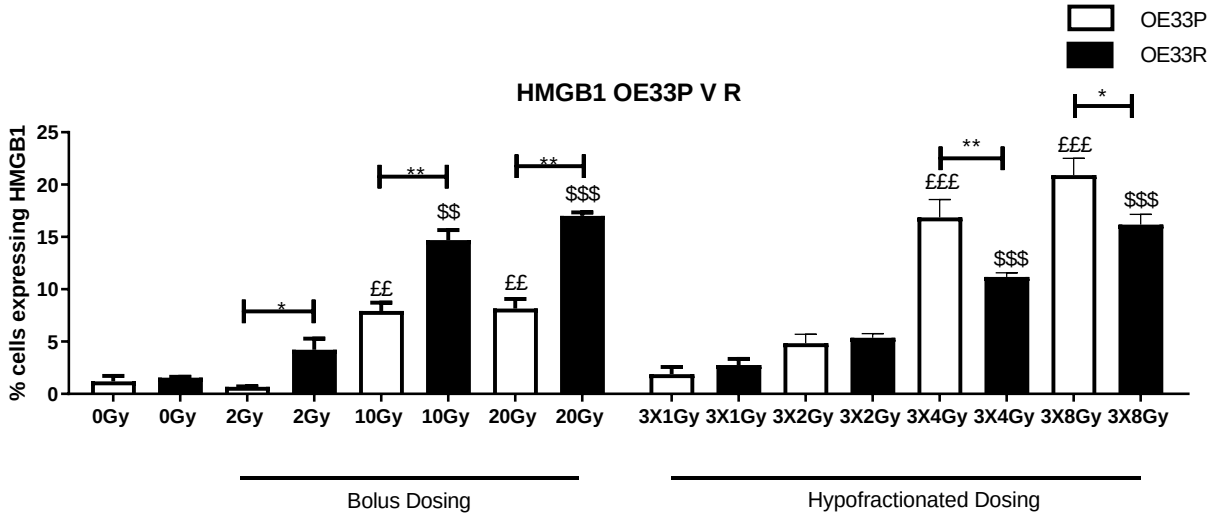

Figure 5.2 HMGB1 is expressed at a higher level on the OE33R cell line compared to the OE33P cell line with bolus dosing and at higher levels on the OE33P cell line with fractionated dosing. OE33P & OE33R cell lines were screened for the surface expression of HMGB1 by flow cytometry. Tukey's multiple comparison testing. Graph shows mean % expression (±SEM) (n=3). * denotes comparison of OE33P and OE33R, * P<0.05, ** p<0.01, *** P<0.001, **** P<0.0001. £ denotes comparison of dosing with 0 Gy on OE33P, £ p<0.05, ££ p<0.01, £££ p<0.001. $ denotes comparison of dosing with 0 Gy on OE33R, $ P<0.05, $$ P<0.01, $$$ P<0.001.

In the OE33P cell line, there was a significantly higher expression of HMGB1 in response to 10 Gy (7.93±0.79), 20 Gy (8.16±0.92), 3x4 Gy (16.87±1.7), 3x8 Gy (20.0±1.6) compared to 0 Gy (1.2±0.53) p<0.01, p<0.001, p<0.001, p<0.01, p<0.001 respectively (Figure 5.2).

In the OE33R cell line, there was a significantly higher expression of HMGB1 in response to 10 Gy (14.7±0.96), 20 Gy (17±0.35), 3x4 Gy (11.17±0.41) and 3x8 Gy (16.17±0.98) compared to 0 Gy (1.55±0.09) p<0.01, p<0.001, p<0.01, p<0.01, respectively. There is a higher expression of HMGB1 on OE33R with bolus dosing; 2 Gy (4.23±1.05), 10 Gy (14.7±0.96) and 20 Gy (17±0.35) compared to OE33P; 2 Gy (0.67±0.05), 10 Gy (7.93±0.79) and 20 Gy (8.16±0.91) p<0.05, p<0.01, p<0.01 respectively. There was a higher expression of HMGB1 with fractionated dosing 3x4 Gy in the OE33P cell line (16.87±1.7) and 3x8 Gy (20.9±1.6) compared to the OE33R cell line; 3x4 Gy (11.17±0.41) and 3x8 Gy (16.17±0.98) p<0.01, p<0.05 respectively (Figure 5.2). Further significance between the dosing regimens are available in Appendix Table 2.

5.3 Damage Associated Molecular Pattern Expression by age and passage matched OE33 P and OE33 R (model of radioresistance) cells following bolus and hypofractionated radiotherapy dosing under conditions of the Tumour Microenvironment (TME).

Glutamine is crucial for T cell activation, while glucose metabolism and aerobic glycolysis delivers intermediates for biosynthesis pathways, which is necessary for differentiation and proliferation of T cells. In hypoxia, cancer cells switch to glycolytic metabolism, which contributes to the acidification of the tumour microenvironment. These glycolytic metabolites including lactate can then be utilised by cancer cells and be pro-tumourigenic. The hypoxic microenvironment is also diverse with a vast supply of immune cells, with the tumour active in recruitment from the circulation. Of note, hypoxic cancer cells produce signalling molecules that promote the transformation of fibroblasts into cancer associated fibroblasts (CAFs). Often, hypoxia leads to the dysregulation of all immune cells in such a way that supports progression and subsequent metastases. For example, fibroblasts can be transformed into tumour-prone CAFs, vascularisation process facilitates cancer progression, and antitumour immune function becomes generally repressed. Hence all three factors, nutrient deprivation and hypoxia are of significant translational and clinical interest for their effects on their immunomodulatory effects on the immune system and are explored below.

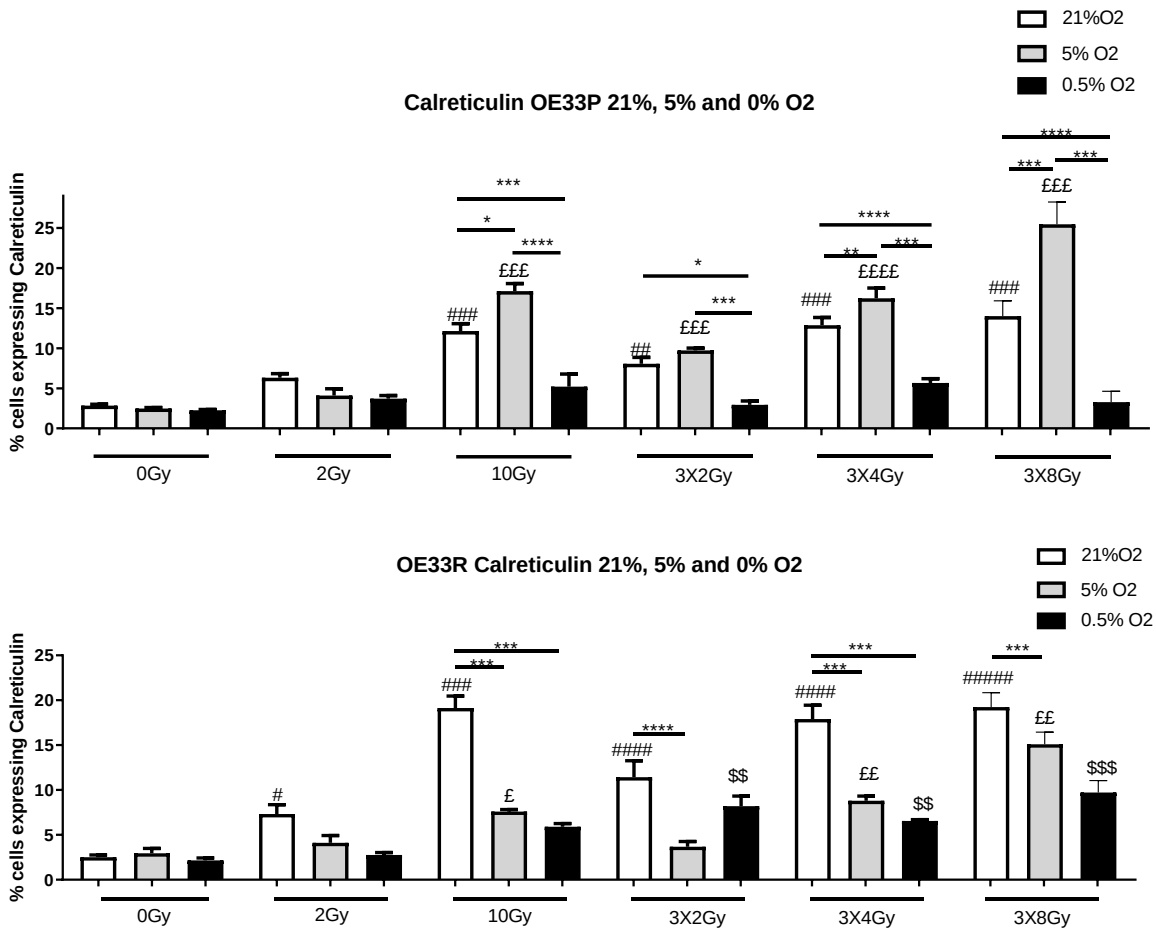

Figure 5.3. Calreticulin is expressed at a higher level under 5% Oxygenation in the OE33P cell line, with higher expression of Calreticulin under normal oxygenation compared to 5% and 0.5% hypoxia in the OE33R cell line. OE33P and OE33R cell lines were screened for the surface expression of Calreticulin by flow cytometry following bolus and fractionated radiation and culture under differing concentrations of oxygen. 21%=Normal oxygenation, 5%=mild hypoxia, 0.5%=severe hypoxia. Bolus dosing was administered once daily over three consecutive days. Staining of cancer cells took place 24hrs after last fraction of radiation. Tukey's multiple comparison testing. Graph shows mean % expression (±SEM) (n=3). * denotes comparison between oxygen levels for each radiation dosing regimen, * P<0.05, ** p<0.01, *** P<0.001, **** P<0.0001. # denotes comparison of dosing with 0 Gy at 21% 02, # P<0.05, ## p<0.01, ### P<0.001, #### P<0.0001. £ denotes comparison of dosing with 0 Gy at 5% O_2, £ p<0.05, ££ p<0.01, £££ p<0.001. $ denotes comparison of dosing with 0 Gy at 0.5% O_2, $ P<0.05, $$ P<0.01, $$$ P<0.001.

In the OE33P cell line, there was a significant increase in expression of Calreticulin in response to 10 Gy irradiation (12.13±0.92), fractionated dosing 3x2 Gy (8.05±0.81), 3x4 Gy (12.86±0.98) and 3x8 Gy (14±1.11) compared to non-irradiated cells (2.34±0.87) $p<0.001$, $p<0.01$, $p<0.001$, $p<0.001$ respectively. There was a significant increase in expression of Calreticulin with 10 Gy at 5% O_2 (5.21±1.58), 3x2 Gy at 5% O_2 (9.73±0.29), 3x4 Gy at 5%O_2 (16.23±1.27), 3x8 Gy at 5% O_2 (25.47±1.61) compared to 0 Gy 5% O_2 (2.49±0.11) $p<0.001$, $p<0.01$, $p<0.01$, $p<0.001$ respectively. There was a significantly higher expression of Calreticulin in response to 10 Gy 5% O_2 (17.13±0.93) compared to 10 Gy (12.13±0.93) with normal oxygen concentrations $p<0.05$, and 10 Gy 0.5% O_2 (5.21±1.58) $P<0.001$ and 10 Gy 5% O_2 compared to 10 Gy 0.5% O_2 $p<0.001$. There was a significantly increased expression of Calreticulin at 3x2 Gy under normal oxygenation (8.05±0.81) compared to 3x2 Gy 5% O_2 (9.72±0.29) $p<0.001$) and 3x2 Gy 5% O_2 compared to 3x2 Gy 0.5% O_2 (2.94±0.48) $p<0.001$. There was a significantly higher expression of Calreticulin at 3x4 Gy normoxia (12.86±0.98) compared to 3x4 Gy 5% O_2 (16.23±1.27) $p<0.01$ and 3x4 Gy 0.5% O_2 (5.67±0.52) $p<0.001$ and a significantly higher expression of Calreticulin at 3x4 Gy 5% O_2 compared to 0.5% O_2 $p<0.001$. There was a significantly higher expression of Calreticulin at 3x8 Gy normal oxygenation (14±1.11) compared to 3x8 Gy 5% O_2 (25.47±1.61) $p<0.001$, 3x8 Gy 5% O_2 compared to 0.5% O2 (3.28±0.77) $p<0.001$, and 3x8 Gy 5% O_2 compared to 3x8 Gy 0.5% O_2 $p<0.001$ (Figure 5.3).

In the OE33 R cell line there was a significant increase in expression of Calreticulin in response to 2 Gy irradiation (7.32±1.03), 10 Gy irradiation (19.13±2.32), fractionated dosing 3x2 Gy (11.44±1.82), 3x4 Gy (17.9±1.55) and 3x8 Gy (19.23±0.93) compared to

non-irradiated cells (0 Gy) (2.3±0.25) $p<0.01$, $p<0.001$, $p<0.001$, $p<0.001$, $p<0.001$ respectively. There was a significant increase in expression of Calreticulin in response to 10 Gy at 5% O_2 (7.59±0.24), 3x4 Gy at 5% O_2 (8.8±0.52), 3x8 Gy at 5% O_2 compared to 0 Gy 5% O_2 (2.95±0.54) $p<0.05$, $p<0.01$, $p<0.01$ respectively. There was a significant increase in expression of Calreticulin with 3x2 Gy at 0.5% O_2 (8.2±1.13), 3x4 Gy 0.5% O_2 (6.55±0.14) and 3x8 Gy 0.5% O_2 (9.71±0.78) compared to 0 Gy 0.5% O_2 (2.15±0.27) $p<0.01$, $p<0.01$, $p<0.001$ respectively. There was a significantly higher expression of Calreticulin in response to 10Gy with normal oxygen concentrations (19.13±2.32) compared to 10 Gy 5% O_2 (7.59±0.24) $p<0.001$, and 10 Gy 0.5% O_2 (5.9±0.36) $p<0.001$. There was a significantly increased expression of Calreticulin at 3x2 Gy under normal oxygenation (11.44±1.82) compared to 3x2 Gy 5% O_2 (3.68±0.59) $p<0.001$). There was a significantly higher expression of Calreticulin at 3x4 Gy normoxia (17.9±1.55) compared to 3x4 Gy 5% O_2 (8.8±0.52) $p<0.001$ and 3x4 Gy 0.5% O_2 (6.55±0.14) $p<0.001$. There was a significantly higher expression of Calreticulin in response to 3x8 Gy normal oxygenation (19.23±0.93) compared to 3x8 Gy 5% O_2 (15.1±0.78) $p<0.001$ (Figure 5.3). Further significance between the dosing regimens and conditions of the TME are available in Appendix Table 3.

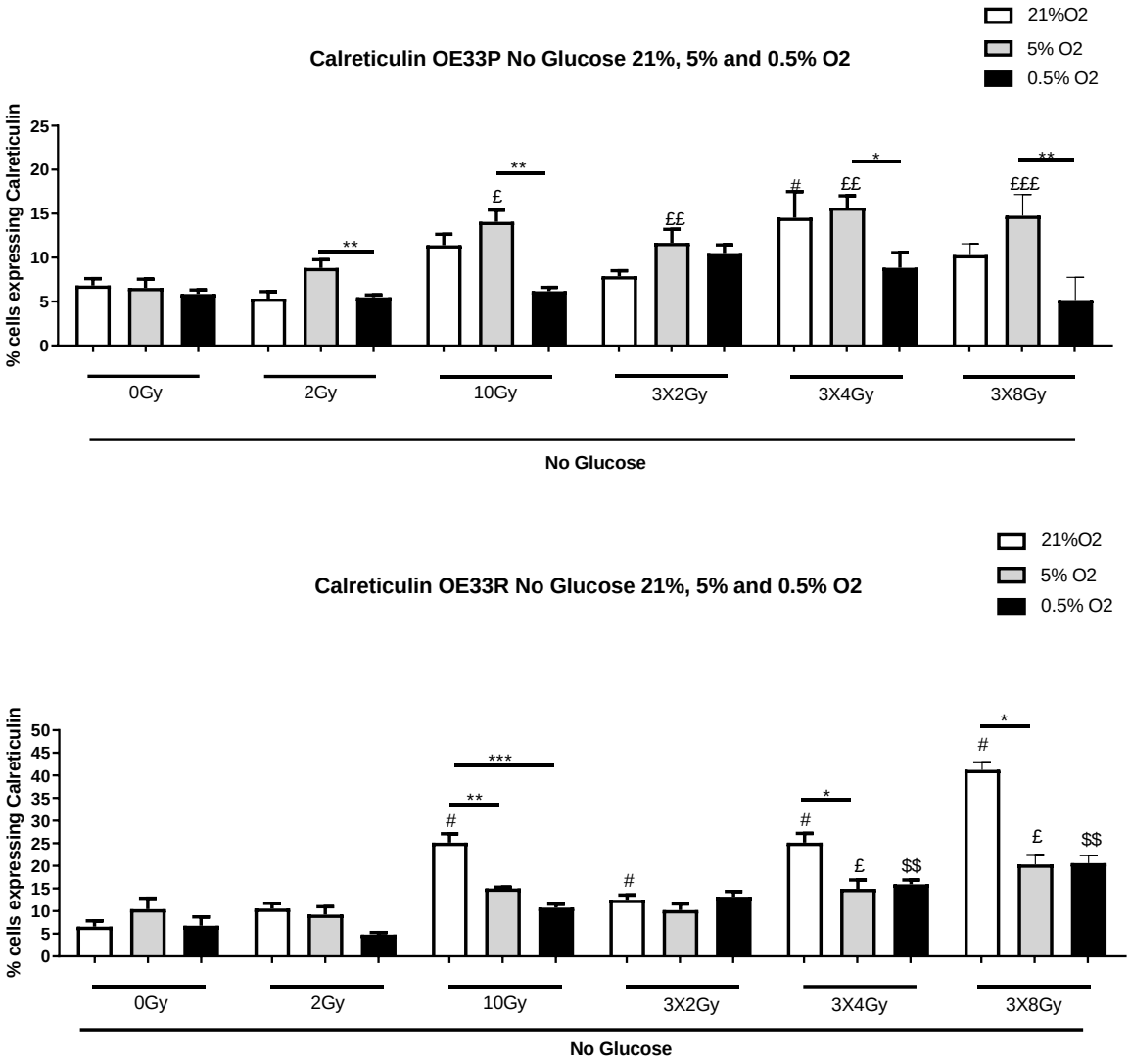

Figure 5.4. Calreticulin is expressed at a higher level under 5% Oxygenation no Glucose in the OE33P cell line, with higher expression of Calreticulin under normal oxygenation no Glucose compared to 5% O_2 no Glucose and 0.5% O_2 no Glucose in the OE33R cell line. OE33P and OE33R cell lines were screened for the surface expression of Calreticulin by flow cytometry. 21%=Normal oxygenation, 5%=mild hypoxia, 0.5%=severe hypoxia. Bolus dosing was administered once daily over three consecutive days. Staining of cancer cells took place 24hrs after last fraction of radiation. Tukey's multiple comparison testing. Graph shows mean % expression (±SEM) (n=3). * denotes comparison between oxygen levels for each radiation dosing regimen, * P<0.05, ** p<0.01, *** P<0.001, **** P<0.0001. # denotes comparison of dosing with 0Gy at 21% O_2, # P<0.05, ## p<0.01, ### P<0.001, #### P<0.0001. £ denotes comparison of

dosing with 0 Gy at 5% O_2, £ p<0.05, ££ p<0.01, £££ p<0.001. $ denotes comparison of dosing with 0 Gy at 0.5% O_2, $ P<0.05, $$ P<0.01, $$$ P<0.001.

In the OE33P cell line there was a significant increase in expression of Calreticulin in response to 10 Gy at 5% O_2 (14.07±1.33), 3x2 Gy at 5% O_2 (11.68±1.54), 3x4 Gy at 5% O_2 (15.7±1.33), 3x8 Gy at 5% O_2 (14.77±1.39) compared to 0 Gy 5% O_2 (6.55±0.99) p<0.05, p<0.01, p<0.01, p<0.001 respectively. There was a significantly higher expression of Calreticulin in response to 2 Gy 5% O_2 (8.82±0.95) compared to 2 Gy 0.5% O_2 (5.49±0.27) p<0.01, 10 Gy 5% (14.07±1.33) compared to 10 Gy 0.5% O_2 (6.18±0.43) p<0.01, 3x4 Gy 5% (15.7±1.33) compared to 3x4 Gy 0.5% (8.85±1.74) p<0.05, and 3x8 Gy 5% (14.77±1.39) compared to 3x8 Gy 0.5% O_2 (5.18±1.49) p<0.01 (Figure 5.4).

In the OE33R cell line there was a significant increase in expression of Calreticulin in response to 10 Gy (25.13±1.96), 3x2 Gy (12.5±1.04), 3x4 Gy (25.13±2.07), and 3x8 Gy (41.23±1.02) compared to non-irradiated cells (6.55±1.3), p<0.05. There was a significantly higher expression of Calreticulin at 3x4 Gy 5% O_2 (14.93±-1.94), 3x8 Gy 5% O_2 (20.3±1.29) compared to non-irradiated cells at 5% O_2 (10.42±2.44) p<0.05. There was also a significantly higher expression of Calreticulin at 3x4 Gy 0.5% O_2 (15.93±0.97), 3x8 Gy 0.5% O2 (20.6±1) compared to non-irradiated cells (6.78±1.94) p<0.01. There was also a significantly higher expression of Calreticulin in response to 10 Gy normoxia (25.13±1.96) compared to 10 Gy 5% O_2 (15±0.3) p<0.01 and 10 Gy 0.5% O_2 (10.77±0.78) P<0.001. There was a significantly higher expression of Calreticulin at 3x4 Gy normoxia (25.13±2.07) compared to 3x4 Gy 5% O_2 (14.93±1.94) p<0.05 and 3x8 Gy normoxia (41.23±1.02) compared to 3x8 Gy 5% O_2 (10.77±0.78) P<0.05 (Figure 5.4).

Further significance between the dosing regimens and conditions of the TME are available in Appendix Table 4.

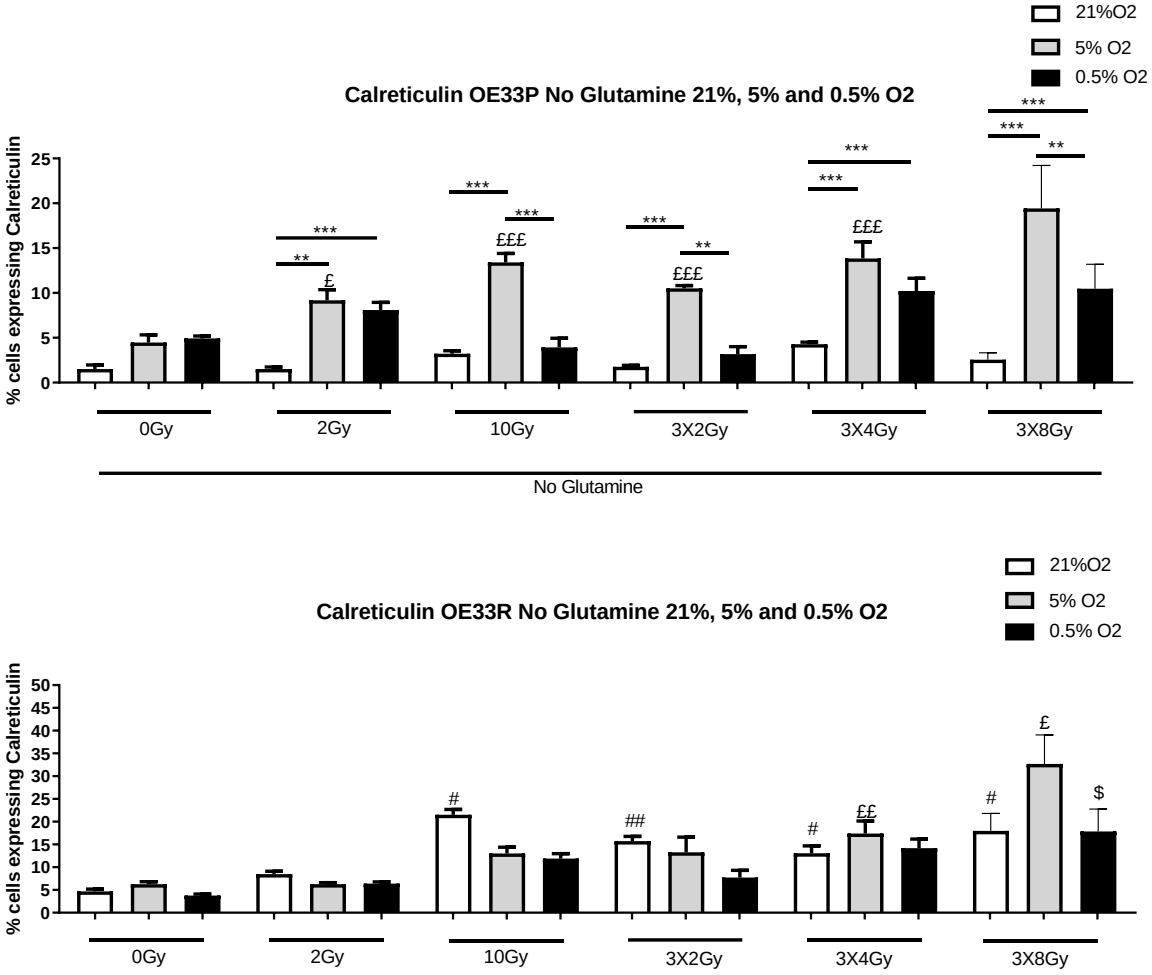

Figure 5.5 Calreticulin is expressed at a higher level under 5% Oxygenation no Glutamine and O.5% Oxygenation no Glutamine in the OE33P cell line, with a mixed pattern of expression of Calreticulin in the OE33R cell line. OE33P & OE33R cell lines were screened for the surface expression of Calreticulin by flow cytometry. 21%=Normal oxygenation, 5%=mild hypoxia, 0.5%=severe hypoxia. Bolus dosing was administered once daily over three consecutive days. Staining of cancer cells took place 24hrs after last fraction of radiation. Tukey's multiple comparison testing. Graph shows mean % expression (±SEM) (n=3). * denotes comparison between oxygen levels for each radiation dosing regimen, * P<0.05, ** p<0.01, *** P<0.001, **** P<0.0001. # denotes comparison of dosing with 0Gy at 21% 02, # P<0.05, ## p<0.01, ### P<0.001, ####

P<0.0001. £ denotes comparison of dosing with 0 Gy at 5% O2, £ p<0.05, ££ p<0.01, £££ p<0.001. $ denotes comparison of dosing with 0 Gy at 0.5% O2, $ P<0.05, $$ P<0.01, $$$ P<0.001.

In the OE33P cell line there was a significant increase in expression of Calreticulin no glutamine with 2 Gy at 5% O_2 (9.18±1.19), 10Gy at 5% O_2 (13.4±1), 3x2 Gy at 5% O_2 (10.5±0.32), 3x4 Gy at 5% O_2 (13.83±1.86), compared to 0 Gy 5% O_2 (4.46±0.86) p<0.05, p<0.01, p<0.05, p<0.001, p<0.001, p<0.001 respectively. There is a significantly higher expression of Calreticulin at 2 Gy 5% O_2 no glutamine (9.18±1.19) and 2 Gy 0.5% O_2 no glutamine (8.1±0.85) compared to 2 Gy normoxia (1.53±0.22) p<0.01, p<0.001 respectively. There is a significantly higher expression of Calreticulin at 10 Gy 5% O_2 (13.4±1) compared to 10 Gy normoxia (3.22±0.33) p<0.001 and 10 Gy 0.05% O_2 (3.94±1.1) p<0.001. There is a significantly higher expression of Calreticulin at 3x2 Gy 5% O_2 (10.4±0.32) compared to 3x2 Gy normoxia (1.75±0.17) p<0.01 and 3x2 Gy 0.5% O_2 (3.18±0.82) p<0.001. The expression of Calreticulin is significantly higher with 3x4 Gy 5% O_2 no glutamine (13.83±1.86) and 3x4 Gy 0.5% O_2 no glutamine (10.21±1.42) compared to 3x4 Gy normoxia (4.27±0.24) p<0.001. There was also a significantly higher expression of Calreticulin at 3x8 Gy 5% O_2 no glutamine (19.43±2.76) and 3x8 Gy 0.5% O_2 no glutamine (10.48±1.58) compared to 3x8 Gy normoxia no glutamine (2.56±.44) p<0.001 (Figure 5.5).

In the OE33R cell line there was a significantly higher expression of Calreticulin in response to 10 Gy no glutamine (21.5±1.19), 3x2 Gy no glutamine (15.73±1.04), 3x4 Gy no glutamine (13.05±1.65) and 3x8 Gy no glutamine (17.7±2.83) compared to 0 Gy no glutamine (4.68±0.49) p<0.05, p<0.01, p<0.05, p<0.05 respectively. There was a

significantly higher expression of Calreticulin at 3x4 Gy 5% O_2 no glutamine (17.5±2.75) and 3x8 Gy 5% O_2 no glutamine (32.7±3.67) compared to 0 Gy 5% O_2 no glutamine (6.25±0.58) $p<0.01$, $p<0.05$ respectively. There was an increased expression of Calreticulin at 3x8 Gy 0.5% O_2 no glutamine (17.87±2.83) compared to 0 Gy 0.5% O_2 no glutamine (3.76±0.35) $p<0.05$ (Figure 5.5). Further significance between the dosing regimens and conditions of the TME are available in Appendix Table 5.

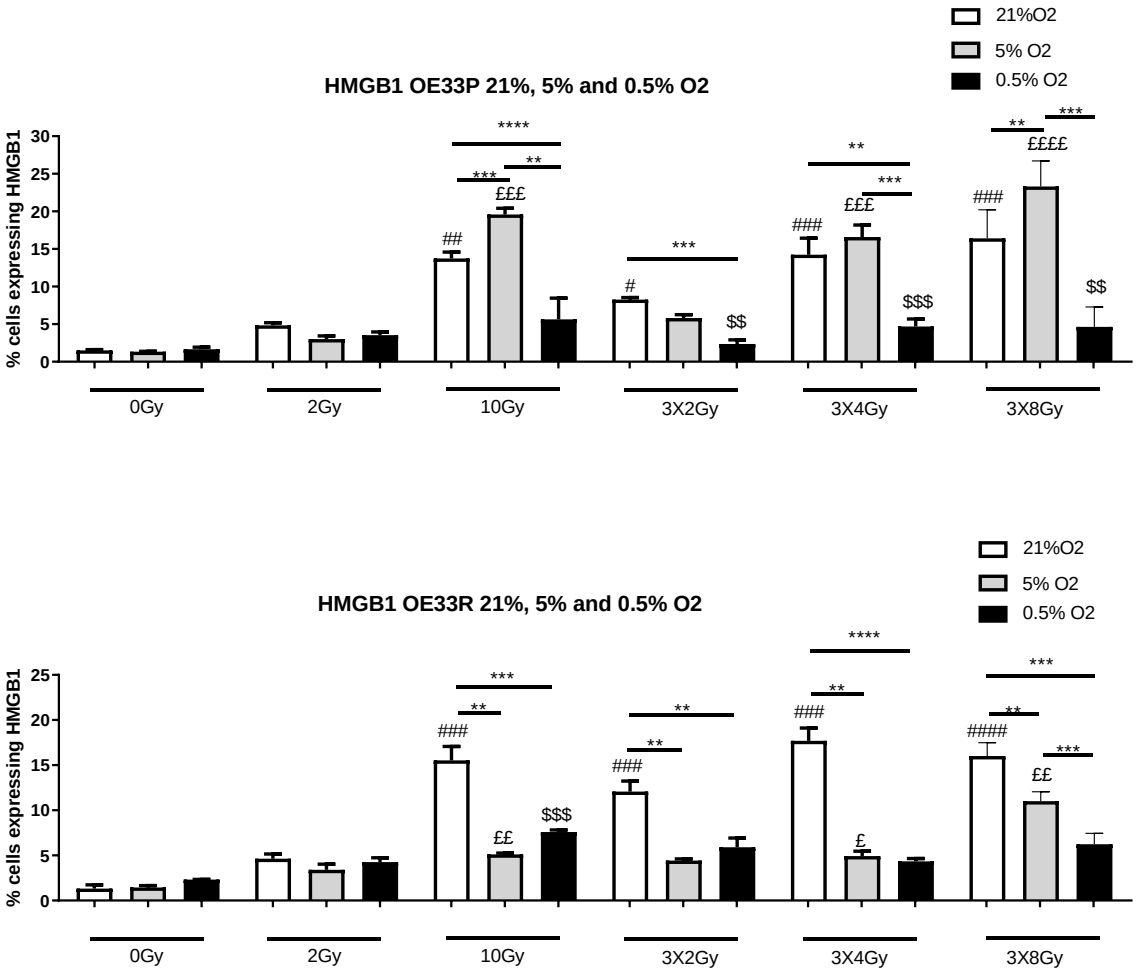

Figure 5.6. HMGB1 is expressed at a higher level under 5% Oxygenation no Glucose in the OE33P cell line, with a higher expression of HMGB1 under normal oxygenation in the OE33R cell line. OE33P and OE33R cell lines were screened for the surface expression of HMGB1 by flow cytometry. 21%=Normal oxygenation, 5%=mild hypoxia, 0.5%=severe hypoxia. Bolus dosing was administered once daily over three

consecutive days. Staining of cancer cells took place 24hrs after last fraction of radiation. Tukey's multiple comparison testing. Graph shows mean % expression (±SEM) (n=3). * denotes comparison between oxygen levels for each radiation dosing regimen, * $p<0.05$, ** $p<0.01$, *** $p<0.001$, **** $p<0.0001$. # denotes comparison of dosing with 0 Gy at 21% O_2, # $p<0.05$, ## $p<0.01$, ### $p<0.001$, #### $p<0.0001$. £ denotes comparison of dosing with 0 Gy at 5% O_2, £ $p<0.05$, ££ $p<0.01$, £££ $p<0.001$. $ denotes comparison of dosing with 0 Gy at 0.5% O_2, $ $p<0.05$, $$ $p<0.01$, $$$ $p<0.001$.

In the 0E33P cell line there was a significantly higher expression of HMGB1 in response to 10 Gy normoxia (13.73±0.86), 3x2 Gy normoxia (8.26+/-0.28), 3x4 Gy normoxia (14.23±2.2), 3x8Gy normoxia (16.4±2.2) compared to 0 Gy normoxia (1.51±0.12) $p<0.01$, $p<0.05$, $p<0.001$, $p<0.001$ respectively. There was also a significantly higher expression of HMGB1 at 10 Gy 5% O_2 (19.6±0.82), 3x4 Gy 5% O_2 (16.6±1.59), 3x8 Gy 5% O_2 (23.2±1.97) compared to 0 Gy 5% O_2 (1.33±0.05) $p<0.001$, $p<0.001$, $p<0.001$. There is a significantly higher expression of HMGB1 at 3x2 Gy 0.5% O_2 (2.36±0.55), 3x4 Gy 0.5% O_2 (4.68±1.01) and 3x8 Gy 0.5% O_2 (4.65±1.52) compared to 0 Gy 0.5% O_2 (1.67±0.26) $p<0.01$, $p<0.001$, $p<0.01$ respectively. There was a significantly higher expression of HMGB1 at 10 Gy 5% O_2 (19.6±0.82) compared to 10 Gy normoxia (13.73±0.86) $p<0.001$ and 10 Gy 0.5% O_2 (5.64±2.83) $p<0.001$. There was a significantly higher expression of HMGB1 at 3x2 Gy normoxia (8.26±0.28) compared to 3x2 Gy 0.5% O_2 (2.36±0.55) $p<0.001$. There was also a significantly higher expression of HMGB1 at 3x4 Gy normoxia (14.23±2.2) and 3x4 Gy 5% O_2 (16.6±1.59) compared to 3x4 Gy 0.5% O_2 (4.68±1) $p<0.01$, $p<0.001$ respectively. There was a significantly higher expression of HMGB1 at 3x8 Gy 5% O_2 (23.3±1.97) compared to 3x8 Gy normoxia (16.4±2.2) $p<0.01$ and 3x8 Gy 0.5% O_2 (4.65±1.52) $p<0.001$ (Figure 5.6).

In the OE33R cell line, there was a significantly higher expression of HMGB1 in response to 10 Gy (15.53±1.55), 3x2 Gy (12.07±1.17), 3x4 Gy (17.7±1.42) and 3x8 Gy (16±0.86) compared to 0 Gy normoxia (1.32±0.43) $p<0.001$, $p<0.001$, $p<0.001$, $p<0.0001$ respectively. There is a significantly higher expression of HMGB1 in response to 10 Gy 5% O_2 (5.11±0.44), 3x4 Gy 5% O_2 (4.92±0.55) and 3x8 Gy 5% O_2 (11±0.61) compared to 0 Gy 5% O_2 (1.45±0.2) $p<0.01$, $p<0.05$, $p<0.01$ respectively. There was also a significantly higher expression of HMGB1 at 10 Gy 0.5% O_2 (7.59±0.24) compared to 0 Gy 0.5% O_2 (2.32±0.3) $p<0.01$. There was a significantly higher expression of HMGB1 in response to 10 Gy normoxia (15.53±1.55) compared to 10 Gy 5% O_2 (5.11±0.14) $p<0.01$ and 10 Gy 0.5% O_2 (7.59±0.24) $p<0.001$. There was also a significantly higher expression of HMGB1 at 3x2 Gy normoxia (12.07±1.17) compared to 3x2 Gy 5% O_2 (4.42±0.19) $p<0.01$ and 3x2 Gy 0.5% O_2 (5.91±1.02) $p<0.01$. There was a significantly higher expression of HMGB1 at 3x4 Gy normoxia (17.7±1.42) compared to 3x4 Gy 5% O_2 (4.92±0.55) $p<0.001$ and 3x4 Gy 0.5% O_2 (4.35±0.31) $p<0.001$. There was a significantly higher expression of HMGB1 at 3x8 Gy normoxia (16±0.86) compared to 3x8 Gy 5% O_2 (11±0.61) $p<0.001$ and 3x8 Gy 0.5% O_2 (6.24±0.69) $p<0.001$ (Figure 5.6). Further significance between the dosing regimens and different levels of oxygenation are available in Appendix Table 6.

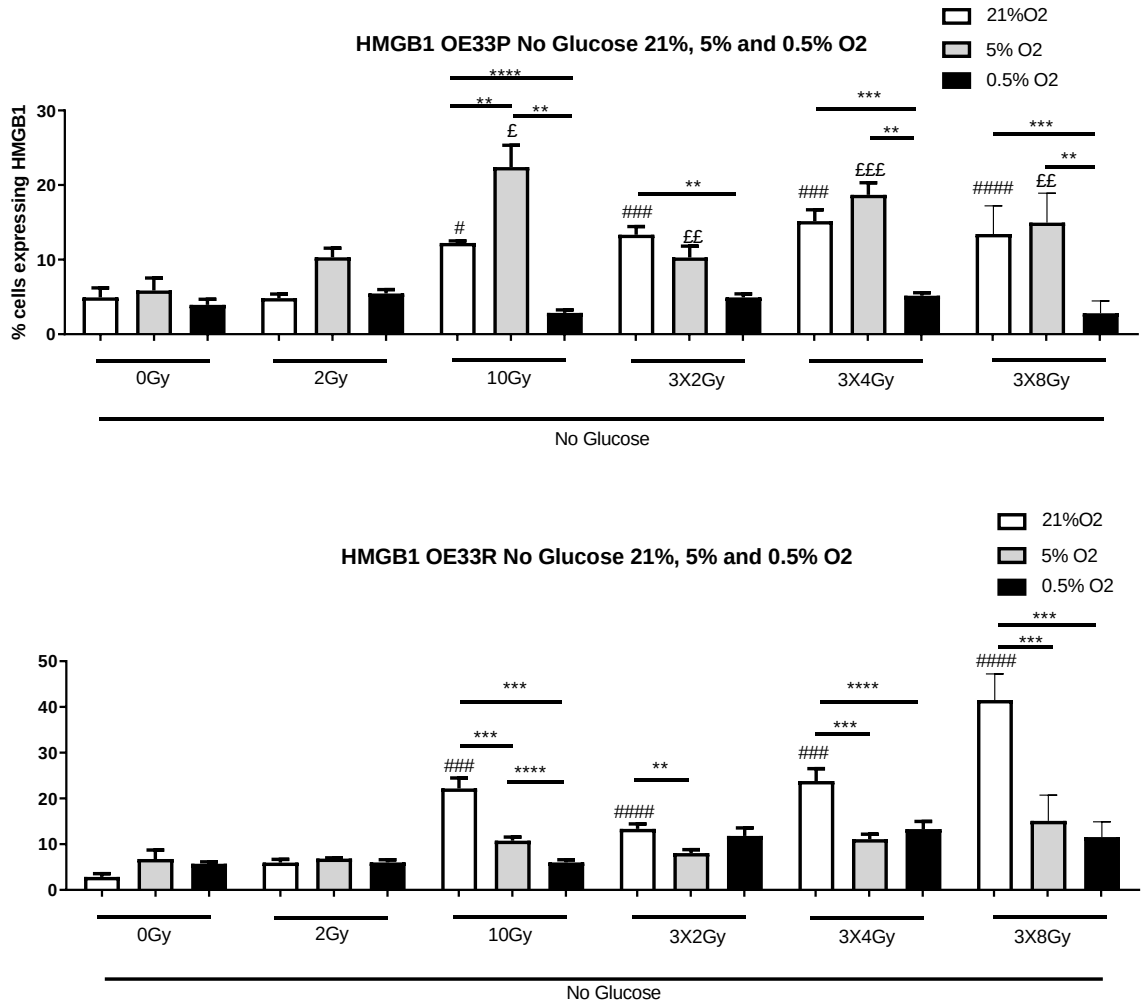

Figure 5.7. HMGB1 is expressed at a higher level under 5% Oxygenation no Glucose in the OE33P cell line, with a higher expression of HMGB1 under normal oxygenation in the OE33R cell line. OE33P and OE33R cell lines were screened for the surface expression of HMGB1 by flow cytometry. 21%=Normal oxygenation, 5%=mild hypoxia, 0.5%=severe hypoxia. Bolus dosing was administered once daily over three consecutive days. Staining of cancer cells took place 24hrs after last fraction of radiation. Tukey's multiple comparison testing. Graph shows mean % expression (±SEM) (n=3). * denotes comparison between oxygen levels for each radiation dosing regimen, * P<0.05, ** p<0.01, *** p<0.001, **** p<0.0001. # denotes comparison of dosing with 0Gy at 21% O_2, # p<0.05, ## p<0.01, ### p<0.001, #### p<0.0001. £ denotes comparison of dosing with 0Gy

at 5% O_2, £ $p<0.05$, ££ $p<0.01$, £££ $p<0.001$. $ denotes comparison of dosing with 0Gy at 0.5% O_2, $ $p<0.05$, $$ $p<0.01$, $$$ $p<0.001$.

In the OE33 P cell line, there was a significantly increased expression of HMGB1 in response to 10 Gy normoxia no glucose (12.23±0.27), 3x2 Gy (13.33±1.11), 3x4 Gy (15.17±1.52) and 3x8 Gy (13.44±2.18) compared to 0 Gy normoxia no glucose (4.95±1.25) $p<0.05$, $p<0.001$, $p<0.001$, $p<0.0001$ respectively. There was a significantly higher expression of HMGB1 in response to 10 Gy 5% O_2 no glucose (22.4±2.94), 3x2 Gy 5% O_2 no glucose (10.28±1.53), 3x4 Gy 5%O_2 no glucose (18.7±1.6) and 3x8 Gy 5% O_2 no glucose (14.97±2.28) $p<0.05$, $p<0.01$, $p<0.001$, $p<0.01$ respectively. There was a significantly higher expression of HMGB1 in response to 10 Gy 5% O_2 no glucose (22.4±2.94) compared to 10 Gy normoxia no glucose (12.23±0.27) $p<0.01$ and 10 Gy 0.5% O_2 no glucose (2.86±0.41) $p<0.001$. There was a significantly higher expression of HMGB1 at 3x2 Gy normoxia no glucose (13.33±1.11) compared to 3x2 Gy 0.5% O_2 no glucose (4.95±0.47) $p<0.01$. There was a significantly lower expression of HMGB1 at 3x8 Gy 0.5% O_2 no glucose (2.81±0.95) compared to 3x8 Gy normoxia no glucose (13.44±2.18) $p<0.001$ and 3x8 Gy 5% O_2 no glucose (14.97±2.28) $p<0.01$ (Figure 5.7).

In the OE33R cell line there was a significantly higher expression of HMGB1 in response to 10 Gy normoxia no glucose (22.17±2.31), 3x2 Gy (13.33±1.11), 3x4 Gy (23.8±2.71) and 3x8 Gy (41.53±3.28) compared to 0 Gy normoxia no glucose (2.83 ±0.71) $p<0.001$, $p<0.001$, $p<0.0001$, $p<0.001$ respectively. There was a significantly higher expression of HMGB1 at 10 Gy normoxia no glucose (22.17±2.31) compared to 10 Gy 5% O_2 no glucose (10.77±0.78) $p<0.001$, and 10 Gy 0.5% O_2 no glucose (6.03±0.59)

p<0.001. Additionally, there was a significantly higher expression of HMGB1 in response to 10 Gy 5% O_2 no glucose (10.77±0.78) compared to 10 Gy 0.5% O_2 no glucose (6.03±0.59) p<0.01. There was a significantly higher expression of HMGB1 at 3x2 Gy normoxia no glucose (13.33±1.11) compared to 3x2 Gy 5% O_2 no glucose (8.08±0.74) p<0.01. There was a significantly higher expression of HMGB1 at 3x8 Gy normoxia no glucose (41.53±3.28) compared to 3x8 Gy 5% O_2 no glucose (15.1±3.25) p<0.001 and 3x8 Gy 0.5% O_2 no glucose (11.56±1.93) p<0.0001 (Figure 5.7). Further significance between the dosing regimens, different levels of oxygenation and glucose deprivation are available in Appendix Table 7.

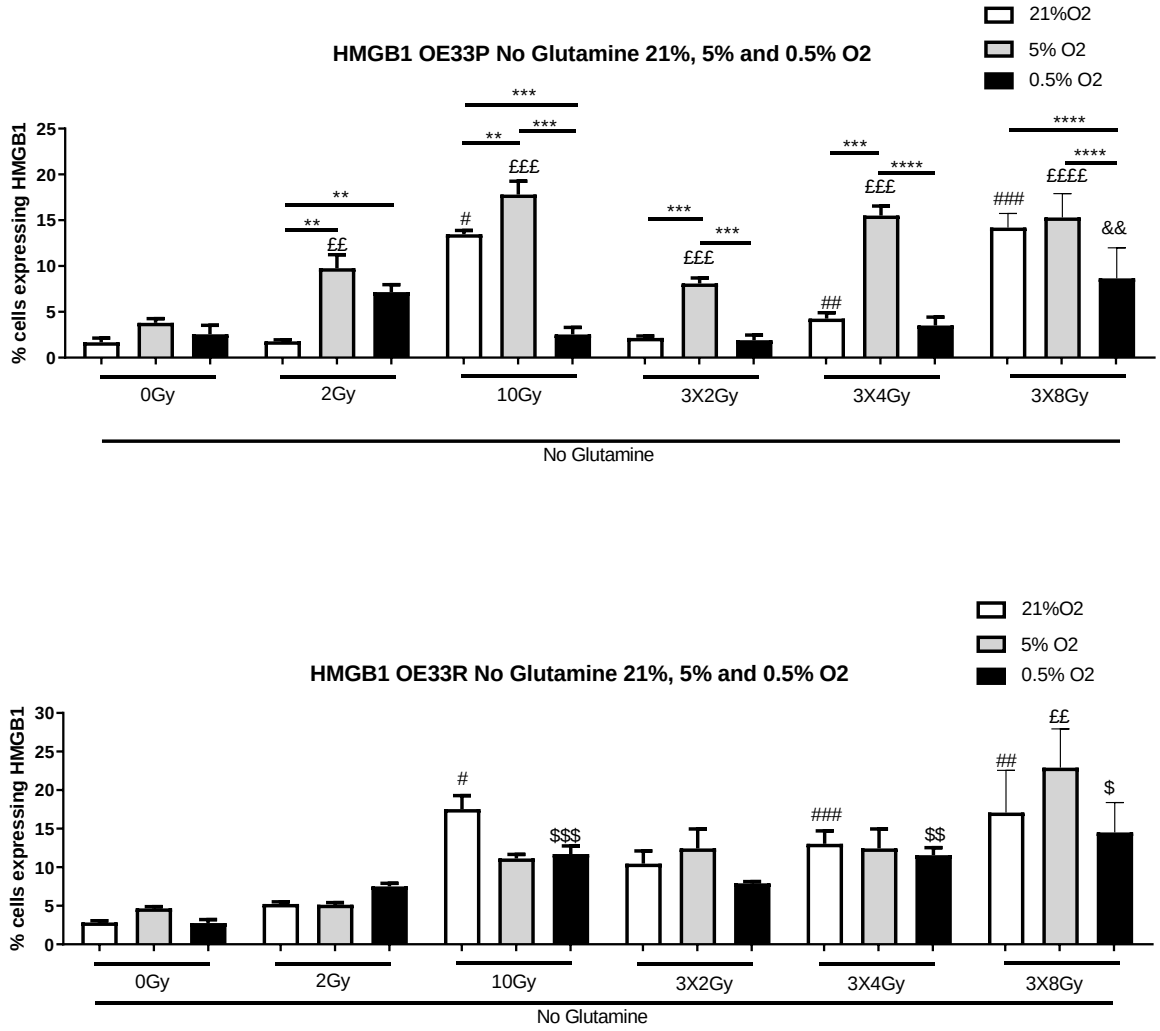

Figure 5.8. HMGB1 is expressed at a higher level under 5% Oxygenation no Glutamine in the OE33P cell line, with a mixed pattern of expression of HMGB1 in the OE33R cell line. OE33P & OE33R cell lines were screened for the surface

expression of HMGB1 by flow cytometry. 21%=Normal oxygenation, 5%=mild hypoxia, 0.5%=severe hypoxia. Bolus dosing was administered once daily over three consecutive days. Staining of cancer cells took place 24hrs after last fraction of radiation. Tukey's multiple comparison testing. Graph shows mean % expression (±SEM) (n=3). * denotes comparison between oxygen levels for each radiation dosing regimen, * $p<0.05$, ** $p<0.01$, *** $p<0.001$, **** $p<0.0001$. # denotes comparison of dosing with 0 Gy at 21% 02, # $p<0.05$, ## $p<0.01$, ### $p<0.001$, #### $p<0.0001$. £ denotes comparison of dosing with 0 Gy at 5% O_2, £ $p<0.05$, ££ $p<0.01$, £££ $p<0.001$. $ denotes comparison of dosing with 0 Gy at 0.5% O_2, $ $p<0.05$, $$ $p<0.01$, $$$ $p<0.001$.

In the OE33P cell line there was a significantly higher expression of HMGB1 in response to 10 Gy normoxia no glutamine (13.47±0.41) and 3x4 Gy normoxia no glutamine (4.26±0.62) and 3x8Gy normoxia no glutamine (14.2+/-0.89) compared to 0 Gy normoxia no glutamine (1.68±0.46) $p<0.05$, $p<0.01$, $p<0.001$ respectively. There was significantly increased expression of HMGB1 in response to 2 Gy 5% O_2 no glutamine (9.76±1.49), 10 Gy 5% O_2 no glutamine (17.8±1.46), 3x2 Gy 5% O_2 no glutamine (8.09±0.61), 3x4 Gy 5% O_2 no glutamine (15.5±1.06) and 3x8 Gy 5% O_2 no glutamine (15.3±1.5) $p<0.01$, $p<0.001$, $p<0.001$, $p<0.001$, $p<0.0001$ respectively. There was also increased expression of HMGB1 at 3x8 Gy 0.5% O_2 no glutamine (8.65±1.63) compared to 0 Gy 0.5% O_2 no glutamine (2.56±0.96) $p<0.01$. There was increased expression of HMGB1 at 2 Gy 5% O_2 no glutamine (9.79±1.49) compared to 2 Gy normoxia no glutamine (1.78±0.17) $p<0.01$ and 2 Gy 0.5% O_2 no glutamine (7.15±0.82) $p<0.01$. There was increased expression of HMGB1 at 10 Gy 5% O_2 no glutamine (17.8±1.46) compared to 10 Gy normoxia no glutamine (13.47±0.41) $p<0.01$ and 10 Gy 0.5% O_2 no glutamine (2.54±0.76) $p<0.001$. There was a significantly higher expression of HMGB1 at 3x2 Gy 5% O_2 no glutamine (8.09±0.61) compared to 3x2 Gy normoxia no glutamine (2.15±0.21) $p<0.001$ and 3x2 Gy 0.5% O_2 no glutamine (1.91±0.55) $p<0.001$ and 3x4 Gy

5% O_2 no glutamine (15.5±1.06) compared to 3x4 Gy normoxia no glutamine (4.26±0.65) $p<0.001$ and 3x4 Gy 0.5% O_2 no glutamine (3.51±0.92) $p<0.001$. There was significantly less HMGB1 expressed at 3x8 Gy 0.5% O_2 no glutamine (8.65±1.93) compared to 3x8 Gy 5% O_2 no glutamine (15.3±1.5) $p<0.001$ and 3x8 Gy normoxia no glutamine (14.2±0.89) $p<0.001$ (Figure 5.8).

In the OE33 R cell line, there was significantly higher expression of HMGB1 in response to 10 Gy normoxia no glutamine (17.53±1.76), 3x4 Gy normoxia no glutamine (13.05±1.65), 3x8 Gy normoxia no glutamine (17.1±3.16) compared to 0 Gy normoxia no glutamine (2.85±0.22) $p<0.05$, $p<0.001$, $p<0.01$ respectively. There was significantly higher expression of HMGB1 at 3x8 Gy 5% O_2 no glutamine (22.9±2.9) compared to 0 Gy 5% O_2 no glutamine (4.66±0.23) $p<0.05$. There was significantly higher expression of HMGB1 at 10 Gy 0.5% O_2 no glutamine (11.7±1.06), 3x4 Gy 0.5% no glutamine (11.57±0.97) and 3x8 Gy 0.5% O_2 no glutamine (14.5±2.25) compared to 0 Gy 0.5% O_2 no glutamine (2.75±0.46) $p<0.001$, $p<0.01$, $p<0.05$ respectively (Figure 5.8). Further significance between the dosing regimens, different levels of oxygenation and glutamine deprivation are available in Appendix Table 8.

5.4 Basal expression of DAMPs on the surface of peripheral blood and tumour-infiltrating T cells, $CD45^-$ and $CD45^+$ cells in treatment-naïve OAC patients.

In order to determine the basal expression of DAMPs *ex vivo* patient samples were taken at endoscopy pre conventional chemo(radio)therapy, the current standards of care in OAC.

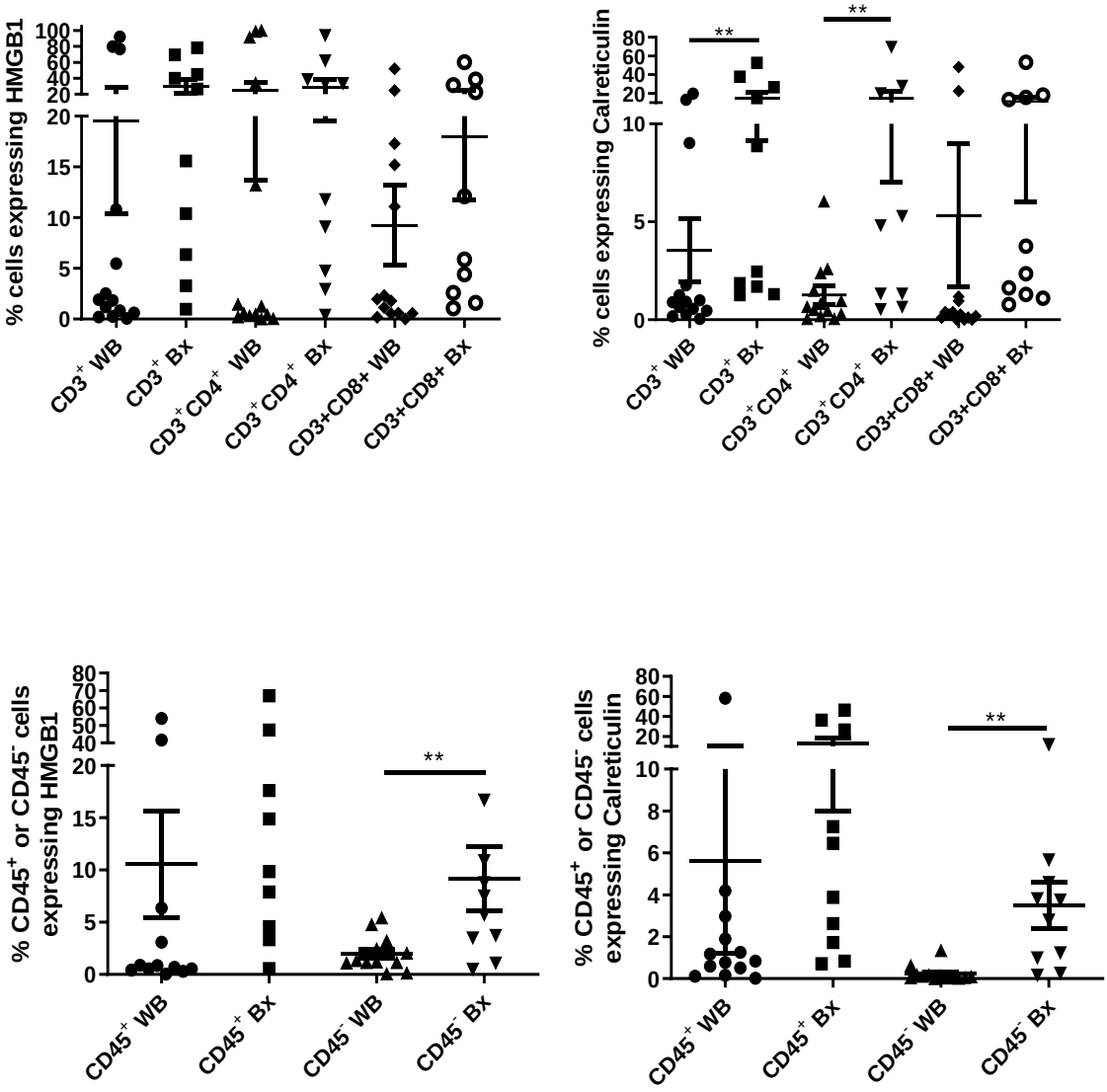

Figure 5.9: Expression of DAMPS on the surface of peripheral blood and tumour-infiltrating T cells, CD45$^-$ and CD45$^+$ cells in treatment-naïve OAC patients. The expression of HMGB1 and Calreticulin was determined on the surface of peripheral blood and tumour-infiltrating CD3$^+$, CD3$^+$CD4$^+$, CD3$^+$CD8$^+$, CD45$^-$ and CD45$^+$ cells in treatment-naïve OAC whole blood (n=14) and tumour biopsy tissue (n=10) *ex vivo* by flow cytometry. WB=Whole Blood, Bx=Biopsy. Wilcoxon rank test, *<0.05, **<0.001 and ***<0.0001.

For pre-treatment samples, the expression of CD3$^+$ HMGB1 was higher on tumour tissue (29.56±8.76) than on whole blood (19.58±9.23). There was also an increased expression of CD3$^+$CD4 $^+$HMGB1 on tumour tissue (29.1±9.56) compared to whole blood

(24.42±10.76). There was also a higher expression of $CD3^{+}CD8^{+}$HMGB1 on tumour tissue (18.01±6.28) compared to whole blood (9.24±3.91) (Figure 5.9). The expression of $CD3^{+}$ Calreticulin was significantly higher on tumour tissue (18.26±5.78) compared to whole blood (3.56±1.61) $p<0.01$. $CD3^{+}CD4^{+}$ Calreticulin was significantly higher on tumour tissue (14.59±7.59) than on whole blood (1.26±0.46) $p<0.01$. There was also a higher expression of $CD3^{+}CD8^{+}$Calreticulin on tumour tissue (11.15±5.14) compared to whole blood (5.33±3.66). There was a higher expression of $CD45^{+}$ HMGB1 on tumour tissue (20.95±6.99) compared to whole blood (10.56±5.09). There was a significantly higher expression of $CD45^{-}$ HMGB1 on tumour tissue (9.18±3.1) compared to whole blood (2±0.45) $p<0.01$. There was a higher expression of $CD45^{+}$ Calreticulin on tumour tissue (13.29±5.31) compared to whole blood (5.6±4.4) and a significantly higher expression of $CD45^{-}$ Calreticulin on tumour tissue (3.52±1.11) compared to whole blood (0.22±0.1) $p<0.01$ (Figure 5.9).

5.5 Basal expression of DAMPs on the surface of peripheral blood and tumour-infiltrating T cells, CD45$^-$ and CD45$^+$ cells in post-treatment OAC patients (FLOT chemotherapy, CROSS chemoradiotherapy)

Post treatment samples, 7 of which were matched from pre treatment samples were examined for DAMP expression to determine if chemo(radiotherapy) induced immunogenic cell death.

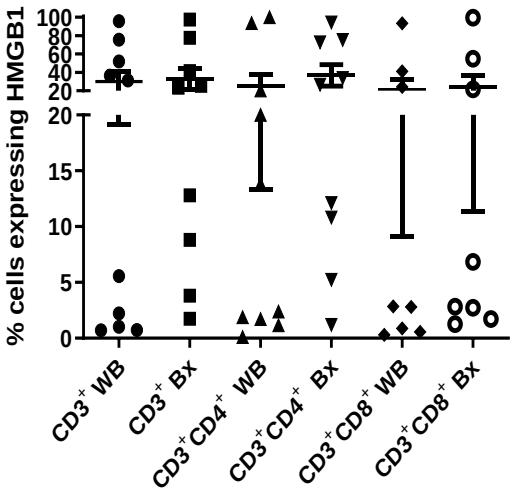

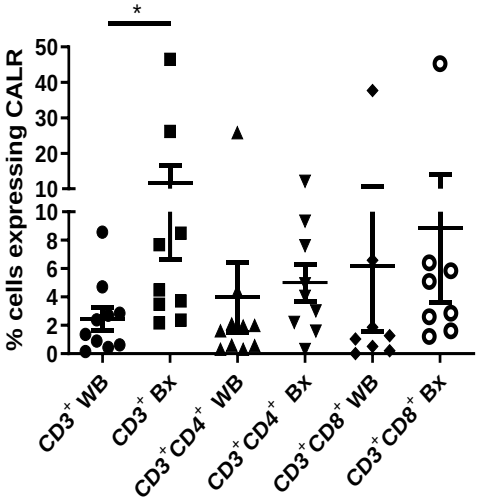

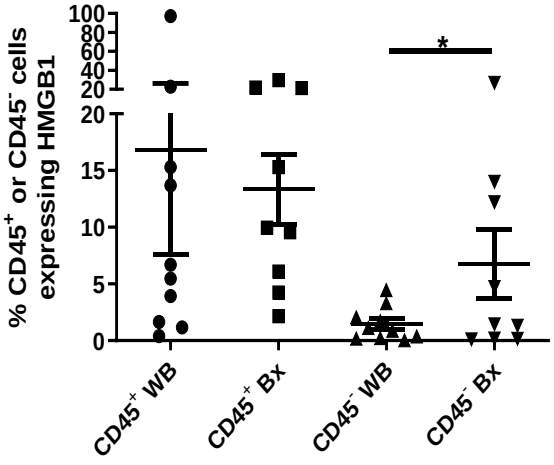

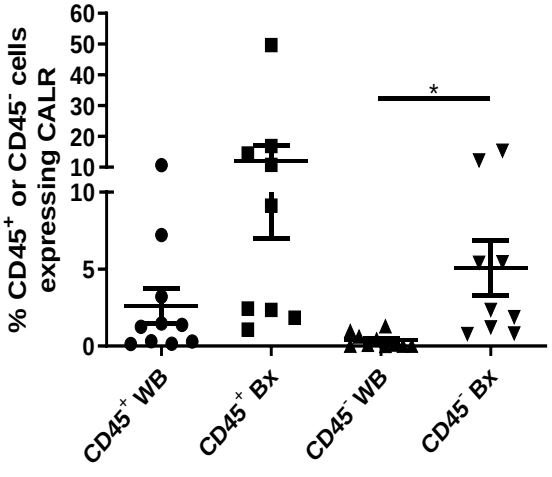

Figure 5.10. Expression of DAMPS on the surface of peripheral blood and tumour infiltrating T cells, $CD45^-$ and $CD45^+$ cells in post-treatment OAC patients. The expression of HMGB1 and Calreticulin was determined on the surface of peripheral blood and tumour-infiltrating $CD3^+$, $CD3^+$ $CD4^+$, $CD3^+$ $CD8^+$, $CD45^-$ and $CD45^+$ cells in post treatment whole blood (n=10) and tumour biopsy tissue (n=9) *ex vivo* by flow cytometry (Wilcoxon ranked test). Treatments: FLOT n=5 and CROSS n=5.

For post treatment samples, there was a higher expression of $CD3^+$ HMGB1 on tumour tissue (32.44±11.28) compared to whole blood (30.11±10.97), $CD3^+CD4^+$ HMGB1 on tumour tissue (36.83±11.61) compared to whole blood (25.49±12.14) and $CD4^+CD8^+$ HMGB1 on tumour tissue (23.91±12.57) compared to whole blood (20.75±11.62). There was a higher expression of $CD45^+$ HMGB1 on whole blood (16.83±9.24) compared to tumour tissue (13.35±3.1), with a higher expression of $CD45^-$ HMGB1 on tumour tissue (6.78±3.08) compared to whole blood (1.44±0.47). There was a significantly higher expression of $CD3^+$ Calreticulin on tumour tissue (11.68±2.68) compared to whole blood (2.47±0.81) $p<0.05$ (Figure 5.10). There was a higher expression of $CD3^+CD4^+$ Calreticulin on tumour tissue (5.04±1.3) compared to whole blood (3.97±2.46) and also $CD4^+CD8^+$ Calreticulin on tumour tissue (8.87±5.25) compared to whole blood (6.15±4.57). There was a higher expression of $CD45^+$ Calreticulin on tumour tissue (12.08±5.09) compared to whole blood (2.61±1.13) and also a significantly higher expression of $CD45^-$ Calreticulin on tumour tissue (5.06±1.77) compared to whole blood (0.36±0.15) $p<0.05$ (Figure 5.10).

5.6 Assessing DAMPs on matched pre and post treatment fresh tumour samples

In order to determine if conventional treatment strategies induce immunogenic cell death, matched pre and post patient whole blood and tumour biopsies (n=5) were compared.

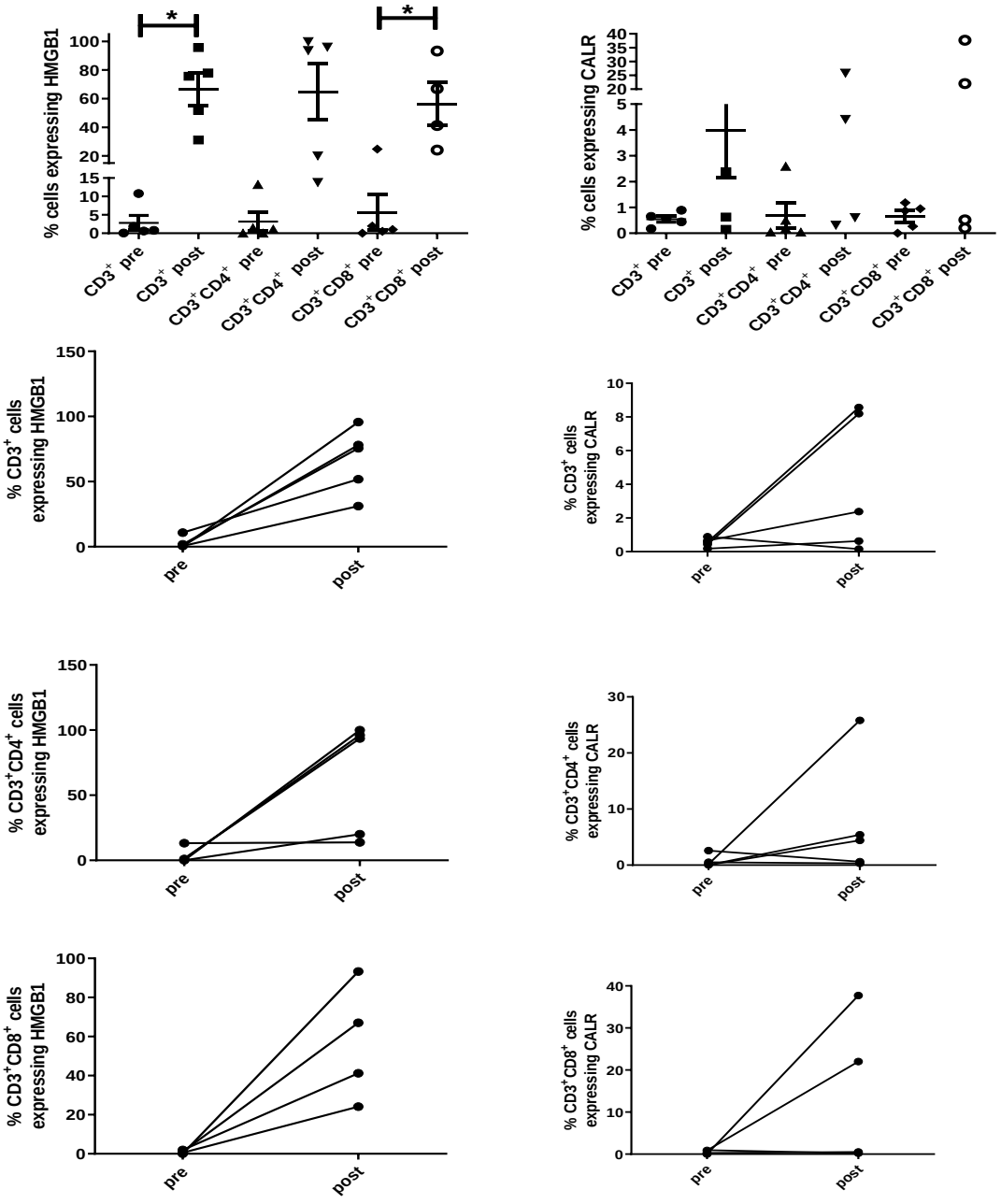

Figure 5.11. Expression of DAMPS on the surface of matched peripheral blood T cells, pre and post-treatment OAC patients. The expression of HMGB1 and Calreticulin (CALR) was determined on the surface of peripheral blood $CD3^+$, $CD3^+$

$CD4^+$, $CD3^+$ $CD8^+$, $CD45^-$ and $CD45^+$ cells in matched pre and post treatment whole blood (n=5) *ex vivo* by flow cytometry.

There was a significantly increased expression of $CD3^+$HMGB1 on whole blood post treatment (66.46±11.25) compared to pre-treatment samples (2.82±2.02) $p<0.05$ (Figure 5.11). The expression of $CD3^+CD4^+$HMGB1 was higher on post treatment whole blood (64.66±19.55) compared to pre-treatment samples (3.16±2.53). There was a significantly higher expression of $CD4^+CD8^+$ HMGB1 on post treatment whole blood (59.5±10.1) compared to pre-treatment (5.66±4.8) $p<0.01$. There was a higher expression of $CD3^+$Calreticulin on post treatment whole blood (3.98±1.83) compared to pre treatment (0.54±0.12), $CD3^+CD4^+$Calreticulin (7.31±4.73) post treatment compared to pre treatment levels (0.67±0.47). There was also higher expression of $CD3^+CD8^+$Calreticulin on post treatment whole blood (15.11±9.09) compared to pre treatment levels (0.65±0.22) (Figure 5.11).

5.7 Examining the Expression of DAMPS on the surface of peripheral blood $CD45^+$ and $CD45^-$ cells pre and post-treatment OAC patients.

CD45 is a critical regulator of signalling thresholds in immune cells and is moving rapidly back into the spotlight as a drug target and central regulator involved in autoimmunity and antiviral immunity. In this section the expression of DAMPs was assessed on CD45+ and CD45- cells in pre and post treatment samples.

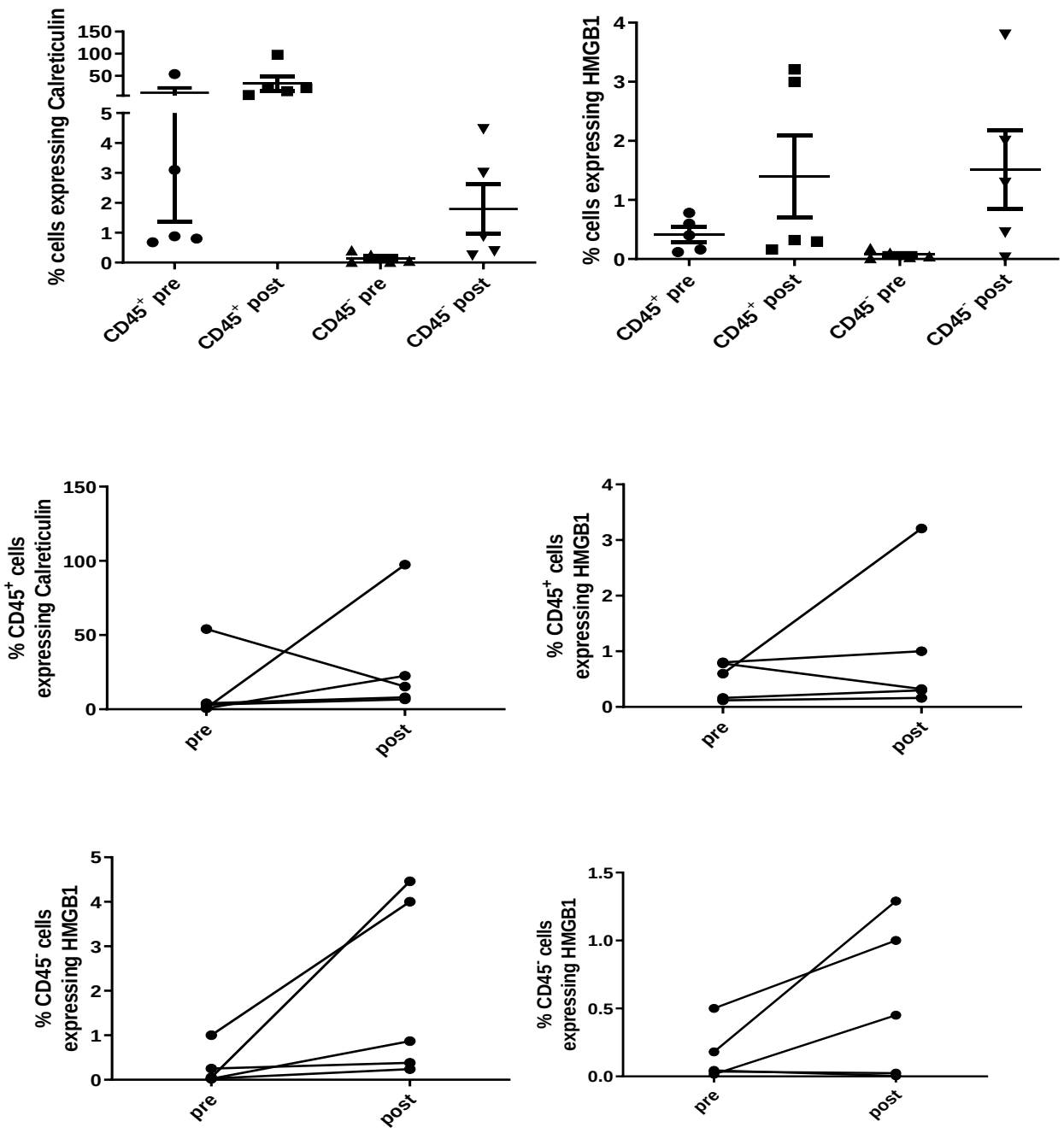

Figure 5.12. Expression of DAMPS on the surface of peripheral blood CD45$^+$ and CD45$^-$ cells pre and post-treatment OAC patients. The expression of HMGB1 and CALR was determined on the surface of peripheral blood CD45$^+$ and CD45$^-$ cells in matched pre and post treatment (CROSS) whole blood (n=5) *ex vivo* by flow cytometry.

There was a higher expression of CD45$^+$ HMGB1 on post treatment whole blood (30±17.09) compared to pre treatment (12.55±10.41) and a higher expression of CD45$^-$

HMGB1 (1.99±0.92) on post treatment whole blood compared to pre-treatment samples (0.27±0.19). (Figure 5.12) Similarly, there was a higher expression of $CD45^{+}$Calreticulin post treatment (0.99±0.57) compared to pre-treatment samples (0.49±0.15). There was also an increased expression of $CD45^{-}$Calreticulin on post treatment whole blood (0.55±0.26) compared to pre treatment samples (0.16±0.09) (Figure 5.12).

5.8 Expression of DAMPS on the surface of peripheral blood and tumour infiltrating T cells, based on treatment modality in OAC patients.

The two main treatment modalities alluded to earlier remain the FLOT chemotherapy alone or CROSS chemoradiotherapy. In order to determine if there is a difference in the immunogenic potential effects of either modality, these were compared in post treatment samples (n=5 CROSS, n=5 FLOT).

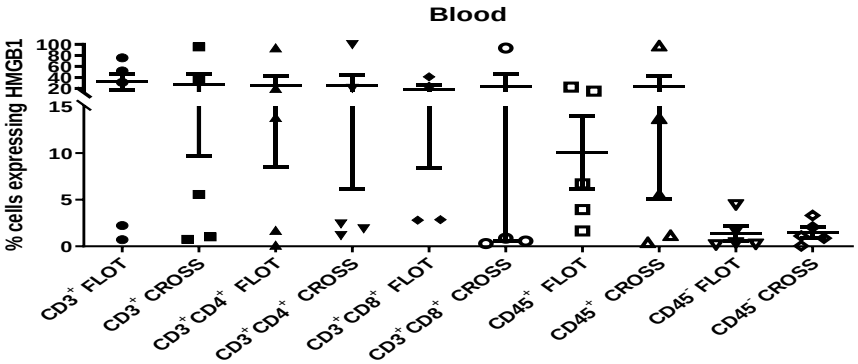
Blood
% cells expressing HMGB1
100
80
60
40
20
15
10
5
0
CD3+ FLOT
CD3+ CROSS
CD3+CD4+ FLOT
CD3+CD4+ CROSS
CD3+CD8+ FLOT
CD3+CD8+ CROSS
CD45+ FLOT
CD45+ CROSS
CD45- FLOT
CD45- CROSS

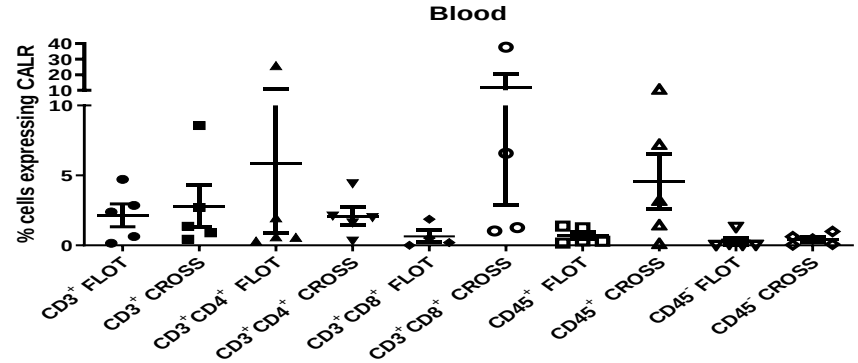
Blood
% cells expressing CALR
40
30
20
10
10
5
0
CD3+ FLOT
CD3+ CROSS
CD3+CD4+ FLOT
CD3+CD4+ CROSS
CD3+CD8+ FLOT
CD3+CD8+ CROSS
CD45+ FLOT
CD45+ CROSS
CD45- FLOT
CD45- CROSS

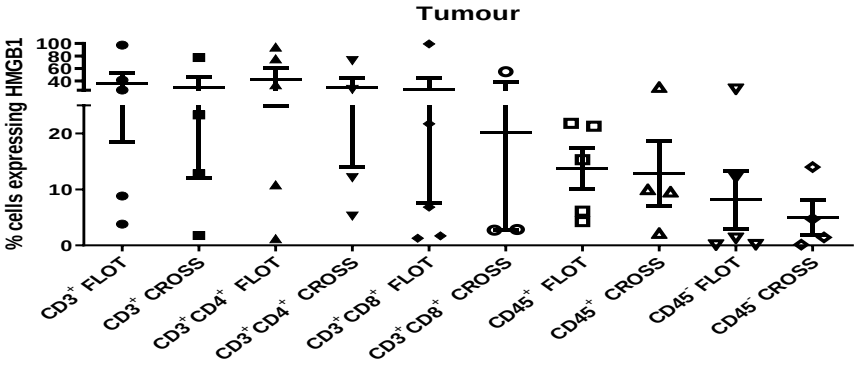
Tumour
% cells expressing HMGB1
100
80
60
40
20
10
0
CD3+ FLOT
CD3+ CROSS
CD3+CD4+ FLOT
CD3+CD4+ CROSS
CD3+CD8+ FLOT
CD3+CD8+ CROSS
CD45+ FLOT
CD45+ CROSS
CD45- FLOT
CD45- CROSS

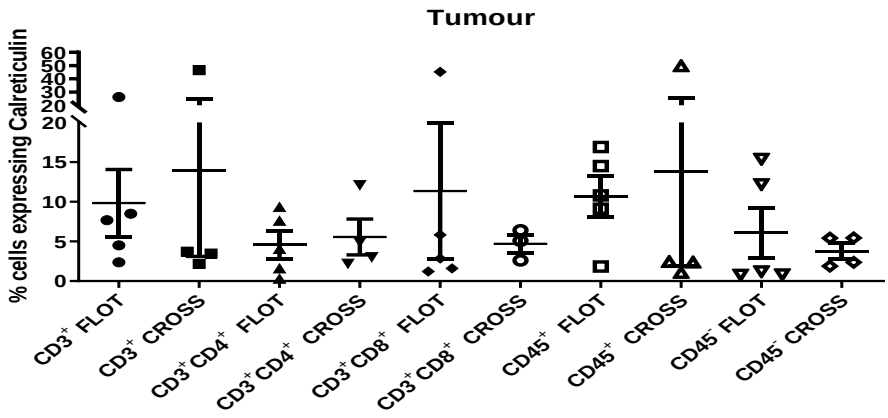

Figure 5.13. Expression of DAMPS on the surface of peripheral blood and tumour infiltrating T cells, based on treatment modality in OAC patients. The expression of HMGB1 and CALR was determined on the surface of peripheral blood and tumour-infiltrating $CD3^+$, $CD3^+$ $CD4^+$, $CD3^+$ $CD8^+$, $CD45^-$ and $CD45^+$ cells in post treatment FLOT (n=5 Blood, n=5 biopsies) and post treatment CROSS (n=5 Blood, n=4 biopsies) *ex vivo* by flow cytometry.

There was a higher expression of $CD3^+$HMGB1 in whole blood in patients who received FLOT (32.31±14.42) compared to CROSS (27.9±18.21), a higher expression of $CD3^+CD4^+$HMGB1 in those who received FLOT (25.84±17.34) compared to CROSS (25.13±19.03) (Figure 5.13). There was a higher expression of $CD3^+CD8^+$HMGB1 in those who received CROSS (23.76±23.18) compared to FLOT (17.74±9.29). There was a higher expression of $CD45^+$HMGB1 in the whole blood of those who received CROSS (23.63±18.59) compared to FLOT (10.04±3.9) (Figure 5.13). There was a higher expression of $CD45^-$HMGB1 in the whole blood of those who received CROSS (1.48±0.56) compared to those who received FLOT (1.4±0.82).

There was a higher expression of $CD3^+$Calreticulin in whole blood in patients who received CROSS (2.79±1.49) compared to FLOT (2.15±0.82), a higher expression of

$CD3^+CD4^+$Calreticulin in those who received FLOT (5.85±4.99) compared to CROSS (2.08±0.66) (Figure 5.13). There was a higher expression of $CD3^+CD8^+$Calreticulin in those who received CROSS (11.65±8.78) compared to FLOT (0.65±0.42). There was a higher expression of $CD45^+$Calreticulin in the whole blood of those who received CROSS (4.54±1.95) compared to FLOT (0.68±0.26). There was a higher expression of $CD45^-$Calreticulin in the whole blood of those who received CROSS (0.43±0.18) compared to those who received FLOT (0.29±0.25) (Figure 5.13).

There was a higher expression of $CD3^+$HMGB1 in tumour tissue in patients who received FLOT (35.34±16.86) compared to CROSS (28.81±16.78), a higher expression of $CD3^+CD4^+$HMGB1 in those who received FLOT (43.02±18.07) compared to CROSS (29.08±15.14). There was a higher expression of $CD3^+CD8^+$HMGB1 in those who received FLOT (26.18±18.67) compared to CROSS (20.12±17.34) (Figure 5.13). There was a higher expression of $CD45^+$HMGB1 in the tumour tissue of those who received FLOT (13.75±3.7) compared to CROSS (12.84±5.9). There was a higher expression of $CD45^-$HMGB1 in the tumour tissue of those who received FLOT (8.14±5.21) compared to those who received CROSS (5.08±3.13).

There was a higher expression of $CD3^+$Calreticulin in tumour tissue in patients who received CROSS (13.97±10.85) compared to FLOT (9.85±4.23), a higher expression of $CD3^+CD4^+$Calreticulin in those who received CROSS (5.56±2.25) compared to FLOT (4.57±1.72). There was a higher expression of $CD3^+CD8^+$Calreticulin in those who received FLOT (11.36±8.52) compared to CROSS (4.7±1.11). There was a higher expression of $CD45^+$Calreticulin in the whole blood of those who received CROSS (13.89±11.94) compared to FLOT (10.63±2.59). There was a higher expression of $CD45^-$

Calreticulin in the whole blood of those who received CROSS (3.78+/-0.96) compared to those who received FLOT (6.09±3.19) (Figure 5.13).

5.9. Correlations of DAMP expression in whole blood and tumour samples with clinicopathological characteristics

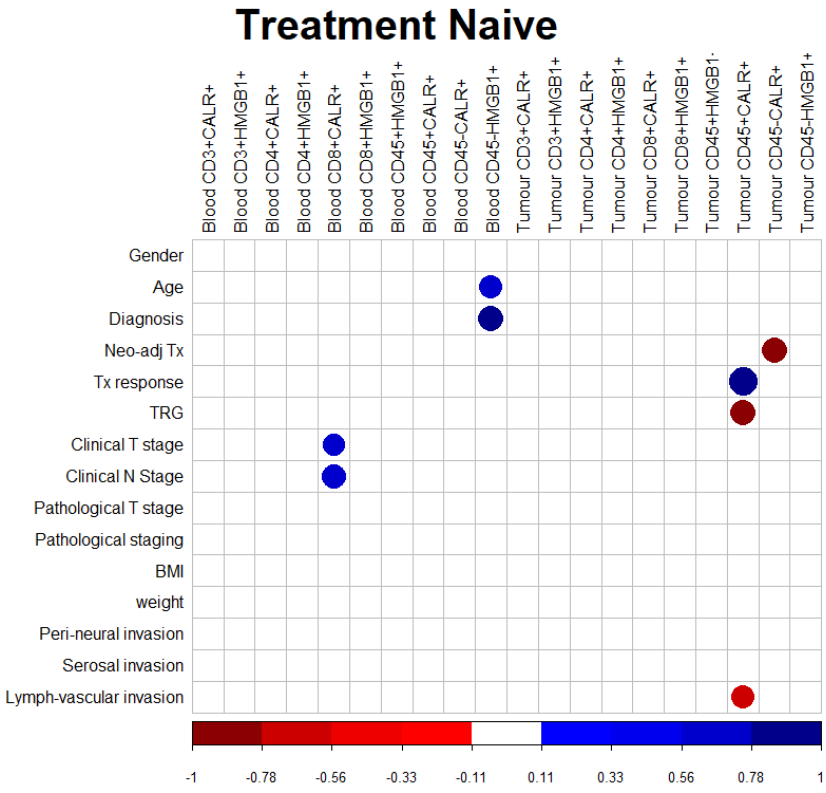

Figure 5.14 Tumour CD45^{+}CALR^{+} positively correlated with Tumour Regression Grade and Lymphovascular invasion as does Tumour CD45-CALR+ with Neoadjuvant treatment modality. Corrplots illustrating the correlation values for the expression and co-expression of immune checkpoints in OAC tumour samples correlated with clinical demographics and characteristics. Patient clinical features included age, weight (pre-treatment, kg), BMI (pre-treatment, kg/m^2), neo-adjuvant treatment received, treatment response (determined by radiographic features using PET/CT), tumour regression grade (TRG), clinical tumour stage and nodal involvement, pathological tumour stage and nodal involvement, BMI (post-treatment, kg/m^2), weight (post-treatment, kg), serosal invasion and lymph-vascular invasion. Blue indicates a positive correlation, red negative correlation. Non-parametric Spearman correlation. Significant

data shown only. Spearman r 0.4-0.59 moderate, 0.6-0.79 strong and 0.8-1 very strong. *p<0.05.

The expression of $CD45^{+}$Calreticulin on treatment naïve tumour tissue positively correlates with the Tumour Regression Grade (TRG) and also with lymphovascular invasion. The expression of $CD45^{-}$Calreticulin positively correlates with the neoadjuvant treatmwnt modality received pre -operatively (Figure 5.14). Tumour $CD8^{+}CALR^{+}$ positively correlated with tumour overall clinical stage, neoadjuvant treatment modality pathological T stage, and Tumour CD45+HMGB1- positively correlates with serosal invasion. Tumour $CD3^{+}CALR^{+}$ positively correlated with Tumour Regression Grade (Figure 5.15).

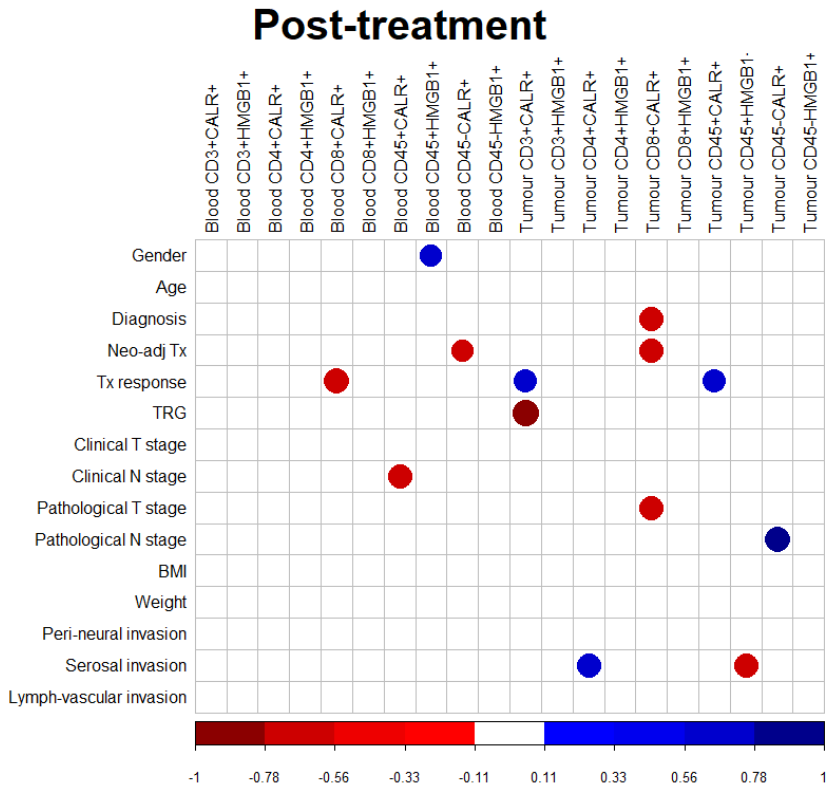

Figure 5.15 Tumour CD8$^+$CALR$^+$ positively correlated with Tumour overall clinical stage, neoadjuvant treatment modality pathological T stage, and Tumour CD45+HMGB1- positively correlates with serosal invasion. Tumour CD3+CALR+ positively correlated with Tumour Regression Grade. Corrplots illustrating the correlation values for the expression and co-expression of immune checkpoints in OAC tumour samples correlated with clinical demographics and characteristics. Patient clinical features included age, weight (pre-treatment, kg), BMI (pre-treatment, kg/m^2), neo-adjuvant treatment received, treatment response (determined by radiographic features using PET/CT), tumour regression grade (TRG), clinical tumour stage and nodal involvement, pathological tumour stage and nodal involvement, BMI (post-treatment, kg/m^2), weight (post-treatment, kg), serosal invasion and lymph-vascular invasion. Blue indicates a positive correlation, red negative correlation. Non-parametric Spearman correlation. Significant data shown only. Spearman r 0.4-0.59 moderate, 0.6-0.79 strong and 0.8-1 very strong. *p<0.05.

5.10 Cell viability in the context of radiation, the tumour microenvironment and immune checkpoint blockade

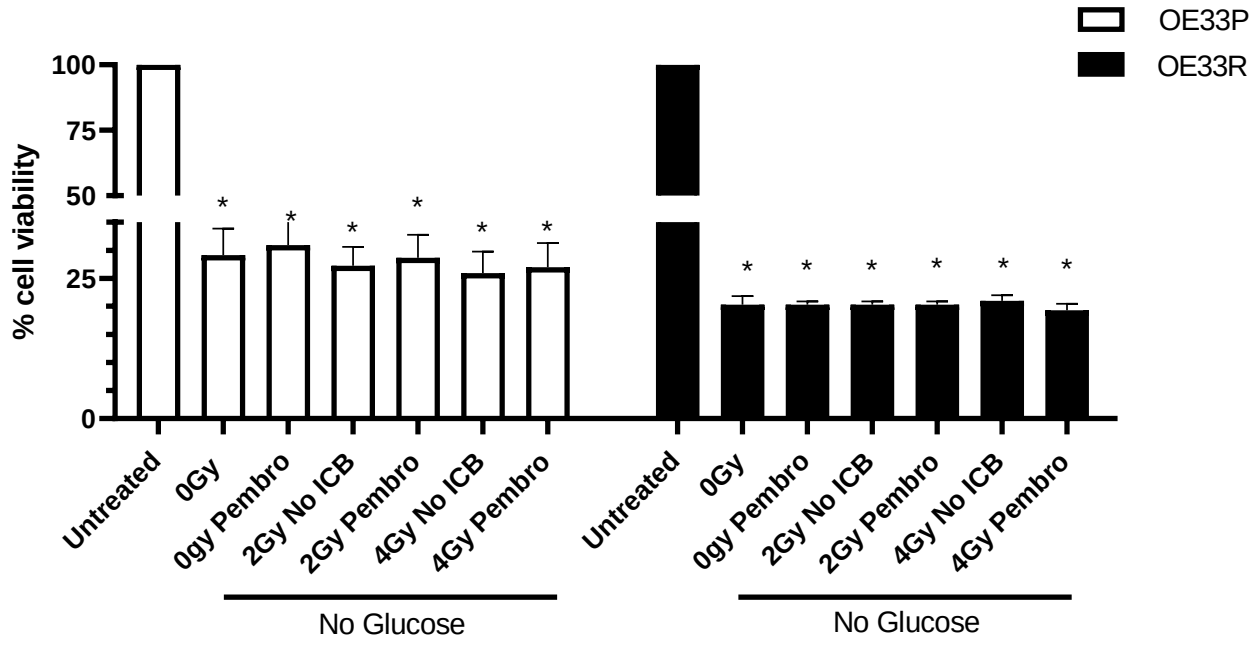

Figure 5.16; Ionising radiation with Pembrolizumab and Glucose deprivation. The % viability (±SEM) of OE33P and OE33R cells were assessed using a CCK8 assay with or without radiation (0, 2 or 4 Gy), in the absence of Glucose and with or without immune checkpoint inhibitor Pembrolizumab (Pembro), (n=3) 24 hrs after irradiation. Tukey's multiple comparison testing. * $p<0.05$.

There was a significantly reduced viability of OE33P and OE33R cells with nutrient deprivation in the absence of radiation (29.12±2.75) with no significant alteration in viability with Pembrolizumab alone (30.92±2.37) or 2 Gy radiation (27.23±1.95) or 4 Gy irradiation (25.94±2.22) or in combination with pembrolizumab and glucose deprivation. There was no difference in cell viability in the OE33R cell line with or without radiation and pembrolizumab and glucose deprivation (Figure 5.16). Further significance between

the dosing regimens, Pembrolizumab and glucose deprivation are available in Appendix Table 9.

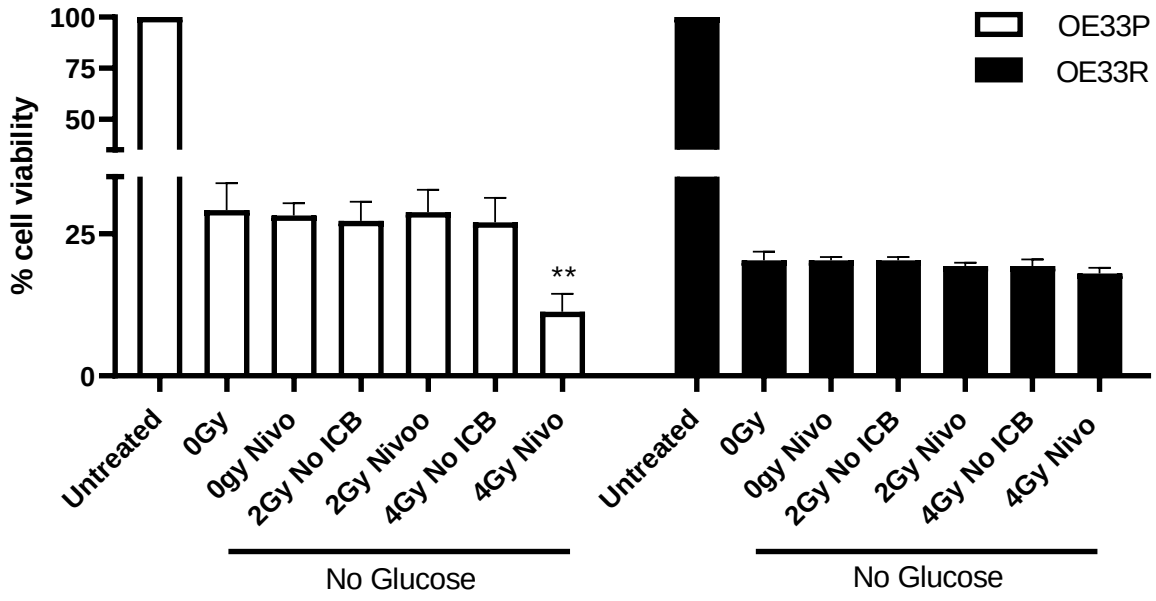

Figure 5.17; Ionising radiation with Nivolumab and Glucose deprivation. The % viability (±SEM) of OE33P and OE33R cells were assessed using a CCK8 assay with or without radiation (0, 2 or 4 Gy) and with or without immune checkpoint inhibitor Nivolumab (Nivo), (n=3) 24 hrs after irradiation. Tukey's multiple comparison testing. * $p<0.05$, ** $p<0.01$.

There was a significantly reduced viability of OE33P and OE33R cells with nutrient deprivation in the absence of radiation (29.12±2.75) with no significant alteration in viability with Nivolumab alone (30.92±2.37) or 2 Gy radiation (27.23±1.95) or 4 Gy irradiation (25.94±2.22) or in combination with Nivolumab 2 Gy and glucose deprivation (28.75±2.3). There was a significantly reduced viability with 4 Gy irradiation and Nivolumab (11.29±1.82) $p<0.01$. There was no difference in cell viability in the OE33R cell line with or without radiation and Nivolumab and glucose deprivation (Figure 5.17).

Further significance between the dosing regimens, Nivolumab and glucose deprivation are available in Appendix Table 10.

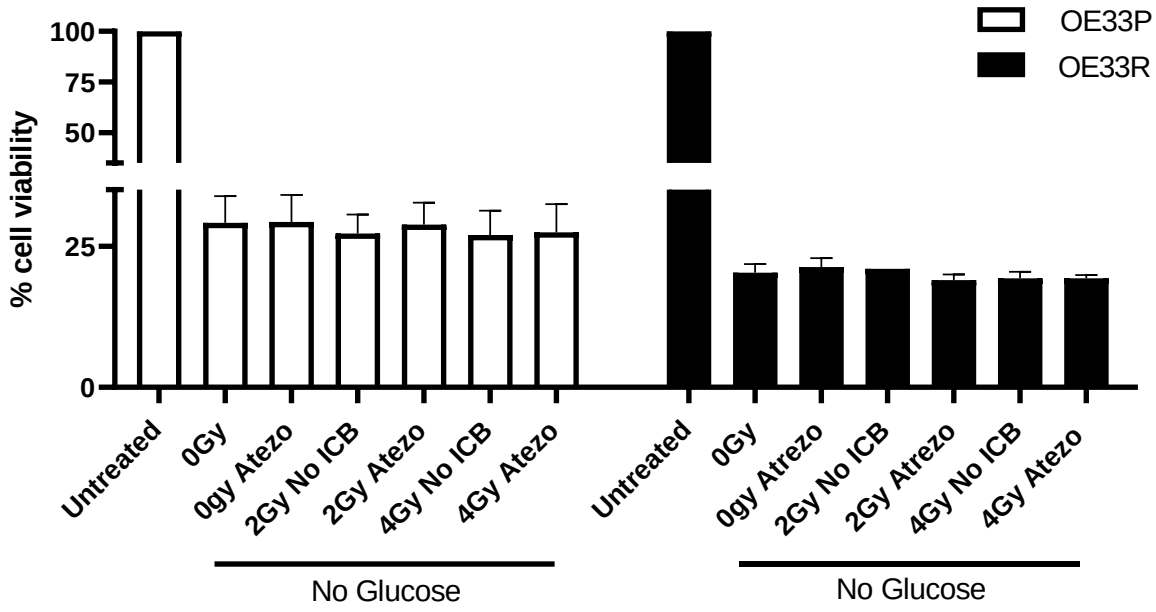

Figure 5.18; Ionising radiation with Atezolizumab and Glucose deprivation. The % viability (±SEM) of OE33P and OE33R cells were assessed using a CCK8 assay with or without radiation (0, 2 or 4 Gy) and with or without immune checkpoint inhibitor Atezolizumab (Atezo), (n=3) 24 hrs after irradiation. Tukey's multiple comparison testing. * $p<0.05$, ** $p<0.01$, *** $p<0.001$.

There was a significantly reduced viability of OE33P and OE33R cells with nutrient deprivation in the absence of radiation (29.12±2.75) with no significant alteration in viability with Atezolizumab alone (29.14±3.27) or 2 Gy radiation (32.12±2.95) or 4 Gy irradiation (27.48±3.22) or in combination with Atezolizumab 2 Gy or 4 Gy and glucose deprivation (26.98±2.3). There was no difference in cell viability in the OE33R cell line

with or without radiation and Atezolizumab and glucose deprivation (Figure 5.18). Further significance between the dosing regimens, Atezolizumab and glucose deprivation are available in Appendix Table 11.

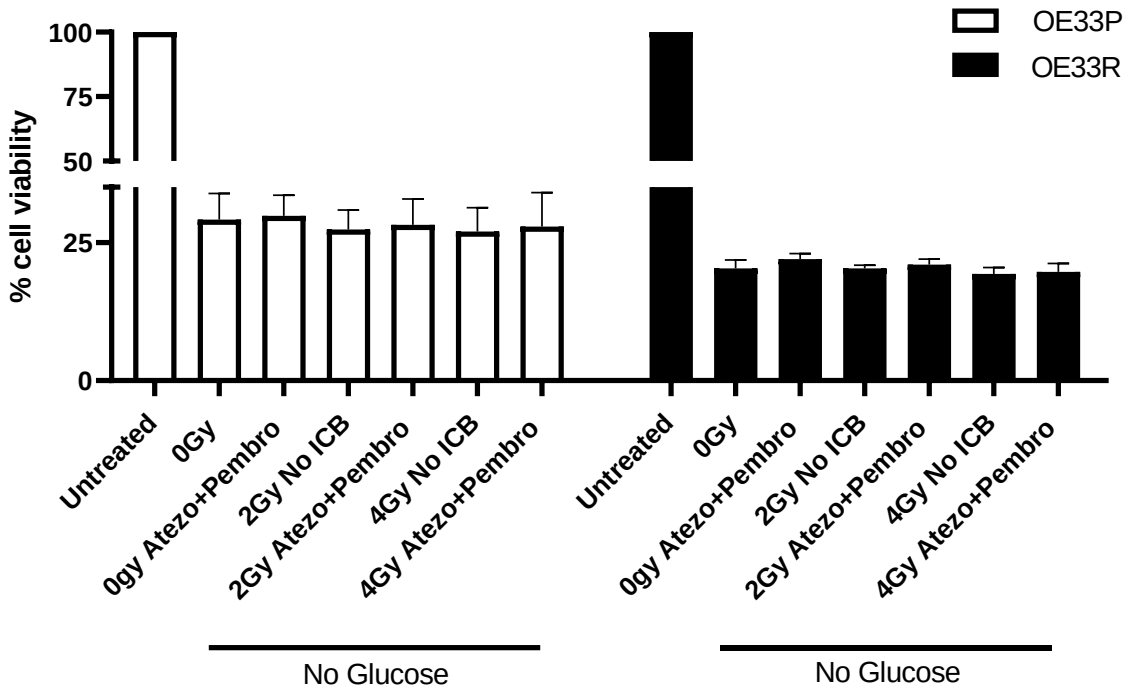

Figure 5.19; Ionising radiation with Atezolizumab & Pembrolizumab and Glucose deprivation. The % viability (±SEM) of OE33P and OE33R cells were assessed using a CCK8 assay with or without radiation (0, 2 or 4 Gy) and with or without immune checkpoint inhibitor Atezolizumab and Pembrolizumab (Atezo & Pembro), (n=3) 24 hrs after irradiation. Tukey's multiple comparison testing. *$p<0.05$, ** $p<0.01$, *** $p<0.001$.

There was a significantly reduced viability of OE33P and OE33R cells with nutrient deprivation in the absence of radiation (29.12±2.75) with no significant alteration in viability with Atezolizumab and Pembrolizumab alone (31.14±2.24) or 2 Gy radiation (31.43±2.75) or 4 Gy irradiation (31.48±3.76) or in combination with Atezolizumab and

Pembrolizumab 2 Gy or 4 Gy and glucose deprivation (28.35±2.79). There was no difference in cell viability in the OE33R cell line with or without radiation and Atezolizumab and Pembrolizumab and glucose deprivation (Figure 5.19). Further significance between the dosing regimens, Atezolizumab and Pembrolizumab and glucose deprivation are available in Appendix Table 12.

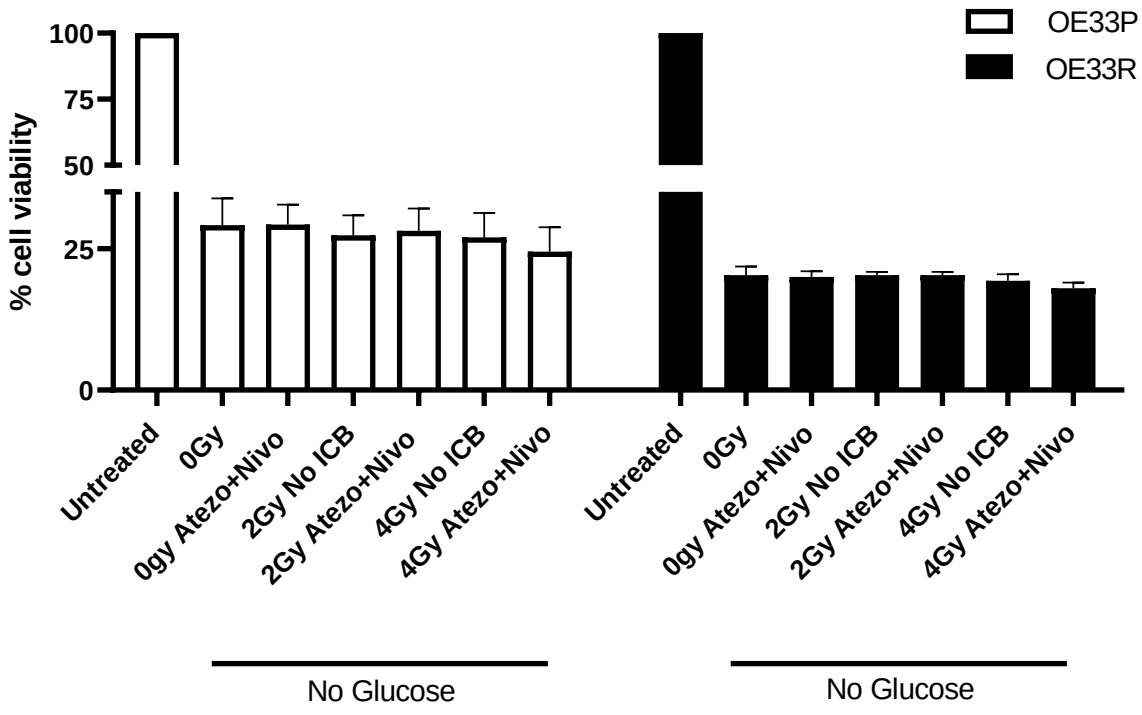

Figure 5.20; Ionising radiation with Atezolizumab & Nivolumab and Glucose deprivation. The % viability (±SEM) of OE33P and OE33R cells were assessed using a CCK8 assay with or without radiation (0, 2 or 4 Gy) and with or without immune checkpoint inhibitor Atezolizumab and Nivolumab (Atezo & Nivo), (n=3) 24 hrs after irradiation. Tukey's multiple comparison testing. * $p<0.05$, ** $p<0.01$, *** $p<0.001$.

There was a significantly reduced viability of OE33P and OE33R cells with nutrient deprivation in the absence of radiation (27.12±2.75) with no significant alteration in

viability with Atezolizumab and Nivolumab alone (28.57-2.86) or 2 Gy radiation (29.83±2.46) or 4 Gy irradiation (27.42±2.53) or in combination with Atezolizumab and Nivolumab 2 Gy or 4 Gy and glucose deprivation (24.24±2.45). There was no difference in cell viability in the OE33R cell line with or without radiation and Atezolizumab and Nivolumab and glucose deprivation (Figure 5.20). Further significance between the dosing regimens, Atezolizumab and Nivolumab and glucose deprivation are available in Appendix Table 13.

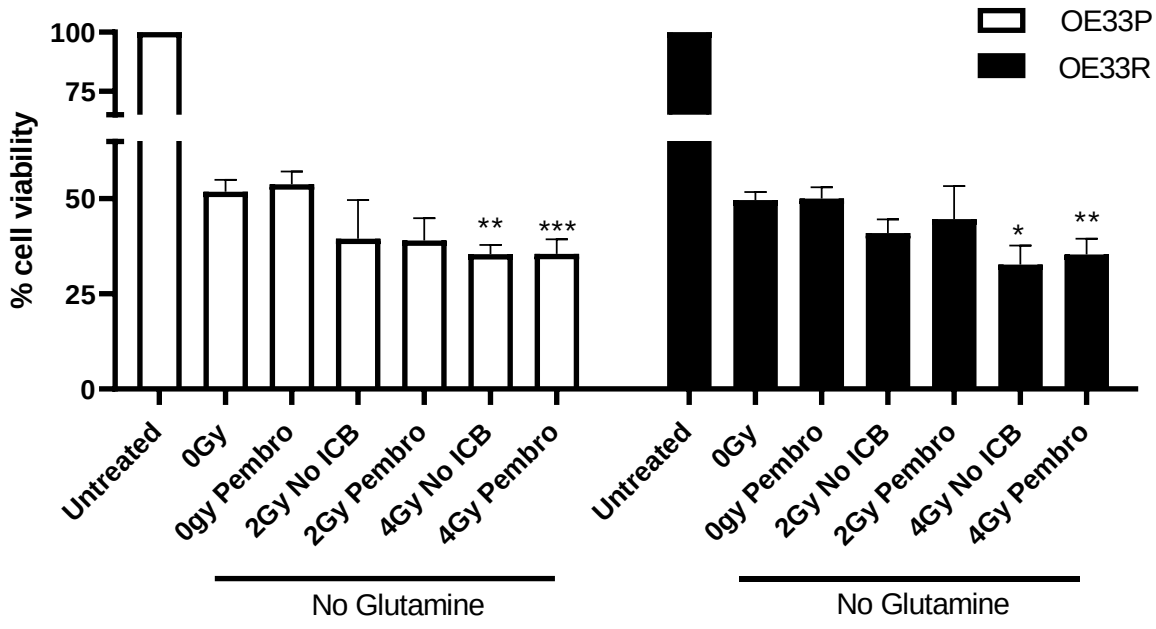

Figure 5.21; Ionising radiation with Pembrolizumab and Glutamine deprivation. The % viability (±SEM) of OE33P and OE33R cells were assessed using a CCK8 assay with or without radiation (0, 2 or 4 Gy) and with or without immune checkpoint inhibitor Pembrolizumab (Pembro), (n=3) 24 hrs after irradiation. Tukey's multiple comparison testing. * $p<0.05$, ** $p<0.01$, *** $p<0.001$

There was a significantly reduced viability of OE33P and OE33R cells with nutrient deprivation in the absence of radiation (51.81±1.25) with no significant alteration in

viability with Pembrolizumab alone (53.76±2.97) or 2 Gy radiation (39.48±4.95). There was a significant reduced viability with 4 Gy irradiation (35.42±1.4) $p<0.001$ or in combination with pembrolizumab and glutamine deprivation (35.48±2.21) $p<0.01$. There was a significant reduction in cell viability in the OE33R cell line with 4 Gy radiation alone (33.67±2.9) $p<0.05$) pembrolizumab and glutamine deprivation (34.33±2.04) $p<0.01$ (Figure 5.21). Further significance between the dosing regimens, Pembrolizumab and glutamine deprivation are available in Appendix Table 14.

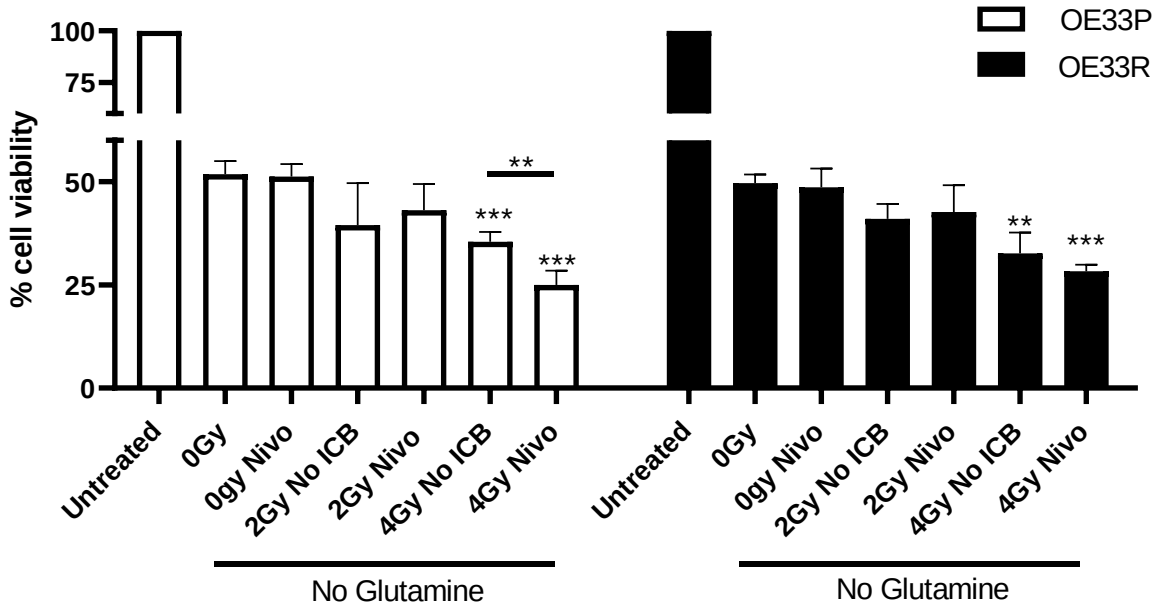

Figure 5.22; Ionising radiation with Nivolumab and Glutamine deprivation. The % viability (±SEM) of OE33P and OE33R cells were assessed using a CCK8 assay with or without radiation (0, 2 or 4 Gy) and with or without immune checkpoint inhibitor Nivolumab (Nivo), (n=3) 24 hrs after irradiation. Tukey's multiple comparison testing. * $p<0.05$, ** $p<0.01$, *** $p<0.001$

There was a significantly reduced viability of OE33P and OE33R cells with nutrient deprivation in the absence of radiation (51.81±1.25) with no significant alteration in

viability with Nivolumab alone (51.26±1.74) or 2 Gy radiation (39.48±4.95). There was a significant reduced viability with 4 Gy irradiation (35.42±1.4) $p<0.001$ or in combination with Nivolumab and glutamine deprivation (24.97±2.21) $p<0.001$. There was a significant reduction in viability between 4 Gy alone and 4 Gy Nivolumab ($p<0.01$). There was a significant reduction in cell viability in the OE33R cell line with 4 Gy radiation alone (32.67±2.9) $p<0.05$) Nivolumab and glutamine deprivation (28.33±0.88) $p<0.01$ (Figure 5.22). Further significance between the dosing regimens, Nivolumab and glutamine deprivation are available in Appendix Table 15.

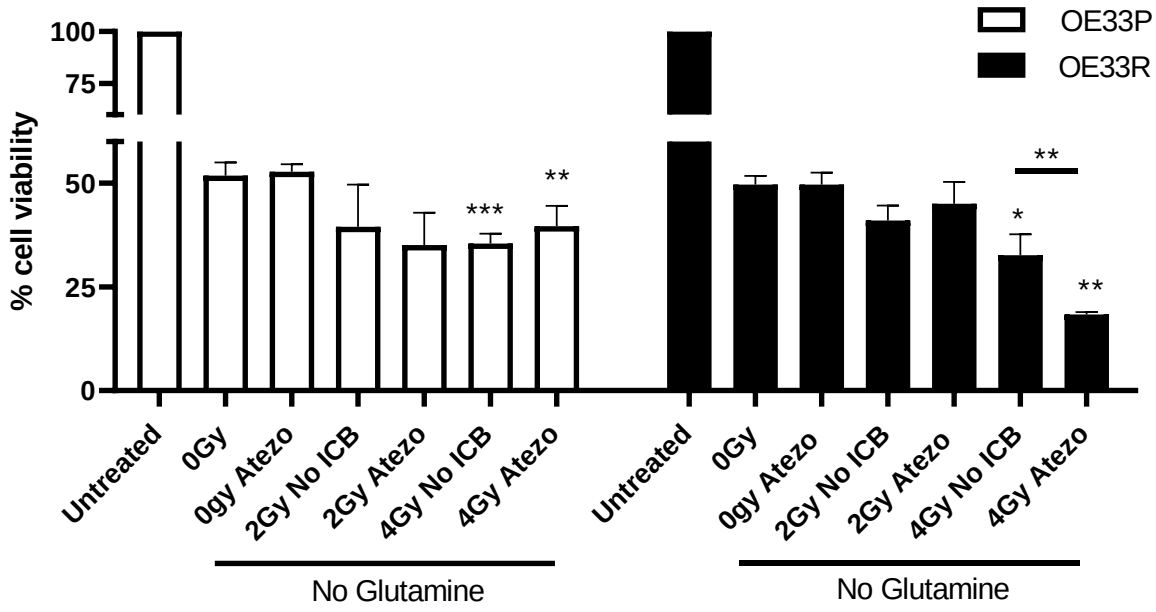

Figure 5.23; Ionising radiation with Atezolizumab and Glutamine deprivation. The % viability (±SEM) of OE33P and OE33R cells were assessed using a CCK8 assay with or without radiation (0, 2 or 4 Gy) and with or without immune checkpoint inhibitor Atezolizumab (Atezo), (n=3) 24 hrs after irradiation. Tukey's multiple comparison testing. * $p<0.05$, ** $p<0.01$, *** $p<0.001$.

There was a significantly reduced viability of OE33P and OE33R cells with nutrient deprivation in the absence of radiation (51.81±1.25) with no significant alteration in

viability with Atezolizumab alone (52.72±1.04) or 2 Gy radiation (39.48±4.95). There was a significant reduced viability with 4 Gy irradiation (35.41±4.5) $p<0.001$ or in combination with Atezolizumab and glutamine deprivation (39.6±2.83) $p<0.01$. There was a significant reduction in cell viability in the OE33R cell line with 4 Gy radiation alone (32.67±2.9) $p<0.05$) Atezolizumab and glutamine deprivation (18.33±0.33) $p<0.01$. There was a significant reduction in viability between 4 Gy alone and 4 Gy Atezolizumab ($p<0.01$) (Figure 5.23). Further significance between the dosing regimens, Atezolizumab and glutamine deprivation are available in Appendix Table 16.

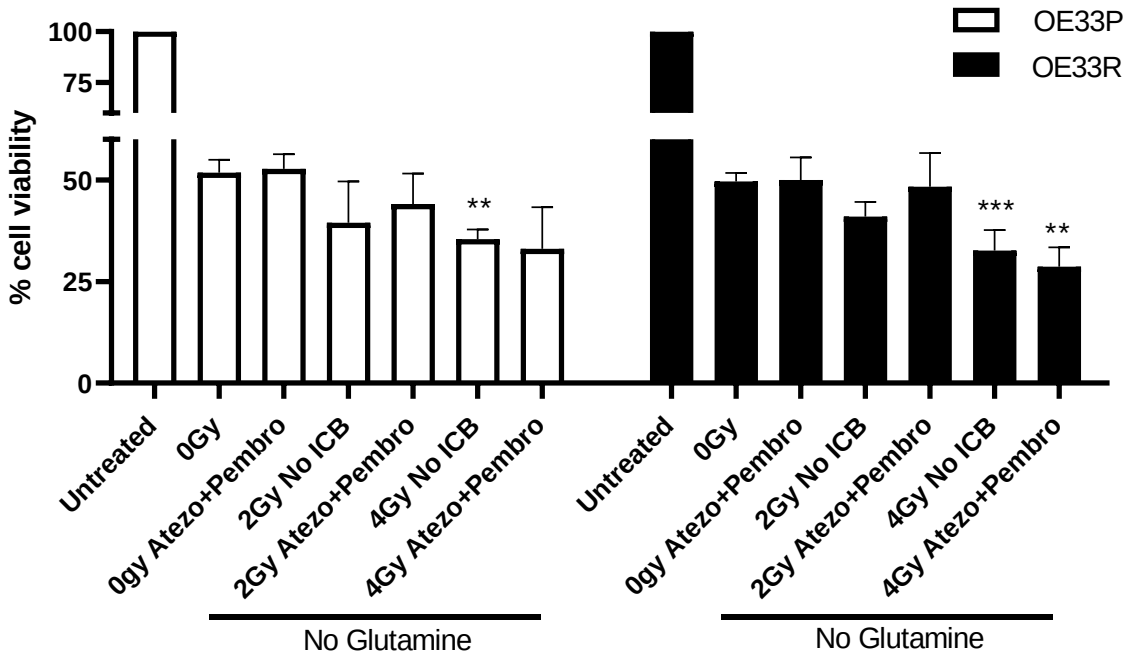

Figure 5.24; Ionising radiation with Atezolizumab and Pembrolizumab and Glutamine deprivation. The % viability (±SEM) of OE33P and OE33R cells were assessed using a CCK8 assay with or without radiation (0, 2 or 4 Gy) and with or without immune checkpoint inhibitor Atezolizumab and Pembrolizumab (Atezo and Pembro), (n=3) 24 hrs after irradiation. Tukey's multiple comparison testing. * $p<0.05$, ** $p<0.01$, *** $p<0.001$

There was a significantly reduced viability of OE33P and OE33R cells with nutrient deprivation in the absence of radiation (51.81±1.25) with no significant alteration in viability with Atezolizumab and Pembrolizumab alone (52.76±2.08) or 2 Gy radiation (39.48±4.95). There was a significant reduced viability with 4 Gy irradiation (35.41±4.5) $p<0.01$. There was a significant reduction in cell viability in the OE33R cell line with 4 Gy radiation alone (32.67±2.9) $p<0.001$) Atezolizumab and Pembrolizumab and glutamine deprivation (28.67±2.73) $p<0.01$. (Figure 5.24). Further significance between the dosing regimens, Atezolizumab and Pembrolizumab and glutamine deprivation are available in Appendix Table 17.

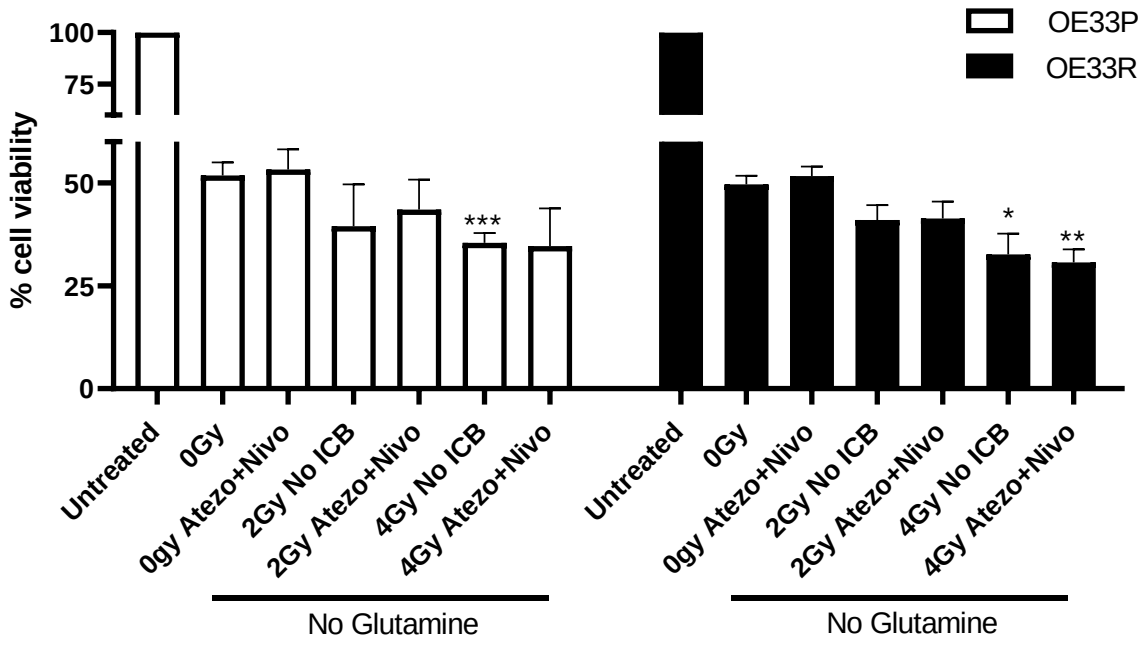

Figure 5.25; Ionising radiation with Atezolizumab and Nivolumab and Glutamine deprivation. The % viability (±SEM) of OE33P and OE33R cells were assessed using a CCK8 assay with or without radiation (0, 2 or 4 Gy) and with or without immune

checkpoint inhibitor Atezolizumab and Nivolumab (Atezo and Nivo), (n=3) 24 hrs after irradiation. Tukey's multiple comparison testing. * $p<0.05$, ** $p<0.01$, *** $p<0.001$

There was a significantly reduced viability of OE33P and OE33R cells with nutrient deprivation in the absence of radiation (51.81±1.25) with no significant alteration in viability with Atezolizumab and Nivolumab alone (53.24±2.84) or 2 Gy radiation (39.48±4.95). There was a significant reduced viability with 4 Gy irradiation (35.41±4.5) $p<0.01$. There was a significant reduction in cell viability in the OE33R cell line with 4 Gy radiation alone (32.67±2.9) $p<0.05$ and Atezolizumab and Nivolumab and glutamine deprivation (30.67±1.86) $p<0.01$. (Figure 5.25). Further significance between the dosing regimens, Atezolizumab and Nivolumab and glutamine deprivation are available in Appendix Table 18.

5.11 Discussion

It has been demonstrated that solid neoplasms are highly heterogenous and develop, progress, and respond to local and systemic therapies in the context of intricate crosstalk with the host immune system (288). It must be borne in mind that distinct phenotypic and behavioural features generally co-exist, and often multiple non-transformed cells are co-opted by growing cancers to support their needs. There is accumulating evidence that the efficacy of most chemo- and radiotherapeutic agents commonly employed in the clinic are dependent on the propagation of anti-tumour-targeting immune responses (313). Consequently, mechanistically, conventional therapeutics such as chemotherapy and radiotherapy can evoke a therapeutically relevant, adaptive immune response against malignant cells and is referred to as "immunogenic cell death." Radiation therapy induces changes in the phenotype and microenvironment of tumour cells after exposure to irradiation, chemotherapeutic agents, and immune modulating agents rendering the tumour more immunogenic with the induction of abscopal effects and this varies widely with the model systems and the radiation regimen utilised (314). There have been previous studies in the literature suggesting interactions and synergies of radiation therapy are essentially dependent on type-I interferons (produced by the cyclic GMP-AMP synthase (cGAS)/stimulator of interferon genes (STING) axis), APCs, and cytotoxic $CD8^+$ T cells, are the result of high single doses (10–20 Gy) (315). However, more recently, on the contrary, a recent study suggests that fractionated dosing such as 3 × 8 Gy may be optimal (316). However in reality, clinically abscopal tumour lesion responses remain elusive and exceedingly rare, likely because comparable hypofractionation (fractions of >5 Gy) are rarely used in the radiotherapeutic routine.

The findings of significantly higher calreticulin expression with radiation in the OE33R when compared to the OE33P cell line is interesting and suggest an immunogenic type

of cell death induced by radiation in the radioresistant cell line providing a foundation for immune modulating agents to enhance the established anti-tumour response particularly with adverse biology such as radioresistance. There were similar findings for HMGB1 with a higher expression of HMGB1 in the OE33R cell line with bolus dosing, however, there was a significantly higher expression of HMGB1 with fractionated dosing regimens of 3x4 Gy and 3x8 Gy in the OE33P cell line compared to the OE33R cell line. The increased expression of both DAMPS post radiotherapy *in vivo* and *ex vivo* post conventional therapies suggest promise of oesophageal adenocarcinoma as an immunogenic tumour entity and therefore a potential target for systemic immunotherapies. In addition to this, the increased expression of Calreticulin and HMGB1 post radiation with hypoxia, notably 5% O_2 and nutrient deprivation, represent further exciting data and reaffirm the hypothesis that oesophageal cancer is a viable phenotype for enhancing the anti-tumour immune response. On the contrary, it is also important to note that the properties of the intrinsic tumour microenvironment, such as hypoxia or nutrient deprivation, endemic of tumours, could alter the action of ICD stressors and modulate the immunomodulatory properties of DAMPs (317). Furthermore, it was previously demonstrated that hypoxia leads to HMGB1 release, which can contribute to tumour invasiveness (318). DAMPs are released from cells under stress due to these harsh conditions of the tumour microenvironment including nutrient deprivation and hypoxia, or secondary to treatment with chemotherapy or radiotherapy and when released can have a double edged sword activating innate immunity, providing a pathway to a systemic inflammatory response or can be manipulated in regulating inflammation in the tumour microenvironment, promoting angiogenesis and increasing autophagy with immune evasion and avoidance of apoptosis, facilitating progression and or dissemination (319).

There is evidence in the literature of high Calreticulin levels in cancer cells correlating with favourable disease outcome in a cohort of 68 neuroblastoma patients as a consequence of radiation therapy inducing immunogenic cell death (295) and also in a cohort of lung cancer patients (320). In addition to this, increased CALR expression by cancer cells has been associated with tumour infiltration by $CD45RO^{+}$ memory T cells and improved 5-year overall survival in patients with advanced colorectal carcinoma (CRC) (321). HMGB1 has been demonstrated to have both pro and anti-tumour modulating effects and is overexpressed in precancerous states such as liver cirrhosis and gastric dysplasia (322) in addition to a wide range of tumours and may induce inflammatory responses that promote tumourigenesis and/or progression (322, 323). HMGB1 triggers the recruitment of neutrophils, subsequent inflammation and amplification of injury in multiple injury models (324). In one study, high levels of HMGB1 expression in cancer cells have been shown to correlate with improved overall survival in 88 patients with oesophageal squamous cell carcinoma subjected to neo-adjuvant chemoradiotherapy and surgical resection, as well as in 76 subjects with resectable gastric adenocarcinoma (325). However, in colorectal cancer, elevated HMGB1 in serum correlated with incidence, progression or unfavourable disease outcome in a cohort of 219 colorectal cancer patients demonstrating the diverse prognostic or predictive value of high intratumoural and circulating levels of HMGB1 (321). Interestingly, in this study, there were two distinct subgroups with high and low expressors of DAMPs, and this correlated with tumour regression grade and lymphatic invasions. Patients who were high expressors of HMGB1 had a significantly better Tumour Regression Grade (TRG 1-2) compared to low expressors. Similarly, patients who had an increase in Calreticulin post treatment had a better TRG (1-2).

A deeper understanding of the diverse roles of DAMPs is needed to exploit therapeutic strategies, and it is postulated that these therapeutic approaches might incorporate both activation and inhibition of DAMP signalling pathways. Furthermore, drawing conclusions about the clinical applicability of DAMPs as biomarkers is currently still restricted by the small size of these studies, heterogeneous patient populations (i.e., disease stage), and treatment differences such as chemoradiotherapy combinations and dosing and therefore further work is needed to elucidate mechanistics and therapeutic potential.

Chapter 6: The impact of conventional therapies and immune checkpoint blockade on the immune profile in Oesophageal Adenocarcinoma

Donlon NE, Sheppard A, Davern M, O'Connell F, Phelan JJ, Power R, Nugent T, Dinneen K, Aird J, Greene J, Nevins Selvadurai P, Bhardwaj A, Foley EK, Ravi N, Donohoe CL, Reynolds JV, Lysaght J, O'Sullivan J, Dunne MR. Linking Circulating Serum Proteins with Clinical Outcomes in Esophageal Adenocarcinoma-An Emerging Role for Chemokines. Cancers (Basel). 2020 Nov 13;12(11):3356. doi: 10.3390/cancers12113356. PMID: 33202734; PMCID: PMC7698106.

6.1 Introduction

Adenocarcinoma of the oesophagus (OAC) or the oesophagogastric junction (OGJ) are particularly aggressive cancer types and are rapidly increasing in the Western world in line with growing obesity rates (326). In locally advanced disease, the addition of neoadjuvant chemoradiotherapy or perioperative chemotherapy (neo-CT) to surgical resection provides a modest overall survival (OS) benefit (5, 212, 327). This benefit is mainly restricted to the 10–15% of patients who display a pathological complete response (pCR) to treatment in the resected tumour (328). As prognosis is poor (20) and systemic therapy is associated with significant morbidity (6), the ability to predict a response to neoadjuvant treatment could allow a more tailored approach to multimodal therapy.

The pathological response to neo-CT treatment can be measured by the tumour regression grade (TRG) (329). Use of the Mandard TRG classification system, first described in 1994 (226), is recommended by UK and Irish guidelines (330). This system is based on the amount of residual tumour and the degree of fibrosis at the primary tumour site and uses a five-point scale, where a score of one corresponds to complete tumour regression with no tumour cells detectable and a score of five denotes no evidence of tumour regression. A pathological response to neo-CT, as defined by a Mandard TRG score of 1–2, is associated with prolonged disease-free survival (DFS) and OS in retrospective studies (331-333) and prolonged OS in a secondary analysis of a randomized trial (228). Other morphological markers, including downstaging of lymph node status, present strong independent prognostic markers in OAC (334), particularly in patients without a local pathological response (228). Adverse pathological features described on resected tumour samples, including poor differentiation, mucinous or signet ring features, and perineural, vascular and lymphovascular invasion are also negatively

associated with DFS (335-338) and have the potential to be used alongside TRG in patient stratification.

Activation of the effector immune response is now recognized to be involved in the response to chemoradiotherapy (339). Immunogenic cell death is a key mediator of this and can be induced by radiotherapy and cytotoxic chemotherapies employed in the neoadjuvant setting (340, 341). This therapy-induced anti-tumour immunity may predict tumour regression, for example a tumour gene expression signature of the DNA damage immune response, including programmed cell death ligand 1 (PD-L1) and several inflammatory cytokines (CXCL9, CXCL13, CXCL10/IP-10, CXCL11, CCL5, CCL18), has been shown to predict tumour regression in OAC (342). Interestingly, expression of such DNA damage immune response markers was also associated with increased levels of $CD8^+$ tumour-infiltrating lymphocytes in resected tumours, which have independently been associated with pathologic response in OAC (343). However, the association between pathological responses and blood-derived immune profiles has not been previously explored in detail in OAC. Chronic inflammation has been implicated in OAC development and presents a possible mechanism of resistance to neoadjuvant therapy (260). Circulating proteins can be quantified easily as a measure of systemic events, such as inflammation and angiogenesis and are more amenable to routine interrogation than tumour tissues. Circulating factors such as C-reactive protein (CRP) (344), soluble interleukin-6 receptor (sIL-6R) (345) and vascular endothelial growth factor (VEGF) (346) have demonstrated prognostic potential in oesophageal cancer, however most studies to date have focused on squamous cell type oesophageal tumours. We aimed to assess whether such serum protein profiles also had a prognostic or predictive ability in the OAC setting, as well as assessing the immunomodulatory effect of radiation on effector immune cells.

This body of work had three aims;

1. quantification of levels of 54 serum markers from OAC/OGJ patients, and assessment of links with clinicopathological outcomes, e.g., overall survival (OS), TRG, adverse events and immune cell infiltration into tumours.
2. Assess the impact of ionising radiation on OAC patient treatment naïve Peripheral blood mononuclear cells.
3. Determine the effects of multimodal treatment with radiation to the tumour and ICB administration to patient PBMCs cells on cytolysis of tumour cells.

Through this, we aimed to better understand systemic immune and angiogenic profiles linked with clinical outcomes.

6.2 Results

6.2.1 Lower TRG Scores and Node Negativity Are Associated with Longer Overall Survival (OS) Time

OS time was visualized using a Kaplan–Meier curve, dividing patients into low (TRG1–2) and high (TRG3–5) groups or based on treatment response and nodal status, as shown in Figure 6.1. Log-rank testing showed that low TRG scores were associated with a longer survival time (median 70.4 months) compared to high scores (median 33.5 months), $p < 0.05$ (Figure 6.1A). OAC patients with node positive disease showed shorter survival times (median 22.4 months) than node negative (94.6 months) or pathological complete response (pCR) (70.1 months) cohorts (Figure 6.1B).

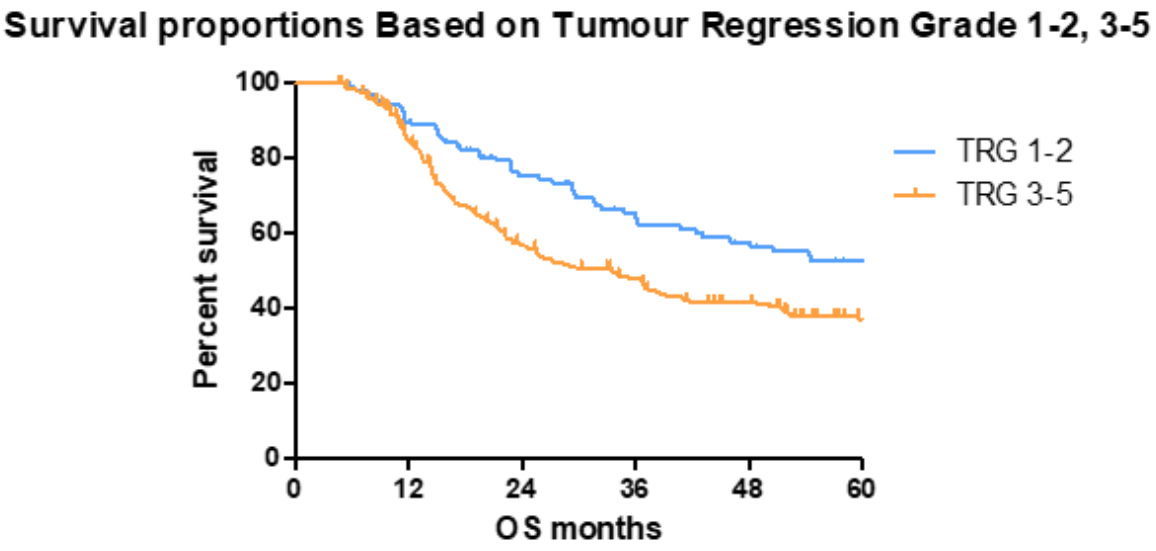

	TRG 1-2			TRG 3-5		
Survival (years)	No at risk	Deaths	% survival	No at risk	Deaths	% survival
1	110	11	90	240	34	85
3	97	25	65	182	75	48
5	62	11	53	91	19	37

Median Survival; TRG 1-2; 70.43, TRG 3-5; 33.47**, P<0.05**

(A)

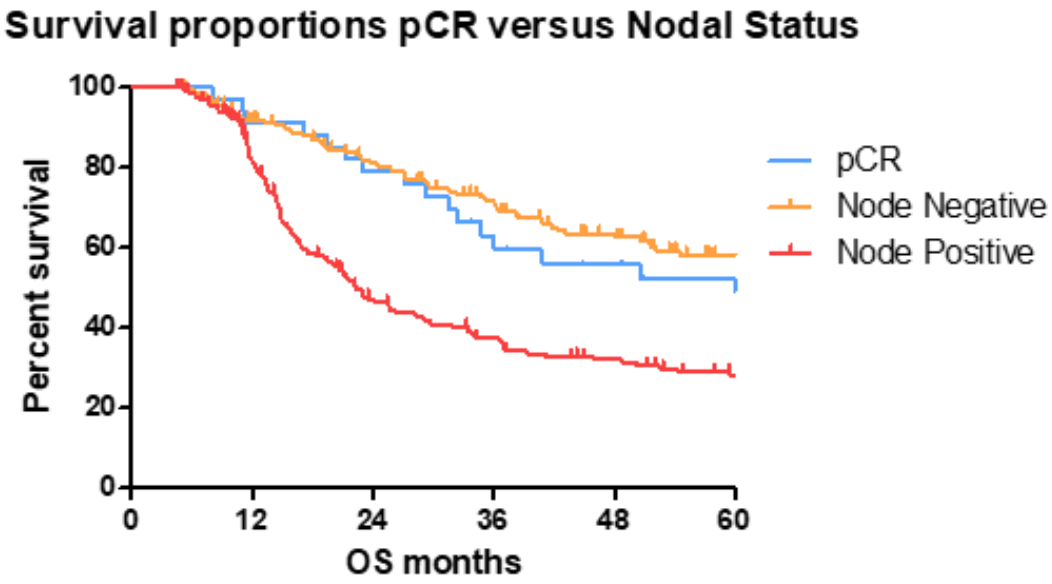

	pCR			Node Negative			Node Positive		
Survival (years)	No at risk	Deaths	% survival	No at risk	Deaths	% survival	No at risk	Deaths	% survival
1	34	3	91	161	13	92	189	32	82
3	31	9	63	141	29	72	138	71	38
5	19	3	52	98	17	58	55	13	28

Median Survival; pCR; 70.1 months, Node Negative 94.57 months, Node Positive 22.4 Months
P<0.001

(B)

Figure 6.1. Lower TRG scores and node negativity are associated with longer overall survival time. A cohort of 80 OAC/OGJ patients was divided according to low (TRG1–2) or high (TRG3–5) TRG scores (**A**), or nodal status and pCR (**B**) and OS time in months was visualized using a Kaplan–Meier curve. Log-rank (Mantel–Cox) tests were performed to assess median survival time differences between groups. TRG = Tumour Regression Grade, OS = Overall Survival, pCR = Pathological Complete Response.

6.3 CCL4 Is Lower and Tie2 and CRP Levels Higher in Pre-Treatment Serum of Patients with a Subsequent Poor Response to Neo-Adjuvant Treatment

Given the considerable survival differences observed between low (TRG1–2) and high (TRG3–5) groups, these divisions were used to assess differences in the levels of pre-treatment serum cytokines (Figure 6.2). Patients with a favourable response to neo-CT, i.e., a low TRG score, showed higher levels of circulating CCL4 ($p < 0.01$) (Figure 6.2a). A further subdivision of TRG groups showed that levels were significantly higher in the TRG1/2 cohort when compared to TRG3 ($p < 0.05$) and TRG4/5 ($p < 0.01$) groups individually (Figure 6.2b). Levels of angiogenic factor Tie2 ($p < 0.05$) and inflammatory factor CRP ($p < 0.05$) were significantly higher in poor responders (Figure 6.2c–f). For Tie2, this difference was most apparent when TRG1/2 and TRG4/5 groups were compared.

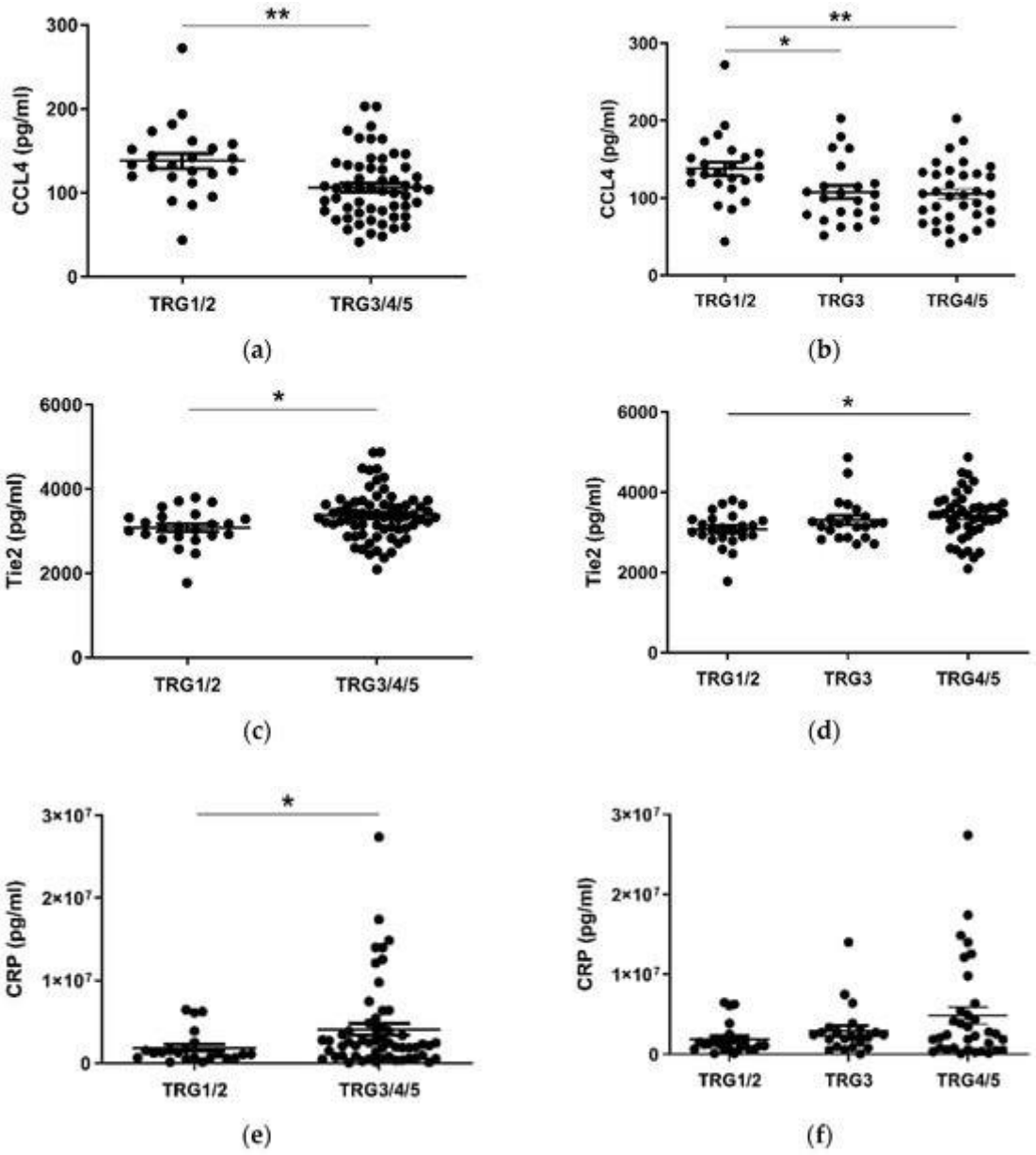

Figure 6.2. CCL4, Tie2 and CRP levels are altered in pre-treatment serum between TRG treatment response groups. Levels of cytokines were measured in serum of 80 patients using multiplex ELISA and grouped by TRG score. Two group data sets were analyzed by Mann–Whitney test, and three group data sets were analyzed by ANOVA (Kruskal–Wallis test with Dunn's multiple comparisons). * $p < 0.05$. ** $p < 0.01$. CRP = C Reactive Protein.

6.4. Pre-Treatment Serum IL-10 Is Associated with Reduced Overall Survival, while CCL22 and CCL26 Are Associated with Prolonged Overall Survival

After observing that levels of certain serum proteins measured at a pre-treatment timepoint were associated with TRG scores, we next investigated whether protein levels were also associated with OS time. Patients were divided into high and low expressing cohorts based on median expression value of each protein, and associations were assessed by log-rank test and visualized using Kaplan–Meier curves (Figure 6.3). As shown in Figure 6.3, levels greater than the median of the immunosuppressive cytokine IL-10 were significantly associated with poorer OS ($p = 0.0055$, hazard ratio (HR) = 0.378, 95% confidence interval (CI) = 0.1818–0.786), whereas higher than median levels of the chemokines CCL22 ($p = 0.0101$, HR = 2.301, 95% CI = 1.183–4.475) and CCL26 ($p = 0.0163$, HR = 2.254, 95% CI = 1.14–4.456) were associated with longer OS.

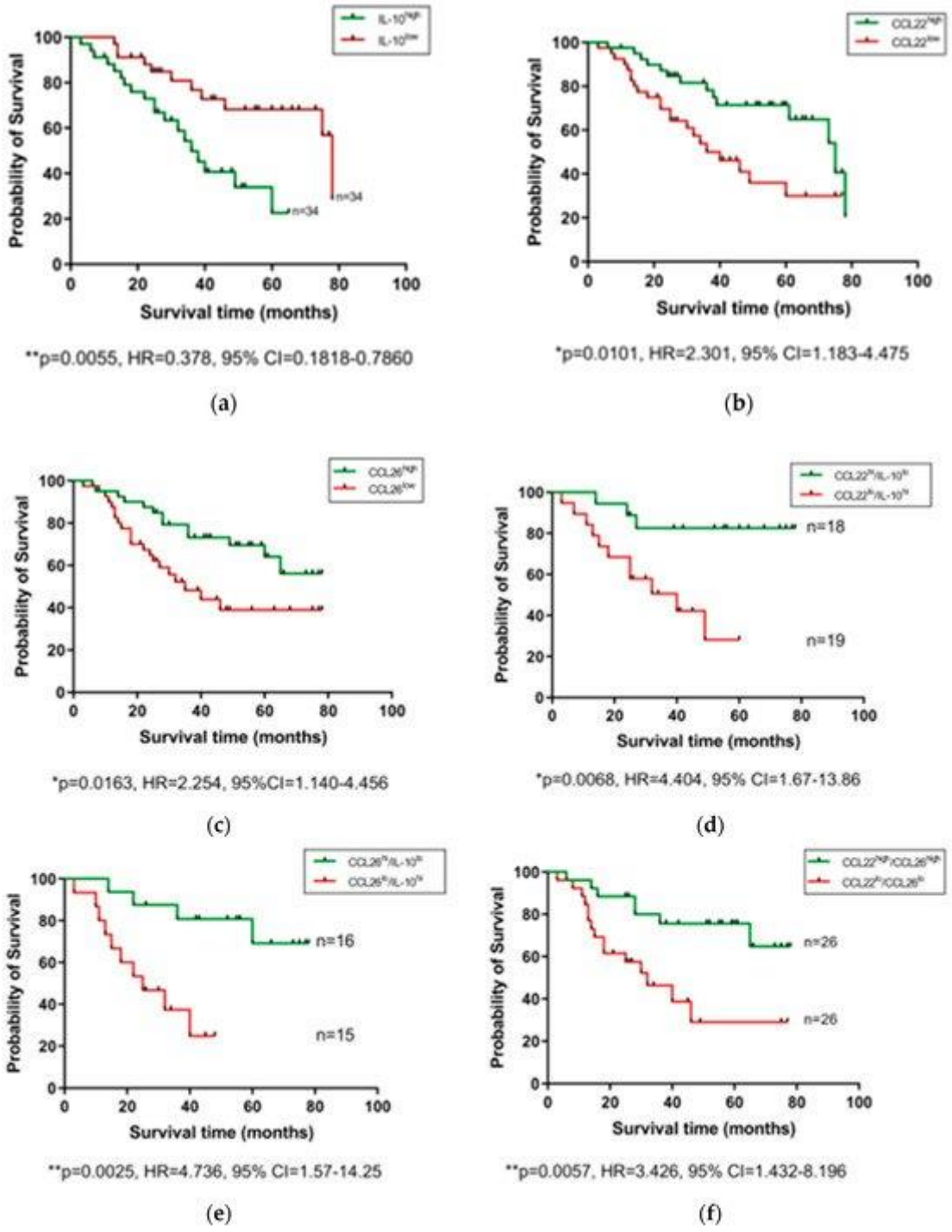

Figure 6.3. Serum IL-10, CCL22, and CCL26 levels are associated with overall survival. Groups were divided into cytokine high and low populations using the median cytokine level as a cut-off and OS was visualized using Kaplan–Meier curves. Log-rank (Mantel–Cox) tests were performed to assess median survival time differences between groups and data were visualized using Kaplan–Meier curves. OS = Overall Survival, IL = Interleukin.

6.5. Reduced Levels of Circulating CCL3, CCL4, IL-1α and IL-12/IL-23p40 and Elevated Levels of Tie2 and VEGF Are Associated with Adverse Tumour Features

We sought to investigate differences in the levels of circulating factors in the serum of patients with or without adverse features. Adverse pathological features included poor tumour differentiation, mucinous or signet ring features, and evidence of perineural, vascular and lymphovascular invasion. Patients were divided into three cohorts; 0, 1–2 and 3–4 adverse features. As shown in Figure 6.4, levels of CCL3, CCL4, IL-1α, and IL-12/IL-23p40 were observed to be highest in those with no adverse features compared to the groupings with adverse features. Conversely, levels of Tie2 and VEGF were lowest in those with no adverse features present.

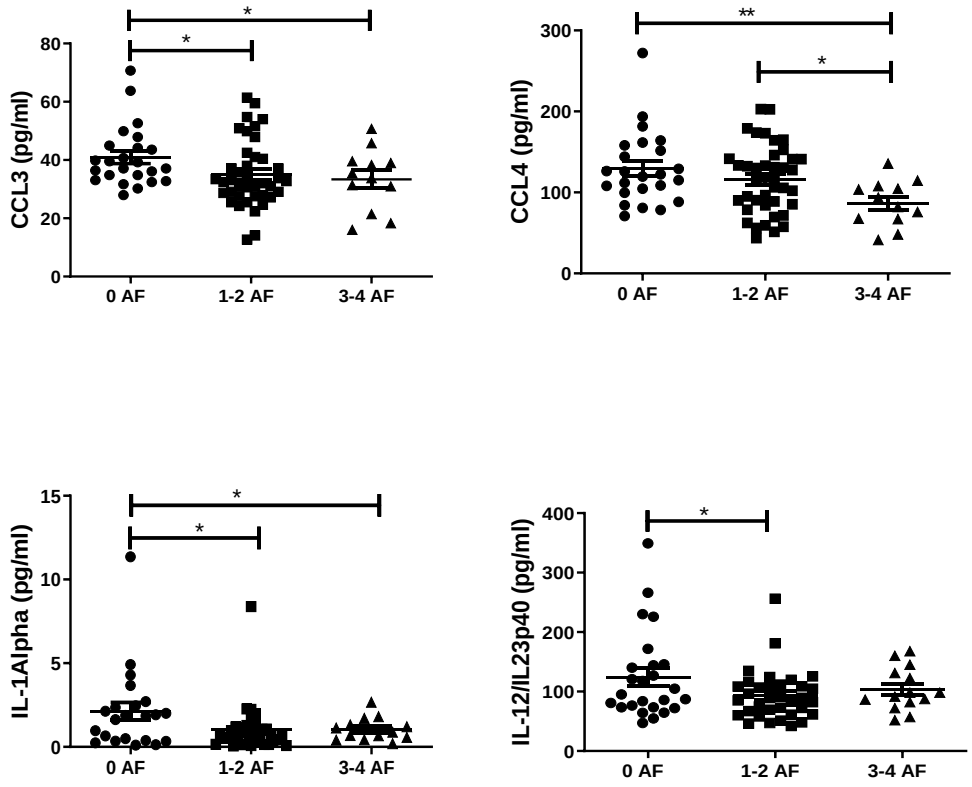

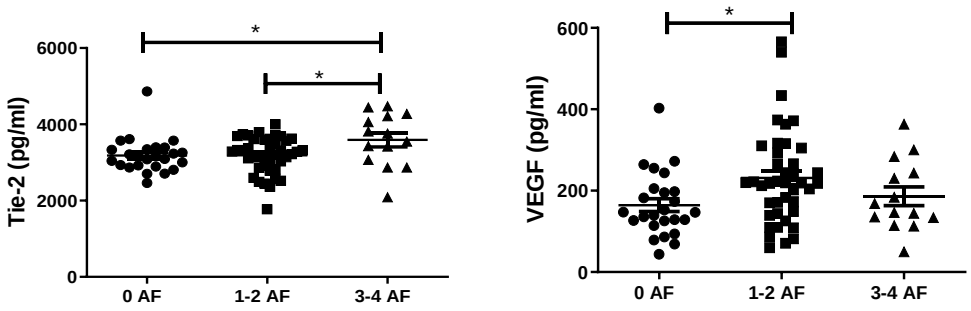

Figure 6.4. In OAC patients with no adverse features of tumour biology, CCL3, CCL4, IL-1α, and IL-12/IL-23p40 levels were significantly higher in serum, with the contrary evident for Tie2 and VEGF. Groups were divided according to adverse features of tumour biology, with groupings of 0 adverse features, 1–2 adverse features or 3–4 adverse features. Data were analysed by ANOVA (Kruskal–Wallis test with Dunn's multiple comparisons). * $p < 0.05$. ** $p < 0.01$. IL = Interleukin, VEGF = Vascular Endothelial Growth Factor.

6.6. Neo-Adjuvant Treatment Increases Serum Pro-Inflammatory Cytokines and Decreases Anti-Angiogenic Mediators

Given extensive evidence in the literature outlining the various pro- and anti-tumour effects of chemotherapy and radiotherapy on anti-tumour immunity, we compared the expression of circulating serum levels of immune-based proteins before and after neo-CT treatment in order to further elucidate the effect of neo-adjuvant treatment on systemic immunity. Serum specimens were collected at a pre- and post-treatment timepoint for n = 28 donors (11 donors received CROSS regimen, 7 received FLOT and 10 received MAGIC), and levels of 54 circulating proteins were quantified on the same plate, within a single assay run. As shown in Figure 6.5, significant elevations were observed after treatment in the levels of PlGF ($p < 0.0001$), CCL3, IL-21, IL-12/IL-23p40, GM-CSF, bFGF, TNF-α, IFN-γ, CXCL10, CCL4, and IL-5, whereas angiogenic factor VEGFC was

significantly decreased ($p < 0.0001$) when data were analyzed using a Wilcoxon matched pairs signed rank test.

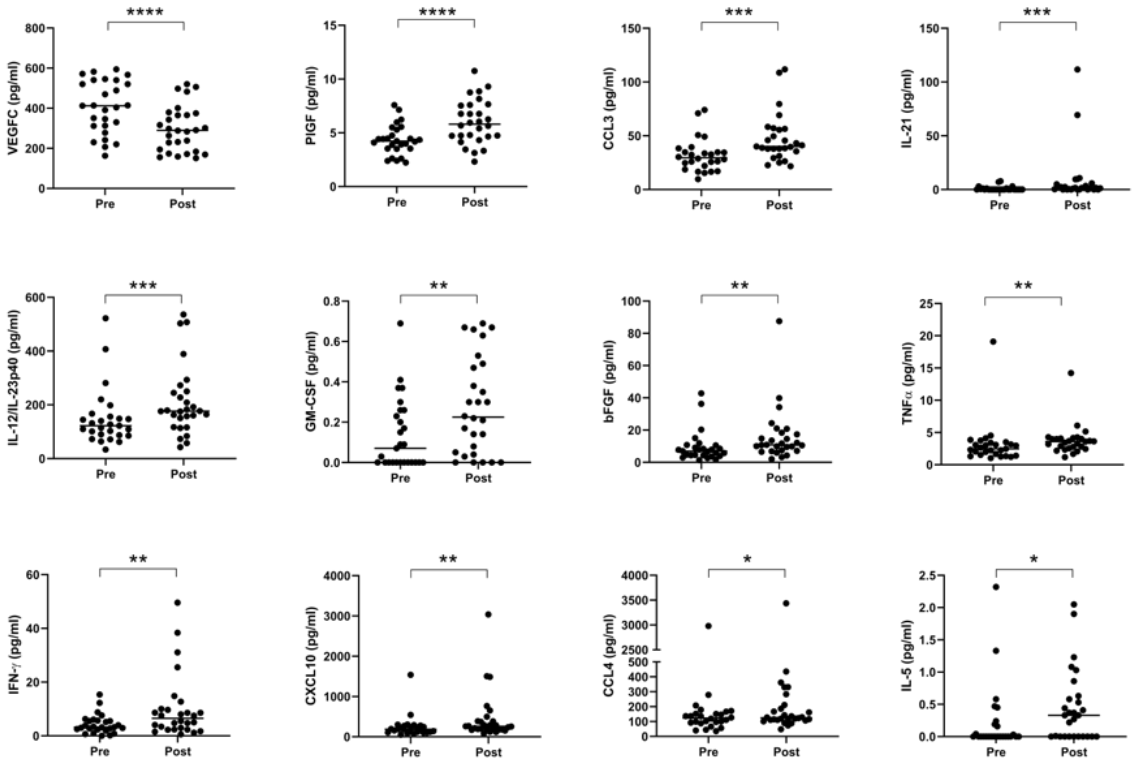

Figure 6.5. Serum pro-inflammatory cytokines are increased, and anti-angiogenic cytokines are decreased following neo-adjuvant treatment. Cytokines were measured before and after treatment in a cohort of 28 matched donors. Pre- and post-treatment datasets were compared using a Wilcoxon matched pairs signed rank test, * $p < 0.05$, ** $p < 0.01$, *** $p < 0.001$, **** $p < 0.0001$. VEGF = Vascular Endothelial Growth Factor, PlGF = Placental Growth Factor, IL = Interleukin, GM-CSF = Granulocyte-Macrophage Colony-Stimulating Factor, bFGF = Basic Fibroblast Growth Factor, TNF = Tumour Necrosis Factor, IFN = Interferon.

6.7. Tumours with High Lymphocytic Infiltration Showed Higher Levels of Circulating TNF-β, CCL4, CCL13 and IL-27 in pre treatment samples

Hematoxylin and eosin stained tumour pre-treatment biopsy slides were available for a subset of n = 32 patients who underwent serum cytokine analysis. Within this cohort, consensus scoring from two pathologists showed an overall low level of tumour stroma

(only 3/32 tumours scored >50%) and high levels of overall inflammation (29/32 donors scoring highly). Infiltration of lymphocytes, plasma cells, neutrophils, and eosinophils was also classified into high (>50%) and low (0–50%) groups. When patients were grouped into lymphocyte high (>50% infiltration) and low (<50%) cohorts, it was observed that individuals with lymphocyte high tumours also showed elevated levels of serum CCL4 ($p < 0.05$), CCL13 ($p < 0.05$), IL-27 ($p < 0.05$), and TNF-β ($p < 0.01$) (Figure 6.6). No significant differences were observed when levels were compared for other cytokines, or with infiltration of other immune cell types, i.e., plasma cells, eosinophils, or neutrophils.

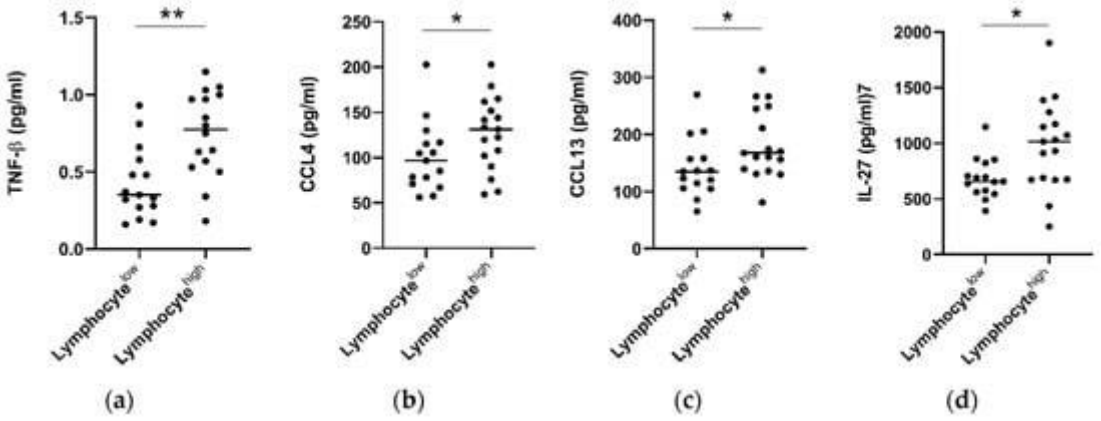

Figure 6.6. Patients with high tumour lymphocyte infiltration show elevated serum TNF-β, CCL4, CCL13, and IL-27. Tumour diagnostic biopsies were scored for lymphocytic infiltration in a cohort of n = 32 patients and divided into low (<50% infiltration, n = 15) and high (>50%, n = 17) cohorts. Pre-treatment cytokine levels were analysed between groups. A Mann–Whitney test was used to compare lymphocyte low and high populations, * $p < 0.05$, ** $p < 0.01$. TNF = Tumour Necrosis Factor, IL = Interleukin.

6.8. Correlation Analysis of Cytokines with Patient Clinical Outcomes

To determine if treatment-naïve protein expression levels identified by 54-plex ELISA correlated with patient clinical features, Spearman correlations were performed and visualized using the R package "CorrPlot" (Figure 6.7a). Nine cytokines with fewer than 40 detectable readings (i.e., half the total cohort tested) were excluded from analysis.

The corresponding Spearman r values and *p* values associated with each correlation are summarized in Figure 6.7b. Age at time of diagnosis indicated weak significant positive correlations with secretion of IL-12/IL-23p40 (r = 0.2702, *p* = 0.015), IL-6 (r = 0.3404, *p* = 0.002), CCL3 (r = 0.2622, *p* = 0.02), PlGF (r = 0.2902, *p* = 0.009), and TNF-α (r = 0.2387, *p* = 0.032). Perineural invasion showed a weak negative correlation with CXCL10 (r = −0.268, *p* = 0.016). Lymphatic invasion showed weak positive correlations with IL-1RA (r = 0.2363, *p* = 0.035) and IL-27 (r = 0.2298, *p* = 0.04) and serosal involvement showed weak negative correlations with CCL4 (r=−0.2513, *p* = 0.027) and VEGF (r=−0.2822, *p* =0.013). Clinical TNM stage showed weak positive correlations with IFN-γ (r =0.3229, *p* = 0.024) and CCL2 (r=0.3274, *p* = 0.017), while pathologic T stage yielded weak negative correlations with CXCL10 (r = −0.223, *p* = 0.048), CCL4 (r = −0.2793, *p* = 0.013), and PlGF (r = −0.2767, *p* = 0.014), with pathologic N stage showing weak negative correlations with CCL11 (r = −0.2234, *p* = 0.048), IL-22 (r = −0.2517, *p* = 0.029), and positive weak correlations with IL-17B (r=0.2554, *p* = 0.027). TRG indicated weak negative correlations with CCL4 (r = −0.2694, *p* = 0.016) and CCL17 (r = −0.2257, *p* = 0.046), with disease recurrence showing weak positive correlation with IL-1β (r = 0.2923, *p* = 0.027), also yielding weak negative correlations with CCL17 (r = −0.2503, *p* = 0.026) and TNF-β (r = −0.2323, *p* = 0.046). No other significant associations were identified between treatment naive protein expression and matched clinical features.

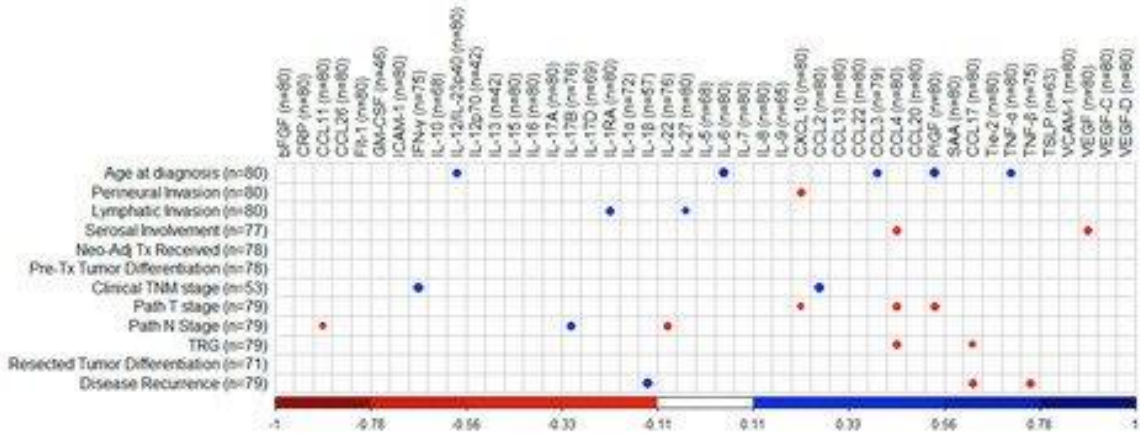

(a)

Clinical Factor	Protein	Spearman r	*p* Value (Two-Tailed)
Age at diagnosis	IL-12/IL-23p40	0.2702	0.015
	IL-6	0.3404	0.002
	CCL3 (n = 79)	0.2622	0.020
	PlGF	0.2902	0.009
	TNF-α	0.2387	0.032
Perineural Invasion	CXCL10	−0.2680	0.016
Lymphatic Invasion	IL-1RA	0.2363	0.035
	IL-27	0.2298	0.040
Serosal Involvement	CCL4	−0.2513	0.027
	VEGF	−0.2822	0.013
Clinical TNM stage	IFN-γ (n = 75)	0.3229	0.024
	CCL2	0.3274	0.017
Pathologic T stage	CXCL10	−0.2230	0.048
	CCL4	−0.2793	0.013
	PlGF	−0.2767	0.014
Pathologic N Stage	CCL11	−0.2234	0.048
	IL-17B (n = 76)	0.2554	0.027
	IL-22 (n = 76)	−0.2517	0.029
TRG	CCL4	−0.2694	0.016
	CCL17	−0.2257	0.046
Disease Recurrence	IL-1β (n = 57)	0.2923	0.027
	CCL17	−0.2503	0.026
	TNF-β (n = 75)	−0.2323	0.046

(b)

Figure 6.7. Correlation of cytokine levels with clinical parameters. (a) CorrPlot illustrating positive correlations identified between age at diagnosis with IL-12/IL-23p40, IL-6, CCL3, PlGF, and TNF-α, lymphatic invasion with IL-1RA and IL-27, clinical TNM stage with IFN-γ and CCL2, pathologic N stage with IL-17B and disease recurrence with IL-1β. Negative correlations also illustrated were identified between perineural invasion with CXCL10, serosal involvement with CCL4 and VEGF, pathologic T stage with CXCL10, CCL4, and PlGF, pathologic N stage with CCL11 and IL-22, TRG with CCL4 and CCL17 and disease recurrence with CCL17 and TNF-β. (**b**) Table summarizing correlation values including Spearman r and *p*-values. Cohort n = 80, unless stated otherwise. All reported *p* values were also adjusted for false discovery rate

using the Holm–Bonferroni method. TNM = Tumour Node Metastasis, TRG = Tumour Regression Grade. IL = Interleukin, PlGF = Placental Growth Factor, TNF = Tumour Necrosis Factor, VEGF = Vascular Endothelial Growth Factor, IFN = Interferon.

6.9: Immune checkpoint expression on $CD3^+$, $CD3^+CD4^+$, $CD3^+CD8^+$ cells following bolus and hypofractionated radiotherapy dosing in the presence of nutrient deprivation.

The impact of radiation in the presence of nutrient deprivation on immune function has yet to be elucidated. Proliferating cancer cells induce a microenvironment of nutrient deprivation, however, immune cells must exist and function in the same setting but the impact of nutrient deprivation and radiation are yet to be examined in detail. In order to mimic the conditions of nutrient deprivation that often prevails in the tumour microenvironment we evaluated the expression of ICs, cytokines and DAMPs under conditions of no glucose and no glutamine as well as under normal culture nutrient supply.

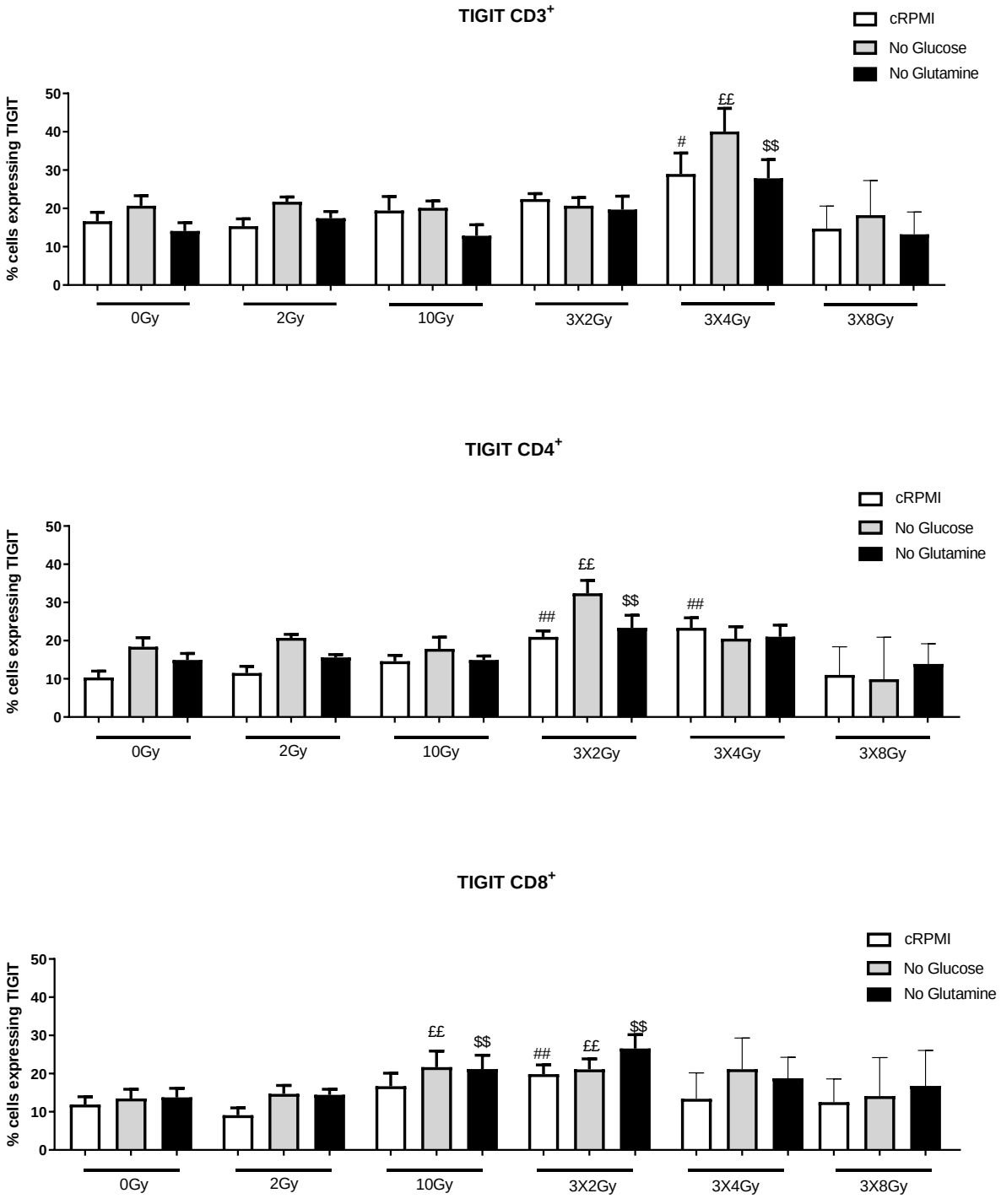

Figure 6.8: The expression of TIGIT was determined on the surface of peripheral blood $CD3^+$, $CD3^+CD4^+$, $CD3^+CD8^+$ cells in treatment naïve whole blood (n=6) with and without radiation and in the presence or absence of nutrient deprivation (glucose and glutamine deprivation) by flow cytometry. Tukey's multiple comparison testing. # denotes comparison of dosing with 0 Gy normal nutrient supply, # $p<0.05$, ## $p<0.01$. £ denotes comparison of dosing with 0 Gy and Glucose deprivation, £ $p<0.05$, ££ $p<0.01$, £££ $p<0.001$. $ denotes comparison of dosing with 0 Gy at and Glutamine deprivation, $ $p<0.05$, $$ $p<0.01$, $$$ $p<0.001$.

There was a significant increase in $CD3^+$ TIGIT at 3x4 Gy normal nutrient supply (28.97±8.3), 3x4 Gy no Glucose (40.07±7.6), 3x4 Gy no Glutamine (27.83±5.91), compared to 0 Gy normal nutrient supply (16.67±5.4) 0 Gy no Glucose (20.7±3.67), 0Gy no Glutamine (14.1±3.29), $p<0.05$, $p<0.01$, $p<0.01$, respectively. There was a significant increase in $CD3^+CD4^+$ TIGIT at 3x2 Gy normal nutrient supply (20.97±13.2), 3x2 Gy no Glucose (32.38±11.2), 3x2 Gy no Glutamine (23.33±7.51), compared to 0 Gy normal nutrient supply (10.34±7.4) 0 Gy no Glucose (18.38±3.4), 0 Gy no Glutamine (14.93±3.86), $p<0.01$, $p<0.01$, $p<0.01$, respectively and 3x4 Gy normal nutrient supply (23.35±5.89) $p<0.01$ (Figure 6.8).

There was a significant increase in $CD3^+CD8^+$ TIGIT 10 Gy no Glucose (21.68±8.07), compared to 0 Gy no Glucose (11.23±7.02) and 10 Gy no Glutamine (21.2±3.63) compared to 0 Gy no Glutamine (13.78±4.59) $p<0.01$, $p<0.01$, respectively. There was a significant increase in $CD3^+CD8^+$ TIGIT at 3x2 Gy normal nutrient supply (19.85±5.91), 3x2 Gy no Glucose (21.08±6.77), and 3x2 Gy no Glutamine (26.57±11.2) compared to 0 Gy normal nutrient supply (11.88±6.2), 0 Gy no Glucose (11.23±7.02), 0 Gy no Glutamine (13.78±14.1), $p<0.01$, $p<0.01$, $p<0.01$, respectively (Figure 6.8).

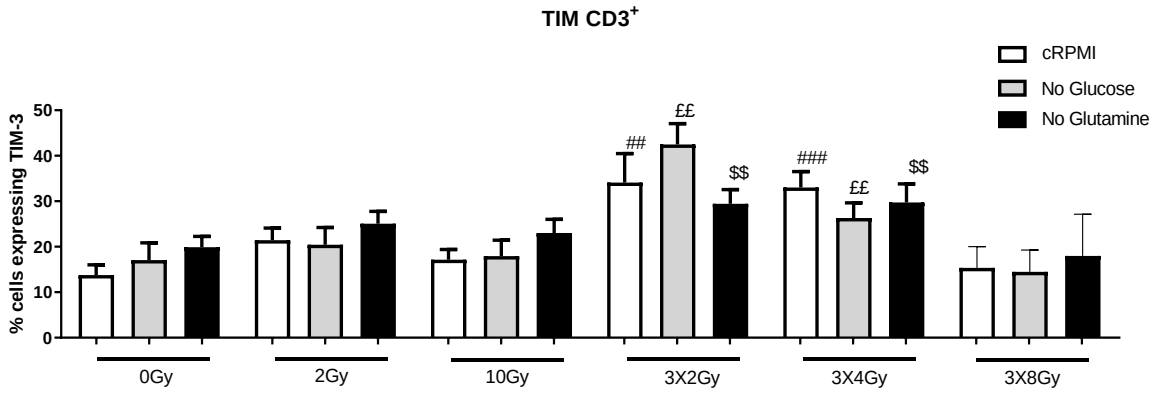

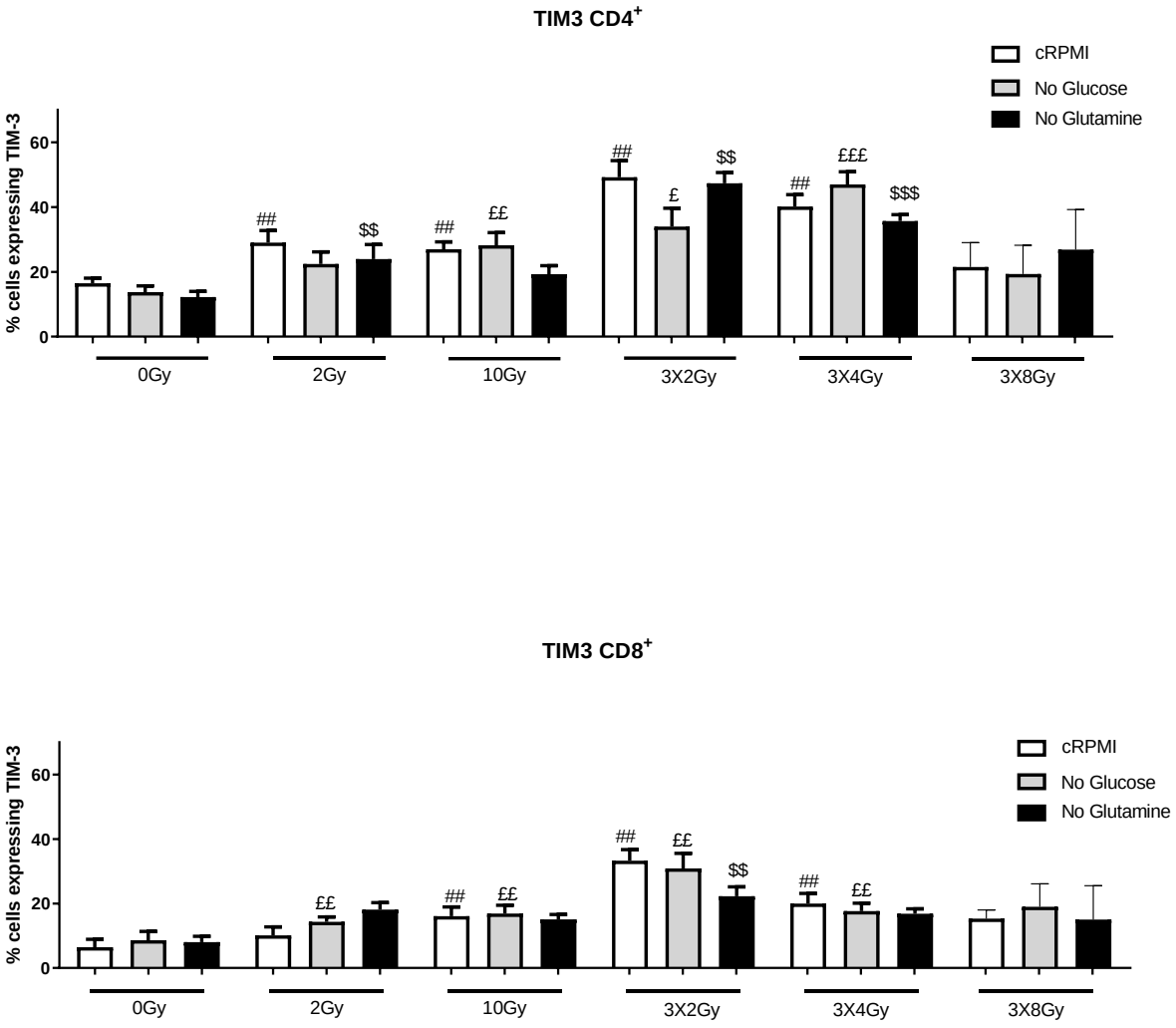

Figure 6.9: The expression of TIM-3 was determined on the surface of peripheral blood $CD3^+$, $CD3^+CD4^+$, $CD3^+CD8^+$ cells in treatment naïve whole blood (n=6) with and without radiation and with and without nutrient deprivation (glucose and glutamine deprivation) by flow cytometry. Tukey's multiple comparison testing. # denotes comparison of dosing with 0 Gy normal nutrient supply, # $p<0.05$, ## $p<0.01$. £ denotes comparison of dosing with 0 Gy and Glucose deprivation, £ $p<0.05$, ££ $p<0.01$. $ denotes comparison of dosing with 0 Gy at and Glutamine deprivation, $ $p<0.05$, $$ $p<0.01$.

There was a significant increase in $CD3^+$ TIM3 at 3x2 Gy normal nutrient supply (34.08±12.45), 3x2 Gy no Glucose (42.48±11.1) 3x2 Gy no Glutamine (29.42±7.72) and 3x4 Gy normal nutrient supply (33.02±8.62), 3x4 Gy no Glucose (26.3±7.54), 3x4 Gy no

Glutamine (29.73±9.99), compared to 0 Gy normal nutrient supply (13.75±4.98) 0 Gy no Glucose (17.05±6.78), 0 Gy no Glutamine (19.88±4.54), $p<0.001$, $p<0.001$, $p<0.001$, $p<0.001$, $p<0.001$, $p<0.001$, respectively (Figure 6.9).

There was a significant increase in $CD3^+CD4^+$ TIM3 at 2 Gy normal nutrient supply (29±9.18) 2 Gy no Glutamine (23.93±10.97), 10Gy (26.97±5.63), 10 Gy no Glucose (28.22±9.48), 10 Gy no Glutamine (19.3±6.43), 3x2 Gy normal nutrient supply (47.33±8.17), 3x2 Gy no Glucose (34.12±13.83), 3x2 Gy no Glutamine (47.33±8.17), 3x4 Gy normal nutrient supply (40.17±9.61), 3x4 Gy no Glucose (47.12±8.99), 3x4 Gy no Glutamine (35.7±4.79), compared to 0 Gy normal nutrient supply (16.47±3.93) 0 Gy no Glucose (13.75±4.73), 0 Gy no Glutamine (12.22±4.33), $p<0.01$, $p<0.01$, $p<0.01$, $p<0.01$, $p<0.01$, $p<0.05$, $p<0.01$, $p<0.01$, $p<0.001$, $p<0.001$ respectively (Figure 6.9).

There was a significant increase in $CD3^+CD8^+$ TIM3 at 2 Gy no Glucose (14.34+/-3.66), 10 Gy normal nutrient supply (16.05±7.11), 10 Gy no Glucose (16.89±6.24), 3x2 Gy normal nutrient supply (33.3+/-8.35), 3x2 Gy no Glucose (30.88+/-11.47), and 3x2 Gy no Glutamine (22.27±7.07), 3x4 Gy normal nutrient supply (19.95±7.82) and 3x4 Gy no Glucose (19.1±7.13) compared to 0 Gy normal nutrient supply (11.88±6.2), 0 Gy no Glucose (11.23±7.02), 0 Gy no Glutamine (13.78±14.1), $p<0.01$, $p<0.01$, $p<0.01$, $p<0.01$, $p<0.01$, $p<0.01$, $p<0.01$, $p<0.01$ respectively (Figure 6.9).

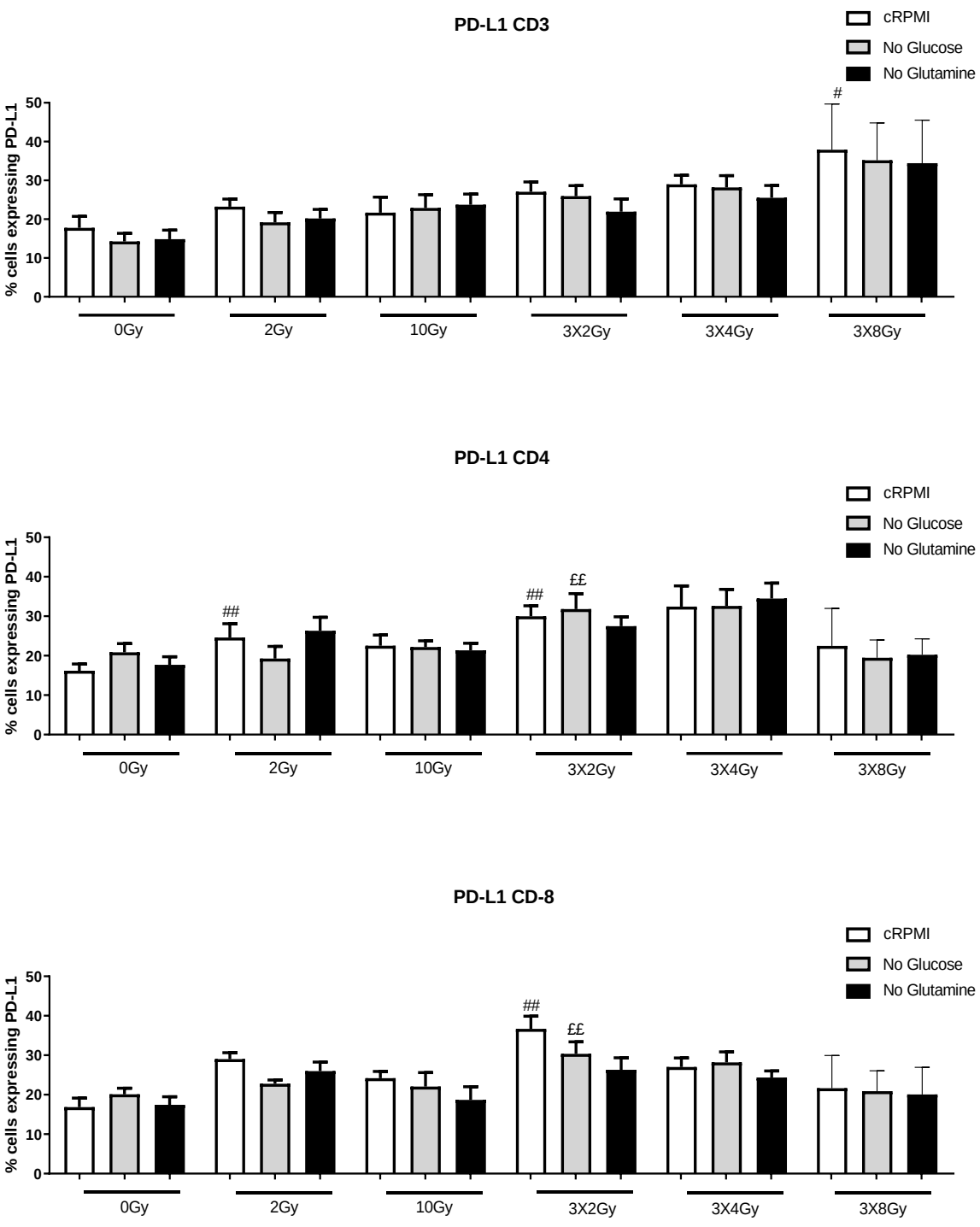

Figure 6.10: The expression of PD-L1 was determined on the surface of peripheral blood $CD3^+$, $CD3^+CD4^+$, $CD3^+CD8^+$ cells in treatment naïve whole blood (n=6) with and without radiation and with and without nutrient deprivation (glucose and glutamine deprivation) by flow cytometry. Tukey's multiple comparison testing. # denotes comparison of dosing with 0 Gy normal nutrient supply, # $p<0.05$, ## $p<0.01$. £ denotes comparison of dosing with 0 Gy and Glucose deprivation, £ $p<0.05$, ££ $p<0.01$, £££ $p<0.001$. $ denotes comparison of dosing with 0 Gy at and Glutamine deprivation, $ $p<0.05$, $$ $p<0.01$.

There was a significant increase in $CD3^+$ PD-L1 at 3x8 Gy (37.89±11.23) to 0 Gy normal nutrient supply (16.65±5.89) $p<0.01$ (Figure 6.10).

There was a significant increase in $CD3^+$ $CD4^+$ PD-L1 at 2 Gy normal nutrient supply (24.6±7.89), 3x2 Gy normal nutrient supply (29.97±6.59), 3x2 Gy no Glucose (31.82±8.76), compared to 0 Gy normal nutrient supply (16.17±4.22) 0 Gy no Glucose (20.85±5.42), $p<0.01$, $p<0.01$, $p<0.01$, respectively (Figure 6.10).

There was a significant increase in $CD3^+$ $CD8^+$ PD-L1 at 3x2 Gy normal nutrient supply (36.67±7.92), 3x2 Gy no Glucose (30.33±7.24), compared to 0 Gy normal nutrient supply (16.83±5.71), 0 Gy no Glucose (20.12±3.2), $p<0.01$, $p<0.01$, respectively (Figure 6.10).

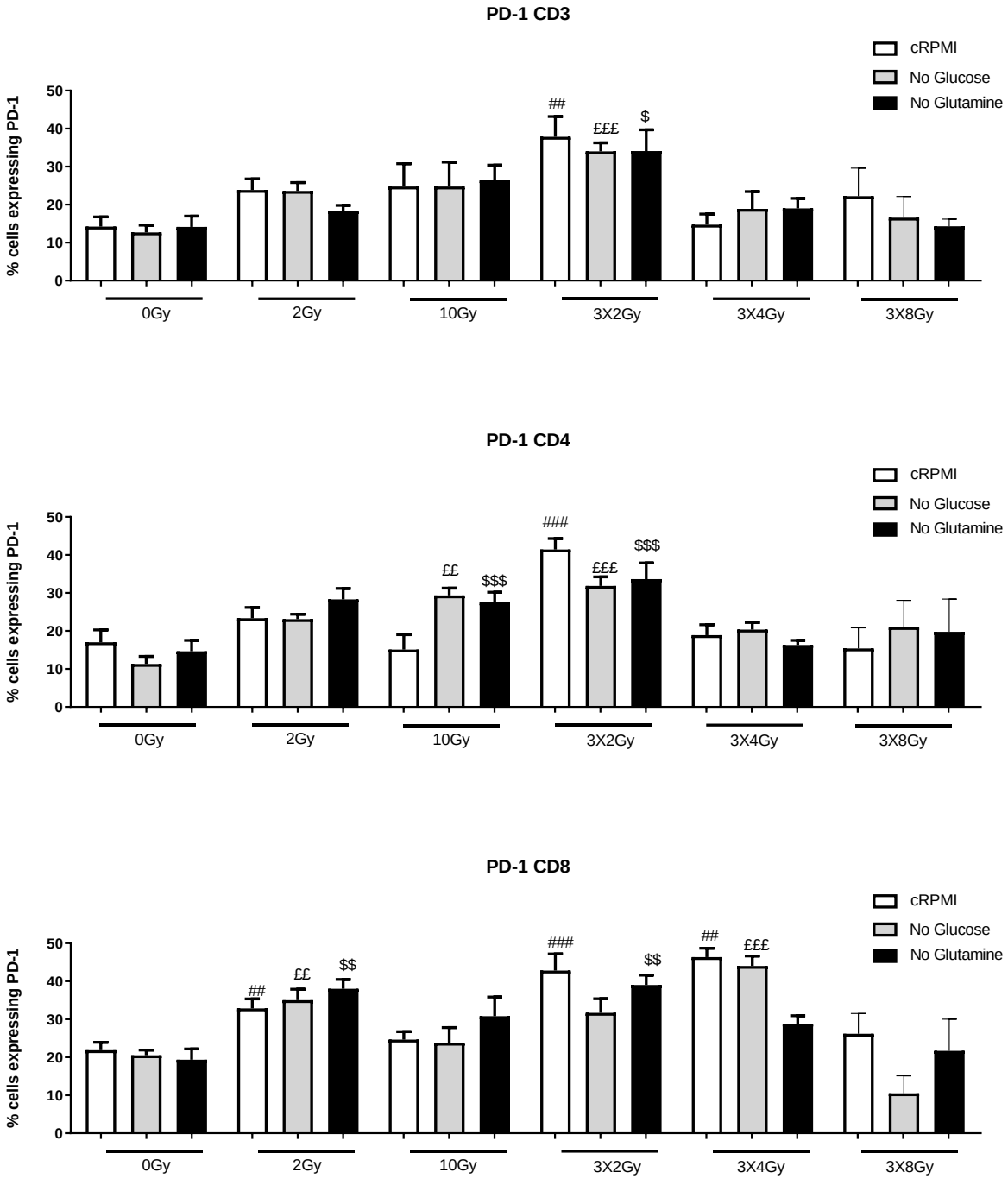

Figure 6.11:The expression of PD-1 was determined on the surface of peripheral blood CD3^{+}, CD3^{+} CD4 $^{+}$, CD3 $^{+}$ CD8 $^{+}$ cells in treatment naïve whole blood (n=6) with and without radiation and with and without nutrient deprivation (glucose and glutamine deprivation) by flow cytometry. Tukey's multiple comparison testing. # denotes comparison of dosing with 0 Gy normal nutrient supply, # $p<0.05$, ## $p<0.01$. £ denotes comparison of dosing with 0 Gy and Glucose deprivation, £ $p<0.05$, ££ $p<0.01$, £££ $p<0.001$. $ denotes comparison of dosing with 0 Gy at and Glutamine deprivation, $ $p<0.05$, $$ $p<0.01$, $$$ $p<0.001$.

There was a significant increase in $CD3^+$ PD-1 at 3x2 Gy normal nutrient supply (37.85±5.89), 3x2 Gy no Glucose (34.03±5.49) 3x2 Gy no Glutamine (34.12±11.23) compared to 0Gy normal nutrient supply (14.23±3.56) 0 Gy no Glucose (12.67±4.72), 0 Gy no Glutamine (14.14±5.67), $p<0.01$, $p<0.01$, $p<0.01$, respectively (Figure 6.11).

There was a significant increase in $CD3^+CD4^+$ PD-1 at 10 Gy no Glucose (29.37±4.67) 10 Gy no Glutamine (27.5±6.56), 3x2 Gy normal nutrient supply (41.5±7.05), 3x2 Gy no Glucose (31.87±5.81), 3x2 Gy no Glutamine (33.6±4.23), compared to 0 Gy normal nutrient supply (17±4.5) 0 Gy no Glucose (11.32±4.87), 0 Gy no Glutamine (14.63±3.78), $p<0.01$, $p<0.01$, $p<0.01$, $p<0.001$, $p<0.01$, $p<0.001$, $p<0.001$ respectively (Figure 6.11).

There was a significant increase in $CD3^+CD8^+$ PD-1 at 2 Gy normal nutrient supply (32.83±6.15), 2 Gy no Glucose (35.12±7.13), 2 Gy no Glutamine (37.6±6.07), 3x2 Gy normal nutrient supply (42.8±5.67), and 3x2 Gy no Glutamine (39.14±6.36), 3x4 Gy normal nutrient supply (19.95±7.82), 3x4 Gy normal nutrient supply (46.33±5.79) and 3x4 Gy no Glucose (44.23±6.45) compared to 0 Gy normal nutrient supply (21.83±5.12), 0 Gy no Glucose (20.5±3.45), 0 Gy no Glutamine (19.33±2.93), $p<0.01$, $p<0.01$, $p<0.01$, $p<0.001$, $p<0.01$, $p<0.01$, $p<0.001$, respectively (Figure 6.11).

6.10: Cytokine expression by $CD3^+$, $CD3^+CD4^+$, $CD3^+CD8^+$ cells following bolus and hypofractionated radiotherapy dosing in the presence of nutrient deprivation.

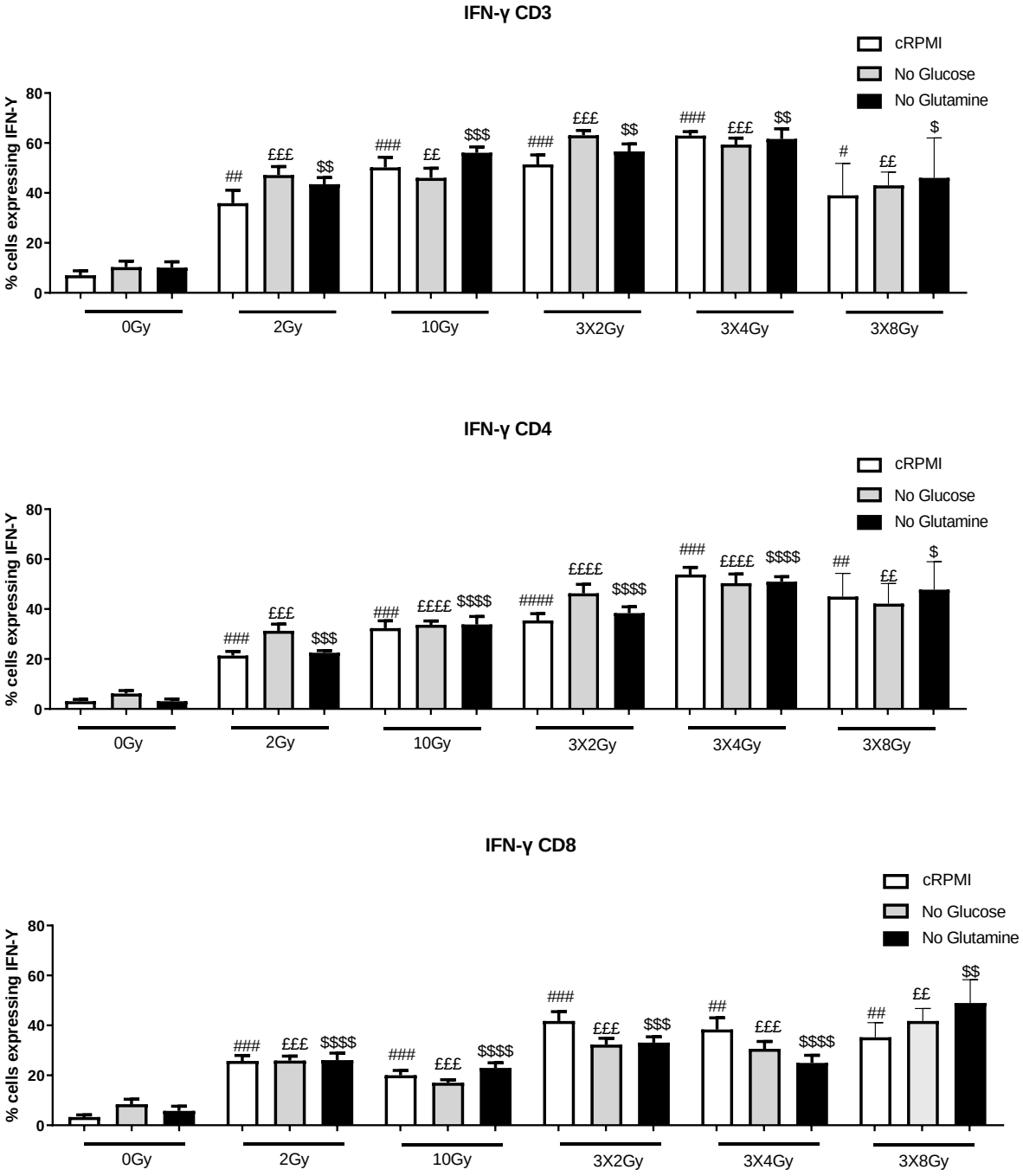

Figure 6.12: The expression of IFN-γ was determined on the surface of peripheral blood $CD3^+$, $CD3^+CD4^+$, $CD3^+CD8^+$ cells in treatment naïve whole blood (n=6) with and without radiation and with and without nutrient deprivation (glucose and glutamine deprivation) by flow cytometry. Tukey's multiple comparison testing. # denotes comparison of dosing with 0Gy normal nutrient supply, # $p<0.05$, ## $p<0.01$, ### $p<0.001$, #### $p<0.0001$. £ denotes comparison of dosing with 0Gy and Glucose

deprivation, £ p<0.05, ££ p<0.01, £££ p<0.001. $ denotes comparison of dosing with 0Gy at and Glutamine deprivation, $ p<0.05, $$ p<0.01, $$$ p<0.001.

There was a significant increase in $CD3^+$ IFN-γ at 2 Gy (35.87±5.24), 10 Gy (50.22±4.08), 3x2 Gy (51.4±3.83), 3x4 Gy (62.93±1.63), 3x8 Gy (39.03±5.22) compared to 0 Gy (7.04±1.77), p<0.01, p<0.001, p<0.001, p<0.001, p<0.01 respectively. There was a significant increase in $CD3^+$ IFN-γ at 2 Gy no Glucose (47.18±3.36), 10 Gy no Glucose (46±3.92), 3x2 Gy no Glucose (63.1±1.96), 3x4 Gy no Glucose (59.35±2.6) and 3x8 Gy no Glucose (43.02±2.17) compared to 0 Gy no Glucose (10.31±2.42), p<0.001, p<0.001, p<0.001, p<0.001, p<0.01 respectively. There was a significant increase in $CD3^+$ IFN-γ at 2 Gy no Glutamine (43.5±2.69), 10 Gy no Glutamine (56.07±2.39), 3x2 Gy no Glutamine (56.6±3.06), 3x4 Gy no Glutamine (61.63±4.08) and 3x8 Gy no Glutamine (46.03±6.54) compared to 0 Gy no Glutamine (10.08±2.37), p<0.01, p<0.001, p<0.01, p<0.01, p<0.05 respectively (Figure 6.12).

There was a significant increase in $CD3^+$ $CD4^+$ IFN-γ at 2 Gy (21.35±1.68), 10 Gy (32.38±2.93), 3x2 Gy (35.4±2.77), 3x4 Gy (53.8±2.88), 3x8 Gy (44.93±3.81) compared to 0 Gy (3.09±2.33), p<0.001, p<0.001, p<0.001, p<0.001, p<0.01 respectively. There was a significant increase in $CD3^+CD4^+$ IFN-γ at 2 Gy no Glucose (31.32±2.65), 10 Gy no Glucose (33.72±1.52), 3x2 Gy no Glucose (46.27±3.66), 3x4 Gy no Glucose (50.35±3.67) and 3x8 Gy no Glucose (42,17±3.45) compared to 0 Gy no Glucose (6.17±2.1), p<0.001, p<0.01, p<0.001, p<0.001, p<0.01 respectively. There was a significant increase in $CD3^+$ $CD4^+$ IFN-γ at 2 Gy no Glutamine (22.52±0.92), 10 Gy no Glutamine (33.8±3.25), 3x2 Gy no Glutamine (38.37±2.55), 3x4 Gy no Glutamine

(50.94±2.15) and 3x8 Gy no Glutamine (47.75±4.59) compared to 0 Gy no Glutamine (4.1±2.3), $p<0.001$, $p<0.001$, $p<0.001$, $p<0.001$, $p<0.05$ respectively (Figure 6.12).

There was a significant increase in $CD3^+$ $CD8^+$ IFN-γ at 2 Gy (25.75±2.65), 10 Gy (20.02±1.97), 3x2 Gy (41.77±3.73), 3x4 Gy (48.98±3.8), 3x8 Gy (30.62±2.95) compared to 0 Gy (4.39±3.55), $p<0.001$, $p<0.001$, $p<0.001$, $p<0.01$, $p<0.01$ respectively. There was a significant increase in $CD3^+CD8^+$ IFN-γ at 2 Gy no Glucose (25.88±1.91), 10 Gy no Glucose (17.05±3.56), 3x2 Gy no Glucose (35.22±2.4), 3x4 Gy no Glucose (32.27±2.54) and 3x8 Gy no Glucose (30.62±2.95) compared to 0 Gy no Glucose (8.45±1.951), $p<0.001$, $p<0.001$, $p<0.001$, $p<0.001$, $p<0.01$ respectively. There was a significant increase in $CD3^+$ $CD8^+$ IFN-γ at 2 Gy no Glutamine (26.13±2.74), 10 Gy no Glutamine (22.93±2.12), 3x2 Gy no Glutamine (41.77±2.05), 3x4 Gy no Glutamine (33.1±2.31) and 3x8 Gy no Glutamine (24.93±3.08) compared to 0 Gy no Glutamine (5.78±1.89), $p<0.001$, $p<0.001$, $p<0.001$, $p<0.001$, $p<0.01$ respectively (Figure 6.12).

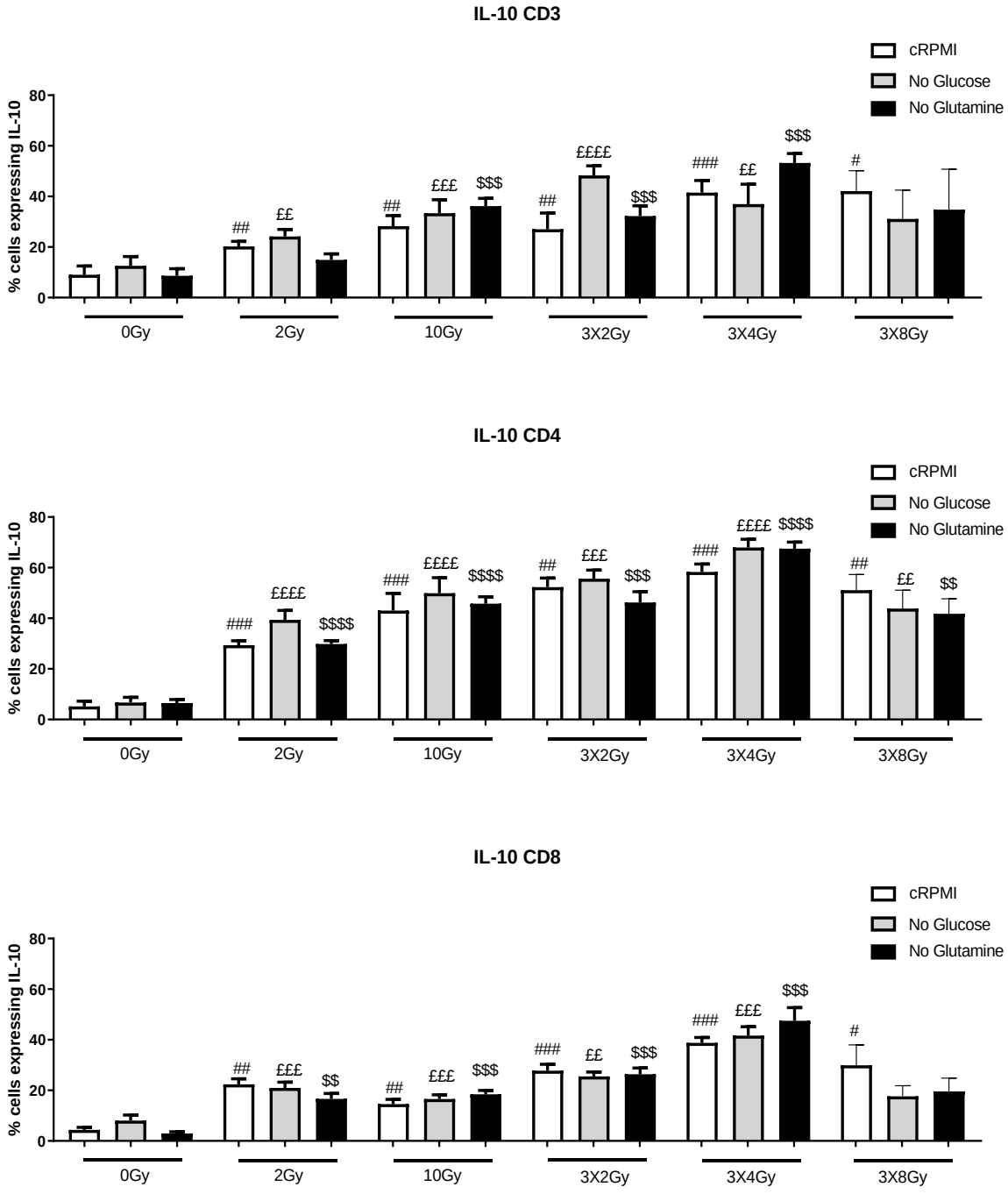

Figure 6.13: The expression of IL-10 was determined on the surface of peripheral blood $CD3^+$, $CD3^+CD4^+$, $CD3^+CD8^+$ cells in treatment naïve whole blood (n=6) with and without radiation and with and without nutrient deprivation (glucose and glutamine deprivation) by flow cytometry. Tukey's multiple comparison testing. # denotes comparison of dosing with 0Gy normal nutrient supply, # $p<0.05$, ## $p<0.01$, ### $p<0.001$, #### $p<0.0001$. £ denotes comparison of dosing with 0 Gy and Glucose deprivation, £ $p<0.05$, ££ $p<0.01$, £££ $p<0.001$. $ denotes comparison of dosing with 0 Gy at and Glutamine deprivation, $ $p<0.05$, $$ $p<0.01$, $$$ $p<0.001$.

There was a significant increase in $CD3^+$ IL-10 at 2 Gy (23.53±2.65), 10 Gy (28.25±4.18), 3x2 Gy (27.03±6.38), 3x4 Gy (41.5±4.77), 3x8 Gy (42.08±3.29) compared to 0 Gy (5.4±2.17), $p<0.01$, $p<0.01$, $p<0.01$, $p<0.001$, $p<0.01$ respectively. There was a significant increase in $CD3^+$ IL-10 at 2 Gy no Glucose (27.47±4.19), 10 Gy no Glucose (33.38±5.31), 3x2 Gy no Glucose (48.3±3.83), and 3x4 Gy no Glucose (36.97±7.84) compared to 0 Gy no Glucose (8.75+/-3.24), $p<0.01$, $p<0.001$, $p<0.0001$, $p<0.01$ respectively. There was a significant increase in $CD3^+$ IL-10 at 10 Gy no Glutamine (36.17±3.07), 3x2 Gy no Glutamine (32.22±4.1), and 3x4 Gy no Glutamine (53.22±3.77) compared to 0 Gy no Glutamine (5.46±1.53), $p<0.001$, $p<0.001$, $p<0.001$ respectively (Figure 6.13).

There was a significant increase in $CD3^+$ $CD4^+$ IL-10 at 2 Gy (29.38±1.72), 10 Gy (43.02±6.8), 3x2 Gy (52.27±3.62), 3x4 Gy (58.28±3.16), 3x8 Gy (51.08±2.53) compared to 0 Gy (5.17±2.07), $p<0.001$, $p<0.001$, $p<0.01$, $p<0.001$, $p<0.01$ respectively. There was a significant increase in $CD3^+CD4^+$ IL-10 at 2 Gy no Glucose (39.37±3.75), 10 Gy no Glucose (49.87±6.15), 3x2 Gy no Glucose (55.63±3.41), 3x4 Gy no Glucose (67.95±3.25) and 3x8 Gy no Glucose (43.8±2.97) compared to 0 Gy no Glucose (6.67±2.09), $p<0.001$, $p<0.001$, $p<0.001$, $p<0.001$, $p<0.01$ respectively. There was a significant increase in $CD3^+$ $CD4^+$ IL-10 at 2 Gy no Glutamine (29.83±2.34), 10 Gy no Glutamine (45.78±2.69), 3x2 Gy no Glutamine (46.2±4.29), 3x4 Gy no Glutamine (67.48±2.61) and 3x8 Gy no Glutamine (41.77±2.41) compared to 0 Gy no Glutamine (6.48±1.43), $p<0.001$, $p<0.001$, $p<0.001$, $p<0.001$, $p<0.01$ respectively (Figure 6.13).

There was a significant increase in $CD3^+$ $CD8^+$ IL-10 at 2 Gy (22.37±2.23), 10 Gy (14.58±1.86), 3x2 Gy (27.78±2.49), 3x4 Gy (38.78±2.09), 3x8 Gy (29.92±3.28)

compared to 0 Gy (4.33±1.01), $p<0.01$, $p<0.01$, $p<0.001$, $p<0.001$, $p<0.05$ respectively. There was a significant increase in $CD3^{+}CD8^{+}$ IL-10 at 2 Gy no Glucose (20.93±2.98), 10 Gy no Glucose (16.53±2.09), 3x2 Gy no Glucose (25.5±1.73), and 3x4 Gy no Glucose (41.65±3.54) compared to 0 Gy no Glucose (8.1±4.3), $p<0.001$, $p<0.001$, $p<0.001$, $p<0.001$ respectively. There was a significant increase in $CD3^{+}$ $CD8^{+}$ IL-10 at 2 Gy no Glutamine (16.62±2.17), 10 Gy no Glutamine (18.4±1.57), 3x2 Gy no Glutamine (26.33±4.3), and 3x4 Gy no Glutamine (47.47±5.20) compared to 0 Gy no Glutamine (2.98±5.4), $p<0.01$, $p<0.001$, $p<0.001$, $p<0.001$ respectively (Figure 6.13).

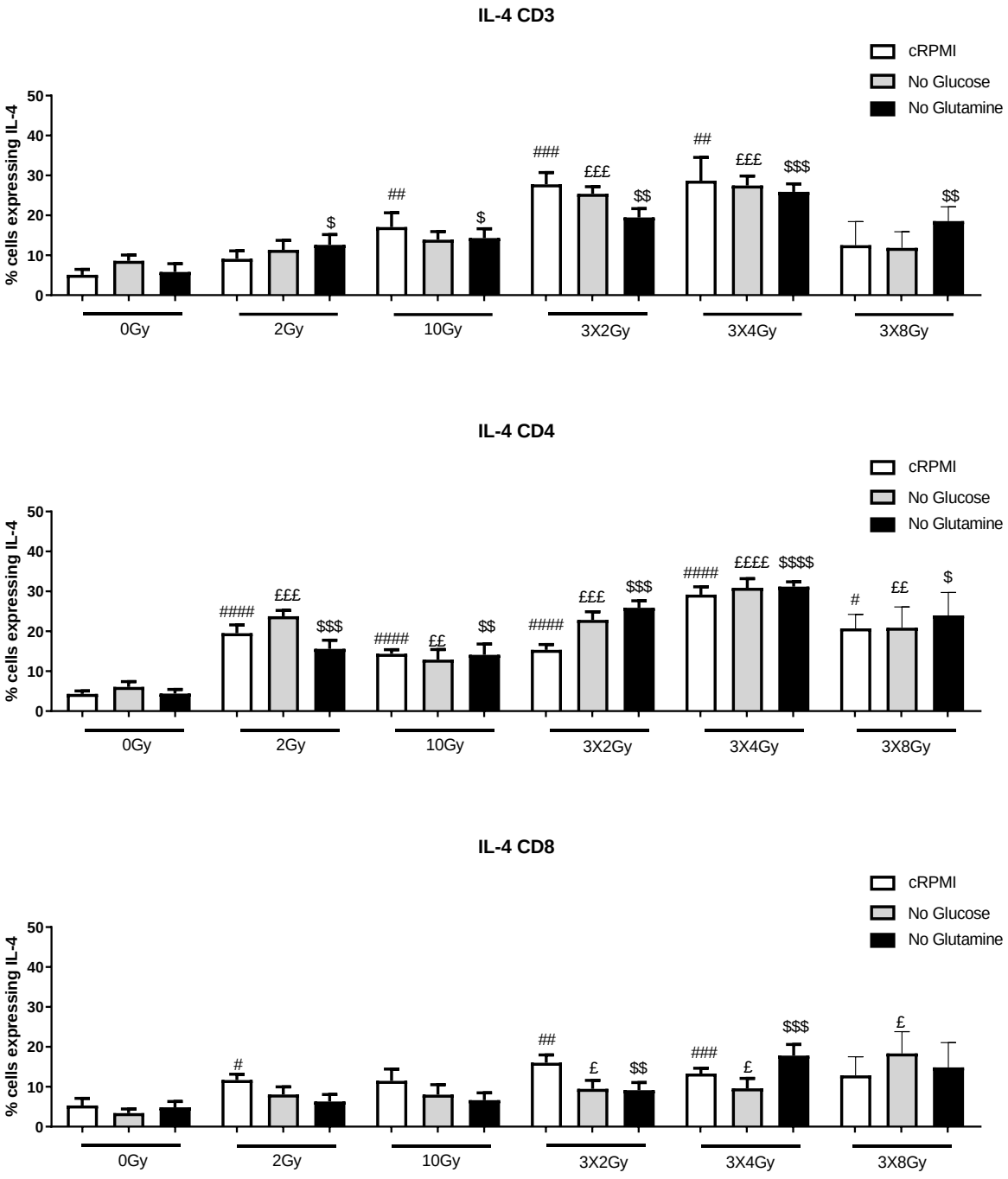

Figure 6.14: The expression of IL-4 was determined on the surface of peripheral blood CD3$^+$, CD3$^+$ CD4 $^+$, CD3 $^+$ CD8 $^+$ cells in treatment naïve whole blood (n=6) with and without radiation and with and without nutrient deprivation (glucose and glutamine deprivation) by flow cytometry. Tukey's multiple comparison testing. # denotes comparison of dosing with 0 Gy normal nutrient supply, # p<0.05, ## p<0.01, ### p<0.001, #### p<0.0001. £ denotes comparison of dosing with 0 Gy and Glucose deprivation, £ p<0.05, ££ p<0.01, £££ p<0.001. $ denotes comparison of dosing with 0 Gy at and Glutamine deprivation, $ p<0.05, $$ p<0.01, $$$ p<0.001.

There was a significant increase in $CD3^+$ IL-4 at 10 Gy (17.05±3.58), 3x2 Gy (27.78±2.96), 3x4 Gy (28.67±5.86) compared to 0 Gy (8.61±1.49), $p<0.01$, $p<0.001$, $p<0.01$ respectively. There was a significant increase in $CD3^+$ IL-4 at 3x2 Gy no Glucose (25.38±1.98), and 3x4 Gy no Glucose (27.48±2.98) compared to 0 Gy no Glucose (8.61±1.47), $p<0.001$, $p<0.001$, respectively. There was a significant increase in $CD3^+$ IL-4 at 2 Gy no Glutamine (12.58±2.78) 10 Gy no Glutamine (14.24±2.37), 3x2 Gy no Glutamine (19.48±2.28), and 3x4 Gy no Glutamine (25.88±2.39) and 3x8 Gy no Glutamine (18.57±2.35) compared to 0 Gy no Glutamine (5.81±2.07), $p<0.05$, $p<0.05$, $p<0.01$, $p<0.001$, $p<0.01$ respectively (Figure 6.14).

There was a significant increase in $CD3^+$ $CD4^+$ IL-4 at 2 Gy (19.5±2.1), 10 Gy (14.33±1.98), 3x2 Gy (15.33±2.4), 3x4 Gy (29.17±1.96), 3x8 Gy (20.73±1.43) compared to 0 Gy (4.32±1.1), $p<0.001$, $p<0.001$, $p<0.01$, $p<0.001$, $p<0.05$ respectively. There was a significant increase in $CD3^+CD4^+$ IL-4 at 2 Gy no Glucose (23.77±1.5), 10 Gy no Glucose (14.08±2.74), 3x2 Gy no Glucose (22.83±2.05), 3x4 Gy no Glucose (30.9±2.29) and 3x8 Gy no Glucose (20.9±2.13) compared to 0 Gy no Glucose (6.06±1.34), $p<0.001$, $p<0.01$, $p<0.001$, $p<0.001$, $p<0.01$ respectively. There was a significant increase in $CD3^+$ $CD4^+$ IL-4 at 2 Gy no Glutamine (15.62±2.65), 10 Gy no Glutamine (14.08±2.74), 3x2 Gy no Glutamine (25.88±1.78), 3x4 Gy no Glutamine (31.17±1.98) and 3x8 Gy no Glutamine (23.97±3.67) compared to 0 Gy no Glutamine (5.89±3.44), $p<0.01$, $p<0.01$, $p<0.001$, $p<0.01$, $p<0.01$ respectively (Figure 6.14).

There was a significant increase in $CD3^+$ $CD8^+$ IL-4 at 2 Gy (11.7±1.5), 3x2 Gy (16.4±3.49), 3x4 Gy (13.29±1.78) compared to 0 Gy (5.33±3.2), $p<0.05$, $p<0.01$, $p<0.001$ respectively. There was a significant increase in $CD3^+CD8^+$ IL-4 at 3x2 Gy no Glucose

(9.49±3.12), 3x4 Gy no Glucose (9.89±2.52) and 3x8 Gy no Glucose (18.33±2.23) compared to 0 Gy no Glucose (3.4±1.87), $p<0.05$, $p<0.05$, $p<0.05$ respectively. There was a significant increase in $CD3^+$ $CD8^+$ IL-4 at 3x2 Gy no Glutamine (9.13±1.98), and 3x4 Gy no Glutamine (17.8±.82) compared to 0 Gy no Glutamine (4.85±1.45), $p<0.01$, $p<0.001$, respectively (Figure 6.14).

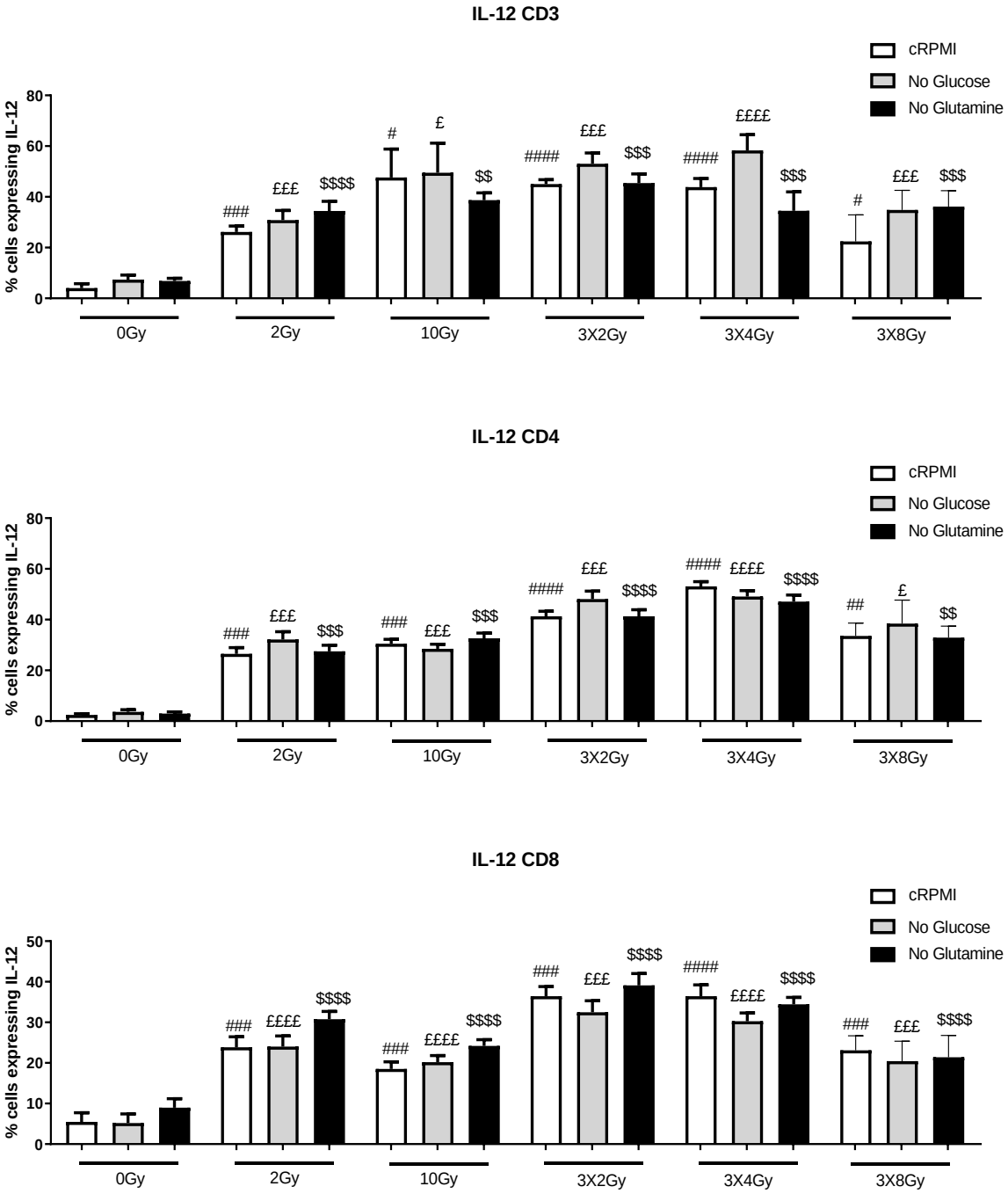

Figure 6.15: The expression of IL-12 was determined on the surface of peripheral blood $CD3^+$, $CD3^+CD4^+$, $CD3^+$ $CD8^+$ cells in treatment naïve whole blood (n=6) with and without radiation and with and without nutrient deprivation (glucose and glutamine deprivation) by flow cytometry. Tukey's multiple comparison testing. # denotes comparison of dosing with 0 Gy normal nutrient supply, # p<0.05, ## p<0.01, ### p<0.001, ####p<0.0001. £ denotes comparison of dosing with 0 Gy and Glucose deprivation, £ p<0.05, ££ p<0.01, £££ p<0.001. $ denotes comparison of dosing with 0 Gy at and Glutamine deprivation, $ p<0.05, $$ p<0.01, $$$ p<0.001.

There was a significant increase in $CD3^+$ IL-12 at 2 Gy (26.18±-2.3), 10 Gy (47.63±11.23), 3x2 Gy (53.02±4.27), 3x4 Gy (58.32±6.2), 3x8 Gy (34.85±3.9) compared to 0 Gy (7.33±2.89), p<0.001, p<0.05, p<0.001, p<0.001, p<0.001 respectively. There was a significant increase in $CD3^+$ IL-12 at 2 Gy no Glucose (30.82±3.8), 10 Gy no Glucose (49.47±11.67), 3x2 Gy no Glucose (48.3±3.83), and 3x4 Gy no Glucose (36.97±7.84) and 3x8 Gy no Glucose (34.85±3.9) compared to 0 Gy no Glucose (8.75±3.24), p<0.01, p<0.001, p<0.0001, p<0.001, p<0.001 respectively. There was a significant increase in $CD3^+$ IL-12 at 2 Gy no Glutamine (34.43±7.6), 10 Gy no Glutamine (38.72±5.8), 3x2 Gy no Glutamine (45.43±9.7), and 3x4 Gy no Glutamine (34.48±8.78), and 3x8 Gy no Glutamine (36.15±6.5) compared to 0 Gy no Glutamine (5.46±1.53), p<0.001, p<0.01, p<0.001, p<0.001 respectively (Figure 6.15).

There was a significant increase in $CD3^+$ $CD4^+$ IL-12 at 2 Gy (24.3±9.5), 10 Gy (30.6±5.67), 3x2 Gy (41.32±6.7), 3x4 Gy (49.45±-6.5), 3x8 Gy (34.57±5.45) compared to 0 Gy (4.17±4.07), p<0.001, p<0.001, p<0.01, p<0.001, p<0.01 respectively. There was a significant increase in $CD3^+CD4^+$ IL-12 at 2 Gy no Glucose (27.6±11.2), 10 Gy no Glucose (26.5±6.15), 3x2 Gy no Glucose (48.12±13.2), 3x4 Gy no Glucose (49.1±7.89) and 3x8 Gy no Glucose (34.45±-5.78) compared to 0 Gy no Glucose (4.67±7.5), p<0.001,

$p<0.001$, $p<0.001$, $p<0.001$, $p<0.01$ respectively. There was a significant increase in $CD3^+$ $CD4^+$ IL-12 at 2 Gy no Glutamine (27.48±3.2), 10 Gy no Glutamine (32.67±11.2), 3x2 Gy no Glutamine (41.3±12.3), 3x4 Gy no Glutamine (47.1±4.8) and 3x8 Gy no Glutamine (32.88±4.98) compared to 0 Gy no Glutamine (4.48±2.73), $p<0.001$, $p<0.001$, $p<0.001$, $p<0.001$, $p<0.001$ respectively (Figure 6.15).

There was a significant increase in $CD3^+$ $CD8^+$ IL-12 at 2 Gy (23.83±8.76), 10 Gy (18.58±5.68), 3x2 Gy (36.45±6.76), 3x4 Gy (36.43±3.23), 3x8 Gy (23.08±9.87) compared to 0 Gy (5.47±3.99), $p<0.001$, $p<0.01$, $p<0.001$, $p<0.001$, $p<0.001$ respectively. There was a significant increase in $CD3^+CD8^+$ IL-12 at 2 Gy no Glucose (24.93±6.98), 10 Gy no Glucose (20.2±12.3) 3x2 Gy no Glucose (32.48±6.78), and 3x4 Gy no Glucose (30.25±5.17) compared to 0 Gy no Glucose (9.2±9.6), $p<0.001$, $p<0.001$, $p<0.001$, $p<0.001$ respectively. There was a significant increase in $CD3^+$ $CD8^+$ IL-12 at 2 Gy no Glutamine (30.78±2.4), 10 Gy no Glutamine (24.18±3.78), 3x2 Gy no Glutamine (39.12±9.6) and 3x4 Gy no Glutamine (34.45±5.91) compared to 0 Gy no Glutamine (8.98±4.4), $p<0.01$, $p<0.001$, $p<0.001$, $p<0.001$ respectively (Figure 6.15).

6.11; DAMP expression on $CD3^+$, $CD3^+CD4^+$, $CD3^+CD8^+$ cells following bolus and hypofractionated radiotherapy dosing in the presence of nutrient deprivation.

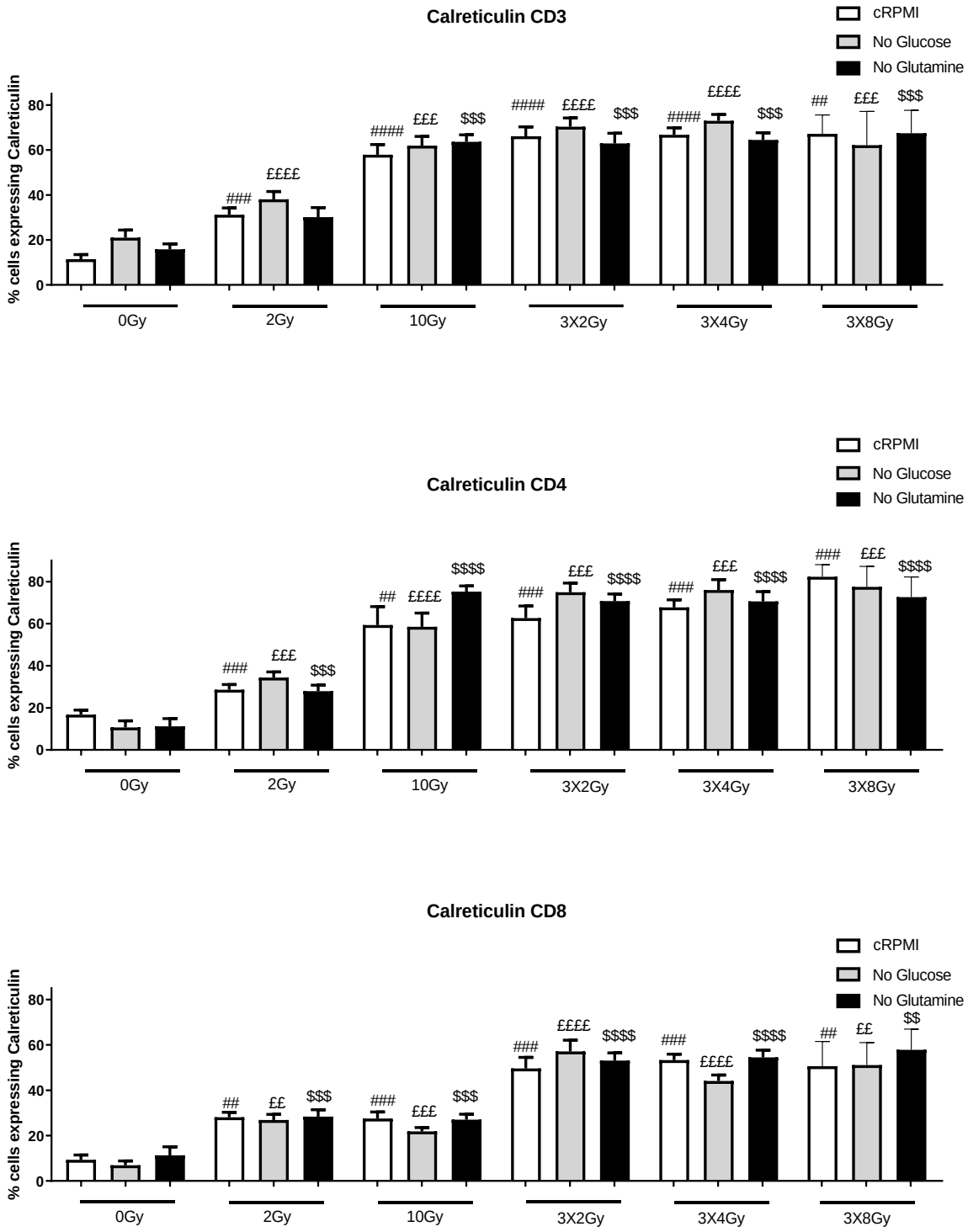

Figure 6.16: The expression of Calreticulin was determined on the surface of peripheral blood $CD3^+$, $CD3^+$ $CD4^+$, $CD3^+$ $CD8^+$ cells in treatment naïve whole blood (n=6) with and without radiation and with and without nutrient deprivation

(glucose and glutamine deprivation) by flow cytometry. Tukey's multiple comparison testing. # denotes comparison of dosing with 0Gy normal nutrient supply, # p<0.05, ## p<0.01, ### p<0.001, #### p<0.0001. £ denotes comparison of dosing with 0Gy and Glucose deprivation, £ p<0.05, ££ p<0.01, £££ p<0.001. $ denotes comparison of dosing with 0Gy at and Glutamine deprivation, $ p<0.05, $$ p<0.01, $$$ p<0.001.

There was a significant increase in $CD3^+$ Calreticulin at 2 Gy (31.2±7.48), 2 Gy no Glucose (38.05±8.54), 10 Gy (57.88±11.09), 10 Gy no Glucose (61.92±7.67), 10 Gy no Glutamine (63.67±7.56) compared to 0 Gy (11.42±5.03) 0 Gy no Glucose (21±-8.31) and 0 Gy no Glutamine (15.82±5.96), p<0.001, p<0.001, p<0.001, p<0.001, p<0.001 respectively. There was a significant increase in $CD3^+$ Calreticulin at 3x2 Gy (66.15±10.25) 3x2 Gy no Glucose (70.37±9.56), 3x2 Gy no Glutamine (62.95±11.15) 3x4 Gy (66.78±7.5), and 3x4 Gy no Glucose (73.02±6.83), 3x4 Gy no Glutamine (64.5±7.82), 3x8 Gy (67.18±8.47), 3x8 Gy no Glucose (62.15±15.03) and 3x8 Gy no Glutamine (67.48±10.21) compared to 0 Gy (11.42±5.03) 0Gy no Glucose (21±8.32) and 0Gy no Glutamine (15.82±5.96), p<0.001, p<0.001, p<0.001, p<0.001, p<0.001, p<0.001, p<0.01, p<0.01, p<0.01 respectively (Figure 6.16).

There was a significant increase in $CD3^+CD4^+$ Calreticulin at 2 Gy (28.58±6.07), 2 Gy no Glucose (34.42±6.48), 2 Gy no Glutamine (27.95±6.92), 10 Gy (58.5±16.16), 10 Gy no Glucose (59.5±15.6), 10 Gy no Glutamine (75.23±16.54) compared to 0 Gy (16.78±5.36) 0 Gy no Glucose (10.67±7.72) and 0 Gy no Glutamine (11.22±8.95), p<0.001, p<0.001, p<0.001, p<0.001, p<0.001 respectively. There was a significant increase in $CD3^+$ $CD4^+$ Calreticulin at 3x2 Gy (62.68±14.19) 3x2 Gy no Glucose (74.97±10.65), 3x2 Gy no Glutamine (70.73±8.4) 3x4 Gy (67.77±8.88), and 3x4 Gy no Glucose (76.02±12.09), 3x4 Gy no Glutamine (70.58±11.46), 3x 8Gy (82.3±5.82), 3x 8Gy no Glucose (77.5±9.73) and 3x8 Gy no Glutamine (72.65±9.58) compared to 0 Gy

(16.78±5.36) 0 Gy no Glucose (10.67±7.72) and 0 Gy no Glutamine (11.22±8.95), p<0.001, p<0.001, p<0.001, p<0.001, p<0.001, p<0.001, p<0.01, p<0.01, p<0.01 respectively (Figure 6.16).

There was a significant increase in $CD3^{+}CD8^{+}$ Calreticulin at 2 Gy (28.08±5.43), 2 Gy no Glucose (26.85±.07), 2 Gy no Glutamine (28.37±7.54), 10 Gy (27.5±7.09), 10 Gy no Glucose (21.83±4.17), 10 Gy no Glutamine (27.04±5.97) compared to 0 Gy (9.32±5.21) 0 Gy no Glucose (6.88±4.78) and 0 Gy no Glutamine (11.28±9.28), p<0.001, p<0.001, p<0.001, p<0.001, p<0.001 respectively. There was a significant increase in $CD3^{+}$ $CD8^{+}$ Calreticulin at 3x2 Gy (49.65±11.84) 3x2 Gy no Glucose (57.1±12.23), 3x2 Gy no Glutamine (53.1±8.29) 3x4 Gy (53.28±6.43), and 3x4 Gy no Glucose (44.07±6.51), 3x4 Gy no Glutamine (54.5±7.87), 3x8 Gy (50.62±10.89), 3x8 Gy no Glucose (51.08±9.94) and 3x8 Gy no Glutamine (57.83±9.11) compared to 0 Gy (9.32±5.21) 0 Gy no Glucose (6.88±4.78) and 0 Gy no Glutamine (11.28±9.28), p<0.001, p<0.001, p<0.001, p<0.001, p<0.001, p<0.001, p<0.01, p<0.01, p<0.01 respectively (Figure 6.16).

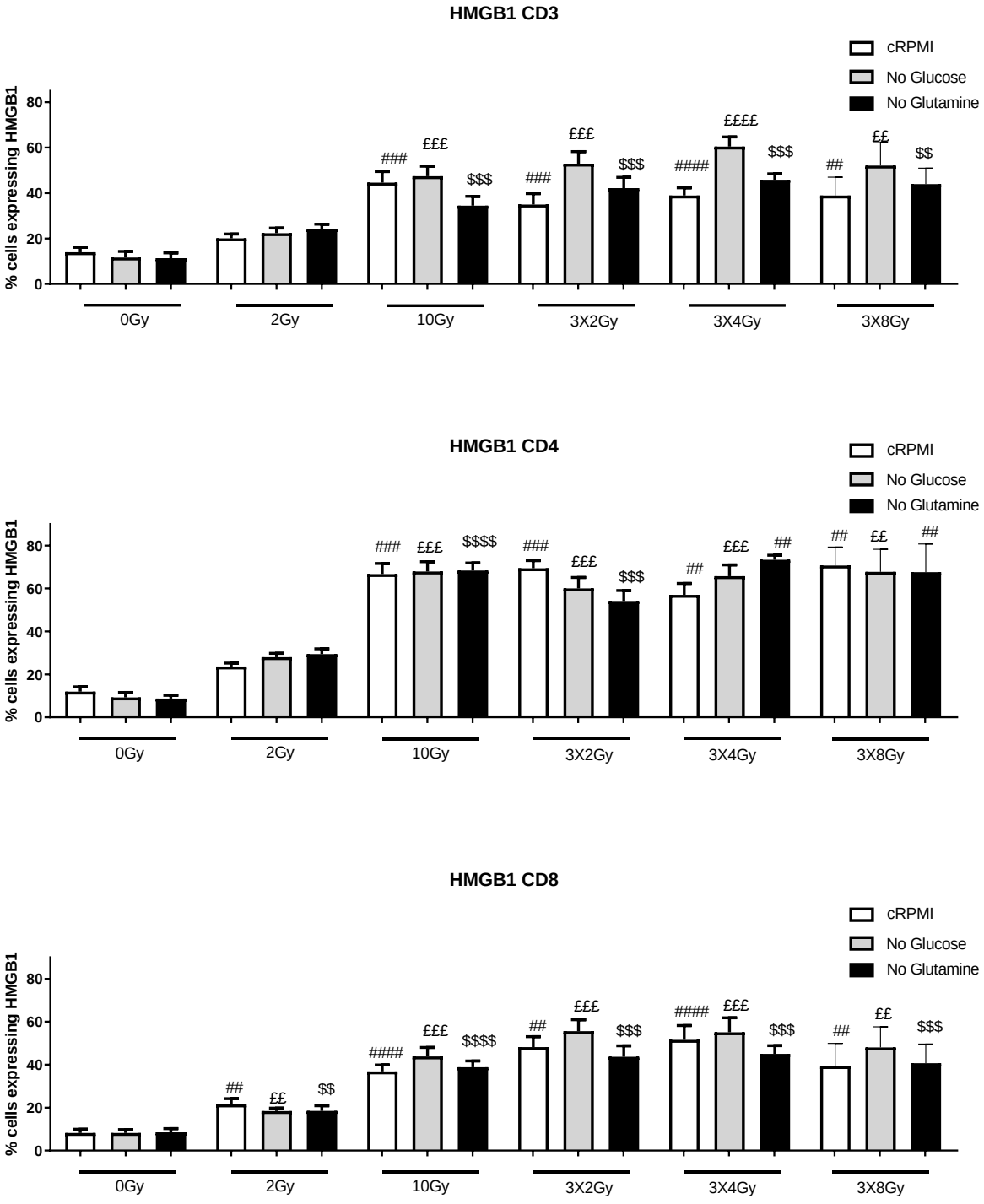

Figure 6.17: The expression of HMGB1 was determined on the surface of peripheral blood $CD3^+$, $CD3^+CD4^+$, $CD3^+CD8^+$ cells in treatment naïve whole blood (n=6) with and without radiation and with and without nutrient deprivation (glucose and glutamine deprivation) by flow cytometry. Tukey's multiple comparison testing. # denotes comparison of dosing with 0 Gy normal nutrient supply, # $p<0.05$, ## $p<0.01$, ### $p<0.001$, #### $p<0.0001$. £ denotes comparison of dosing with 0 Gy and Glucose deprivation, £ $p<0.05$, ££ $p<0.01$, £££ $p<0.001$. $ denotes comparison of dosing with 0 Gy at and Glutamine deprivation, $ $p<0.05$, $$ $p<0.01$, $$$ $p<0.001$.

There was a significant increase in $CD3^+$ HMGB1 at 10 Gy (44.62±11.83), 10 Gy no Glucose (47.42±10.71), 10 Gy no Glutamine (34.43±10.17) 3x2 Gy (34.98±11.68) 3x2 Gy no Glucose (52.95±11.23), 3x2 Gy no Glutamine (42.2±11.62) compared to 0 Gy (13.97±5.27) 0 Gy no Glucose (11.68±6.48) and 0 Gy no Glutamine (11.33±5.82), $p<0.001$, $p<0.001$, $p<0.001$, $p<0.001$, $p<0.001$, $P<0.01$ respectively. There was a significant increase in $CD3^+$ HMGB1 at 3x4 Gy (38.92±8.33), and 3x4 Gy no Glucose (60.47±10.31), 3x4 Gy no Glutamine (45.88±6.45), 3x8 Gy (38.92±8.1), 3x8 Gy no Glucose (52.07±4.14) and 3x8 Gy no Glutamine (43.97±6.98) compared to 0 Gy (13.97±5.27) 0 Gy no Glucose (11.68±6.48) and 0 Gy no Glutamine (11.33±5.82), $p<0.001$, $p<0.001$, $p<0.001$, $p<0.001$, $p<0.001$, $p<0.001$, respectively (Figure 6.17).

There was a significant increase in $CD3^+CD4^+$ HMGB1 at 10 Gy (68.75±12.20), 10 Gy no Glucose (64.35±8.6), 10 Gy no Glutamine (75.23±8.11) compared to 0 Gy (11.95±5.5) 0 Gy no Glucose (9.27±5.64) and 0 Gy no Glutamine (8.7±3.72), $p<0.001$, $p<0.001$, $p<0.001$, respectively. There was a significant increase in $CD3^+$ $CD4^+$ HMGB1 at 3x2 Gy (69.42±8.81) 3x2 Gy no Glucose (60.03±5.13), 3x2 Gy no Glutamine (54.2±4.84), 3x4 Gy (57.03±5.32), and 3x4 Gy no Glucose (65.72±12.91), 3x4 Gy no Glutamine (73.37±5.22), 3x8 Gy (70.68±8.62), 3x8 Gy no Glucose (67.75±10.52) and 3x8 Gy no Glutamine (67.58±12.14) compared to 0 Gy (11.95±5.5) 0 Gy no Glucose (9.27±5.64) and 0 Gy no Glutamine (8.7±3.72), $p<0.001$, $p<0.001$, $p<0.001$, $p<0.001$, $p<0.001$, $p<0.001$, $p<0.01$, $p<0.01$, $p<0.01$ respectively (Figure 6.17).

There was a significant increase in $CD3^+CD8^+$ HMGB1 at 2 Gy (21.47±6.68), 2 Gy no Glucose (18.42±2.37), 2 Gy no Glutamine (18.52±5.88), 10 Gy (36.87±7.33), 10 Gy no Glucose (43.8±10.39), 10 Gy no Glutamine (38.82±8.07) compared to 0 Gy (8.18±4.32)

0 Gy no Glucose (8.01±3.88) and 0 Gy no Glutamine (8.9±4.22), p<0.001, p<0.001, p<0.001, p<0.001, p<0.001, p<0.001, p<0.001 respectively. There was a significant increase in $CD3^+$ $CD8^+$ HMGB1 at 3x2 Gy (48.18±11.9) 3x2 Gy no Glucose (55.6±13.01), 3x2 Gy no Glutamine (43.7±12.54) 3x4 Gy (51.53±6.54), and 3x4 Gy no Glucose (55.07±6.9), 3x4 Gy no Glutamine (45±9.55), 3x8 Gy (39.37±10.55), 3x8 Gy no Glucose (48.02±9.59) and 3x8Gy no Glutamine (40.67±9.98) compared to 0Gy (8.18±4.32) 0Gy no Glucose (8.01±3.88) and 0 Gy no Glutamine (8.9±4.22), p<0.001, p<0.001, p<0.001, p<0.001, p<0.001, p<0.001, p<0.01, p<0.01, p<0.001 respectively (Figure 6.17).

6.12 The effects of multimodal treatment with radiation to the tumour and ICB administration to patient PBMCs cells on cytolysis of tumour cells.

To mimic the local effects of radiotherapy in conjunction with immunotherapy and OAC patient PBMCs trafficked to the tumour, ionising radiation was administered to tumour cells OE33P, OE33R, FLO-1 and FLO1-LM cell lines and PBMC's treated with immune checkpoint inhibitors.

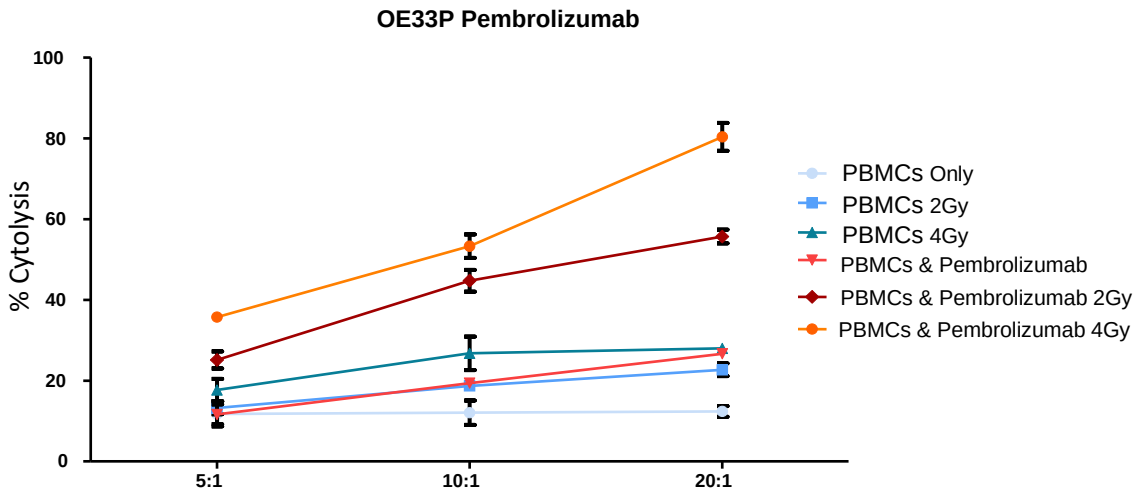
OE33P Pembrolizumab
% Cytolysis
100
80
60
40
20
0
5:1
10:1
20:1
PBMCs Only
PBMCs 2Gy
PBMCs 4Gy
PBMCs & Pembrolizumab
PBMCs & Pembrolizumab 2Gy
PBMCs & Pembrolizumab 4Gy

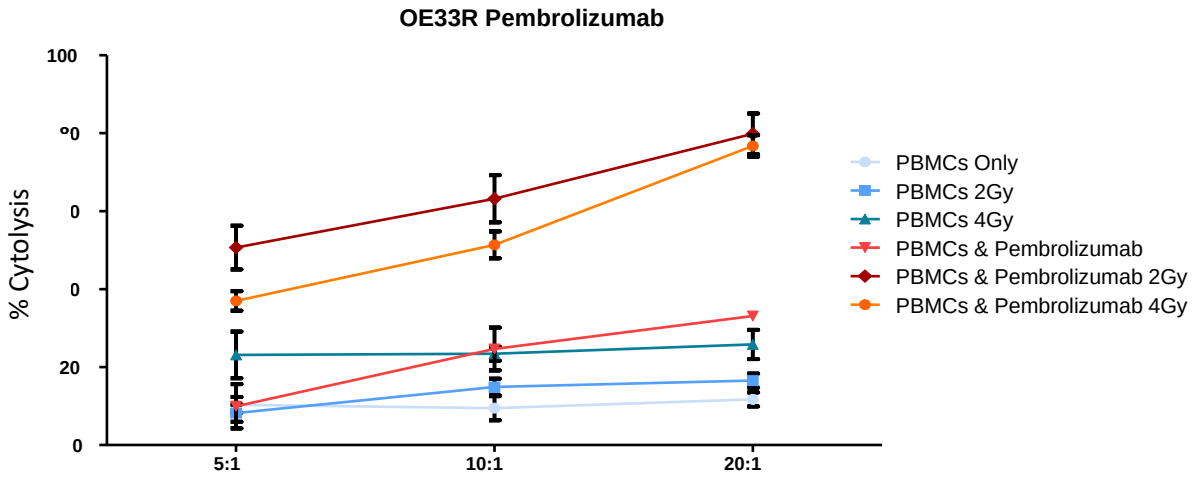
OE33R Pembrolizumab
% Cytolysis
100
0
0
20
0
5:1
10:1
20:1
PBMCs Only
PBMCs 2Gy
PBMCs 4Gy
PBMCs & Pembrolizumab
PBMCs & Pembrolizumab 2Gy
PBMCs & Pembrolizumab 4Gy

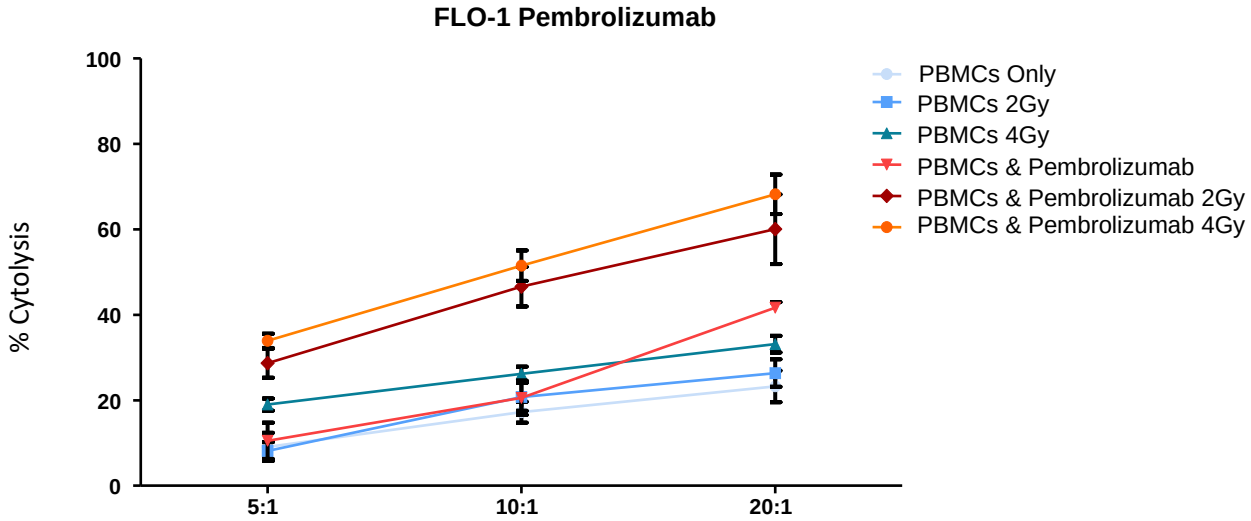
FLO-1 Pembrolizumab
% Cytolysis
100
80
60
40
20
0
5:1
10:1
20:1
PBMCs Only
PBMCs 2Gy
PBMCs 4Gy
PBMCs & Pembrolizumab
PBMCs & Pembrolizumab 2Gy
PBMCs & Pembrolizumab 4Gy

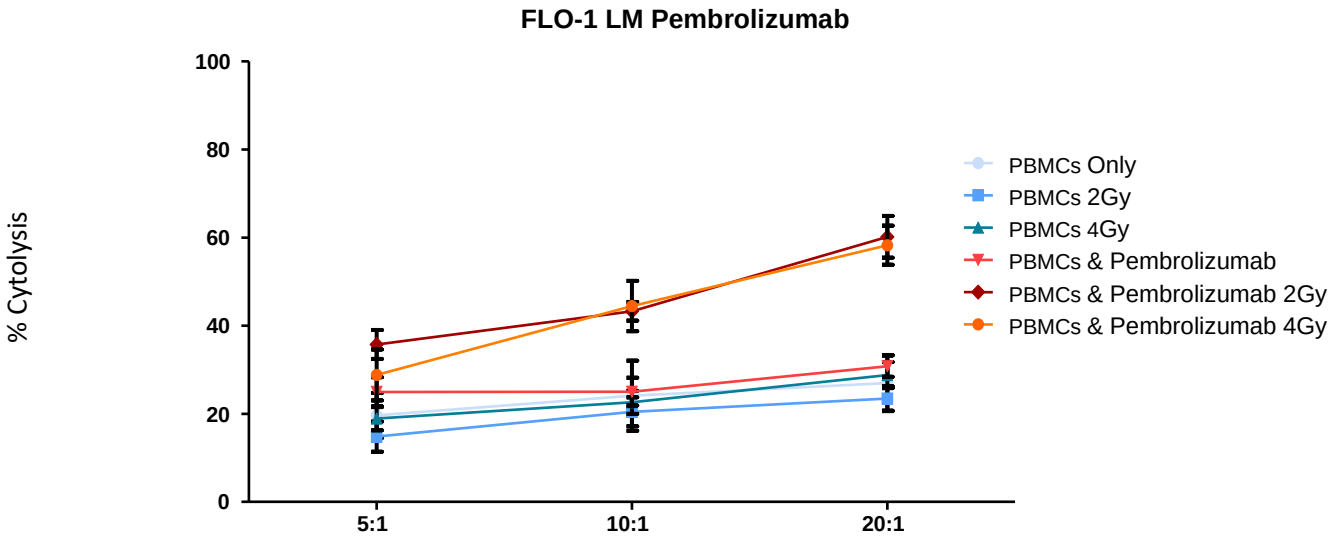

Figure 6.18: The cytolytic effects on OE33P, OE33R, FLO-1, FLO-1 LM cell lines treated with and without radiation in the presence and absence of Pembrolizumab (n=5), Wilcoxon ranked test, by CCK8 Assay. A ratio of 5;1, 10;1, 20;1 of PBMCs were treated with immune checkpoint blocker Pembrolizumab for 5 days and then added to cancer cells.

There was a significantly increased level of cytolysis in the OE33P cell line with radiation in conjunction with Pembrolizumab at 2 Gy 10:1 PBMCs (42.2±6.73) compared to PBMCs alone (14.45±5.45) $p<0.001$, PBMCs at 2 Gy (18.76±6.5) $p<0.01$, PBMCs 4Gy (22.1±14.32) $p<0.01$ and PBMCs with Pembrolizumab alone (19.2±3.4) $p<0.001$. There was also a significantly increased level of cytolysis with 4 Gy 10:1 PBMCs (51.34±7.5) compared to PBMCs alone (14.45±5.45) $p<0.001$, PBMCs at 2 Gy (18.76±6.5) $p<0.001$, PBMCs 4 Gy (22.1±14.32) $p<0.001$ and PBMCs with Pembrolizumab alone (19.2±3.4) $p<0.001$. There was a significantly increased level of cytolysis in the OE33P cell line with radiation in conjunction with Pembrolizumab at 2 Gy 20:1 PBMCs (49.2±5.53) compared to PBMCs alone (13.72±4.35) $p<0.001$, PBMCs at 2 Gy (22.44±5.32) $p<0.001$, PBMCs 4 Gy (22.6±3.13) $p<0.001$ and PBMCs with Pembrolizumab alone (22.2±2.6)

p<0.001. There was a significantly increased level of cytolysis in the OE33P cell line with radiation in conjunction with Pembrolizumab at 4 Gy 20:1 PBMCs (78.56±11.25) compared to PBMCs alone (13.72±4.35) p<0.001, PBMCs at 2Gy (22.44±5.32) p<0.001, PBMCs 4Gy (22.6±3.13) p<0.001 and PBMCs with Pembrolizumab alone (22.2±2.6) p<0.001. There was a significant increase in cytolysis form 2 Gy Pembrolizumab 20:1 PBMCs (49.2±5.53) to 4Gy Pembrolizumab 20:1 PBMCs (78.56±11.25) p<0.001 (Figure 6.18).

There was a significantly increased level of cytolysis in the OE33R cell line with radiation in conjunction with Pembrolizumab at 2 Gy 10:1 PBMCs (49.34±9.54) compared to PBMCs alone (10.35±6.37) p<0.01, PBMCs at 2 Gy (14.47±9.98) p<0.01, PBMCs 4 Gy (21.34±2.41) p<0.001 and PBMCs with Pembrolizumab alone (22,34±1.74) p<0.001. There was also a significantly increased level of cytolysis with 4 Gy 10:1 PBMCs (62.37±14.46) compared to PBMCs alone (10.35±6.37) p<0.01, PBMCs at 2 Gy (14.47±9.98) p<0.01, PBMCs 4 Gy (21.34±2.41) p<0.001 and PBMCs with Pembrolizumab alone (22.34±1.74) p<0.001. There was a significantly increased level of cytolysis in the OE33R cell line with radiation in conjunction with Pembrolizumab at 2 Gy 20:1 PBMCs (75.62±3,21) compared to PBMCs alone (10.41±2.78) p<0.001, PBMCs at 2 Gy (18.34±3.21) p<0.001, PBMCs 4 Gy (23.9±6.23) p<0.001 and PBMCs with Pembrolizumab alone (26.9±4.56) p<0.001. There was a significantly increased level of cytolysis in the OE33R cell line with radiation in conjunction with Pembrolizumab at 4 Gy 20:1 PBMCs (79.89±9.42) compared to PBMCs alone (10.41±2.78) p<0.001, PBMCs at 2 Gy (18.34±3.21) p<0.001, PBMCs 4 Gy (23.9±6.23) p<0.001 and PBMCs with Pembrolizumab alone (26.9±4.56) p<0.001 (Figure 6.18).

There was a significantly increased level of cytolysis in the FLO-1 cell line with radiation in conjunction with Pembrolizumab at 2 Gy 10:1 PBMCs (41.32±11.51) compared to PBMCs alone (16.63±7.49) $p<0.01$, PBMCs at 2 Gy (18.97±3.27) $p<0.0001$, PBMCs 4 Gy (23.58±3.63) $p<0.01$ and PBMCs with Pembrolizumab alone (19,12±1.96) $p<0.001$. There was also a significantly increased level of cytolysis with 4 Gy 10:1 PBMCs (48.35±12.27) compared to PBMCs alone (16.63±7.49) $p<0.01$, PBMCs at 2 Gy (18.97±3.27) $p<0.001$, PBMCs 4 Gy (23.58±3.63) $p<0.001$ and PBMCs with Pembrolizumab alone (19,12±1.96) $p<0.001$. There was a significantly increased level of cytolysis in the FLO-1 cell line with radiation in conjunction with Pembrolizumab at 2 Gy 20:1 PBMCs (58.2±15.45) compared to PBMCs alone (21.5±6.45) $p<0.05$, PBMCs at 2 Gy (24.23±3.21) $p<0.01$, PBMCs 4 Gy (23.9±6.23) $p<0.01$ and PBMCs with Pembrolizumab alone (38.78±2.56) $p<0.05$. There was a significantly increased level of cytolysis in the FLO-1 cell line with radiation in conjunction with Pembrolizumab at 4 Gy 20:1 PBMCs (68.45±12.56) compared to PBMCs alone (21.5±6.45) $p<0.01$, PBMCs at 2 Gy (24.23±3.21) $p<0.01$, PBMCs 4 Gy (23.9±6.23) $p<0.01$ and PBMCs with Pembrolizumab alone (38.78±2.56) $p<0.01$ (Figure 6.18).

There was a significantly increased level of cytolysis in the FLO-1 LM cell line with radiation in conjunction with Pembrolizumab at 2 Gy 10:1 PBMCs (43.2±15.4) compared to PBMCs alone (21.3±3.67) $p<0.05$, PBMCs at 2 Gy (19.27±5.63) $p<0.01$, PBMCs 4 Gy (21.34±4.59) $p<0.01$ and PBMCs with Pembrolizumab alone (21.98±3.47) $p<0.01$. There was also a significantly increased level of cytolysis with 4 Gy 10:1 PBMCs (44.2±10.9) compared to PBMCs alone (23.83±4.2) $p<0.01$, PBMCs at 2 Gy (19.98±4.3)

$p<0.05$, PBMCs 4 Gy (20.04±5.9) $p<0.01$ and PBMCs with Pembrolizumab alone (24.99±4.07) $p<0.01$. There was a significantly increased level of cytolysis in the FLO-1 LM cell line with radiation in conjunction with Pembrolizumab at 2 Gy 20:1 PBMCs (56.8±7.34) compared to PBMCs alone (21.5±6.45) $p<0.001$, PBMCs at 2 Gy (24.23±3.21) $p<0.01$, PBMCs 4 Gy (23.9±6.23) $p<0.01$ and PBMCs with Pembrolizumab alone (24.5±2.6) $p<0.05$. There was a significantly increased level of cytolysis in the FLO-1 cell line with radiation in conjunction with Pembrolizumab at 4 Gy 20:1 PBMCs (58.9.45±9.6) compared to PBMCs alone (21.5±6.45) $p<0.01$, PBMCs at 2 Gy (24.23±3.21) $p<0.01$, PBMCs 4 Gy (23.9±6.23) $p<0.01$ and PBMCs with Pembrolizumab alone (24.5±2.6) $p<0.01$ (Figure 6.18).

6.13. Discussion

TRG scoring upon surgical resection represents a promising candidate for stratifying patients into good and poor prognostic groups after neo-CT treatment. Previous multicenter cohort studies have demonstrated the independent prognostic value of the Mandard classification of TRG for both neoadjuvant chemotherapy and chemoradiotherapy (331-333). We observed in a cohort of n = 80 patients, that those with a low TRG score have a longer survival compared to those with high TRG. Previous studies on chemoradiotherapy-treated patients found that a three-point scale (TRG 1 vs. TRG 2–3 vs. TRG 4–5) provided the best discriminant fit (347), while a more recent large (n = 1,293) multicenter analysis of neoadjuvant chemotherapy concluded that separating patients into TRG 1–2 and TRG 3–5 had a greater prognostic value (334). We also observed that splitting TRG cohorts in the latter, two-tiered manner gave the strongest prognostic result and therefore used this approach throughout this study. While the TRG score appears to have a consistent prognostic ability, there is an urgent clinical need to implement non-invasive stratification approaches into routine clinical practice at the pre-treatment stage in order to identify patients who are likely to benefit from neoadjuvant treatment and those who are not. Patients in the non-responsive group could then proceed immediately to surgical intervention or alternative treatment approaches and would avoid undesirable side effects and delays to surgery, which often leads to tumour upstaging and worse prognosis in those who fail to benefit from neoadjuvant treatment. We therefore investigated levels of 54 circulating serum cytokines, in order to assess their potential association with clinical outcomes.

Analysis of 54 markers in treatment-naive serum showed associations between several circulating factors and clinical outcomes. Of note, chemokines CCL22, CCL26, and CCL4 were all associated with favorable outcomes, with elevated CCL22 and CCL26

associated with longer OS time and higher CCL4 observed in patients who responded well to neoadjuvant therapy (TRG 1–2). CCL4 was particularly prominent throughout our analysis, being also observed at the highest levels in patients with no adverse features (alongside CCL3, IL-1α, and IL-12/IL-23p40), elevated in patients with high tumour lymphocyte infiltration and negatively associated with serosal invasion and pathologic tumour stage. In terms of adverse clinical associations, IL-10 was higher in the serum of patients with a shorter survival time, and Tie2 and CRP were higher in pre-treatment serum of patients who had a subsequent poor response to neo-CT therapy. The angiogenic factors Tie2 and VEGF were also elevated in the serum of patients with adverse features.

Chemokines form part of a complex network of chemotactic molecules, responsible for orchestrating immune cell migration and infiltration into tissues and display high levels of redundancy. Levels of various chemokines have previously been associated with clinical outcomes including OS and tumour recurrence, but whether such associations are favorable or adverse appears to depend on the tumour type and whether the chemokine is measured in the local tumour environment or in circulation (348). Prognostic analysis of data from The Human Protein Atlas showed that CCL22 expression in tumours was favorably associated with survival in colorectal, endometrial cancers, and in head and neck cancers (349). Elevated serum CCL22 was also linked with improved survival in a cohort of 1208 patients with glioma (349); however, serum CCL22 was found to be elevated in advanced tumour stages in breast cancer (350) and was associated with metastatic spread and recurrence in gastric cancer patients (351). We observed that higher than median levels of serum CCL22 were associated with prolonged OS in the OAC/OGJ setting ($p = 0.0101$, HR = 2.301, 95% CI = 1.18–4.48). CCL22 is produced by macrophages, dendritic cells and tumour cells and is a chemoattractant for several cell types including regulatory T cells and T helper type 2 cells, as evidenced by their

expression of the CCL22 receptor, CCR4 (352). The presence of elevated systemic CCL22 may also indicate uninhibited function of antigen presenting cells, which are important for orchestrating anti-tumour responses and therefore result in a net positive effect when elevated in the periphery. Indeed, previous work by our colleagues has demonstrated that CCL22 expression in OAC tumours is relatively low compared to OAC serum (353). Much less is known about the role of CCL26 in cancer, however elevated levels of this chemokine in tumours have been reported in later stage colorectal cancer and has been associated with worse prognosis (354). We observed that higher than median levels of serum CCL26 were associated with prolonged overall survival ($p = 0.0163$, HR = 2.254, 95% CI = 1.14–4.45). CCL26 is responsible for recruitment of eosinophils to the mucosa, and is strongly upregulated in the chronic inflammatory condition, eosinophilic esophagitis (355) and therefore, its abundance in the circulation in the OAC setting could also reflect mucosal inflammation.

CCL4, also known as macrophage inflammatory protein-1β (MIP-1β) is a CC chemokine expressed by various immune cells, with specificity for CCR5 receptors. Elevated expression of CCL4 in tumours was associated with unfavourable prognosis in renal carcinoma, but favorable prognosis when detected in colorectal, endometrial, and melanoma tumours (348) and oesophageal squamous cell carcinoma (356). In the latter study, expression of CCL4 in tumours was associated with higher cytotoxic T cell infiltration and expression of cytolytic effector molecules perforin and granzyme (356). Interestingly, we observed that patients with high lymphocytic tumour infiltration showed elevated serum CCL4 ($p < 0.05$), when compared to those with low infiltration. Although we observed no significant association between serum CCL4 and OS, we observed higher CCL4 levels in patients with a good treatment response ($p < 0.01$), those with no adverse features, and found a negative association with serosal invasion and

pathologic tumour stage, implicating CCL4 as a marker of favorable anti-tumour immune responses in OAC. CCL4 expression in serum was observed to be higher in OAC patients compared to squamous cell tumours in one study, suggesting potential differences in the immune response between these histological cancer subtypes (357).

Conflicting studies on the prognostic potential of chemokines highlight the stark differences in the prognostic value between different cancer types and measurement locations, perhaps reflecting a context-dependent role of the immune cells these chemokines recruit to tumours. The strong male predominance in our OAC cohort may also add a further layer of complexity to these observations, which needs to be addressed in future studies. Growing evidence suggests that chemokines represent useful biomarkers in the oesophageal cancer setting (356). However, given the high level of redundancy and complexity of chemokines, it is likely that profiles composed of multiple chemokines will prove more prognostically useful than any single player alone. Indeed, a study on oesophageal squamous cell carcinoma showed that elevated tumour expression of CCL4 predicted for prolonged survival, but a $CCL4^{high}/CCL20^{low}$ group demonstrated better overall survival, whereas $CCL4^{low}/CCL20^{low}$ and $CCL4^{low}/CCL20^{high}$ groups showed the worst overall survival (358). Although we did not observe any link between CCL4, CCL20, and OS in our OAC cohort (even when analysed in combination), we did however observe improved OS time when favourable cytokine profiles ($CCL22^{high}$, $CCL26^{high}$, and $IL\text{-}10^{low}$) were analysed in combination, reinforcing the idea that multiple markers enhance prognostic efficacy.

In terms of markers with negative clinical associations, levels of pre-treatment serum CRP and Tie2 were increased in patients with a subsequent poor treatment response to neoadjuvant therapy. CRP is an acute phase protein and general indicator of inflammation and has previously been linked with poor prognosis, recurrence and

response to therapy in several malignancies, including OAC (359, 360). Such observations led to development of the modified Glasgow Prognostic Score, which combines indices of decreased plasma albumin and elevated CRP. Although this scoring approach has been shown to have prognostic ability in other gastrointestinal cancer types (361), a prognostic effect has not been demonstrated in oesophageal cancer, where an association with advanced stage but no independent prognostic significance or impact on operative outcomes was observed in a cohort of 223 patients (362). We did not observe any association between CRP levels and OS in our cohort, possibly due to the cohort size (n = 80), which was smaller than that of studies by Ikeda et al. (n = 356) (359) and Nozoe et al. (n = 262) (360). However, CRP was observed to be higher in patients with a poor response to neo-CT (TRG3–5), suggesting a negative role for systemic inflammation in the treatment response in this cohort.

We also observed that patients with a poor treatment response had elevated pre-treatment levels of Tie2, a tyrosine kinase that acts as a cell surface receptor for angiopoietins and plays an important role in angiogenesis. Circulating Tie2 is a vascular response biomarker in bevacizumab-treated ovarian and metastatic colorectal cancer patients (363). The angiopoietin/Tie2 axis is therefore an attractive target for cancer therapy, since it is involved in inflammation, metastasis and lymphangiogenesis, and drugs such as trebananib have been designed to block Tie2 receptor interaction with angiopoeitin ligands (364). We observed that patients with adverse features showed a higher pre-treatment level of angiogenic factors Tie2 and VEGF, however these cytokines showed no significant difference when other clinical parameters were assessed. A higher than median expression of the immunosuppressive cytokine IL-10 in treatment-naive serum was associated with a shortened survival time, in agreement with other studies in gastrointestinal cancers and a meta-analysis of 21 studies on 1788 patients with

various cancer types, which showed that high serum IL-10 was associated with worse clinical outcomes (365).

Proinflammatory cytokines IL-1α and IL-12/IL-23p40 and chemoattractant molecules CCL3 and CCL4 were detected at lower levels in the treatment-naive serum of patients with adverse tumour features when compared to those with no adverse tumour features, potentially indicating a lack of an effective anti-tumour response, and instead reflecting an immune environment which promotes disease progression and the acquisition of adverse tumour features. Alternatively, the presence of adverse tumour features may reflect a more aggressive and immunosuppressive tumour microenvironment which actively dampens anti-tumour immunity. IL-1 acts downstream of inflammasome signalling and as such plays a vital role in innate immunity and can act as a damage associated molecular pattern (DAMP) (366). Conversely, significantly higher levels of tumour-promoting, pro-angiogenic factors Tie2 and VEGF were detected in the pre-treatment serum of patients who had adverse tumour features following neo-adjuvant treatment which are associated with poorer responses and prognoses (209).

Chemotherapy and radiotherapy can have profound effects on reshaping the tumour microenvironment and immune response to cancer, leading to either an enhancement or suppression of anti-tumour immune responses (367), which depend on a myriad of tumour–host interactions. Of note, we demonstrated an increase in immune checkpoint expression in all three compartments (CD3, CD4, CD8) with 3x2 Gy radiation dosing across all checkpoints (TIGIT, TIM3, PD-1 and PD-L1). In addition to this there was an increase in DAMP expression (Calreticulin and HMGB1) on the surface of OAC patient PBMCs post ionising radiation. We also found that ionising radiation induced the upregulation of IFN-γ, suggestive of a more anti-tumour immune landscape, as IFN-γ induces MHC molecule expression, promotes DC antigen presentation as well and

encouraging $CD8^+$ T cell responses as well as an increase in interleukin 12 (IL-12), which is crucial for initiation of the differentiation of naive $CD4^+$ T cells to T helper type 1 (Th1) cells. On the contrary there is a simultaneous increase in Th2 pro-tumour cytokines as a consequence of radiation, with a significant increase in IL-4 and IL-10 which may propagate an immunosuppressive milieu. Immunosuppressive IL-10 inhibits the differentiation and activation of DCs, which are key activators of anti-tumour effector cells of the adaptive immune system, including cytotoxic $CD8^+$ T cells.

A number of previous studies have demonstrated that nutrient deprivation suppressed the proliferation of Peripheral Blood Lymphocytes (PBL's), and fostered the secretion of IL-4 and reduced secretion of IFN-γ. It is therefore possible that glucose-deficient microenvironments in local cancer tissues cause a partial immunodeficiency, which is advantageous to cancer growth (358), The net result of these alterations in immune function could result in a Th1/Th2 imbalance in favour of an immunosuppressive phenotype.

We also investigated levels of immune serum proteins before and after neo-CT treatment to help elucidate the net effect of neoadjuvant therapy on systemic immunity. Of the 54 mediators measured, twelve showed significant alterations following neo-CT treatment, including: VEGFC, PlGF, CCL3, IL-21, IL-12/IL-23p40, GM-CSF, bFGF and TNF-α, IFN-γ, CXCL10, CCL4 and IL-5, with VEGFC being lower after treatment, whereas all other effectors were elevated at the post-treatment, pre-surgical time point. Such factors comprise a mixture of pro- and anti-tumour immune effector molecules, highlighting the double-edged sword effects of chemoradiotherapy. Interestingly, while we did not observe any significant changes in levels of VEGF family members, in VEGFA and VEGFD after neo-CT treatment, in line with previous studies (368), levels of the family member VEGFC were greatly reduced after neo-CT treatment.

Chemoradiotherapy concomitantly induces damage to tumour cells as well as the tumour vasculature (369), therefore an increase in systemic vascular damage proteins and pro-survival growth factors including bFGF and PlGF following neoadjuvant treatment is logical. bFGF has a myriad of cellular functions, including proliferation, cell survival, differentiation, and motility and has specific roles in wound healing and tissue repair, which may have adverse implications for tumour progression (370). Studies in oesophageal cancer studies have demonstrated that FGF2 overexpression is associated with a risk of recurrence of disease as well as reduced OS post-surgical resection (259).

Cytolytic activity is an important process for eliminating intracellular pathogens and cancer cells. Pembrolizumab (Keytruda) has been already approved for use in combination with platinum and fluoropyrimidine-based chemotherapy for patients with metastatic or locally advanced esophageal or gastroesophageal carcinoma and is based on data from the KEYNOTE-590 (NCT03189719) trial. Interestingly, the cytolytic assay which is an *in vitro* model of the trafficking of activated T cells to the tumour site following radiation shows promise of the synchronised and potent anti tumour effect of combining radiation with immune checkpoint blockade. The other important caveat to mention is the improved cytolytic activity noted with 4 Gy radiation and Pembrolizumab. Furthermore, with the promising results from the Checkmate-577 trial, this provides a robust rationale for the use of ICBs in the curative setting and warrants interrogation in well designed trials.

In summary, the data show that non-invasive serum cytokine signatures differ based on treatment response as determined by Mandard TRG score, overall survival time, adverse tumour features, and immune cell infiltration into tumours. In particular, we show that several chemokines are linked with favourable outcomes, including OS (CCL22, CCL26) and treatment response (CCL4), implicating a role for immune cell trafficking

in the immune response to OAC. CCL4 in particular was linked with several favourable clinical indicators, but not OS, highlighting a need for further studies to understand the underlying biology of this chemokine in OAC.

A better understanding of immune signatures associated with favourable clinical outcomes in OAC will help build a clearer picture of the critical pathways involved in anti-tumour immunity. Moreover, the effects of ICB in combination with radiation hold promise and may offer new insights, further improving patient outcomes in OAC.

Chapter 7: General Discussion

The incidence of Oesophageal adenocarcinoma (OAC) is exponentially rising, it is the seventh most common cancer and the sixth leading cause of cancer-related mortality worldwide (371). Despite improvements in the multimodal treatment and advances in minimally invasive treatments, the prognosis remains poor compared with other solid tumour types: the 5-year overall survival (OS) rate remains 45–50% for patients who can be treated with curative intent, and 15–25% for all stages of disease (372). Radiotherapy continues to represent one of the principal treatment modalities in the management of a plethora of cancer subtypes for the past century. It is used in approximately 50% of cancer patients in the neoadjuvant, adjuvant, curative or palliative settings (19). Tri-modality treatment of surgery, chemotherapy and radiotherapy is the standard of care in oesophageal adenocarcinoma (OAC). Radiation triggers DNA damage-induced cell death in cancer cells, and it is now known that radiotherapy can induce immunogenic cell death which can propagate anti-tumour immunity.

Targeted immune therapy represents a major advance in the management of metastatic cancer, with significant benefit for selected patients. Although most focus has been on malignant melanoma and non-small cell lung cancer (NSCLC), there is increasing literature on its efficacy in other cancer types including gastrointestinal cancer. Attention has shifted now to its role in the curative approach to cancer, and hence a scientific and clinical understanding of its interaction with surgery, radiation therapy, chemotherapy and the tumour microenvironment is of great current interest. It is known for example that immunotherapy combined with radiotherapy, results in synergistic immunogenic effects on local and systemic tumour control (373). Its optimum use in the curative setting and with surgery is less studied, therefore understanding this intricate interplay and anti-tumour immunity will be key in leveraging effective combination regimens.

It is long established that complex major surgery fuels a multitude of metabolic, endocrine, neuro-endocrine, procoagulant and immune-inflammatory responses, which may result in an early systemic inflammatory response and subsequently a global state of immune paralysis or suppression (374). This milieu in the context of cancer surgery may be permissive of tumour-cell shedding and production of pro-angiogenic and/or growth factors, with the risk of progression of pre-existing micrometastases and the initiation of new metastases, while simultaneously compromising immune control over residual malignant cells (216). The optimal timing for delivery of immunotherapies to enable synergies for immunostimulation and anti-metastatic efficacy is still unclear (245). At this time, it is also unclear whether immunotherapy has therapeutic benefit during the potentially immunosuppressive perioperative period (246). In theory however, the peri-operative period provides a therapeutic window to potentially arrest metastatic growth, enhance immune function, achieve metabolic reprograming of the tumour microenvironment (TME) and potentiate anticancer immune responses (247). This is timely in view of the recently published Checkmate-577 trial, which demonstrated significant disease-free survival in carcinoma of the gastroesophageal junction with the use of adjuvant anti-programmed cell death protein 1(PD-1) immunotherapy (180).

The success of targeted immune therapies is based on the revitalisation of existing anti-tumour immune responses by disrupting suppressive immune checkpoint pathways, tilting the balance in favour of tumour elimination. It has been demonstrated that solid neoplasms are highly heterogenous and develop, progress, and respond to local and systemic therapies in the context of intricate crosstalk with the host immune system (288). It must be borne in mind that distinct phenotypic and behavioural features generally co-exist, and often multiple non-transformed cells are co-opted by growing cancers to support their needs. There is accumulating evidence that the efficacy of most chemo- and

radiotherapeutic agents commonly employed in the clinic are dependent on the propagation of anti-tumour-targeting immune responses (313). Consequently, mechanistically, conventional therapeutics such as chemotherapy and radiotherapy can evoke a therapeutically relevant, adaptive immune response against malignant cells and is referred to as "immunogenic cell death (ICD)." However, the failures as much as the successes of immune checkpoint blockade (ICB) have led to a more nuanced view of cancer and the immune system, in addition to the physical characteristics of the TME (stromal barriers, hypoxia, pH, nutrient levels) which are critical modulators in tumour-immune interactions (375).

The findings of significantly higher calreticulin expression with radiation in OE33R cells compared to OE33P cells is interesting and suggest an immunogenic type of cell death induced by radiation, providing a foundation for immune modulating agents to enhance established anti-tumour responses in radioresistant tumours. There were similar findings for HMGB1 with a higher expression of HMGB1 in the OE33R cell line with bolus dosing, however, there was a significantly higher expression of HMGB1 with fractionated dosing regimens of 3x4 Gy and 3x8 Gy in the OE33P cell line compared to the OE33R cell line. The increased expression of both DAMPS post-radiotherapy *in vivo* and *ex vivo* post conventional therapies suggest promise of oesophageal adenocarcinoma as an immunogenic tumour entity and therefore a potential target for systemic immunotherapies.

In addition to this, the increased expression of Calreticulin and HMGB1 post-radiation under hypoxia, notably 5% O_2 and nutrient deprivation, represent further exciting data and reaffirm the hypothesis that oesophageal cancer is a viable phenotype for enhancing the anti-tumour immune response. On the contrary, it is also important to note that the properties of the intrinsic tumour microenvironment, such as hypoxia or nutrient

deprivation, endemic of solid tumours, could alter the action of ICD stressors and modulate the immunomodulatory properties of DAMPs (317). Furthermore, it was previously demonstrated that hypoxia leads to HMGB1 release, which can contribute to tumour invasiveness (318). DAMPs are released from cells under stress due to these harsh conditions of the tumour microenvironment, including nutrient deprivation and hypoxia, or secondary to treatment with chemotherapy or radiotherapy and when released can have a double edged sword activating innate immunity, providing a pathway to a systemic inflammatory response or can be manipulated in regulating inflammation in the tumour microenvironment, promoting angiogenesis and increasing autophagy with immune evasion and avoidance of apoptosis, facilitating progression and or dissemination (319).

Co-stimulatory and immune checkpoint molecules can have both immunostimulatory and immunosuppressive effects. In this thesis a range of soluble immune checkpoint receptors and ligands were significantly downregulated following treatment of OAC tumour explants with 4 Gy radiation. However, the role of soluble receptors and ligands on immune regulation and cancer treatment is largely unknown. Also we observed a significant down regulation of soluble PD-1, PD-L1, TIM-3 and TIGIT and this was paralleled by a concomitant increase in OAC cell line surface expression and in a cohort of OAC tumour explants, which may go some way to explain the decrease in the soluble forms of these immune checkpoint proteins post irradiation. B7-H3 (also known as CD276) is an immune checkpoint molecule in the epithelial mesenchymal transition (EMT) pathway, with many cancers exhibiting aberrant overexpression and such upregulation is associated with aggressiveness and a poor clinical prognosis (197). Furthermore, there are studies demonstrating a crucial role for B7-H3 in promoting carcinogenesis and metastasis and playing an essential role in cell proliferation, invasion and migration (197-199). CD276 serves as a T cell inhibitor to promote tumour

proliferation and invasion, in contrast to its role as a T cell stimulatory molecule as previously thought (200). In addition, soluble B7-H3 was found to promote the invasion and metastasis of pancreatic carcinoma cells through the TLR4/NF-κB pathway (50).

The co-stimulatory molecule CD28 is essential in the augmentation of T cell activation and metabolism, driving tumour-infiltrating T cell glycolysis to promote inflammation. It is antagonized by the inhibitory and checkpoint immunotherapy receptors CTLA-4 and PD-1 (201). In the current study, soluble CD28 is reduced with radiation, which may be immunosuppressive. Soluble CD80-Fc (where extracellular domains of human or mouse CD80 are fused to the Fc domain of IgG1) have been found to sustain IFN-γ production by human and murine PD-1^+ activated T cells even in the presence of PD-$L1^+$ human or mouse tumour cells (202). Soluble Glucocorticoid-induced TNF receptor (GITR), which was reduced in this study, is an emerging immunotherapy target expressed at high levels on regulatory T cells (203, 204). Recent phase 1 trials have demonstrated the safe pharmacological profile of agonistic anti-GITR antibodies. Phase II trials are ongoing, evaluating its combination with radiotherapy and anti-PD-1 therapy (NCT04225039). New promising approaches are focusing on the activation of co-stimulatory pathways to enhance antitumour immune responses. GITR activation can promote effector T cell function and inhibit regulatory T cell (Treg) function (203), and may also provide theoretical basis for the clinical application of combinations with monoclonal antibody therapy such as bFGF in molecular targeted therapies (205).

OX40 has a critical role in the maintenance of an immune response beyond the initial few days boosting T cell clonal expansion, effector differentiation, and survival (206). OX40 activation could augment the downstream signaling of TCR mainly through the PI3-K/PKB pathway, accounting for T cell division, survival and cytokine production. OX40 activated in conjunction with TCR signaling could increase calcium influx, promote

nuclear factor of activated T cells (NFAT) activation and enhance several cytokines secretion, such as IL-2, IL-4, IL-5, and IFN-γ (207). OX40 triggering regressed Treg cells, allowing DCs to reach the draining lymph nodes and prime the specific CD8 lymphocytes response to the tumour (208).

Although the focus of immunotherapy to date has been on the local microenvironment, the primary tumour-draining lymph node (TDLN) may have a key role in anti-tumour immunity (376, 377). TDLNs are a primary metastatic site for many cancers, and radical excision of TDLNs is a key element of curative surgery for many cancer sites (378, 379). From an immune cell perspective, $CD4^+$ and $CD8^+$ T cell priming by DCs occurs in the TDLN, and this represents a critical step in the cancer immunity cycle that is potentiated by ICB, in particular CTLA-4 blockade (232). Recent preclinical studies are in keeping with resection of TDLNs augmenting surgery-induced immunosuppression (380). For example, in mouse models of colorectal cancer, ablation of the TDLN resulted in abrogation of anti-tumour efficacy of PD-1 blockade, indicating that this structure is indispensable for the action of an agent primarily active in the local immune TME (240). Surgical resection of TDLNs in mice decreased immune infiltration in the TME and abolished tumour regression in response to ICB (239). Collectively, these studies suggest that TDLNs are pivotal in mounting a response to ICB therapy, and similar results are seen when TDLNs are irradiated (75). Clinical data, however, is lacking and the immunological effects of surgical lymph node dissection have not been evaluated extensively to date in trials. Nevertheless, this provides a rationale for exploring the balance between anti-metastatic and immunosuppressive effects of radical lymph node dissection. We demonstrated that nodal involvement has superior prognostic value than clinical and pathological tumour staging, and soluble mediators within the LNME and TME correlated with clinical tumour stage suggesting the important role of both the

LNME and TME in OAC progression and pathogenesis. These results also highlight the immunosuppressive nature of the TME as demonstrated by higher percentages of T cells co-expressing multiple ICs in the TME compared to the LNME. However, the higher levels of pro-angiogenic mediators found within the LNME suggests an attempt by the local TME to remodel the TDLN toward a pre-metastatic permissive niche. Moreover, tumour-promoting inflammation was identified as an adverse prognostic factor, however, a pro-inflammatory LNME negatively correlated with adverse tumour features. T cells in the LNME and TME expressing inhibitory ICs positively correlated with clinical tumour stage and clinical nodal involvement, respectively, which suggests that combination therapeutic blockade of PD-1, TIM-3 and TIGIT may have therapeutic rationale for boosting response rates in OAC. In our study, the frequency of $CD3^{+}TIM\text{-}3^{+}$ and $CD3^{+}PD\text{-}1^{+}$ cells present in TDLNs positively correlated with clinical tumour stage and the percentage of tumour-infiltrating $CD3^{+}CD8^{+}PD\text{-}1^{+}$ and $CD3^{+}CD8^{+}TIGIT^{+}$ cells positively correlated with clinical tumour nodal metastasis. These findings highlight the central role of the TDLNs in immune-mediated disease, control and potentially represent new methods of biomarker-driven patient stratification. Furthermore, ICBs targeting one or more immune checkpoints such as PD-1, TIM-3 and TIGIT to the tumour draining lymph node may represent a more effective and personalised rational approach for treating oesophagogastric cancer patients.

As an understanding of the relationship between cancer and the immune system has developed, ICB has been incorporated into clinical practice. However, little is known about the influence of oncological surgery on checkpoint expression and DAMP release perioperatively (381). Cancer patients undergoing major oesophageal surgery receive

neoadjuvant chemotherapy or chemoradiation which may alter the immune TME mainly through the release of pattern associated molecular patterns (PAMPs) and DAMPs, upregulation of Tregs, cancer-associated fibroblasts (CAFs), MDSCs, and lymphodepletion.

In the current body of work, intriguingly, there is an increase in the expression of both DAMPS, calreticulin and HMGB1 in all three T cell compartments in the immediate post-operative period, which would suggest an anti-tumour response however, paradoxically in a study on patients undergoing cytoreductive surgery, increased plasma levels of DAMPs were associated with immune suppression and postoperative infections in patients undergoing cytoreductive surgery (277, 278). Therefore, the concomitant increase in soluble checkpoints and DAMPS may represent the perfect timing for administration of immune checkpoint blockade to offset the prevailing immunosuppressive milieu. Th1 cells are drivers of cellular immunity, whereas Th2 cells regulate humoral immunity (382). Alterations in Th1/Th2 balance towards a Th2 phenotype is linked to immunosuppression, metastasis and disease progression (383). Th1 cell responses against a tumour antigen are essential for clinical responses to immunotherapy (384). Surgical stress largely promotes differentiation to a Th2 phenotype, suggesting that cell-mediated immunity is down-regulated and antibody-mediated immunity is up-regulated after surgery, consistent with an increased risk of metastasis or progression (385). The disruption in this Th1/Th2 balance is associated with surgical trauma, where for example a significant shift towards Th2 phenotype is observed following major gastrointestinal cancer resection and may continue for up to two weeks (386).

Following major trauma induced by surgery, endogenous synthesis of glutamine does not fulfil the physiological requirements and the lower concentration adversely affects immune cell functions (387). Similarly, the utilisation of glucose is higher during this critical postoperative phase. Glutamine is essential for the production of CD25, CD45RO and CD71 and also for the synthesis of the cytokines (IFN-γ, TNF-α, and IL-6) (388). Glutamine is crucial for T cell activation, while glucose metabolism and aerobic glycolysis delivers intermediates for biosynthesis pathways, which is necessary for differentiation and proliferation of T cells (389). Glycolysis is essential for effector T cell function and is related to inflammatory cytokine production, mostly IL-2 and IFN-α (390). Therefore, a higher glycolytic activity is important for Th1 differentiation. However, while glutamine is essential for the aforementioned processes there is ongoing research in the administration of drugs resulting in glutamine depletion such as phenylacetate, which is an aromatic fatty acid metabolite of phenylalanine (391). Of note we demonstrated that ionising radiation induced the upregulation of IFN-γ, suggestive of a more anti-tumour immune landscape, as IFN-γ induces MHC molecule expression, promotes DC antigen presentation and $CD8^+$ T cell responses, as well as increasing *i*nterleukin-12 (IL-12), which is crucial for initiation of the differentiation of naive $CD4^+$ T cells to T helper type 1 (Th1) cells. On the contrary, there is a simultaneous increase in Th2 pro-tumour cytokines as a consequence of radiation, with a significant increase in IL-4 and IL-10, which may propagate an immunosuppressive milieu. Immunosuppressive IL-10 inhibits the differentiation and activation of DCs, which are key activators of anti-tumour effector cells of the adaptive immune system, including cytotoxic $CD8^+$ T cells.

A number of previous studies have demonstrated that nutrient deprivation suppressed the proliferation of Peripheral Blood Lymphocytes (PBL's), and fostered the

secretion of IL-4 and reduced secretion of IFN-γ. It is therefore possible that glucose-deficient microenvironments in local cancer tissues cause a partial immunodeficiency, which is advantageous to cancer growth (41), The net result of these alterations in immune function could result in a Th1/Th2 imbalance in favour of an immunosuppressive phenotype. The interplay of these nutrients in cancer metabolism is yet to be fully understood, but there is potential to harness these pathways to promote anti-tumour immunity in the perioperative period.

In gastrointestinal cancers ICB provides some benefit in selected patient subgroups with improved OS and progression-free survival (PFS). Tumours that are PD-L1^{+}, MSI-high, Epstein-Barr virus positive or have a high tumour mutational burden (TMB) have demonstrated the greatest success for distinguishing responders from non-responders to PD-1 ICB in gastric cancer, acting as surrogate markers of pre-existing anti-tumour immunity (392). A meta-analysis performed by Chen *et al*., showed that addition of ICB to the second- and third-line setting in gastroesophageal cancers improves some, but not all survival endpoints (393). The ORRs for PD-1, PD-L1 and CTLA-4 ICB were 9.9%, 12.0% and 2.1% respectively. The median PFS was 1.6, 1.6 and 2.9 months, respectively and the median OS of the three groups was 6.0, 5.4 and 7.7 months, respectively (393). However, levels of drug resistance due to intratumoural heterogeneity are higher in metastatic tumours and tumour immunogenicity, measured by lymphocyte infiltration, is more pronounced in early stage disease (394).

The use of postoperative adjuvant ICB is highlighted by the CheckMate 577 trial in oesophageal cancer. In patients with residual disease following neoadjuvant chemotherapy and radiation therapy and surgery, adjuvant nivolumab doubled recurrence-free survival compared with placebo. The impact of the timing of adjuvant therapy after surgery is intriguing, specifically when immunotherapy is administered after

10 weeks compared with the cohort who received it less than 10 weeks post-surgery, with hazards ratios (HR) (95%CI) of [0.66 (0.52-0.84)] and [0.84(0.57-1.22)]. This supports the ethos of a deeper understanding of the TME to augment the prevailing immunosuppressive phenotype and identify optimal timing of drug delivery.

7.1 Conclusion

Collectively, this body of work supports a rationale for administering ICB in the first-line setting both preoperatively and perioperatively to harness the power of the immune system boosting the efficacy of conventional regimens but also to eradicate residual disease following surgery. However, outstanding issues remain. We have demonstrated that timing and scheduling of immunotherapy can potentially be of benefit in the neoadjuvant, and perioperative setting. In addition, there is a potential for such treatments to control and harness the putative immunosuppression of the perioperative period. Several clinical trials are underway to help understand the optimal combination and timing of ICB with multimodal regimens in the perioperative setting.Rresults from these trials are eagerly awaited and will offer important insight and guidance into future clinical decision making.

Despite the success in leveraging the combination of immunotherapy for the treatment of upper gastrointestinal cancers, further studies are warranted. There is a lack of studies that directly compare the immunogenicity of different dosing and fractionation regimens. This is seen in both preclinical studies and clinical trials, and not specific to gastrointestinal cancers. Some studies vary the entire dose of radiation but do not ascertain whether this dose would be better delivered in a single ablative dose, a hypofractionated regimen or conventional 1.8-2 Gy fractionation. Well-controlled preclinical studies would provide more clarity on the subtle effects of different

fractionation, while a multi-arm clinical trial would be useful to determine the optimal dosage regimen for clinical practice. These trials should also have translational study endpoints including abscopal response and changes in $CD8^+$ TILs, T_{reg} cells and MDSCs levels in the irradiated and peripheral sites. This would provide a means for dissecting the mechanisms of action and resistance to immuno-radiotherapy, and provide further mechanistic data specific to upper GI cancers. Finally, there is a need for more trials in advanced disease setting. In contrast to single agent ICB, most trials of ICB and radiotherapy are in locally advanced, resectable disease where chemoradiotherapy is a standard of care. However, outcomes are worst in the refractory disease setting and response rates to single agent ICB is low (157). This highlights an unmet need for trials in this population, which could stand to benefit most of this symbiotic combination.

7.2 Future direction

The advent of immune checkpoint blockade has shifted the paradigm in the treatment of solid tumours, but the impact of ICIs on patient outcomes in UGI cancers has been limited. Radiotherapy has the potential to augment responses to ICI through cGAS-STING signalling, immunogenic cell death, upregulation of neoantigen expression and through inflammatory remodelling of the immune microenvironment. Given the extensive pre-existing use of radiation and the modest activity of single agent immunotherapy, gastroesophageal cancers are poised to greatly benefit from a combination of ICIs and radiotherapy. However, questions remain surrounding methods of optimising the radiation dose and timing while minimising toxicity. Most ongoing clinical trials employ conventional radiation fractionation, although preclinical data suggest that hypofractionated regimens are favourable in terms of toxicity and efficacy and this is what needs to be intensively scrutinized. Furthermore ICBs targeting one or more immune checkpoints such as PD-1, TIM-3 and TIGIT to the tumour draining lymph

node may represent a more effective and personalised rational approach for treating oesophagogastric cancer patients and this is an evolving field which needs interrogation.

Signalling events following radiotherapy have profound effects in altering the immune landscape of the TME. Advances have been made in recent years to untangle the biology of radiation induced anti-tumour immunity and how this knowledge can be used to design rational therapeutic approaches. However, issues remain regarding the paradoxical effects of radiation in recruiting suppressive cell populations, the complex effects that radiation invokes on the tumour vasculature and the radiation dosage and fractionation that influences these effects. Although hypofractionated regimens display the most promising immunomodulation in preclinical studies, there needs to be prospective clinical studies that directly compare different approaches. Questions remain around the best way to promote immunostimulatory effects of radiotherapy while minimising immunosuppression. We propose that combining radiation with immunotherapy is a promising approach to shift this balance and exploit the microenvironment's untapped therapeutic potential however, a better understanding of variability in response to immune checkpoint blockade is also required. Future trials should incorporate correlative endpoints to identify predictive biomarkers of response as this will help to select patients likely to benefit from radiation and immunotherapy and facilitate a precision oncology approach.

References

1. Arnold M, Laversanne M, Brown LM, Devesa SS, Bray F. Predicting the Future Burden of Esophageal Cancer by Histological Subtype: International Trends in Incidence up to 2030. Am J Gastroenterol. 2017;112(8):1247-55.
2. Bray F, Ferlay J, Soerjomataram I, Siegel RL, Torre LA, Jemal A. Global cancer statistics 2018: GLOBOCAN estimates of incidence and mortality worldwide for 36 cancers in 185 countries. CA Cancer J Clin. 2018;68(6):394-424.
3. O'Sullivan J, Lysaght J, Donohoe CL, Reynolds JV. Obesity and gastrointestinal cancer: the interrelationship of adipose and tumour microenvironments. Nat Rev Gastroenterol Hepatol. 2018;15(11):699-714.
4. van Hagen P, Hulshof MC, van Lanschot JJ, Steyerberg EW, van Berge Henegouwen MI, Wijnhoven BP, et al. Preoperative chemoradiotherapy for esophageal or junctional cancer. N Engl J Med. 2012;366(22):2074-84.
5. Cunningham D, Allum WH, Stenning SP, Thompson JN, Van de Velde CJ, Nicolson M, et al. Perioperative chemotherapy versus surgery alone for resectable gastroesophageal cancer. N Engl J Med. 2006;355(1):11-20.
6. Al-Batran SE, Homann N, Pauligk C, Goetze TO, Meiler J, Kasper S, et al. Perioperative chemotherapy with fluorouracil plus leucovorin, oxaliplatin, and docetaxel versus fluorouracil or capecitabine plus cisplatin and epirubicin for locally advanced, resectable gastric or gastro-oesophageal junction adenocarcinoma (FLOT4): a randomised, phase 2/3 trial. Lancet. 2019;393(10184):1948-57.
7. Low DE, Kuppusamy MK, Alderson D, Cecconello I, Chang AC, Darling G, et al. Benchmarking Complications Associated with Esophagectomy. Ann Surg. 2019;269(2):291-8.
8. Lagergren J, Smyth E, Cunningham D, Lagergren P. Oesophageal cancer. Lancet. 2017;390(10110):2383-96.
9. Reynolds JV, Donohoe CL, McGillycuddy E, Ravi N, O'Toole D, O'Byrne K, et al. Evolving progress in oncologic and operative outcomes for esophageal and junctional cancer: lessons from the experience of a high-volume center. J Thorac Cardiovasc Surg. 2012;143(5):1130-7.e1.
10. Biere SS, van Berge Henegouwen MI, Maas KW, Bonavina L, Rosman C, Garcia JR, et al. Minimally invasive versus open oesophagectomy for patients with oesophageal cancer: a multicentre, open-label, randomised controlled trial. Lancet. 2012;379(9829):1887-92.
11. Mariette C, Markar SR, Dabakuyo-Yonli TS, Meunier B, Pezet D, Collet D, et al. Hybrid Minimally Invasive Esophagectomy for Esophageal Cancer. N Engl J Med. 2019;380(2):152-62.
12. van der Sluis PC, Ruurda JP, van der Horst S, Verhage RJ, Besselink MG, Prins MJ, et al. Robot-assisted minimally invasive thoraco-laparoscopic esophagectomy versus open transthoracic esophagectomy for resectable esophageal cancer, a randomized controlled trial (ROBOT trial). Trials. 2012;13:230.
13. Arnold M, Rutherford MJ, Bardot A, Ferlay J, Andersson TM, Myklebust T, et al. Progress in cancer survival, mortality, and incidence in seven high-income countries 1995-2014 (ICBP SURVMARK-2): a population-based study. Lancet Oncol. 2019;20(11):1493-505.
14. Walsh TN, Noonan N, Hollywood D, Kelly A, Keeling N, Hennessy TP. A comparison of multimodal therapy and surgery for esophageal adenocarcinoma. N Engl J Med. 1996;335(7):462-7.
15. Chang KH, McAnena OJ, Smith MJ, Salman RR, Khan MF, Lowe D. Surgery for oesophageal cancer at Galway University Hospital 1993-2008. Ir J Med Sci. 2010;179(4):521-7.
16. Darvin P, Toor SM, Sasidharan Nair V, Elkord E. Immune checkpoint inhibitors: recent progress and potential biomarkers. Exp Mol Med. 2018;50(12):1-11.

17. Maharaj AD, Holland JF, Scarborough RO, Evans SM, Ioannou LJ, Brown W, et al. The Upper Gastrointestinal Cancer Registry (UGICR): a clinical quality registry to monitor and improve care in upper gastrointestinal cancers. BMJ Open. 2019;9(9):e031434.
18. Kelly RJ. The emerging role of immunotherapy for esophageal cancer. Current Opinion in Gastroenterology. 2019;35(4).
19. Baskar R, Lee KA, Yeo R, Yeoh KW. Cancer and radiation therapy: current advances and future directions. Int J Med Sci. 2012;9(3):193-9.
20. Smyth EC, Lagergren J, Fitzgerald RC, Lordick F, Shah MA, Lagergren P, et al. Oesophageal cancer. Nat Rev Dis Primers. 2017;3:17048.
21. Zemek RM, Chin WL, Nowak AK, Millward MJ, Lake RA, Lesterhuis WJ. Sensitizing the Tumor Microenvironment to Immune Checkpoint Therapy. Front Immunol. 2020;11:223.
22. Barker HE, Paget JTE, Khan AA, Harrington KJ. Erratum: The tumour microenvironment after radiotherapy: mechanisms of resistance and recurrence. Nature Reviews Cancer. 2015;15(8):509-.
23. McBride S, Sherman E, Tsai CJ, Baxi S, Aghalar J, Eng J, et al. Randomized Phase II Trial of Nivolumab With Stereotactic Body Radiotherapy Versus Nivolumab Alone in Metastatic Head and Neck Squamous Cell Carcinoma. Journal of Clinical Oncology. 2020:JCO.20.00290.
24. Dewan MZ, Galloway AE, Kawashima N, Dewyngaert JK, Babb JS, Formenti SC, et al. Fractionated but not single-dose radiotherapy induces an immune-mediated abscopal effect when combined with anti-CTLA-4 antibody. Clin Cancer Res. 2009;15(17):5379-88.
25. Park SS, Dong H, Liu X, Harrington SM, Krco CJ, Grams MP, et al. PD-1 Restrains Radiotherapy-Induced Abscopal Effect. Cancer Immunol Res. 2015;3(6):610-9.
26. Postow MA, Callahan MK, Barker CA, Yamada Y, Yuan J, Kitano S, et al. Immunologic correlates of the abscopal effect in a patient with melanoma. N Engl J Med. 2012;366(10):925-31.
27. Welsh JW, Chen D, Baas P, Chang JY, Verma V, Comeaux N, et al. Radiotherapy to augment pembrolizumab responses and outcomes in metastatic non-small cell lung cancer: Pooled analysis of two randomized trials. Journal of Clinical Oncology. 2020;38(15_suppl):9548-.
28. Ngwa W, Irabor OC, Schoenfeld JD, Hesser J, Demaria S, Formenti SC. Using immunotherapy to boost the abscopal effect. Nat Rev Cancer. 2018;18(5):313-22.
29. Golden EB, Frances D, Pellicciotta I, Demaria S, Helen Barcellos-Hoff M, Formenti SC. Radiation fosters dose-dependent and chemotherapy-induced immunogenic cell death. Oncoimmunology. 2014;3:e28518.
30. Chao MP, Jaiswal S, Weissman-Tsukamoto R, Alizadeh AA, Gentles AJ, Volkmer J, et al. Calreticulin is the dominant pro-phagocytic signal on multiple human cancers and is counterbalanced by CD47. Sci Transl Med. 2010;2(63):63ra94.
31. Apetoh L, Ghiringhelli F, Tesniere A, Obeid M, Ortiz C, Criollo A, et al. Toll-like receptor 4–dependent contribution of the immune system to anticancer chemotherapy and radiotherapy. Nature Medicine. 2007;13(9):1050-9.
32. Ghiringhelli F, Apetoh L, Tesniere A, Aymeric L, Ma Y, Ortiz C, et al. Activation of the NLRP3 inflammasome in dendritic cells induces IL-1beta-dependent adaptive immunity against tumors. Nat Med. 2009;15(10):1170-8.
33. McGranahan N, Furness AJ, Rosenthal R, Ramskov S, Lyngaa R, Saini SK, et al. Clonal neoantigens elicit T cell immunoreactivity and sensitivity to immune checkpoint blockade. Science. 2016;351(6280):1463-9.
34. Dillon MT, Bergerhoff KF, Pedersen M, Whittock H, Crespo-Rodriguez E, Patin EC, et al. ATR Inhibition Potentiates the Radiation-induced Inflammatory Tumor Microenvironment. Clin Cancer Res. 2019;25(11):3392-403.

35. Reits EA, Hodge JW, Herberts CA, Groothuis TA, Chakraborty M, Wansley EK, et al. Radiation modulates the peptide repertoire, enhances MHC class I expression, and induces successful antitumor immunotherapy. J Exp Med. 2006;203(5):1259-71.
36. Sharma A, Bode B, Wenger RH, Lehmann K, Sartori AA, Moch H, et al. gamma-Radiation promotes immunological recognition of cancer cells through increased expression of cancer-testis antigens in vitro and in vivo. PLoS One. 2011;6(11):e28217.
37. Formenti SC, Rudqvist NP, Golden E, Cooper B, Wennerberg E, Lhuillier C, et al. Radiotherapy induces responses of lung cancer to CTLA-4 blockade. Nat Med. 2018;24(12):1845-51.
38. Dovedi SJ, Cheadle EJ, Popple AL, Poon E, Morrow M, Stewart R, et al. Fractionated Radiation Therapy Stimulates Antitumor Immunity Mediated by Both Resident and Infiltrating Polyclonal T-cell Populations when Combined with PD-1 Blockade. Clin Cancer Res. 2017;23(18):5514-26.
39. Arneth B. Tumor Microenvironment. Medicina (Kaunas). 2019;56(1).
40. Matsumura S, Wang B, Kawashima N, Braunstein S, Badura M, Cameron TO, et al. Radiation-induced CXCL16 release by breast cancer cells attracts effector T cells. J Immunol. 2008;181(5):3099-107.
41. Ruocco MG, Pilones KA, Kawashima N, Cammer M, Huang J, Babb JS, et al. Suppressing T cell motility induced by anti-CTLA-4 monotherapy improves antitumor effects. J Clin Invest. 2012;122(10):3718-30.
42. Connolly KA, Belt BA, Figueroa NM, Murthy A, Patel A, Kim M, et al. Increasing the efficacy of radiotherapy by modulating the CCR2/CCR5 chemokine axes. Oncotarget. 2016;7(52):86522-35.
43. Klug F, Prakash H, Huber PE, Seibel T, Bender N, Halama N, et al. Low-dose irradiation programs macrophage differentiation to an iNOS(+)/M1 phenotype that orchestrates effective T cell immunotherapy. Cancer Cell. 2013;24(5):589-602.
44. Sektioglu IM, Carretero R, Bender N, Bogdan C, Garbi N, Umansky V, et al. Macrophage-derived nitric oxide initiates T-cell diapedesis and tumor rejection. Oncoimmunology. 2016;5(10):e1204506.
45. Togashi Y, Shitara K, Nishikawa H. Regulatory T cells in cancer immunosuppression — implications for anticancer therapy. Nature Reviews Clinical Oncology. 2019;16(6):356-71.
46. Mondini M, Loyher PL, Hamon P, Gerbe de Thore M, Laviron M, Berthelot K, et al. CCR2-Dependent Recruitment of Tregs and Monocytes Following Radiotherapy Is Associated with TNFalpha-Mediated Resistance. Cancer Immunol Res. 2019;7(3):376-87.
47. Gabrilovich DI. Myeloid-Derived Suppressor Cells. Cancer Immunol Res. 2017;5(1):3-8.
48. Liang H, Deng L, Hou Y, Meng X, Huang X, Rao E, et al. Host STING-dependent MDSC mobilization drives extrinsic radiation resistance. Nature Communications. 2017;8(1):1736.
49. Deng L, Liang H, Burnette B, Beckett M, Darga T, Weichselbaum RR, et al. Irradiation and anti-PD-L1 treatment synergistically promote antitumor immunity in mice. J Clin Invest. 2014;124(2):687-95.
50. Carlson DJ, Yenice KM, Orton CG. Tumor hypoxia is an important mechanism of radioresistance in hypofractionated radiotherapy and must be considered in the treatment planning process. Med Phys. 2011;38(12):6347-50.
51. Meijer TW, Kaanders JH, Span PN, Bussink J. Targeting hypoxia, HIF-1, and tumor glucose metabolism to improve radiotherapy efficacy. Clin Cancer Res. 2012;18(20):5585-94.
52. Scott KE, Cleveland JL. Lactate Wreaks Havoc on Tumor-Infiltrating T and NK Cells. Cell Metab. 2016;24(5):649-50.
53. Zheng X, Fang Z, Liu X, Deng S, Zhou P, Wang X, et al. Increased vessel perfusion predicts the efficacy of immune checkpoint blockade. J Clin Invest. 2018;128(5):2104-15.

54. Rüegg C, Yilmaz A, Bieler G, Bamat J, Chaubert P, Lejeune FJ. Evidence for the involvement of endothelial cell integrin alphaVbeta3 in the disruption of the tumor vasculature induced by TNF and IFN-gamma. Nat Med. 1998;4(4):408-14.
55. Tian L, Goldstein A, Wang H, Ching Lo H, Sun Kim I, Welte T, et al. Mutual regulation of tumour vessel normalization and immunostimulatory reprogramming. Nature. 2017;544(7649):250-4.
56. Kang Y-K, Boku N, Satoh T, Ryu M-H, Chao Y, Kato K, et al. Nivolumab in patients with advanced gastric or gastro-oesophageal junction cancer refractory to, or intolerant of, at least two previous chemotherapy regimens (ONO-4538-12, ATTRACTION-2): a randomised, double-blind, placebo-controlled, phase 3 trial. The Lancet. 2017;390(10111):2461-71.
57. Fuchs CS, Doi T, Jang RW, Muro K, Satoh T, Machado M, et al. Safety and Efficacy of Pembrolizumab Monotherapy in Patients With Previously Treated Advanced Gastric and Gastroesophageal Junction Cancer: Phase 2 Clinical KEYNOTE-059 Trial. JAMA Oncology. 2018;4(5):e180013-e.
58. Kojima T, Muro K, Francois E, Hsu C-H, Moriwaki T, Kim S-B, et al. Pembrolizumab versus chemotherapy as second-line therapy for advanced esophageal cancer: Phase III KEYNOTE-181 study. Journal of Clinical Oncology. 2019;37(4_suppl):2-.
59. Kato K, Cho BC, Takahashi M, Okada M, Lin C-Y, Chin K, et al. Nivolumab versus chemotherapy in patients with advanced oesophageal squamous cell carcinoma refractory or intolerant to previous chemotherapy (ATTRACTION-3): a multicentre, randomised, open-label, phase 3 trial. The Lancet Oncology.
60. Kato K, Sun JM, Shah MA, Enzinger PC, Adenis A, Doi T, et al. LBA8_PR Pembrolizumab plus chemotherapy versus chemotherapy as first-line therapy in patients with advanced esophageal cancer: The phase 3 KEYNOTE-590 study. Annals of Oncology. 2020;31:S1192-S3.
61. Moehler M, Shitara K, Garrido M, Salman P, Shen L, Wyrwicz L, et al. LBA6_PR Nivolumab (nivo) plus chemotherapy (chemo) versus chemo as first-line (1L) treatment for advanced gastric cancer/gastroesophageal junction cancer (GC/GEJC)/esophageal adenocarcinoma (EAC): First results of the CheckMate 649 study. Annals of Oncology. 2020;31:S1191.
62. Antonia SJ, Villegas A, Daniel D, Vicente D, Murakami S, Hui R, et al. Overall Survival with Durvalumab after Chemoradiotherapy in Stage III NSCLC. New England Journal of Medicine. 2018;379(24):2342-50.
63. Kwon ED, Drake CG, Scher HI, Fizazi K, Bossi A, van den Eertwegh AJ, et al. Ipilimumab versus placebo after radiotherapy in patients with metastatic castration-resistant prostate cancer that had progressed after docetaxel chemotherapy (CA184-043): a multicentre, randomised, double-blind, phase 3 trial. Lancet Oncol. 2014;15(7):700-12.
64. Weichselbaum RR, Liang H, Deng L, Fu YX. Radiotherapy and immunotherapy: a beneficial liaison? Nat Rev Clin Oncol. 2017;14(6):365-79.
65. Jones CM, Spencer K, Hitchen C, Pelly T, Wood B, Hatfield P, et al. Hypofractionated Radiotherapy in Oesophageal Cancer for Patients Unfit for Systemic Therapy: A Retrospective Single-Centre Analysis. Clin Oncol (R Coll Radiol). 2019;31(6):356-64.
66. Spaas M, Lievens Y. Is the Combination of Immunotherapy and Radiotherapy in Non-small Cell Lung Cancer a Feasible and Effective Approach? Frontiers in Medicine. 2019;6:244.
67. Chakraborty M, Abrams SI, Camphausen K, Liu K, Scott T, Coleman CN, et al. Irradiation of Tumor Cells Up-Regulates Fas and Enhances CTL Lytic Activity and CTL Adoptive Immunotherapy. The Journal of Immunology. 2003;170(12):6338.
68. Vanpouille-Box C, Alard A, Aryankalayil MJ, Sarfraz Y, Diamond JM, Schneider RJ, et al. DNA exonuclease Trex1 regulates radiotherapy-induced tumour immunogenicity. Nat Commun. 2017;8:15618.

69. Dorta-Estremera S, Colbert LE, Nookala SS, Yanamandra AV, Yang G, Delgado A, et al. Kinetics of Intratumoral Immune Cell Activation During Chemoradiation for Cervical Cancer. Int J Radiat Oncol Biol Phys. 2018;102(3):593-600.
70. Samstein R, Rimner A, Barker CA, Yamada Y. Combined Immune Checkpoint Blockade and Radiation Therapy: Timing and Dose Fractionation Associated with Greatest Survival Duration Among Over 750 Treated Patients. International Journal of Radiation Oncology • Biology • Physics. 2017;99(2):S129-S30.
71. Demaria S, Ng B, Devitt ML, Babb JS, Kawashima N, Liebes L, et al. Ionizing radiation inhibition of distant untreated tumors (abscopal effect) is immune mediated. Int J Radiat Oncol Biol Phys. 2004;58(3):862-70.
72. Venkatesulu BP, Mallick S, Lin SH, Krishnan S. A systematic review of the influence of radiation-induced lymphopenia on survival outcomes in solid tumors. Crit Rev Oncol Hematol. 2018;123:42-51.
73. Crocenzi T, Cottam B, Newell P, Wolf RF, Hansen PD, Hammill C, et al. A hypofractionated radiation regimen avoids the lymphopenia associated with neoadjuvant chemoradiation therapy of borderline resectable and locally advanced pancreatic adenocarcinoma. Journal for immunotherapy of cancer. 2016;4:45-.
74. Wild AT, Herman JM, Dholakia AS, Moningi S, Lu Y, Rosati LM, et al. Lymphocyte-Sparing Effect of Stereotactic Body Radiation Therapy in Patients With Unresectable Pancreatic Cancer. Int J Radiat Oncol Biol Phys. 2016;94(3):571-9.
75. Marciscano AE, Ghasemzadeh A, Nirschl TR, Theodros D, Kochel CM, Francica BJ, et al. Elective Nodal Irradiation Attenuates the Combinatorial Efficacy of Stereotactic Radiation Therapy and Immunotherapy. Clin Cancer Res. 2018;24(20):5058-71.
76. Louvel G, Bahleda R, Ammari S, Le Péchoux C, Levy A, Massard C, et al. Immunotherapy and pulmonary toxicities: can concomitant immune-checkpoint inhibitors with radiotherapy increase the risk of radiation pneumonitis? European Respiratory Journal. 2018;51(1):1701737.
77. Nagarsheth N, Wicha MS, Zou W. Chemokines in the cancer microenvironment and their relevance in cancer immunotherapy. Nat Rev Immunol. 2017;17(9):559-72.
78. Parkes EE, Walker SM, Taggart LE, McCabe N, Knight LA, Wilkinson R, et al. Activation of STING-Dependent Innate Immune Signaling By S-Phase-Specific DNA Damage in Breast Cancer. Journal of the National Cancer Institute. 2016;109(1):djw199.
79. Spranger S, Dai D, Horton B, Gajewski TF. Tumor-Residing Batf3 Dendritic Cells Are Required for Effector T Cell Trafficking and Adoptive T Cell Therapy. Cancer Cell. 2017;31(5):711-23.e4.
80. Luo R, Firat E, Gaedicke S, Guffart E, Watanabe T, Niedermann G. Cisplatin Facilitates Radiation-Induced Abscopal Effects in Conjunction with PD-1 Checkpoint Blockade Through CXCR3/CXCL10-Mediated T-cell Recruitment. Clinical Cancer Research. 2019;25(23):7243.
81. Di Maggio FM, Minafra L, Forte GI, Cammarata FP, Lio D, Messa C, et al. Portrait of inflammatory response to ionizing radiation treatment. Journal of inflammation (London, England). 2015;12:14-.
82. Hallahan D, Kuchibhotla J, Wyble C. Cell adhesion molecules mediate radiation-induced leukocyte adhesion to the vascular endothelium. Cancer Res. 1996;56(22):5150-5.
83. Formenti SC, Demaria S. Combining Radiotherapy and Cancer Immunotherapy: A Paradigm Shift. JNCI: Journal of the National Cancer Institute. 2013;105(4):256-65.
84. Langley RE, Bump EA, Quartuccio SG, Medeiros D, Braunhut SJ. Radiation-induced apoptosis in microvascular endothelial cells. Br J Cancer. 1997;75(5):666-72.
85. Heckmann M, Douwes K, Peter R, Degitz K. Vascular activation of adhesion molecule mRNA and cell surface expression by ionizing radiation. Exp Cell Res. 1998;238(1):148-54.

86. Paris F, Fuks Z, Kang A, Capodieci P, Juan G, Ehleiter D, et al. Endothelial apoptosis as the primary lesion initiating intestinal radiation damage in mice. Science. 2001;293(5528):293-7.
87. Wang J, Boerma M, Fu Q, Hauer-Jensen M. Significance of endothelial dysfunction in the pathogenesis of early and delayed radiation enteropathy. World J Gastroenterol. 2007;13(22):3047-55.
88. Oh CW, Bump EA, Kim JS, Janigro D, Mayberg MR. Induction of a senescence-like phenotype in bovine aortic endothelial cells by ionizing radiation. Radiat Res. 2001;156(3):232-40.
89. Wang Y, Boerma M, Zhou D. Ionizing Radiation-Induced Endothelial Cell Senescence and Cardiovascular Diseases. Radiation research. 2016;186(2):153-61.
90. Moeller BJ, Cao Y, Li CY, Dewhirst MW. Radiation activates HIF-1 to regulate vascular radiosensitivity in tumors: Role of reoxygenation, free radicals, and stress granules. Cancer Cell. 2004;5(5):429-41.
91. Edwards E, Geng L, Tan J, Onishko H, Donnelly E, Hallahan DE. Phosphatidylinositol 3-kinase/Akt signaling in the response of vascular endothelium to ionizing radiation. Cancer Res. 2002;62(16):4671-7.
92. Abdollahi A, Griggs DW, Zieher H, Roth A, Lipson KE, Saffrich R, et al. Inhibition of alpha(v)beta3 integrin survival signaling enhances antiangiogenic and antitumor effects of radiotherapy. Clin Cancer Res. 2005;11(17):6270-9.
93. Nguemgo Kouam P, Bühler H, Hero T, Adamietz IA. The increased adhesion of tumor cells to endothelial cells after irradiation can be reduced by FAK-inhibition. Radiation Oncology. 2019;14(1):25.
94. Baker DG, Krochak RJ. The response of the microvascular system to radiation: a review. Cancer Invest. 1989;7(3):287-94.
95. Hoving S, Heeneman S, Gijbels MJ, te Poele JA, Russell NS, Daemen MJ, et al. Single-dose and fractionated irradiation promote initiation and progression of atherosclerosis and induce an inflammatory plaque phenotype in ApoE(-/-) mice. Int J Radiat Oncol Biol Phys. 2008;71(3):848-57.
96. Chin MS, Freniere BB, Bonney CF, Lancerotto L, Saleeby JH, Lo YC, et al. Skin perfusion and oxygenation changes in radiation fibrosis. Plast Reconstr Surg. 2013;131(4):707-16.
97. Jain RK. Molecular regulation of vessel maturation. Nat Med. 2003;9(6):685-93.
98. Denekamp J. Vascular endothelium as the vulnerable element in tumours. Acta Radiol Oncol. 1984;23(4):217-25.
99. Garcia-Barros M, Paris F, Cordon-Cardo C, Lyden D, Rafii S, Haimovitz-Friedman A, et al. Tumor response to radiotherapy regulated by endothelial cell apoptosis. Science. 2003;300(5622):1155-9.
100. Kioi M, Vogel H, Schultz G, Hoffman RM, Harsh GR, Brown JM. Inhibition of vasculogenesis, but not angiogenesis, prevents the recurrence of glioblastoma after irradiation in mice. J Clin Invest. 2010;120(3):694-705.
101. Kozin SV, Kamoun WS, Huang Y, Dawson MR, Jain RK, Duda DG. Recruitment of myeloid but not endothelial precursor cells facilitates tumor regrowth after local irradiation. Cancer Res. 2010;70(14):5679-85.
102. Lerman OZ, Greives MR, Singh SP, Thanik VD, Chang CC, Seiser N, et al. Low-dose radiation augments vasculogenesis signaling through HIF-1-dependent and -independent SDF-1 induction. Blood. 2010;116(18):3669-76.
103. Dewhirst MW, Kimura H, Rehmus SW, Braun RD, Papahadjopoulos D, Hong K, et al. Microvascular studies on the origins of perfusion-limited hypoxia. Br J Cancer Suppl. 1996;27:S247-51.

104. Brizel DM, Sibley GS, Prosnitz LR, Scher RL, Dewhirst MW. Tumor hypoxia adversely affects the prognosis of carcinoma of the head and neck. Int J Radiat Oncol Biol Phys. 1997;38(2):285-9.
105. van den Beucken T, Koch E, Chu K, Rupaimoole R, Prickaerts P, Adriaens M, et al. Hypoxia promotes stem cell phenotypes and poor prognosis through epigenetic regulation of DICER. Nat Commun. 2014;5:5203.
106. Al-Assar O, Demiciorglu F, Lunardi S, Gaspar-Carvalho MM, McKenna WG, Muschel RM, et al. Contextual regulation of pancreatic cancer stem cell phenotype and radioresistance by pancreatic stellate cells. Radiotherapy and Oncology. 2014;111(2):243-51.
107. Rockwell S, Dobrucki IT, Kim EY, Marrison ST, Vu VT. Hypoxia and radiation therapy: past history, ongoing research, and future promise. Curr Mol Med. 2009;9(4):442-58.
108. Semenza GL, Wang GL. A nuclear factor induced by hypoxia via de novo protein synthesis binds to the human erythropoietin gene enhancer at a site required for transcriptional activation. Mol Cell Biol. 1992;12(12):5447-54.
109. Kim Y-H, Yoo K-C, Cui Y-H, Uddin N, Lim E-J, Kim M-J, et al. Radiation promotes malignant progression of glioma cells through HIF-1alpha stabilization. Cancer Letters. 2014;354(1):132-41.
110. Luo W, Hu H, Chang R, Zhong J, Knabel M, O'Meally R, et al. Pyruvate Kinase M2 Is a PHD3-Stimulated Coactivator for Hypoxia-Inducible Factor 1. Cell. 2011;145(5):732-44.
111. Semenza GL, Jiang BH, Leung SW, Passantino R, Concordet JP, Maire P, et al. Hypoxia response elements in the aldolase A, enolase 1, and lactate dehydrogenase A gene promoters contain essential binding sites for hypoxia-inducible factor 1. J Biol Chem. 1996;271(51):32529-37.
112. Koukourakis MI, Giatromanolaki A, Panteliadou M, Pouliliou SE, Chondrou PS, Mavropoulou S, et al. Lactate dehydrogenase 5 isoenzyme overexpression defines resistance of prostate cancer to radiotherapy. British journal of cancer. 2014;110(9):2217-23.
113. Brand A, Singer K, Koehl Gudrun E, Kolitzus M, Schoenhammer G, Thiel A, et al. LDHA-Associated Lactic Acid Production Blunts Tumor Immunosurveillance by T and NK Cells. Cell Metabolism. 2016;24(5):657-71.
114. Lee DC, Sohn HA, Park ZY, Oh S, Kang YK, Lee KM, et al. A lactate-induced response to hypoxia. Cell. 2015;161(3):595-609.
115. Singh D, Arora R, Kaur P, Singh B, Mannan R, Arora S. Overexpression of hypoxia-inducible factor and metabolic pathways: possible targets of cancer. Cell & bioscience. 2017;7:62-.
116. Ren L, Yu Y, Wang L, Zhu Z, Lu R, Yao Z. Hypoxia-induced CCL28 promotes recruitment of regulatory T cells and tumor growth in liver cancer. Oncotarget. 2016;7(46):75763-73.
117. Ke X, Chen C, Song Y, Cai Q, Li J, Tang Y, et al. Hypoxia modifies the polarization of macrophages and their inflammatory microenvironment, and inhibits malignant behavior in cancer cells. Oncology letters. 2019;18(6):5871-8.
118. Doedens AL, Stockmann C, Rubinstein MP, Liao D, Zhang N, DeNardo DG, et al. Macrophage expression of hypoxia-inducible factor-1 alpha suppresses T-cell function and promotes tumor progression. Cancer Res. 2010;70(19):7465-75.
119. Corzo CA, Condamine T, Lu L, Cotter MJ, Youn JI, Cheng P, et al. HIF-1alpha regulates function and differentiation of myeloid-derived suppressor cells in the tumor microenvironment. J Exp Med. 2010;207(11):2439-53.
120. Sceneay J, Chow MT, Chen A, Halse HM, Wong CS, Andrews DM, et al. Primary tumor hypoxia recruits CD11b+/Ly6Cmed/Ly6G+ immune suppressor cells and compromises NK cell cytotoxicity in the premetastatic niche. Cancer Res. 2012;72(16):3906-11.
121. Kojima Y, Acar A, Eaton EN, Mellody KT, Scheel C, Ben-Porath I, et al. Autocrine TGF-beta and stromal cell-derived factor-1 (SDF-1) signaling drives the evolution of tumor-

promoting mammary stromal myofibroblasts. Proc Natl Acad Sci U S A. 2010;107(46):20009-14.
122. Liu Y, Meyer C, Muller A, Herweck F, Li Q, Mullenbach R, et al. IL-13 induces connective tissue growth factor in rat hepatic stellate cells via TGF-beta-independent Smad signaling. J Immunol. 2011;187(5):2814-23.
123. Wang Z, Tang Y, Tan Y, Wei Q, Yu W. Cancer-associated fibroblasts in radiotherapy: challenges and new opportunities. Cell communication and signaling : CCS. 2019;17(1):47-.
124. Arnold CR, Mangesius J, Skvortsova, II, Ganswindt U. The Role of Cancer Stem Cells in Radiation Resistance. Front Oncol. 2020;10:164.
125. Boelens MC, Wu TJ, Nabet BY, Xu B, Qiu Y, Yoon T, et al. Exosome transfer from stromal to breast cancer cells regulates therapy resistance pathways. Cell. 2014;159(3):499-513.
126. Park CC, Zhang HJ, Yao ES, Park CJ, Bissell MJ. Beta1 integrin inhibition dramatically enhances radiotherapy efficacy in human breast cancer xenografts. Cancer research. 2008;68(11):4398-405.
127. Sun Y, Campisi J, Higano C, Beer TM, Porter P, Coleman I, et al. Treatment-induced damage to the tumor microenvironment promotes prostate cancer therapy resistance through WNT16B. Nature medicine. 2012;18(9):1359-68.
128. Wujanto C, Vellayappan B, Siva S, Louie AV, Guckenberger M, Slotman BJ, et al. Stereotactic Body Radiotherapy for Oligometastatic Disease in Non-small Cell Lung Cancer. Frontiers in Oncology. 2019;9:1219.
129. Manda K, Glasow A, Paape D, Hildebrandt G. Effects of ionizing radiation on the immune system with special emphasis on the interaction of dendritic and T cells. Frontiers in oncology. 2012;2:102-.
130. Cao MD, Chen ZD, Xing Y. Gamma irradiation of human dendritic cells influences proliferation and cytokine profile of T cells in autologous mixed lymphocyte reaction. Cell Biol Int. 2004;28(3):223-8.
131. Dewey WC, Ling CC, Meyn RE. Radiation-induced apoptosis: Relevance to radiotherapy. International Journal of Radiation Oncology*Biology*Physics. 1995;33(4):781-96.
132. Kachikwu EL, Iwamoto KS, Liao YP, DeMarco JJ, Agazaryan N, Economou JS, et al. Radiation enhances regulatory T cell representation. Int J Radiat Oncol Biol Phys. 2011;81(4):1128-35.
133. Gao H, Dong Z, Gong X, Dong J, Zhang Y, Wei W, et al. Effects of various radiation doses on induced T-helper cell differentiation and related cytokine secretion. Journal of radiation research. 2018;59(4):395-403.
134. Tabi Z, Spary LK, Coleman S, Clayton A, Mason MD, Staffurth J. Resistance of CD45RA- T cells to apoptosis and functional impairment, and activation of tumor-antigen specific T cells during radiation therapy of prostate cancer. J Immunol. 2010;185(2):1330-9.
135. Schaue D, Comin-Anduix B, Ribas A, Zhang L, Goodglick L, Sayre JW, et al. T-cell responses to survivin in cancer patients undergoing radiation therapy. Clin Cancer Res. 2008;14(15):4883-90.
136. Hareyama M, Imai K, Oouchi A, Takahashi H, Hinoda Y, Tsujisaki M, et al. The effect of radiation on the expression of intercellular adhesion molecule-1 of human adenocarcinoma cells. Int J Radiat Oncol Biol Phys. 1998;40(3):691-6.
137. Lugade AA, Moran JP, Gerber SA, Rose RC, Frelinger JG, Lord EM. Local radiation therapy of B16 melanoma tumors increases the generation of tumor antigen-specific effector cells that traffic to the tumor. J Immunol. 2005;174(12):7516-23.
138. Morisada M, Clavijo PE, Moore E, Sun L, Chamberlin M, Van Waes C, et al. PD-1 blockade reverses adaptive immune resistance induced by high-dose hypofractionated but not low-dose daily fractionated radiation. Oncoimmunology. 2018;7(3):e1395996.

139. Lee Y, Auh SL, Wang Y, Burnette B, Meng Y, Beckett M, et al. Therapeutic effects of ablative radiation on local tumor require CD8+ T cells: changing strategies for cancer treatment. Blood. 2009;114(3):589-95.
140. Verbrugge I, Hagekyriakou J, Sharp LL, Galli M, West A, McLaughlin NM, et al. Radiotherapy increases the permissiveness of established mammary tumors to rejection by immunomodulatory antibodies. Cancer Res. 2012;72(13):3163-74.
141. Filatenkov A, Baker J, Mueller AM, Kenkel J, Ahn GO, Dutt S, et al. Ablative Tumor Radiation Can Change the Tumor Immune Cell Microenvironment to Induce Durable Complete Remissions. Clin Cancer Res. 2015;21(16):3727-39.
142. Galon J, Bruni D. Approaches to treat immune hot, altered and cold tumours with combination immunotherapies. Nature Reviews Drug Discovery. 2019;18(3):197-218.
143. Dovedi SJ, Adlard AL, Lipowska-Bhalla G, McKenna C, Jones S, Cheadle EJ, et al. Acquired resistance to fractionated radiotherapy can be overcome by concurrent PD-L1 blockade. Cancer Res. 2014;74(19):5458-68.
144. Tang H, Liang Y, Anders RA, Taube JM, Qiu X, Mulgaonkar A, et al. PD-L1 on host cells is essential for PD-L1 blockade-mediated tumor regression. J Clin Invest. 2018;128(2):580-8.
145. Herbst RS, Soria JC, Kowanetz M, Fine GD, Hamid O, Gordon MS, et al. Predictive correlates of response to the anti-PD-L1 antibody MPDL3280A in cancer patients. Nature. 2014;515(7528):563-7.
146. Maity A, Mick R, Huang AC, George SM, Farwell MD, Lukens JN, et al. A phase I trial of pembrolizumab with hypofractionated radiotherapy in patients with metastatic solid tumours. Br J Cancer. 2018;119(10):1200-7.
147. Tree AC, Jones K, Hafeez S, Sharabiani MTA, Harrington KJ, Lalondrelle S, et al. Dose-limiting Urinary Toxicity With Pembrolizumab Combined With Weekly Hypofractionated Radiation Therapy in Bladder Cancer. Int J Radiat Oncol Biol Phys. 2018;101(5):1168-71.
148. Argyle D, Kitamura T. Targeting Macrophage-Recruiting Chemokines as a Novel Therapeutic Strategy to Prevent the Progression of Solid Tumors. Front Immunol. 2018;9:2629.
149. Formenti SC, Lee P, Adams S, Goldberg JD, Li X, Xie MW, et al. Focal Irradiation and Systemic TGFbeta Blockade in Metastatic Breast Cancer. Clin Cancer Res. 2018;24(11):2493-504.
150. Wennerberg E, Spada S, Rudqvist N-P, Lhuillier C, Gruber S, Chen Q, et al. CD73 blockade promotes dendritic cell infiltration of irradiated tumors and tumor rejection. Cancer Immunology Research. 2020:canimm.0449.2019.
151. McLaughlin M, Patin EC, Pedersen M, Wilkins A, Dillon MT, Melcher AA, et al. Inflammatory microenvironment remodelling by tumour cells after radiotherapy. Nature Reviews Cancer. 2020.
152. Pilié PG, Tang C, Mills GB, Yap TA. State-of-the-art strategies for targeting the DNA damage response in cancer. Nature Reviews Clinical Oncology. 2019;16(2):81-104.
153. Dillon MT, Barker HE, Pedersen M, Hafsi H, Bhide SA, Newbold KL, et al. Radiosensitization by the ATR Inhibitor AZD6738 through Generation of Acentric Micronuclei. Mol Cancer Ther. 2017;16(1):25-34.
154. Vendetti FP, Karukonda P, Clump DA, Teo T, Lalonde R, Nugent K, et al. ATR kinase inhibitor AZD6738 potentiates CD8+ T cell-dependent antitumor activity following radiation. J Clin Invest. 2018;128(9):3926-40.
155. Dillon MT, Boylan Z, Smith D, Guevara J, Mohammed K, Peckitt C, et al. PATRIOT: A phase I study to assess the tolerability, safety and biological effects of a specific ataxia telangiectasia and Rad3-related (ATR) inhibitor (AZD6738) as a single agent and in combination with palliative radiation therapy in patients with solid tumours. Clin Transl Radiat Oncol. 2018;12:16-20.

156. Patel P, Sun L, Robbins Y, Clavijo PE, Friedman J, Silvin C, et al. Enhancing direct cytotoxicity and response to immune checkpoint blockade following ionizing radiation with Wee1 kinase inhibition. Oncoimmunology. 2019;8(11):e1638207.
157. Power R, Lowery MA, Reynolds JV, Dunne MR. The Cancer-Immune Set Point in Oesophageal Cancer. Frontiers in Oncology. 2020;10:891.
158. Lynam-Lennon N, Reynolds JV, Pidgeon GP, Lysaght J, Marignol L, Maher SG. Alterations in DNA repair efficiency are involved in the radioresistance of esophageal adenocarcinoma. Radiat Res. 2010;174(6):703-11.
159. Yao R, Feng WT, Xu LJ, Zhong XM, Liu H, Sun Y, et al. DUXAP10 regulates proliferation and apoptosis of chronic myeloid leukemia via PTEN pathway. Eur Rev Med Pharmacol Sci. 2018;22(15):4934-40.
160. Smyth EC, Lagergren J, Fitzgerald RC, Lordick F, Shah MA, Lagergren P, et al. Oesophageal cancer. Nature Reviews Disease Primers. 2017;3(1):17048.
161. Lagergren J, Smyth E, Cunningham D, Lagergren P. Oesophageal cancer. The Lancet. 2017;390(10110):2383-96.
162. van Hagen P, Hulshof MCCM, van Lanschot JJB, Steyerberg EW, Henegouwen MIvB, Wijnhoven BPL, et al. Preoperative Chemoradiotherapy for Esophageal or Junctional Cancer. New England Journal of Medicine. 2012;366(22):2074-84.
163. Minsky BD, Pajak TF, Ginsberg RJ, Pisansky TM, Martenson J, Komaki R, et al. INT 0123 (Radiation Therapy Oncology Group 94-05) phase III trial of combined-modality therapy for esophageal cancer: high-dose versus standard-dose radiation therapy. J Clin Oncol. 2002;20(5):1167-74.
164. Nemoto K, Kawashiro S, Toh Y, Numasaki H, Tachimori Y, Uno T, et al. Comparison of the effects of radiotherapy doses of 50.4 Gy and 60 Gy on outcomes of chemoradiotherapy for thoracic esophageal cancer: subgroup analysis based on the Comprehensive Registry of Esophageal Cancer in Japan from 2009 to 2011 by the Japan Esopha. Esophagus. 2020;17(2):122-6.
165. Liu L, Yang Y, Guo Q, Ren B, Peng Q, Zou L, et al. Comparing hypofractionated to conventional fractionated radiotherapy in postmastectomy breast cancer: a meta-analysis and systematic review. Radiation Oncology. 2020;15(1).
166. Whelan TJ, Pignol J-P, Levine MN, Julian JA, Mackenzie R, Parpia S, et al. Long-Term Results of Hypofractionated Radiation Therapy for Breast Cancer. New England Journal of Medicine. 2010;362(6):513-20.
167. Murray Brunt A, Haviland JS, Wheatley DA, Sydenham MA, Alhasso A, Bloomfield DJ, et al. Hypofractionated breast radiotherapy for 1 week versus 3 weeks (FAST-Forward): 5-year efficacy and late normal tissue effects results from a multicentre, non-inferiority, randomised, phase 3 trial. The Lancet. 2020;395(10237):1613-26.
168. Widmark A, Gunnlaugsson A, Beckman L, Thellenberg-Karlsson C, Hoyer M, Lagerlund M, et al. Ultra-hypofractionated versus conventionally fractionated radiotherapy for prostate cancer: 5-year outcomes of the HYPO-RT-PC randomised, non-inferiority, phase 3 trial. The Lancet. 2019;394(10196):385-95.
169. Dearnaley D, Syndikus I, Mossop H, Khoo V, Birtle A, Bloomfield D, et al. Conventional versus hypofractionated high-dose intensity-modulated radiotherapy for prostate cancer: 5-year outcomes of the randomised, non-inferiority, phase 3 CHHiP trial. The Lancet Oncology. 2016;17(8):1047-60.
170. Donohoe CL, O'Farrell NJ, Grant T, King S, Clarke L, Muldoon C, et al. Classification of Pathologic Response to Neoadjuvant Therapy in Esophageal and Junctional Cancer: Assessment of Existing Measures and Proposal of a Novel 3-Point Standard. Annals of Surgery. 2013;258(5).
171. Noble F, Lloyd MA, Turkington R, Griffiths E, O'Donovan M, O'Neill JR, et al. Multicentre cohort study to define and validate pathological assessment of response to

neoadjuvant therapy in oesophagogastric adenocarcinoma. BJS (British Journal of Surgery). 2017;104(13):1816-28.
172. Iwai Y, Ishida M, Tanaka Y, Okazaki T, Honjo T, Minato N. Involvement of PD-L1 on tumor cells in the escape from host immune system and tumor immunotherapy by PD-L1 blockade. Proc Natl Acad Sci U S A. 2002;99(19):12293-7.
173. Chen DS, Mellman I. Elements of cancer immunity and the cancer-immune set point. Nature. 2017;541(7637):321-30.
174. Kelly RJ, Ajani JA, Kuzdzal J, Zander T, Van Cutsem E, Piessen G, et al. LBA9_PR Adjuvant nivolumab in resected esophageal or gastroesophageal junction cancer (EC/GEJC) following neoadjuvant chemoradiation therapy (CRT): First results of the CheckMate 577 study. Annals of Oncology. 2020;31:S1193-S4.
175. Donlon NE, Power R, Hayes C, Reynolds JV, Lysaght J. Radiotherapy, immunotherapy, and the tumour microenvironment: Turning an immunosuppressive milieu into a therapeutic opportunity. Cancer Letters. 2021.
176. Deng L, Liang H, Xu M, Yang X, Burnette B, Arina A, et al. STING-Dependent Cytosolic DNA Sensing Promotes Radiation-Induced Type I Interferon-Dependent Antitumor Immunity in Immunogenic Tumors. Immunity. 2014;41(5):843-52.
177. Hou Y, Liang H, Rao E, Zheng W, Huang X, Deng L, et al. Non-canonical NF-κB Antagonizes STING Sensor-Mediated DNA Sensing in Radiotherapy. Immunity. 2018;49(3):490-503.e4.
178. Kugeratski FG, Atkinson SJ, Neilson LJ, Lilla S, Knight JRP, Serneels J, et al. Hypoxic cancer-associated fibroblasts increase NCBP2-AS2/HIAR to promote endothelial sprouting through enhanced VEGF signaling. Sci Signal. 2019;12(567).
179. Ziani L, Buart S, Chouaib S, Thiery J. Hypoxia increases melanoma-associated fibroblasts immunosuppressive potential and inhibitory effect on T cell-mediated cytotoxicity. Oncoimmunology. 2021;10(1):1950953.
180. Kelly RJ, Ajani JA, Kuzdzal J, Zander T, Van Cutsem E, Piessen G, et al. Adjuvant Nivolumab in Resected Esophageal or Gastroesophageal Junction Cancer. N Engl J Med. 2021;384(13):1191-203.
181. Gong J, Le TQ, Massarelli E, Hendifar AE, Tuli R. Radiation therapy and PD-1/PD-L1 blockade: the clinical development of an evolving anticancer combination. J Immunother Cancer. 2018;6(1):46.
182. Zhao Y, Chen D, Wang W, Zhao T, Wen J, Zhang F, et al. Significance of TIM-3 Expression in Resected Esophageal Squamous Cell Carcinoma. Ann Thorac Surg. 2020;109(5):1551-7.
183. Lyu J, Liu T, Li T, Li F, Wang Q, Wang J, et al. Comparison of efficacy, safety, and costs between neoadjuvant hypofractionated radiotherapy and conventionally fractionated radiotherapy for esophageal carcinoma. Cancer Med. 2019;8(8):3710-8.
184. Wang J, Yu J, Jiang Y, Pei D, Zhu H, Wang J. Hypofractionated Radiotherapy in Combination With Chemotherapy Improves Outcome of Patients With Esophageal Carcinoma Tracheoesophageal Groove Lymph Node Metastasis. Front Oncol. 2020;10:1540.
185. Haibe Y, Kreidieh M, El Hajj H, Khalifeh I, Mukherji D, Temraz S, et al. Resistance Mechanisms to Anti-angiogenic Therapies in Cancer. Front Oncol. 2020;10:221.
186. Macarulla T, Montagut C, Sánchez-Martin FJ, Granja M, Verdaguer H, Sastre J, et al. The role of PIGF blockade in the treatment of colorectal cancer: overcoming the pitfalls. Expert Opin Biol Ther. 2020;20(1):15-22.
187. Qian BZ, Zhang H, Li J, He T, Yeo EJ, Soong DY, et al. FLT1 signaling in metastasis-associated macrophages activates an inflammatory signature that promotes breast cancer metastasis. J Exp Med. 2015;212(9):1433-48.

188. Wei SC, Tsao PN, Weng MT, Cao Z, Wong JM. Flt-1 in colorectal cancer cells is required for the tumor invasive effect of placental growth factor through a p38-MMP9 pathway. J Biomed Sci. 2013;20(1):39.
189. Tian Y, Zajac AJ. IL-21 and T Cell Differentiation: Consider the Context. Trends Immunol. 2016;37(8):557-68.
190. Deng S, Sun Z, Qiao J, Liang Y, Liu L, Dong C, et al. Targeting tumors with IL-21 reshapes the tumor microenvironment by proliferating PD-1intTim-3-CD8+ T cells. JCI Insight. 2020;5(7).
191. Li Y, Cong Y, Jia M, He Q, Zhong H, Zhao Y, et al. Targeting IL-21 to tumor-reactive T cells enhances memory T cell responses and anti-PD-1 antibody therapy. Nat Commun. 2021;12(1):951.
192. Davidi S, Fremder E, Kan T, Raviv Z, Timaner M, Karin N, et al. The antiangiogenic role of the pro-inflammatory cytokine interleukin-31. Oncotarget. 2017;8(10):16430-44.
193. Kan T, Feldman E, Timaner M, Raviv Z, Shen-Orr S, Aronheim A, et al. IL-31 induces antitumor immunity in breast carcinoma. J Immunother Cancer. 2020;8(2).
194. Teng MW, Andrews DM, McLaughlin N, von Scheidt B, Ngiow SF, Möller A, et al. IL-23 suppresses innate immune response independently of IL-17A during carcinogenesis and metastasis. Proc Natl Acad Sci U S A. 2010;107(18):8328-33.
195. Yan J, Smyth MJ, Teng MWL. Interleukin (IL)-12 and IL-23 and Their Conflicting Roles in Cancer. Cold Spring Harb Perspect Biol. 2018;10(7).
196. Allin KH, Nordestgaard BG. Elevated C-reactive protein in the diagnosis, prognosis, and cause of cancer. Crit Rev Clin Lab Sci. 2011;48(4):155-70.
197. Liu S, Liang J, Liu Z, Zhang C, Wang Y, Watson AH, et al. The Role of CD276 in Cancers. Front Oncol. 2021;11:654684.
198. Dong P, Xiong Y, Yue J, Hanley SJB, Watari H. B7H3 As a Promoter of Metastasis and Promising Therapeutic Target. Front Oncol. 2018;8:264.
199. Xie C, Liu D, Chen Q, Yang C, Wang B, Wu H. Soluble B7-H3 promotes the invasion and metastasis of pancreatic carcinoma cells through the TLR4/NF-κB pathway. Sci Rep. 2016;6:27528.
200. Dai W, Shen G, Qiu J, Zhao X, Gao Q. Aberrant expression of B7-H3 in gastric adenocarcinoma promotes cancer cell metastasis. Oncol Rep. 2014;32(5):2086-92.
201. Beckermann KE, Hongo R, Ye X, Young K, Carbonell K, Healey DCC, et al. CD28 costimulation drives tumor-infiltrating T cell glycolysis to promote inflammation. JCI Insight. 2020;5(16).
202. Haile ST, Dalal SP, Clements V, Tamada K, Ostrand-Rosenberg S. Soluble CD80 restores T cell activation and overcomes tumor cell programmed death ligand 1-mediated immune suppression. J Immunol. 2013;191(5):2829-36.
203. Zhu MMT, Burugu S, Gao D, Yu J, Kos Z, Leung S, et al. Evaluation of glucocorticoid-induced TNF receptor (GITR) expression in breast cancer and across multiple tumor types. Mod Pathol. 2020;33(9):1753-63.
204. van Beek AA, Zhou G, Doukas M, Boor PPC, Noordam L, Mancham S, et al. GITR ligation enhances functionality of tumor-infiltrating T cells in hepatocellular carcinoma. Int J Cancer. 2019;145(4):1111-24.
205. Liu M, Xing LQ. Basic fibroblast growth factor as a potential biomarker for diagnosing malignant tumor metastasis in women. Oncol Lett. 2017;14(2):1561-7.
206. Redmond WL, Ruby CE, Weinberg AD. The role of OX40-mediated co-stimulation in T-cell activation and survival. Crit Rev Immunol. 2009;29(3):187-201.
207. Willoughby J, Griffiths J, Tews I, Cragg MS. OX40: Structure and function - What questions remain? Mol Immunol. 2017;83:13-22.
208. Weixler B, Cremonesi E, Sorge R, Muraro MG, Delko T, Nebiker CA, et al. OX40 expression enhances the prognostic significance of CD8 positive lymphocyte infiltration in colorectal cancer. Oncotarget. 2015;6(35):37588-99.

209. Donlon NE, Elliott JA, Donohoe CL, Murphy CF, Nugent T, Moran B, et al. Adverse Biology in Adenocarcinoma of the Esophagus and Esophagogastric Junction Impacts Survival and Response to Neoadjuvant Therapy Independent of Anatomic Subtype. Ann Surg. 2020;272(5):814-9.
210. Donlon NE, Sheppard A, Davern M, O'Connell F, Phelan JJ, Power R, et al. Linking Circulating Serum Proteins with Clinical Outcomes in Esophageal Adenocarcinoma-An Emerging Role for Chemokines. Cancers (Basel). 2020;12(11).
211. Tomasello G, Petrelli F, Ghidini M, Pezzica E, Passalacqua R, Steccanella F, et al. Tumor regression grade and survival after neoadjuvant treatment in gastro-esophageal cancer: A meta-analysis of 17 published studies. Eur J Surg Oncol. 2017;43(9):1607-16.
212. Kelsen DP, Ginsberg R, Pajak TF, Sheahan DG, Gunderson L, Mortimer J, et al. Chemotherapy followed by surgery compared with surgery alone for localized esophageal cancer. N Engl J Med. 1998;339(27):1979-84.
213. Korst RJ, Kansler AL, Port JL, Lee PC, Kerem Y, Altorki NK. Downstaging of T or N Predicts Long-Term Survival After Preoperative Chemotherapy and Radical Resection for Esophageal Carcinoma. The Annals of Thoracic Surgery. 2006;82(2):480-5.
214. Matsuyama J, Doki Y, Yasuda T, Miyata H, Fujiwara Y, Takiguchi S, et al. The effect of neoadjuvant chemotherapy on lymph node micrometastases in squamous cell carcinomas of the thoracic esophagus. Surgery. 2007;141(5):570-80.
215. Lou F, Sima CS, Adusumilli PS, Bains MS, Sarkaria IS, Rusch VW, et al. Esophageal cancer recurrence patterns and implications for surveillance. J Thorac Oncol. 2013;8(12):1558-62.
216. Matzner P, Sandbank E, Neeman E, Zmora O, Gottumukkala V, Ben-Eliyahu S. Harnessing cancer immunotherapy during the unexploited immediate perioperative period. Nat Rev Clin Oncol. 2020.
217. Benish M, Ben-Eliyahu S. Surgery as a double-edged sword: a clinically feasible approach to overcome the metastasis-promoting effects of surgery by blunting stress and prostaglandin responses. Cancers (Basel). 2010;2(4):1929-51.
218. Brown M, Assen FP, Leithner A, Abe J, Schachner H, Asfour G, et al. Lymph node blood vessels provide exit routes for metastatic tumor cell dissemination in mice. Science. 2018;359(6382):1408.
219. Pereira ER, Kedrin D, Seano G, Gautier O, Meijer EFJ, Jones D, et al. Lymph node metastases can invade local blood vessels, exit the node, and colonize distant organs in mice. Science. 2018;359(6382):1403.
220. Halsted WS. THE RESULTS OF RADICAL OPERATIONS FOR THE CURE OF CARCINOMA OF THE BREAST.*. Annals of Surgery. 1907;46(1).
221. Rice TW, Ishwaran H, Hofstetter WL, Schipper PH, Kesler KA, Law S, et al. Esophageal Cancer: Associations With (pN+) Lymph Node Metastases. Annals of Surgery. 2017;265(1).
222. Peyre CG, Hagen JA, DeMeester SR, Altorki NK, Ancona E, Griffin SM, et al. The number of lymph nodes removed predicts survival in esophageal cancer: an international study on the impact of extent of surgical resection. Ann Surg. 2008;248(4):549-56.
223. Mariette C, Piessen G, Briez N, Triboulet JP. The number of metastatic lymph nodes and the ratio between metastatic and examined lymph nodes are independent prognostic factors in esophageal cancer regardless of neoadjuvant chemoradiation or lymphadenectomy extent. Ann Surg. 2008;247(2):365-71.
224. Barbour AP, Jones M, Gonen M, Gotley DC, Thomas J, Thomson DB, et al. Refining esophageal cancer staging after neoadjuvant therapy: importance of treatment response. Ann Surg Oncol. 2008;15(10):2894-902.
225. Hölscher AH, Drebber U, Schmidt H, Bollschweiler E. Prognostic classification of histopathologic response to neoadjuvant therapy in esophageal adenocarcinoma. Ann Surg. 2014;260(5):779-84; discussion 84-5.

226. Mandard AM, Dalibard F, Mandard JC, Marnay J, Henry-Amar M, Petiot JF, et al. Pathologic assessment of tumor regression after preoperative chemoradiotherapy of esophageal carcinoma. Clinicopathologic correlations. Cancer. 1994;73(11):2680-6.
227. Noble F, Nolan L, Bateman AC, Byrne JP, Kelly JJ, Bailey IS, et al. Refining pathological evaluation of neoadjuvant therapy for adenocarcinoma of the esophagus. World journal of gastroenterology. 2013;19(48):9282-93.
228. Smyth EC, Fassan M, Cunningham D, Allum WH, Okines AF, Lampis A, et al. Effect of Pathologic Tumor Response and Nodal Status on Survival in the Medical Research Council Adjuvant Gastric Infusional Chemotherapy Trial. J Clin Oncol. 2016;34(23):2721-7.
229. Zanoni A, Verlato G, Giacopuzzi S, Motton M, Casella F, Weindelmayer J, et al. ypN0: Does It Matter How You Get There? Nodal Downstaging in Esophageal Cancer. Ann Surg Oncol. 2016;23(Suppl 5):998-1004.
230. Shapiro J, Biermann K, van Klaveren D, Offerhaus GJA, ten Kate FJW, Meijer SL, et al. Prognostic Value of Pretreatment Pathological Tumor Extent in Patients Treated With Neoadjuvant Chemoradiotherapy Plus Surgery for Esophageal or Junctional Cancer. Annals of Surgery. 2017;265(2).
231. Rotman J, Koster BD, Jordanova ES, Heeren AM, de Gruijl TD. Unlocking the therapeutic potential of primary tumor-draining lymph nodes. Cancer Immunology, Immunotherapy. 2019;68(10):1681-8.
232. Leach DR, Krummel MF, Allison JP. Enhancement of antitumor immunity by CTLA-4 blockade. Science. 1996;271(5256):1734-6.
233. Chen DS, Mellman I. Oncology meets immunology: the cancer-immunity cycle. Immunity. 2013;39(1):1-10.
234. van Pul KM, Vuylsteke RJCLM, van de Ven R, te Velde EA, Rutgers EJT, van den Tol PM, et al. Selectively hampered activation of lymph node-resident dendritic cells precedes profound T cell suppression and metastatic spread in the breast cancer sentinel lymph node. Journal for ImmunoTherapy of Cancer. 2019;7(1):133.
235. van de Ven R, van den Hout MF, Lindenberg JJ, Sluijter BJ, van Leeuwen PA, Lougheed SM, et al. Characterization of four conventional dendritic cell subsets in human skin-draining lymph nodes in relation to T-cell activation. Blood. 2011;118(9):2502-10.
236. Heeren AM, Koster BD, Samuels S, Ferns DM, Chondronasiou D, Kenter GG, et al. High and interrelated rates of PD-L1+CD14+ antigen-presenting cells and regulatory T cells mark the microenvironment of metastatic lymph nodes from patients with cervical cancer. Cancer Immunol Res. 2015;3(1):48-58.
237. van den Hout M, Koster BD, Sluijter BJR, Molenkamp BG, van de Ven R, van den Eertwegh AJM, et al. Melanoma Sequentially Suppresses Different DC Subsets in the Sentinel Lymph Node, Affecting Disease Spread and Recurrence. Cancer Immunol Res. 2017;5(11):969-77.
238. Alonso R, Flament H, Lemoine S, Sedlik C, Bottasso E, Péguillet I, et al. Induction of anergic or regulatory tumor-specific CD4+ T cells in the tumor-draining lymph node. Nature Communications. 2018;9(1):2113.
239. Fransen MF, Schoonderwoerd M, Knopf P, Camps MGM, Hawinkels LJAC, Kneilling M, et al. Tumor-draining lymph nodes are pivotal in PD-1/PD-L1 checkpoint therapy. JCI Insight. 2018;3(23).
240. Chamoto K, Chowdhury PS, Kumar A, Sonomura K, Matsuda F, Fagarasan S, et al. Mitochondrial activation chemicals synergize with surface receptor PD-1 blockade for T cell-dependent antitumor activity. Proc Natl Acad Sci U S A. 2017;114(5):E761-e70.
241. Hebb JPO, Mosley AR, Vences-Catalán F, Rajasekaran N, Rosén A, Ellmark P, et al. Administration of low-dose combination anti-CTLA4, anti-CD137, and anti-OX40 into murine tumor or proximal to the tumor draining lymph node induces systemic tumor regression. Cancer Immunology, Immunotherapy. 2018;67(1):47-60.

242. Donlon NE, Power R, Hayes C, Reynolds JV, Lysaght J. Radiotherapy, immunotherapy, and the tumour microenvironment: Turning an immunosuppressive milieu into a therapeutic opportunity. Cancer Lett. 2021;502:84-96.
243. Donlon NE, Power R, Hayes C, Davern M, Reynolds JV, Lysaght J. Radiation and Immunotherapy in Upper Gastrointestinal Cancers: The Current State of Play. International Journal of Molecular Sciences. 2021;22(3):1071.
244. Hodi FS, O'Day SJ, McDermott DF, Weber RW, Sosman JA, Haanen JB, et al. Improved survival with ipilimumab in patients with metastatic melanoma. N Engl J Med. 2010;363(8):711-23.
245. Aliru ML, Schoenhals JE, Venkatesulu BP, Anderson CC, Barsoumian HB, Younes AI, et al. Radiation therapy and immunotherapy: what is the optimal timing or sequencing? Immunotherapy. 2018;10(4):299-316.
246. Bakos O, Lawson C, Rouleau S, Tai LH. Combining surgery and immunotherapy: turning an immunosuppressive effect into a therapeutic opportunity. J Immunother Cancer. 2018;6(1):86.
247. Sukumar M, Kishton RJ, Restifo NP. Metabolic reprograming of anti-tumor immunity. Curr Opin Immunol. 2017;46:14-22.
248. Horowitz M, Neeman E, Sharon E, Ben-Eliyahu S. Exploiting the critical perioperative period to improve long-term cancer outcomes. Nat Rev Clin Oncol. 2015;12(4):213-26.
249. Smyth E, Knödler M, Giraut A, Mauer M, Nilsson M, Van Grieken N, et al. VESTIGE: Adjuvant Immunotherapy in Patients With Resected Esophageal, Gastroesophageal Junction and Gastric Cancer Following Preoperative Chemotherapy With High Risk for Recurrence (N+ and/or R1): An Open Label Randomized Controlled Phase-2-Study. Front Oncol. 2019;9:1320.
250. Matzner P, Sandbank E, Neeman E, Zmora O, Gottumukkala V, Ben-Eliyahu S. Harnessing cancer immunotherapy during the unexploited immediate perioperative period. Nat Rev Clin Oncol. 2020;17(5):313-26.
251. Donlon NE, Kammili A, Roopnarinesingh R, Davern M, Power R, King S, et al. FLOT-regimen Chemotherapy and Transthoracic en bloc Resection for Esophageal and Junctional Adenocarcinoma. Ann Surg. 2021.
252. Kojima T, Shah MA, Muro K, Francois E, Adenis A, Hsu CH, et al. Randomized Phase III KEYNOTE-181 Study of Pembrolizumab Versus Chemotherapy in Advanced Esophageal Cancer. J Clin Oncol. 2020;38(35):4138-48.
253. Kato K, Cho BC, Takahashi M, Okada M, Lin CY, Chin K, et al. Nivolumab versus chemotherapy in patients with advanced oesophageal squamous cell carcinoma refractory or intolerant to previous chemotherapy (ATTRACTION-3): a multicentre, randomised, open-label, phase 3 trial. Lancet Oncol. 2019;20(11):1506-17.
254. Rahman SA, Walker RC, Lloyd MA, Grace BL, van Boxel GI, Kingma BF, et al. Machine learning to predict early recurrence after oesophageal cancer surgery. Br J Surg. 2020;107(8):1042-52.
255. Kim R, Kawai A, Wakisaka M, Funaoka Y, Tasaka Y, Yasuda N, et al. Immune response induced by preoperative chemotherapy in breast cancer: Role of peripheral natural killer (pNK) cell activity, tumor-infiltrating lymphocytes (TILs), and tumor microenvironment factors (TMEFs). Journal of Clinical Oncology. 2018;36(15_suppl):e12644-e.
256. van Sandick JW, Boermeester MA, Gisbertz SS, ten Berge IJ, Out TA, van der Pouw Kraan TC, et al. Lymphocyte subsets and T(h)1/T(h)2 immune responses in patients with adenocarcinoma of the oesophagus or oesophagogastric junction: relation to pTNM stage and clinical outcome. Cancer Immunol Immunother. 2003;52(10):617-24.
257. Doi T, Piha-Paul SA, Jalal SI, Saraf S, Lunceford J, Koshiji M, et al. Safety and Antitumor Activity of the Anti–Programmed Death-1 Antibody Pembrolizumab in Patients With Advanced Esophageal Carcinoma. Journal of Clinical Oncology. 2017;36(1):61-7.

258. Stolfi C, Pallone F, Macdonald TT, Monteleone G. Interleukin-21 in cancer immunotherapy: Friend or foe? Oncoimmunology. 2012;1(3):351-4.
259. Barclay C, Li AW, Geldenhuys L, Baguma-Nibasheka M, Porter GA, Veugelers PJ, et al. Basic fibroblast growth factor (FGF-2) overexpression is a risk factor for esophageal cancer recurrence and reduced survival, which is ameliorated by coexpression of the FGF-2 antisense gene. Clin Cancer Res. 2005;11(21):7683-91.
260. Buckley AM, Lynam-Lennon N, O'Neill H, O'Sullivan J. Targeting hallmarks of cancer to enhance radiosensitivity in gastrointestinal cancers. Nat Rev Gastroenterol Hepatol. 2020;17(5):298-313.
261. Bailey SR, Nelson MH, Himes RA, Li Z, Mehrotra S, Paulos CM. Th17 Cells in Cancer: The Ultimate Identity Crisis. Frontiers in Immunology. 2014;5:276.
262. Chen D, Hu Q, Mao C, Jiao Z, Wang S, Yu L, et al. Increased IL-17-producing CD4(+) T cells in patients with esophageal cancer. Cell Immunol. 2012;272(2):166-74.
263. Pinchuk IV, Morris KT, Nofchissey RA, Earley RB, Wu J-Y, Ma TY, et al. Stromal cells induce Th17 during Helicobacter pylori infection and in the gastric tumor microenvironment. PloS one. 2013;8(1):e53798-e.
264. Liu Q, Sun Z, Chen L. Memory T cells: strategies for optimizing tumor immunotherapy. Protein Cell. 2020;11(8):549-64.
265. Ando M, Ito M, Srirat T, Kondo T, Yoshimura A. Memory T cell, exhaustion, and tumor immunity. Immunol Med. 2020;43(1):1-9.
266. Berger C, Jensen MC, Lansdorp PM, Gough M, Elliott C, Riddell SR. Adoptive transfer of effector CD8+ T cells derived from central memory cells establishes persistent T cell memory in primates. J Clin Invest. 2008;118(1):294-305.
267. Hinrichs CS, Borman ZA, Cassard L, Gattinoni L, Spolski R, Yu Z, et al. Adoptively transferred effector cells derived from naive rather than central memory CD8+ T cells mediate superior antitumor immunity. Proc Natl Acad Sci U S A. 2009;106(41):17469-74.
268. Najafi M, Hashemi Goradel N, Farhood B, Salehi E, Nashtaei MS, Khanlarkhani N, et al. Macrophage polarity in cancer: A review. J Cell Biochem. 2019;120(3):2756-65.
269. Gu D, Ao X, Yang Y, Chen Z, Xu X. Soluble immune checkpoints in cancer: production, function and biological significance. J Immunother Cancer. 2018;6(1):132.
270. Frigola X, Inman BA, Krco CJ, Liu X, Harrington SM, Bulur PA, et al. Soluble B7-H1: differences in production between dendritic cells and T cells. Immunol Lett. 2012;142(1-2):78-82.
271. Ward FJ, Dahal LN, Wijesekera SK, Abdul-Jawad SK, Kaewarpai T, Xu H, et al. The soluble isoform of CTLA-4 as a regulator of T-cell responses. Eur J Immunol. 2013;43(5):1274-85.
272. Ge W, Li J, Fan W, Xu D, Sun S. Tim-3 as a diagnostic and prognostic biomarker of osteosarcoma. Tumour Biol. 2017;39(7):1010428317715643.
273. Sorensen SF, Demuth C, Weber B, Sorensen BS, Meldgaard P. Increase in soluble PD-1 is associated with prolonged survival in patients with advanced EGFR-mutated non-small cell lung cancer treated with erlotinib. Lung Cancer. 2016;100:77-84.
274. Li N, Jilisihan B, Wang W, Tang Y, Keyoumu S. Soluble LAG3 acts as a potential prognostic marker of gastric cancer and its positive correlation with CD8+T cell frequency and secretion of IL-12 and INF-γ in peripheral blood. Cancer Biomark. 2018;23(3):341-51.
275. Fougeray S, Brignone C, Triebel F. A soluble LAG-3 protein as an immunopotentiator for therapeutic vaccines: Preclinical evaluation of IMP321. Vaccine. 2006;24(26):5426-33.
276. Vanmeerbeek I, Sprooten J, De Ruysscher D, Tejpar S, Vandenberghe P, Fucikova J, et al. Trial watch: chemotherapy-induced immunogenic cell death in immuno-oncology. Oncoimmunology. 2020;9(1):1703449.
277. Leijte GP, Custers H, Gerretsen J, Heijne A, Roth J, Vogl T, et al. Increased Plasma Levels of Danger-Associated Molecular Patterns Are Associated With Immune Suppression and

Postoperative Infections in Patients Undergoing Cytoreductive Surgery and Hyperthermic Intraperitoneal Chemotherapy. Front Immunol. 2018;9:663.
278. Tang F, Tie Y, Tu C, Wei X. Surgical trauma-induced immunosuppression in cancer: Recent advances and the potential therapies. Clin Transl Med. 2020;10(1):199-223.
279. Rabinovich GA, Gabrilovich D, Sotomayor EM. Immunosuppressive strategies that are mediated by tumor cells. Annu Rev Immunol. 2007;25:267-96.
280. Nakayamada S, Takahashi H, Kanno Y, O'Shea JJ. Helper T cell diversity and plasticity. Curr Opin Immunol. 2012;24(3):297-302.
281. Kumar V, Patel S, Tcyganov E, Gabrilovich DI. The Nature of Myeloid-Derived Suppressor Cells in the Tumor Microenvironment. Trends Immunol. 2016;37(3):208-20.
282. Mantovani A, Allavena P, Sica A, Balkwill F. Cancer-related inflammation. Nature. 2008;454(7203):436-44.
283. Loke P, Allison JP. PD-L1 and PD-L2 are differentially regulated by Th1 and Th2 cells. Proc Natl Acad Sci U S A. 2003;100(9):5336-41.
284. Maurer M, von Stebut E. Macrophage inflammatory protein-1. Int J Biochem Cell Biol. 2004;36(10):1882-6.
285. Silva TA, Ribeiro FL, Oliveira-Neto HH, Watanabe S, Alencar Rde C, Fukada SY, et al. Dual role of CCL3/CCR1 in oral squamous cell carcinoma: implications in tumor metastasis and local host defense. Oncol Rep. 2007;18(5):1107-13.
286. Youngs SJ, Ali SA, Taub DD, Rees RC. Chemokines induce migrational responses in human breast carcinoma cell lines. Int J Cancer. 1997;71(2):257-66.
287. Nobel TB, Livschitz J, Xing XX, Barbetta A, Hsu M, Tan KS, et al. Surveillance Implications of Recurrence Patterns in Early Node-Negative Esophageal Adenocarcinoma. Ann Thorac Surg. 2019;108(6):1640-7.
288. Gonzalez H, Hagerling C, Werb Z. Roles of the immune system in cancer: from tumor initiation to metastatic progression. Genes Dev. 2018;32(19-20):1267-84.
289. Janssen LME, Ramsay EE, Logsdon CD, Overwijk WW. The immune system in cancer metastasis: friend or foe? J Immunother Cancer. 2017;5(1):79.
290. Kaur P, Asea A. Radiation-induced effects and the immune system in cancer. Front Oncol. 2012;2:191.
291. Chen HHW, Kuo MT. Improving radiotherapy in cancer treatment: Promises and challenges. Oncotarget. 2017;8(37):62742-58.
292. Sato H, Demaria S, Ohno T. The role of radiotherapy in the age of immunotherapy. Jpn J Clin Oncol. 2021;51(4):513-22.
293. Olivares-Urbano MA, Griñán-Lisón C, Marchal JA, Núñez MI. CSC Radioresistance: A Therapeutic Challenge to Improve Radiotherapy Effectiveness in Cancer. Cells. 2020;9(7).
294. Kim BM, Hong Y, Lee S, Liu P, Lim JH, Lee YH, et al. Therapeutic Implications for Overcoming Radiation Resistance in Cancer Therapy. Int J Mol Sci. 2015;16(11):26880-913.
295. Fucikova J, Moserova I, Urbanova L, Bezu L, Kepp O, Cremer I, et al. Prognostic and Predictive Value of DAMPs and DAMP-Associated Processes in Cancer. Front Immunol. 2015;6:402.
296. Ashrafizadeh M, Farhood B, Eleojo Musa A, Taeb S, Najafi M. Damage-associated molecular patterns in tumor radiotherapy. Int Immunopharmacol. 2020;86:106761.
297. Spel L, Boelens JJ, Nierkens S, Boes M. Antitumor immune responses mediated by dendritic cells: How signals derived from dying cancer cells drive antigen cross-presentation. Oncoimmunology. 2013;2(11):e26403.
298. Gogolák P, Réthi B, Hajas G, Rajnavölgyi E. Targeting dendritic cells for priming cellular immune responses. J Mol Recognit. 2003;16(5):299-317.
299. Gold LI, Eggleton P, Sweetwyne MT, Van Duyn LB, Greives MR, Naylor SM, et al. Calreticulin: non-endoplasmic reticulum functions in physiology and disease. Faseb j. 2010;24(3):665-83.

300. Michalak M, Corbett EF, Mesaeli N, Nakamura K, Opas M. Calreticulin: one protein, one gene, many functions. Biochem J. 1999;344 Pt 2(Pt 2):281-92.
301. Grover A, Troudt J, Foster C, Basaraba R, Izzo A. High mobility group box 1 acts as an adjuvant for tuberculosis subunit vaccines. Immunology. 2014;142(1):111-23.
302. Walle T, Martinez Monge R, Cerwenka A, Ajona D, Melero I, Lecanda F. Radiation effects on antitumor immune responses: current perspectives and challenges. Ther Adv Med Oncol. 2018;10:1758834017742575.
303. Petrova V, Annicchiarico-Petruzzelli M, Melino G, Amelio I. The hypoxic tumour microenvironment. Oncogenesis. 2018;7(1):10.
304. Whiteside TL. The tumor microenvironment and its role in promoting tumor growth. Oncogene. 2008;27(45):5904-12.
305. Otto AM. Metabolic Constants and Plasticity of Cancer Cells in a Limiting Glucose and Glutamine Microenvironment-A Pyruvate Perspective. Front Oncol. 2020;10:596197.
306. Emami Nejad A, Najafgholian S, Rostami A, Sistani A, Shojaeifar S, Esparvarinha M, et al. The role of hypoxia in the tumor microenvironment and development of cancer stem cell: a novel approach to developing treatment. Cancer Cell Int. 2021;21(1):62.
307. Muz B, de la Puente P, Azab F, Azab AK. The role of hypoxia in cancer progression, angiogenesis, metastasis, and resistance to therapy. Hypoxia (Auckl). 2015;3:83-92.
308. Gkiouli M, Biechl P, Eisenreich W, Otto AM. Diverse Roads Taken by (13)C-Glucose-Derived Metabolites in Breast Cancer Cells Exposed to Limiting Glucose and Glutamine Conditions. Cells. 2019;8(10).
309. Lambert AW, Pattabiraman DR, Weinberg RA. Emerging Biological Principles of Metastasis. Cell. 2017;168(4):670-91.
310. Krombach J, Hennel R, Brix N, Orth M, Schoetz U, Ernst A, et al. Priming anti-tumor immunity by radiotherapy: Dying tumor cell-derived DAMPs trigger endothelial cell activation and recruitment of myeloid cells. Oncoimmunology. 2019;8(1):e1523097.
311. Zhou J, Wang G, Chen Y, Wang H, Hua Y, Cai Z. Immunogenic cell death in cancer therapy: Present and emerging inducers. J Cell Mol Med. 2019;23(8):4854-65.
312. Adjemian S, Oltean T, Martens S, Wiernicki B, Goossens V, Vanden Berghe T, et al. Ionizing radiation results in a mixture of cellular outcomes including mitotic catastrophe, senescence, methuosis, and iron-dependent cell death. Cell Death Dis. 2020;11(11):1003.
313. Carvalho HA, Villar RC. Radiotherapy and immune response: the systemic effects of a local treatment. Clinics (Sao Paulo). 2018;73(suppl 1):e557s.
314. Derer A, Deloch L, Rubner Y, Fietkau R, Frey B, Gaipl US. Radio-Immunotherapy-Induced Immunogenic Cancer Cells as Basis for Induction of Systemic Anti-Tumor Immune Responses - Pre-Clinical Evidence and Ongoing Clinical Applications. Front Immunol. 2015;6:505.
315. Storozynsky Q, Hitt MM. The Impact of Radiation-Induced DNA Damage on cGAS-STING-Mediated Immune Responses to Cancer. Int J Mol Sci. 2020;21(22).
316. Habets TH, Oth T, Houben AW, Huijskens MJ, Senden-Gijsbers BL, Schnijderberg MC, et al. Fractionated Radiotherapy with 3 x 8 Gy Induces Systemic Anti-Tumour Responses and Abscopal Tumour Inhibition without Modulating the Humoral Anti-Tumour Response. PLoS One. 2016;11(7):e0159515.
317. Yan W, Chang Y, Liang X, Cardinal JS, Huang H, Thorne SH, et al. High-mobility group box 1 activates caspase-1 and promotes hepatocellular carcinoma invasiveness and metastases. Hepatology. 2012;55(6):1863-75.
318. Tsung A, Klune JR, Zhang X, Jeyabalan G, Cao Z, Peng X, et al. HMGB1 release induced by liver ischemia involves Toll-like receptor 4 dependent reactive oxygen species production and calcium-mediated signaling. J Exp Med. 2007;204(12):2913-23.
319. Boone BA, Lotze MT. Targeting damage-associated molecular pattern molecules (DAMPs) and DAMP receptors in melanoma. Methods Mol Biol. 2014;1102:537-52.

320. Garg AD, Elsen S, Krysko DV, Vandenabeele P, de Witte P, Agostinis P. Resistance to anticancer vaccination effect is controlled by a cancer cell-autonomous phenotype that disrupts immunogenic phagocytic removal. Oncotarget. 2015;6(29):26841-60.
321. Fahmueller YN, Nagel D, Hoffmann RT, Tatsch K, Jakobs T, Stieber P, et al. Immunogenic cell death biomarkers HMGB1, RAGE, and DNAse indicate response to radioembolization therapy and prognosis in colorectal cancer patients. Int J Cancer. 2013;132(10):2349-58.
322. Chung HW, Lee SG, Kim H, Hong DJ, Chung JB, Stroncek D, et al. Serum high mobility group box-1 (HMGB1) is closely associated with the clinical and pathologic features of gastric cancer. J Transl Med. 2009;7:38.
323. Brezniceanu ML, Völp K, Bösser S, Solbach C, Lichter P, Joos S, et al. HMGB1 inhibits cell death in yeast and mammalian cells and is abundantly expressed in human breast carcinoma. Faseb j. 2003;17(10):1295-7.
324. Huebener P, Pradere JP, Hernandez C, Gwak GY, Caviglia JM, Mu X, et al. The HMGB1/RAGE axis triggers neutrophil-mediated injury amplification following necrosis. J Clin Invest. 2015;125(2):539-50.
325. Suzuki Y, Mimura K, Yoshimoto Y, Watanabe M, Ohkubo Y, Izawa S, et al. Immunogenic tumor cell death induced by chemoradiotherapy in patients with esophageal squamous cell carcinoma. Cancer Res. 2012;72(16):3967-76.
326. Hur C, Miller M, Kong CY, Dowling EC, Nattinger KJ, Dunn M, et al. Trends in esophageal adenocarcinoma incidence and mortality. Cancer. 2013;119(6):1149-58.
327. Sjoquist KM, Burmeister BH, Smithers BM, Zalcberg JR, Simes RJ, Barbour A, et al. Survival after neoadjuvant chemotherapy or chemoradiotherapy for resectable oesophageal carcinoma: an updated meta-analysis. Lancet Oncol. 2011;12(7):681-92.
328. Kelsen DP, Winter KA, Gunderson LL, Mortimer J, Estes NC, Haller DG, et al. Long-term results of RTOG trial 8911 (USA Intergroup 113): a random assignment trial comparison of chemotherapy followed by surgery compared with surgery alone for esophageal cancer. J Clin Oncol. 2007;25(24):3719-25.
329. Langer R, Becker K. Tumor regression grading of gastrointestinal cancers after neoadjuvant therapy. Virchows Arch. 2018;472(2):175-86.
330. Allum WH, Blazeby JM, Griffin SM, Cunningham D, Jankowski JA, Wong R. Guidelines for the management of oesophageal and gastric cancer. Gut. 2011;60(11):1449-72.
331. Noble F, Nolan L, Bateman AC, Byrne JP, Kelly JJ, Bailey IS, et al. Refining pathological evaluation of neoadjuvant therapy for adenocarcinoma of the esophagus. World J Gastroenterol. 2013;19(48):9282-93.
332. Schneider PM, Baldus SE, Metzger R, Kocher M, Bongartz R, Bollschweiler E, et al. Histomorphologic tumor regression and lymph node metastases determine prognosis following neoadjuvant radiochemotherapy for esophageal cancer: implications for response classification. Ann Surg. 2005;242(5):684-92.
333. Tong DK, Law S, Kwong DL, Chan KW, Lam AK, Wong KH. Histological regression of squamous esophageal carcinoma assessed by percentage of residual viable cells after neoadjuvant chemoradiation is an important prognostic factor. Ann Surg Oncol. 2010;17(8):2184-92.
334. Noble F, Lloyd MA, Turkington R, Griffiths E, O'Donovan M, O'Neill JR, et al. Multicentre cohort study to define and validate pathological assessment of response to neoadjuvant therapy in oesophagogastric adenocarcinoma. Br J Surg. 2017;104(13):1816-28.
335. Blum Murphy M, Xiao L, Patel VR, Maru DM, Correa AM, F GA, et al. Pathological complete response in patients with esophageal cancer after the trimodality approach: The association with baseline variables and survival-The University of Texas MD Anderson Cancer Center experience. Cancer. 2017;123(21):4106-13.

336. Gao A, Wang L, Li J, Li H, Han Y, Ma X, et al. Prognostic Value of Perineural Invasion in Esophageal and Esophagogastric Junction Carcinoma: A Meta-Analysis. Dis Markers. 2016;2016:7340180.
337. Law SY, Fok M, Wong J. Pattern of recurrence after oesophageal resection for cancer: clinical implications. Br J Surg. 1996;83(1):107-11.
338. Schiefer AI, Schoppmann SF, Birner P. Lymphovascular invasion of tumor cells in lymph node metastases has a negative impact on survival in esophageal cancer. Surgery. 2016;160(2):331-40.
339. Lhuillier C, Rudqvist NP, Elemento O, Formenti SC, Demaria S. Radiation therapy and anti-tumor immunity: exposing immunogenic mutations to the immune system. Genome Med. 2019;11(1):40.
340. McLaughlin M, Patin EC, Pedersen M, Wilkins A, Dillon MT, Melcher AA, et al. Inflammatory microenvironment remodelling by tumour cells after radiotherapy. Nat Rev Cancer. 2020;20(4):203-17.
341. Vacchelli E, Ma Y, Baracco EE, Sistigu A, Enot DP, Pietrocola F, et al. Chemotherapy-induced antitumor immunity requires formyl peptide receptor 1. Science. 2015;350(6263):972-8.
342. Turkington RC, Knight LA, Blayney JK, Secrier M, Douglas R, Parkes EE, et al. Immune activation by DNA damage predicts response to chemotherapy and survival in oesophageal adenocarcinoma. Gut. 2019;68(11):1918-27.
343. Noble F, Mellows T, McCormick Matthews LH, Bateman AC, Harris S, Underwood TJ, et al. Tumour infiltrating lymphocytes correlate with improved survival in patients with oesophageal adenocarcinoma. Cancer Immunol Immunother. 2016;65(6):651-62.
344. Fujiwara H, Suchi K, Okamura S, Okamura H, Umehara S, Todo M, et al. Elevated serum CRP levels after induction chemoradiotherapy reflect poor treatment response in association with IL-6 in serum and local tumor site in patients with advanced esophageal cancer. J Surg Oncol. 2011;103(1):62-8.
345. Makuuchi Y, Honda K, Osaka Y, Kato K, Kojima T, Daiko H, et al. Soluble interleukin-6 receptor is a serum biomarker for the response of esophageal carcinoma to neoadjuvant chemoradiotherapy. Cancer Sci. 2013;104(8):1045-51.
346. Kleespies A, Bruns CJ, Jauch KW. Clinical significance of VEGF-A, -C and -D expression in esophageal malignancies. Onkologie. 2005;28(5):281-8.
347. Donohoe CL, O'Farrell NJ, Grant T, King S, Clarke L, Muldoon C, et al. Classification of pathologic response to neoadjuvant therapy in esophageal and junctional cancer: assessment of existing measures and proposal of a novel 3-point standard. Ann Surg. 2013;258(5):784-92; discussion 92.
348. Vilgelm AE, Richmond A. Chemokines Modulate Immune Surveillance in Tumorigenesis, Metastasis, and Response to Immunotherapy. Front Immunol. 2019;10:333.
349. Zhou M, Bracci PM, McCoy LS, Hsuang G, Wiemels JL, Rice T, et al. Serum macrophage-derived chemokine/CCL22 levels are associated with glioma risk, CD4 T cell lymphopenia and survival time. Int J Cancer. 2015;137(4):826-36.
350. Jafarzadeh A, Fooladseresht H, Minaee K, Bazrafshani MR, Khosravimashizi A, Nemati M, et al. Higher circulating levels of chemokine CCL22 in patients with breast cancer: evaluation of the influences of tumor stage and chemokine gene polymorphism. Tumour Biol. 2015;36(2):1163-71.
351. Wei Y, Wang T, Song H, Tian L, Lyu G, Zhao L, et al. C-C motif chemokine 22 ligand (CCL22) concentrations in sera of gastric cancer patients are related to peritoneal metastasis and predict recurrence within one year after radical gastrectomy. J Surg Res. 2017;211:266-78.
352. Martinenaite E, Munir Ahmad S, Hansen M, Met Ö, Westergaard MW, Larsen SK, et al. CCL22-specific T Cells: Modulating the immunosuppressive tumor microenvironment. Oncoimmunology. 2016;5(11):e1238541.

353. Kavanagh ME, Conroy MJ, Clarke NE, Gilmartin NT, Feighery R, MacCarthy F, et al. Altered T Cell Migratory Capacity in the Progression from Barrett Oesophagus to Oesophageal Adenocarcinoma. Cancer Microenviron. 2019;12(1):57-66.
354. Lan Q, Lai W, Zeng Y, Liu L, Li S, Jin S, et al. CCL26 Participates in the PRL-3-Induced Promotion of Colorectal Cancer Invasion by Stimulating Tumor-Associated Macrophage Infiltration. Mol Cancer Ther. 2018;17(1):276-89.
355. Blanchard C, Wang N, Stringer KF, Mishra A, Fulkerson PC, Abonia JP, et al. Eotaxin-3 and a uniquely conserved gene-expression profile in eosinophilic esophagitis. J Clin Invest. 2006;116(2):536-47.
356. Goto M, Liu M. Chemokines and their receptors as biomarkers in esophageal cancer. Esophagus. 2020;17(2):113-21.
357. Li Z, Qian J, Li J, Zhu C. Clinical Significance of Serum Chemokines in Esophageal Cancer. Med Sci Monit. 2019;25:5850-5.
358. Liu K, Yang K, Wu B, Chen H, Chen X, Chen X, et al. Tumor-Infiltrating Immune Cells Are Associated With Prognosis of Gastric Cancer. Medicine (Baltimore). 2015;94(39):e1631.
359. Ikeda M, Natsugoe S, Ueno S, Baba M, Aikou T. Significant host- and tumor-related factors for predicting prognosis in patients with esophageal carcinoma. Ann Surg. 2003;238(2):197-202.
360. Nozoe T, Saeki H, Sugimachi K. Significance of preoperative elevation of serum C-reactive protein as an indicator of prognosis in esophageal carcinoma. Am J Surg. 2001;182(2):197-201.
361. Leitch EF, Chakrabarti M, Crozier JE, McKee RF, Anderson JH, Horgan PG, et al. Comparison of the prognostic value of selected markers of the systemic inflammatory response in patients with colorectal cancer. Br J Cancer. 2007;97(9):1266-70.
362. Walsh SM, Casey S, Kennedy R, Ravi N, Reynolds JV. Does the modified Glasgow Prognostic Score (mGPS) have a prognostic role in esophageal cancer? J Surg Oncol. 2016;113(7):732-7.
363. Jayson GC, Zhou C, Backen A, Horsley L, Marti-Marti K, Shaw D, et al. Plasma Tie2 is a tumor vascular response biomarker for VEGF inhibitors in metastatic colorectal cancer. Nat Commun. 2018;9(1):4672.
364. Biel NM, Siemann DW. Targeting the Angiopoietin-2/Tie-2 axis in conjunction with VEGF signal interference. Cancer Lett. 2016;380(2):525-33.
365. Zhao S, Wu D, Wu P, Wang Z, Huang J. Serum IL-10 Predicts Worse Outcome in Cancer Patients: A Meta-Analysis. PLoS One. 2015;10(10):e0139598.
366. Cohen I, Rider P, Vornov E, Tomas M, Tudor C, Wegner M, et al. IL-1α is a DNA damage sensor linking genotoxic stress signaling to sterile inflammation and innate immunity. Sci Rep. 2015;5:14756.
367. Barker HE, Paget JT, Khan AA, Harrington KJ. The tumour microenvironment after radiotherapy: mechanisms of resistance and recurrence. Nat Rev Cancer. 2015;15(7):409-25.
368. McDonnell CO, Harmey JH, Bouchier-Hayes DJ, Walsh TN. Effect of multimodality therapy on circulating vascular endothelial growth factor levels in patients with oesophageal cancer. Br J Surg. 2001;88(8):1105-9.
369. Siemann DW. The unique characteristics of tumor vasculature and preclinical evidence for its selective disruption by Tumor-Vascular Disrupting Agents. Cancer Treat Rev. 2011;37(1):63-74.
370. Haugsten EM, Wiedlocha A, Olsnes S, Wesche J. Roles of fibroblast growth factor receptors in carcinogenesis. Mol Cancer Res. 2010;8(11):1439-52.
371. Then EO, Lopez M, Saleem S, Gayam V, Sunkara T, Culliford A, et al. Esophageal Cancer: An Updated Surveillance Epidemiology and End Results Database Analysis. World J Oncol. 2020;11(2):55-64.

372. Morgan E, Soerjomataram I, Gavin AT, Rutherford MJ, Gatenby P, Bardot A, et al. International trends in oesophageal cancer survival by histological subtype between 1995 and 2014. Gut. 2021;70(2):234-42.
373. Jiang W, Chan CK, Weissman IL, Kim BYS, Hahn SM. Immune Priming of the Tumor Microenvironment by Radiation. Trends Cancer. 2016;2(11):638-45.
374. Hogan BV, Peter MB, Shenoy HG, Horgan K, Hughes TA. Surgery induced immunosuppression. Surgeon. 2011;9(1):38-43.
375. Vinay DS, Ryan EP, Pawelec G, Talib WH, Stagg J, Elkord E, et al. Immune evasion in cancer: Mechanistic basis and therapeutic strategies. Seminars in Cancer Biology. 2015;35:S185-S98.
376. Rotman J, Koster BD, Jordanova ES, Heeren AM, de Gruijl TD. Unlocking the therapeutic potential of primary tumor-draining lymph nodes. Cancer Immunol Immunother. 2019;68(10):1681-8.
377. Pereira ER, Jones D, Jung K, Padera TP. The lymph node microenvironment and its role in the progression of metastatic cancer. Semin Cell Dev Biol. 2015;38:98-105.
378. Macalindong SS, Kim KH, Nam BH, Ryu KW, Kubo N, Kim JY, et al. Effect of total number of harvested lymph nodes on survival outcomes after curative resection for gastric adenocarcinoma: findings from an eastern high-volume gastric cancer center. BMC Cancer. 2018;18(1):73.
379. Hsu JT, Le PH, Kuo CJ, Yeh TS, Jan YY. Survival impact of the number of lymph node retrieved on patients with node-negative gastric cancer: more is better? Transl Gastroenterol Hepatol. 2017;2:103.
380. Neeve SC, Robinson BW, Fear VS. The role and therapeutic implications of T cells in cancer of the lung. Clin Transl Immunology. 2019;8(8):e1076.
381. Zarour HM, Ferrone S. Cancer immunotherapy: Progress and challenges in the clinical setting. Eur J Immunol. 2011;41(6):1510-5.
382. Kumar S, Jeong Y, Ashraf MU, Bae YS. Dendritic Cell-Mediated Th2 Immunity and Immune Disorders. Int J Mol Sci. 2019;20(9).
383. Knochelmann HM, Dwyer CJ, Bailey SR, Amaya SM, Elston DM, Mazza-McCrann JM, et al. When worlds collide: Th17 and Treg cells in cancer and autoimmunity. Cell Mol Immunol. 2018;15(5):458-69.
384. Knutson KL, Disis ML. Tumor antigen-specific T helper cells in cancer immunity and immunotherapy. Cancer Immunol Immunother. 2005;54(8):721-8.
385. Decker D, Schondorf M, Bidlingmaier F, Hirner A, von Ruecker AA. Surgical stress induces a shift in the type-1/type-2 T-helper cell balance, suggesting down-regulation of cell-mediated and up-regulation of antibody-mediated immunity commensurate to the trauma. Surgery. 1996;119(3):316-25.
386. Ishikawa M, Nishioka M, Hanaki N, Miyauchi T, Kashiwagi Y, Ioki H, et al. Perioperative immune responses in cancer patients undergoing digestive surgeries. World J Surg Oncol. 2009;7:7.
387. Shah AM, Wang Z, Ma J. Glutamine Metabolism and Its Role in Immunity, a Comprehensive Review. Animals (Basel). 2020;10(2).
388. Newsholme EA, Newsholme P, Curi R. The role of the citric acid cycle in cells of the immune system and its importance in sepsis, trauma and burns. Biochem Soc Symp. 1987;54:145-62.
389. Curi R, Lagranha CJ, Doi SQ, Sellitti DF, Procopio J, Pithon-Curi TC, et al. Molecular mechanisms of glutamine action. J Cell Physiol. 2005;204(2):392-401.
390. Roth E, Oehler R, Manhart N, Exner R, Wessner B, Strasser E, et al. Regulative potential of glutamine--relation to glutathione metabolism. Nutrition. 2002;18(3):217-21.

391. Samid D, Shack S, Myers CE. Selective growth arrest and phenotypic reversion of prostate cancer cells in vitro by nontoxic pharmacological concentrations of phenylacetate. J Clin Invest. 1993;91(5):2288-95.
392. Folprecht G. Tumor mutational burden as a new biomarker for PD-1 antibody treatment in gastric cancer. Cancer Commun (Lond). 2019;39(1):74.
393. Chen C, Zhang F, Zhou N, Gu YM, Zhang YT, He YD, et al. Efficacy and safety of immune checkpoint inhibitors in advanced gastric or gastroesophageal junction cancer: a systematic review and meta-analysis. Oncoimmunology. 2019;8(5):e1581547.
394. Lønning PE. Assessing Novel Therapies Based on Late-Stage Efficacy: A Dangerous Concept? Trends in Cancer. 2020.

Appendix

Appendix Table 1; The effects of bolus dosing and fractionated dosing regimens on the expression of Calreticulin on OE33P and OE33R cell lines. Tukey's multiple comparison testing, n=3.

Tukey's multiple comparisons test	Summary	Tukey's multiple comparisons test	Summary
0Gy vs. 2Gy	**	10Gy vs. 3X8Gy	****
0Gy vs. 10Gy	**	10Gy vs. 20Gy	****
0Gy vs. 10Gy	****	10Gy vs. 3X1Gy	****
0Gy vs. 20Gy	**	10Gy vs. 3X1Gy	****
0Gy vs. 20Gy	****	10Gy vs. 3X2Gy	****
0Gy vs. 3X2Gy	****	10Gy vs. 3X2Gy	***
0Gy vs. 3X4Gy	****	10Gy vs. 3X4Gy	**
0Gy vs. 3X4Gy	****	20Gy vs. 20Gy	****
0Gy vs. 3X8Gy	****	20Gy vs. 3X1Gy	*
0Gy vs. 3X8Gy	****	20Gy vs. 3X4Gy	***
0Gy vs. 10Gy	****	20Gy vs. 3X8Gy	****
0Gy vs. 20Gy	****	20Gy vs. 3X8Gy	****
0Gy vs. 3X2Gy	**	20Gy vs. 3X1Gy	****
0Gy vs. 3X4Gy	****	20Gy vs. 3X1Gy	****
0Gy vs. 3X4Gy	****	20Gy vs. 3X2Gy	****
0Gy vs. 3X8Gy	****	20Gy vs. 3X2Gy	***
0Gy vs. 3X8Gy	****	20Gy vs. 3X4Gy	**
2Gy vs. 2Gy	**	3X1Gy vs. 3X2Gy	****
2Gy vs. 10Gy	**	3X1Gy vs. 3X4Gy	****
2Gy vs. 10Gy	****	3X1Gy vs. 3X4Gy	****
2Gy vs. 20Gy	**	3X1Gy vs. 3X8Gy	****
2Gy vs. 20Gy	****	3X1Gy vs. 3X8Gy	****
2Gy vs. 3X2Gy	****	3X1Gy vs. 3X4Gy	**
2Gy vs. 3X4Gy	****	3X1Gy vs. 3X4Gy	****
2Gy vs. 3X4Gy	****	3X1Gy vs. 3X8Gy	****
2Gy vs. 3X8Gy	****	3X1Gy vs. 3X8Gy	****
2Gy vs. 3X8Gy	****	3X2Gy vs. 3X2Gy	***
2Gy vs. 10Gy	****	3X2Gy vs. 3X4Gy	****
2Gy vs. 20Gy	****	3X2Gy vs. 3X4Gy	****
2Gy vs. 3X1Gy	*	3X2Gy vs. 3X8Gy	****
2Gy vs. 3X4Gy	***	3X2Gy vs. 3X8Gy	****
2Gy vs. 3X8Gy	****	3X2Gy vs. 3X8Gy	****
2Gy vs. 3X8Gy	****	3X2Gy vs. 3X8Gy	****
10Gy vs. 10Gy	****	3X4Gy vs. 3X8Gy	**
10Gy vs. 20Gy	****	3X4Gy vs. 3X8Gy	****
10Gy vs. 3X1Gy	*	3X4Gy vs. 3X8Gy	*
10Gy vs. 3X4Gy	***		
10Gy vs. 3X8Gy	****		

Appendix Table 2; The effects of bolus dosing and fractionated dosing regimens on the expression of HMGB1 on OE33P and OE33R cell lines. Tukey's multiple comparison testing, n=3.

Tukey's multiple comparisons test	Summary	Tukey's multiple comparisons test	Summary
0Gy vs. 10Gy	***	10Gy vs. 3X2Gy	****
0Gy vs. 20Gy	***	10Gy vs. 3X2Gy	****
0Gy vs. 3X4Gy	****	10Gy vs. 3X8Gy	**
0Gy vs. 3X8Gy	****	20Gy vs. 20Gy	****
0Gy vs. 10Gy	****	20Gy vs. 3X1Gy	**
0Gy vs. 20Gy	***	20Gy vs. 3X1Gy	**
0Gy vs. 3X4Gy	****	20Gy vs. 3X4Gy	****
0Gy vs. 3X8Gy	****	20Gy vs. 3X8Gy	****
2Gy vs. 10Gy	***	20Gy vs. 3X8Gy	****
2Gy vs. 10Gy	****	20Gy vs. 3X1Gy	****
2Gy vs. 20Gy	****	20Gy vs. 3X1Gy	****
2Gy vs. 20Gy	****	20Gy vs. 3X2Gy	****
2Gy vs. 3X2Gy	*	20Gy vs. 3X2Gy	****
2Gy vs. 3X4Gy	****	20Gy vs. 3X4Gy	**
2Gy vs. 3X4Gy	****	3X1Gy vs. 3X4Gy	****
2Gy vs. 3X8Gy	****	3X1Gy vs. 3X4Gy	****
2Gy vs. 3X8Gy	****	3X1Gy vs. 3X8Gy	****
2Gy vs. 10Gy	****	3X1Gy vs. 3X8Gy	****
2Gy vs. 20Gy	****	3X1Gy vs. 3X4Gy	****
2Gy vs. 3X4Gy	****	3X1Gy vs. 3X4Gy	****
2Gy vs. 3X4Gy	***	3X1Gy vs. 3X8Gy	****
2Gy vs. 3X8Gy	****	3X1Gy vs. 3X8Gy	****
2Gy vs. 3X8Gy	****	3X2Gy vs. 3X4Gy	****
10Gy vs. 10Gy	***	3X2Gy vs. 3X4Gy	**
10Gy vs. 20Gy	****	3X2Gy vs. 3X8Gy	****
10Gy vs. 3X1Gy	**	3X2Gy vs. 3X8Gy	****
10Gy vs. 3X1Gy	*	3X2Gy vs. 3X4Gy	****
10Gy vs. 3X4Gy	****	3X2Gy vs. 3X4Gy	**
10Gy vs. 3X8Gy	****	3X2Gy vs. 3X8Gy	****
10Gy vs. 3X8Gy	****	3X2Gy vs. 3X8Gy	****
10Gy vs. 20Gy	***	3X4Gy vs. 3X4Gy	**
10Gy vs. 3X1Gy	****	3X4Gy vs. 3X8Gy	****
10Gy vs. 3X1Gy	****	3X4Gy vs. 3X8Gy	*
		3X8Gy vs. 3X8Gy	*

Appendix Table 3; The effects of dosing regimens and different levels of hypoxia on the expression of Calreticulin on OE33P and OE33R cell lines. Tukey's multiple comparison testing, n=3.

Tukey's multiple comparisons test	Summary	Tukey's multiple comparisons test	Summary
OE33P	**P Value**	**OE33R**	**P Value**
2Gy vs. 10Gy	**	0Gy vs. 10Gy 5% O2	*
2Gy vs. 10Gy 5% O2	****	0Gy vs. 3X2Gy 0.5% O2	**
2Gy vs. 3X4Gy	***	0Gy vs. 3X4Gy 5% O2	**
2Gy vs. 3X4Gy 5% O2	****	0Gy vs. 3X8Gy 5% O2	****
2Gy vs. 3X8Gy	****	0Gy vs. 3X8Gy 0.5% 02	***
2Gy vs. 3X8Gy 5% O2	****	0Gy 5% O2 vs. 10Gy	****
2Gy 5% O2 vs. 10Gy	****	0Gy 5% O2 vs. 3X2Gy	****
2Gy 5% O2 vs. 10Gy 5% O2	****	0Gy 5% O2 vs. 3X2Gy 0.5% O2	*
2Gy 5% O2 vs. 3X2Gy 5% O2	**	0Gy 5% O2 vs. 3X4Gy	****
2Gy 5% O2 vs. 3X4Gy	****	0Gy 5% O2 vs. 3X4Gy 5% O2	**
2Gy 5% O2 vs. 3X4Gy 5% O2	****	0Gy 5% O2 vs. 3X8Gy	****
2Gy 5% O2 vs. 3X8Gy	****	0Gy 5% O2 vs. 3X8Gy 5% O2	****
2Gy 5% O2 vs. 3X8Gy 5% O2	****	0Gy 5% O2 vs. 3X8Gy 0.5% 02	***
2Gy 0.5% O2 vs. 10Gy	****	0Gy 0.5% O2 vs. 2Gy	*
2Gy 0.5% O2 vs. 10Gy 5% O2	****	0Gy 0.5% O2 vs. 10Gy	****
2Gy 0.5% O2 vs. 3X2Gy 5% O2	**	0Gy 0.5% O2 vs. 10Gy 5% O2	**
2Gy 0.5% O2 vs. 3X4Gy	****	0Gy 0.5% O2 vs. 3X2Gy	****
2Gy 0.5% O2 vs. 3X4Gy 5% O2	****	0Gy 0.5% O2 vs. 3X2Gy 0.5% O2	**
2Gy 0.5% O2 vs. 3X8Gy	****	0Gy 0.5% O2 vs. 3X4Gy	****
2Gy 0.5% O2 vs. 3X8Gy 5% O2	****	0Gy 0.5% O2 vs. 3X4Gy 5% O2	***
10Gy vs. 3X2Gy 0.5% O2	****	0Gy 0.5% O2 vs. 3X8Gy	****
10Gy vs. 3X4Gy 0.5% O2	***	0Gy 0.5% O2 vs. 3X8Gy 5% O2	****
10Gy vs. 3X8Gy 5% O2	****	0Gy 0.5% O2 vs. 3X8Gy 0.5% 02	****
10Gy vs. 3X8Gy 0.5% 02	****	2Gy vs. 10Gy	****
10Gy 5% O2 vs. 3X2Gy	****	2Gy vs. 3X4Gy	****
10Gy 5% O2 vs. 3X2Gy 5% O2	****	2Gy vs. 3X8Gy	****
10Gy 5% O2 vs. 3X2Gy 0.5% O2	****	2Gy vs. 3X8Gy 5% O2	****
10Gy 5% O2 vs. 3X4Gy 0.5% O2	****	2Gy 5% O2 vs. 10Gy	****
10Gy 5% O2 vs. 3X8Gy 5% O2	****	2Gy 5% O2 vs. 3X2Gy	***
10Gy 5% O2 vs. 3X8Gy 0.5% 02	****	2Gy 5% O2 vs. 3X4Gy	****
10Gy 0.5% O2 vs. 3X4Gy	****	2Gy 5% O2 vs. 3X4Gy 5% O2	*

10Gy 0.5% O2 vs. 3X4Gy 5% O2	****	2Gy 5% O2 vs. 3X8Gy	****
10Gy 0.5% O2 vs. 3X8Gy	****	2Gy 5% O2 vs. 3X8Gy 5% O2	****
10Gy 0.5% O2 vs. 3X8Gy 5% O2	****	2Gy 5% O2 vs. 3X8Gy 0.5% 02	**
3X2Gy vs. 3X4Gy	*	2Gy 0.5% O2 vs. 10Gy	****
3X2Gy vs. 3X4Gy 5% O2	****	2Gy 0.5% O2 vs. 10Gy 5% O2	*
3X2Gy vs. 3X8Gy	**	2Gy 0.5% O2 vs. 3X2Gy	****
3X2Gy vs. 3X8Gy 5% O2	****	2Gy 0.5% O2 vs. 3X2Gy 0.5% O2	**
3X2Gy vs. 3X8Gy 0.5% 02	*	2Gy 0.5% O2 vs. 3X4Gy	****
3X2Gy 5% O2 vs. 3X4Gy 5% O2	***	2Gy 0.5% O2 vs. 3X4Gy 5% O2	**
3X2Gy 5% O2 vs. 3X8Gy 5% O2	****	2Gy 0.5% O2 vs. 3X8Gy	****
3X2Gy 5% O2 vs. 3X8Gy 0.5% 02	***	2Gy 0.5% O2 vs. 3X8Gy 5% O2	****
3X2Gy 0.5% O2 vs. 3X4Gy	****	2Gy 0.5% O2 vs. 3X8Gy 0.5% 02	***
3X2Gy 0.5% O2 vs. 3X4Gy 5% O2	****	10Gy vs. 10Gy 5% O2	****
3X2Gy 0.5% O2 vs. 3X8Gy	****	10Gy vs. 10Gy 0.5% O2	****
3X2Gy 0.5% O2 vs. 3X8Gy 5% O2	****	10Gy vs. 3X2Gy	****
3X4Gy vs. 3X8Gy 5% O2	****	10Gy vs. 3X2Gy 5% O2	****
3X4Gy vs. 3X8Gy 0.5% 02	****	10Gy vs. 3X2Gy 0.5% O2	****
3X4Gy 5% O2 vs. 3X8Gy 5% O2	****	10Gy vs. 3X4Gy 5% O2	****
3X4Gy 5% O2 vs. 3X8Gy 0.5% 02	****	10Gy vs. 3X4Gy 0.5% O2	****
3X4Gy 0.5% O2 vs. 3X8Gy	****	10Gy vs. 3X8Gy 0.5% 02	****
3X4Gy 0.5% O2 vs. 3X8Gy 5% O2	****	10Gy 5% O2 vs. 3X4Gy	****
		10Gy 5% O2 vs. 3X8Gy	****
		10Gy 5% O2 vs. 3X8Gy 5% O2	****
		10Gy 0.5% O2 vs. 3X2Gy	**
		10Gy 0.5% O2 vs. 3X4Gy	****
		10Gy 0.5% O2 vs. 3X8Gy	****
		10Gy 0.5% O2 vs. 3X8Gy 5% O2	****
		3X2Gy vs. 3X2Gy 5% O2	****
		3X2Gy vs. 3X4Gy	***
		3X2Gy vs. 3X4Gy 0.5% O2	*
		3X2Gy vs. 3X8Gy	****
		3X2Gy 5% O2 vs. 3X4Gy	****
		3X2Gy 5% O2 vs. 3X4Gy 5% O2	*
		3X2Gy 5% O2 vs. 3X8Gy	****
		3X2Gy 5% O2 vs. 3X8Gy 5% O2	****

		3X2Gy 5% O2 vs. 3X8Gy 0.5% 02	**
		3X2Gy 0.5% O2 vs. 3X4Gy	****
		3X2Gy 0.5% O2 vs. 3X8Gy	****
		3X2Gy 0.5% O2 vs. 3X8Gy 5% O2	***
		3X4Gy vs. 3X4Gy 5% O2	****
		3X4Gy vs. 3X4Gy 0.5% O2	****
		3X4Gy vs. 3X8Gy 0.5% 02	****
		3X4Gy 5% O2 vs. 3X8Gy	****
		3X4Gy 5% O2 vs. 3X8Gy 5% O2	**
		3X4Gy 0.5% O2 vs. 3X8Gy	****
		3X4Gy 0.5% O2 vs. 3X8Gy 5% O2	****
		3X8Gy vs. 3X8Gy 0.5% 02	****
		3X8Gy 5% O2 vs. 3X8Gy 0.5% 02	*

Appendix Table 4; The effects of dosing regimens and different levels of hypoxia and glucose deprivation on the expression of Calreticulin on OE33P and OE33R cell lines. Tukey's multiple comparison testing, n=3.

Tukey's multiple comparisons test	Summary	Tukey's multiple comparisons test	Summary
OE33P	**P Value**	**OE33R**	**P Value**
0Gy vs. 10Gy 5% O2	*	2Gy vs. 3X4Gy	*
0Gy vs. 3X4Gy 5% O2	**	2Gy vs. 3X4Gy 0.5% O2	*
0Gy vs. 3X8Gy 5% O2	**	2Gy vs. 3X8Gy	*
0Gy 5% O2 vs. 10Gy 5% O2	*	2Gy vs. 3X8Gy 0.5% 02	*
0Gy 5% O2 vs. 3X4Gy	**	2Gy 5% O2 vs. 3X4Gy	***
0Gy 0.5% O2 vs. 10Gy 5% O2	**	2Gy 0.5% O2 vs. 10Gy 5% O2	*
0Gy 0.5% O2 vs. 3X4Gy	**	2Gy 0.5% O2 vs. 3X8Gy	****
0Gy 0.5% O2 vs. 3X4Gy 5% O2	***	2Gy 0.5% O2 vs. 3X8Gy 5% O2	*
0Gy 0.5% O2 vs. 3X8Gy 5% O2	**	10Gy vs. 3X2Gy 5% O2	*
2Gy vs. 10Gy 5% O2	**	10Gy vs. 3X2Gy 0.5% O2	*
2Gy vs. 3X4Gy	**	10Gy 5% O2 vs. 3X8Gy	*
2Gy vs. 3X4Gy 5% O2	***	10Gy 0.5% O2 vs. 3X8Gy	*
2Gy vs. 3X8Gy 5% O2	***	3X2Gy vs. 3X4Gy	*
2Gy 5% O2 vs. 3X4Gy 5% O2	*	3X2Gy vs. 3X4Gy 0.5% O2	*
2Gy 0.5% O2 vs. 10Gy 5% O2	**	3X2Gy vs. 3X8Gy	*
2Gy 0.5% O2 vs. 3X4Gy	**	3X2Gy vs. 3X8Gy 0.5% 02	*
2Gy 0.5% O2 vs. 3X4Gy 5% O2	***	3X2Gy 5% O2 vs. 3X8Gy	*
2Gy 0.5% O2 vs. 3X8Gy 5% O2	**	3X2Gy 5% O2 vs. 3X8Gy 5% O2	*
10Gy 5% O2 vs. 3X8Gy 0.5% 02	**	3X2Gy 0.5% O2 vs. 3X8Gy	*
10Gy 0.5% O2 vs. 3X4Gy	**	3X2Gy 0.5% O2 vs. 3X8Gy 0.5% 02	*
10Gy 0.5% O2 vs. 3X4Gy 5% O2	***	3X4Gy 0.5% O2 vs. 3X8Gy	*
10Gy 0.5% O2 vs. 3X8Gy 5% O2	**	3X4Gy 0.5% O2 vs. 3X8Gy 0.5% 02	*
3X2Gy vs. 3X4Gy 5% O2	*		
3X2Gy vs. 3X8Gy 5% O2	*		
3X4Gy vs. 3X8Gy 0.5% 02	***		
3X4Gy 5% O2 vs. 3X4Gy 0.5% O2	*		
3X4Gy 5% O2 vs. 3X8Gy 0.5% 02	***		
3X8Gy 5% O2 vs. 3X8Gy 0.5% 02	***		

Appendix Table 5; The effects of dosing regimens and different levels of hypoxia and glutamine deprivation on the expression of Calreticulin on OE33P and OE33R cell lines. Tukey's multiple comparison testing, n=3.

Tukey's multiple comparisons test	Summary	Tukey's multiple comparisons test	Summary
OE33P	**P Value**	**OE33R**	**P Value**
0Gy vs. 2Gy 5% O2	**	0Gy 5% O2 vs. 10Gy	***
0Gy vs. 2Gy 0.5% O2	*	0Gy 5% O2 vs. 3X4Gy 5% O2	*
0Gy vs. 10Gy 5% O2	****	0Gy 5% O2 vs. 3X8Gy	**
0Gy vs. 3X2Gy 5% O2	***	0Gy 5% O2 vs. 3X8Gy 5% O2	****
0Gy vs. 3X4Gy 5% O2	****	0Gy 5% O2 vs. 3X8Gy 0.5% 02	**
0Gy vs. 3X4Gy 0.5% O2	***	2Gy vs. 10Gy	**
0Gy vs. 3X8Gy 5% O2	****	2Gy vs. 3X8Gy 5% O2	****
0Gy vs. 3X8Gy 0.5% 02	***	2Gy 5% O2 vs. 10Gy	***
0Gy 5% O2 vs. 10Gy 5% O2	***	2Gy 5% O2 vs. 3X4Gy 5% O2	*
0Gy 5% O2 vs. 3X2Gy 5% O2	*	2Gy 5% O2 vs. 3X8Gy	**
0Gy 5% O2 vs. 3X8Gy 5% O2	****	2Gy 5% O2 vs. 3X8Gy 5% O2	****
0Gy 5% O2 vs. 3X8Gy 0.5% 02	*	2Gy 5% O2 vs. 3X8Gy 0.5% 02	**
0Gy 0.5% O2 vs. 10Gy 5% O2	***	2Gy 0.5% O2 vs. 10Gy	***
0Gy 0.5% O2 vs. 3X4Gy 5% O2	***	2Gy 0.5% O2 vs. 3X4Gy 5% O2	*
0Gy 0.5% O2 vs. 3X8Gy 5% O2	****	2Gy 0.5% O2 vs. 3X8Gy	**
2Gy vs. 2Gy 5% O2	**	2Gy 0.5% O2 vs. 3X8Gy 5% O2	****
2Gy vs. 2Gy 0.5% O2	*	2Gy 0.5% O2 vs. 3X8Gy 0.5% 02	**
2Gy vs. 10Gy 5% O2	****	10Gy vs. 3X2Gy 0.5% O2	***
2Gy vs. 3X2Gy 5% O2	***	10Gy vs. 3X8Gy 5% O2	*
2Gy vs. 3X4Gy 5% O2	****	10Gy 5% O2 vs. 3X8Gy 5% O2	****
2Gy vs. 3X4Gy 0.5% O2	***	10Gy 0.5% O2 vs. 3X8Gy 5% O2	****
2Gy vs. 3X8Gy 5% O2	****	3X2Gy vs. 3X8Gy 5% O2	****
2Gy vs. 3X8Gy 0.5% 02	***	3X2Gy 5% O2 vs. 3X8Gy 5% O2	****
2Gy 5% O2 vs. 10Gy	*	3X2Gy 0.5% O2 vs. 3X8Gy	*
2Gy 5% O2 vs. 3X2Gy	**	3X2Gy 0.5% O2 vs. 3X8Gy 5% O2	****
2Gy 5% O2 vs. 3X2Gy 0.5% O2	*	3X2Gy 0.5% O2 vs.3X8Gy .5%02	*
2Gy 5% O2 vs. 3X8Gy	*	3X4Gy vs. 3X8Gy 5% O2	****
2Gy 5% O2 vs. 3X8Gy 5% O2	****	3X4Gy 5% O2 vs. 3X8Gy 5% O2	***
2Gy 0.5% O2 vs. 3X2Gy	*	3X4Gy 0.5% O2 vs. 3X8Gy 5% O2	****
2Gy 0.5% O2 vs. 3X8Gy 5% O2	****		
10Gy vs. 10Gy 5% O2	****		
10Gy vs. 3X2Gy 5% O2	**		
10Gy vs. 3X4Gy 5% O2	****		
10Gy vs. 3X4Gy 0.5% O2	**		
10Gy vs. 3X8Gy 5% O2	****		
10Gy vs. 3X8Gy 0.5% 02	**		
10Gy 5% O2 vs. 10Gy 0.5% O2	****		
10Gy 5% O2 vs. 3X2Gy	****		
10Gy 5% O2 vs. 3X2Gy 0.5% O2	****		
10Gy 5% O2 vs. 3X4Gy	***		
10Gy 5% O2 vs. 3X8Gy	****		
10Gy 5% O2 vs. 3X8Gy 5% O2	*		

10Gy 0.5% O2 vs. 3X2Gy 5% O2	*		
10Gy 0.5% O2 vs. 3X4Gy 5% O2	****		
10Gy 0.5% O2 vs. 3X4Gy 0.5% O2	*		
10Gy 0.5% O2 vs. 3X8Gy 5% O2	****		
10Gy 0.5% O2 vs. 3X8Gy 0.5% 02	*		
3X2Gy vs. 3X2Gy 5% O2	***		
3X2Gy vs. 3X4Gy 5% O2	****		
3X2Gy vs. 3X4Gy 0.5% O2	***		
3X2Gy vs. 3X8Gy 5% O2	****		
3X2Gy vs. 3X8Gy 0.5% 02	***		
3X2Gy 5% O2 vs. 3X2Gy 0.5% O2	**		
3X2Gy 5% O2 vs. 3X4Gy	*		
3X2Gy 5% O2 vs. 3X8Gy	**		
3X2Gy 5% O2 vs. 3X8Gy 5% O2	***		
3X2Gy 0.5% O2 vs. 3X4Gy 5% O2	****		
3X2Gy 0.5% O2 vs. 3X4Gy 0.5% O2	**		
3X2Gy 0.5% O2 vs. 3X8Gy 5% O2	****		
3X2Gy 0.5% O2 vs. 3X8Gy 0.5% 02	**		
3X4Gy vs. 3X4Gy 5% O2	****		
3X4Gy vs. 3X4Gy 0.5% O2	*		
3X4Gy vs. 3X8Gy 5% O2	****		
3X4Gy vs. 3X8Gy 0.5% 02	*		
3X4Gy 5% O2 vs. 3X8Gy	****		
3X4Gy 0.5% O2 vs. 3X8Gy	**		
3X4Gy 0.5% O2 vs. 3X8Gy 5% O2	***		
3X8Gy vs. 3X8Gy 5% O2	****		
3X8Gy vs. 3X8Gy 0.5% 02	**		
3X8Gy 5% O2 vs. 3X8Gy 0.5% 02	***		

Appendix Table 6; The effects of dosing regimens and different levels of hypoxia on the expression of Calreticulin on OE33P and OE33R cell lines. Tukey's multiple comparison testing, n=3.

Tukey's multiple comparisons test	Summary	Tukey's multiple comparisons test	Summary
OE33P	**P Value**	**OE33R**	**P Value**
0Gy vs. 10Gy 5% O2	****	0Gy vs. 10Gy 0.5% O2	***
0Gy vs. 3X4Gy 5% O2	****	0Gy vs. 3X2Gy 0.5% O2	*
0Gy vs. 3X8Gy 5% O2	****	0Gy vs. 3X8Gy 5% O2	****
0Gy 5% O2 vs. 10Gy	****	0Gy vs. 3X8Gy 0.5% 02	**
0Gy 5% O2 vs. 3X2Gy	*	0Gy 5% O2 vs. 10Gy	****
0Gy 5% O2 vs. 3X4Gy	****	0Gy 5% O2 vs. 10Gy 0.5% O2	***
0Gy 5% O2 vs. 3X4Gy 5% O2	****	0Gy 5% O2 vs. 3X2Gy	****
0Gy 5% O2 vs. 3X8Gy	****	0Gy 5% O2 vs. 3X2Gy 0.5% O2	*
0Gy 5% O2 vs. 3X8Gy 5% O2	****	0Gy 5% O2 vs. 3X4Gy	****
0Gy 0.5% O2 vs. 10Gy	****	0Gy 5% O2 vs. 3X8Gy	****
0Gy 0.5% O2 vs. 10Gy 5% O2	****	0Gy 5% O2 vs. 3X8Gy 0.5% 02	**
0Gy 0.5% O2 vs. 3X4Gy	****	0Gy 0.5% O2 vs. 10Gy	****
0Gy 0.5% O2 vs. 3X4Gy 5% O2	****	0Gy 0.5% O2 vs. 3X2Gy	****
0Gy 0.5% O2 vs. 3X8Gy	****	0Gy 0.5% O2 vs. 3X4Gy	****
0Gy 0.5% O2 vs. 3X8Gy 5% O2	****	0Gy 0.5% O2 vs. 3X8Gy	****
2Gy vs. 10Gy	**	0Gy 0.5% O2 vs. 3X8Gy 5% O2	****
2Gy vs. 10Gy 5% O2	****	2Gy vs. 10Gy	****
2Gy vs. 3X4Gy	**	2Gy vs. 3X2Gy	****
2Gy vs. 3X4Gy 5% O2	****	2Gy vs. 3X4Gy	****
2Gy vs. 3X8Gy	****	2Gy vs. 3X8Gy	****
2Gy vs. 3X8Gy 5% O2	****	2Gy vs. 3X8Gy 5% O2	****
2Gy 5% O2 vs. 10Gy	***	2Gy 5% O2 vs. 10Gy	****
2Gy 5% O2 vs. 10Gy 5% O2	****	2Gy 5% O2 vs. 10Gy 0.5% O2	*
2Gy 5% O2 vs. 3X4Gy	****	2Gy 5% O2 vs. 3X2Gy	****
2Gy 5% O2 vs. 3X4Gy 5% O2	****	2Gy 5% O2 vs. 3X4Gy	****
2Gy 5% O2 vs. 3X8Gy	****	2Gy 5% O2 vs. 3X8Gy	****
2Gy 5% O2 vs. 3X8Gy 5% O2	****	2Gy 5% O2 vs. 3X8Gy 5% O2	****
2Gy 0.5% O2 vs. 10Gy	***	2Gy 0.5% O2 vs. 10Gy	****
2Gy 0.5% O2 vs. 10Gy 5% O2	****	2Gy 0.5% O2 vs. 3X2Gy	****
2Gy 0.5% O2 vs. 3X4Gy	***	2Gy 0.5% O2 vs. 3X4Gy	****
2Gy 0.5% O2 vs. 3X4Gy 5% O2	****	2Gy 0.5% O2 vs. 3X8Gy	****
2Gy 0.5% O2 vs. 3X8Gy	****	2Gy 0.5% O2 vs. 3X8Gy 5% O2	****
2Gy 0.5% O2 vs. 3X8Gy 5% O2	****	10Gy vs. 10Gy 5% O2	****
10Gy vs. 10Gy 0.5% O2	**	10Gy vs. 10Gy 0.5% O2	****
10Gy vs. 3X2Gy 5% O2	*	10Gy vs. 3X2Gy 5% O2	****
10Gy vs. 3X2Gy 0.5% O2	****	10Gy vs. 3X2Gy 0.5% O2	****
10Gy vs. 3X4Gy 0.5% O2	**	10Gy vs. 3X4Gy 5% O2	****
10Gy vs. 3X8Gy 5% O2	***	10Gy vs. 3X4Gy 0.5% O2	****
10Gy vs. 3X8Gy 0.5% 02	**	10Gy vs. 3X8Gy 5% O2	*
10Gy 5% O2 vs. 10Gy 0.5% O2	****	10Gy vs. 3X8Gy 0.5% 02	****
10Gy 5% O2 vs. 3X2Gy	****	10Gy 5% O2 vs. 3X2Gy	****
10Gy 5% O2 vs. 3X2Gy 5% O2	****	10Gy 5% O2 vs. 3X4Gy	****
10Gy 5% O2 vs. 3X2Gy 0.5% O2	****	10Gy 5% O2 vs. 3X8Gy	****
10Gy 5% O2 vs. 3X4Gy 0.5% O2	****	10Gy 5% O2 vs. 3X8Gy 5% O2	***
10Gy 5% O2 vs. 3X8Gy 0.5% 02	****	10Gy 0.5% O2 vs. 3X2Gy	*

10Gy 0.5% O2 vs. 3X4Gy	**	10Gy 0.5% O2 vs. 3X4Gy	****
10Gy 0.5% O2 vs. 3X4Gy 5% O2	****	10Gy 0.5% O2 vs. 3X8Gy	****
10Gy 0.5% O2 vs. 3X8Gy	***	3X2Gy vs. 3X2Gy 5% O2	****
10Gy 0.5% O2 vs. 3X8Gy 5% O2	****	3X2Gy vs. 3X2Gy 0.5% O2	***
3X2Gy vs. 3X4Gy 5% O2	**	3X2Gy vs. 3X4Gy	***
3X2Gy vs. 3X8Gy	**	3X2Gy vs. 3X4Gy 5% O2	****
3X2Gy vs. 3X8Gy 5% O2	****	3X2Gy vs. 3X4Gy 0.5% O2	****
3X2Gy 5% O2 vs. 3X4Gy	**	3X2Gy vs. 3X8Gy 0.5% 02	***
3X2Gy 5% O2 vs. 3X4Gy 5% O2	***	3X2Gy 5% O2 vs. 3X4Gy	****
3X2Gy 5% O2 vs. 3X8Gy	***	3X2Gy 5% O2 vs. 3X8Gy	****
3X2Gy 5% O2 vs. 3X8Gy 5% O2	****	3X2Gy 5% O2 vs. 3X8Gy 5% O2	****
3X2Gy 0.5% O2 vs. 3X4Gy	****	3X2Gy 0.5% O2 vs. 3X4Gy	****
3X2Gy 0.5% O2 vs. 3X4Gy 5% O2	****	3X2Gy 0.5% O2 vs. 3X8Gy	****
3X2Gy 0.5% O2 vs. 3X8Gy	****	3X2Gy 0.5% O2 vs. 3X8Gy 5% O2	**
3X2Gy 0.5% O2 vs. 3X8Gy 5% O2	****	3X4Gy vs. 3X4Gy 5% O2	****
3X4Gy vs. 3X4Gy 0.5% O2	***	3X4Gy vs. 3X4Gy 0.5% O2	****
3X4Gy vs. 3X8Gy 5% O2	**	3X4Gy vs. 3X8Gy 5% O2	****
3X4Gy vs. 3X8Gy 0.5% 02	***	3X4Gy vs. 3X8Gy 0.5% 02	****
3X4Gy 5% O2 vs. 3X4Gy 0.5% O2	****	3X4Gy 5% O2 vs. 3X8Gy	****
3X4Gy 5% O2 vs. 3X8Gy 0.5% 02	****	3X4Gy 5% O2 vs. 3X8Gy 5% O2	***
3X4Gy 0.5% O2 vs. 3X8Gy	****	3X4Gy 0.5% O2 vs. 3X8Gy	****
3X4Gy 0.5% O2 vs. 3X8Gy 5% O2	****	3X4Gy 0.5% O2 vs. 3X8Gy 5% O2	****
		3X8Gy vs. 3X8Gy 5% O2	**
		3X8Gy vs. 3X8Gy 0.5% 02	****
		3X8Gy 5% O2 vs. 3X8Gy 0.5% 02	**

Appendix Table 7; The effects of dosing regimens and different levels of hypoxia and glucose deprivation on the expression of HMGB1 on OE33P and OE33R cell lines. Tukey's multiple comparison testing, n=3.

Tukey's multiple comparisons test	Summary	Tukey's multiple comparisons test	Summary
OE33P	**P Value**	**OE33R**	**P Value**
0Gy vs. 10Gy 5% O2	****	0Gy vs. 3X4Gy 0.5% O2	*
0Gy vs. 3X4Gy 5% O2	****	0Gy vs. 3X8Gy 5% O2	**
0Gy vs. 3X8Gy 5% O2	**	0Gy 5% O2 vs. 10Gy	****
0Gy 5% O2 vs. 3X2Gy	*	0Gy 5% O2 vs. 3X4Gy	****
0Gy 5% O2 vs. 3X4Gy	**	0Gy 5% O2 vs. 3X8Gy	****
0Gy 5% O2 vs. 3X8Gy	*	0Gy 0.5% O2 vs. 10Gy	****
0Gy 0.5% O2 vs. 10Gy	*	0Gy 0.5% O2 vs. 3X4Gy	****
0Gy 0.5% O2 vs. 10Gy 5% O2	****	0Gy 0.5% O2 vs. 3X8Gy	****
0Gy 0.5% O2 vs. 3X2Gy	**	0Gy 0.5% O2 vs. 3X8Gy 5% O2	*
0Gy 0.5% O2 vs. 3X4Gy	***	2Gy vs. 10Gy	****
0Gy 0.5% O2 vs. 3X4Gy 5% O2	****	2Gy vs. 3X4Gy	****
0Gy 0.5% O2 vs. 3X8Gy	**	2Gy vs. 3X8Gy	****
0Gy 0.5% O2 vs. 3X8Gy 5% O2	***	2Gy vs. 3X8Gy 5% O2	*
2Gy vs. 10Gy 5% O2	****	2Gy 5% O2 vs. 10Gy	****
2Gy vs. 3X4Gy	***	2Gy 5% O2 vs. 3X4Gy	****
2Gy vs. 3X4Gy 5% O2	****	2Gy 5% O2 vs. 3X8Gy	****
2Gy vs. 3X8Gy	*	2Gy 0.5% O2 vs. 10Gy	****
2Gy vs. 3X8Gy 5% O2	**	2Gy 0.5% O2 vs. 3X4Gy	****
2Gy 5% O2 vs. 10Gy 5% O2	****	2Gy 0.5% O2 vs. 3X8Gy	****
2Gy 5% O2 vs. 10Gy 0.5% O2	*	10Gy vs. 10Gy 5% O2	**
2Gy 5% O2 vs. 3X4Gy 5% O2	*	10Gy vs. 10Gy 0.5% O2	****
2Gy 5% O2 vs. 3X8Gy 0.5% 02	*	10Gy vs. 3X2Gy 5% O2	***
2Gy 0.5% O2 vs. 10Gy 5% O2	****	10Gy vs. 3X2Gy 0.5% O2	*
2Gy 0.5% O2 vs. 3X2Gy	*	10Gy vs. 3X4Gy 5% O2	**
2Gy 0.5% O2 vs. 3X4Gy	**	10Gy vs. 3X8Gy	****
2Gy 0.5% O2 vs. 3X4Gy 5% O2	****	10Gy vs. 3X8Gy 0.5% 02	**
2Gy 0.5% O2 vs. 3X8Gy	*	10Gy 5% O2 vs. 3X4Gy	***
2Gy 0.5% O2 vs. 3X8Gy 5% O2	**	10Gy 5% O2 vs. 3X8Gy	****
10Gy vs. 10Gy 5% O2	**	10Gy 0.5% O2 vs. 3X4Gy	****
10Gy vs. 10Gy 0.5% O2	**	10Gy 0.5% O2 vs. 3X8Gy	****
10Gy vs. 3X8Gy 0.5% 02	**	3X2Gy vs. 3X4Gy	*
10Gy 5% O2 vs. 10Gy 0.5% O2	****	3X2Gy vs. 3X8Gy	****
10Gy 5% O2 vs. 3X2Gy	**	3X2Gy 5% O2 vs. 3X4Gy	****
10Gy 5% O2 vs. 3X2Gy 5% O2	****	3X2Gy 5% O2 vs. 3X8Gy	****
10Gy 5% O2 vs. 3X2Gy 0.5% O2	****	3X2Gy 0.5% O2 vs. 3X4Gy	**
10Gy 5% O2 vs. 3X4Gy 0.5% O2	****	3X2Gy 0.5% O2 vs. 3X8Gy	****
10Gy 5% O2 vs. 3X8Gy	**	3X4Gy vs. 3X4Gy 5% O2	***
10Gy 5% O2 vs. 3X8Gy 0.5% 02	****	3X4Gy vs. 3X4Gy 0.5% O2	*
10Gy 0.5% O2 vs. 3X2Gy	***	3X4Gy vs. 3X8Gy	****
10Gy 0.5% O2 vs. 3X4Gy	****	3X4Gy vs. 3X8Gy 0.5% 02	**
10Gy 0.5% O2 vs. 3X4Gy 5% O2	****	3X4Gy 5% O2 vs. 3X8Gy	****
10Gy 0.5% O2 vs. 3X8Gy	***	3X4Gy 0.5% O2 vs. 3X8Gy	****
10Gy 0.5% O2 vs. 3X8Gy 5% O2	****	3X8Gy vs. 3X8Gy 5% O2	****
3X2Gy vs. 3X2Gy 0.5% O2	*	3X8Gy vs. 3X8Gy 0.5% 02	****
3X2Gy vs. 3X4Gy 0.5% O2	*		

3X2Gy vs. 3X8Gy 0.5% 02	***
3X2Gy 5% O2 vs. 3X4Gy 5% O2	*
3X2Gy 5% O2 vs. 3X8Gy 0.5% 02	*
3X2Gy 0.5% O2 vs. 3X4Gy	**
3X2Gy 0.5% O2 vs. 3X4Gy 5% O2	****
3X2Gy 0.5% O2 vs. 3X8Gy	*
3X2Gy 0.5% O2 vs. 3X8Gy 5% O2	**
3X4Gy vs. 3X4Gy 0.5% O2	**
3X4Gy vs. 3X8Gy 0.5% 02	****
3X4Gy 5% O2 vs. 3X4Gy 0.5% O2	****
3X4Gy 5% O2 vs. 3X8Gy 0.5% 02	****
3X4Gy 0.5% O2 vs. 3X8Gy	*
3X4Gy 0.5% O2 vs. 3X8Gy 5% O2	**
3X8Gy vs. 3X8Gy 0.5% 02	***
3X8Gy 5% O2 vs. 3X8Gy 0.5% 02	****

Appendix Table 8; The effects of dosing regimens and different levels of hypoxia and glutamine deprivation on the expression of HMGB1 on OE33P and OE33R cell lines. Tukey's multiple comparison testing, n=3.

Tukey's multiple comparisons test	Summary	Tukey's multiple comparisons test	Summary
OE33P	P Value	OE33R	P Value
0Gy vs. 2Gy 5% O2	***	0Gy vs. 10Gy 5% O2	ns
0Gy vs. 2Gy 0.5% O2	*	0Gy vs. 10Gy 0.5% O2	*
0Gy vs. 10Gy 5% O2	****	0Gy vs. 3X2Gy 5% O2	*
0Gy vs. 3X2Gy 5% O2	**	0Gy vs. 3X4Gy 5% O2	*
0Gy vs. 3X4Gy 5% O2	****	0Gy vs. 3X4Gy 0.5% O2	*
0Gy vs. 3X8Gy 5% O2	****	0Gy vs. 3X8Gy 5% O2	****
0Gy vs. 3X8Gy 0.5% 02	**	0Gy vs. 3X8Gy 0.5% 02	**
0Gy 5% O2 vs. 10Gy	****	0Gy 5% O2 vs. 10Gy	***
0Gy 5% O2 vs. 3X8Gy	****	0Gy 5% O2 vs. 3X8Gy	***
0Gy 0.5% O2 vs. 2Gy 5% O2	***	0Gy 5% O2 vs. 3X8Gy 5% O2	****
0Gy 0.5% O2 vs. 10Gy	****	0Gy 5% O2 vs. 3X8Gy 0.5% 02	*
0Gy 0.5% O2 vs. 10Gy 5% O2	****	0Gy 0.5% O2 vs. 10Gy	****
0Gy 0.5% O2 vs. 3X2Gy 5% O2	*	0Gy 0.5% O2 vs. 10Gy 0.5% O2	*
0Gy 0.5% O2 vs. 3X4Gy 5% O2	****	0Gy 0.5% O2 vs. 3X2Gy 5% O2	*
0Gy 0.5% O2 vs. 3X8Gy	****	0Gy 0.5% O2 vs. 3X4Gy	**
0Gy 0.5% O2 vs. 3X8Gy 5% O2	****	0Gy 0.5% O2 vs. 3X4Gy 5% O2	*
2Gy vs. 10Gy	****	0Gy 0.5% O2 vs. 3X4Gy 0.5% O2	*
2Gy vs. 10Gy 5% O2	****	0Gy 0.5% O2 vs. 3X8Gy	****
2Gy vs. 3X2Gy 5% O2	**	0Gy 0.5% O2 vs. 3X8Gy 5% O2	****
2Gy vs. 3X4Gy 5% O2	****	0Gy 0.5% O2 vs. 3X8Gy .5% 02	**
2Gy vs. 3X8Gy	****	2Gy vs. 10Gy	***
2Gy vs. 3X8Gy 5% O2	****	2Gy vs. 3X8Gy	**
2Gy vs. 3X8Gy 0.5% 02	**	2Gy vs. 3X8Gy 5% O2	****
2Gy 5% O2 vs. 10Gy 5% O2	***	2Gy vs. 3X8Gy 0.5% 02	*
2Gy 5% O2 vs. 10Gy 0.5% O2	***	2Gy 5% O2 vs. 10Gy	***
2Gy 5% O2 vs. 3X2Gy	***	2Gy 5% O2 vs. 3X8Gy	***
2Gy 5% O2 vs. 3X2Gy 0.5% O2	***	2Gy 5% O2 vs. 3X8Gy 5% O2	****
2Gy 5% O2 vs. 3X4Gy	*	2Gy 5% O2 vs. 3X8Gy 0.5% 02	*
2Gy 5% O2 vs. 3X4Gy 5% O2	*	2Gy 0.5% O2 vs. 10Gy	*
2Gy 5% O2 vs. 3X4Gy 0.5% O2	**	2Gy 0.5% O2 vs. 3X8Gy	*
2Gy 5% O2 vs. 3X8Gy 5% O2	*	2Gy 0.5% O2 vs. 3X8Gy 5% O2	****
2Gy 0.5% O2 vs. 10Gy	**	10Gy vs. 3X2Gy 0.5% O2	*
2Gy 0.5% O2 vs. 10Gy 5% O2	****	10Gy 5% O2 vs. 3X8Gy 5% O2	**
2Gy 0.5% O2 vs. 3X2Gy 0.5% O2	*	10Gy 0.5% O2 vs. 3X8Gy 5% O2	**

2Gy 0.5% O2 vs. 3X4Gy 5% O2	****	3X2Gy vs. 3X8Gy 5% O2	***
2Gy 0.5% O2 vs. 3X8Gy	**	3X2Gy 5% O2 vs. 3X8Gy 5% O2	**
2Gy 0.5% O2 vs. 3X8Gy 5% O2	***	3X2Gy 0.5% O2 vs. 3X8Gy	*
10Gy vs. 3X2Gy	****	3X2Gy 0.5% O2 vs. 3X8Gy 5% O2	****
10Gy vs. 3X2Gy 5% O2	*	3X4Gy vs. 3X8Gy 5% O2	*
10Gy vs. 3X2Gy 0.5% O2	****	3X4Gy 5% O2 vs. 3X8Gy 5% O2	**
10Gy vs. 3X4Gy	****	3X4Gy 0.5% O2 vs. 3X8Gy 5% O2	**
10Gy vs. 3X4Gy 0.5% O2	****		
10Gy 5% O2 vs. 10Gy 0.5% O2	****		
10Gy 5% O2 vs. 3X2Gy	****		
10Gy 5% O2 vs. 3X2Gy 5% O2	****		
10Gy 5% O2 vs. 3X2Gy 0.5% O2	****		
10Gy 5% O2 vs. 3X4Gy	****		
10Gy 5% O2 vs. 3X4Gy 0.5% O2	****		
10Gy 5% O2 vs. 3X8Gy 0.5% 02	****		
10Gy 0.5% O2 vs. 3X2Gy 5% O2	*		
10Gy 0.5% O2 vs. 3X4Gy 5% O2	****		
10Gy 0.5% O2 vs. 3X8Gy	****		
10Gy 0.5% O2 vs. 3X8Gy 5% O2	****		
10Gy 0.5% O2 vs. 3X8Gy 0.5% 02	**		
3X2Gy vs. 3X4Gy 5% O2	****		
3X2Gy vs. 3X8Gy	****		
3X2Gy vs. 3X8Gy 5% O2	****		
3X2Gy vs. 3X8Gy 0.5% 02	**		
3X2Gy 5% O2 vs. 3X4Gy 5% O2	***		
3X2Gy 5% O2 vs. 3X8Gy	**		
3X2Gy 5% O2 vs. 3X8Gy 5% O2	***		
3X2Gy 0.5% O2 vs. 3X4Gy 5% O2	****		
3X2Gy 0.5% O2 vs. 3X8Gy	****		
3X2Gy 0.5% O2 vs. 3X8Gy 5% O2	****		
3X2Gy 0.5% O2 vs. 3X8Gy .5% 02	**		
3X4Gy vs. 3X4Gy 5% O2	****		
3X4Gy vs. 3X8Gy	****		
3X4Gy vs. 3X8Gy 5% O2	****		
3X4Gy 5% O2 vs. 3X8Gy 0.5% 02	**		
3X4Gy 0.5% O2 vs. 3X8Gy	****		
3X4Gy 0.5% O2 vs. 3X8Gy 5% O2	****		

Appendix Table 9; The effects of Pembrolizumab and different levels of glucose deprivation on the cell viability on OE33P and OE33R cell lines. Tukey's multiple comparison testing, n=3.

Tukey's multiple comparisons test	Summary
Untreated vs. 0Gy	****
Untreated vs. 0gy Pembro	****
Untreated vs. 2Gy No ICB	****
Untreated vs. 2Gy Pembro	****
Untreated vs. 4Gy No ICB	****
Untreated vs. 4Gy Pembro	****
Untreated vs. 0Gy	****
Untreated vs. 0gy Pembro	****
Untreated vs. 2Gy No ICB	****
Untreated vs. 2Gy Pembro	****
Untreated vs. 4Gy No ICB	****
Untreated vs. 4Gy Pembro	****
0Gy vs. Untreated	****
0Gy vs. 0Gy	*
0Gy vs. 0gy Pembro	*
0Gy vs. 2Gy No ICB	*
0Gy vs. 2Gy Pembro	*
0Gy vs. 4Gy Pembro	**
0gy Pembro vs. Untreated	****
0gy Pembro vs. 0Gy	**
0gy Pembro vs. 0gy Pembro	**
0gy Pembro vs. 2Gy No ICB	**
0gy Pembro vs. 2Gy Pembro	**
0gy Pembro vs. 4Gy No ICB	**
0gy Pembro vs. 4Gy Pembro	**
2Gy No ICB vs. Untreated	****
2Gy Pembro vs. Untreated	****
2Gy Pembro vs. 0Gy	*
2Gy Pembro vs. 0gy Pembro	*
2Gy Pembro vs. 2Gy No ICB	*
2Gy Pembro vs. 2Gy Pembro	*
2Gy Pembro vs. 4Gy Pembro	*
4Gy No ICB vs. Untreated	****
4Gy Pembro vs. Untreated	****
Untreated vs. 0Gy	****
Untreated vs. 0gy Pembro	****
Untreated vs. 2Gy No ICB	****
Untreated vs. 2Gy Pembro	****
Untreated vs. 4Gy No ICB	****
Untreated vs. 4Gy Pembro	****

Appendix Table 10; The effects of Nivolumab and different levels of glucose deprivation on the cell viability on OE33P and OE33R cell lines. Tukey's multiple comparison testing, n=3.

Tukey's multiple comparisons test	Summary
Untreated vs. 0Gy	****
Untreated vs. 0gy Nivo	****
Untreated vs. 2Gy No ICB	****
Untreated vs. 2Gy Nivoo	****
Untreated vs. 4Gy No ICB	****
Untreated vs. 4Gy Nivo	****
Untreated vs. 0Gy	****
Untreated vs. 0gy Nivo	****
Untreated vs. 2Gy No ICB	****
Untreated vs. 2Gy Nivo	****
Untreated vs. 4Gy No ICB	****
Untreated vs. 4Gy Nivo	****
0Gy vs. 4Gy Nivo	***
0Gy vs. Untreated	****
0Gy vs. 4Gy Nivo	*
0gy Nivo vs. 4Gy Nivo	**
0gy Nivo vs. Untreated	****
0gy Nivo vs. 4Gy Nivo	*
2Gy No ICB vs. 4Gy Nivo	**
2Gy No ICB vs. Untreated	****
2Gy Nivoo vs. 4Gy Nivo	**
2Gy Nivoo vs. Untreated	****
2Gy Nivoo vs. 4Gy Nivo	*
4Gy No ICB vs. 4Gy Nivo	**
4Gy No ICB vs. Untreated	****
4Gy Nivo vs. Untreated	****
Untreated vs. 0Gy	****
Untreated vs. 0gy Nivo	****
Untreated vs. 2Gy No ICB	****
Untreated vs. 2Gy Nivo	****
Untreated vs. 4Gy No ICB	****
Untreated vs. 4Gy Nivo	****

Appendix Table 11; The effects of Atezolizumab and different levels of glucose deprivation on the cell viability on OE33P and OE33R cell lines. Tukey's multiple comparison testing, n=3.

Tukey's multiple comparisons test	Summary
Untreated vs. 0Gy	****
Untreated vs. 0gy Atezo	****
Untreated vs. 2Gy No ICB	****
Untreated vs. 2Gy Atezo	****
Untreated vs. 4Gy No ICB	****
Untreated vs. 4Gy Atezo	****
Untreated vs. 0Gy	****
Untreated vs. 0gy Atezo	****
Untreated vs. 2Gy No ICB	****
Untreated vs. 2Gy Atezo	****
Untreated vs. 4Gy No ICB	****
Untreated vs. 4Gy Atezo	****
0Gy vs. Untreated	****
0Gy vs. 2Gy Atezo	*
0Gy vs. 4Gy No ICB	*
0Gy vs. 4Gy Atezo	*
0gy Atezo vs. Untreated	****
0gy Atezo vs. 0Gy	*
0gy Atezo vs. 2Gy Atezo	*
0gy Atezo vs. 4Gy No ICB	*
0gy Atezo vs. 4Gy Atezo	*
2Gy No ICB vs. Untreated	****
2Gy Atezo vs. Untreated	****
2Gy Atezo vs. 2Gy Atezo	*
2Gy Atezo vs. 4Gy No ICB	*
2Gy Atezo vs. 4Gy Atezo	*
4Gy No ICB vs. Untreated	****
4Gy Atezo vs. Untreated	****
Untreated vs. 0Gy	****
Untreated vs. 0gy Atezo	****
Untreated vs. 2Gy No ICB	****
Untreated vs. 2Gy Atezo	****
Untreated vs. 4Gy No ICB	****
Untreated vs. 4Gy Atezo	****

Appendix Table 12; The effects of Atezolizumab and Pembrolizumab and different levels of glucose deprivation on the cell viability on OE33P and OE33R cell lines. Tukey's multiple comparison testing, n=3.

Tukey's multiple comparisons test	Summary
Untreated vs. 0Gy	****
Untreated vs. 0gy Atezo+Pembro	****
Untreated vs. 2Gy No ICB	****
Untreated vs. 2Gy Atezo+Pembro	****
Untreated vs. 4Gy No ICB	****
Untreated vs. 4Gy Atezo+Pembro	****
Untreated vs. 0Gy	****
Untreated vs. 0gy Atrezo+Pembro	****
Untreated vs. 2Gy No ICB	****
Untreated vs. 2Gy Atrezo+Pembro	****
Untreated vs. 4Gy No ICB	****
Untreated vs. 4Gy Atezo+Pembro	****
0Gy vs. Untreated	****
0Gy vs. 4Gy No ICB	*
0Gy vs. 4Gy Atezo+Pembro	*
0gy Atezo+Pembro vs. Untreated	****
0gy Atezo+Pembro vs. 0Gy	*
0gy Atezo+Pembro vs. 2Gy No ICB	*
0gy Atezo+Pembro vs. 4Gy No ICB	*
0gy Atezo+Pembro vs. 4Gy Atezo+Pembro	*
2Gy No ICB vs. Untreated	****
2Gy Atezo+Pembro vs. Untreated	****
4Gy No ICB vs. Untreated	****
4Gy Atezo+Pembro vs. Untreated	****
Untreated vs. 0Gy	****
Untreated vs. 0gy Atrezo+Pembro	****
Untreated vs. 2Gy No ICB	****
Untreated vs. 2Gy Atrezo+Pembro	****
Untreated vs. 4Gy No ICB	****
Untreated vs. 4Gy Atezo+Pembro	****

Appendix Table 13; The effects of Atezolizumab and Nivolumab and different levels of glucose deprivation on the cell viability on OE33P and OE33R cell lines. Tukey's multiple comparison testing, n=3.

Tukey's multiple comparisons test	Summary
Untreated vs. 0Gy	****
Untreated vs. 0gy Atezo+Nivo	****
Untreated vs. 2Gy No ICB	****
Untreated vs. 2Gy Atezo+Nivo	****
Untreated vs. 4Gy No ICB	****
Untreated vs. 4Gy Atezo+Nivo	****
Untreated vs. 0Gy	****
Untreated vs. 0gy Atrezo+Nivo	****
Untreated vs. 2Gy No ICB	****
Untreated vs. 2Gy Atrezo+Nivo	****
Untreated vs. 4Gy No ICB	****
Untreated vs. 4Gy Atezo+Nivo	****
0Gy vs. Untreated	****
0gy Atezo+Nivo vs. Untreated	****
2Gy No ICB vs. Untreated	****
2Gy Atezo+Nivo vs. Untreated	****
4Gy No ICB vs. Untreated	****
4Gy Atezo+Nivo vs. Untreated	****
Untreated vs. 0Gy	****
Untreated vs. 0gy Atrezo+Nivo	****
Untreated vs. 2Gy No ICB	****
Untreated vs. 2Gy Atrezo+Nivo	****
Untreated vs. 4Gy No ICB	****
Untreated vs. 4Gy Atezo+Nivo	****

Appendix Table 14; The effects of Pembrolizumab and different levels of glutamine deprivation on the cell viability on OE33P and OE33R cell lines. Tukey's multiple comparison testing, n=3.

Tukey's multiple comparisons test	Summary
Untreated vs. 0Gy	****
Untreated vs. 0gy Pembro	****
Untreated vs. 2Gy No ICB	****
Untreated vs. 2Gy Pembro	****
Untreated vs. 4Gy No ICB	****
Untreated vs. 4Gy Pembro	****
Untreated vs. 0Gy	****
Untreated vs. 0gy Pembro	****
Untreated vs. 2Gy No ICB	****
Untreated vs. 2Gy Pembro	****
Untreated vs. 4Gy No ICB	****
Untreated vs. 4Gy Pembro	****
0Gy vs. 4Gy No ICB	*
0Gy vs. 4Gy Pembro	*
0Gy vs. Untreated	****
0Gy vs. 4Gy No ICB	**
0Gy vs. 4Gy Pembro	*
0gy Pembro vs. 2Gy Pembro	*
0gy Pembro vs. 4Gy No ICB	**
0gy Pembro vs. 4Gy Pembro	*
0gy Pembro vs. Untreated	****
0gy Pembro vs. 4Gy No ICB	***
0gy Pembro vs. 4Gy Pembro	**
2Gy No ICB vs. Untreated	****
2Gy Pembro vs. Untreated	****
4Gy No ICB vs. Untreated	****
4Gy Pembro vs. Untreated	****
Untreated vs. 0Gy	****
Untreated vs. 0gy Pembro	****
Untreated vs. 2Gy No ICB	****
Untreated vs. 2Gy Pembro	****
Untreated vs. 4Gy No ICB	****
Untreated vs. 4Gy Pembro	****
0Gy vs. 4Gy No ICB	*
0gy Pembro vs. 4Gy No ICB	**
0gy Pembro vs. 4Gy Pembro	*

Appendix Table 15; The effects of Nivolumab and different levels of glutamine deprivation on the cell viability on OE33P and OE33R cell lines. Tukey's multiple comparison testing, n=3.

Tukey's multiple comparisons test	Summary
Untreated vs. 0Gy	****
Untreated vs. 0gy Nivo	****
Untreated vs. 2Gy No ICB	****
Untreated vs. 2Gy Nivo	****
Untreated vs. 4Gy No ICB	****
Untreated vs. 4Gy Nivo	****
Untreated vs. 0Gy	****
Untreated vs. 0gy Nivo	****
Untreated vs. 2Gy No ICB	****
Untreated vs. 2Gy Nivo	****
Untreated vs. 4Gy No ICB	****
Untreated vs. 4Gy Nivo	****
0Gy vs. 4Gy No ICB	*
0Gy vs. 4Gy Nivo	***
0Gy vs. Untreated	****
0Gy vs. 4Gy No ICB	**
0Gy vs. 4Gy Nivo	***
0gy Nivo vs. 4Gy No ICB	*
0gy Nivo vs. 4Gy Nivo	***
0gy Nivo vs. Untreated	****
0gy Nivo vs. 4Gy No ICB	**
0gy Nivo vs. 4Gy Nivo	***
2Gy No ICB vs. Untreated	****
2Gy Nivo vs. 4Gy Nivo	*
2Gy Nivo vs. Untreated	****
2Gy Nivo vs. 4Gy Nivo	*
4Gy No ICB vs. Untreated	****
4Gy Nivo vs. Untreated	****
4Gy Nivo vs. 0Gy	***
4Gy Nivo vs. 0gy Nivo	**
4Gy Nivo vs. 2Gy Nivo	*
Untreated vs. 0Gy	****
Untreated vs. 0gy Nivo	****
Untreated vs. 2Gy No ICB	****
Untreated vs. 2Gy Nivo	****
Untreated vs. 4Gy No ICB	****
Untreated vs. 4Gy Nivo	****
0Gy vs. 4Gy No ICB	*
0Gy vs. 4Gy Nivo	***
0gy Nivo vs. 4Gy No ICB	*
0gy Nivo vs. 4Gy Nivo	**

Appendix Table 16; The effects of Atezolizumab and different levels of glutamine deprivation on the cell viability on OE33P and OE33R cell lines. Tukey's multiple comparison testing, n=3.

Tukey's multiple comparisons test	Summary
Untreated vs. 0Gy	****
Untreated vs. 0gy Atezo	****
Untreated vs. 2Gy No ICB	****
Untreated vs. 2Gy Atezo	****
Untreated vs. 4Gy No ICB	****
Untreated vs. 4Gy Atezo	****
Untreated vs. 0Gy	****
Untreated vs. 0gy Atezo	****
Untreated vs. 2Gy No ICB	****
Untreated vs. 2Gy Atezo	****
Untreated vs. 4Gy No ICB	****
Untreated vs. 4Gy Atezo	****
0Gy vs. 2Gy Atezo	**
0Gy vs. 4Gy No ICB	**
0Gy vs. Untreated	****
0Gy vs. 4Gy No ICB	**
0Gy vs. 4Gy Atezo	****
0gy Atezo vs. 2Gy Atezo	**
0gy Atezo vs. 4Gy No ICB	**
0gy Atezo vs. Untreated	****
0gy Atezo vs. 4Gy No ICB	***
0gy Atezo vs. 4Gy Atezo	****
2Gy No ICB vs. Untreated	****
2Gy No ICB vs. 4Gy Atezo	***
2Gy Atezo vs. Untreated	****
2Gy Atezo vs. 0Gy	*
2Gy Atezo vs. 0gy Atezo	*
2Gy Atezo vs. 4Gy Atezo	**
4Gy No ICB vs. Untreated	****
4Gy No ICB vs. 0Gy	*
4Gy No ICB vs. 0gy Atezo	*
4Gy No ICB vs. 4Gy Atezo	**
4Gy Atezo vs. Untreated	****
4Gy Atezo vs. 4Gy Atezo	***
Untreated vs. 0Gy	****
Untreated vs. 0gy Atezo	****
Untreated vs. 2Gy No ICB	****
Untreated vs. 2Gy Atezo	****
Untreated vs. 4Gy No ICB	****
Untreated vs. 4Gy Atezo	****
0Gy vs. 4Gy No ICB	**
0Gy vs. 4Gy Atezo	****
0gy Atezo vs. 4Gy No ICB	**
0gy Atezo vs. 4Gy Atezo	****
2Gy No ICB vs. 4Gy Atezo	****
2Gy Atezo vs. 4Gy Atezo	****
4Gy No ICB vs. 4Gy Atezo	*

Appendix Table 17; The effects of Atezolizumab and Pembrolizumab and different levels of glutamine deprivation on the cell viability on OE33P and OE33R cell lines. Tukey's multiple comparison testing, n=3.

Tukey's multiple comparisons test	Summary
Untreated vs. 0Gy	****
Untreated vs. 0gy Atezo+Pembro	****
Untreated vs. 2Gy No ICB	****
Untreated vs. 2Gy Atezo+Pembro	****
Untreated vs. 4Gy No ICB	****
Untreated vs. 4Gy Atezo+Pembro	****
Untreated vs. 0Gy	****
Untreated vs. 0gy Atezo+Pembro	****
Untreated vs. 2Gy No ICB	****
Untreated vs. 2Gy Atezo+Pembro	****
Untreated vs. 4Gy No ICB	****
Untreated vs. 4Gy Atezo+Pembro	****
0Gy vs. 4Gy Atezo+Pembro	*
0Gy vs. Untreated	****
0Gy vs. 4Gy No ICB	*
0Gy vs. 4Gy Atezo+Pembro	**
0gy Atezo+Pembro vs. 4Gy No ICB	*
0gy Atezo+Pembro vs. 4Gy Atezo+Pembro	*
0gy Atezo+Pembro vs. Untreated	****
0gy Atezo+Pembro vs. 4Gy No ICB	*
0gy Atezo+Pembro vs. 4Gy Atezo+Pembro	**
2Gy No ICB vs. Untreated	****
2Gy Atezo+Pembro vs. Untreated	****
4Gy No ICB vs. Untreated	****
4Gy Atezo+Pembro vs. Untreated	****
Untreated vs. 0Gy	****
Untreated vs. 0gy Atezo+Pembro	****
Untreated vs. 2Gy No ICB	****
Untreated vs. 2Gy Atezo+Pembro	****
Untreated vs. 4Gy No ICB	****
Untreated vs. 4Gy Atezo+Pembro	****
0Gy vs. 4Gy Atezo+Pembro	**
0gy Atezo+Pembro vs. 4Gy No ICB	*
0gy Atezo+Pembro vs. 4Gy Atezo+Pembro	**
2Gy Atezo+Pembro vs. 4Gy Atezo+Pembro	*

Appendix Table 18; The effects of Atezolizumab and Nivolumab and different levels of glutamine deprivation on the cell viability on OE33P and OE33R cell lines. Tukey's multiple comparison testing, n=3.

Tukey's multiple comparisons test	Summary
Untreated vs. 0Gy	****
Untreated vs. 0gy Atezo+Nivo	****
Untreated vs. 2Gy No ICB	****
Untreated vs. 2Gy Atezo+Nivo	****
Untreated vs. 4Gy No ICB	****
Untreated vs. 4Gy Atezo+Nivo	****
Untreated vs. 0Gy	****
Untreated vs. 0gy Atezo+Nivo	****
Untreated vs. 2Gy No ICB	****
Untreated vs. 2Gy Atezo+Nivo	****
Untreated vs. 4Gy No ICB	****
Untreated vs. 4Gy Atezo+Nivo	****
0Gy vs. 4Gy No ICB	*
0Gy vs. 4Gy Atezo+Nivo	*
0Gy vs. Untreated	****
0Gy vs. 4Gy No ICB	**
0Gy vs. 4Gy Atezo+Nivo	**
0gy Atezo+Nivo vs. 4Gy No ICB	*
0gy Atezo+Nivo vs. 4Gy Atezo+Nivo	**
0gy Atezo+Nivo vs. Untreated	****
0gy Atezo+Nivo vs. 4Gy No ICB	**
0gy Atezo+Nivo vs. 4Gy Atezo+Nivo	***
2Gy No ICB vs. Untreated	****
2Gy Atezo+Nivo vs. Untreated	****
4Gy No ICB vs. Untreated	****
4Gy No ICB vs. 0gy Atezo+Nivo	*
4Gy Atezo+Nivo vs. Untreated	****
4Gy Atezo+Nivo vs. 0gy Atezo+Nivo	*
Untreated vs. 0Gy	****
Untreated vs. 0gy Atezo+Nivo	****
Untreated vs. 2Gy No ICB	****
Untreated vs. 2Gy Atezo+Nivo	****
Untreated vs. 4Gy No ICB	****
Untreated vs. 4Gy Atezo+Nivo	****
0Gy vs. 4Gy No ICB	*
0Gy vs. 4Gy Atezo+Nivo	**
0gy Atezo+Nivo vs. 4Gy No ICB	**
0gy Atezo+Nivo vs. 4Gy Atezo+Nivo	**

Appendix Figure 1; Gating strategy for Immune checkpoint cells on OE33P cells. Gate 1 included all cells in the FSC versus SSCA plot, doublet cells were then excluded using FSC-H versus FSC-A plot, dead cells were excluded using zombie aqua viability marker.

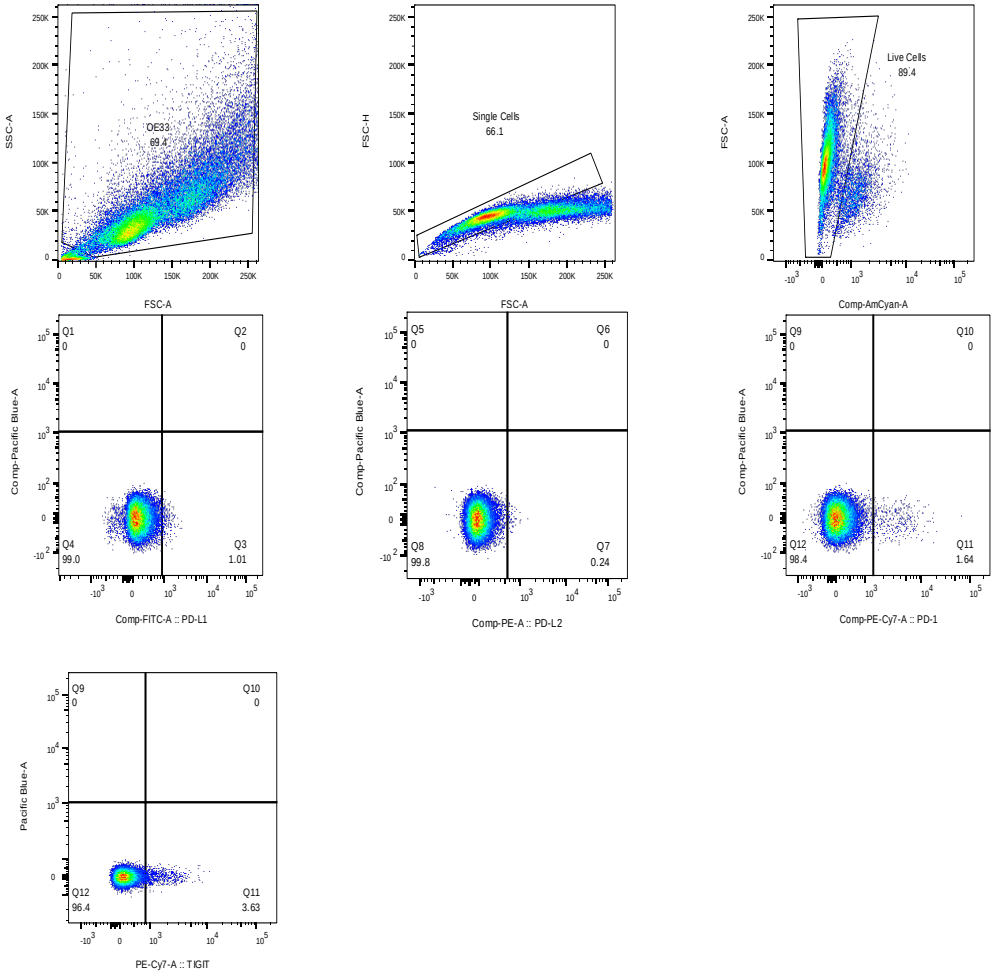

Appendix Figure 2; Gating strategy for DAMPS expression on OE33P cell line.
Gate 1 included all cells in the FSC versus SSCA plot, doublet cells were then excluded using FSC-H versus FSC-A plot, dead cells were excluded using zombie aqua viability marker.

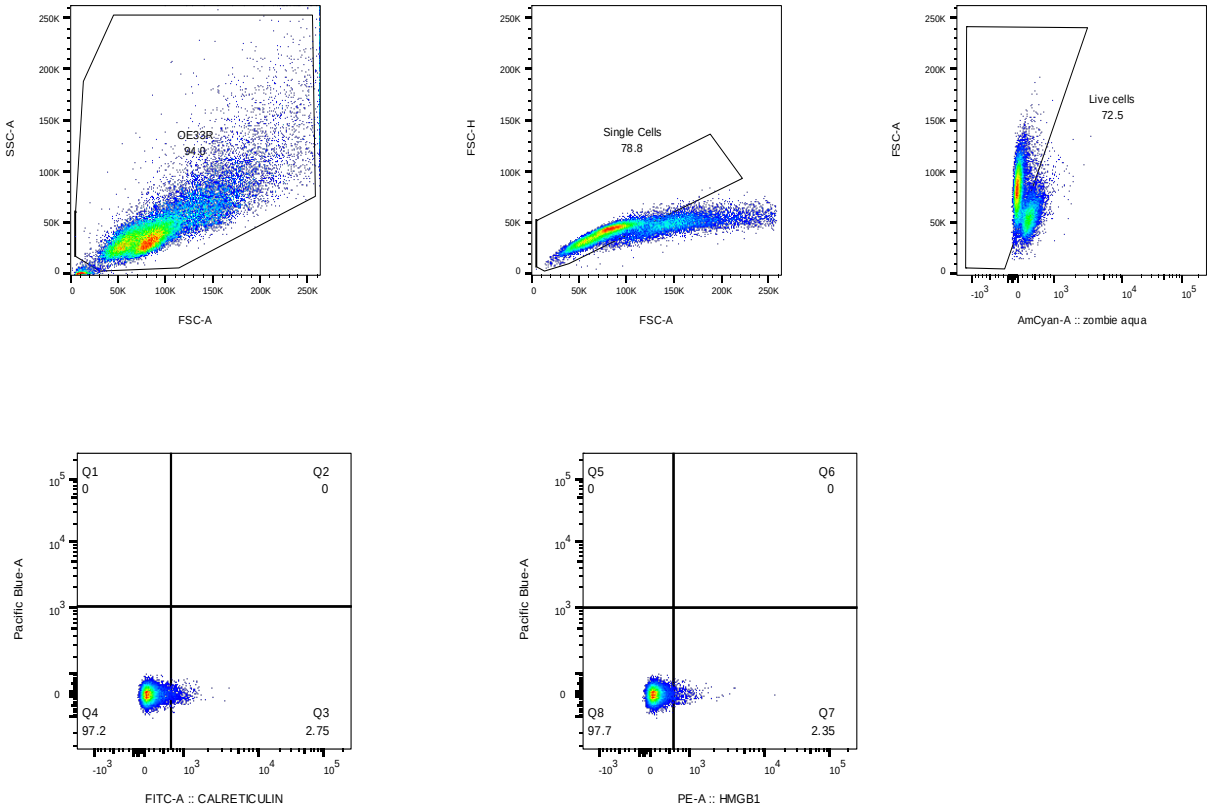

Appendix Figure 3; Gating strategy and representative dot plots for assessing the effect of radiation on cytokine production by T cells. Gate 1 included all cells in the FSC versus SSCA plot, doublet cells were then excluded using FSC-H versus FSC-A plot, dead cells were excluded using Zombie aqua viability marker. The intracellular surface expression of IFN-γ, TNF-α and IL-2 was assessed on CD3+, CD3+CD4+cells and CD3+CD8+cells. Representative dot plots are shown for IL-2, IL-10 and for IFN-γ gated on CD3+CD4+ cells post 2Gy irradiation.

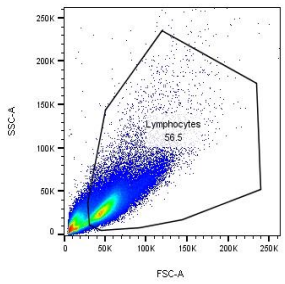

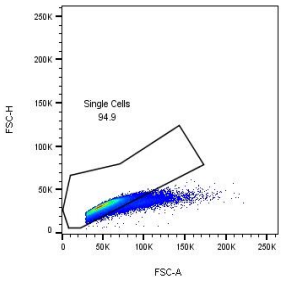

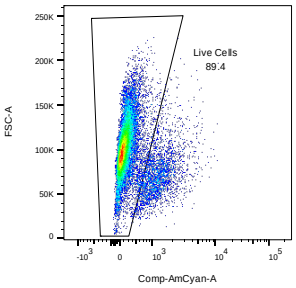

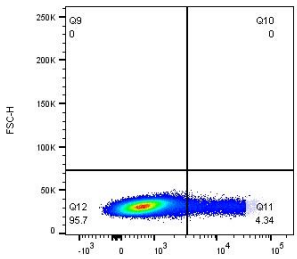

IFN- γ

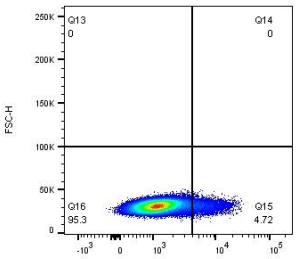

IL-2

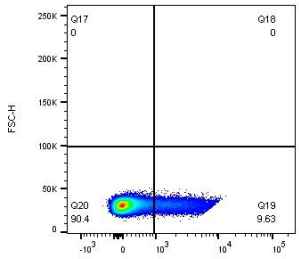

IL-10

Appendix Figure 4; Gating strategy for assessing direct effects of surgery on immune checkpoint expression perioperatively on T cells by flow cytometry. Gate 1 included all cells in the FSC versus SSCA plot, doublet cells were then excluded using FSC-H versus FSC-A plot, dead cells were excluded using zombie aqua viability marker. The expression of the checkpoints were assessed on all CD3+CD4+ and CD3+ CD8+ cells.